Benzylic Organosulfides and Analogues: Greener Synthesis, Anti-cancer Activities and the Feasibilities of H_2S Donation

A Thesis

Submitted in Partial Fulfilment of the

Requirements for the Degree of

Doctor of Philosophy

by

Debojit Bhattacherjee

Centre for the Environment

Indian Institute of Technology Guwahati

Assam – 781039, India

September 2022

Benzylic Organosulfides and Analogues: Greener Synthesis, Anti-cancer Activities and the Feasibilities of H_2S Donation

A Thesis

Submitted in Partial Fulfilment of the

Requirements for the Degree of

Doctor of Philosophy

by

Debojit Bhattacherjee

Roll no. - 166152101

Centre for the Environment

Indian Institute of Technology Guwahati

Assam – 781039, India

September 2022

Dedicated To

All the souls deceased of cancer

Indian Institute of Technology Guwahati

Centre for the Environment

Guwahati

Assam – 781039

STATEMENT

I hereby declare that the research work described in the thesis entitled "***Benzylic Organosulfides and Analogues: Greener Synthesis, Anti-cancer Activities and the Feasibilities of H_2S Donation***" is the outcome of investigations carried out by me under the supervision of **Dr. Krishna P. Bhabak** and **Prof. Tapas K. Mandal** at Centre for the Environment, Indian Institute of Technology Guwahati, India, for the award of degree of Doctor of Philosophy.

In keeping with the general practice of reporting scientific observations, due acknowledgements have been made wherever the work described in this thesis is based on the findings of other investigators. Any omission that might have occurred by oversight or mistake is unintentional and gravely regretted.

_____

Debojit Bhattacherjee

Roll No: 166152101

Indian Intitute of Technology Guwahati

Centre for the Environment

Guwahati

Assam – 781039

CERTIFICATE

This is to certify that the research work presented in the thesis entitled "***Benzylic Organosulfides and Analogues: Greener Synthesis, Anti-cancer Activities and the Feasibilities of H_2S Donation***" by **Mr. Debojit Bhattacherjee** (Roll no: 166152101) for the award of the degree of Doctor of Philosophy is an authentic record of the results obtained from the research work carried out under our supervision in Centre for the Environment, Indian Institute of Technology Guwahati, India. The research work reported in his thesis is original and the same has not been submitted elsewhere for a degree.

Prof. Tapas K. Mandal

(Co-supervisor)

Professor
Department of Chemical Engineering
Indian Institute of Technology Guwahati
Assam – 781039

Dr. Krishna P. Bhabak

(Supervisor)

Associate Professor
Department of Chemistry
Indian Institute of Technology Guwahati
Assam – 781039

Acknowledgements

I would like to take this opportunity to appreciate the kind help and support of all the people around me to make the journey, a very memorable one. Without their help, it would not have been possible to achieve this goal.

First and foremost, I would like to express my deepest gratitude towards my thesis supervisor **Dr. Krishna P. Bhabak** for his constant and persistent support, motivation and guidance throughout the entire tenure of my research work. His perseverant support, unparalleled efforts and never-ending patience, even in the midst of COVID-19 pandemic, proved to be extremely important for fulfilling this goal. Moreover, his mindful scrutiny and scrupulous suggestions of manuscripts were invaluable assets in this journey. Under his close supervision, the ideals of a true researcher have been inculcated within me. It has been, indeed, a very nice and pleasant experience in working with him.

My deepest gratitude goes out to my co-supervisor, **Prof. Tapas K. Mandal**, who has been a constant support and mentor throughout my Ph.D. tenure. His meticulous scrutiny and thoughtful suggestions were essential to my success. It has been, indeed, a very nice and pleasant experience in working with him.

I would like to extend my acknowledgement to my doctoral committee members **Prof. Subhendu S. Bag** (Chairman), **Dr. Animesh Das** (Member) and **Dr. Rajkumar P. Thummer** (Member) for taking their time out of their busy schedule to review my progress and also to share their knowledge, provide invaluable suggestions to overall improve my research.

I am thankful to **Indian Institute of Technology Guwahati** for providing me fellowship, and to the **Centre for the Environment**, **Central Instruments Facility** (**CIF**) for providing me with instrumental facilities for nuclear magnetic resonance (NMR) and single crystal X-ray diffraction (SC-XRD) experiments. Additionally, I would like to acknowledge all the instrument operators and non-teaching staffs of Department of Chemistry, Centre for the Environment and Administrative building, IIT Guwahati for extending their kind help in whichever ways, as applicable.

I would like to specially acknowledge my colleague **Dr. Kaustav Banerjee**, for his homely care, other professional help and moral support in every academic and personal perspectives, during the ups and downs of my PhD journey. I am forever grateful and

thankful towards other lab members **Mr. Sulendar K. Mahato**, **Mr. Abu Sufian** and **Ms. Shivani Marandi**, **Ms. Pallavi Barman**, **Mr. Rahul Kesarwani**, **Mr. Roopjyoti Misra**, **Mr. MD. Badirujjaman** for bearing with me throughout the entirety of my research journey.

Next I would like to thank all the project students **Ms. Queen Bhardwaj**, **Mr. Nirmal Kumar**, **Mr. Niladri Sekhar Mondal**, **Mr. Partha Sarathi Karmakar**, **Ms. Ankita Sahu**, **Ms. Sharmistha De**, and **Mr. Devarshi Bharadwaj** for their contributions towards my research work.

I would like to specially acknowledge my collaborators **Ms. Khyati Raina**. and **Dr. Rajkumar P. Thummer**, Dept. of Biosciences and Bioengineering, Indian Institute of Technology Guwahati, for their active collaborative effort. Additionally, I would also like to extend my sincere acknowledgements towards **Dr**. **Chitra Basu** and **Dr**. **Runa Sur**, Calcutta University, for their significant collaborative contribution. Furthermore, I would like to extend my sincere gratitude to Late **Dr. Hemant K. Srivastava** for his unforgettable support during the computational studies. Further, I would like to thank **Ms. Samiyara Begum** for performing the computational studies.

I would like to extend my thanks to all of my batch mates, friends and juniors specially **Dr. Nirmalya Pradhan**, **Dr. Soutick Nandi**, **Mr. Gaurav Bhatt**, **Ms. Chandrima Das**, **Ms. Gloria Narayan**, **Mr. Riddhi Banerjee** and **Mr. H. Krishna Kumar** for providing me professional assistance out of their busy schedule.

Next, most importantly I would like to thank my family. I would like to mention my father **Mr. Ramkrishna Bhattacharya** and my mother **Mrs. Debjani Bhattacharjee** and my grandmother **Late. Ila Mukherjee** for raising me into who I am. Last but not the least, I must acknowledge the unparalleled motivation and constant encouragement I received from **Ms. Maitreyee Ganguly** and **Dr. Sourav Mal** during my difficult times. Finally, I would like to thank the Almighty God for making this possible and giving me the strength, perseverance and determination to work.

Sd/-_____

Debojit Bhattacherjee

Table of Contents

		Page
	Abbreviations	i - iv
	Synopsis	v - xvi
Chapter 1	***Introduction***	
1.1	Hydrogen sulfide (H_2S) and its origin	3
	1.1.1. Environmental sources of H_2S	4
	1.1.2. H_2S production by sulfate-reducing microbes (SRM)	5
	1.1.3. Dietary sources of H_2S	6
1.2	Regulation and metabolism of H_2S	7
	1.2.1. Biosynthesis of H_2S	7
	1.2.2. Metabolism of H_2S *via* oxidation	9
1.3	Chemical donors of H_2S	10
	1.3.1. Inorganic donors of H_2S	10
	1.3.2. Naturally occurring H_2S donors	10
	1.3.3. Synthetic OSCs as H_2S donors	12
	1.3.3.1. Hydrolysis-triggered donors	12
	1.3.3.2. Thiol-triggered donors	13
	1.3.3.3. Light-triggered donors	14
	1.3.3.4. Enzyme-triggered donors	15
1.4	Methods of detection of H_2S	16
	1.4.1. Spectrophotometric method	16
	1.4.2. Electrochemical method	17
	1.4.3. Fluorogenic detection methods	19
1.5	Chemical biology of H_2S	21
	1.5.1. Interaction with metalloenzymes	21
	1.5.2. Protein persulfidation	22
1.6	Role of H_2S in cancer	23
	1.6.1. Proangiogenic role of H_2S agents	24
	1.6.2. H_2S-mediated persulfidation	25

1.6.3. Apoptotic effect of H_2S 25
1.6.4. Modulation of glucose uptake process by H_2S donors 26
1.6.5. H_2S suppresses cell survival-related signaling pathways 26
1.6.6. H_2S induces cell cycle arrest 26
1.7 Biological activities of garlic-derived H_2S donors 26
1.8 Thesis objective 28
1.9 Thesis overview 29
1.10 References 29

Chapter 2 ***Design, Synthesis and Anti-cancer Activities of Benzylic Derivatives of Diallyl Disulfide (DADS) and the Corresponding Diselenide***
2.1 Introduction 41
2.2 Outline of the chapter 42
2.3 Results and discussion 43
2.3.1. Synthesis of disulfides and diselenides 43
2.3.2. Important structural features in disulfide **2.3** and diselenide **2.8** 44
2.3.3. Anti-proliferative activities of disulfides and diselenides 46
2.3.4. Anti-proliferative activities in different organ-specific cancer cell lines 49
2.3.5. Cellular morphology analysis using DAPI 49
2.3.6. Evaluation of the anti-migratory activity of compound **2.8** 50
2.3.7. *In vitro* antioxidant activities of disulfides and diselenides 51
2.3.8. Generation of intracellular reactive oxygen species (ROS) by the test compounds 52
2.3.9. Western blot experiment 53
2.4 Conclusions 54
2.5 Experimental section 55
2.5.1. Materials and methods 55
2.5.2. General synthesis of disulfides DBDS, **2.2**-**2.5** 55
2.5.3. General synthesis of diselenides **2.6**-**2.10** 57
2.5.4. GSH–GSSG coupled assay 58

2.5.5. Crystallography 58
2.5.6. Cell lines and culture 59
2.5.7. Cell viability assay 59
2.5.8. Cellular morphology study by a nuclear staining dye DAPI 59
2.5.9. Wound healing (scratch) assay 60
2.5.10. Measurement of intracellular ROS levels in MCF-7 cells 60
2.5.11. Western blot analysis 60
2.5.12. Statistical analysis 61
2.6 References 61

Chapter 3 ***Selective Synthetic Methodologies and Preliminary Anti-proliferative Activities of Symmetrical Organodisulfides and Organotrisulfides***

3.1 Introduction 67
3.2 Outline of the chapter 70
3.3 Results and discussion 70
3.3.1. Optimization of trisulfide synthesis 70
3.3.2. Substrate scope of trisulfides 73
3.3.3. Optimization and substrate scope of disulfides DBDS, DADS and **3.1a-3.19a** 74
3.3.4. Characterization of trisulfide, disulfide and monosulfide 77
3.3.5. Mechanistic investigation 78
3.3.6. Theoretical investigation 81
3.3.7. Anti-proliferative activities of trisulfides 83
3.3.8. Estimation of the H_2S donation capacity of **3.4** and DATS 87
3.4 Conclusions 89
3.5 Experimental Procedure 89
3.5.1. Materials and method 89
3.5.2. Synthesis of Bunte salts 90
3.5.3. General synthetic method for trisulfides 90
3.5.4. Bulk-scale synthesis of a representative trisulfide **3.4** 94
3.5.5. Synthesis of unsymmetrical trisulfide **3.22** 95

3.5.6. General synthesis of disulfides 95
3.5.7. Synthesis of unsymmetrical disulfide **3.22a** 99
3.5.8. Synthesis of monosulfide **3.11b** 100
3.5.9. HPLC analysis 100
3.5.10. DFT calculations 101
3.5.11. X-Ray crystallography 101
3.5.12. Cell culture 101
3.5.13. Cellular morphology and viability studies 102
3.5.14. Detection of Hydrogen sulfide (H_2S) release by MB assay 103
3.5.15. H_2S release from **3.4** in cellular medium and its detection using fluorescent probe NAP-N_3 103
3.6 References 103

Chapter 4 ***Anti-cancer Activity of Benzylic Organotrisulfides in Triple-negative Breast Cancer: Inactivation of Wnt/β-catenin Signaling Cascade and Contribution of the Released Hydrogen Sulfide***

4.1 Introduction 109
4.2 Outline of the chapter 111
4.3 Results and discussion 111
4.3.1. Synthesis of symmetrical organopolysulfides 111
4.3.2. Preliminary anti-proliferative activities 112
4.3.3. Modulation of cell cycle of TNBC cells by compound **4.1** 116
4.3.4. Apoptosis study and the expression of key cancer marker proteins in TNBC cells 118
4.3.5. Regulation of Wnt/β-catenin signaling by compound **4.1** 120
4.3.6. Mechanistic insights for the inhibition of β-catenin by compound **4.1** 121
4.3.7. Feasibility of H_2S donation from compound **4.1**, DBTS and DATS 124
4.3.8. Sustained release of H_2S from organic donors and its anti-proliferative activity 126
4.3.9. Modulation of p53 and P21 expression by the released H_2S 130

from compound **4.1**

4.3.10. Proposed mechanistic pathway for the anti-proliferative activity of compound **4.1** 132

4.4 Conclusions 133

4.5 Experimental section 134

4.5.1. Materials and method 134

4.5.2. Synthesis of Bunte salts 134

4.5.3. Synthesis of compound **4.1** 135

4.5.4. Synthesis of compound **4.2** 135

4.5.5. Synthesis of compound **4.3** 136

4.5.6. Synthesis of compound **4.5** 136

4.5.7. HPLC analysis 137

4.5.8. Detection of H_2S release by MB assay 137

4.5.9. Measurement of the released H_2S using the turn-on fluorogenic probe **WSP2** 137

4.5.10. Cell culture 138

4.5.11. Cell viability assay 138

4.5.12. Effect of compound **4.1** on cellular morphology 138

4.5.13. GFP-lentivirus production and evaluation of cellular morphology 139

4.5.14. Wound healing (Scratch) assay 140

4.5.15. Cell cycle analysis 140

4.5.16. FITC-Annexin V/ PI dead cell apoptosis assay 140

4.5.17. Estimation of ROS profile after treatment with **4.1** 141

4.5.18. Intracellular H_2S detection 141

4.5.19. Western blot analysis 142

4.5.20. Subcellular fractionation 142

4.5.21. Molecular docking studies 143

4.5.21.1. Protein preparation 143

4.5.21.2. Ligand preparation 143

4.5.21.3. Receptor grid generation and docking method 143

4.5.22. Statistical analysis 144

4.6 References 144

Annexure I	Thesis overview and future perspectives	149
Annexure II	List of publications and conferences	153
Annexure III	Supplementary data of Chapter 2	157
Annexure IV	Supplementary data of Chapter 3	173
Annexure V	Supplementary data of Chapter 4	231

Abbreviations

Å	Angstrom
ACE	Angiotensin-converting enzyme
AE	Anion exchanger
Ag	Silver
Akt	Protein kinase B
AMPK	5' AMP-activated protein kinase
ANOVA	Analysis of variance
AP-1	Activator protein-1
APS	Adenosine-5'-phosphate
ARG	L-Arginine
AS	Atherosclerosis
ASN	L-Asparagine
ASR	Assimilatory sulfate reduction
atm	Atmosphere
ATP	Adenosine triphosphate
Bcl2	B-cell lymphoma 2
CA	Carbonic anhydrase
CaSKi	Human chorionic gonadotropin
CAT	Cysteine amino transferase
CBS	Cystathionine-β-synthase
$CDCl_3$	Chloroform-d_3
CdS	Cadmium sulfide
CK-1α	Casein kinase 1α
CO_2	Carbon dioxide
Con A	Concanavalin A
CoQ	Coenzyme Q
COS	Carbonyl sulfide
COX-2	Cyclooxygenase-2
CSE	Cystathionine-γ-lyase
CuS	Copper sulfide
CYP	Cytochrome P450
Cys	L-Cysteine
CysC	Adenylyl-sulfate kinase
CysDN	Sulfate adenylyl transferase
CysH	PAPS reductase
CysIJ	Sulfite reductase
DADS	Diallyl disulfide
DAO	Diamine oxidase
DAS	Diallyl monosulfide
DATS	Diallyl trisulfide
DBDS	Dibenzyl disulfide
DBMS	Dibenzyl monosulfide
DBTS	Dibenzyl trisulfide
DCFH-DA	Dichloro-dihydro-fluorescein diacetate
DFT	Density functional theory
DLD-1	Colorectal adenocarcinoma cell line
DMEM	Dulbecco's modified Eagle medium
DMSO	Dimethyl sulfoxide

DPBS	Dulbecco's phosphate buffered saline
DSR	Dissimilatory sulfate reduction
DTT	1,4-Dithiothreitol
DTTS	Diallyl tetrasulfide
E3	Ubiquitin ligase
EGFR	Epidermal growth factor receptor
ER+	Estrogen receptor positive
ERK	Extracellular signal-regulated kinase
ESI-MS	Electrospray ionization mass spectroscopy
ETHE1	Sulfur dioxygenase
FACS	Fluorescence-activated single cell sorting
FBS	Fetal bovine serum
g	Gram
GAPDH	Glyceraldehyde-3-phosphate dehydrogenase
GFP	Green fluorescent protein
GLU	L-Glutamic acid
GSH	Glutathione reduced
GSK-3β	Glycogen synthase kinase-3β
GSSG	Glutathione disulfide
GSSH	Glutathione persulfide
GSTP-1	Glutathione S-transferase pi 1
h	Hour(s)
H_2S	Hydrogen sulfide
H_2SO_4	Sulfuric acid
HAT	H-atom transfer
HCC	Hepatocellular carcinoma
HCT-116	Human colorectal carcinoma cell
HEK-293	Human embryonic kidney cells
HepG2	Human hepatoma cells
HIF-1α	Hypoxia inducible factor-1α
His	L-Histidine
HOCl	Hypochlorus acid
HPLC	High performance liquid chromatography
HS^-	Hydrosulfide
Hz	Hertz
IC_{50}	Inhibitory concentration 50%
IRC	Intrinsic reaction coordinate
ISE	Ion-selective electrode
K	Kelvin
LC-MS	Liquid chromatography-mass spectrometry
LDL	low-density lipoprotein
LiCl	Lithium chloride
LOD	Limit of detection
LRP5/6	Low-density lipoprotein-related receptors 5
LYS	L-Lysine
M	Molar
M.P.	Melting point
MB	Methylene blue
mBBr	Monobromobimane

MCF-7	Michigan cancer foundation-7
MG-63	Human osteosarcoma
MHz	Mega hertz
Min	Minute(s)
mL	Millilitre
mM	Milimolar
mM	Milimolar
mm	Millimetre
mmol	Milimole
MMP	Matrix metalloprotease protein
MS	Methionine synthase
3-MST	3-Mercaptopyruvate sulfurtransferase
mTOR	Mammalian target of rapamycin
MTT	Cell viability assay
Na_2S	Sodium sulfide
Na_2Se_2	Disodium diselenide
NAC	*N*-acetyl L-cysteine
$NADP^+$	Nicotinamide adenine dinucleotide phosphate oxidized
NADPH	Nicotinamide adenine dinucleotide phosphate reduced
NaSH	Sodium hydrosulfide
NEM	*N*-ethylmaleimide
NHE	Sodium/proton exchanger
NKE	Normal kidney epithelial cells
NMR	Nuclear magnetic resonance
NO	Nitric oxide
Nrf2	Nuclear factor erythroid 2-releated factor 2
NSAIDs	Non-steroidal anti-inflammatory drugs
^oC	Degree Celsius
$OH^{\cdot}$	Hydroxyl radical
ORTEP	Oak ridge thermal ellipsoid plot
OSCs	Organosulfur compounds
PAG	*D,L*-Propargylglycine
PAPS	3'-Phospho-adenosine-5'-phosphate
PARP	Poly (ADP-ribose) polymerase
PBS	Phosphate Buffer Saline
PC3	Prostate cancer cells
PDB	Protein data bank
Pet. Ether	Petroleum ether (60 – 80)
Ph	Phenyl
PI	Propidium iodide
PI3K	Phosphoinositide 3-kinase
PMSF	Phenylmethylsulfonyl fluoride
ppb	Parts per billion
ppm	Parts per million
PTEN	Phosphatase and tensin homologue
Q-TOF	Quadrupole time-of-flight
RIPA	Radio-immunoprecipitation assay P (Lysis buffer)
RNS	Reactive nitrogen species
ROS	Reactive oxygen species

rt/RT	Room temperature
$S_2O_3^{2-}$	Thiosulfate
SAC	S-allyl cysteine
SARS-CoV-2	Severe acute respiratory syndrome coronavirus 2
SdB	Sulfide dibimane
SDS	Sodium dodecyl sulfate
SO	Sulfide oxidase
SO_2	Sulfur dioxide
SO_4^{2-}	Sulfate
SQR	Sulfide quinone reductase
SRM	Sulfate-reducing microbes
STAT-3	Signal transducer and activator of transcription 3
TCF/LEF-1	T-cell factor/lymphoid enhancer factor
TiO_2	Titanium dioxide
TLC	Thin layer chromatography
TML	Trimethyl lock
TNBC	Triple-negative breast cancer
TNF-α	Tissue necrosis factor-α
TRIM	Tripartite motif
TrxR	Thioredoxin reductase
TS	Transition state
TST	Thiosulfate sulfurtransferase
UV-Vis	Ultra-violet visible
VEGF	Vascular endothelial growth factor
WHO	World health organisation
Wnt	Wingless-related integration site
β-Trcp	β-Transducin repeat-containing protein
δ	Chemical shift (ppm)
ΔOD	Difference in optical density
µg	Microgram
µL	Microliter
µM	Micromolar

In the year of 1777, a Swedish-German chemist Carl Wilhelm Scheele, discovered an essential bio-active gaseous molecule popularly known as hydrogen sulfide (H_2S).[1] Approximately 100 years later of this discovery, H_2S producing bacteria was isolated and cultured. Interestingly, the synthesis of H_2S generally occurred from the elemental sulfur source or sulfur-containing amino acids, majorly found in living systems of the earth. The active catabolism of H_2S is found to be essential for plants, bacteria and mammalian systems. Since then, an array of research has been conducted to understand the biological importance of H_2S towards the different form of life on the earth. In mammals, H_2S producing enzymes such as, cystathionine gamma-lyase (CSE), cystathionine β-synthase (CBS) and 3-Mercaptopyruvate sulfurtransferase (3-MST) have been found to be crucial for the cellular growth and proliferation.[2] The active research on the exploration of detailed biological applications of inorganic and organic H_2S donors began after 1980.[3] Mainly, the H_2S donors are classified into two major categories such as inorganic donors (sulfide and bisulfide salts) and organic donors (various organosulfur compounds including trisulfides, disulfides, isothiocyanates, dithiophosphines, thiones, thiocarbonates etc). However, the detailed biological activities of inorganic H_2S donors (Na_2S and NaHS) revealed several limitations due to the instantaneous release of H_2S from the inorganic salts. To counter the problem, higher doses of the salts (up to millimolar concentration) have been used to maintain the level of H_2S in the study, which is therapeutically injudicious. Moreover, the supporting literature has identified the limitations of fast-release H_2S donors over the sustained-release H_2S donors, especially for the treatment of cancer. Therefore, the various organosulfur compounds capable of releasing H_2S have been developed in the last two decades for the sustained H_2S delivery. Among them, garlic-derived organosulfur compounds were majorly explored as organic donors of H_2S and applied in many disease models. Among the established polysulfides, diallyl sulfide (DAS), diallyl disulfide (DADS), and diallyl trisulfide (DATS) are commonly studied as antioxidants in several diseases including cancer.[4] Studies showed that a higher dose of DADS could promote anti-cancer activities in different organ-specific cell types. In late 2000, Lin *et al*. reported DADS-induced apoptosis in human cervical cancer cells (Ca Ski) *via* the generation of reactive oxygen species (ROS) and Ca^{2+}-dependent mitochondrial apoptosis.[5] Furthermore, DAS treatment with other chemotherapeutic drugs served as an adjuvant therapeutic strategy to protect the cellular redox balance by decreasing the ROS-mediated cell damages in normal tissues.[6] An

organopolysulfide such as DATS have been screened as a potent H_2S donor towards many disease conditions. Among the other pharmacological activities, DATS was also found to be a prominent cytotoxic and chemopreventive molecule against cancer and inflammatory diseases. In 2005, Herman-Antosiewicz and co-workers have reported the cell cycle-specific activities of DATS in human prostate cancer cells. They have shown that, upon the treatment of DATS, activation of DNA damage checkpoint markers such as checkpoint kinase 1 and checkpoint kinase 2 took place.[7]

The burden of cancer incidence increases largely across the globe. According to the GLOBOCAN report, the cancer burden is expected to be 28.4 million in 2040, a 47% rise from 2020 with a risk of a high mortality rate. The global statistics stated that the heterogeneity of breast cancer is the most common cause of death in a woman population. Among all the types of cancers, triple-negative breast cancer (TNBC) showed very high invasiveness and very low response to medicines due to the absence of major receptor targets (Estrogen, progesterone and HER-2). Therefore, development of small-molecule anti-cancer therapeutics is certainly important and challenging for the treatment of breast cancer in general and triple-negative sub-type of particular.

The present thesis, entitled "***Benzylic Organosulfides and Analogues: Greener Synthesis, Anti-cancer Activities and the Feasibilities of H_2S Donation***" consists of four chapters, based on the results of experimental and computational works performed during the complete course of Ph.D. research tenure.

Chapter 1: Introduction

The **first chapter** contains general introduction relevant to H_2S and its donors. A brief history and chemical properties of H_2S and its impact on environmental ambiances are discussed here (Figure 1). The introduction section has been divided into four sections, firstly, a brief and concise review has been made regarding the different sources (bacterial, plant and dietary) of H_2S. Secondly, the detailed biochemical aspects of H_2S catabolism and metabolism have been elaborated. Thirdly, owing to the emergence of H_2S research in medical science, methods for an accurate and quantitative detection of H_2S in the biological samples has been discussed. Finally, detailed pharmacological activities of H_2S towards many disease models have been discussed with appropriate examples. Furthermore, the impact of H_2S donation towards the progression and metastasis of cancer and the possible association with the modes of H_2S delivery rate (fast

or sustained delivery) from the chemical donors (inorganic and organic) have been discussed. The synthetic H_2S donors are mainly designed to combat different disease states and the controlled/sustained donation of H_2S has been shown to be crucial for the beneficial impacts of H_2S in the field of drug delivery. Discussion has been made on the development of various stimuli-triggered organic donors of H_2S such as (i) hydrolysis-based H_2S donors (ii) biothiol-triggered H_2S donors (iii) light-triggered H_2S donors (iv) enzyme-triggered H_2S donors etc.[8-10] Over the last two decades, physiological and pharmacological effects of H_2S using different organic donors have been explored to a large extent. Herein, the detailed overview of H_2S-mediated biological effects on different disease conditions (nervous system, cardiovascular system, neurological disorders, ion channels and inflammatory responses) have been explored in addition to its impact on cancer. Growing evidences support the dual role of H_2S towards progression and growth of cancer.[11] The detailed signaling aspects upon the donation of H_2S have been discussed in this section. Furthermore, the proangiogenic and anti-cancer effect of different H_2S donors have been highlighted.

Inspired by the previous reports on organopolysulfide-mediated H_2S donation toward cancer treatment, we developed an interest in designing a selective synthetic strategy for the synthesis of garlic-inspired organopolysulfides. Further, we screened their H_2S donation capacities in a cellular medium and studied detailed mechanistic insights towards for its anti-cancer activities. The current thesis explored the following possibilities:

1. It is not clear whether the anti-cancer activity of the organosulfur compounds in garlic could be enhanced further with some synthetic analogues or not.
2. Can organopolysulfides be synthesized in a very selective and convenient manner?
3. The correlation between the ease of H_2S release from organopolysulfides and their anti-cancer activities is missing.
4. Detailed mechanistic pathways for the anti-cancer activities of organopolysulfides and the possible involvement of the released H_2S is absent.

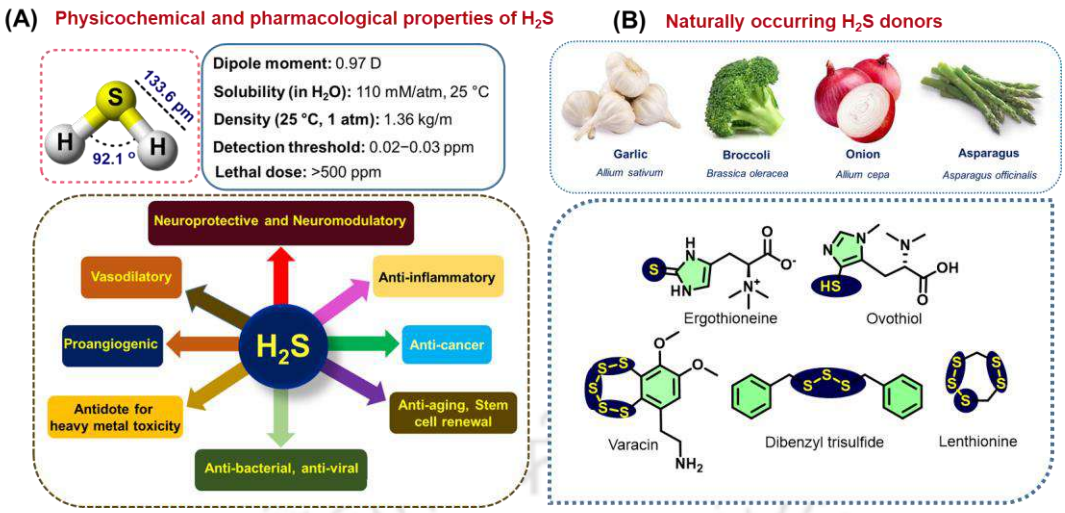

Figure 1. (A) General physicochemical and pharmacological properties of H_2S. (B) Chemical structures of some representative organosulfur compounds present in *allium* vegetables and other natural sources.

Chapter 2: Design, Synthesis and Anti-cancer Activities of Benzylic Derivatives of Diallyl Disulfide (DADS) and the Corresponding Diselenide

As discussed in last section, although a number of reports describe the medicinal impacts of different garlic-derived organosulfur compounds including allyl sulfides, the synthesis followed by the bio-evaluation of the structural analogues of allyl sulfides for detailed structure-activity correlations is rare in the literature. In search of developing newer derivatives with potential anti-cancer activities, we have synthesized a series of benzylic disulfide derivatives of DADS with different substituents at the *para*-position of benzene ring (compounds **1**-**5**, Figure 2).

Furthermore, to understand the importance of sulfur atom in DADS and in its benzylic derivatives **1-5** towards their anti-proliferative activities the corresponding selenium analogues (**6-10**) were also synthesized for a detailed structure-activity correlation studies (Figure 2). The synthesized disulfides and diselenides were evaluated for their anti-proliferative activities in breast adenocarcinoma cells (MCF-7). The preliminary anti-proliferative activity revealed significantly higher potency of diselenides over the corresponding disulfides as a general trend. Our study further revealed that the activity of organodisulfides/diselenides could be increased several-folds upon the introduction of a cyano group at the para-position of the benzene ring. The 4-cyano derivative was found to be more selective towards ER+ human breast cancer cell line

(MCF-7) over the non-cancerous normal kidney epithelial cells (NKE). The 4-cyano substituted disulfide **3** showed much higher potency than DADS, indicating the importance of 4-cyano group in enhancing the effectiveness of disulfide compounds. Interestingly, all the benzylic diselenides exhibited almost 9-16 fold higher anti-proliferative activity than the well-known organoselenium compound ebselen (2-Phenyl-1,2-benzoselenazol-3(2*H*)-one) against the MCF-7 cells.

To further investigate the mechanistic aspect of few potent compounds, estimation of the intracellular ROS level (DCF-DA assay) was studied using flow cytometry. Interestingly, compound **8** exhibited an increased ROS level in the malignant cells as compared to the non-malignant cells. Furthermore, the anti-migratory activity of compound **8** was evaluated using conventional scratch assay in MCF-7 cells. Interestingly, a significantly higher anti-migratory behaviour of the cells was observed in the presence of compound **8** (0.5 and 1.0 µM) as compared to the vehicle control. Finally, the western blot analysis was performed to estimate the expression level of several cancer promoting proteins. Upon the treatment of compound **8** (0.5 and 1.0 µM), a significant down-regulation of Procaspase 3, Bcl2 and Survivin were observed in comparison with the loading control.

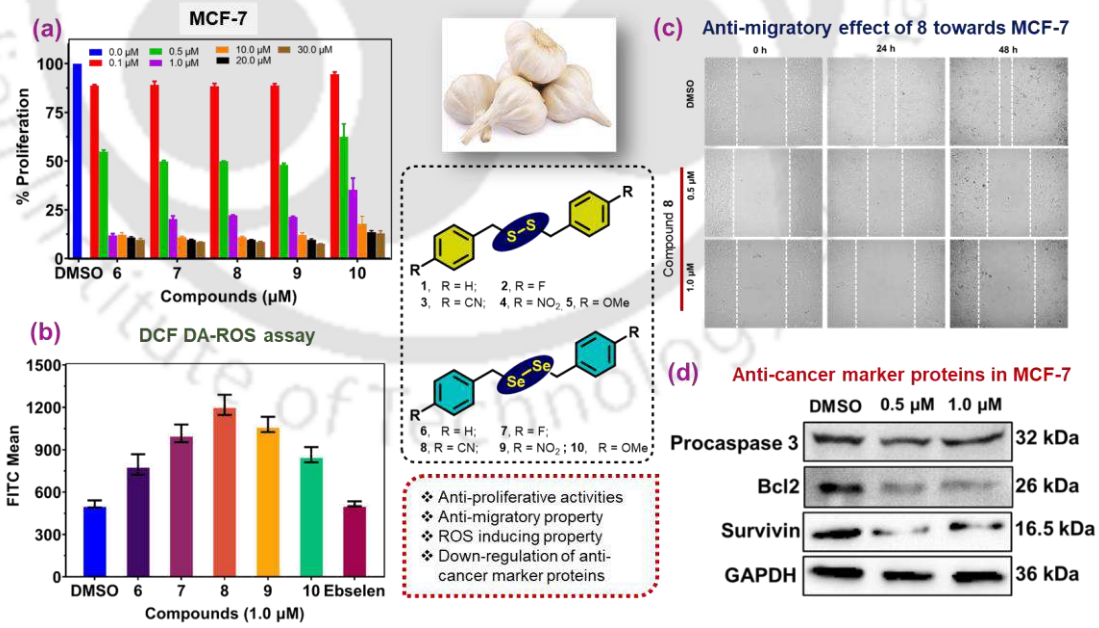

Figure 2. Brief highlights of chapter 2; (a) Comparative dose-dependent (0.0, 0.1, 0.5, 1.0, 10.0, 20.0 and 30.0) anti-proliferative activities of compounds **6-10** in MCF-7 cells

over 24 h. (b) Estimation of the intracellular ROS level in MCF-7 cells in the presence of compounds **6-10** and ebselen using flow cytometry. (c) Anti-migratory effect of compound **8** against MCF-7 cells. (d) Western blot experiments for the modulation of the expression level of few key cancer-related marker proteins in MCF-7 cells upon the treatment of compound **8** (0.5 and 1.0 µM) after an incubation for 48 h.

Chapter 3: Selective Synthetic Methodologies and Preliminary Anti-proliferative Activities of Symmetrical Organodisulfides and Organotrisulfides

The organic sulfur compounds (OSCs) present in garlic play key roles for its notable medicinal properties particularly towards cancer. Among the lipid soluble allyl sulfides (DAS, DADS and DATS) present in crushed garlic, DATS is reported to have much superior anti-cancer activities than the corresponding disulfide and monosulfide. However, an effective and selective synthetic method for these allyl sulfides is much difficult firstly owing to their co-formation in most conventional synthetic methods and secondly due to their similar polarities that further complicate their separation.

In the present study, we describe a very simple and convenient method for the selective synthesis of these allyl sulfides and related derivatives utilizing alkyl, alkenyl and benzylic halides as precursors under a greener and catalyst-free condition (Figure 3). We show herein for the first time that a selectivity among symmetrical trisulfides, disulfides and monosulfides can be achieved using Na_2S as a sulfur-transfer agent by the variation of reaction conditions. Feasibility of these selective processes was studied by experimental and computational methods. Upon the synthesis of symmetrical trisulfides, they were evaluated for the preliminary anti-proliferative activities in a representative breast cancer cell line (MCF-7). The preliminary results on the morphological changes of MCF-7 cells and the anti-proliferative activity led to the identification of few trisulfides with excellent anti-proliferative activities (Figure 4). Moreover, 4-methyl substituted benzylic trisulfide **16** was found to be the most potent compound with an IC_{50} of around 1.0 µM. The compound **16** was evaluated further for its ability to release H_2S in the presence of biothiols such as GSH in the aqueous as well as cellular medium. Interestingly, the compound was found to donate H_2S in a sustained manner in the aqueous medium (data not shown) and also donated H_2S in the cellular medium in the presence of endogenous biothiol (Figure 4). The released H_2S from compound **16** in the

cellular medium was detected using the azide-based turn-on fluorogenic probe (**NAP-N_3**), which reacted with H_2S and produced the green fluorogenic probe **NAP-NH_2** (Figure 4).

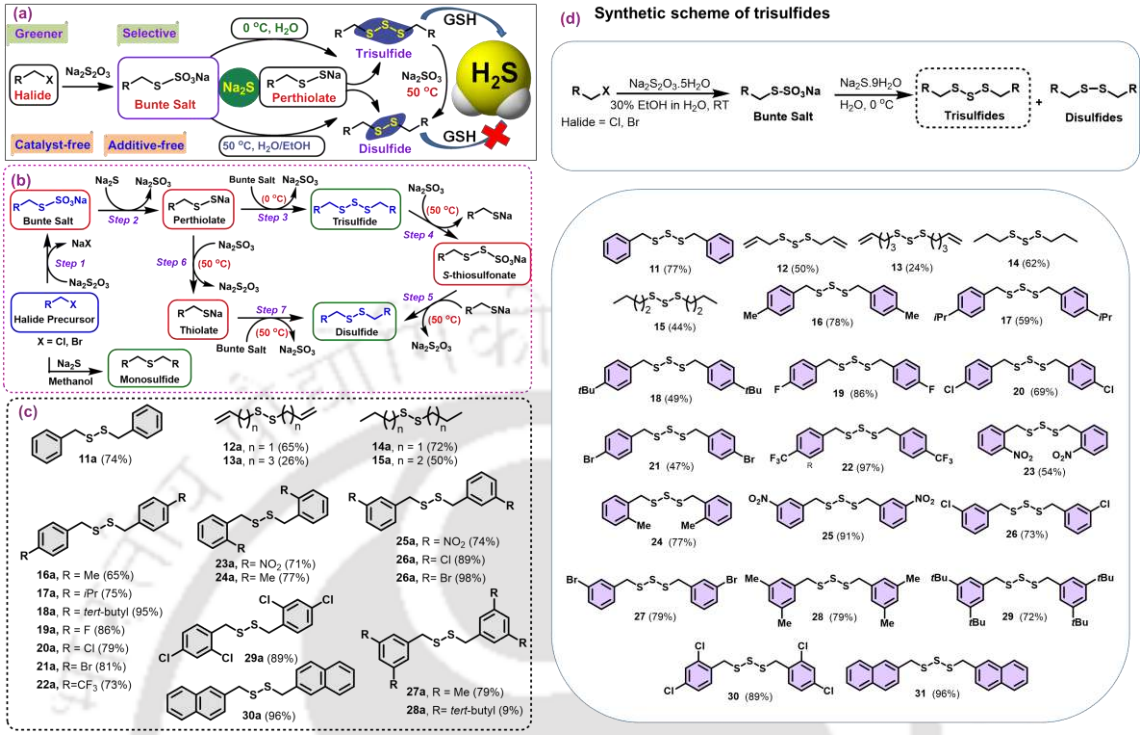

Figure 3. Brief highlights of chapter 3; (a) Schematic representation of the selective synthetic routes to symmetrical trisulfides, disulfides and monosulfides. (b) Proposed mechanistic pathways of monosulfide, disulfide and trisulfide synthesis and substrate scopes for the synthesis of (c) organodisulfides and (d) trisulfides, respectively.

A convenient and selective synthetic methodology for symmetrical trisulfides, disulfide and monosulfides along with the preliminary outcome on potent anti-proliferative activities of some key organotrisulfides towards breast cancer cells would be very much useful for developing newer generation chemotherapeutic and chemopreventive compounds capable of donating H_2S in a sustained manner.

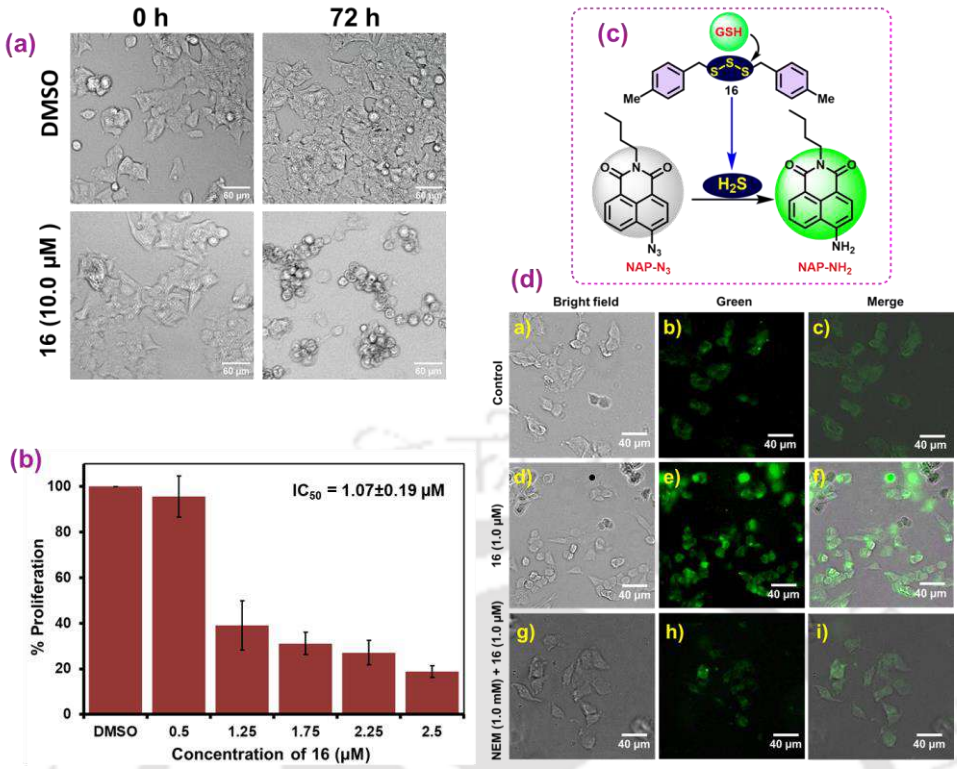

Figure 4. (a) Morphological changes of MCF-7 cells after incubation of compound **16** (10.0 μM) for 72 h. The scale bar represents 60 μm (b) Dose-dependent anti-proliferative activity of compound **16** against MCF-7 cells after an incubation period of 72 h. (c) Schematic representation of H_2S releasing mechanism and H_2S sensing reaction with **NAP-N$_3$** probe. (d) The H_2S level was estimated using the turn-on fluorogenic probe **NAP-N3** (5.0 μM); (a-c) control, (d-f) trisulfide **16** (1.0 μM); (g-i) NEM (1.0 mM) + **16** (1.0 μM). Scale bar represents 40 μm.

Chapter 4: Anti-cancer Activity of Benzylic Organotrisulfides in Triple-negative Breast Cancer: Inactivation of Wnt/β-catenin Signaling Cascade and Contribution of the Released Hydrogen Sulfide

The potent anti-cancer activity of the naturally occurring organopolysulfides has attracted wide research attention over the last two decades. Sustained donation of H_2S from organopolysulfides is found to be beneficial for the treatment of several organ-specific cancers. In the present study, for the first time, the mechanism of action for the potent anti-cancer activity of bis(3,5-dimethoxybenzyl) trisulfide **32** against the highly aggressive triple-negative breast cancer cells (MDA-MB-231) is described. Preliminary *in vitro* studies revealed potent anti-proliferative activity of the trisulfide **32** against triple-negative breast cancer with an IC_{50} value of 1.0 μM. Mechanistic studies reveal that the

compound exhibited anti-cancer activity, primarily by targeting and suppressing the Wnt/β-catenin signaling pathway. The inactivation of the β-catenin level was associated with the cell cycle arrest in the G2/M phase and the significant down-regulation of downstream signaling genes such as Cyclin D1 and c-Myc expression. Several control experiments with the analogous organosulfur compounds and the key enzyme inhibitors reveal that the presence of a trisulfide unit in the compound is crucial for the desired inactivation of β-catenin expression, which is promoted by GSK-3β-induced phosphorylation of β-catenin and its proteasomal degradation.

Moreover, the trisulfide unit or the released H_2S induced the down-regulation of p53 expression with the possible S-sulfhydration process and led to p53-independent up-regulation of p21 expression. Therefore, the key results of this study highlighting the potency of synthetic benzylic organotrisulfide **32** and the released H_2S towards the growth inhibition of triple-negative breast cancer *via* Wnt/β-catenin signaling pathway would certainly be helpful for further studies and understanding while developing small-molecule anti-cancer therapeutics in future.

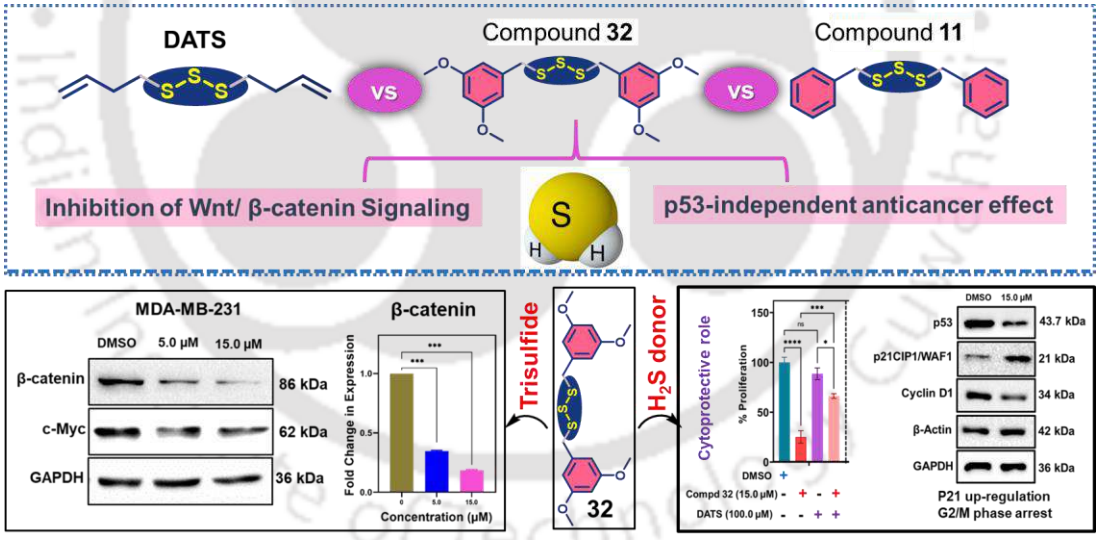

Figure 5. Brief highlights of chapter 4; Down-regulation of β-catenin and c-Myc in MDA-MB-231 cells upon the treatment of compound **32** (5.0 and 15.0 μM). Involvement of the released H_2S from compound **32** and its impacts on the expression levels of p53, p21 and Cyclin D1 in MDA-MB-231 cells.

The potent anti-proliferative activity of the trisulfide **32** and the related derivatives in MDA-MB-231 cells and further experiments regarding the mechanistic investigations provided few useful information. A significant reduction in β-catenin expression by

compound **32** appears to target the canonical Wnt/β-catenin pathway. β-catenin is degraded by proteasomes as a result of GSK-3β-mediated phosphorylation. In addition, the suppression of β-catenin levels could also be tuned by COX-2 expression, as well as several oncogenic proteins such as procaspase 3, Bcl2, and Survivin. According to the cell cycle analysis, compound **32** arrested the cells in G2/M phase and down-regulated Cyclin D1, which regulates mitosis and β-catenin downstream. The impact of the released H_2S from compound **32** and DATS on several oncogenic proteins was studied by western blot analyses and provided useful information. The induction of S-glutathionylation of p53 by GSTP1 expression, which is probably positively regulated by the released H_2S from compound **32** or DATS and could be suppressed by the potent inhibitor of GSTP1 (NBD-HEX). Compound **32** could also regulate the expression of p53 by direct S-sulfhydration process. Considering these deciphering events, a mechanistic pathway for the overall anti-cancer activity of compound **32** against the TNBC cells is proposed in Scheme 1. Interestingly, the thiol intermediate **33** did not exhibit any inhibitory activities towards Wnt/β-catenin pathway.

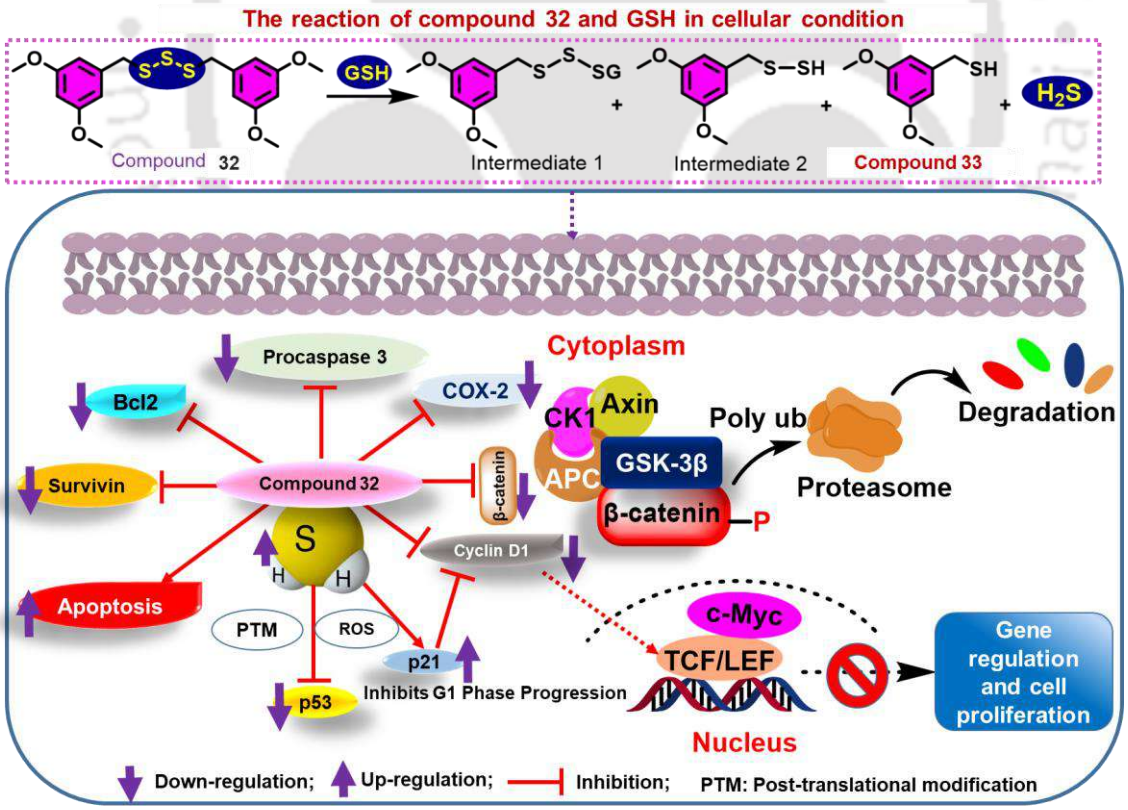

Scheme 1. Proposed mechanistic pathway for the anti-cancer activity of compound **32** against MDA-MB-231 cells.

Conclusions

In chapter 2, we presented a series of 4-substituted benzylic derivatives of DADS as well as their diselenide analogues for detailed structure-activity relationship (SAR) studies regarding their anti-cancer properties against ER+ breast cancer cell lines (MCF-7) and other organ-specific cancer cells. The SAR study revealed that the anti-cancer activity of the organodisulfides/diselenides could be enhanced significantly upon the incorporation of 4-cyano group on the benzene ring (compounds **3** and **8**). In chapter 3, we described a very simple and convenient method for the selective synthesis of garlic-derived allyl sulfides and related derivatives utilizing a wide variety of alkyl, alkenyl, and benzyl halides as precursors under a greener and catalyst-free condition. We show for the first time that, the selectivity among symmetrical trisulfides, disulfides, and monosulfides could be achieved by variation of several reaction parameters. Our study further revealed that the reaction temperature and solvent were two crucial parameters for an effective selectivity toward trisulfides and disulfides. The detailed mechanistic studies by experimental and computational methods indicated that the co-formation of disulfides along with trisulfides is due to the formation of sodium sulfite (Na_2SO_3) as a by-product that interfere in the reaction. Furthermore, results from the preliminary anti-proliferative activities by trisulfides towards breast cancer cells (MCF-7) revealed potent anti-cancer activities of most of the trisulfides in general. Importantly, the 4-methyl substituted trisulfide **16** exhibited the highest anti-proliferative activity in MCF-7 cells and it was capable of donating H_2S in a sustained manner in the presence of biothiols. The mechanistic investigations on the potent anti-proliferative activity of the benzylic organotrisulfide **32** against the highly aggressive triple-negative breast cancer cells (MDA-MB-231) was carried out in chapter 4. The compound exhibited the anti-cancer activity mainly by targeting and suppressing the Wnt/β-catenin signaling pathway. The detailed mechanistic studies revealed that compound **32** facilitated the GSK-3β-induced phosphorylation of β-catenin and subsequent proteasomal degradation, which was supported by the G2/M phase arrest of the cell cycle and the down-regulation of downstream signaling genes such as Cyclin D1 and c-Myc. Unlike the disulfide and monosulfide moieties, the presence of a trisulfide unit facilitated the release of H_2S, which was found to be important for the desired inactivation of β-catenin expression. Moreover, the trisulfide **32** or the released H_2S induced down-regulation of the p53 gene, possibly through S-sulfhydration process.

References

1. B. Meyer, in *Sulfur, Energy, and Environment*, ed. B. Meyer, Elsevier, 1977, DOI: https://doi.org/10.1016/B978-0-444-41595-0.50005-X, pp. 21-37.
2. K. R. Olson and K. D. Straub, *Physiology* **2015**, *31*, 60-72.
3. P. Nicholls and J. K. Kim, *Canadian Journal of Biochemistry and Physiology* **1982**, *60*, 613-623.
4. M. M. Cerda, M. D. Hammers, M. S. Earp, L. N. Zakharov and M. D. Pluth, *Organic Letters* **2017**, *19*, 2314-2317.
5. Y.-T. Lin, J.-S. Yang, S.-Y. Lin, T.-W. Tan, C.-C. Ho, T.-C. Hsia, T.-H. Chiu, C.-S. Yu, H.-F. Lu, Y.-S. Weng and J.-G. Chung, *Anticancer Research* **2008**, *28*, 2791.
6. P. S. S. Rao, N. M. Midde, D. D. Miller, S. Chauhan, A. Kumar and S. Kumar, *Current Drug Metabolism* **2015**, *16*, 486-503.
7. A. Herman-Antosiewicz and S. V. Singh, *Journal of Biological Chemistry* **2005**, *280*, 28519-28528.
8. C. R. Powell, K. M. Dillon and J. B. Matson, *Biochemical Pharmacology* **2018**, *149*, 110-123.
9. M. D. Hammers, L. Singh, L. A. Montoya, A. D. Moghaddam and M. D. Pluth, *Synlett* **2016**, *27*, 1349-1353.
10. C. R. Powell, J. C. Foster, B. Okyere, M. H. Theus and J. B. Matson, *Journal of the American Chemical Society* **2016**, *138*, 13477-13480.
11. X. Cao, L. Ding, Z.-z. Xie, Y. Yang, M. Whiteman, P. K. Moore and J.-S. Bian, *Antioxidant Redox Signaling* **2018**, *31*, 1-38.

Introduction

1.1. Hydrogen sulfide (H_2S) and its origin

Hydrogen sulfide is a colorless gaseous chemical compound with the formula H_2S. It is characterized by a strong foul odor of rotten eggs at ambient conditions. In 1777, Swedish-German chemist Carl Wilhelm Scheele discovered the chemical composition of pure hydrogen sulfide.[1] In the prebiotic earth (3.8 billion years ago), the abundance of sulfur and its reduced form such as H_2S played a significant role in the origin of life on earth and contributed as a rate-limiting source of energy.[2] H_2S is known to have its toxic nature at higher doses towards the living systems.[3] For example, it has been documented that excessive H_2S exposure (>500 ppm) causes immediate unconsciousness followed by death in humans.[4] Despite the challenging conditions, H_2S-rich environments offer ecological opportunities through increased resource availability, decreased competition, and reduced exposure to natural adversaries. Majority of H_2S in the atmosphere is produced naturally by bacteria, volcanoes, and underwater thermal vents.[5] Since life began, H_2S impacted with a greater extent as an important versatile gaseous molecule.

Similar to water (H_2O), the geometry of H_2S is tetrahedral. However, unlike water, H_2S has completely different physicochemical properties. The specific gravity of H_2S (molar mass of 34.08 g/mol) is 1.19 at 15 °C, making it slightly heavier than air. However, H_2S is known to be corrosive, explosive (at 4.3-4.5% in air), and flammable (ignition temperature: 260 °C) in general. While not as polar as water, H_2S has a similar structure and is moderately soluble in water.[5] The oxidation state of sulfur in H_2S is -2 and thus it acts as a reducing agent in general. It acts as a weak acid (pK_a = 6.9 at 18 °C) and in the presence of a base, deprotonation takes place with the formation of hydrosulfide (SH^-) ion, which is soluble in water. It reacts with many transition metal ions to form solid metal sulfides, which are mostly insoluble and often dark in color. For example, the papers soaked with lead (II) acetate is used commonly to detect H_2S because it reacts readily with lead (II) ion and forms lead (II) sulfide, which is black in color. Besides the chemical hazardous nature of H_2S, it exerts multiple biological activities ranging from bacterial to mammals (Figure 1.1). It acts as a gasotransmitter and exhbits multiple biological implications. For example, it shows promising vasodilatory activity by targeting K_{ATP} channels in the smooth muscle cells.[6] Similarly, H_2S-treated cells exhibit promising neuroprotective activities during the oxidative stress-induced cell damages.[7] In addition to the cytoprotective effect, sustained release of H_2S showed encouraging outcomes by inhibiting the growth of malignant cells over the non-malignant cells.[8]

Moreover, recent studies have shown the anti-bacterial and anti-viral effect of H_2S against antibiotic resistant *Staphylococcus aureus* and SARS-CoV-2, respectively.[9] Therefore, the multidimensional effectiveness of H_2S encouraged us to explore various properties of H_2S and its chemical donors towards various disease conditions (Figure 1.1).

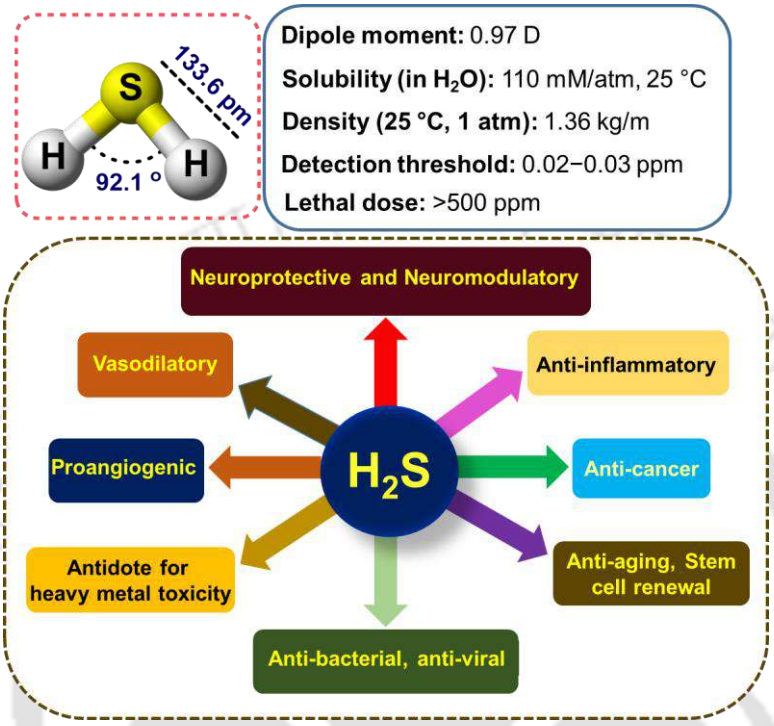

Figure 1.1. General physicochemical pharmacological properties of H_2S.

1.1.1. Environmental sources of H_2S

Anaerobic bacteria can perform the natural breakdown of H_2S to sulfate (SO_4^{2-}) ion. H_2S can be produced artificially through the industrial processes and biochemical degradation of sulfur-containing proteins.[5, 10] It can be converted to sulfuric acid (H_2SO_4) and sulfur dioxide (SO_2) by the hydroxyl radical ($OH^{\bullet}$). After combustion of H_2S, elemental sulfur (S^0) and SO_2 are formed as the final end products. Mostly, sulfur-reducing bacteria can reduce elemental sulfur (S^0) to H_2S *via* enzymatic pathway (Figure 1.2).[5] The concentration of H_2S in urban areas and background sources can be reached up to 1 ppb and 0.33 ppb, respectively. According to the World Health Organizaion (WHO) report, annual H_2S emissions from land-based sources range between 53 and 100 million metric tons of sulfur, while oceanic emissions range from 27 to 150 million metric tons.[11] The H_2S and other toxic compounds are produced by the combination with gases within magma (CO_2, SO_2, N_2, CO, S_8, Ar, Cl_2, and F) or by hydrogen and water

during geothermal activity.[12] The production of H_2S is biotic and well-connected to the metabolism of sulfate-reducing microbes in marine sediments, cold seeps, and some freshwater sources. It has been discovered that the consumption of sulfate by microbes as a terminal electron acceptor takes place for metabolizing methane, hydrocarbons, or organic materials in anoxic conditions and produces H_2S as a by-product.[5]

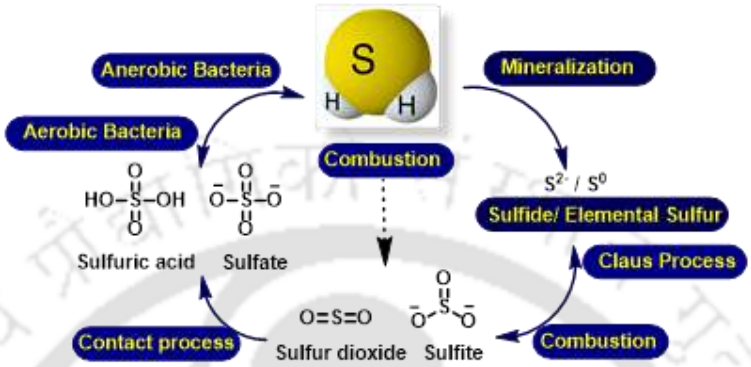

Figure 1.2. Participation of H_2S in the global sulfur cycle.

1.1.2. H_2S production by sulfate-reducing microbes (SRM)

In early 1877, H_2S producing bacteria was first discovered. Gut bacteria appears to play an important role in the production of H_2S, especially on host physiology and pathophysiology. Interestingly, sulfate-reducing microbes (SRM) are found to be a significant component of the normal gut microbiota. In this connection, *Desulfovibrio*, *Desulfobacter*, *Desulfolobus*, and *Desulfotomaculum* have been considered as the most common genera found in the gut.[13] Primarily, enzymatic H_2S production has been considered as a primary function of SRMs, that include bacteria, archaea and fungi.[14] The SRMs are commonly found in sludge or biofilm from high-sulfate industrial waste water treatment systems. SRM-mediated sulfate reduction, with the goal of reducing sulfate to sulfide is commonly governed by two sulfate-reducing pathways, known as assimilatory sulfate reduction (ASR) and dissimilatory sulfate reduction (DSR) pathways, respectively. Both of these processes take place in inaerobic condition and in both the methods, the substrate is sulfate, which undergoes further transformation to adenosine-5′-phosphosulfate (APS) in the presence of ATP with the final reduction to sulfide species. However, there are some differences in the enzymatic processes involved in ASR and DSR pathways. For example, while the DSR pathway uses APS reductase for the reduction of sulfate to sulfite, in ASR pathway, APS is further phosphorylated to 3'-phosphoadenosine 5'-phosphosulfate (PAPS) before the final

reduction to sulfide. Once the sulfate anion is transported to the cells *via* sulfate transporter, sulfate adenylyltransferase (CysDN) catalyses the formation of APS from ATP. Another conversion of APS to PAPS is catalysed by sulfate adenynyl kinase (CysC) enzyme. Finally, the reductions of sulfate to sulfite and sulfite to sulfide are catalyzed by a series of reducing enzymes like PAPS reductase (CysH) and sulfite reductase (CysIJ), respectively (Figure 1.3).

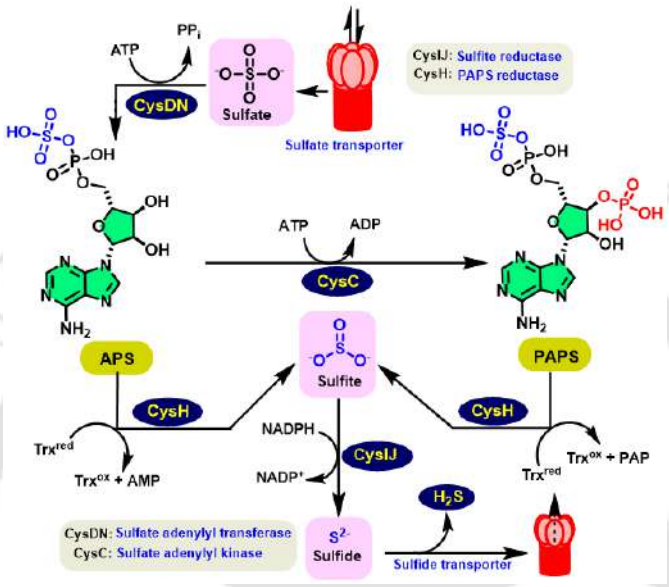

Figure 1.3. The pathways for assimilatory sulfate reduction.

1.1.3. Dietary sources of H_2S

Organosulfur compounds (OSCs) are prevalent in the *allium*- and cruciferous-family of vegetables. More than 33 different OSCs have been identified in garlic itself. Organosulfides in the allium family include oil-soluble polysulfides and water-soluble thiosulfinates with profound medical benefits. The OSCs, present in garlic (*Allium sativum* L.) possess several important therapeutic properties, which led to the identification of garlic as a traditional medicinal vegetable. Organopolysulfides are the major classes of OSCs present in garlic and many of them have several pharmaceutical and pharmacological implications. Additionally, several polar OSCs such as allicin, alliin, methyl-allyl thiosulfinate (**1.1**), S-allyl cysteine (**1.2**) etc are also present in garlic. Among the established polysulfides, diallyl sulfide (DAS), diallyl disulfide (DADS), diallyl trisulfide (DATS) are commonly studied as antioxidants in several diseases including cancer (Figure 1.4). Other OSCs such as sulforaphane and benzyl isothiocyanate (**1.3**) are discovered in cruciferous vegetables such as broccoli, brussels

sprouts, and cabbage. A promising chemoprotective effect of sulforaphane is reported to be connected with the activation of nuclear factor erythroid 2-related factor 2 (Nrf2) protein expression (Figure 1.4).[15] Onion, which is a widely consumed dietary vegetable around the globe, contains numerous phytochemicals, such as polysaccharides, saponins, phenolic compounds, and OSCs are present in onions. Notably, onionin A, cycloalliin, methiin and propiin in onion are reported to have antioxidant, anti-inflammatory and anti-cancer activities.[16] Asparaptine is a newly discovered compound in asparagus that inhibits the angiotensin-converting enzyme (ACE).[17] The compound asparaptine, which is a conjugate of arginine and asparagusic acid is found to be beneficial in lowering the blood pressure. The importance of asparaptine has thus increased lately, requiring further research.

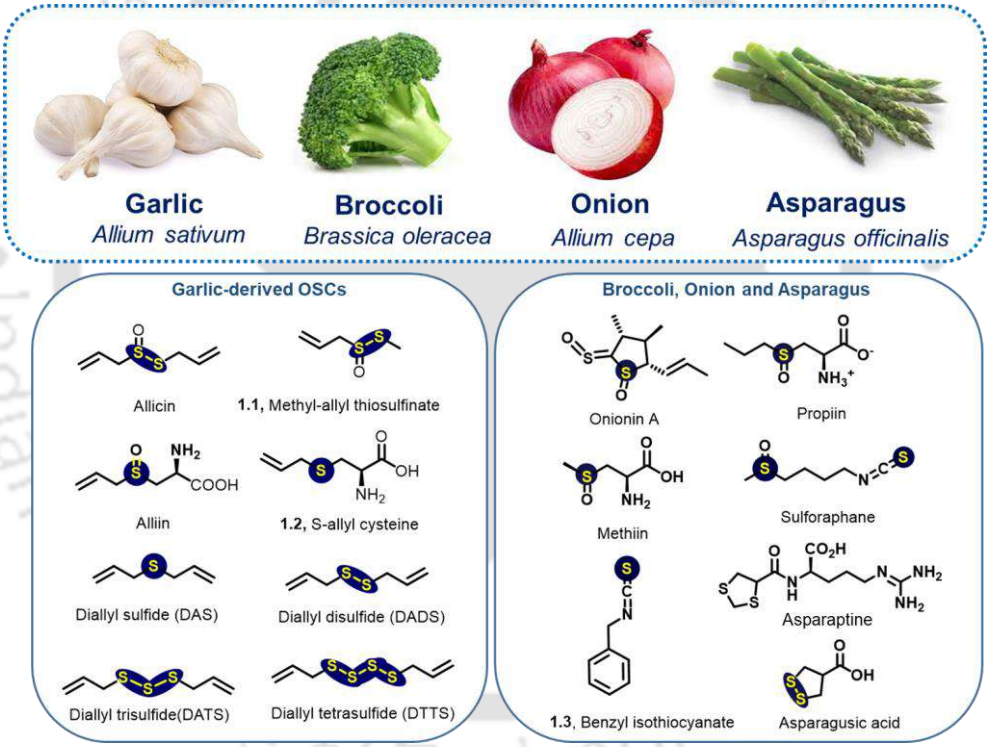

Figure 1.4. Some of the dietary vegetables and the chemical structures of some key OSCs present in those vegetables.

1.2. Regulation and metabolism of H_2S

1.2.1. Biosynthesis of H_2S

Enzymatic synthesis of H_2S is strictly restricted to few enzymes such as cystathionine-β-synthase (CBS), cystathionine-γ-lyase (CSE), and cysteine aminotransferase (CAT) in association with 3-mercaptopyruvate sulfurtransferase (3-MST).[18] Recent literatures

have shown that D-amino acid oxidase (DAO) in association with 3-MST can also produce H_2S by utilizing D-cysteine as the substrate (Figure 1.5).[19] Recently, it has been discovered that 3-MST is responsible for approximately 90% of H_2S produced in the brain. Interestingly, 3-MST, which is primarily found in the mitochondria, generates H_2S enzymatically from α-ketoglutarate and L-cysteine *via* metabolic interplay with CAT.[20] It has been found that, 3-MST in neurons is crucial for much of the brain's H_2S production and CBS is found in astrocytes, suggesting the importance of CBS towards H_2S signalling in other organelles (Figure 1.5).[21] Metabolism of H_2S in mitochondria plays a vital role for the energy supplementation of eukaryotic cells.[22] Similar to nitric oxide (NO), H_2S has been shown to regulate the metabolic demand in mitochondria.[23] However, it is commonly believed that H_2S production is solely regulated in the cytoplasm and further utilised *via* oxidation in the mitochondria. Moreover, H_2S has been shown to have protective roles towards mitochondria and regulates several functions like respiration, redox balance amd metabolism.[24] Recent reports on the treatment of human colon cancer has suggested that, low concentration of sulfide (as an energetic substrate) is effective, with minimum toxicity.[25]

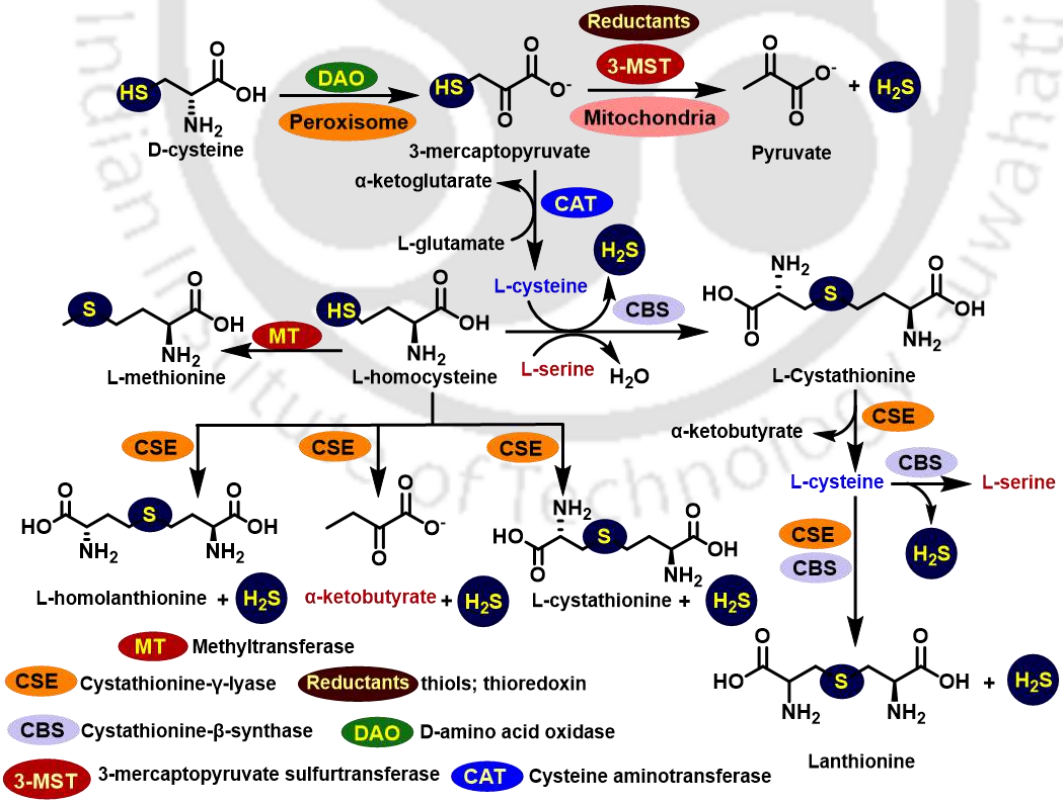

Figure 1.5. Biosynthetic pathways of H_2S production in mammalian cells.

1.2.2. Metabolism of H_2S *via* oxidation

The metabolism of H_2S has been initiated by sulfide-quinone reductase (SQR), which catalyzes the breakdown of H_2S to produce the corresponding sulfane sulfur (S^0) molecule. Subsequently, SQR utilizes coenzyme Q (CoQ) to maintain the supply of energy into electron-transport chain. Finally, sulfane sulfur has been found to be converted essentially to glutathione (GSH), sulfite (SO_3^{2-}), cysteine, and homocysteine, respectively. In physiological condition, the formation of glutathione persulfide (GSSH) from GSH has been catalysed by SQR. Further, sulfur dioxygenase (*ETHE1*) catalyses the SQR-mediated catabolism of GSH to yield sulfite. Finally, Thiosulfate sulfurtransferase (TST) and sulfite oxidase (SO) were discovered and they were found to be activated in the metabolism of sulfite to thiosulfate and sulfate, respectively (Figure 1.6).[18]

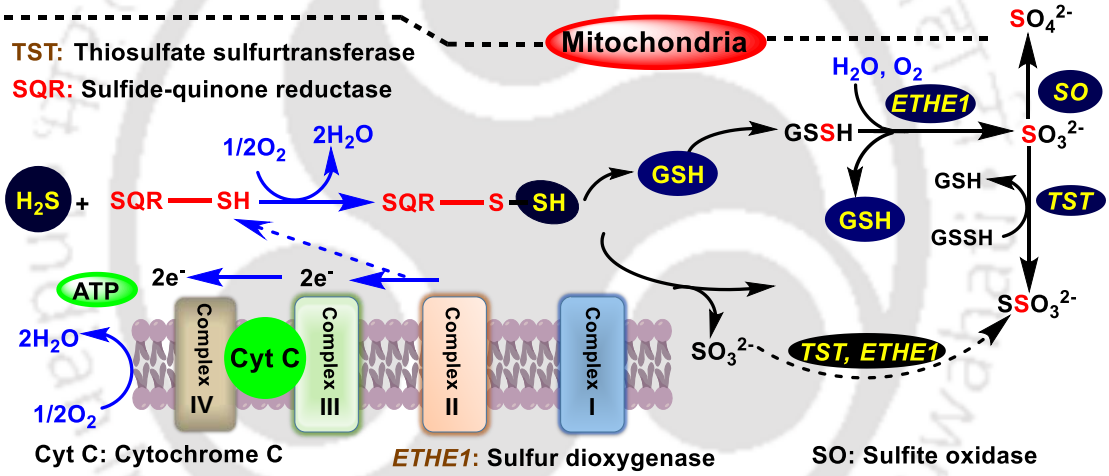

Figure 1.6. Schematic representation of H_2S metabolism in mammalian cells.

1.3. Chemical donors of H_2S

An active therapeutic contribution of H_2S in mammalian systems has been extensively explored in the last few decades. Interestingly, a landmark contribution by Abe and Kimura (1996) highlighted the capability of the endogenously produced H_2S in cell signaling and regulating cellular processes.[26] Biosynthesis of H_2S is very crucial for the cellular redox balance and cellular homeostasis, and a dysregulation of its concentration leads to many diseases.[27] Therefore, in the event of a deficiency cellular H_2S, exogenous donation of H_2S is considered for maintaining its optimal cellular concentration.

1.3.1. Inorganic donors of H_2S

Most commonly administered inorganic donors of H_2S in the biological system are sulfide salts such as sodium hydrosulfide (NaSH) and sodium sulfide (Na_2S). Use of sulfide salts has been an integral therapeutic tool for understanding the signalling processes of H_2S. However, the sulfide salts are capable of generating H_2S instantaneously upon their administration and they tend to establish the equilibrium between H_2S, HS^- and S^{2-} species, while the evaporation of H_2S may take place almost instantaneously. Therefore, the desired concentration of H_2S is hard to achieve from the inorganic salts.[28] In 2001, Wang and co-workers studied the rat aortic ring response upon administration of NaSH solution.[29] Interestingly, the administration of NaSH ensured the release of H_2S, which resulted in more than 60% relaxation over the control sample set. The data suggested significant vasorelaxant property of NaHS as a H_2S donor. In another report, NaHS was shown to exhibit antioxidant property when hypochlorous acid (HOCl)-mediated oxidative stress was induced in the human neuroblastoma cells as a model of myeloperoxidase-mediated HOCl induction causing brain damage and Alzheimer's disease.[30] Interestingly, exogenous administration of NaSH inhibited lipid peroxidation, protein oxidation and prevented cytotoxicity. Aqueous solution of sulfide salts exhibited cytoprotection and healing property in ulcer by quenching the reactive nitrogen species (RNS).[31] Despite all the therapeutic benefits the donation of H_2S from inorganic sulfide salts has major drawbacks, mainly with the instantaneous delivery of H_2S. Under acidic condition (e.g. cancer cells are acidic in nature) volatilization of H_2S caused significant dose fluctuations. Further an aerial oxidation of HS^- caused rapid reduction of H_2S concentration in the physiological conditions.[32] Therefore, sulfide salts as therapeutic substances require high doses of salts and that engage several off-target side-effects in the biological system. Moreover, the ionic nature of the sulfide salts lacks major selectivity towards target proteins, as major ion channels are also dealing with cationic/anionic ions for several pharmacological activities.[28]

1.3.2. Naturally occurring H_2S donors

Garlic and onions are believed to be crucial for the treatment of cardiovascular diseases, hypertension, thrombosis, and diabetes. While the pharmaceutically active constituents of garlic contains several H_2S releasing compounds that contribute to the overall health

benefit,[33] S-allyl cysteine sulfoxide (SAC) and S-allyl mercapto cysteine are the most pungent volatile compounds found naturally in garlic. An enzyme called alliinase [EC 4.4.1.4] is activated and secreted upon the crushing of garlic that converts alliin into allicin. A variety of organopolysulfides including DATS, DADS and DAS are produced after the hydrolysis of alliin to allicin.[34,35] While many linear and cyclic polysulfide-based H_2S donors have been discovered and isolated from variety of plant-based sources, garlic stands as the most explored among them. Mechanistically, the release of H_2S from polysulfides occurred upon the nucleophilic attack of a thiol (GSH, L-cysteine, L-homocysteine, *N*-acetylcysteine etc) at the -S-$(S)_n$-S- linkers of the garlic-derived polysulfides.[36] Unlike the presence of polysulfides in garlic, organic isothiocyanates (H_2S donors) are abundant in cruciferous vegetables such as broccoli, watercress, mustard, and garden cress. For example, sulforaphane, benzyl isothiocyanate (**1.3**), erucin are the major compounds capable of supplying exogenous H_2S from dietary sources (Figure 1.7). Furthermore, few animal-based OSCs as sources of H_2S are ovothiol (from sea urchin eggs) and varacin (from *marine ascidiacea*). A microbial source of H_2S is *streptomyces* that synthesizes an organosulfur compound leinamycin, which is also a naturally occurring compound, capable of donating H_2S. In fungi, some more H_2S donors such as ergothioneine and lenthionine have been found.[37] In this connection, *Petiveria alliacea L.*, a shrub widely used to treat a variety of conditions, including arthritis, asthma, and cancer, contains the main active ingredient dibenzyl trisulfide (DBTS) (Figure 1.7).[38]

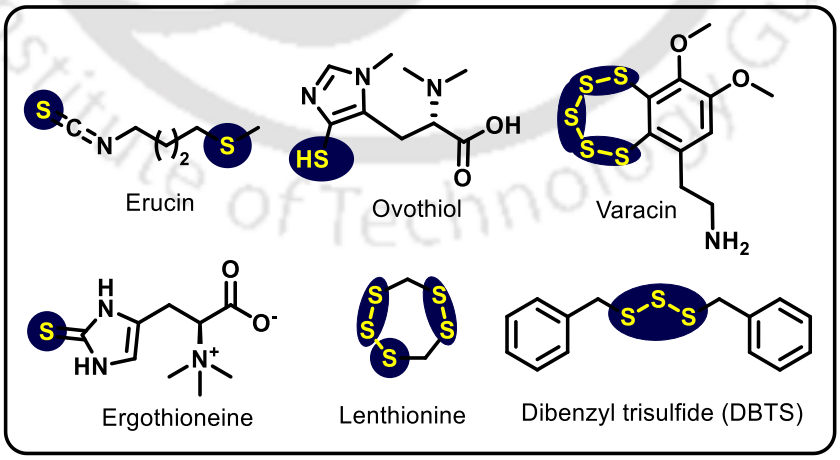

Figure 1.7. Chemical structures of some naturally occurring major OSCs capable of donating H_2S.

1.3.3. Synthetic OSCs as H_2S donors

1.3.3.1. Hydrolysis-triggered donors

As discussed in the previous sections, different classes of H_2S donors have drawn wider research attention as they possess fewer side effects in comparison to the commercial chemotherapeutic drugs that are relevant for future clinical purposes.[39] Despite their numerous utilities, naturally occurring H_2S donors have several limitations that prevent them from being developed further for clinical purposes. Notably, among many drawbacks of DATS, DADS, and DAS, poor water solubility, low bioavailability, and chemical instability impacted the overall biological activities. Moreover, synthetic donors provide sustained release of H_2S profile, which may benefit different disease models.[36b] The release of H_2S from the synthetic donors involves different chemical reactions (Figure 1.8). For example, a Lawesson's reagent (LR) is a commercially available sustained donor of H_2S capable of releasing H_2S for longer. Furthermore, a water-soluble LR derivative such as GYY4137 was developed that released H_2S in a sustained manner under the physiological condition. Interestingly, administration of an aqueous solution of GYY4137 in rats showed significantly higher plasma sulfide levels after 30 mins of treatment and sustained for 2 h.[36b, 40] Another set of hydrolysis-based H_2S donors are known as 1,2-dithiole-3-thiones (DTTs). The reaction of anethole with elemental sulfur produces DTT. In recent times, conjugation of DTTs with other molecules or drugs to make drug-DTT scaffolds has become a prevalent drug delivery approach. However, the H_2S release mechanism from these platforms is still unclear. The hydrolysis of DTTs under physiological conditions showed a slow release profile of H_2S, while the complete hydrolysis of DTT-based molecules required 48 h at 120 °C in a DMSO/H_2O mixture.[41] It is noteworthy that a DTT analogue, ADT-OH, used as a chemotherapeutic treatments in different types of aggressive cancers.[42] Similarly, ADT-OH was coupled with several NSAIDs to develop NSAID-hybrids for the treatment of acute inflammatory diseases. The released H_2S from the hybrids was intended to minimize the NSAID-induced ulcers in the gastrointestinal tract.[43] Recently, a DTT derivative AP-39 linked with a mitochondria-targeting triphenylphosphonium tail was reported to monitor real-time H_2S concentration in mouse endothelial brain cells.[44] Separate reports by Pluth and Anna Sparatore have successfully designed amide linker-based DTT-NSAID conjugate (ACS-15, ACS-14 and ACS-83) to deliver the COX-2 inhibitor for treating acute inflammatory diseases.[45]

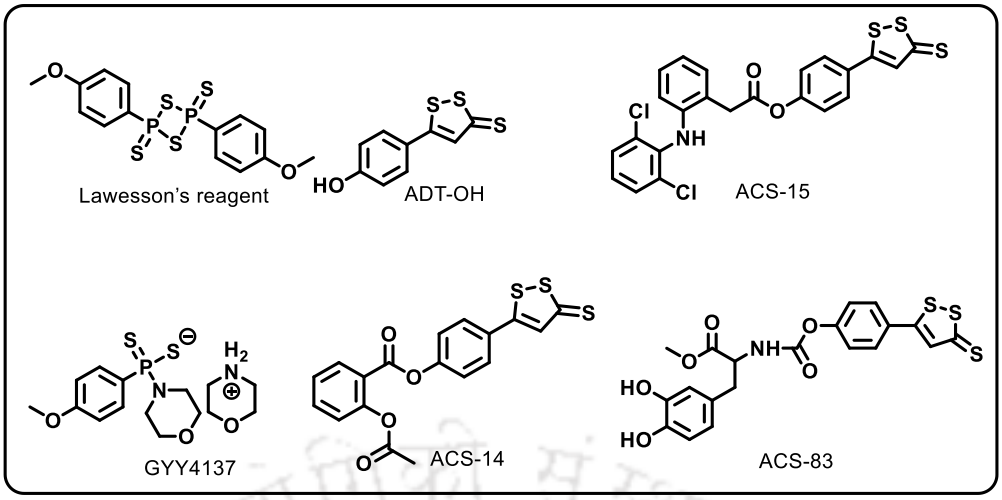

Figure 1.8. Chemical structures of some representative hydrolysis-triggered H_2S donors.

1.3.3.2. Thiol-triggered donors

The release of H_2S from the thiol-triggered H_2S donors occurs upon the nucleophilic attack by thiols at the electrophilic sites within the compounds. Thiol-triggered donors are advantageous over other classes of donors as biothiols (glutathione, L-cysteine, and L-homocysteine) are abundant in the mammalian cellular environment. Firstly, garlic-derived polysulfides (DATS and DTTS) are known to release H_2S in the presence of biothiols in the cellular environment. The nucleophilic attack at the middle sulfur of the trisulfide-linkage leads to rapid thiol exchange reactions and releases H_2S.[46]. Among many nucleophilic reaction-based H_2S donors, a series of *N*-(benzoylthio)benzamides reported by Ming Xian and co-workers was one of the important series of thiol-triggered donors of H_2S till date (Figure 1.9).[47] The rate of release of H_2S from various derivatives in the presence of L-cysteine was assessed. *N*-(benzoylthio)benzamide derivative (**1.5**) is a new class of thiol-triggered H_2S donors that undergo a disulfide exchange reaction to facilitate H_2S release. Interestingly, this class of compound showed negligible cytotoxicity even at higher concentrations.[37] For example, penicillamine perthiol (**1.6**) was synthesized first by Ming Xian and co-workers. Penicillamine-based donors demonstrated a better response in H_2S production in the presence of thiols than cysteine-based donors, which could only release trace amounts of H_2S. The two adjacent methyl groups of penicillamine-based donors, which prevent thiols from cleaving the disulfide bonds, likely contribute to the two different behaviors.[37] Martelli and co-workers examined the H_2S-releasing capabilities of a few aryl isothiocyanates and studied their

vascular impact in rat coronary arteries. A slow release of H_2S was observed in the tested compound phenyl isothiocyanate (**1.7**) when exposed to organic thiols such as L-cysteine.[48] Furthermore, compound **1.7** have shown potent vasorelaxant effects on coronary arteries. In another study, Li and co-workers tested the effectiveness of delayed therapy using a novel H_2S donor, JK-2 (**1.8**), on cardiac function in a murine model for pressure overload-induced heart failure.[49] Finally, synthetic phenylic analogueues of garlic-based alkyl tetrasulfides were reported by Pluth and co-workers, and that was found to exhibit good H_2S donation capacity.[50] In 2020, Bhabak and co-workers developed biothiol-triggered trisulfide-linked fluorogenic donors of H_2S compatible with both aqueous and cellular media. As H_2S and fluorophore are released concurrently, it was possible to monitor intracellular H_2S release and its subsequent trafficking to the lysosomes.[51]

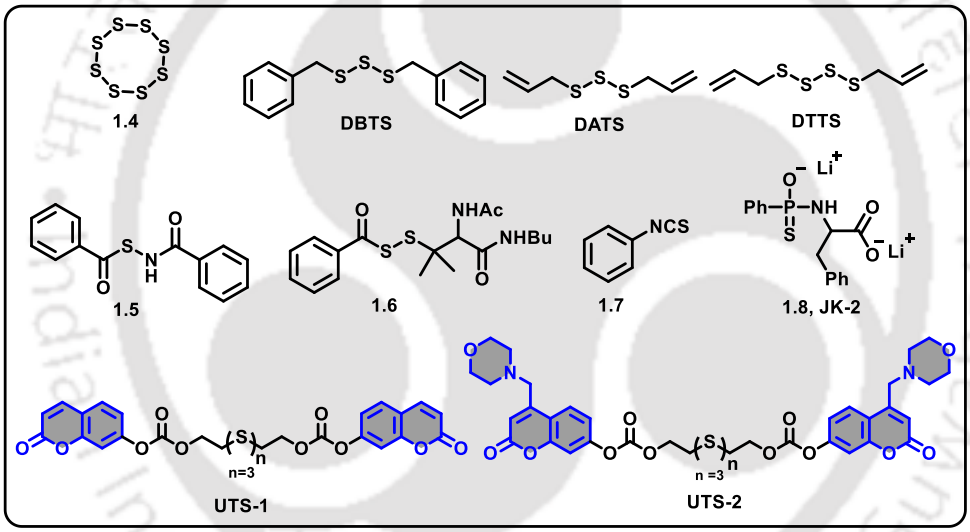

Figure 1.9. Chemical structures of some reprensentative thiol-triggered H_2S donors.

1.3.3.3. Light-triggered donors

Recently, the development of light-triggered prodrug strategies has attracted wide research attention. The light-triggered prodrugs are advantageous over the bio-analyte-responsive drug release strategies as they do not affect any biochemical process to deliver the drugs. After administration of the prodrug, photons of a particular wavelength can trigger the release of drugs at a specific site of interest with the minimized off-target side-effects and toxicities. Over the years, researchers have developed light-triggered donors of H_2S as a vital therapeutic tool for many disease models (Figure 1.10).[52] For example, UV-light responsive photocages such as geminal

dithiol (**1.9**) and ketoprofenate (**1.11**) and are reported as light-triggered H_2S donors. [53,52] They decompose to afford a reasonable amount of H_2S upon the irradiation with UV-light of specific wavelengths (365 nm). In 2017, Pluth and co-workers have reported the light-triggered H_2S donor (**1.12**) that contained a photocleavable *o*-nitrobenzyl group to unmask the caged thiocarbamate.[54] Interestingly, the release of H_2S from compound **1.12** involves two steps. The initial photocleavage leads to the generation of carbonyl sulfide (COS), which could be degraded to H_2S in the presence of carbonic anhydrase (CA).[54] In 2018, Singh and co-workers reported an ESIPT-based light-activated H_2S donor (**1.13**) using a *p*-hydroxyphenacyl moiety as a photo-triggering group. The ESIPT process helped in the self-monitoring and uncaging of H_2S by producing an excellent fluorescence emission with biocompatibility, cellular internalization, and less cytotoxicity towards HeLa cells.[55]

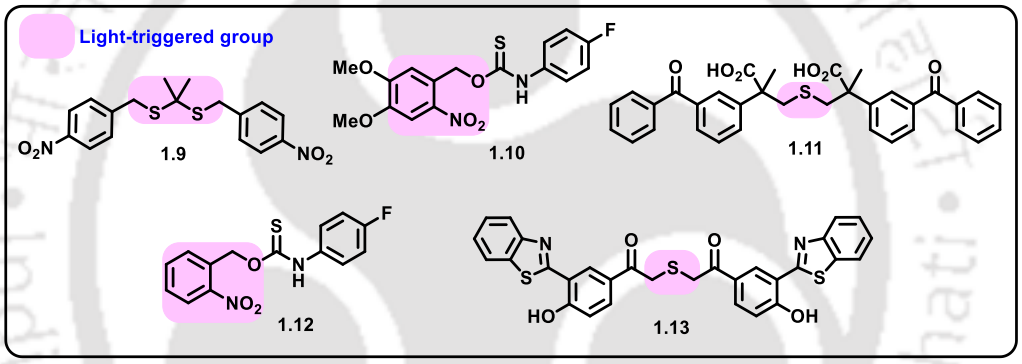

Figure 1.10. Chemical structures of some representative light-triggered H_2S donors.

1.3.3.4. Enzyme-triggered donors

Utilizing enzymes to deliver drug molecules offers several advantages over other stimuli-responsive prodrug systems. It is well-known that enzymes are highly substrate-specific and selectively localized in tissues. Under disease conditions, overexpression of many enzymes is commonly observed; therefore, the development of enzyme-triggered prodrug systems are essential therapeutic tools in medical science. Some reprsentative enzyme-triggered H_2S donors are shown in Figure 1.11. The first example of enzyme-triggered H_2S donor (**1.14**) was reported by Li and co-workers in 2016. [56] The release of H_2S from the donors mainly relied on the lactonization reaction, known as trimethyl lock (TML, **1.14**). The TML strategy was used for the delivery of a variety of drugs. Here, authors have developed thioester-based H_2S donors, which release H_2S upon the lactonization of the ester group. This specialized system is strictly substrate-specific;

hence, the absence of any group may hamper the cyclization process and slow down the H_2S release process. Furthermore, several NSAID-TML hybrids were synthesized subsequently and evaluated for their anti-inflammatory activities upon the inhibition of TNF-α secretion.[57,58] In 2017, Matson and co-workers demonstrated the COS-mediated donation of H_2S upon the activation by CA.[59] Additionally, several thiocarbamate-based COS releasing prodrugs (**1.15-1.16**) have recently been reported.[58] Earlier this year, Bhabak and co-workers reported an organopolysulfide-based near-infrared (NIR) fluorogenic H_2S donor (**1.17**). [60] The probe could be activated by the mammalian antioxidant enzyme thioredoxin reductase (TrxR). Self-immolative cyclization process released H_2S with the simultaneous turn-on fluroscence.

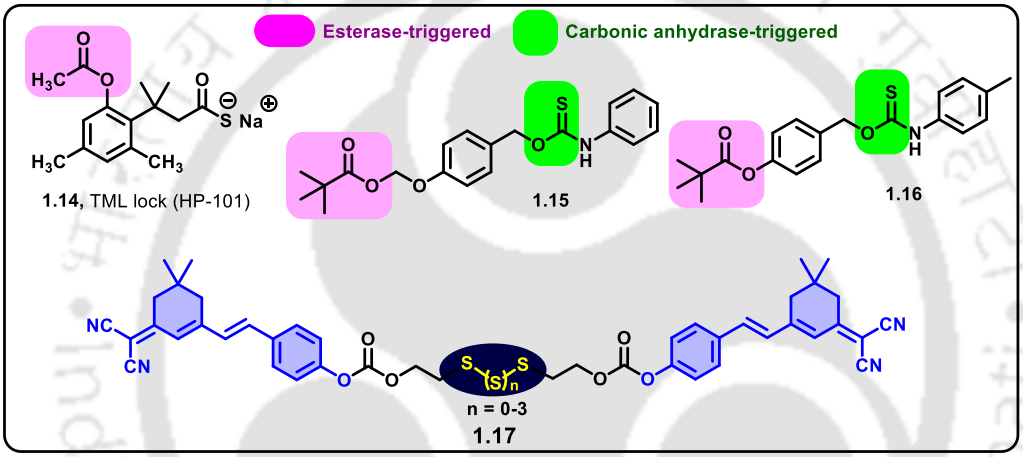

Figure 1.11. Chemical structures of some representative enzyme-triggered H_2S donors.

1.4. Methods of detection of H_2S

Precise quantification of H_2S at the cellular level is very important as the dysregulation of its intracellular concentration is associated with various disease states.[61] Therefore, several methods are developed for estimating H_2S concentration in aqueous and cellular medium.[62] Some of the commonly used methods are elaborately described in the subsequent sections.

1.4.1. Spectrophotometric method

Among many H_2S detection methods, methylene blue assay (MB Assay) is considered as one of the traditional/conventional methods of H_2S quantification.[63] In this method, the iron (III) chloride ($FeCl_3$)-catalyzed electrophilic aromatic substitution at *p*-(dimethylamino)aniline (**1.18**) with hydrosulfide anion (analyte) yields methylene blue

(MB) dye, which exhibits a typical absorbance pattern at 670 nm in UV-Vis spectrophotometric experiment (Scheme 1.1A).[62c] Despite its wide application, recent studies have shown that the value of detection limit (LOD) for MB assay is quite high (~1.0 µM).[63-64] It should be mentioned here that the formation of MB requires an acidic condition and therefore, the assay is generally performed under acidic medium, which may restrict its application in the cellular medium.[65] Another spectroscopic method used for the detection of H_2S is the monobromobimane (mBBr) method.[62c] This method exhibits more reliable results and is compatible with cellular medium. Under the alkaline condition, two equivalents of mBBr (**1.19**) react with H_2S to form a symmetrical and fluorogenic sulfide dibimane (SdB, **1.20**). A high fluorescent emission signal from SdB enables easy detection of H_2S by fluorescence spectroscopy.[65] However, non-specific reactions with thiols is one of the limitations of this method.[62c] Despite this, mBBr assay has been used widely to detect the released H_2S from polysulfides and persulfides from the pool of different sulfane sulfur-based compounds. The detection limit of this method is reported to be as low as 2.0 nM.[66]

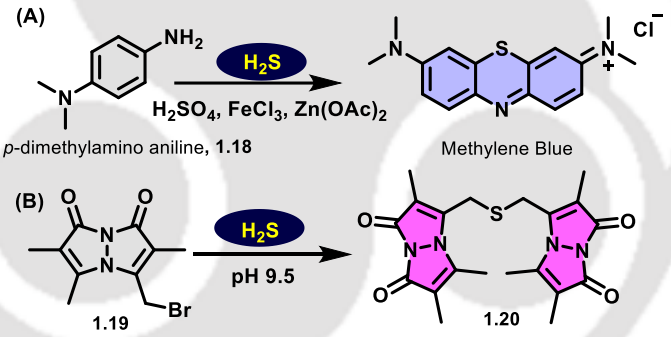

Scheme 1.1. (a) Schematic representation for the formation of methylene blue dye from *p*-(dimethylamino)aniline; (b) Schematic representation for the reaction of H_2S with monobromobimane (mBBr, **1.19**) with the formation of monosulfide **1.20**, used for the detection and quantification of H_2S.

1.4.2. Electrochemical method

The electrochemical method for the selective detection of hydrosulfide (HS^-) or sulfide ions (S^{2-}) has been reported using ion-selective electrodes (ISEs). Electrodes contain the specific HS^- / S^{2-} ion-selective membrane that selective by allow the ions from the solution. Here, the reduction of ferricyanide $[Fe(CN)_6^{3-}]$ to ferrocyanide $[Fe(CN)_6^{4-}]$ by a dianionic sulfide ion (S^{2-}) takes place in a strongly alkaline condition and subsequently

gets re-oxidized at the platinum electrode and finally produces the relevant current based on the concentration of H_2S. The key feature of this method is its compatibility to the mammalian tissue culture systems. This technique, however, cannot detect the H_2S production and its transport within cells.[67] In order to estimate sulfide ions (S^{2-}) with almost perfect selectivity and low LOD (100.0 nM), ISEs have been widely used for serum samples.[67-68] In order to shift the proton dissociation equilibrium from H_2S to S^{2-} (pK_{a1} = 6.9, pK_{a2} = 13.8) and deplete acid-labile sulfide pools, samples must first be pre-treated with alkaline solutions. Two-electron oxidation with elemental sulfur (S^0) as the product allows direct detection of H_2S and hydrosulfide (HS^-).[69] A photo-electrochemical method for determining aqueous H_2S *in situ* has been developed by Li *et al*. (2012) by depositing CdS nanoclusters on TiO_2 nanotubes. According to their study, TiO_2 alone produces a very low amount of photocurrent as compared to TiO_2 and CdS films.[70] The photocurrent increased as more CdS nanoclusters were added to TiO_2 nanotubes exposed to $CdSO_4$ solution and Na_2S solution, respectively. The detection limit was lower than the other methods. The main benefits of this method are its high sensitivity, wide linear range, and low detection limit.[71] Recently, graphene and Ag nanoparticles were utilized to develop an electrochemical sensor for H_2S. The detection limit for this sensor was as low as 100 ppb despite the presence of other substances like CH_4, CO_2, N_2, and O_2. It demonstrated high selectivity for H_2S. The developed sensor also showed a quick response time of (1 s) and a quick recovery time of (20 s) at room temperature, allowing for real-time monitoring of H_2S concentration and dynamics.[72] Despite its high selectivity, repeatability, and low cost compared to other sensors, electrochemical sensors are extremely sensitive to temperature changes. In 2018, a potentiometric sensor with a solid Yttria-stabilized zirconia electrolyte and a delicate La_2NiO_4 working electrode was demonstrated by Hao X and co-workers.[73] At a hydrogen sulfide concentration of 500 ppb, the authors were able to obtain the La_2NiO_4 microstructure with the highest sensitivity. The recovery time of the sensor was found to be decreased from 1200 s to roughly 150 s. Throughout the study, the sensor demonstrated good operational stability and selectivity to hydrogen sulfide.[73] Potentiometric ion-selective electrodes and polarographic sensors have been widely used for H_2S determination in biological samples among various electrochemical sensor types.[67] One of the most popular potentiometric techniques for measuring the sulfide ion in biological systems is the Ag/Ag_2S ion-selective electrode (ISE). Mason *et al.* first

described this technique for determining the sulfide concentration in plasma (1974), however provided only few technical details.[74] Amperometric H_2S sensors can detect H_2S concentrations in whole blood and tissues without modifying the samples in real-time.[75] Jeroschewski *et al*. developed the electrode based on a standard Clark-type oxygen electrode for H_2S measurement in aquatic environments with a detection limit as low as 2.0 µM.[76] Using polarographic oxygen sensors, Doeller and Kraus measured H_2S gas under anoxic conditions at nanomolar levels in real-time.[77]

1.4.3. Fluorogenic detection methods

In the last few years, the development of reaction-based probes for the detection of H_2S have been explored to a large extent. Such probes are typically developed with some H_2S sensitive functional groups in the presence of suitable chromophorics. The probes are designed such that fluorescence is turned-on upon the reaction of the probe with H_2S enabling very sensitive measurement of H_2S concentration using fluorescence spectrophotometric methods. However, these chemical reactions are generally irreversible and can only measure the final accumulated product rather than the real-time H_2S dynamics.[62c] Despite these drawbacks, fluorogenic probes are extremely useful for detecting endogenous H_2S concentration in mammalian cells and tissues at sub-micromolar levels and with significantly higher spatiotemporal resolution. Most of the reported H_2S-sensitive probes contain suitably connected azido-group (R-N_3) with very weak or no fluorescence. In the presence of H_2S, the azide group undergoes reduction to the corresponding amine (R-NH_2) with the turn-on fluorescence (Figure 1.12A). For example, in 2013, Tang and co-workers have reported the coumarin-linked azide-based probe C-7Az (**1.21**), which exhibited excellent selectivity over the biologically relevant analytes and capable of detecting H_2S in the cellular medium.[78] Moreover, **1.21** was successfully used to visualize H_2S in the cardiac tissues of rats with normal and atherosclerosis (AS) conditions.[79] In 2013, Binghe Wang and co-workers have reported a second generation dansyl azide-based flurogenic probe (**1.22**) for the detection of H_2S under physiological conditions.[80] In comparison to the previously reported probe 1,5-dansyl azide-based probes exhibited a significantly higher fluorescence emission in the aqueous medium (>100-fold with 10 M of sulfides) without the addition of any surfactant.[80] A ratiometric fluorescent probe (**1.23**) for H_2S detection based on a coumarin-benzopyrylium core was developed in 2015, by Duan and co-workers. [78] The reported probe (**1.23**) combines an intramolecular spirocyclization reaction with a

selective acyl azide/amide conversion to provide high sensitivity and ratiometric response to H_2S. The proposed coumarin-benzopyrylium probe (**1.23**), which uses the acyl azide as the recognition moiety instead of the conventional azide-based H_2S probes found to be responsive towards H_2S. In a recent study, Qiao and co-workers (2014) developed a lysosome-targeting fluorescent probe (**1.24**) for the detection and the fate of lysosomal H_2S in a real-time manner.[81] Upon the reaction with H_2S, a significant fluorescence enhancement was observed due to the reduction of azide group to the amine. Compared to the previously reported H_2S fluorogenic sensors, this probe showed promising biocompatibility with negligible toxicity toward the cervical cancer cell line (HeLa). However, a common drawback of such azide-based probes are the non-selective reactions with biothiols with false fluroscence signal.[80] Apart from the azide-based probes, several nitro-group containing turn-on fluorogenic probes (**1.25**-**1.26**) are also reported (Figure 1.12B).[82] The nitro group in such types react with the H_2S and undergo reduction to the corresponding amine with turn-on fluorescence. It should be mentioned the reduction of nitro group to amine is highly dependent on the pH of the medium.

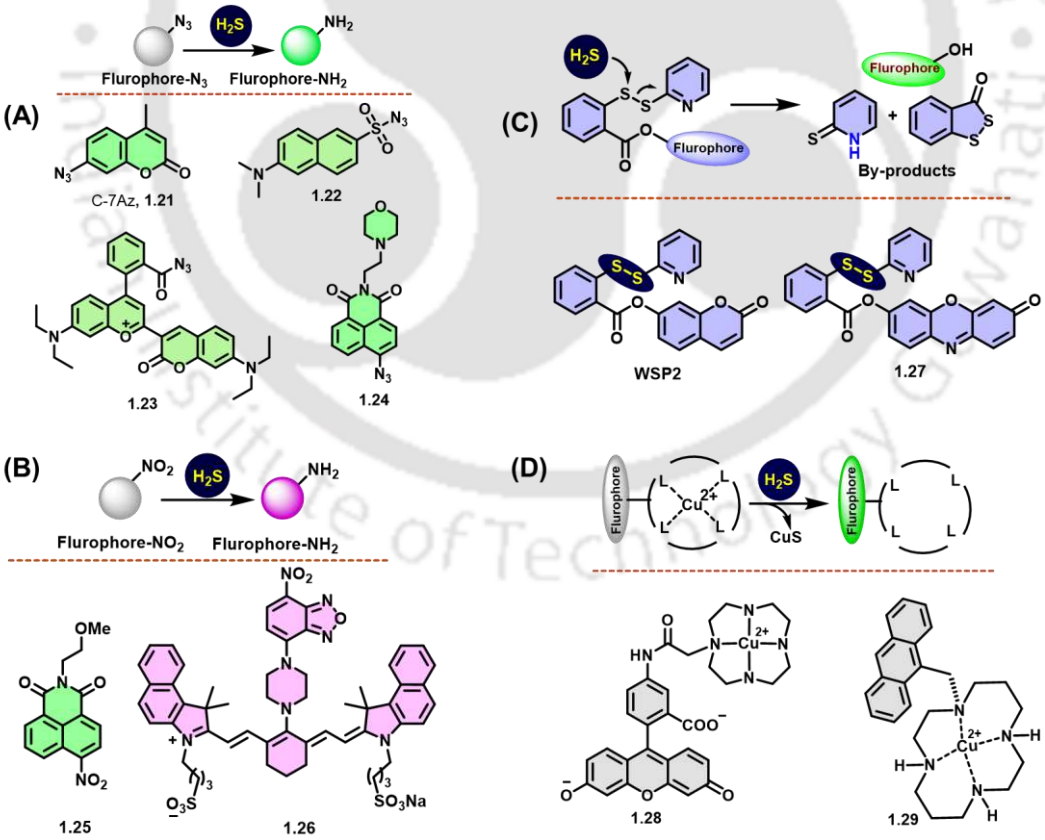

Figure 1.12. Chemical structures of different classes of turn-on fluorogenic probes for detecting H_2S.

Considering some of the non-selective reactions of the above fluorogenic probes with other bio-analytes other than H_2S, nucleophilic-reaction-based probes and such as **WSP2** and **1.27** were developed.[83] These probes were found to be more selective towards H_2S. For example, in 2012, Ming Xian and co-workers reported a highly sensitive disulfide-based ester-linked fluorophore tagged H_2S sensitive probe (**WSP2**, **1.27**). Similarly, **1.27** showed significant detection limit at 47.0 nM which worked well under normal biological pH ranges (pH: 6–9). However, **1.27** showed increased background fluorescence under pH-10, which might be due to the hydrolysis of the ester linkage under this pH value.[83b] The nucleophilic attack of H_2S at the electrophilic sulfur center cleaves the disulfide bond with the subsequent intramolecular cyclization and the release of the fluorophoric unit. Unlike the azide-based probes, the side-reaction of such probes with biothiols is not feasible as the cyclization, and the release of fluorophoric unit is not feasible in the reaction with thiols (Figure 1.12C). Furthermore, turn-on fluorogenic organometallic complexes are also reported for the selective detection of H_2S. Reaction of the metal ion with H_2S produces the insoluble metal sulfide, precipitating from the system with the turn-on fluorescence. For example, copper (II) complexes **1.28** and **1.29** were reported, which would react with H_2S resulting in black insoluble copper sulfide (CuS) precipitate and the turn-on fluorogenic response (Figure 1.12D).[84]

1.5. Chemical biology of H_2S

A growing shred of evidence on the biological role of H_2S attracted a large scientific community to solve many questions regarding the involvement of H_2S in various disease models. Based on its chemical properties, three significant pathways are emphasised.[85]

I. Interaction with metalloenzymes

II. Oxidative modification of protein cysteines

1.5.1. Interaction with metalloenzymes

The binding of H_2S at the metal centers of metalloproteins is well studied in biochemistry. It interacts with metal ions in various ways and alters the protein's active site and activity. For instance, H_2S (^-SH) can react with metal ions when it is present in physiological conditions. Further, H_2S can reduce the metal centers and concomitantly form different oxidized forms of sulfur. For example, heme porphyrin was found to be modified covalently by H_2S and produced an iron-sulfur complex under physiological

conditions.[85] It has been reported that H_2S can modify the metal center (Cu^{II} and Fe^{III}) of cytochrome c oxidase at different concentrations of H_2S.[86] At a low concentration of H_2S, it binds to ferric heme a3 complex and reduces to form SH radical, which further reacts with another H_2S.[87] At a moderate concentration of H_2S, it reacts with the Cu_B^+ center and forms a stable Cu_B-SH^- complex. However, the orientation of Cu_B-SH^- is challenging to stabilize under physiological conditions. Finally, at a higher concentration of H_2S, it can modify both the Cu_B^+ and Fe_B^+ centers as a model of irreversible inhibitor. Interestingly, H_2S-induced reduction of cytochrome c oxidase has been reported to modulate the overall cellular respiration process.[88] Furthermore, X-ray crystal structure of the α-subunit of human hemoglobin with SH^- is reported, indicating the existence of the interaction of SH^- ion with under physiological conditions.[85, 89]

1.5.2. Protein persulfidation

During the post-translational modification, protein thiols (R-SH) are converted to the corresponding (R-SSH) persulfides due to the transformation of cysteine residues. Formation of RSSH/RSS^- in proteins *via* H_2S requires strong oxidants. For examples, under oxidative stress, protein thiols undergo oxidation and produce sulfenic acid (R-SOH). Further reaction of H_2S with sulfinic acid generates perthiolated product of protein (Scheme 1.2).[90] The DNA binding domain in p53 contains 10 cysteine residues, which found to be crucial for the redox regulation. Moreover, Cys 176 and Cys 242 can virtually form a disulfide bond after zinc removal (Scheme 1.2).[91] An extreme oxidative stress condition is found to be crucial for the irreversible protein misfolding and is associated with protein aggregations. The aggregation of the misfolded proteins does not revert to the native form due to oxidative damages.[86] In 2009, Mustafa *et al*. demonstrated the endogenous H_2S-mediated modifications of cysteine residues in numerous proteins, such as glyceraldehyde-3-phosphate dehydrogenase (GAPDH) and β-actin, by converting cysteine-SH groups to cysteine-SSH groups.[91] It is interesting to note that H_2S accelerated the GAPDH activity by promoting the S-sulfhydration of cysteine residues, which eventually led to the reduced GAPDH activity.[92]

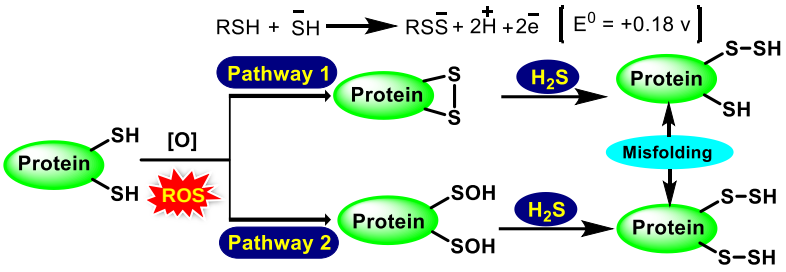

Scheme 1.2. Plausible mechanism of protein persulfidation by H_2S.

1.6. Role of H_2S in cancer

Cancer is a heterogeneous disease that can propagate by the dysregulation of several proteins. Cancer-promoting endogenous and exogenous stimuli can shift the paradigm of a normal cell to cancerous. Many clinical shreds of evidence suggest the dual role of H_2S in cancer progression and metastasis. Several studies have shown that, an altered expression of H_2S-producing enzymes in cancer cells is possibly one of the reasons for the uncontrolled growth and division of cancer cells. However, other reports have highlighted the therapeutic values of H_2S and demonstrated the anti-cancer activities towards different organ-specific cancer cells. Growing pieces of evidence reported the correlation of the concentration of H_2S and its dual role in cancer progression and growth (Figure 1.13).[18] For example, Yanzhang and co-workers (2017) have studied the dual behavior of H_2S in hepatocellular carcinoma (HCC) cells.[93] Their report has suggested the dual mechanism of H_2S towards cellular growth and migration rate towards HCC cells. While NaHS at an elevated concentration showed apoptotic behavior, exhibited proangiogenic behaviour at a lower concentration *via* promotion of tumor growth and blood vessel formation *via* modulating EGFR/ERK/MMP-2 and PTEN/AKT signaling pathways (Figure 1.14).[94]

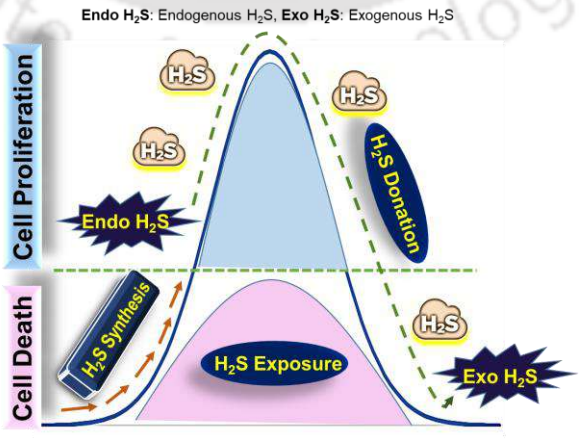

Figure 1.13. The bell-shaped model for the dual role of H_2S in cancer development.

It appears to be debatable about the role of H_2S towards the development of cancer. An appropriate model system is highly desirable to explain why H_2S exerts opposing effects in cancer cells in different experimental studies. In accordance with this phenomenon, Hellmich *et al.* recently depicted a logical bell-shaped model to explain the effects of H_2S in cancer cells (Figure 1.13). The model uses a bell-shaped curve to describe how H_2S affects the proliferation of cancer cells at different concentrations.[8] The endogenous H_2S or treatment with relatively low levels of exogenous H_2S for a relatively short duration could promote or maintain cancer cell growth, whereas relatively high concentrations of H_2S donors for a relatively long period may exhibit anti-cancer effects.[18]

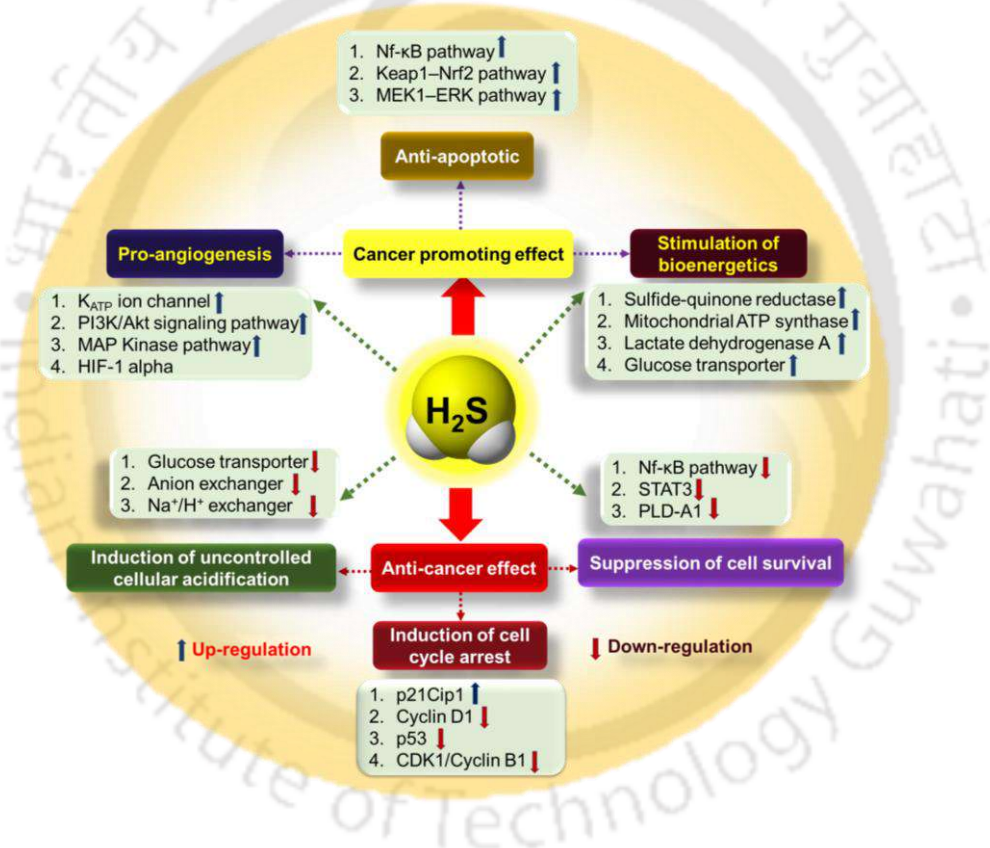

Figure 1.14. Possible molecular mechanisms relevant to the dual role of H_2S in cancer biology.

1.6.1. Proangiogenic role of H_2S

Angiogenesis refers to a critical step for cancer metastasis. A sudden up-regulation of angiogenic stimulators can promote the formation of new blood vessels, providing tumors with sufficient O_2 supply and nutrients for their growth and development. In late 2000, it was reported that NaHS could promote oncogenic stimulators and accelerate cell

proliferation and migration.[95] Moreover, pharmacological inhibition or deletion of CSE showed VEGF-mediated angiogenesis suggesting the effect of H_2S. Two independent groups have reported H_2S-mediated endothelial cell proliferation and migration in either transformed or primary endothelial cells (Cai *et al*. 2007; Papapetropoulos *et al*. 2009).[95b, 95c] The up-regulation of VEGF expression was found to be controlled by the activation of Akt-dependent pathway. The endothelial wound healing and tube-like structure formation were controlled by the activator signaling molecule phosphatidylinositol 3-kinase (PI3K). *In vitro* studies have shown a concentration-dependent increase in cell number in response to H_2S donor (NaHS) (Li *et al*. 2006; Ozsvári *et al*. 2010).[96] The detailed mechanistic studies have shown that the proangiogenic effect of H_2S was associated with the significant phosphorylation of Akt protein followed by a decrease in cytochrome c oxidase activity in RF/6A endothelial cells.[96a]

1.6.2. H_2S-mediated persulfidation

It has long been recognized that K_{ATP} channels are potential targets of H_2S-mediated protein sulfhydration. Many reports have reported that cardioprotection, vasorelaxation and hyperpolarization are the significant benefits of H_2S liberation.[97] Interestingly, H_2S-driven persulfidation of the K_{ATP} channel up-regulates the downstream signals such as p38 and promotes cell survival and proangiogenic effects. Notably, H_2S-mediated persulfidation activates HIF-1α, which helps tumor cells to gain nutrients and oxygen for their growth and metastasis.[98]

1.6.3. Apoptotic effect of H_2S

Despite the proangiogenic effect of H_2S as evidenced from the previous discussions, recent studies have demonstrated that a sustained donation of H_2S for long-term medication may promote programmed cell death of malignant tissues without affecting the normal cells.[18] Controlled doses of exogenous H_2S in cancer cells exhibit PARP-induced DNA damage and cellular death.[99] Furthermore, H_2S-mediated autophagy has been documented in malignant tissues, where it is associated with dose-dependent up-regulation of LC3-II protein expression and significant inhibition of *p*-PI3K, *p*-Akt, and mTOR proteins.[100]

1.6.4. Modulation of glucose uptake process by H_2S donors

One of the utmost hallmarks of cancer is to utilize glucose uptake *via* inhibition of the glycolysis process. Eventually, a higher rate of glycolysis process enhanced the conversion of glucose to lactate production.[101] To maintain the micro-environment of malignant tissues, lactic acid production helps cancer cells to promote angiogenesis. It was reported that the slow-release of H_2S from GYY4137 (200-1000 µM) enhances the glucose uptake and meanwhile suppresses the export of intracellular acids by disrupting the anion exchanger (AE) and sodium/proton exchanger (NHE). Accumulation of excess acids in the cells caused apparent cellular death.[102] Interestingly, GYY4137 did not harm the intracellular acid balance mechanism in non-malignant fibroblast cells (MCF10A).[103]

1.6.5. H_2S suppresses cell survival-related signaling pathways

Cancer cells dysregulate the homeostasis between cell survival and apoptotic genes balance by modulating the pro-survival signaling pathways. For instance, GYY4137, a synthetic analogueue of Lawesson's reagent, causes apoptosis in HCC cells. It is reported to suppress the signal transducer and activator of transcription 3 (STAT3) and VEGF proteins by the down-regulation of Bcl2, Survivin, and VEGF proteins.[104]

1.6.6. H_2S induces cell cycle arrest

Dysregulation of cell cycle events in cancer cells has been shown as one of the critical pathways of cancer cell progression and division. Therefore, modulating the cancer cell division and progression is a valuable strategy for cancer prognosis.[105] Many reports have suggested that H_2S donation at a specific dose may cause cell cycle arrest in cancer cells. For example, S-propargyl cysteine, a H_2S donor, showed cell cycle arrest at G1/S phase in the gastric cancer cell line (SGC-790).[106] Another report has suggested that NaSH (0.4-1.0 mM) treatment led to the suppression of G1/S phase in which progression, possibly by up-regulating p21cip1/WAF1 expression in colon cancer cells.[107] Furthermore, Lu *et al*. found GYY4137 mediated cell cycle arrest at G2/M phase by down-regulation of Cyclin D1 expression in HCC cells.[104]

1.7. Biological activities of garlic-derived H_2S donors

The OSCs in Garlic (*Allium sativum* L.) possess several vital therapeutic properties, which led to the identification of garlic as a traditional medicinal drug.[108] The main bioactive OSCs in garlic are organopolysulfides. Among these, diallyl sulfide (DAS),

diallyl disulfide (DADS), and diallyl trisulfide (DATS) are primarily studied in several diseases, including cancer.[36a] Notably, the trisulfide DATS has been reported as a potential donor of H_2S in physiological conditions, which correlates well with its chemopreventive, cytoprotective, and anti-cancer activities.[35] In 2005, Herman-Antosiewicz and co-workers reported the cell cycle-specific activities of DATS in human prostate cancer cells.[109] Activation of checkpoint kinases 1 and 2 was observed following DATS treatment. DATS-induced Ser216 phosphorylation of Cdc25C protein caused G2/M phase mitotic arrest and inhibited cell proliferation and migration.[109] In 2013, Tsai and co-workers reported very high antioxidant activity of DATS in hyperglycemia-induced diabetic cardiomyocytes. It has been shown that, DATS has suppressed the ROS-induced cardiac cell damage *via* up-regulation of the redox-sensitive transcription factor Nrf-2.[110] In 2017, Choi and co-workers have reported the therapeutic importance of DATS in gastric carcinoma cells.[111] The anti-cancer activity of DATS was enhanced by the induction of ROS profiles selectively in cancer cells over normal cells *via* activation of the AMP-activated protein kinase (AMPK), which was associated with the cell cycle arrest at G2/M phase. Collectively, these findings suggest that DATS exhibited cell-type-specific activities by the complex interplay among cellular mechanisms governing redox homeostasis, apoptosis, and cell cycle arrest. In 2021, Ding and co-workers reported the cytoprotective effect of DATS against the concanavalin A (Con A)-induced acute liver injury.[112] The cytoprotective activity of DATS was associated with the induction of Bcl2/Bax expression in the liver of Con A-injected mice *via* down-regulation of TNF-α-mediated oxidative stress and inflammatory responses. While, DATS can release H_2S upon the nucleophilic attack of nucleophilic biothiols or nucleophilic enzymes, ther release of H_2S from the corresponding disulfide DADS is not feasible as it requires a nucleophilic attack at the α-carbon of the disulfide moiety.[113] However, the studies showed that DADS also exhibits anti-cancer activity in different organ-specific cells at a higher dose. For example, in 2008, Lin *et al*. reported DADS-induced apoptosis in human cervical cancer cells (CaSki) *via* the generation of ROS and Ca^{2+}-dependent mitochondrial apoptosis pathway.[114] The effect of DADS was found to be detrimental as the higher concentration of DADS promoted DNA damage-mediated up-regulation of p53 and p21 expression levels. Furthermore, DADS treatment abrogated the mitochondrial membrane potential by increasing ROS and Ca^{2+} levels, respectively. In a recent study (2019), Yue Z *et al*. reported that, DADS induced

autophagy and apoptosis in human osteosarcoma (MG-63) cells *via* PI3K/Akt/mTOR pathway and the over-expression of LC3-II and Caspase 3 level.[115] Finally, the therapeutic efficacy of DAS was studied extensively in cancer, HIV, and metabolism-related pathways. Interestingly, DAS treatment with chemotherapeutic drugs serves as an adjuvant therapeutic strategy to protect the cellular redox balance *via* minimizing the ROS-mediated cell damage in normal tissues.[116] It is well established that DAS-treated cells are efficacious in preventing CYP2E1 activity, and as a result, the toxicity caused by xenobiotics is significantly reduced. Interestingly, DAS therapy has been shown to lessen the disease pathogenesis and toxicity linked to CYP2E1 overexpression or CYP2E1-mediated side effects in pathological conditions such as diabetes/hyperlipidemia, Parkinson's, HIV, and cancer.[117] Additionally, the antioxidant/anti-inflammatory activities of DAS was highlighted in several reports, which reveal the correlation with the up-regulation of several antioxidant enzymes to combat the redox imbalances in cells.[117]

1.8. Thesis objective

The literature reports reveal the potent anti-cancer activities of garlic in general. It has also been shown that the OSCs present in garlic in general and the organopolysulfides of particular mainly account for the potent anti-cancer activity of garlic. However, as the organopolysulfides present in garlic are very non-polar and volatile, there is no convenient and greener methodology reported for their selective synthesis. Moreover, the organopolysulfides present in garlic are reported to act as sustained donors of H_2S in the presence of biothiols. However, few aspects are still unclear and worth further understanding. For example, (i) it is not clear whether the anti-cancer activity of the OSCs in garlic could be enhanced further with some synthetic analogueues or not; (ii) whether organopolysulfides could be synthesized in a very selective and convenient method or not; (iii) the correlation between the ease of H_2S release from organopolysulfides and their anti-cancer activities; (iv) detailed mechanistic pathways for the anti-cancer activities of organopolysulfides and the possible involvement of the released H_2S. The present thesis explored the rational design, synthetic strategies, characterizations, and the underlying mechanistic pathways of several synthetic analogueues of garlic-based OSCs for their anti-cancer activities with a possible correlation with the release of H_2S.

1.9. Thesis overview

The thesis comprises four chapters. **chapter 1** highlights the general introduction of H_2S and its role in biological systems. This chapter briefly discusses the production, metabolism, and biochemical pathways of H_2S regulation and its detection techniques. Furthermore, the chapter also focuses on the synthetic and natural donors of H_2S and their biological implications in different diseases, notably cancer. In **chapter 2**, a series of synthetic disulfide and diselenide analogueues of the garlic-base disulfide DADS was explored. Possible structure-activity correlation studies towards their antioxidant and anti-proliferative activities were studied against ER+ breast cancer cell line (MCF-7) with the identification of the lead compound. In **chapter 3**, we took the initiative to develop a very convenient, catalyst-free and additive-free method for the selective synthesis of a wide variety of substrates analogueous to the garlic-based allylic disulfide (DADS) and trisulfide (DATS). The preliminary anti-proliferative activities of all the synthesized organotrisulfides against breast cancer cells (MCF-7), and the feasibility of H_2S release were studied. Finally, in **chapter 4**, was devoted in understanding the molecular mechanism for the potent anti-cancer activity of a synthetic benzylic organotrisulfide in triple-negative breast cancer cells (TNBC). The detailed mechanism of action of the synthesized trisulfide and the involvement of the released H_2S were considered in understanding the expression level of key marker proteins and the observed anti-cancer activity.

1.10. References

1. Meyer, B., Chapter 2 - History. In *Sulfur, Energy, and Environment*, Meyer, B., Ed. Elsevier: 1977; pp 21.

2. Olson, K. R.; Straub, K. D., *Physiology* **2015,** *31*, 60.

3. Beauchamp, R. O.; Bus, J. S.; Popp, J. A.; Boreiko, C. J.; Andjelkovich, D. A.; Leber, P., *CRC Critical Reviews in Toxicology* **1984,** *13*, 25.

4. Reiffenstein, R. J.; Hulbert, W. C.; Roth, S. H., *Annual Review of Pharmacology and Toxicology* **1992,** *32*, 109.

5. Malone Rubright, S. L.; Pearce, L. L.; Peterson, J., *Nitric oxide : biology and chemistry* **2017,** *71*, 1.

6. Bhatia, M., *IUBMB Life* **2005,** *57*, 603.

7. Panthi, S.; Chung, H.-J.; Jung, J.; Jeong, N. Y., *Oxidative medicine and cellular longevity* **2016,** *2016*, 9049782.

8. Hellmich, M. R.; Coletta, C.; Chao, C.; Szabo, C., *Antioxidants & Redox Signaling* **2014,** *22*, 424.

9. (a) Zhang, Y.; Yue, T.; Gu, W.; Liu, A.; Cheng, M.; Zheng, H.; Bao, D.; Li, F.; Piao, J.-G., *Journal of Nanobiotechnology* **2022,** *20*, 55; (b) Citi, V.; Martelli, A.; Brancaleone, V.; Brogi, S.; Gojon, G.; Montanaro, R.; Morales, G.; Testai, L.; Calderone, V., *British Journal of Pharmacology* **2020,** *177*, 4931.

10. Sievert, S. M.; Kiene, R. P.; Schulz-Vogt, H. N., *Oceanography* **2007,** *20*, 117.

11. Malone Rubright, S. L.; Pearce, L. L.; Peterson, J., *Nitric oxide : biology and chemistry* **2017,** *71*, 1.

12. Shinohara, H.; Kazahaya, K.; Saito, G.; Matsushima, N.; Kawanabe, Y., *Earth, Planets and Space* **2002,** *54*, 175.

13. Wallace, J. L.; Motta, J.-P.; Buret, A. G., *American Journal of Physiology-Gastrointestinal and Liver Physiology* **2017,** *314*, G143.

14. Linden, D. R., *Antioxidants & Redox Signaling* **2013,** *20*, 818.

15. M. de Figueiredo, S.; S. Binda, N.; A. Nogueira-Machado, J.; A. Vieira-Filho, S.; B. Caligiorne, R., *Recent Patents on Endocrine, Metabolic & Immune Drug Discovery* **2015,** *9*, 24.

16. Zhao, X.-X.; Lin, F.-J.; Li, H.; Li, H.-B.; Wu, D.-T.; Geng, F.; Ma, W.; Wang, Y.; Miao, B.-H.; Gan, R.-Y., *Frontiers in Nutrition* **2021,** *8*.

17. Miyoshi, K.; Enomoto, Y.; Fukusaki, E.; Shimma, S., *Analytical Sciences* **2018,** *34*, 997.

18. Cao, X.; Ding, L.; Xie, Z.-z.; Yang, Y.; Whiteman, M.; Moore, P. K.; Bian, J.-S., *Antioxid Redox Signaling* **2018,** *31*, 1.

19. (a) Shibuya, N.; Koike, S.; Tanaka, M.; Ishigami-Yuasa, M.; Kimura, Y.; Ogasawara, Y.; Fukui, K.; Nagahara, N.; Kimura, H., *Nature Communications* **2013,** *4*, 1366; (b) Pluth, M. D.; Bailey, T. S.; Hammers, M. D.; Hartle, M. D.; Henthorn, H. A.; Steiger, A. K., *Synlett* **2015,** *26*, 2633.

20. Shibuya, N.; Tanaka, M.; Yoshida, M.; Ogasawara, Y.; Togawa, T.; Ishii, K.; Kimura, H., *Antioxidants & Redox Signaling* **2008,** *11,* 703.

21. Nicholson, C. K.; Calvert, J. W., *Pharmacological research* **2010,** *62,* 289.

22. Blackstone, E.; Morrison, M.; Roth Mark, B., *Science* **2005,** *308,* 518.

23. Liu, D. K.; Chang, S. G., *Canadian Journal of Chemistry* **1987,** *65,* 770.

24. Searcy, D. G., *Cell Research* **2003,** *13,* 229.

25. Goubern, M.; Andriamihaja, M.; Nübel, T.; Blachier, F.; Bouillaud, F., *The FASEB Journal* **2007,** *21,* 1699.

26. Abe, K.; Kimura, H., *The Journal of Neuroscience* **1996,** *16,* 1066.

27. Wang, R., *The FASEB Journal* **2002,** *16,* 1792.

28. Powell, C. R.; Dillon, K. M.; Matson, J. B., *Biochem Pharmacol* **2018,** *149,* 110.

29. Zhao, W.; Zhang, J.; Lu, Y.; Wang, R., *The EMBO journal* **2001,** *20,* 6008.

30. Whiteman, M.; Cheung, N. S.; Zhu, Y.-Z.; Chu, S. H.; Siau, J. L.; Wong, B. S.; Armstrong, J. S.; Moore, P. K., *Biochemical and Biophysical Research Communications* **2005,** *326,* 794.

31. Whiteman, M.; Armstrong, J. S.; Chu, S. H.; Jia-Ling, S.; Wong, B.-S.; Cheung, N. S.; Halliwell, B.; Moore, P. K., *Journal of Neurochemistry* **2004,** *90,* 765.

32. Hughes, M. N.; Centelles, M. N.; Moore, K. P., *Free Radical Biology and Medicine* **2009,** *47,* 1346.

33. Bayan, L.; Koulivand, P. H.; Gorji, A., *Avicenna journal of phytomedicine* **2014,** *4,* 1.

34. Lawson, L. D.; Wood, S. G.; Hughes, B. G., *Planta Medica* **1991,** *57,* 263.

35. Brodnitz, M. H.; Pascale, J. V.; Van Derslice, L., *Journal of Agricultural and Food Chemistry* **1971,** *19,* 273.

36. (a) Benavides, G. A.; Squadrito, G. L.; Mills, R. W.; Patel, H. D.; Isbell, T. S.; Patel, R. P.; Darley-Usmar, V. M.; Doeller, J. E.; Kraus, D. W., *Proceedings of the National Academy of Sciences of the United States of America* **2007,** *104,* 17977; (b) Powell, C. R.; Dillon, K. M.; Matson, J. B., *Biochemical Pharmacology* **2018,** *149,* 110.

37. Corvino, A.; Frecentese, F.; Magli, E.; Perissutti, E.; Santagada, V.; Scognamiglio, A.; Caliendo, G.; Fiorino, F.; Severino, B., *Antioxidants* **2021,** *10.*

38. Murray, J.; Picking, D.; Lamm, A.; McKenzie, J.; Hartley, S.; Watson, C.; Williams, L.; Lowe, H.; Delgoda, R., *Fitoterapia* **2016,** *111,* 138.

39. Lee, Z.-W.; Deng, L.-W., Role of H2S Donors in Cancer Biology. In *Chemistry, Biochemistry and Pharmacology of Hydrogen Sulfide*, Moore, P. K.; Whiteman, M., Eds. Springer International Publishing: Cham, 2015; pp 243.

40. Li, L.; Whiteman, M.; Guan, Y. Y.; Neo, K. L.; Cheng, Y.; Lee, S. W.; Zhao, Y.; Baskar, R.; Tan, C.-H.; Moore, P. K., *Circulation* **2008,** *117*, 2351.

41. Zanatta, S. D.; Jarrott, B.; Williams, S. J., *Australian Journal of Chemistry* **2010,** *63*, 946.

42. Perrino, E.; Cappelletti, G.; Tazzari, V.; Giavini, E.; Soldato, P. D.; Sparatore, A., *Bioorganic & Medicinal Chemistry Letters* **2008,** *18*, 1893.

43. Li, L.; Rossoni, G.; Sparatore, A.; Lee, L. C.; Del Soldato, P.; Moore, P. K., *Free Radical Biology and Medicine* **2007,** *42*, 706.

44. Szczesny, B.; Módis, K.; Yanagi, K.; Coletta, C.; Le Trionnaire, S.; Perry, A.; Wood, M. E.; Whiteman, M.; Szabo, C., *Nitric oxide : biology and chemistry* **2014,** *41*, 120.

45. (a) Hammers, M. D.; Singh, L.; Montoya, L. A.; Moghaddam, A. D.; Pluth, M. D., *Synlett* **2016,** *27*, 1349; (b) Sparatore, A.; Santus, G.; Giustarini, D.; Rossi, R.; Del Soldato, P., *Expert Review of Clinical Pharmacology* **2011,** *4*, 109.

46. Bhattacherjee, D.; Sufian, A.; Mahato, S. K.; Begum, S.; Banerjee, K.; De, S.; Srivastava, H. K.; Bhabak, K. P., *Chemical Communications* **2019,** *55*, 13534.

47. Zhao, Y.; Wang, H.; Xian, M., *Journal of the American Chemical Society* **2011,** *133*, 15.

48. Martelli, A.; Testai, L.; Citi, V.; Marino, A.; Bellagambi, F. G.; Ghimenti, S.; Breschi, M. C.; Calderone, V., *Vascular Pharmacology* **2014,** *60*, 32.

49. Li, Z.; Carnal, J.; Kang, J.; Xian, M.; Lefer, D. J., *The FASEB Journal* **2018,** *32*, 698.3.

50. Cerda, M. M.; Hammers, M. D.; Earp, M. S.; Zakharov, L. N.; Pluth, M. D., *Org Lett* **2017,** *19*, 2314.

51. Mahato, S. K.; Bhattacherjee, D.; Bhabak, K. P., *Chemical Communications* **2020,** *56*, 7769.

52. Devarie-Baez, N. O.; Bagdon, P. E.; Peng, B.; Zhao, Y.; Park, C.-M.; Xian, M., *Organic Letters* **2013,** *15*, 2786.

53. Fukushima, N.; Ieda, N.; Sasakura, K.; Nagano, T.; Hanaoka, K.; Suzuki, T.; Miyata, N.; Nakagawa, H., *Chemical Communications* **2014,** *50*, 587.

54. Zhao, Y.; Bolton, S. G.; Pluth, M. D., *Organic Letters* **2017,** *19,* 2278.

55. Venkatesh, Y.; Das, J.; Chaudhuri, A.; Karmakar, A.; Maiti, T. K.; Singh, N. D. P., *Chemical Communications* **2018,** *54,* 3106.

56. (a) Zheng, Y.; Yu, B.; Ji, K.; Pan, Z.; Chittavong, V.; Wang, B., *Angewandte Chemie International Edition* **2016,** *55,* 4514; (b) Borchardt, R. T.; Cohen, L. A., *Journal of the American Chemical Society* **1972,** *94,* 9175.

57. Li, Z.; Organ, C. L.; Zheng, Y.; Wang, B.; Lefer, D. J., *Circulation* **2016,** *134,* A17903.

58. Steiger, A. K.; Zhao, Y.; Pluth, M. D., *Antioxidants & Redox Signaling* **2018,** *28,* 1516.

59. Powell, C. R.; Foster, J. C.; Okyere, B.; Theus, M. H.; Matson, J. B., *J Am Chem Soc* **2016,** *138,* 13477.

60. Mahato, S. K.; Bhattacherjee, D.; Barman, P.; Bhabak, K. P., *Journal of Materials Chemistry B* **2022,** *10,* 2183.

61. Bhatia, M.; Wong, F. L.; Fu, D.; Lau, H. Y.; Moochhala, S. M.; Moore, P. K., *The FASEB Journal* **2005,** *19,* 1.

62. (a) Olson, K. R., *Antioxidants & Redox Signaling* **2011,** *17,* 32; (b) Wang, R., *Physiological Reviews* **2012,** *92,* 791; (c) Hartle, M. D.; Pluth, M. D., *Chemical Society Reviews* **2016,** *45,* 6108; (d) Takano, Y.; Shimamoto, K.; Hanaoka, K., *Journal of clinical biochemistry and nutrition* **2016,** *58,* 7.

63. Lawrence, N. S.; Davis, J.; Jiang, L.; Jones, T. G. J.; Davies, S. N.; Compton, R. G., *Electroanalysis* **2000,** *12,* 1453.

64. Brown, M. D.; Hall, J. R.; Schoenfisch, M. H., *Analytica Chimica Acta* **2019,** *1045,* 67.

65. Shen, X.; Peter, E. A.; Bir, S.; Wang, R.; Kevil, C. G., *Free Radical Biology and Medicine* **2012,** *52,* 2276.

66. Ida, T.; Sawa, T.; Ihara, H.; Tsuchiya, Y.; Watanabe, Y.; Kumagai, Y.; Suematsu, M.; Motohashi, H.; Fujii, S.; Matsunaga, T.; Yamamoto, M.; Ono, K.; Devarie-Baez Nelmi, O.; Xian, M.; Fukuto Jon, M.; Akaike, T., *Proceedings of the National Academy of Sciences* **2014,** *111,* 7606.

67. Xu, T.; Scafa, N.; Xu, L.-P.; Zhou, S.; Abdullah Al-Ghanem, K.; Mahboob, S.; Fugetsu, B.; Zhang, X., *Analyst* **2016,** *141,* 1185.

68. (a) Furne, J.; Saeed, A.; Levitt, M. D., *American Journal of Physiology-Regulatory, Integrative and Comparative Physiology* **2008,** *295,* R1479; (b) Whitfield, N. L.; Kreimier, E. L.; Verdial, F. C.; Skovgaard, N.; Olson, K. R., *American Journal of Physiology-Regulatory, Integrative and Comparative Physiology* **2008,** *294,* R1930.

69. Yang, G.; Wu, L.; Jiang, B.; Yang, W.; Qi, J.; Cao, K.; Meng, Q.; Mustafa Asif, K.; Mu, W.; Zhang, S.; Snyder Solomon, H.; Wang, R., *Science* **2008,** *322,* 587.

70. Li, H.; Tian, Y.; Deng, Z.; Liang, Y., *Analyst* **2012,** *137,* 4605.

71. Hu, X.; Mutus, B., *Reviews in Analytical Chemistry* **2013,** *32,* 247.

72. Ovsianytskyi, O.; Nam, Y.-S.; Tsymbalenko, O.; Lan, P.-T.; Moon, M.-W.; Lee, K.-B., *Sensors and Actuators B: Chemical* **2018,** *257,* 278.

73. Hao, X.; Wang, B.; Ma, C.; Liu, F.; Yang, X.; Liu, T.; Liang, X.; Yang, C.; Zhu, H.; Lu, G., *Sensors and Actuators B: Chemical* **2018,** *255,* 1173.

74. Mason, J.; Cardin, C. J.; Dennehy, A., *Research in Veterinary Science* **1978,** *24,* 104.

75. Olson, K. R.; DeLeon, E. R.; Liu, F., *Nitric oxide : biology and chemistry* **2014,** *41,* 11.

76. Jeroschewski, P.; Steuckart, C.; Kühl, M., *Analytical Chemistry* **1996,** *68,* 4351.

77. Kraus, D. W.; Doeller, J. E., *Journal of Experimental Biology* **2004,** *207,* 3667.

78. Duan, Y.-W.; Yang, X.-F.; Zhong, Y.; Guo, Y.; Li, Z.; Li, H., *Analytica Chimica Acta* **2015,** *859,* 59.

79. Chen, B.; Li, W.; Lv, C.; Zhao, M.; Jin, H.; Jin, H.; Du, J.; Zhang, L.; Tang, X., *Analyst* **2013,** *138,* 946.

80. Wang, K.; Peng, H.; Ni, N.; Dai, C.; Wang, B., *Journal of Fluorescence* **2014,** *24,* 1.

81. Qiao, Q.; Zhao, M.; Lang, H.; Mao, D.; Cui, J.; Xu, Z., *RSC Advances* **2014,** *4,* 25790.

82. (a) Montoya, L. A.; Pluth, M. D., *Chemical Communications* **2012,** *48,* 4767; (b) Wang, R.; Yu, F.; Chen, L.; Chen, H.; Wang, L.; Zhang, W., *Chemical Communications* **2012,** *48,* 11757.

83. (a) Liu, C.; Peng, B.; Li, S.; Park, C.-M.; Whorton, A. R.; Xian, M., *Organic Letters* **2012,** *14,* 2184; (b) Peng, B.; Chen, W.; Liu, C.; Rosser, E. W.; Pacheco, A.; Zhao, Y.; Aguilar, H. C.; Xian, M., *Chemistry – A European Journal* **2014,** *20,* 1010.

84. Lin, V. S.; Chen, W.; Xian, M.; Chang, C. J., *Chemical Society Reviews* **2015,** *44*, 4596.

85. Filipovic, M. R.; Zivanovic, J.; Alvarez, B.; Banerjee, R., *Chemical Reviews* **2018,** *118*, 1253.

86. Kabil, O.; Banerjee, R., *Journal of Biological Chemistry* **2010,** *285*, 21903.

87. Chance, B.; Schoener, B., *Journal of Biological Chemistry* **1966,** *241*, 4567.

88. Wedmann, R.; Bertlein, S.; Macinkovic, I.; Böltz, S.; Miljkovic, J. L.; Muñoz, L. E.; Herrmann, M.; Filipovic, M. R., *Nitric oxide : biology and chemistry* **2014,** *41*, 85.

89. Nicholls, P.; Kim, J. K., *Biochimica et Biophysica Acta (BBA) - Bioenergetics* **1981,** *637*, 312.

90. Koppenol, W. H.; Bounds, P. L., *Archives of Biochemistry and Biophysics* **2017,** *617*, 3.

91. Kim, D.-H.; Kundu, J. K.; Surh, Y.-J., *Molecular Carcinogenesis* **2011,** *50*, 222.

92. Mustafa Asif, K.; Gadalla Moataz, M.; Sen, N.; Kim, S.; Mu, W.; Gazi Sadia, K.; Barrow Roxanne, K.; Yang, G.; Wang, R.; Snyder Solomon, H., *Science Signaling* **2009,** *2*, ra72.

93. Wu, D.; Si, W.; Wang, M.; Lv, S.; Ji, A.; Li, Y., *Nitric oxide : biology and chemistry* **2015,** *50*, 38.

94. Wu, D.; Li, M.; Tian, W.; Wang, S.; Cui, L.; Li, H.; Wang, H.; Ji, A.; Li, Y., *Scientific Reports* **2017,** *7*, 5134.

95. (a) Liu, Y.-H.; Lu, M.; Hu, L.-F.; Wong, P. T. H.; Webb, G. D.; Bian, J.-S., *Antioxidants & Redox Signaling* **2012,** *17*, 141; (b) Cai, W.-J.; Wang, M.-J.; Moore, P. K.; Jin, H.-M.; Yao, T.; Zhu, Y.-C., *Cardiovascular Research* **2007,** *76*, 29; (c) Papapetropoulos, A.; Pyriochou, A.; Altaany, Z.; Yang, G.; Marazioti, A.; Zhou, Z.; Jeschke Mark, G.; Branski Ludwik, K.; Herndon David, N.; Wang, R.; Szabó, C., *Proceedings of the National Academy of Sciences* **2009,** *106*, 21972.

96. (a) Ózsvári, B.; Puskás, L. G.; Nagy, L. I.; Kanizsai, I.; Gyuris, M.; Madácsi, R.; Fehér, L. Z.; Gerö, D.; Szabó, C., *Int J Mol Med* **2010,** *25*, 525; (b) Li, H.-B.; Ge, Y.-K.; Zhang, L.; Zheng, X.-X., *Life Sciences* **2006,** *79*, 1186.

97. (a) Johansen, D.; Ytrehus, K.; Baxter, G. F., *Basic Research in Cardiology* **2006,** *101*, 53; (b) Tang, G.; Wu, L.; Liang, W.; Wang, R., *Molecular Pharmacology* **2005,** *68*, 1757; (c) Zhang, Z.; Huang, H.; Liu, P.; Tang, C.; Wang, J., *Canadian Journal of*

Physiology and Pharmacology **2007,** *85*, 1248; (d) Zhao, W.; Zhang, J.; Lu, Y.; Wang, R., *The EMBO journal* **2001,** *20*, 6008.

98. Bir, S. C.; Kolluru, G. K.; McCarthy, P.; Shen, X.; Pardue, S.; Pattillo, C. B.; Kevil, C. G., *Journal of the American Heart Association 1*, e004093.

99. Zhao, K.; Ju, Y.; Li, S.; Altaany, Z.; Wang, R.; Yang, G., *EMBO reports* **2014,** *15*, 792.

100. Wang, S. S.; Chen, Y. H.; Chen, N.; Wang, L. J.; Chen, D. X.; Weng, H. L.; Dooley, S.; Ding, H. G., *Cell Death & Disease* **2017,** *8*, e2688.

101. (a) Hanahan, D.; Weinberg, Robert A., *Cell* **2011,** *144*, 646; (b) Schulze, A.; Harris, A. L., *Nature* **2012,** *491*, 364; (c) Gerweck, L. E.; Seetharaman, K., *Cancer Research* **1996,** *56*, 1194.

102. Lee, Z. W.; Zhou, J.; Chen, C.-S.; Zhao, Y.; Tan, C.-H.; Li, L.; Moore, P. K.; Deng, L.-W., *PLOS ONE* **2011,** *6*, e21077.

103. Lee, Z. W.; Teo, X. Y.; Tay, E. Y. W.; Tan, C. H.; Hagen, T.; Moore, P. K.; Deng, L. W., *British Journal of Pharmacology* **2014,** *171*, 4322.

104. Lu, S.; Gao, Y.; Huang, X.; Wang, X., *International Journal of Oncology* **2014,** *44*, 1259.

105. Malumbres, M.; Barbacid, M., *Nature Reviews Cancer* **2009,** *9*, 153.

106. Ma, K.; Liu, Y.; Zhu, Q.; Liu, C.-h.; Duan, J.-L.; Tan, B. K. H.; Zhu, Y. Z., *PLOS ONE* **2011,** *6*, e20525.

107. Wu, Y. C.; Wang, X. J.; Yu, L.; Chan, F. K. L.; Cheng, A. S. L.; Yu, J.; Sung, J. J. Y.; Wu, W. K. K.; Cho, C. H., *PLOS ONE* **2012,** *7*, e37572.

108. Fleischauer, A. T.; Arab, L., *The Journal of Nutrition* **2001,** *131*, 1032S.

109. Herman-Antosiewicz, A.; Singh, S. V., *Journal of Biological Chemistry* **2005,** *280*, 28519.

110. Tsai, C.-Y.; Wang, C.-C.; Lai, T.-Y.; Tsu, H.-N.; Wang, C.-H.; Liang, H.-Y.; Kuo, W.-W., *International Journal of Cardiology* **2013,** *168*, 1286.

111. Choi, Y. H., *Biomedicine & Pharmacotherapy* **2017,** *94*, 63.

112. Ding, Y.; Yu, Z.; Zhang, C., *Life Sciences* **2021,** *278*, 119631.

113. Liang, D.; Wu, H.; Wong, M. W.; Huang, D., *Organic Letters* **2015,** *17*, 4196.

114. Lin, Y.-T.; Yang, J.-S.; Lin, S.-Y.; Tan, T.-W.; Ho, C.-C.; Hsia, T.-C.; Chiu, T.-H.; Yu, C.-S.; Lu, H.-F.; Weng, Y.-S.; Chung, J.-G., *Anticancer Research* **2008,** *28*, 2791.

115. Yue, Z.; Guan, X.; Chao, R.; Huang, C.; Li, D.; Yang, P.; Liu, S.; Hasegawa, T.; Guo, J.; Li, M., *Molecules (Basel, Switzerland)* **2019,** *24,* 2665.

116. Na, H.-K.; Kim, E.-H.; Choi, M.-A.; Park, J.-M.; Kim, D.-H.; Surh, Y.-J., *Biochemical Pharmacology* **2012,** *84,* 1241.

117. Rao, P. S. S.; Midde, N. M.; Miller, D. D.; Chauhan, S.; Kumar, A.; Kumar, S., *Current drug metabolism* **2015,** *16,* 486.

Design, Synthesis and Anti-cancer Activities of Benzylic Derivatives of Diallyl Disulfide (DADS) and the Corresponding Diselenide

2.1. Introduction

As described in the previous chapter, medicinally enriched garlic (*Allium sativum*) contains several organosulfur compounds that exert various pharmacological properties including anti-microbial, antioxidant, cardiovascular, anti-carcinogenic, and many more.[1] In 1988, You *et al*. reported the preventive role of *allium* vegetables towards many organ-specific cancers (stomach, gastric, colon and breast) among the Chinese community.[2] Subsequently, the preventive roles of garlic toward colorectal cancer and cancer of the head and neck were reported in several case studies. Further detailed investigations have shown that both hydrophilic and lipophilic organosulfur compounds in garlic exert promising anti-tumorigenic properties against a variety of cancer cell lines.[3] Interestingly, compound **2.1** and alliin are reported to be present in whole raw garlic samples. Upon the enzymatic decomposition by *alliinase*, alliin gets converted to allicin and it further undergoes rapid degradation to form the most stable allyl sulfides such as DAS, DADS and DATS etc (Figure 2.1).[4]

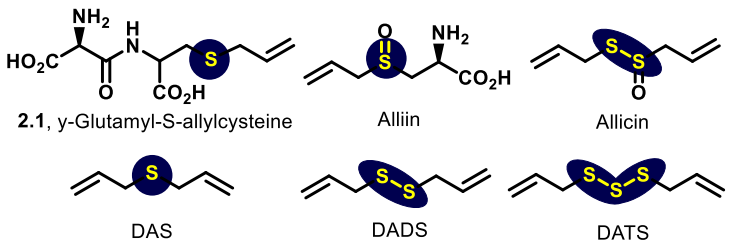

Figure 2.1. Chemical structures of some key organosulfur compounds present in garlic.

The pharmacological potentials of garlic-derived organosulfides were studied by several researchers. For example, Singh *et al*. have reported the anti-cancer potential of DAS in DMBA-induced (7,12-dimethylbenz(a)anthracene) skin carcinogenesis models of Swiss albino mice.[5] The scheduled treatment with DAS reflected an effective delay of the onset of tumorigenesis and reduced the cumulative number of tumors per mouse. This study validates the effectiveness of DAS and the reduction of tumor burden in the higher animal models. Similarly, DADS and its analogues were found to be effective in reducing the levels of oxidized low-density lipoprotein (ox-LDL), lipid peroxidation as well as NF-kβ activity, showing good anti-inflammatory and antioxidant properties in Wistar rat models.[6] Recently, Hosono *et al*. have studied the anti-cancer effect of garlic by using human colon cancer cell lines such as HCT-15 and DLD-1.[7] Another study by Lei and co-workers revealed the growth inhibitory effect of DADS against breast cancer cell line (MCF-7) in a dose-dependent manner.[8] The treatment of DADS (50, 100, 200,

300, or 400 μmol L^{-1}) against MCF-7 for 24 h of exposure showed survival rate of 99%, 91%, 83%, 59%, and 52%, respectively. Detailed studies by the same authors revealed the possible anti-proliferative property of DADS *via* attenuation of ERK-phosphorylation and the activation of SAPK/JNK and p38 pathways.[9] Similarly, in early 2000, Knowles and co-workers have reported DADS-mediated G2/M phase cell cycle arrest *via* reduction of kinase activity of the CDK1/Cyclin B1 complex in human colon cancer cells.[10] Unlike DADS, corresponding trisulfide DATS significantly suppressed the growth of cancer cells *via* arresting the G2/M phase of the cell cycle.[11] Further research on DADS by Dasgupta and co-workers (2013) demonstrated a novel pathway that induces cancer cell apoptosis and G2/M phase arrest *via* induction of NF-κβ-dependent p21waf1/cip1 pathway.[12] In addition to this, DATS has exhibited several other activities such as inhibition of tubulin polymerization, disruption of microtubule network formation, and some specific oxidative modifications of cysteine residues for DATS-treated tubulins, etc. Furthermore, Singh and co-workers have shown that DATS is very much effective in inducing apoptosis in human prostate cancer cells.[13] The allyl sulfides such as DAS, DADS, and DATS were found to inhibit the migration and invasion of human colon cancer cells (colo-205) in the order of DATS > DADS > DAS through the inhibition of matrix metalloproteinase (MMP) expression.[13] Therefore, understanding the exact mechanism of action or the difference in activities of these allyl sulfides towards their anti-tumorigenesis potentials would be very much helpful in understanding the medicinal importance of garlic.

2.2. Outline of the chapter

As discussed in the last section, although several reports describe the medicinal impacts of different garlic-derived organosulfur compounds including allyl sulfides, synthesis followed by the bio-evaluation of structural analogues of allyl sulfides for the detailed structure-activity correlation is rare in the literature. In search of developing newer derivatives with potential anti-cancer activities, we have synthesized a series of benzyl analogues of DADS with the variation of substituents at the para-position of the benzene ring (DBDS and **2.2-2.5**, Figure 2.2). Furthermore, to understand the importance of sulfur atoms in DADS, the corresponding diselenide compounds **2.6-2.10** were also considered for detailed structure-activity correlation studies. Understanding the anti-proliferative activities of these compounds might help in developing more potent disulfide/diselenide analogues for anti-cancer therapy. Our study reveals that the activity

of organodisulfides/diselenides can be increased by several factors upon the introduction of a cyano group at the *para*-position. The 4-cyano substituted disulfide/diselenide derivatives were found to be more selective towards the ER+ human breast cancer cell line (MCF-7) over the non-cancerous normal kidney epithelial cells (NKE). Interestingly, compound **2.3** exhibited much higher potency than DADS, which indicates the importance of the 4-cyano group in enhancing the effectiveness of organodisulfides. It has been observed that, the benzylic diselenides showed almost 9-16 fold potent anti-proliferative activities than the well-known organoselenium compound ebselen against MCF-7 cells. To further investigate the mechanistic aspects of those potent compounds (**2.3** and **2.8**), intracellular ROS inducing abilities was studied using DCF-DA assay. Compound **2.8** exhibited increased ROS levels in malignant cells as compared to the non-malignant cells. The modulation of expression level of key cancer marker proteins in MCF-7 cells by the lead compound **2.8** was studied and the results indicated a dose-dependent down-regulation of Procaspase 3, Bcl2 and Survivin.

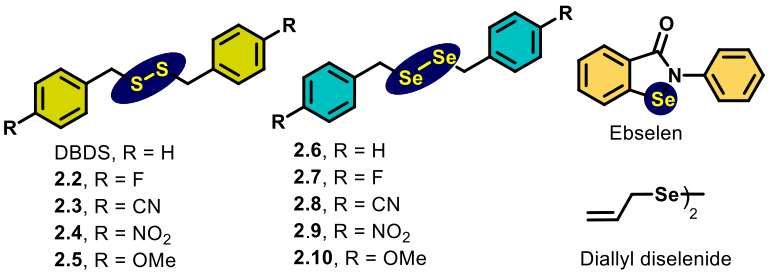

Figure 2.2. Chemical structures of the substituted benzyl disulfides DBDS, **2.2-2.5** and the corresponding diselenides **2.6-2.10** along with ebselen and diallyl diselenide.

2.3. Results and discussion

2.3.1. Synthesis of disulfides and diselenides

The aliphatic, aromatic and benzylic symmetrical disulfides can be synthesized by direct oxidation of thiols.[14] However, the application of these synthetic methods is relatively limited due to the unpleasant and obnoxious smell of most of the aliphatic, benzylic, and aromatic thiols. Therefore, in our present study, the substituted benzyl disulfides DBDS, **2.2-2.5** were prepared following a different method utilizing the corresponding halides as precursors in the presence of thiourea as the sulfur-transfer reagent and manganese dioxide as mild oxidant in a micellar SDS solution with reasonably good yields (Scheme 2.1).[14] The synthesized compounds were finally purified using silica gel column chromatographic techniques. On the other hand, the corresponding diselenides **2.6-2.10**

were synthesized starting from the halides by the reaction with the readily synthesized disodium diselenide (Na_2Se_2) following the literature method with slight modifications. The reagent Na_2Se_2 was prepared *in situ* by the reduction of elemental selenium powder with sodium borohydride.[15] The nucleophilic attack of Na_2Se_2 on two molecules of substituted benzyl halides led to the formation of the corresponding symmetrical diselenides (Scheme 2.1). Very recently, Panduranga *et al*. have reported an interesting method for the synthesis of a series of symmetrical benzyl disulfides and diselenides using the corresponding alcohols as precursors in the presence of sulfur and selenium transfer reagents.[16] This method also provided very good yields to a diverse sets of organodisulfides and diselenides. The cyclic selenenyl amide ebselen was prepared from anthranilic acid following the standard literature method.[17] All the disulfides DBDS, **2.2-2.5** and diselenides **2.6-2.10** were successfully characterized by NMR (^1H, ^{13}C and ^{77}Se) spectroscopic and ESI-MS spectrometric analyses. We attempted to prepare diallyl diselenide corresponding to DADS. Unfortunately, the product was found to be unstable and led to decomposition during the purification step. Therefore, this compound could not be used for further studies.

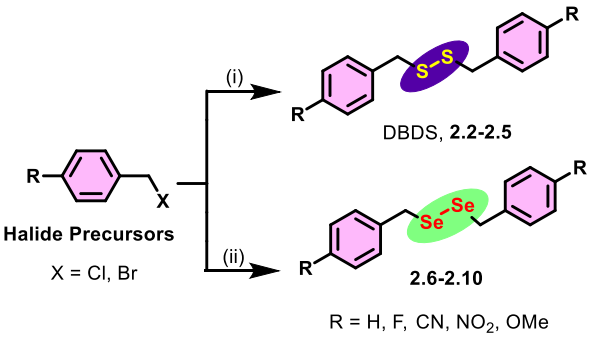

Scheme 2.1. Synthetic schemes for substituted benzyl disulfides (DBDS, **2.2-2.5**) and the corresponding diselenides (**2.6-2.10**). Reagents and conditions: (i) Thiourea, MnO_2, Na_2CO_3, SDS, water, RT; (ii) Na_2Se_2, EtOH, 80 °C.

2.3.2. Important structural features in disulfide 2.3 and diselenide 2.8

In addition to the spectral characterization of all the disulfides and diselenides, a representative disulfide and a diselenide having 4-cyano substitution were characterized by single crystal X-ray diffraction studies. The ORTEP diagrams of compounds **2.3** and **2.8** along with some important bond lengths and angles are shown in Figure 2.3. The X-ray structures of both of these compounds exhibited some interesting features. For example, although no intramolecular interaction was detected due to the presence of electron withdrawing heteroatom at *para*-position of benzene rings, different

intermolecular non-bonded interactions were observed in both the disulfide and diselenide compounds and these interactions led to the formation of extended network-like structural patterns as shown in Figure 2.3 and Table 2.1.

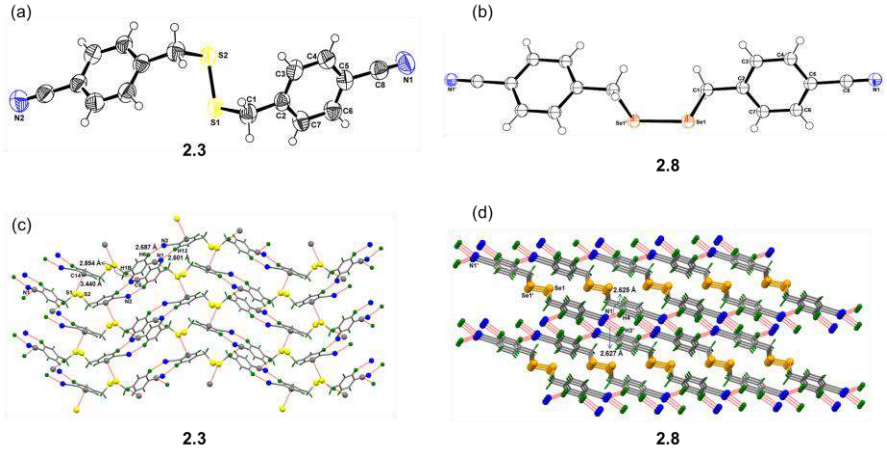

Figure 2.3. (a-b) ORTEP diagrams of compounds **2.3** and **2.8** along with some important bond lengths and bond angles. Displacement ellipsoids are drawn at 50% probability level and hydrogen atoms are shown as small spheres of arbitrary radii. (c-d) Network-like wavy structural pattern of compounds **2.3** and **2.8** showing different non-bonding interactions and the expansion in two orthogonal directions.

Table 2.1. Some important bond angles and distances in the X-ray structures of compound **2.3** and **2.8**.

Entry	Bond distance (Å)		Bond angles (°)	
Compound **2.3**	S1-S2	2.028 Å	C1-S1-S2	103.10°
	C1-S1	1.816 Å	C5-C8-N1	178.64°
	C8-N1	1.136 Å		
Compound **2.8**	Se1-Se1'	2.320 Å	C1-Se1-Se1'	100.65°
	C1-Se1	1.970 Å	C5-C8-N1	179.83°
	C8-N1	1.135 Å		

As shown in Figure 2.3, several intermolecular interactions have been detected in disulfide **2.3**. For example, the electronegative nitrogen atom of cyano group interacted with C-H moiety of benzene ring of another molecule to form N1···H12-C12 linkages (dN1···H12: 2.601 Å). The H-bonding interaction has been further strengthened by the formation of a complimentary H-bond with the formation of N2···H6-C6 linkages (dN2···H6: 2.687 Å). These two H-bonding interactions build an extended wavy chain-like network pattern in one direction. Interestingly, the individual chain networks are connected to each other by two additional inter-layer interactions with C1-S1···C14

(dS1···C14: 3.440 Å) and C8···H1B-C1 (dC8···H1B: 2.854 Å) linkages (Figure 2.3c). These additional interactions link the wave-like chains and extend them in orthogonal directions. A similar wavy-like structural pattern was also reported for the trisulfide analogue of 4-fluoro substituted disulfide (**2.2**).[18]

Similar to the disulfide **2.3**, non-bonding interactions were also detected in the corresponding diselenide **2.8** although the pattern of interactions were found to be different. In this compound, the terminal nitrogen atoms of cyano groups were involved in two intermolecular H-bonding interactions with the benzene ring C-H atoms of two different diselenide units with the formation of N1···H4-C4 (dN1···H4 = 2.625Å) and N1···H3'-C3' (dN1···H3' = 2.627Å) linkages. Similarly, the N' atom of another -CN group of the diselenide unit is also involved in two intermolecular H-bonding interactions with the ring H-atoms. Due to the presence of these four intermolecular H-bonding interactions, the molecule adopts a network-like structural pattern in two directions as shown in Figure 2.3d. The non-bonded interactions observed in the disulfide **2.3** and the corresponding diselenide **2.8** are in contrast to the interactions present in most of the *ortho*-substituted diaryl diselenides reported earlier.[19] In case of *ortho*-substituted diaryl diselenides, mainly intra-molecular non-bonded interactions were observed between the electron withdrawing heteroatoms and Se-centers.

2.3.3. Anti-proliferative activities of disulfides and diselenides

To evaluate the anti-proliferative activities of benzyl analogues of DADS, and their selenium analogues, an MTT assay has been performed after 24 h of compound exposure against human breast cancer cells (MCF-7). The garlic-derived disulfide DADS was considered a standard reference for the evaluation of the anti-proliferative activity of disulfides DBDS and **2.2**-**2.5**. As shown in Figure 2.4, DADS was found to be significantly active as compared to most of the disulfides except disulfide **2.3** having a cyano group at 4-position of benzene ring. Dose-dependent experiments have shown the IC_{50} of compound **2.3** to be 3.55 μM. While a moderate anti-proliferative activity was observed for the dibenzyl disulfide (DBDS), the activity could be altered by the introduction of different electron withdrawing and electron donating groups such as, -F, -CN, -NO_2, or -OMe groups at the 4-position of the benzene ring (Table 2.2). For example, 4-F substituted disulfide **2.2** exhibited almost similar cytotoxicity as similar to compound DBDS. However, a decrease in potency was observed upon the incorporation of 4-NO_2 and 4-OMe groups. Unlike other substitutions, as shown here, a dramatic

enhancement in anti-proliferative activity was observed upon the replacement of 4-H with the 4-CN group (compound **2.3**). The activity of compound **2.3** was (IC_{50}: 3.50 µM) to be increased almost ~14 fold in comparison to compound DBDS (IC_{50}: 43.60 µM)..

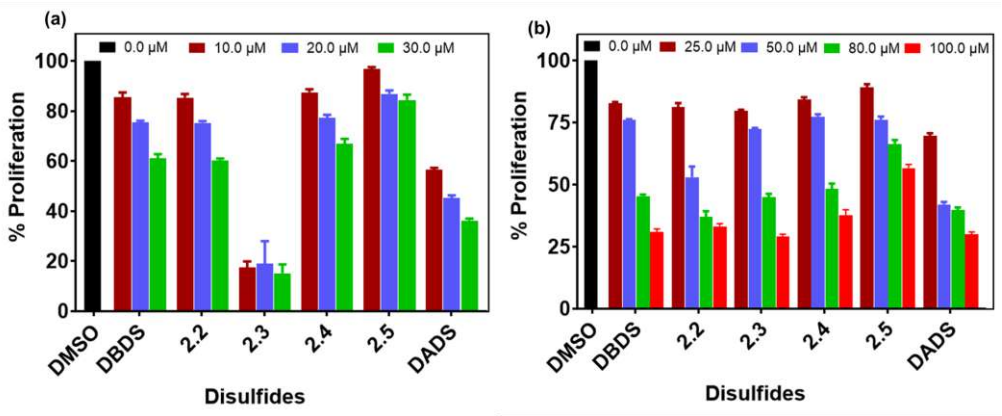

Figure 2.4. Percentage proliferation of (a) MCF-7 and (b) NKE cells treated with the test compounds (DBDS, **2.2**-**2.5** and DADS) in a dose-dependent manner after an incubation for 24 h. Different concentrations of the test compounds were used in MCF-7 and NKE cells.

Inspired by the potencies of the organodisulfides in MCF-7 cells the corresponding selenium analogues **2.6**-**2.10** have been evaluated with the standard cytoprotective organoselenium compound ebselen. Interestingly, the diselenides exhibited almost 9-16 fold higher anti-proliferative activities than the reference compound Ebselen (Figure 2.5, Table 2.2). As shown in the Table 2.2, the IC_{50} values of the all the diselenides were found to be lower than 1.0 µM, which were remarkably lower as compared to ebselen as well as DADS. The effect of different at 4-position of benzene ring is also reflected in diselenides although the effect is relatively less significant than that in disulfides. Unlike other substituents, the incorporation of 4-OMe group (**2.10**) in dibenzyl diselenide **2.6** led to a decrease in the anti-proliferative activity. To understand the toxicity and selectivity of the synthesized compounds **2.6**-**2.10** towards the normal cell over the cancer cell, all the compounds were evaluated further in a representative normal kidney epithelial cell line (NKE). Interestingly, all the diselenides and exhibited significantly lower potency in NKE cells (Table 2.2, Figure 2.5).

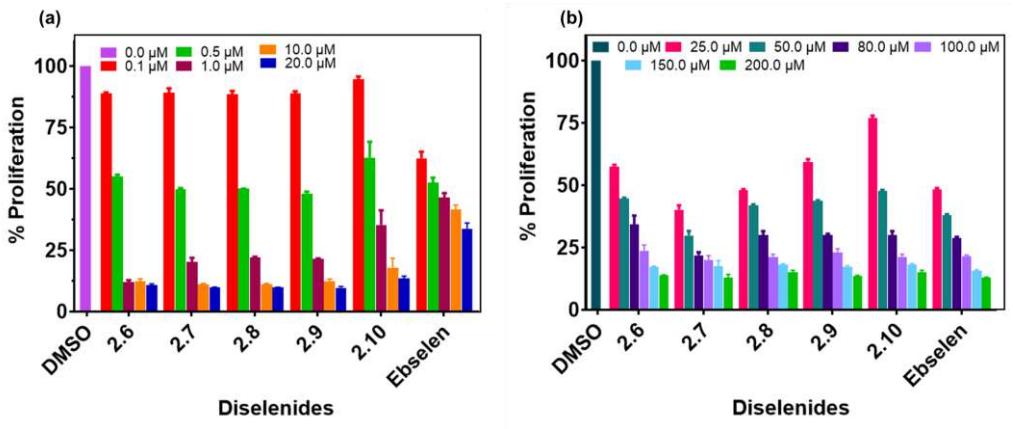

Figure 2.5. Percentage proliferation of (a) MCF-7 and (b) NKE cells treated with the test compounds (**2.6**-**2.10** and Ebselen) in a dose-dependent manner after an incubation for 24 h. Different concentrations of the test compounds were used for MCF-7 and NKE cells.

The IC_{50} of DADS and compound **2.3** were almost 2.7- and 18.5-fold higher in NKE cell, respectively. As expected, DADS and compound **2.3** were shown to be less active towards NKE cells. In contrast to most of the disulfides, the IC_{50} values of all diselenides were at least 50-fold higher in NKE cells as compared to their activities in MCF-7 cell line (Table 2.2). These results strongly support that the substituted benzyl diselenides have dramatically higher potencies for their anti-proliferative activities in breast cancer cells (MCF-7) with enhanced selectivity over normal cells.

Table 2.2. Anti-proliferative activities of disulfides and diselenides along with ebselen against MCF-7 and NKE cells as determined by MTT assay.

Compound	IC_{50} (µM)[a]		Compound	IC_{50} (µM)[a]	
	MCF-7[b]	NKE[c]		MCF-7[b]	NKE[c]
DADS	17.0 ± 0.4	45 ± 2	Ebselen	7 ± 1	28.0 ± 0.3
DBDS	44 ± 2	70 ± 1	**2.6**	0.43 ± 0.10	36 ± 1
2.2	43 ± 2	56 ± 4	**2.7**	0.45 ± 0.20	21 ± 2
2.3	**3 ± 1**	**66 ± 1**	**2.8**	**0.46 ± 0.10**	**30.0 ± 0.4**
2.4	55 ± 3	82 ± 8	**2.9**	0.44 ± 0.10	35.0 ± 0.3
2.5	94 ± 2	102 ± 4	**2.10**	1.0 ± 0.1	42 ± 1

[a]Cell proliferation determined by the MTT assay from the dose-response curves in triplicates after 24 h of incubation at 37 °C. [b] Breast cancer cell line. [c] Normal kidney epithelial cell line.

2.3.4. Anti-proliferative activities in different organ-specific cancer cell lines

Upon the evaluation of all synthesized disulfides and diselenides in MCF-7 and NKE cell lines, we have further evaluated the most active disulfide (**2.3**) and diselenide (**2.8**) against other organ-specific cell lines such as liver (HepG2), prostate (PC-3) and colon (HCT-116) cancer cells. Additionally, the cells were incubated with different compounds for a duration of 48 h to estimate the effect of the exposure time of the compounds. We have selected compounds **2.3**, **2.8**, DADS, and ebselen as reference compounds for better comparison purposes. As shown in Figure 2.6, compound **2.8** an organoselenium compound has shown to be more potent in all the organ-specific cell lines than the active disulfide compound **2.3**. Furthermore, comparative activities of these representative compounds in MCF-7 cells with an incubation of 24 h (Table 2.2) and 48 h (Figure 2.6) reveal that the variation of incubation time from 24 h to 48 h does not have significant impact on their anti-proliferative activities in MCF-7 cells.

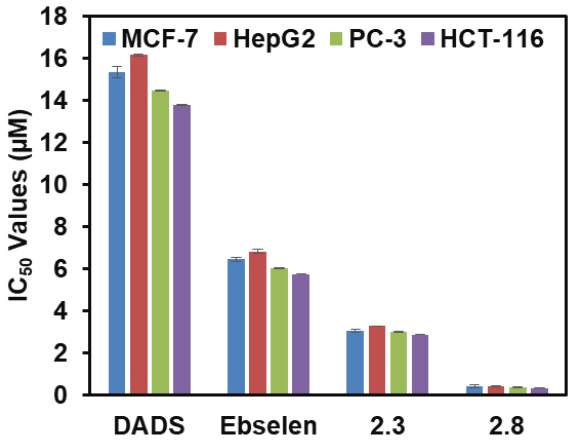

Figure 2.6. Cell proliferation determined by the MTT assay from the dose-response curves after 48 h of incubation at 37 °C. About 3×10^3/100.0 µl/well were seeded in 96-well culture plates and treated with various concentrations of test compounds (**2.3**, **2.8**, DADS and Ebselen) for 48 h at 37 °C.

2.3.5. Cellular morphology analysis using DAPI

The purpose of this study was to determine whether compound **2.8** (1.0 µM) has any effect on the morphology and viability of MCF-7 cells after 48 h of incubation. The changes in nuclear architecture were evidenced by staining the **2.8** treated cells with DAPI and comparing that with the untreated cells. As shown in Figure 2.7, treatment of cells with **2.8** (1.0 µM) over 48 h led to nuclear aberration with possible indication of DNA damage and programmed cell death as visualized upon DAPI-staining.

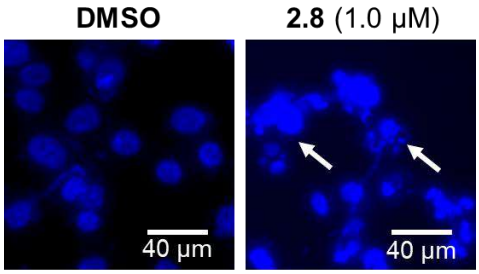

Figure 2.7. Evaluation of the changes in nuclear morphology of MCF-7 cells using DAPI upon the treatment of cells with compound **2.8** for 48 h. Scale bar represents 40 µm.

2.3.6. Evaluation of the anti-migratory activity of compound 2.8

The anti-migratory activity of compound **2.8** has been examined by scratch assay. The cellular monolayer was mechanically scratched and compound **2.8** (0.5 and 1.0 µM) was added for 48 h and the cellular distribution was imaged and measured at different time intervals. In the absence of any compound (DMSO control), the cells migrated to the scratched area over 48 h and almost compensated the vacant space. However, compound **2.8** prevented the cellular migration in a dose-dependent manner over time. It has been observed that compound **2.8** exhibited an anti-migratory activity at 1.0 µM after 24 h of incubation (Figure 2.8). The same anti-migratory property of compound **2.8** persisted even after 48 h of incubation. These observations indicate the potent anti-migratory activity of compound **2.8** in MCF-7 cells.

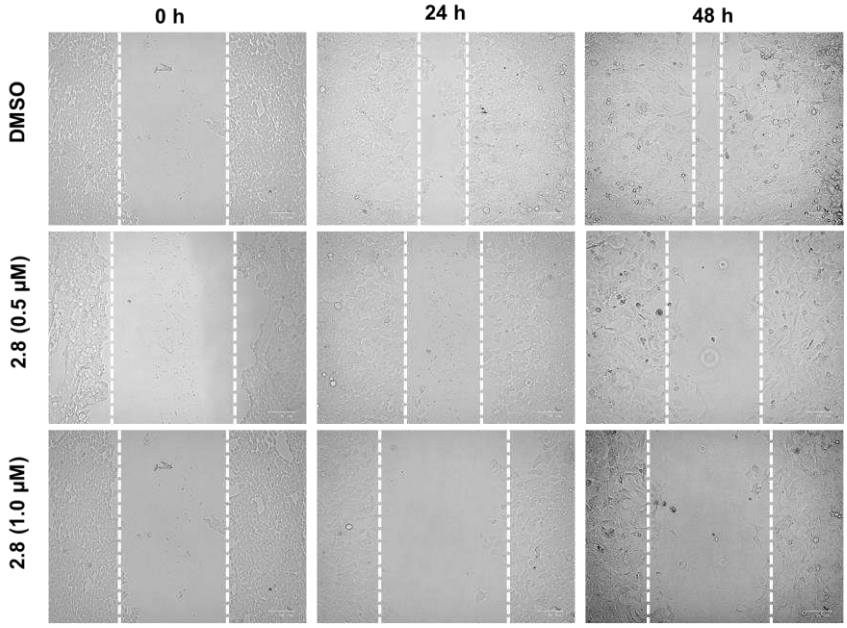

Figure 2.8. Anti-migratory activity of compound **2.8** in MCF-7 cells. The compound **2.8** (0.5 and 1.0 µM) was incubated upto 48 h and images were captured at 0, 12, 24 and 48 h. Scale bar represents 100 µm.

2.3.7. *In vitro* antioxidant activities of disulfides and diselenides

To understand the capability of the test compounds to catalytically reduce H_2O_2, an initial rate of reduction of the same was evaluated spectrophotometrically using a glutathione/glutathione disulfide (GSH/GSSG) coupled assay system in presence of synthesized benzyl derivatives of disulfides and diselenide compounds. Previous reports have suggested that the antioxidant activities of organochalcogen compounds play an important role in reducing tumor progression.[19c] To understand the mode of anti-proliferative activities of disulfides and diselenides in cancer cells, an evaluation of *in vitro* antioxidant activity would be beneficial. It has also been shown that the reduction of peroxides can be efficiently performed by various diaryl diselenides.[19c] Therefore, to understand the antioxidant properties of disulfides and diselenides, we have determined their potencies for the catalytic reduction of H_2O_2 using the well-established GSH/GSSG coupled assay method.[19c, 20] The catalytic reduction of H_2O_2 by disulfides and diselenides along with anti-inflammatory organoselenium compound ebselen was studied by using GSH as the co-substrate. The initial rate (v_0) for the reaction in the presence and absence of sulfur/selenium compounds was determined by following the oxidation of reduced nicotinamide adenine dinucleotide phosphate (NADPH) at 340 nm using UV-Vis spectroscopic method in a phosphate buffer medium and the results are shown in Table 2.3. In this assay, the reactions of disulfides/diselenides with GSH are expected to produce the corresponding catalytically active thiols/selenols for the reduction of peroxide. As shown below, the initial rate for the catalytic reduction of H_2O_2 by garlic-derived disulfide DADS was found to be higher than the control reaction without any sulfur/selenium compound. However, most of the benzyl derivatives of DADS were found to be inactive or exhibited very weak antioxidant activities. The antioxidant activity of standard organoselenium compound ebselen was found to be much higher than the control reaction, which is in agreement with the previously reported data.[21] Whereas, the benzyl derivatives of diselenides were found to exhibit relatively weaker antioxidant activities. However, their activities were slightly higher than the corresponding disulfide analogues. In general, these results indicate that organodisulfides (DBDS, **2.2-2.5**) and diselenides (**2.6-2.10**) used in the present study exhibit very weak antioxidant activities as compared to the standard compound ebselen for the *in vitro* reduction of ROS such as H_2O_2.

Table 2.3. Initial rates (v_o) for the reduction of H_2O_2 by GSH in the presence of disulfides, diselenides and ebselen.

Compound	Initial rate (v_o) [μM min^{-1}][a]	Compound	Initial rate (v_o) [μM min^{-1}][a]
Control	11 ± 1	Control	11 ± 1
DADS	27 ± 1	Ebselen	108 ± 8
DBDS	10 ± 2	**2.6**	22 ± 15
2.2	10.0 ± 0.5	**2.7**	23 ± 3
2.3	9 ± 1	**2.8**	15 ± 10
2.4	12 ± 4	**2.9**	12 ± 6
2.5	13 ± 4	**2.10**	33 ± 5

[a]The reactions were carried out in phosphate buffer (100 mM, pH 7.4) at 25 °C. Test compounds: 50.0 μM; GSH: 2.0 mM; NADPH: 0.4 mM; ethylenediaminetetraacetate disodium salt (EDTA): 1.0 mM; glutathione disulfide reductase: 1.7 units/mL; hydrogen peroxide: 1.6 mM. The control reactions were performed under identical conditions in the absence of sulfur/selenium compounds.

2.3.8. Generation of intracellular ROS by the test compounds

It is well known that generation of intracellular ROS is an influential mechanism for the organoselenium compound-induced cytotoxicity in cancer cells. High concentration of ROS induces cell death of cancer cells by damaging genomic DNA, proteins and lipids.[22] To determine whether disulfides DBDS, **2.2-2.5** diselenides **2.6-2.10** cause any cell death by generating ROS in MCF-7 cells, the DCF-DA assay was carried out and the amount of ROS generated when cells were incubated with disulfides or diselenides was measured using flow cytometry. Upon the reaction of non-fluorescent DCF-DA with the intracellular ROS, the green-emitting fluorogenic dye DCF was produced, which was detected by a built-in green channel in FACS. Interestingly, diselenides **2.6-2.10** (1.0 μM) exhibited an enhancement of ROS level in the range of 1.54-2.54 fold as compared to the control as shown in Figure 2.9. Notably, compound **2.8** that exhibited the highest anti-proliferative activity, showed the highest increase (2.36-fold) in DCF intensity (Figure 2.9). It should be noted that no detectable enhancement of ROS level was observed in the presence of a 1.0 μM concentration of ebselen which is much lower than the IC_{50} of ebselen (7.30 μM). Further, a 2.0-fold enhancement of ROS level was observed in the presence of a 10.0 μM concentration of ebselen. On the other hand, the increase in ROS level was found to be almost negligible in the presence of disulfides

(10.0 and 50.0 µM) except compound **2.3**, which increased the ROS level by 2.1 fold at higher concentration (50.0 µM). These data suggest that, diselenides and disulfides have a different mode of action to exhibit the anti-proliferative activity.

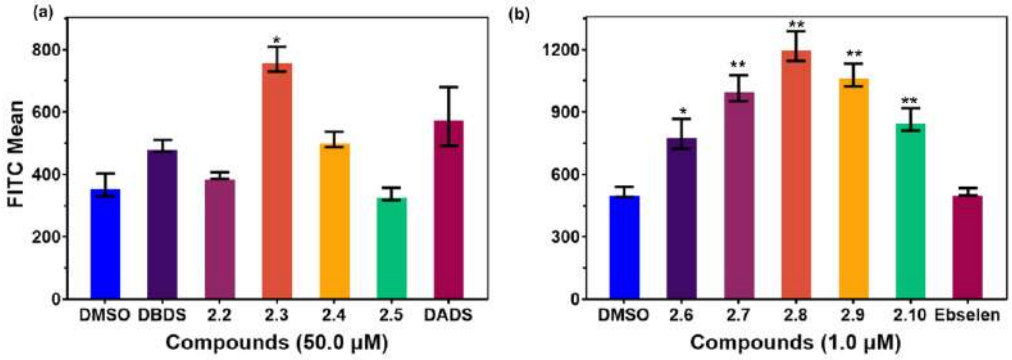

Figure 2.9. Estimation of the intracellular ROS production in MCF-7 cells in the presence of different (a) disulfides and (b) diselenides. All data are represented as mean ± SD of three independent experiments and differences between the mean values were assessed by paired *t*-test. **p*<0.05 and ***p*<0.01 indicate the significant difference compared with the control group.

2.3.9. Western blot experiment

To understand the mode of action of compound **2.8** in the MCF-7 cell line, we have performed a western blot experiment to estimate the expression level of some key proteins that is responsible for cancer progression. The MCF-7 cells were incubated compound **2.8** (0.5 and 1.0 µM) for 48 h using of DMSO as vehicle control. A cytosolic protein GAPDH was used as a housekeeping marker for loading control for the experiment. As shown in Figure 2.10, the expression levels of some key proteins such as procaspase 3, Bcl2, and Survivin were studied in the presence of compound **2.8**. It is well evident that Survivin and Bcl2 act as anti-apoptotic markers, responsible for the progression and survival of cancer. Herein, the effect of compound **2.8** was found to be noticeable as the down-regulation of Survivin and Bcl2 was markedly observed in a dose-dependent manner. Additionally, compound **2.8** reduces the expression of procaspase 3. Procaspase 3 is a well-known protein marker responsible for the apoptosis and is a zymogen of caspase 3, which can activate an executioner protein called caspase 3. Therefore, the dose-dependent down-regulation of procaspase 3 in the presence of **2.8** indicates the activation of caspase 3, which promotes apoptosis.

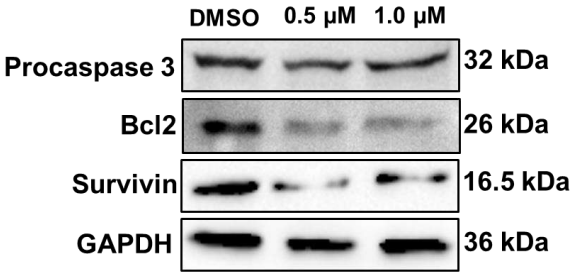

Figure 2.10. Western blot analysis for the estimation of key protein expression levels in MCF-7 cells in the presence of compound **2.8** at different concentrations (0.0, 0.5 and 1.0 μM) for 48 h. Equal protein loading was confirmed by the analysis of GAPDH expression.

2.4. Conclusions

In summary, we reported herein a series of 4-substituted benzyl derivatives of DADS and the corresponding diselenide analogues for detailed structure-activity correlation studies towards their anti-cancer properties against ER+ breast cancer cell line (MCF-7). The potent compounds were evaluated further in other organ-specific malignant cell lines. Activities of both the sets of sulfur and selenium compounds were studied separately along with the reference compounds such as DADS and Ebselen, respectively. The study revealed that the anti-proliferative activity dramatically enhanced upon the incorporation of a cyano group at the 4-position of a benzene ring (compound **2.3**). Interestingly, compound **2.3** was found to be more potent than the garlic-derived disulfide DADS. Moreover, all the benzylic diselenides exhibited much higher potencies than DADS and the corresponding organodisulfides and the well-known cytoprotective compound ebselen. In contrast to most disulfides, all the diselenides exhibited enhanced selectivity towards cancer cells (MCF-7) over normal cells (NKE cells). Further investigations revealed the notable increase in intracellular ROS level upon the administration of diselenides towards MCF-7 cells correlating with their anti-proliferative activity. Finally, SAR studies reveal that anti-cancer activity of garlic-derived compound DADS can be dramatically increased either by replacing the allyl group with the 4-cyanobenzyl group (compound **2.3**) also by the replacement of sulfur by selenium (compound **2.8**) atom. Treatment of compound **2.8** in MCF-7 cells induced prominent nuclear fragmentation as evaluated by the staining with DAPI. Additionally, **2.8** promotes apoptosis of MCF-7 cells. Upon treatment of **2.8**, dose-

dependent down-regulation of several oncogenic marker proteins (Bcl2, Survivin, and Procaspase 3) was observed. However, further mechanistic studies would be necessary to understand the molecular pathways associated with the anti-cancer activities of organodisulfides/diselenides analogues of DADS.

2.5. Experimental Section

2.5.1. Materials and Methods

Thin layer chromatographic (TLC) analyses were carried out on pre-coated silica gel on aluminum sheets. All the final products were purified by silica gel or neutral aluminum oxide column chromatography using the freshly distilled solvents. The NMR spectra ^{1}H (400 or 600 MHz), ^{13}C (100 or 150 MHz) and ^{77}Se (114 MHz) NMR spectra were obtained on Varian Mercury plus 400 MHz or Bruker 400 MHz spectrometer at 298 K. Chemical shifts are cited with respect to Me_4Si (^{1}H and ^{13}C) as internal standard and Me_2Se (^{77}Se) as external standards. Mass spectral studies were carried out on an Agilent Accurate-Mass Q-TOF LC/MS 6520 spectrometer, and peaks are given in *m*/*z* (% of basis peak). Cell viability assay was performed using Thermo Scientific Multiskan™ GO Microplate spectrophotometer. Cellular morphology was visualized and imaged under Bio-Rad ZOE™ fluorescent cell imager.

2.5.2. General synthesis of disulfides DBDS, 2.2-2.5

The disulfides in the present study were synthesized following the literature method with minor modifications.[14, 23] To a micellar solution of sodium dodecyl sulfate (SDS, 0.2 M, and 1.6 equiv), thiourea (1.5 equiv), manganese dioxide (1.0 equiv) and sodium carbonate (1.5 equiv) was added the corresponding benzyl halide derivative (1.0 equiv) dropwise at room temperature. The reaction mixture was stirred magnetically overnight. A dark brown colored suspension was observed. The progress of reaction was monitored by TLC analysis until the benzyl halide derivative was consumed. The reaction mixture was diluted with ethyl acetate and filtered through celite pad to remove the suspension of manganese dioxide. The filtrate was extracted with water. The organic layer was washed with brine and dried over anhydrous sodium sulfate. The solvent was evaporated to afford the crude product. The crude mixture was purified by silica gel column chromatography using hexane and ethyl acetate as eluents.

Compound DBDS:[24] Benzyl bromide (7.20 g, 42.00 mmol) was used to yield the disulfide DBDS as white amorphous solid. Reaction time: 5 h, Yield: 70% (7.25 g); M.P: 68 - 70 ºC; R_f = 0.5 (100% hexane). ^{1}H NMR ($CDCl_3$, 600 MHz): δ (ppm) = 3.61 (s, 2H), 7.25 -7.35 (m, 5H). ^{13}C NMR ($CDCl_3$, 150 MHz): δ (ppm) = 43.5, 127.7, 128.7, 129.2, 137.6. ESI-MS: *m*/*z* calcd for $C_{14}H_{15}S_2$ $[M+H]^+$: 247.06; observed: 247.06.

Compound **2.2**:[25] 4-Fluorobenzyl bromide (2.28 g, 12.06 mmol) was used to yield the disulfide **2.2** as white amorphous solid. Reaction time: 4 h, Yield: 90% (4.03 g); M.P: 99 - 100 ºC; R_f = 0.5 (100 % hexane). ^{1}H NMR ($CDCl_3$, 600 MHz): δ (ppm) = 3.58 (s, 2H), 7.02 (t, *J* = 8.6 Hz, 2H), 7.21 - 7.20 (m, 2H). ^{13}C NMR ($CDCl_3$, 150 MHz): δ (ppm) = 41.9, 130.4, 130.5, 132.6, 132.7, 160.9, 162.6. ESI-MS: *m*/*z*: calcd for $C_{14}H_{15}S_2F_2$ $[M+H]^+$: 283.06; found: 283.04.

Compound **2.3**:[26] 4-Cyanobenzyl bromide (4.00 g, 20.00 mmol) was used to yield the disulfide **2.3** as light pink amorphous solid. Reaction time: 5 h, Yield: 59% (3.56 g); M.P: 144 - 145 ºC; R_f = 0.5 (100% benzene). ^{1}H NMR ($CDCl_3$, 600 MHz): δ (ppm) = 3.73 (s, 4H), 7.21 (d, *J* = 8.0 Hz, 2H), 7.53 (d, *J* = 8.0 Hz, 2H). ^{13}C NMR ($CDCl_3$, 150 MHz): δ (ppm) = 42.6, 111.2, 118.6, 129.7, 132.4, 143.1. ESI-MS: *m*/*z*: calcd for $C_{16}H_{13}N_2S_2$ $[M+H]^+$: 297.05; found: 297.05.

Compound **2.4**:[26] 4-Nitrobenzyl bromide (4.32 g, 20.00 mmol) was used to yield the disulfide **2.4** as light grey amorphous solid. Reaction time: 3 h, Yield: 35% (2.35 g); M.P: 124-125 ºC; R_f = 0.6 (10% ethyl acetate in hexane). ^{1}H NMR ($CDCl_3$, 600 MHz): δ (ppm) = 3.69 (s, 2H), 7.39 (d, *J* = 8.6 Hz, 2H), 8.20 (d, *J* = 8.6 Hz, 2H). ^{13}C NMR ($CDCl_3$, 150 MHz): δ (ppm) = 42.4, 124.0, 130.3, 144.9, 147.5. ESI-MS: *m*/*z*: calcd for $C_{14}H_{15}N_2O_4S_2$ $[M+H]^+$: 337.02; found: 337.03.

Compound **2.5**:[26] 4-Methoxybenzyl chloride (0.57 g, 3.67 mmol) was used to yield the disulfide **2.5** as white amorphous solid. Reaction time: 2 h, Yield: 27% (0.31 g); M.P: 122 - 123 ºC; R_f = 0.6 (5% ethyl acetate in hexane). ^{1}H NMR ($CDCl_3$, 600 MHz): δ (ppm) = 3.58 (s, 2H), 3.80 (s, 3H), 6.86 (d, *J* = 8.6 Hz, 2H), 7.17 (d, *J* = 8.6 Hz, 2H). ^{13}C NMR ($CDCl_3$, 150 MHz): δ (ppm) = 42.3, 54.8, 113.4, 128.9, 130.1, 158.5. ESI-MS: *m*/*z*: calcd for $C_{16}H_{19}O_2S_2$ $[M+H]^+$: 307.08; found: 307.08.

2.5.3. General synthesis of diselenides 2.6-2.10

The diselenides in the present study were synthesized following the literature method with minor modifications.[15-16] To a stirring suspension of selenium powder (1.4 equiv) in ethanol (150.0 ml) at 0 °C, sodium borohydride (1.0 equiv) was added all at once and stirring was continued for 15 min under argon atmosphere. The reaction mixture was refluxed for 1.5 h during which the selenium powder was dissolved with an appearance of wine red colored solution. To the prepared ethanolic solution of disodium diselenide, was added the corresponding substituted benzyl halide derivatives (0.9 equiv) and the solution was refluxed for 4 h. The progress of reaction was monitored by TLC analysis until the benzylic halide was consumed. The reaction mixture was diluted and extracted with ethyl acetate and washed with brine (200.0 mL) solution and dried over anhydrous sodium sulfate. The mixture was purified by neutral alumina column chromatography using hexane and ethyl acetate as eluents. During the column chromatography 2% triethylamine was added to the eluting solvent to retain the stability of some the diselenides during the chromatographic separation.

Compound **2.6**:[27] Benzyl bromide (0.5 g, 2.92 mmol) was used to yield the diselenide **2.6** as light brown amorphous solid. Reaction time: 2 h, Yield: 46% (0.45 g); M.P: 258-260 ºC, R_f = 0.5 (100% hexane). ^{1}H NMR ($CDCl_3$, 600 MHz): δ (ppm) = 3.83 (s, 2H) 7.22 - 7.31 (m, 5H); ^{13}C NMR ($CDCl_3$, 150 MHz): δ (ppm) = 32.8, 127.3, 128.7, 129.2, 139.2. ^{77}Se NMR ($CDCl_3$, 114 MHz): δ (ppm) = 401. ESI- MS: *m/z*: calcd for $C_{14}H_{15}Se_2$ $[M+H]^+$: 341.95, found. 341.21.

Compound **2.7**:[28] 4-Fluorobenzyl bromide (0.76 g, 4.02 mmol) was used to yield the diselenide **2.7** as light yellow amorphous solid. Reaction time: 3 h, Yield: 60% (0.9 g); M.P: 255-256 ºC; R_f = 0.5 (100% hexane). ^{1}H NMR ($CDCl_3$, 600 MHz): δ (ppm) = 3.81 (s, 2H), 6.99 (t, *J* = 8.6 Hz, 2H), δ 7.17 (dd, *J* = 8.4, 5.5 Hz, 2H). ^{13}C NMR ($CDCl_3$, 150 MHz): δ (ppm) = 31.8, 115.6, 130.7, 135.0, 161.4, 163.0.^{77}Se NMR ($CDCl_3$, 114 MHz): δ = 404.

Compound **2.8**:[28] 4-Cyanobenzyl bromide (0.60 g, 3.06 mmol) was used to yield the diselenide **2.8** as light orange amorphous solid. Reaction time: 4 h, Yield: 72% (0.85 g); M.P: 262-263 ºC; R_f = 0.8 (100% benzene). ^{1}H NMR ($CDCl_3$, 600 MHz): δ (ppm) = 4.30 (s, 2H), 7.17 (d, *J* = 8.0 Hz, 2H), 7.50 (d, *J* = 8.0 Hz, 2H), ^{13}C NMR ($CDCl_3$, 150

MHz): δ (ppm) = 31.7, 111.1, 118.9, 129.8, 132.5, 144.6. ^{77}Se NMR ($CDCl_3$, 114 MHz): δ (ppm) = 425. ESI- MS: *m*/*z*: calcd for $C_{16}H_{16}N_3Se_2$ $[M+NH_4]^+$:409.96, found: 409.97.

Compound **2.9**:[29] 4-Nitrobenzyl bromide (0.50 g, 2.31 mmol) was used to yield the. diselenide **2.9** as brownish red amorphous solid. Reaction time: 3 h, Yield: 23% (0.22 g); M.P: 256 - 257 ºC; R_f = 0.5 (10% ethyl acetate in hexane). ^{1}H NMR ($CDCl_3$, 600 MHz): δ (ppm) = 3.92 (s, 2H), 7.35 (d, *J* = 8.4 Hz, 2H), 8.18 - 8.19 (d, *J* = 8.4 Hz, 2H). ^{13}C NMR ($CDCl_3$, 150 MHz): δ (ppm) = 31.4, 123.9, 129.8, 146.7. ^{77}Se NMR ($CDCl_3$, 114 MHz): δ (ppm) = 428. ESI- MS: *m*/*z*: calcd for $C_{14}H_{12}N_2O_4Se_2Na$ $[M+Na]^+$: 454.90, found: 454.90.

Compound **2.10**:[28] 4-Methoxybenzyl chloride (0.57 g, 3.67 mmol) was used to yield the diselenide **2.10** as pale orange crystalline solid. Reaction time: 2 h, Yield: 12% (0.17 g); M.P: 265-266 ºC; R_f = 0.6 (1% ethyl acetate in hexane). ^{1}H NMR ($CDCl_3$, 600 MHz): δ (ppm) = 3.83 (s, 2H) 3.79 (s, 3H), 6.84 (d, *J* = 8.4 Hz, 2H), 7.16 (d, *J* = 8.4 Hz, 2H). ^{13}C NMR ($CDCl_3$, 150 MHz): δ (ppm) = 32.4, 55.5, 114.1, 130.3, 131.3, 158.9. ^{77}Se NMR ($CDCl_3$, 114 MHz): δ (ppm) = 397. ESI- MS: *m*/*z*: calcd for $C_{16}H_{22}NO_2Se_2$ $[M+NH_4]^+$: 419.99, found. 420.00.

2.5.4. GSH–GSSG coupled assay[30]

The GP_x-like antioxidant activity of the synthetic organoselenium and organodisulfide compounds was screened spectrophotometrically. The test mixture contained GSH (2.0 mM), EDTA (1.0 mM), glutathione disulfide reductase (1.7 units/mL) and NADPH (0.4 mM) in 0.1 M potassium phosphate buffer at pH 7.4. Disulfide/diselenide compounds (50 mM) was added to the test mixture at room temperature, and the reaction was started by the addition of H_2O_2 (1.6 mM). The initial reduction rate was calculated from the rate of NADPH oxidation at 340 nm. Each initial rate was measured at least 3 times and calculated from the first 5–10% of the reaction by using 6.22 $mM^{-1}cm^{-1}$ as the molar extinction coefficient for NADPH.

2.5.5. Crystallography

Single crystal X-ray diffraction data was collected on a Bruker AXS SMART APEX CCD diffractometer at room temperature (293 K). The X-ray generator was operated at 50 KV and 35 mA using Mo-Kα radiation (λ = 0.71073 Å). The data was collected using

SMART software package. The data were reduced by SAINTPLUS, an empirical absorption correction was applied using the package SADABS and XPREP were used to determine the space group. The crystal structure was solved by direct methods using SIR92 and refined by full-matrix least-squares method using SHELXL97.[31] All non-hydrogen atoms were refined anisotropically and hydrogen atoms were assigned at idealized locations. **CCDC- 1535430** (compound **2.3**) and **CCDC- 1535431** (compound **2.8**) contain the supplementary crystallographic data for this paper. These data can be obtained free of charge from The Cambridge Crystallographic Data Centre *via* www.ccdc.cam.ac.uk/data_request/cif.

2.5.6. Cell lines and culture

Human breast carcinoma cell line MCF-7 was obtained from the National Centre for Cell Science (NCCS), India and normal kidney epithelium cell (NKE) was obtained from the laboratory of Dr. Mahadeb Pal, Bose Institute, Kolkata, India. MCF-7 cells were cultured in DMEM medium and NKE cells were cultured in RPMI medium supplemented with 10% (v/v) fetal bovine serum (FBS), 1 % Pen-strep and Amphotericin B. Cells were cultured as a monolayer in a humidified incubator at 37 °C in the presence of 5% CO_2 concentration.

2.5.7. Cell viability assay[32]

Cell viability was investigated by MTT assay. Initially, 3×10^3 cells were seeded in each well of a 96-well plate and incubated for 24 h in a humidified incubator at 37 °C and in the presence of 5% CO_2. Cells were treated with or without different compounds or the vehicle for 24 h. MTT was added to the wells and the resulting purple formazan that was formed was dissolved using DMSO followed by quantification using spectrophotometer at a wavelength of 570 nm.

2.5.8. Cellular morphology study by a nuclear staining dye DAPI

MDA-MB-231 cells (2×10^4 cells/ 2.0 mL) were plated in 35 mm dishes and maintained in a CO_2-regulated humidified (95% air/5% CO_2 atmosphere) incubator at 37 °C. The next day, cells were treated with text compounds **2.8** (0.5 and 1.0 µM), and DMSO as vehicle control. The cells were imaged (Bright field) under fluorescent cell imager after 48 h of time intervals. The nuclear aberration was analyzed upon staining the compound (5.0 and 15.0 µM) treated cells with DAPI. After the treatment with compound **2.8** for

48 h, cells were washed with ice-cold DPBS for three times and fixed the cells with 4 % formaldehyde (Merck) and incubated for 10 min at room temperature. After the incubation, cells were washed and incubated further for 10 min with DAPI (Sigma Aldrich). Finally, cells were washed with DPBS for three times and imaged under fluorescent imager.

2.5.9. Wound healing (scratch) assay

MCF-7 cells were seeded in a 24-well plate at a concentration of 6×10^5 cells per 0.5 mL per well and incubated in a CO_2 incubator at 37 °C to form a cellular monolayer. The cells were pre-incubated in serum-free medium (DMEM without FBS) for 6 h. Using a 10.0 µL tip, a scratch was made on the monolayer and the debris was removed by washing with DPBS (1X). Cells were treated with the test compound (0.5 and 1.0 µM) and the scratch was observed under microscopy at regular intervals (0, 12, 24 and 48 h).

2.5.10. Measurement of intracellular ROS levels in MCF-7 cells

The level of intracellular ROS in MCF-7 cells was determined by DCFH-DA staining followed by analysis by flow cytometry according to a previously described method.[22] Initially, each well of a 6-well plate was seeded with 3×10^5 cells and incubated for 24 h. Cells were treated with the vehicle as control or with different compounds. After 2 h of treatment, cells were washed with PBS followed by staining with 20.0 µM of DCFH-DA. Cells were then incubated for 30 min at 37 °C in a CO_2 incubator. ROS generation was measured using FACS Verse (Becton Dickinson).

2.5.11. Western blot analysis

MCF-7 cells (5×10^5 cells per 5.0 mL) were treated with test compounds and incubated for respected time points. After treatment, cells were washed with cold DPBS for three times. Finally, the whole-cell protein was extracted using RIPA cell lysis buffer (150.0 mM of NaCl, 1% (v/v) NP-40 (Himedia), 0.5% Sodium deoxycholate (Himedia), 0.1% SDS, 25.0 mM of Tris, 10 mg/ml PMSF (Sigma Aldrich). Equal volumes of protein was loaded and separated on 2% sodium dodecyl sulfate (SDS)-polyacrylamide gel by electrophoresis and transferred to a nitrocellulose membrane (Bio-Rad). Protein transfer was confirmed by Ponceau-S (HiMedia) staining. The blots were blocked with 5% (w/v) non-fat dry milk in 1X TBST buffer for 1 h at room temperature. Finally, the blots were

incubated with the primary antibodies specific for Survivin, Procaspase 3, Bcl2, GAPDH (Cell Signaling, Abcam, Invitrogen) overnight at 4 °C. Following the primary antibody incubation (1:5000), the blots were washed with TBST (1X) buffer and incubated with IgG-HRP-conjugated secondary antibodies (anti-rabbit) (1:10000) (Abcam/Cell signaling) for 1 h and developed using Clarity™ Western ECL Substrate (Bio-Rad) and imaged using ChemiDoc XRS+ System equipped with Image Lab software (Bio-Rad, California, USA). The housekeeping genes such as GAPDH was used as a loading control.

2.5.12. Statistical analysis

The statistical analysis was performed using KyPlot version 2.0 beta 15 (32 bit). When A1 = IC_{50}, Y = response (Y = 100 % when X = 0), X = inhibitory concentration, then IC_{50} values were calculated by the following formula, $Y = 100 \times A1/(X + A1)$. The IC_{50} values were compared by paired *t*-test. $P < 0.05$ was considered significant.

2.6. References

1. Corzo-Martínez, M.; Corzo, N.; Villamiel, M., *Trends in Food Science & Technology* **2007**, *18*, 609-625.
2. You, W. C.; Blot, W. J.; Chang, Y. S.; Ershow, A. G.; Yang, Z. T.; An, Q.; Henderson, B.; Xu, G. W.; Fraumeni, J. F.; Wang, T. G., *Cancer Research* **1988**, *48*, 3518-3523.
3. Fleischauer, A. T.; Arab, L., *The Journal of Nutrition* **2001**, *131*, 1032S-1040S.
4. Song, K.; Milner, J. A., *The Journal of Nutrition* **2001**, *131*, 1054S-1057S.
5. Singh, A.; Shukla, Y., *Biomedical and Environmental Sciences* **1998**, *11*, 258-263.
6. Rai, S. K.; Sharma, M.; Tiwari, M., *Life Sciences* **2009**, *85*, 211-219.
7. Hosono, T.; Fukao, T.; Ogihara, J.; Ito, Y.; Shiba, H.; Seki, T.; Ariga, T., *Journal of Biological Chemistry* **2005**, *280*, 41487-41493.
8. 9. Lei, X.-y.; Yao, S.-q.; Zu, X.-y.; Huang, Z.-x.; Liu, L.-j.; Zhong, M.; Zhu, B.-y.; Tang, S.-s.; Liao, D.-f., *Acta Pharmacologica Sinica* **2008**, *29*, 1233-1239.
10. Knowles, L. M.; Milner, J. A., *Carcinogenesis* **2000**, *21*, 1129-1134.
11. Hosono, T.; Fukao, T.; Ogihara, J.; Ito, Y.; Shiba, H.; Seki, T.; Ariga, T., *Journal of Biological Chemistry* **2005**, *280*, 41487-41493.

12. Donaldson, M. S., *Nutrition Journal* **2004**, *3*, 19.
13. Xiao, D.; Herman-Antosiewicz, A.; Antosiewicz, J.; Xiao, H.; Brisson, M.; Lazo, J. S.; Singh, S. V., *Oncogene* **2005**, *24*, 6256-6268.
14. Firouzabadi, H.; Iranpoor, N.; Abbasi, M., *Bulletin of the Chemical Society of Japan* **2010**, *83*, 698-702.
15. Oliveira, A. R. M. d.; Piovan, L.; Simonelli, F.; Barison, A.; Santos, M. d. F. C.; de Mello, M. B. M., *Journal of Organometallic Chemistry* **2016**, *806*, 54-59.
16. Panduranga, V.; Prabhu, G.; Basavaprabhu; Panguluri, N. R.; Sureshbabu, V. V., *Synthesis* **2016**, *48*, 1711-1718.
17. Engman, L.; Hallberg, A., *The Journal of Organic Chemistry* **1989**, *54*, 2964-2966.
18. An, H.; Hu, X.; Gu, J.; Chen, L.; Xu, W.; Mo, X.; Xu, W.; Wang, X.; Xu, X., *AAPS PharmSciTech* **2008**, *9*, 551-556.
19. (a) Bhabak, K. P.; Mugesh, G., *Chemistry – A European Journal* **2009**, *15*, 9846-9854; (b) Bhabak, K. P.; Mugesh, G., *Chemistry – An Asian Journal* **2009**, *4*, 974-983; (c) Bhabak, K. P.; Mugesh, G., *Chemistry – A European Journal* **2008**, *14*, 8640-8651.
20. Liou, G.-Y.; Storz, P., *Free Radical Research* **2010**, *44*, 479-496.
21. (a) Sarma, B. K.; Mugesh, G., *Journal of the American Chemical Society* **2005**, *127*, 11477-11485; (b) Bhabak, K. P.; Mugesh, G., *Chemistry – A European Journal* **2007**, *13*, 4594-4601.
22. Panja, S.; Ghate, N. B.; Mandal, N., *Cancer Cell International* **2016**, *16*, 51.
23. (a) Firouzabadi, H.; Abbassi, M.; Karimi, B., *Synthetic Communications* **1999**, *29*, 2527-2531; (b) Witt, D., *Synthesis* **2008**, *2008*, 2491-2509.
24. McKillop, A.; Koyunçu, D.; Krief, A.; Dumont, W.; Renier, P.; Trabelsi, M., *Tetrahedron Letters* **1990**, *31*, 5007-5010.
25. Bao, Y.; Mo, X.; Xu, X.; He, Y.; Xu, X.; An, H., *Journal of Pharmaceutical and Biomedical Analysis* **2008**, *48*, 664-671.
26. Bandgar, B. P.; Uppalla, L. S.; Sadavarte, V. S., *Tetrahedron Letters* **2001**, *42*, 6741-6743.
27. Klayman, D. L.; Griffin, T. S., *Journal of the American Chemical Society* **1973**, *95*, 197-199.

28. Chen, F.; Li, F.; Zeng, Q., *European Journal of Organic Chemistry* **2021**, *2021*, 5605-5608.

29. Price, T. S.; Jones, L. M., *Journal of the Chemical Society, Transactions* **1909**, *95*, 1729-1738.

30. Wilson, S. R.; Zucker, P. A.; Huang, R. R. C.; Spector, A., *Journal of the American Chemical Society* **1989**, *111*, 5936-5939.

31. (a) Sheldrick, G. M., *Acta Crystallographica Section C* **2015**, *71*, 3-8; (b) Altomare, A.; Cascarano, G.; Giacovazzo, C.; Guagliardi, A.; Burla, M. C.; Polidori, G.; Camalli, M., *Journal of Applied Crystallography* **1994**, *27*, 435-435.

32. Bhattacherjee, D.; Sufian, A.; Mahato, S. K.; Begum, S.; Banerjee, K.; De, S.; Srivastava, H. K.; Bhabak, K. P., *Chemical Communications* **2019**, *55*, 13534-13537.

Selective Synthetic Methodologies and Preliminary Anti-proliferative Activities of Symmetrical Organodisulfides and Organotrisulfides

3.1. Introduction

Organopolysulfides are the major classes of organic sulfur compounds (OSCs) and many of them have important pharmaceutical and medicinal implications.[1] While the occurrence of disulfide formation is well-established in many proteins, natural products and bio-molecules, evidences for the presence of trisulfides, tetrasulfides and higher homologues are relatively rare. Some representative examples include the naturally occurring enediyne antibiotics such as esperamicins, epipolythiodiketopiperazine alkaloid such as (+)-Luteoalbusin B, plant-isolated dibenzyl trisulfide (DBTS) and garlic-derived diallyl trisulfides (DATS) (Figure 3.1).[2] Although evidence for the presence of trisulfide (-S-S-S-) linkage in recombinant protein is rare, studies have shown the feasibility of such connectivity in proteins and enzymes.[3] The complex trisulfide-based natural products or simpler garlic-derived organosulfur compounds as shown in Figure 3.1 act as antitumor antibiotics, cytotoxic agents or anti-cancer as well as chemopreventive agents.[4] As described in chapters 1 and 2, garlic-derived organopolysulfides exhibit potent medicinal properties for several disease conditions such as, cancer, Parkinson disease, cardiovascular disease, Alzheimer's disease and many others.[5] A number of aliphatic organotrisulfides such as DATS, allyl methyl trisulfide and dimethyl trisulfide are present in garlic (*Allium sativum*) along with many other organosulfur compounds having potent pharmacological activities.[6,7] Besides the superior anti-cancer activities of the garlic-derived trisulfides including DATS, the trisulfides have been considered recently as precursors of H_2S, a gasotransmitter having implications towards neurotransmission, vasodilation, apoptosis and many other physiological processes.[8] In 2017, Kiesel and co-workers have reported the ability of DATS to suppress the proliferation of various breast cancer cell lines (MCF-7 and MDA-MB-231).[9] Treatment with 40.0 μM DATS significantly reduced the cellular viability by approximately 53% compared to the vehicle control, *via* down-regulation of two important alpha secretases (ADAM10 and ADAM17) in breast cancer cells.[9] Similarly, another report by Liu and co-workers have shown the TrxR inhibitory activity of DATS in triple-negative breast cancer cells.[10] Consistently, the *in vivo* model suggested that DATS-mediated suppression of MMP2/9 and NF-κβ expression was due to the down-regulation and NF-κβ expression was due to the down-regulation of TrxR-1 expression the down-regulation of TrxR-1 expression.

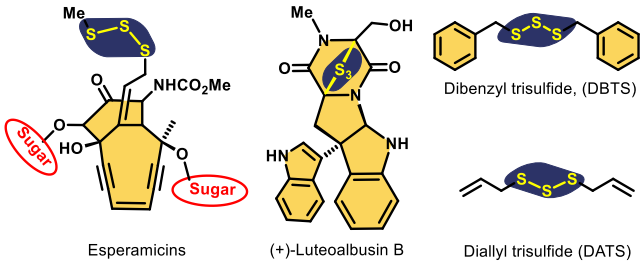

Figure 3.1. Chemical structures of some naturally occurring organotrisulfides.

Considering the potent pharmaceutical implications of the organopolysulfides, it is important to develop a convenient and improved method for the synthesis of Organosulfides (OSCs) in general and organotrisulfides in particular. The reported methods of synthesis of organotrisulfides use either of the organic thiols or the corresponding halides as the precursors with suitable electrophilic or nucleophilic sulfur-transfer agents (Scheme 3.1).[11] Several aliphatic and aromatic tri- and tetrasulfides have been synthesized using thiol as precursors in the presence of electrophilic sulfur-transfer reagents such as sulfur dichloride (SCl_2) and sulfur monochloride (S_2Cl_2).[12] For example, in 2003, Harpp and co-workers developed a method for synthesizing symmetrical aromatic trisulfides and tetrasulfides in higher yields and purity.[8a] The method included pyridine as a base which improved the overall reaction yield and purity by the formation of the insoluble pyridinium salt. Upon addition of the yellow chlorosulfane to the thiol/pyridine solution, immediate conversion to a white precipitate was reported. It was anticipated that formation of pyridinium salt byproduct drives the reaction to completion. However, it is important to explore alternative approaches to greener perspectives in research today owing to the foul smell of thiol and the use of hazardous chemicals, such as SCl_2 and S_2Cl_2. Additionally, the synthetic exploration of hydropolysulfides showed many interesting routes toward the synthesis of penta- and heptasulfides.[13] In 2019, Pluth and co-workers reported another thiol route for the synthesis of symmetrical benzyl trisulfides using thiol as a precursor. Reaction with methoxycarbonylsulfenyl chloride with benzyl mercaptan readily afforded the desired precursor benzyl sulfenylthiocarbonate compound. Further, treatment with potassium *tert*-butoxide (KO^tBu) in methanol provided an inseparable mixture of benzyl disulfide and benzyl trisulfides (Scheme 3.1).[14] However, such methods are mostly abandoned or obsolete owing to no more commercial availability of above-mentioned electrophilic sulfur-transfer reagents as well as due to the unpleasant smell of majority of organic thiols. Therefore, alternate methods for trisulfides utilizing nucleophilic sulfur-transfer

agents and electrophilic precursors became important. The use of nucleophilic sulfur-transfer reagent was first reported in 1946 by Fuson *et al.* for the preparation of bis(2-hydroxyethyl)trisulfide from ethylene chlorohydrin in the presence of disodium trisulfide (Na_2S_3).[15] Subsequently, the use of nucleophilic sulfur-transfer reagents for the preparation of disulfides and trisulfides was further explored by Milligan and co-workers during 1960s. They showed that trisulfides could be prepared by the reaction of sodium S-alkyl thiolsulfates (R-S-SO_3Na) and sodium sulfide (Na_2S). However, the method had limited substrate scope and the trisulfides were accompanied by a significant amount of disulfides and tetrasulfides as mixtures.[16] After almost four decades, in 2001, Roy and co-workers have reported a different method for symmetrical organotrisulfides starting from the corresponding halides in the presence of elemental sulfur and inorganic salts such as tin(II) chloride and copper(II) chloride.[17] However, the method was not selective towards trisulfides as a mixed product with significant amount of tetrasulfide analogues were observed. In 2013, Wirth and co-workers have reported the synthesis of symmetrical disulfides and trisulfides utilizing flow-chemistry using variable ratio of sulfur powder to sodium sulfide in the presence of phase-transfer catalysts.[15] Although the reaction time was very short, the method was not selective to trisulfides as the reaction led to the formation of a mixture of disulfide to pentasulfide compounds. To the best of our knowledge, all the reported methods for symmetrical trisulfides suffer from selectivity issue and the substrate scope has not been explored well as there is no generalized method available for an exclusive preparation of symmetrical trisulfides. Similar to organotrisulfides, symmetrical organodisulfides are conventionally prepared either from the corresponding thiols or halides. While the oxidation of aromatic and aliphatic thiols generally produces disulfides selectively, aliphatic or benzylic halides can be effectively converted to disulfides in the presence of sulfur transfer agents such as thiourea and carbon disulfide. Very recently, Soleiman-Beigi and co-workers have described a greener methodology mainly for dialkyl disulfides using a heterocyclic polar sulfur transfer reagent (PMOxT).[18] Formation of few trisulfides were reported when a secondary and tertiary alkyl group was used instead of primary alkyl groups. Considering the enormous pharmacological importance of organosulfides in general and the garlic-based organosulfides of particular, it is important to develop a greener and convenient method for the selective synthesis of OSCs.

3.2. Outline of the chapter

In this chapter, we describe a straightforward and convenient method for the selective synthesis of garlic-derived allyl sulfides and related derivatives utilizing a wide variety of alkyl, alkenyl, and benzyl halides as precursors under greener and catalyst-free and additive-free conditions. Selectivity among symmetrical trisulfides and disulfides with wider substrate scopes could be enhanced using sodium sulfide as a key sulfur-transfer agent with a slight variation of reaction parameters. Our study further reveals that, while the selective formation of trisulfides was feasible at a lower temperature (0 °C), the corresponding disulfides were the sole products at a relatively higher temperature (50 °C) (Scheme 3.2). The detailed mechanistic studies involving experimental and computational methods indicate that the by-product sodium sulfite (Na_2SO_3) plays a crucial role in trisulfide and disulfide co-formation. Furthermore, computational studies revealed a relatively lower energy barrier for the synthesis of trisulfides over the disulfides. Following synthesis, all the synthesized organotrisulfides were evaluated for their preliminary anti-proliferative activities on ER+ breast cancer (MCF-7) cells. The study of identified few organotrisulfides that showed excellent anti-cancer activities (less than 10.0 µM) in MCF-7 cell lines. Additionally, bis(4-methylbenzyl) trisulfide was found to be the most potent anti-proliferative compound that exhibited a sustained H_2S release profile.

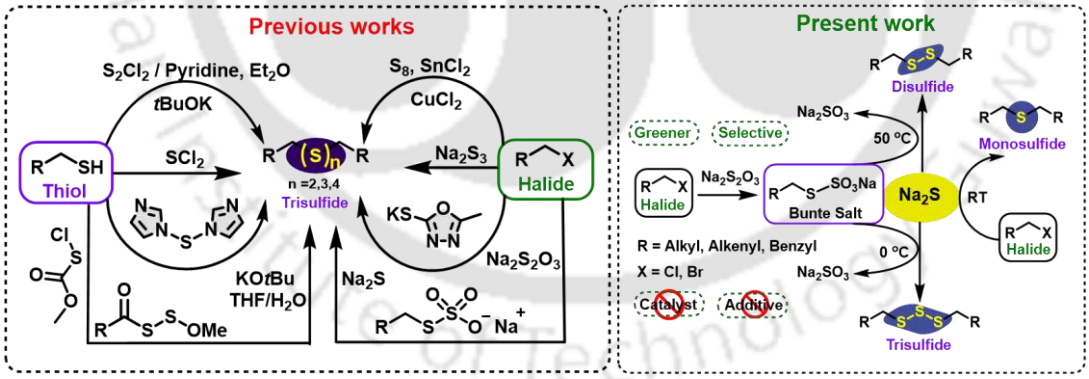

Scheme 3.1. Some of the previously reported synthetic schemes to symmetrical organopolysulfides (*previous work*) and the optimized synthetic schemes to trisulfides, disulfides and monosulfides (*present work*).

3.3. Results and discussion

3.3.1. Optimization of trisulfide synthesis

The selective synthesis of the unsubstituted benzyl trisulfide DBTS was attempted first. The synthesis of DBTS needs an initial reaction of benzyl bromide with $Na_2S_2O_3.5H_2O$

producing the corresponding Bunte salt and a subsequent reaction with $Na_2S.9H_2O$ (Scheme 3.2). As the preparation of Bunte salt is well-established, second step was optimized mainly for the selective synthesis of DBTS (Table 3.1).

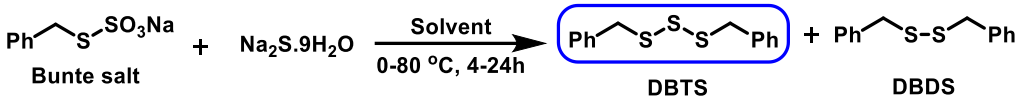

Scheme 3.2. Optimization of the synthesis of the trisulfide DBTS.

Attempts with other sulfur-transfer agents (thiourea, NaHS and ZnS) were unsuccessful as they afforded mostly corresponding disulfide DBDS. Use of 0.5 equiv Na_2S with respect to Bunte salt produced DBTS predominantly (59%) but with some DBDS (7%). With decreased Na_2S equivalence, overall yield was reduced and an increased equivalence rather produced higher disulfide content (Table 3.1). As the second step is more crucial for a selective formation of trisulfide, all possible factors were considered to achieve an optimized reaction condition. A freshly prepared and column purified S-benzyl thiosulfate was used as precursor in all the optimization reactions and results are summarized in Table 3.1. It is evident from the reaction scheme in Scheme 3.2 that an exclusive formation of DBTS theoretically demands the reaction of one molecule of Na_2S with two molecules of Bunte salt. Therefore, to understand the effect of Na_2S towards the formation of trisulfides, we varied the relative molar equivalence of Na_2S with reference to Bunte salt from 0.5 equiv to 3.0 equiv (entry 1-4, Table 3.1). The reactions were carried out in water at room temperature for 24 h. As shown in Table 3.1, an exclusive formation of the trisulfide DBTS with a trace amount of the corresponding disulfide DBDS was observed with 0.1-0.5 equiv of Na_2S. A further increase of Na_2S equivalence led to an increase in disulfide formation (entry 3-4) (Table 3.1). As the crude yield of trisulfide was highest with 0.5 equiv of Na_2S that is in accordance to stoichiometric requirement for trisulfide formation (entry 1), we have considered 0.5 equiv of Na_2S for further optimization process. To investigate the effect of solvent on the ease of trisulfide formation, the reaction was performed in different polar and water miscible solvents (entry 5-9) as shown in Table 3.1. Surprisingly, an exclusive formation of DBDS with a trace amount of DBTS was detected in almost all the organic solvents used in the present study. While the reaction in methanol led to the formation of disulfide (63%) with minor amount of trisulfide (9%) (entry 5), similar in ethanol (entry 6) led to the formation of slightly higher amount of trisulfide (21%) formation with (60%) of disulfide component. However, reaction in 1,4-dioxane (entry 7) afforded a

completely selective formation of disulfide under identical reaction condition. Formation of a trace amount of higher polysulfide (dibenzyl tetrasulfide) along with trisulfide and disulfide was observed when the reaction was carried out in ACN and DMSO. A similar formation of tetrasulfide and disulfide as minor impurity was reported in the recent report for the synthesis of DBTS utilizing benzyl mercaptan as precursor and methoxycarbonylsulfenyl chloride as sulfur-transfer agent.[14] Based on these observations, water was chosen as the best solvent for a selective formation of trisulfide with significantly good yield.

Table 3.1. Different optimization condition for the synthesis of trisulfide DBTS.

Entry	Na_2S	Solvent	Temp (°C)	Time (h)	Yield of DBTS (%)[a]	Yield of DBDS (%)[a]
1	0.5	H_2O	RT	24	59	7
2	0.1	H_2O	RT	24	19	1
3	1.0	H_2O	RT	24	27	6
4	3.0	H_2O	RT	24	37	21
5	0.5	MeOH	RT	24	9	63
6	0.5	EtOH	RT	24	21	60
7	0.5	Dioxane	RT	24	0	73
8	0.5	ACN	RT	24	30	40
9	0.5	DMSO	RT	24	8	65
10	0.5	H_2O	RT	4	61	5
11	0.5	H_2O	RT	8	70	6
12	0.5	H_2O	RT	12	66	6
13	0.5	H_2O	RT	16	70	6
14	**0.5**	**H_2O**	**0**	**8**	**77**	**1**
15	0.5	H_2O	0	12	68	2
16	0.5	H_2O	80	4	41	27

[a]Yields are calculated from the peak intensities of -S-CH_2- group in ^{1}H NMR spectra of the product mixture.

After optimizing the solvent system, we further optimized the time of the reaction by varying the reaction time from 4 h to 16 h at room temperature. Formation of trisulfide DBTS (61%) was significant within 4 h and was improved further (70%) over 8-16 h (Table 3.1). However, to minimize the DBDS content further, the reaction temperature was tuned. Interestingly, reaction at 0 °C produced DBTS exclusively (77%) with a trace of DBDS (1%) within 8 h (entry 14). Formation of DBDS was enhanced either with

longer reaction time at 0 °C (2%) or by increasing the temperature (27%) within 4 h (entry 15-16). Therefore, the reaction at lower temperature (0 °C) was considered optimized to synthesize DBTS selectively (entry 14). As the normal phase column chromatography co-elutes DBTS and DBDS, the relative yields of DBTS and DBDS in the mixture was calculated from the relative peak intensity of -SCH_2- groups in ^{1}H NMR spectra.

3.3.2. Substrate scope of trisulfides

The optimized condition was used for synthesizing DATS and various alkyl, alkenyl and substituted benzylic compounds (Figure 3.2). While DATS was synthesized at good yield (50%) with a complete selectivity, the yield was relatively lower for the longer chain alkenyl trisulfide **3.1** (24%) and with trace of disulfide **3.1a** (2%). Interestingly, complete selectivity with good yields was observed for alkyl trisulfides **3.2** (62%) and **3.3** (44%). The scope was extended further to various substituted benzyl trisulfides **3.4**-**3.19** containing various electron donating and withdrawing groups. For example, 4-substituted benzylic trisulfides (**3.4**-**3.10**) were synthesized with significantly good yields. The yield was found to be higher for the 4-methyl substituted trisulfide **3.4** (78%), the yield decreased slightly for 4-isopropyl- and 4-*tert*-butyl-substituted trisulfides **3.5** (59%) and **3.6** (49%), respectively with traces of the corresponding disulfides. In contrast, the yields of trisulfides **3.8**-**3.10** containing electron withdrawing groups on the benzene ring were relatively higher (69-97%) with better selectivity except the 4-Br substituted compound **3.9** (47%). To understand the effect of different substituents at various positions on the benzene ring towards the overall selectivity and yield of trisulfides, a series of benzylic trisulfides (**3.11**-**3.18**) were synthesized using similar optimized condition. Representative 2-nitro- and 2-methyl-substituted benzylic trisulfides **3.11** (54%) and **3.12** (77%) were synthesized with good selectivity and yields. Particularly, trisulfide **3.11** was found to have slight difference in the relative polarity from the corresponding disulfide **3.11a** and therefore **3.11** could be purified by column chromatography. Moreover, its chemical structure was further confirmed by X-ray studies. Similarly, 3-substituted benzylic trisulfides (**3.13**-**3.15**) were synthesized at good yields with enhanced selectivity. Interestingly, a complete selectivity with excellent yields was observed for 3,5-disubstituted and 2,4-disubstituted benzylic trisulfides **3.16**-**3.18** (Figure 3.2). Finally, the scope was expanded further with a naphthalene-based trisulfide **3.19** (96%) with complete selectivity. Therefore, the proposed method was

found to be highly selective towards trisulfide synthesis with a wider substrate scope. The trace amount of co-produced disulfides (≤5%) for few substrates could be separated by reverse-phase column chromatography. Further, the method was validated with a gram-scale synthesis of **3.4** (3.24 g, 82%) with a complete selectivity. The purity of compound **3.4** was evaluated by NMR and analytical HPLC methods.

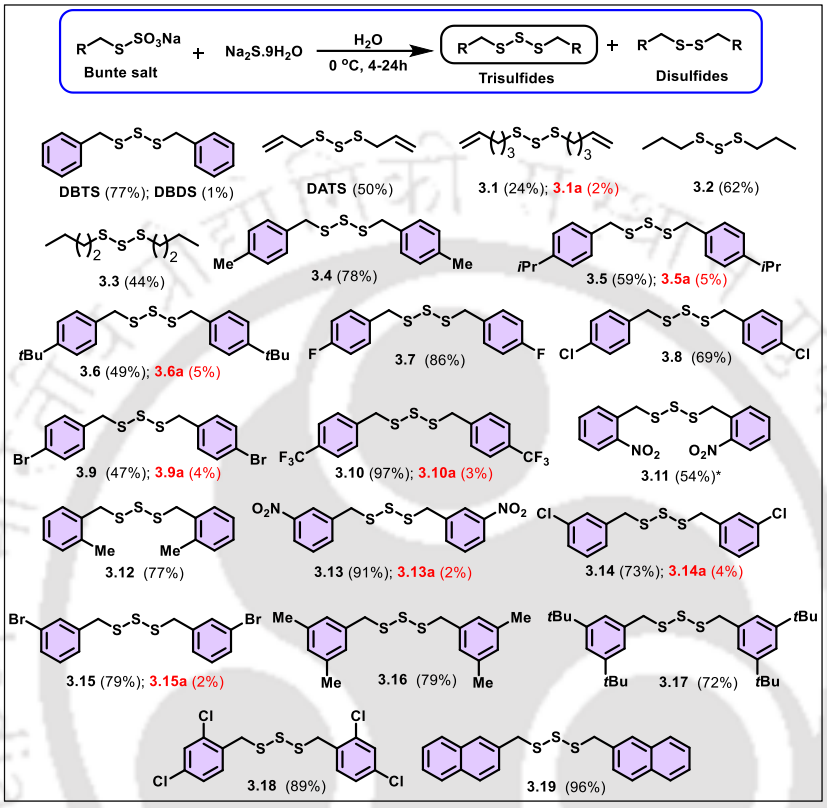

Figure 3.2. Chemical structures of the synthesized symmetrical trisulfides DBTS, DATS and **3.1**-**3.19**. *Yields of the trisulfides and disulfides are calculated from the peak intensities of -S-CH_2- group in ^{1}H NMR spectra of product mixture. *Yield of the trisulfide **3.11** was calculated after purification.

3.3.3. Optimization and substrate scope of disulfides DBDS, DADS and 3.1a-3.19a

In Table 3.1, it has been shown that under certain reaction conditions, particularly with the variation of solvent and temperature, the percentage of dibenzyl disulfide (DBDS) could be enhanced as compared to DBTS. This was the initial clue to optimize the synthetic condition for the selective synthesis of disulfide DBDS with the slight variation of reaction conditions (Scheme 3.3).

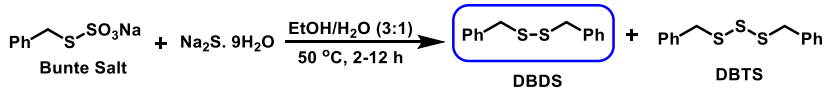

Scheme 3.3. Optimization of reaction conditions for the synthesis of DBDS.

However, considering the greener aspects, we retained the water component and mixed EtOH to initiate optimization (Table 3.2). Firstly, keeping all the parameters intact only temperature was varied to investigate the disulfide formation. Interestingly, a complete selectivity towards DBDS was observed at 50 °C or above within 4 h in EtOH-H_2O (3:1) system. This condition was utilized successfully to synthesize alkenyl, alkyl and substituted benzylic disulfides DBDS, **3.1a**-**3.19a** with good yields and complete selectivity (Table 3.2). The garlic-based disulfide DADS was synthesized exclusively with 65% yield. The structure of disulfide **3.11a** was further confirmed by X-ray study.

Table 3.2. Optimization of the reaction conditions for the selective synthesis of the DBDS. In this study EtOH-H_2O system was taken for the optimization.

Entry	Na_2S	EtOH-H_2O	Temp (°C)	Time (h)	Yield of DBDS (%)[a]	Yield of DBTS (%)[a]
1	0.5	100:0	RT	4	5	61
2	0.5	75:25	RT	4	17	54
3	0.5	50:50	RT	4	31	35
4	0.5	25:75	RT	4	71	5
5	0.5	0:100	RT	4	36	21
6	0.5	25:75	0	4	43	22
7	0.5	25:75	50	4	66	0
8	0.5	25:75	80	4	62	0
9	0.5	25:75	50	2	64	0
10	**0.5**	**25:75**	**50**	**8**	**79**	**0**
11	0.5	25:75	50	12	62	0

[a]Yields are calculated from the peak intensities of -S-CH_2- group in ^{1}H NMR spectra of the product mixture.

Selectivity towards the disulfide was significantly enhanced upon slight increase in the temperature. For example, the reaction exhibited complete disulfide formation (66%) without any co-formation of trisulfide at 50 °C (entry 7). A further increase in reaction temperature (80 °C) did not improve the yield of disulfide. To optimize the condition further, the reaction time was varied from 2 h to 12 h at 50 °C. As shown in Table 3.2, the yield of selective disulfide formation was further enhanced (79%) at 50 °C for 8 h of

reaction time (entry 10). This condition was considered as optimized for a selective preparation of disulfides. While a complete selectivity towards disulfide has been observed for all the benzylated compounds, aliphatic substrates led to the co-formation of trisulfides along with desired disulfides. For example, while the synthesis of the long chain alkenyl disulfide **3.3a** contained around 10% of the corresponding trisulfide **3.3**, DADS showed complete selectivity with good yield (65%). The scope was extended further to various substituted benzyl disulfides **3.4a-3.19a**. For example, 4-substituted benzylic disulfides (**3.4a-3.10a**) were synthesized with significantly good yields. However, *tert*-butyl benzyl substrate showed minor amount of trisulfide component **3.6** (5%). Unlike compound **3.17a**, a complete selectivity with excellent yields was observed for 3,5-disubstituted compound **3.16a** with a good yield (79%). The trisulfide component of **3.17a** was found to be predominant due to the hydrophobic nature of the compound. It has been observed that, a better selectivity towards disulfides could be achieved upon the reaction of the trisulfides with sulfite (SO_3^{2-}) for the substrates that afforded a mixture of disulfides and the corresponding trisulfides under the optimized conditions.

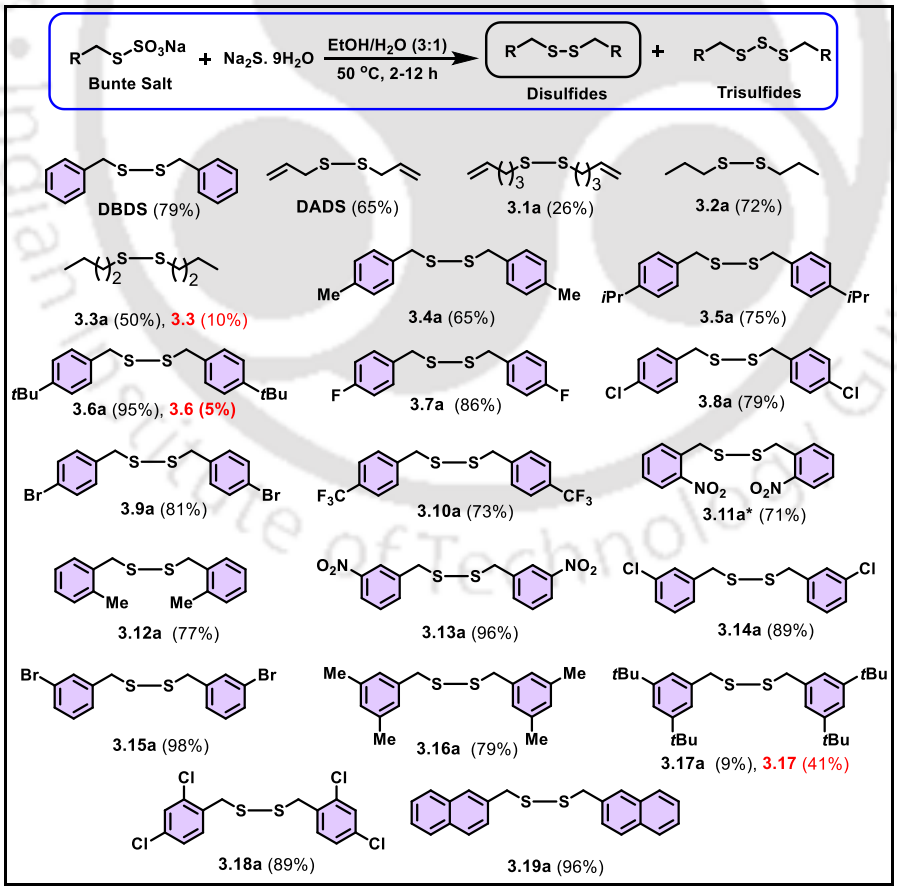

Figure 3.3. Chemical structures of the synthesized symmetrical disulfides DBDS, DADS and **3.1a-3.19a**. Yields are calculated from the peak intensities of -S-CH_2- group in ^{1}H

NMR spectra of product mixture. *Yield of the disulfide **3.11a** was calculated after purification.

3.3.4. Characterization of trisulfide, disulfide and monosulfide

Based on the optimized reaction conditions, a selective synthetic method for trisulfides and disulfides has been developed in the present study. While an exclusive formation of trisulfides was obtained by carrying out the reaction at a lower temperature (0 °C) in water. Similarly, disulfides have been obtained as almost the sole product upon performing the reaction at a relatively higher temperature (50 °C) in a binary solvent comprising of water and ethanol (1:3) using Na_2S as a sulfur-transfer agent. In addition to the trisulfides and disulfides, synthesis of the corresponding symmetrical monosulfides was also attempted by a direct reaction of Na_2S with halides in an ethanolic medium at room temperature. Owing to the very less difference in polarities of most of the alkyl, alkenyl, and benzylic trisulfides, disulfides, and monosulfides, it was practically impossible to monitor their formation from simple thin-layer chromatographic (TLC) analyses. Therefore, ^{1}H NMR spectroscopic experiments were carried out to identify them mainly by monitoring the signal of the -SCH_2- groups. Owing to the presence of 2-nitro group in the disulfide **3.11a**, the corresponding monosulfide **3.11b** was prepared and characterized for a comparative study as shown in Figure 3.4. The chemical shift of the -SCH_2- group in the ^{1}H NMR spectrum of crude trisulfide **3.11** appeared at 4.32 ppm with a co-appearance of a small signal at 4.03 ppm for the -SCH_2- group of the corresponding disulfide **3.11a**. Both of these products were formed when the reaction was carried out at room temperature. The intensity of the peak corresponding to disulfide at 4.03 ppm was significantly minimized when the reaction was carried out at 0 °C in an aqueous medium with an enormous selectivity towards trisulfide **3.11**. In contrast, the complete disappearance of a signal at 4.32 ppm corresponding to trisulfide **3.11** was observed in the reaction at an elevated temperature (50 °C) in a binary solvent. While the chemical shift value of -SCH_2- a group of trisulfide is significantly down-field shifted as compared to the corresponding disulfide, this difference was found to be negligible between the disulfide and the corresponding monosulfide, and even for some substrates, it was almost indistinguishable. For example, the chemical shift value of -SCH_2- group of disulfide **3.11a** at 4.03 ppm was found to be shifted marginally to the up-field to 4.02 ppm for the corresponding monosulfide **3.11b**. In addition to the chemical shift values of -SCH_2- protons, a

difference in the signal pattern of aromatic protons is also observed for disulfide **3.11a** and monosulfide **3.11b** (Figure 3.4).

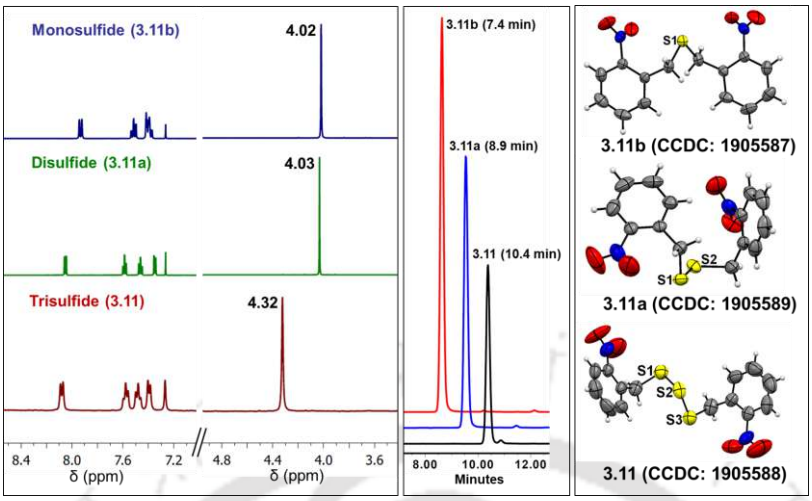

Figure 3.4. ^{1}H NMR spectra (A), reverse-phase HPLC chromatogram (B) and ORTEP diagrams (C) of compounds **3.11**, **3.11a** and **3.11b**. The compounds used here for NMR and HPLC studies was purified by column chromatographic method.

All these representative OSCs (**3.11**, **3.11a** and **3.11b**) having 2-nitro substitution were further analyzed by reverse-phase analytical HPLC method to understand their relative retention time. As shown in Figure 3.4B, the retention time was increased gradually on going from monosulfide **3.11b** (7.4 min) to disulfide **3.30** (8.9 min) to trisulfide **3.11** (10.4 min), which is expected as per their relative polarity is concerned. Furthermore, these representative compounds were characterized by single crystal X-ray analyses. The ORTEP diagrams of trisulfide **3.11** (**CCDC: 1905588**), disulfide **3.11a** (**CCDC: 1905589**) and monosulfide **3.11b** (**CCDC: 1905587**) clearly confirmed their geometries and sulfur content (Figure 3.4C).

3.3.5. Mechanistic investigation

Based on the observation on the exclusive formation of trisulfides at low temperature (0 °C) and disulfides at a relatively higher temperature (50 °C), we have proposed the following mechanistic pathways as outlined in Scheme 3.4. The alkyl, alkenyl or benzyl halides react with the commercially available $Na_2S_2O_3.5H_2O$ in aqueous ethanolic solution leading to an exclusive formation of the corresponding Bunte Salts (Step 1). The produced Bunte salts further react with $Na_2S.9H_2O$ in an aqueous solution leading to the formation of symmetrical trisulfides at lower temperature (0 °C) with a co-formation

of Na_2SO_3 *via* an intermediary of sodium perthiolates (Steps 2 and 3). However, an exclusive formation of symmetrical disulfides was observed when the reaction was carried out at an elevated temperature (≥ 50 °C) in an aqueous ethanolic solvent. The formation of disulfides under this condition was proposed *via* two different possible pathways. At an elevated temperature, the sodium perthiolates may react with both of Bunte salts and sodium sulfite in a competitive manner. Firstly, the reaction of sodium perthiolate with the by-product Na_2SO_3 would produce the thiolate intermediate (step 4), which could react subsequently with the remaining Bunte salt leading to the formation of the corresponding disulfide (step 5). Secondly, the reaction of perthiolate with the Bunte salt would produce trisulfide (step 3), which could react further with the co-produced Na_2SO_3 at a higher temperature to generate the thiolate and the S-thiosulfonate intermediates (step 6). The subsequent reaction of thiolate with S-thiosulfonate would produce the disulfide as final product (step 7) (Scheme 3.4).

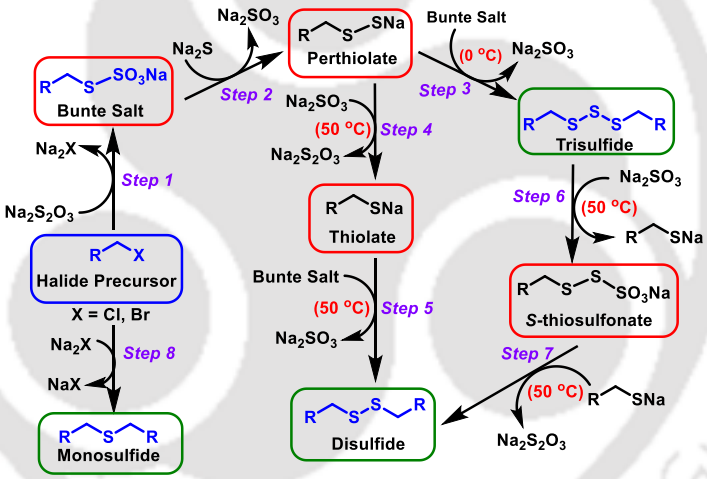

Scheme 3.4. Proposed mechanistic pathways to symmetrical trisulfides, disulfides and the corresponding monosulfides. While step 3 is predominant at lower temperature leading to the formation of trisulfides, steps 4-7 was found to be feasible at higher temperature to afford disulfides as exclusive products. Step 8 was feasible at room temperature for the selective formation of the monosulfides.

Several control experiments have been performed to propose the above mechanism. To track and isolate the right intermediate in the above processes, we have synthesized and purified two Bunte salts (**3.20** and **3.21**) corresponding to 4-methylbenzyl bromide and 4-isopropylbenzyl bromide, respectively and reacted with sodium sulfide under the condition of trisulfide and disulfide formation. When the mixture (1:1) of these two Bunte salts was treated with an equivalent amount of Na_2S under an optimized reaction

condition at 0 °C, three products were obtained as evidenced by ^{1}H NMR, HPLC and ESI-MS analyses. The products were assigned to the two symmetrical trisulfides **3.4** and **3.5** along with a mixed trisulfide **3.22** (Figure 3.5 and Scheme 3.5).

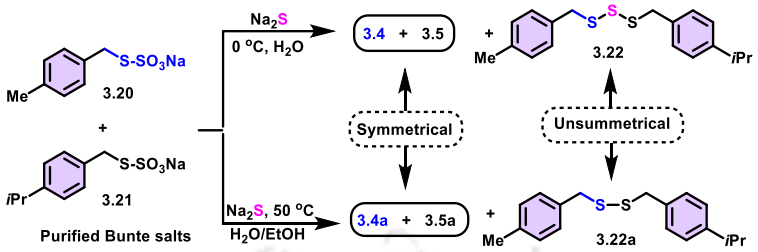

Scheme 3.5. Schematic representation for the synthesis of mixed trisulfide **3.22** and disulfide **3.22a** during the reaction of Na_2S with two different Bunte salts **3.20** and **3.21**.

The formation of mixed trisulfide **3.22** in the above experiment indicates the involvement of stepwise reaction sequences of Bunte salts in the presence of Na_2S *via* an intermediary of sodium perthiolate as shown in Schemes 3.4 and 3.5. Reaction of Na_2S with both the Bunte salts and the formation of a mixed trisulfide **3.22** is also a symbolic of the trapping of perthiolate intermediate. Interestingly, when a similar reaction was conducted at an elevated temperature (50 °C) in aqueous ethanolic medium, the formation of three disulfides (**3.22a**, **3.4a** and **3.5a**) was observed. All the synthesized products were characterized by ^{1}H NMR, HPLC and ESI-MS methods (Figure 3.5).

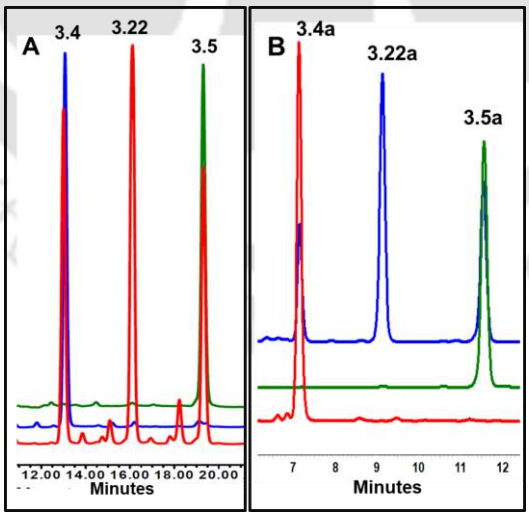

Figure 3.5. (A) HPLC chromatogram of pure symmetrical trisulfides (**3.4** and **3.5**) and the crude trisulfide mixture containing unsymmetrical trisulfide **3.22** and symmetrical trisulfide **3.4**, **3.5**. Compounds were analyzed using (85 to 97%) acetonitrile and (15 to 3%) water system for 10 min. (B) HPLC chromatogram of pure symmetrical disulfides

(**3.4a** and **3.5a**) and trisulfide mixture containing unsymmetrical disulfide **3.22a**. Compounds were analyzed using acetonitrile (92 to 98%) and water (8 to 2%) in a linear gradient mode for 10 min followed by (98:2) ratio of acetonitrile and water in an isocratic mode for another 10 min.

3.3.6. Theoretical investigation

To understand and support our experimental outcomes about the selective formation of trisulfides and disulfides, we performed the density functional theory (DFT) calculations on these reaction sequences. The reaction of a representative precursor halide (benzyl bromide) with $Na_2S_2O_3$ and Na_2S to form trisulfide DBTS and disulfide DBDS was studied using M06/6-31+G(d) level of theory (see computational methodology section for further details). As shown in Scheme 3.4, step 1 was the reaction of precursor halide with $Na_2S_2O_3$ to form the reactant complex **Bn-R1**. The Bunte salt and sodium bromide complex (**Bn-P1**) was formed *via* transition state **Bn-TS1** with an energy barrier of 14.01 kcal mol^{-1}. This step was associated with a cleavage of C-Br bond and a formation of C-S bond by the nucleophilic attack of $Na_2S_2O_3$ to benzyl bromide. In step 2, the produced Bunte salt reacts with sodium sulfide and this reactant complex **Bn-R2** produces the perthiolate intermediate (**Bn-P2**) *via* transition state **Bn-TS2** with an energy barrier of 8.88 kcal mol^{-1}. Co-formation of sodium sulfite (Na_2SO_3) takes place along with the perthiolate intermediate in this step. In step 3, the generated perthiolate reacts with another molecule of Bunte salt leading to the formation of the symmetrical trisulfide **DBTS**. The reactant complex comprising of the perthiolate and Bunte salt (**Bn-R3**) produces the trisulfide and sodium sulfite complex (**Bn-P3**) through the transition state **Bn-TS3** with an energy barrier of 5.04 kcal mol^{-1}. It should be noted here that, the energy barrier in all these steps are moderate to nominal and the products such as **Bn-P1**, **Bn-P2** and **Bn-P3** are significantly more stable than the corresponding reactants **Bn-R1**, **Bn-R2** and **Bn-R3**, indicating clear feasibility of these reactions at ambient temperature (Figure 3.6). Moreover, as the energy barrier in third step (5.04 kcal mol^{-1}) is lower than that in the second step (8.89 kcal mol^{-1}), a spontaneous transformation of the perthiolate intermediate to the trisulfide in the presence of Bunte salt is feasible at 0 °C with a significantly high yield (Step 3).

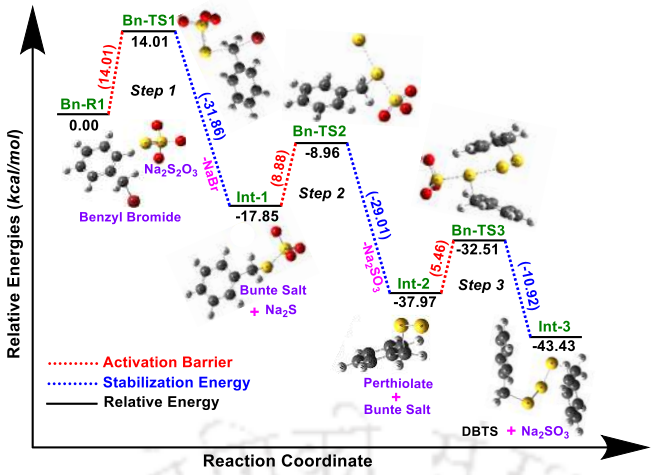

Figure 3.6. Energy profile diagram for the formation of the trisulfide DBTS. Sodium ions are not depicted here for a better clarity in the representation; however, they are present in calculations. All the reported energy values (kcal mol^{-1}) were calculated at the M06/6-31+G (d) level of DFT in water solvent.

To understand the feasibility of the formation of disulfide DBDS from the Bunte salt at a higher temperature (50 °C), the energy profile for these reactions were also studied using same computational method (Figures 3.6 and 3.7). As evident from Scheme 3.4, there are two probable pathways for the formation of disulfides along with trisulfides. According to the first pathway, the perthiolate intermediate once generated, may have two possible options to react further. Either it can react with the Bunte salt to form the corresponding trisulfide as shown above (step 3, Scheme 3.4 and Figure 3.6) or it can react with the co-produced Na_2SO_3 *via* a transition state of **Bn-TS4** leading to the formation of thiolate and thiosulfate complex (**Bn-P4**, step 4, Scheme 3.4 and Figure 3.7). The produced thiolate then reacts with the Bunte salt leading to the formation of the corresponding disulfide DBDS (Step 5, Scheme 3.4 or Figure 3.7). As the energy barrier for step 3 (5.04 kcal mol^{-1}) to produce trisulfide is relatively lower than that of step 4 (7.92 kcal mol^{-1}) and step 5 (8.92 kcal mol^{-1}), trisulfide becomes the major product with the co-formation of a very trace amount of disulfide at a lower temperature (Figures 3.7A and 3.7B). This is indeed in agreement with our experimental finding that trisulfides were almost exclusive products at 0 °C and the amount of disulfides was increased when the reaction was carried out at higher temperature.

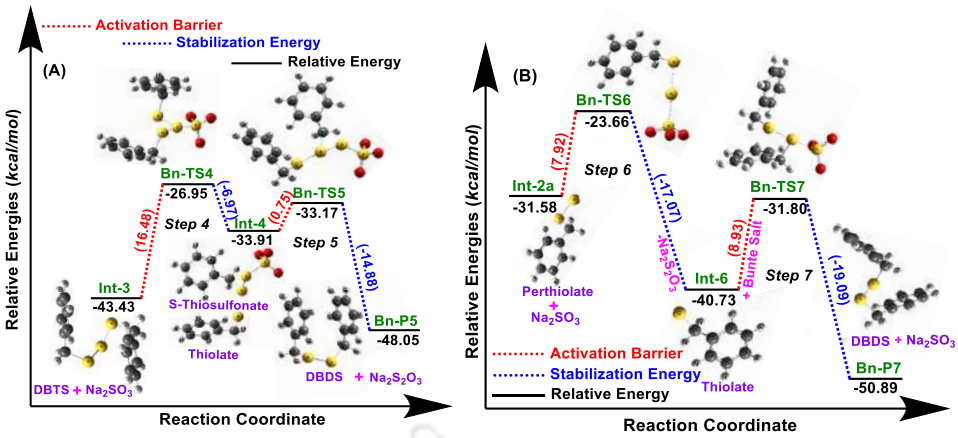

Figure 3.7. Energy profile diagram for the reaction of trisulfide DBTS (A) and perthiolate intermediate (B) with the co-produced Na_2SO_3 to form the disulfide DBDS. Sodium ions are not depicted here for clarity in the representation. All the reported energy values (kcal/mol) were calculated at M06/6-31+G (d) level of DFT in water solvent.

A second possible pathway is the reaction of trisulfide (DBTS) with co-produced Na_2SO_3 (step 6, Scheme 3.4). They react to generate product complex **Bn-P6** *via* the transition state of **Bn-TS6**. The product complex reacts further between themselves leading to the formation of disulfide (DBDS) along with sodium thiosulfate (**Bn-P7**) *via* the transition state of **Bn-TS7**. It should be noted here that the energy barrier in step 6 is relatively higher (15.71 kcal mol^{-1}) and the product **Bn-P6** is less stable than reactants **Bn-P3**, indicating a lesser feasibility of this step at a lower temperature. This is in agreement with our experimental observation that trisulfide is almost unreactive towards Na_2SO_3 at 0 °C. However, the product complex **Bn-P6** reacts immediately to form the highly stable disulfide complex **Bn-P7** with very small energy barrier (0.75 kcal mol^{-1}) and thus making the overall transformation feasible and favourable, especially at an elevated temperature. In general, both of these processes (steps 4-7) probably work simultaneously at an elevated temperature (50 °C) leading to an exclusive formation of the disulfide.

3.3.7. Anti-proliferative activities of trisulfides

The medicinal impacts of consuming garlic and other *Allium* vegetables towards many chronic conditions including diabetes, cardiovascular diseases, inflammation and cancer is well-known from ancient times.[19] Particularly, the anti-cancer effects of garlic is shown to arise mainly due to the presence of lipid-soluble OSCs (allyl sulfides) than the water-soluble compounds.[20] Furthermore, it has also been shown that the number of

sulfur atoms as well as the allyl group in these lipid-soluble compounds are proportional to their anti-cancer potentials.[21] For example, it has been reported that organotrisulfide (DATS) is more potent than the corresponding disulfide (DADS) and monosulfide (DAS) towards prostate and breast cancers.[22] Therefore, the anti-cancer activity of DATS has been studied extensively in different organ specific cancer cells as well as in many animal models. To understand the importance of allyl group in DATS as well as to develop a more potent trisulfide compound, we took the initiative to screen all the synthesized trisulfides (DBTS, DATS and **3.1**-**3.19**) in our study towards a representative breast cancer cell line (MCF-7) for a preliminary structure-activity relationship (SAR) study. The anti-cancer activity profiles of these compounds was first qualitatively evaluated by studying the changes in cellular morphology of MCF-7 cells over a duration of 72 h upon the treatment of these crude trisulfides (DBDS, DADS and **3.1a**-**3.19a**) at concentrations of 10.0 µM and 25.0 µM. The morphology and the killing profile of cells was monitored by capturing the images of treated cells with reference to the untreated controls at an interval of each 24 h. The changes of cellular morphology of MCF-7 cells over 72 h upon the treatment with compound **3.4** is shown in Figure 3.8.

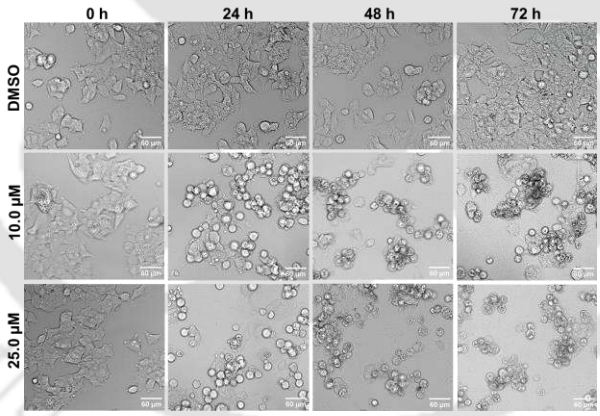

Figure 3.8. Morphological changes of MCF-7 cells upon the treatment of compound **3.4**. Scale bar represents 60 µm.

Finally, cell viability experiment (MTT assay) was carried out for all the sets to understand their relative anti-cancer activities over 72 h. Interestingly, the changes in morphology was found to correlate well with their anti-proliferative activities after 72 h (Figures 3.8 and 3.9).

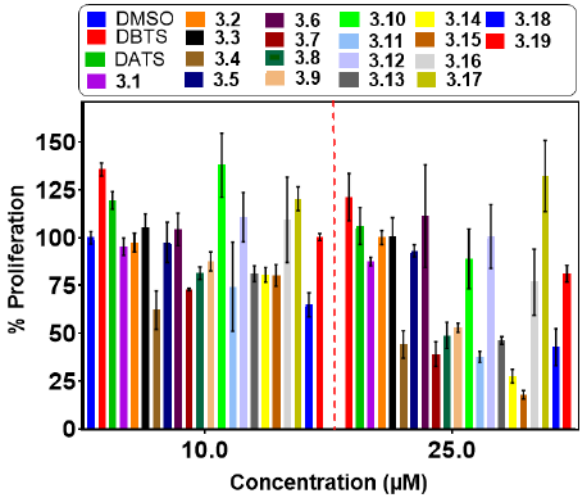

Figure 3.9. Percentage proliferation of MCF-7 cells in the presence of trisulfides (DBTS, DATS and **3.1**-**3.19**) at a concentration of 10.0 and 25.0 μM after an incubation of 72 h at 37 °C. All data are represented by mean ± SD values and differences between the mean values.

After the careful analysis of the cellular morphology of MCF-7 cells upon the treatment of trisulfides. It has been observed that, few trisulfides such as **3.7, 3.8**, **3.9**, **3.11, 3.13-3.15** and **3.18** damaged the cellular morphology significantly at 10.0 μM concentration. The cells become more agglomerated over time up to 72 h. The apoptotic nature of those agglomerated and rounded cells was further evident from the cell viability results after 72 h. The crude trisulfides that exhibited significant anti-proliferative activities in the cell viability assay were chosen further to understand their actual potency. As shown in Figure 3.2 that some of the synthesized trisulfides accompanied a trace amount of disulfides, which were difficult to separate by normal chromatographic method. Therefore, the short-listed potent crude trisulfides were purified further by reverse-phase HPLC method. Upon the final purification of these key compounds, they were evaluated further towards their anti-proliferative activities in MCF-7 cells over 72 h. Some selected compounds were further evaluated and IC_{50} concentrations were determined against MCF-7 cell line. Interestingly, our synthesized organotrisulfides showed significantly improved antiproliferative activity compared to garlic DATS. Finally, organotrisulfides containing different functional groups showed higher potency than unsubstituted DBTS on MCF-7 cells. Remarkably, compound **3.4** a 4-methylbenzyl substituted compound showed maximum potency. However, compound **3.18**, which is a 2,4-dichloro substituted benzyl trisulfide failed to exhibit potent anti-proliferative activity (Table 3.3).

Table 3.3. Determination of IC_{50} values of few selected trisulfides/disulfides in MCF-7 cells after the incubation for 72 h.

Compound	IC_{50} (µM)	Compound	IC_{50} (µM)
3.4	1.07	**3.11a**	1.80
3.7	3.03	**3.13**	4.34
3.8	2.77	**3.14**	3.70
3.9a	5.33	**3.18**	8.31

It should be noted that the anti-proliferative activity of DATS was much lesser up upto a concentration of 25.0 µM under the identical condition as evidenced by the preliminary screening by morphological studies followed by anti-proliferative activity profiles. The relatively moderate to lower potency of DATS towards MCF-7 cells was in agreement with the reports published earlier.[23] Similarly, to understand the anti-proliferative activity of the corresponding disulfides, we have screened several disulfides against MCF-7 cells. Interestingly, compound **3.9a** and **3.11a** were found to be most potent even at 10.0 µM concentration. Therefore, we decided to purify these compounds by HPLC and evaluated their IC_{50} towards MCF-7 cells. Interestingly, 2-nitro substituted compound **3.11a** exhibited much higher potency (IC_{50}: 1.80 µM) than compound **3.9a** (IC_{50}: 5.33 µM) after 72 h of incubation (Figure 3.10, Table 3.3).

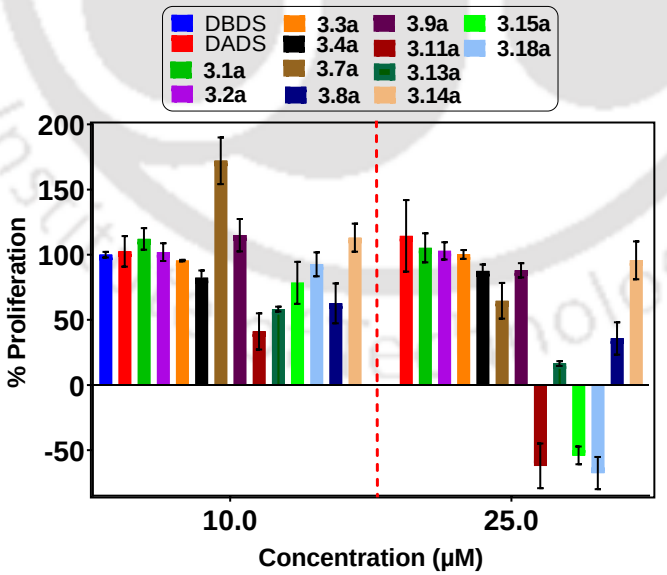

Figure 3.10. Percentage proliferation of MCF-7 cells in the presence of purified disulfides (DBDS, DADS and **3.1a**-**3.18a**) at a concentration of 10.0 and 25.0 µM after an incubation of 72 h at 37 °C.

The preliminary results with very high anti-proliferative activities of few trisulfides/disulfides in this study reveal that the basic skeletons as well as the functional groups present on the trisulfide (-S-S-S-)and disulfide (-S-S-) linkages are significantly important for the observed anti-proliferative activities and this observation further indicate that better chemotherapeutic or chemopreventive compounds can be developed upon the suitable modification of organic moieties and functional groups in garlic-derived organosulfur compounds. However, this warrants further detailed studies towards their mode of actions in cellular as well as in animal models.

3.3.8. Estimation of the H_2S donation capacity of trisulfide 3.4 and DATS

Inspired by the potent anti-proliferative activities of some synthesized trisulfides, a representative trisulfide (**3.4**), was studied further for its H_2S donation efficacy in the presence of GSH using MB assay and compared to the corresponding disulfide **3.4a** and DATS. While the disulfide **3.4a** (50.0 µM) was found to be inactive, a moderate and sustained H_2S release profile was observed for the trisulfide **3.4** (50.0 µM), under the identical condition. However, a much higher, but less sustained H_2S release profile was observed for DATS at 50.0 µM and thus a lower concentration (25.0 µM) was used (Figure 3.11).

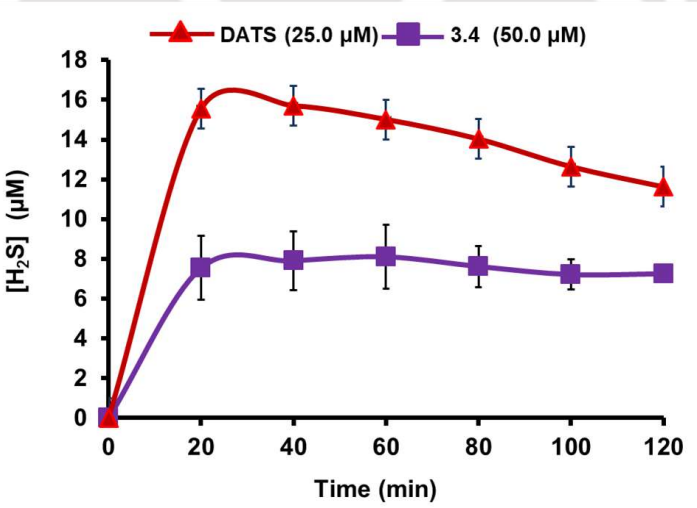

Figure 3.11. The H_2S release profile of compound **3.4** (50.0 µM) and DATS (25.0 µM) in the presence of GSH (500 µM) using MB assay.

The endogenous thiol-mediated H_2S release profile of **3.4** in cellular medium (MCF-7) and its detection was also studied using H_2S-sensitive turn-on fluorogenic probe **NAP-N_3**. Initially, the azide-based fluorogenic probe was incubated to MCF-7 cells and the

fluorescence emission was imaged in Bio-Rad ZOE^{TM} fluorescence imager. Initial fluorescence emission indicated the level of intracellular H_2S. However, a more intense green fluorescence emission from **NAP-NH$_2$** (reduction of **NAP-N$_3$** by H_2S) indicated the release of H_2S from the trisulfide **3.4** by endogenous thiols (Figure 3.12). These observations indicate that, suitably designed organotrisulfides could be good candidates for developing potent anti-cancer agents providing H_2S-mediated cellular protections. However, due to the unavailability of a suitable method for estimating the real-time 'in-cell' H_2S concentration, the proper correlation with anti-proliferative activities and the H_2S donations from synthesized different organotrisulfides could not be determined. Based on the previous literature reports on the detailed mechanistic studies have suggested that the anti-proliferative activity of organotrisulfides could be associated with the contribution of both the released H_2S and the perthiol intermediate formation and followed by the interactions with several target proteins and enzymes.[24]

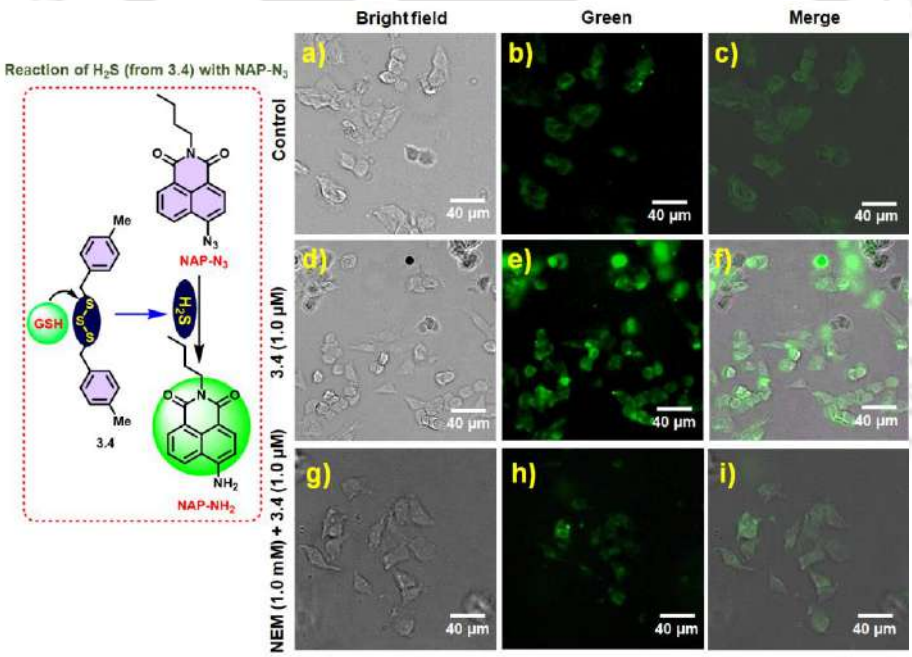

Figure 3.12. Fluorescent microscopic images (bright field, green channel and merged) of MCF-7 cells for the visualization of endogenous H_2S level and upon the exogenous donation from the trisulfide **3.4** (1.0 μM). The H_2S level was estimated using the turn-on fluorogenic probe **NAP-N$_3$** (5.0 μM); (a-c) control, (d-f) trisulfide **3.4** (1.0 μM); (g-i) NEM (1.0 mM) + **3.4** (1.0 μM). Scale bar represents 40 μm.

3.4. Conclusions

In summary, we describe herein a convenient method for the selective synthesis of garlic-derived allyl sulfides and related derivatives utilizing a wide variety of alkyl, alkenyl, and benzyl halides as precursors under a greener and catalyst-free condition. We show for the first time that, the selectivity among symmetrical trisulfides, disulfides, and monosulfides can be achieved by variation of sodium sulfide and the reaction parameters. Our study further reveals that reaction temperature and solvent are two crucial parameters for an effective selectivity toward trisulfides and disulfides. The detailed mechanistic studies by experimental and computational methods have indicated that the co-formation of disulfides along with trisulfides is due to the formation of sodium sulfite as a by-product that was responsible for the mixture. Furthermore, preliminary anti-proliferative activities for the synthesized trisulfides and disulfides in breast cancer cells (MCF-7) identified few potent trisulfides including trisulfide **3.4** with excellent anti-cancer activity (IC_{50} 1.07 μM). Additionally, the trisulfide **3.4** exhibited sustained H_2S release profile unlike the garlic-based trisulfide DATS. Taken together, the greener and selective synthetic strategy of organosulfides along with the excellent anti-proliferative activities of some key trisulfides would certainly be advantageous for elucidating their detailed medicinal and pharmacological implications in near future.

3.5. Experimental Section

3.5.1. Materials and Methods

Thin layer chromatographic (TLC) analyses were carried out on pre-coated silica gel on aluminium sheets. All the solvents used for chromatographic separations were distilled before use. Melting point of the synthesized compounds was recorded in a Büchi B540 melting point apparatus and the values are uncorrected. The NMR spectra were recorded with a Bruker Ascend^{TM} 400 and 600 spectrometers or Varian Mercury plus 400 MHz NMR Spectrometer. Chemical shifts are cited with respect to Me_4Si as internal standard. High resolution mass spectra (HRMS) and GC-MS were obtained using an Agilent 6520 Accurate-Mass Quadrupole Time-of-Flight (Q-TOF) LC/MS spectrometer and PerkinElmer Clarus 680 GC/600C MS, respectively. CHNS analysis was performed by using Thermo Finnigan CHNS (O) Analyzer (Model: FLASH EA 1112 series). Finally, cells were incubated in CO_2 incubator (Eppendorf, Galaxy CO-170S). Purity of the synthesized compounds was analyzed by high-performance liquid chromatography

(HPLC) using Waters 2489 instrument having waters 600 controller and 600 pump or Agilent 1220 infinity II LC system using reverse-phase C-18 column (Luna ®, 5μM, 100 Å, 205×4.6 mm). Cell viability assay was performed using Thermo Scientific Multiskan™ GO Microplate spectrophotometer. Cellular morphology was visualized and imaged under Bio-Rad ZOE™ fluorescent cell imager. The fluorescent sensor of H_2S (**NAP-N_3**) was synthesized following the reported method.[25]

3.5.2. Synthesis of Bunte salts

Bunte salts were prepared following the literature method with minor modifications.[26] To a stirred solution of sodium thiosulfate pentahydrate (1.77 mmol, 1.3 equiv) in 30% of ethanol-water mixture (5.0 mL), was added the corresponding halide precursor (1.36 mmol, 1.0 equiv) and stirred at room temperature for 4-5 h. Progress of the reaction was monitored by TLC study. Upon completion of the reaction, ethanol component was removed under reduced pressure and the residue was used for the next step in general without any further purification. The crude Bunte salt could also be purified using neutral alumina column chromatographic method with ethyl acetate and methanol as eluents. The Bunte salt corresponding to benzyl bromide was purified by the above method and was used in the optimization reactions of trisulfides and disulfides.

3.5.3. General synthetic method for trisulfides

To a stirred solution of the crude Bunte salt (1.36 mmol, 1.0 equiv, considering 100% conversion of halides to Bunte salts) in water (20.0 mL), was added an aqueous solution (25.0 mL) of sodium sulfide nonahydrate (0.68 mmol, 0.5 equiv) at 0 °C in a drop-wise manner and the mixture was stirred at that temperature for the required duration. A white colored suspension appeared upon completion of the addition of sodium sulfide. The progress of the reaction was monitored by TLC study. Upon the completion of the reaction, the mixture was diluted with ethyl acetate and washed with brine solution. The combined organic layer was dried over anhydrous sodium sulfate and the solvent was evaporated under reduced pressure to afford crude trisulfides.

Compound DBTS: Benzyl bromide (0.25 g, 1.36 mmol) was used as a precursor to yield the trisulfide DBTS as white amorphous solid. Reaction time: 8 h, Yield: 77% (0.16 g); M.P: 44 - 46 ºC; R_f = 0.5 (100 % petroleum ether). ^{1}H NMR ($CDCl_3$, 400 MHz,): δ (ppm): 4.02 (s, 2H), 7.33 - 7.25 (m, 5H); ^{13}C NMR ($CDCl_3$, 100 MHz): δ (ppm): 43.1,

127.6, 128.6, 129.4, 136.5. ESI-MS: *m/z* calcd for $C_{14}H_{15}S_3$ $[M+H]^+$: 279.0330; observed $[M+H]^+$: 279.0589.

Compound DATS:[27] Allyl bromide (1.00 g, 8.46 mmol) was used as a precursor to yield the trisulfide DATS as a yellow liquid. Reaction time: 5 h, Yield: 50% (0.40 g); R_f = 0.9 (100 % petroleum ether). ^{1}H NMR ($CDCl_3$, 600 MHz) δ (ppm): 3.51 (d, *J* = 7.3 Hz, 2H), 5.20 - 5.25 (m, 2H), 5.85 - 5.91 (m, 1H). ^{13}C NMR ($CDCl_3$, 150 MHz) δ (ppm): 41.6, 119.1, 132.7.

Compound **3.1**:[28] 5-Bromopent-1-ene (0.50 gm, 3.35 mmol) was used as a precursor to yield the trisulfide **3.1** as a yellow liquid. Reaction time: 12 h, Yield: 24% (0.10 g); R_f = 0.8 (100 % petroleum ether). ^{1}H NMR ($CDCl_3$, 400 MHz) δ (ppm): 1.82 – 1.89 (m, 2H), 2.16 – 2.21 (m, 2H), 2.88 (t, *J* = 7.2 Hz, 2H) 4.98 – 5.08 (m, 2H), 5.74 – 5.85 (m, 2H). ^{13}C NMR ($CDCl_3$, 100 MHz) δ (ppm): 27.2, 31.4, 37.3, 114.3, 136.6.

Compound **3.2**: *n*-Propyl bromide (0.50 g, 4.06 mmol) was used as a precursor to yield the trisulfide **3.2** as liquid product. Reaction time: 6 h, Yield: 62% (0.23 g); R_f = 0.8 (100 % petroleum ether). ^{1}H NMR ($CDCl_3$, 400 MHz) δ (ppm): 1.02 (t, *J* = 7.3 Hz, 3H), 1.74 – 1.83 (m, 2H), 2.85 (t, *J* = 9.6 Hz, 2H). ^{13}C NMR ($CDCl_3$, 100 MHz) δ (ppm): 13.3, 22.3, 41.0. ESI-MS: *m/z* calcd for $C_6H_{15}S_3$ $[M+H]^+$: 183.0330; observed $[M+H]^+$: 183.1127.

Compound **3.3**: *n*-Butyl bromide (5.08 g, 49.8 mmol) was used as a precursor to yield the trisulfide **3.3** as liquid product. Reaction time: 6 h, Yield: 44% (1.57 g); R_f = 0.7 (100 % petroleum ether). ^{1}H NMR ($CDCl_3$, 400 MHz) δ (ppm): 0.94 (t, *J* = 7.4 Hz, 3H), 1.41 – 1.47 (m, 2H), 1.69 – 1.76 (m, 2H), 2.87 (t, *J* = 7.3 Hz, 3H). ^{13}C NMR ($CDCl_3$, 100 MHz) δ (ppm): 13.6, 21.7, 30.9, 38.6. ESI-MS: *m/z* calcd for $C_8H_{19}S_3$ $[M+H]^+$: 211.0643; observed $[M+H]^+$: 211.1322.

Compound **3.4**: 4-Methylbenzyl bromide (0.25 g, 1.36 mmol) was used as a precursor to yield the trisulfide **3.4** as white amorphous solid. Reaction time: 3 h, Yield: 78% (0.16 g); M.P: 61 - 63 ºC; R_f = 0.5 (100 % petroleum ether). ^{1}H NMR ($CDCl_3$, 400 MHz): δ (ppm): 2.33 (s, 3H), 4.01 (s, 2H), 7.13 (d, *J* = 6.4 Hz, 2H), 7.20 (d, *J* = 7.2 Hz, 2H). ^{13}C NMR ($CDCl_3$, 150 MHz): δ (ppm): 21.2, 42.9, 129.3, 129.3, 133.4, 137.3. ESI-MS: *m/z* calcd for $C_{16}H_{18}S_3$ K $[M+K]^+$: 345.0202; observed $[M+K]^+$: 345.0171.

Compound **3.5**: 4-Isopropylbenzyl bromide (0.28 g, 1.36 mmol) was used as a precursor to yield the trisulfide **3.5** as viscous liquid. Reaction time: 3 h, Yield: 59% (0.15 g); R_f =

0.5 (100 % petroleum ether). ^{1}H NMR ($CDCl_3$, 400 MHz): δ (ppm): 1.22 (d, *J* = 6.8 Hz, 3H), 2.86 - 2.90 (m, 1H) 4.01 (s, 2H), 7.18 (d, *J* = 7.8 Hz, 2H), 7.23 (d, *J* = 8.1 Hz, 2H); ^{13}C NMR ($CDCl_3$, 100 MHz): δ (ppm): 23.9, 33.8. 43.0, 126.7, 129.4, 133.8, 148.3. ESI-MS: *m/z* calcd for $C_{20}H_{30}NS_3$ $[M+NH_4]^+$: 380.1534; observed $[M+NH_4]^+$: 380.1540.

Compound **3.6**: 4-*tert*-Butylbenzyl chloride (0.25 g, 1.36 mmol) was used as a precursor to yield the trisulfide **3.6** as semi solid product. Reaction time: 3 h, Yield: 49% (0.15 g); R_f = 0.5 (100 % petroleum ether). ^{1}H NMR ($CDCl_3$, 600 MHz): δ (ppm): 1.30 (s, 9H), 4.01 (s, 2H), 7.25 – 7.23 (m, 1H), 7.35 – 7.33 (m, 1H). ^{13}C NMR ($CDCl_3$, 150 MHz): δ (ppm): 31.3, 34.5, 42.9, 125.4, 125.6, 129.1, 133.4, 150.6. ESI-MS: *m/z* calcd for $C_{22}H_{34}NS_3$ $[M+NH_4]^+$: 408.1848; observed $[M+NH_4]^+$: 408.1831.

Compound **3.7**: 4-Flurobenzyl bromide (0.26 g, 1.36 mmol) was used as a precursor to yield the trisulfide **3.7** as white amorphous solid. Reaction time: 3 h, Yield: 86% (0.18 g); M.P: 63 - 65 ºC; R_f = 0.5 (100 % petroleum ether). ^{1}H NMR ($CDCl_3$, 400 MHz) δ (ppm): 4.00 (s, 2H), 7.04 – 6.97 (m, 2H), 7.24 - 7.28 (m, 2H). ^{13}C NMR ($CDCl_3$, 100 MHz) δ (ppm): 42.2, 115.4, 115.6, 131.0, 131.1, 132.2, 132.3, 161.1, 163.5. ESI-MS: *m/z* calcd for $C_{14}H_{12}F_2S_3$ $[M]^+$: 314.0069; observed: 314.0790. Anal. calcd for $C_{16}H_{12}F_6S_3$: C, 53.48, H, 3.85, S, 30.59. Found, C, 53.51, H, 3.78, S, 30.16.

Compound **3.8**: 4-Chlorobenzyl chloride (0.22 g, 1.36 mmol) was used as a precursor to yield the trisulfide **3.8** as off-white amorphous solid. Reaction time: 4 h, Yield: 69% (0.22 g); M.P: 82 – 84 ºC; R_f = 0.5 (100 % petroleum ether). ^{1}H NMR ($CDCl_3$, 600 MHz) δ (ppm): 3.98 (s, 2H), 7.23 (d, *J* = 8.4 Hz, 2H), 7.30 (d, *J* = 8.4 Hz, 2H). ^{13}C NMR ($CDCl_3$, 150 MHz) δ (ppm): 42.2, 128.7, 130.7, 133.5, 134.9. Anal. calcd for $C_{14}H_{12}Cl_2S_3$: C, 48.41; H, 3.48; S, 27.69. Found, C, 48.43, H, 3.70, S, 27.78.

Compound **3.9**: 4-Bromobenzyl bromide (0.34 g, 1.36 mmol) was used as a precursor to yield the trisulfide **3.9** as white amorphous solid. Reaction time: 4 h, Yield: 47% (0.15 g); M.P: 70 – 72 ºC; R_f = 0.5 (100 % petroleum ether). ^{1}H NMR ($CDCl_3$, 400 MHz) δ (ppm): 3.96 (s, 2H), 7.17 (d, *J* = 8.2 Hz, 2H), 7.45 (d, *J* = 8.2 Hz, 2H). ^{13}C NMR ($CDCl_3$, 100 MHz) δ (ppm): 42.3, 121.6, 131.1, 131.7, 135.5. Anal. calcd for $C_{14}H_{12}Br_2S_3$: C, 38.55; H, 2.77; S, 22.05. Found, C, 38.38, H, 2.25, S, 22.44.

Compound **3.10**: 4-Trifluromethyl benzyl bromide (0.26 g, 1.36 mmol) was used as a precursor to yield the trisulfide **3.10** as viscous liquid. Reaction time: 4 h, Yield: 97% (0.24 g); R_f = 0.5 (100 % petroleum ether).^{1}H NMR ($CDCl_3$, 600 MHz) δ (ppm): 4.04 (s,

2H), 7.41 (d, *J* = 8.1 Hz, 2H), 7.58 (d, *J* = 8.2 Hz, 2H). ^{13}C NMR ($CDCl_3$, 150 MHz) δ (ppm): 42.2, 121.3 – 126.8 (q, *J* = 270.0 Hz), 125.5 – 125.6 (q, *J* = 10.5 Hz), 129.5-130.1 (q, *J* = 96.0 Hz), 129.7, 140.5. Anal. calcd for $C_{16}H_{12}F_6S_3$: C, 46.37, H, 2.92, F, 27.50, S, 23.21. Found, C, 46.03, H, 3.33, S, 22.45.

Compound **3.11**: 2-Nitrobenzyl bromide (0.10 g, 1.36 mmol) was used as a precursor to afford the trisulfide **3.11** as white amorphous solid with along with some disulfide. The crude product was purified by silica gel column chromatography to afford the pure trisulfide as white amorphous solid. Reaction time: 2 h, Yield: 54% (0.05 g); M.P: 105-107 ºC; R_f = 0.5 (10 % ethyl acetate in petroleum ether). ^{1}H NMR ($CDCl_3$, 400 MHz) δ (ppm): 4.32 (s, 2H), 7.39 (d, *J* = 7.3 Hz, 1H), 7.48 (t, *J* = 7.5 Hz, 1H), 7.57 (t, *J* = 7.2 Hz, 1H), 8.08 (d, *J* = 7.9 Hz, 1H). ^{13}C NMR ($CDCl_3$, 150 MHz) δ (ppm): 40.8, 125.8, 128.9, 132.5, 133.0, 133.4, 133.4, 147.7. ESI-MS: *m/z* calcd for $C_{14}H_{12}N_2O_4S_3Na$; observed: $[M+Na]^+$: 390.9851; observed $[M+Na]^+$: 390.9850.

Compound **3.12**: 2-Methylbenzyl bromide (0.25 g, 1.36 mmol) was used as a precursor to yield the trisulfide **3.12** as white amorphous solid. Reaction time: 6 h, Yield: 77% (0.16 g); M.P: 38 - 40 ºC; R_f = 0.7 (100 % petroleum ether 60 – 80). ^{1}H NMR ($CDCl_3$, 400 MHz): δ (ppm): 2.39 (s, 3H), 4.07 (s, 2H), 7.15 – 7.23 (m, 2H). ^{13}C NMR ($CDCl_3$, 150 MHz): δ (ppm): 19.2, 41.1, 126.0, 128.0, 130.6, 130.6, 134.0, 137.0. ESI-MS: *m/z* calcd for $C_{16}H_{19}S_3$ $[M+H]^+$: 307.0643; observed $[M+H]^+$: 307.0676.

Compound **3.13**: 3-Nitrobenzyl bromide (0.28 g, 1.36 mmol) was used as a precursor to yield the trisulfide **3.13** as white amorphous solid. Reaction time: 3 h, Yield: 91% (0.27 g); M.P: 110 - 112 ºC; R_f = 0.5 (10 % ethyl acetate in petroleum ether).^{1}H NMR ($CDCl_3$, 400 MHz) δ (ppm): 4.09 (s, 2H), 7.52 (t, *J* = 7.8 Hz, 1H), 7.62 (d, *J* = 7.6 Hz, 1H), 8.16 (d, *J* = 9.0 Hz, 2H). ^{13}C NMR ($CDCl_3$, 100 MHz) δ (ppm): 41.8, 122.7, 124.3, 129.6, 135.5, 138.5, 148.4. ESI-MS: *m/z* calcd for $C_{14}H_{12}N_2O_4S_3Na$ $[M+Na]^+$: 390.9851; observed $[M+Na]^+$: 390.9820.

Compound **3.14**: 3-Chlorobenzyl chloride (0.22 g, 1.36 mmol) was used as a precursor to yield the trisulfide **3.14** as white amorphous solid. Reaction time: 3 h, Yield: 73% (0.18 g); M.P: 43 – 45 ºC; R_f = 0.5 (10 % petroleum ether).^{1}H NMR ($CDCl_3$, 400 MHz) δ (ppm): 3.97 (2H, s), 7.18 - 7.19 (m, 1H), 7.26 (d, *J* = 5.1 Hz, 2H), 7.30 (s, 1H). ^{13}C NMR ($CDCl_3$, 100 MHz) δ (ppm): 42.4, 127.6, 127.8, 129.5, 129.8, 134.4, 138.5. ESI-MS: *m/z* calcd for $C_{14}H_{12}Cl_2S_3$ Na $[M+Na]^+$: 368.9370; observed $[M+Na]^+$: 368.4329.

Compound **3.15**: 3-Bromobenzyl bromide (0.34 g, 1.36 mmol) was used as a precursor to yield the trisulfide **3.15** as white amorphous solid. Reaction time: 3 h, Yield: 79% (0.24 g); M.P: 57 - 59 ºC; R_f = 0.5 (100 % petroleum ether).^{1}H NMR ($CDCl_3$, 400 MHz) δ (ppm): 3.96 (s, 2H), 7.17 – 7.24 (m, 2H), 7.41 (d, *J* = 7.3 Hz, 2H), 7.46 (s, 1H). ^{13}C NMR ($CDCl_3$, 100 MHz) δ (ppm): 42.4, 122.6, 128.1, 130.2, 130.7, 132.4, 138.8. ESI-MS: *m/z* calcd for $C_{14}H_{12}Br_2S_3K$ $[M+K]^+$: 472.8099; observed $[M+K]^+$: 472.4377.

Compound **3.16**: 3,5-Dimethylbenzyl bromide (0.25 g, 1.36 mmol) was used as a precursor to yield the trisulfide **3.16** as white amorphous solid. Reaction time: 3 h, Yield: 79% (0.18 g); M.P: 69 - 71 ºC; R_f = 0.5 (100 % petroleum ether 60 – 80). ^{1}H NMR ($CDCl_3$, 400 MHz): δ (ppm): 2.30 (s, 6H), 3.98 (s, 2H), 6.90 (s, 1H). 6.93 (s, 2H). ^{13}C NMR ($CDCl_3$, 100 MHz): δ (ppm): 21.2, 43.3, 127.2, 129.3, 136.3, 138.2. ESI-MS: *m/z* calcd for $C_{18}H_{26}N\,S_3$ $[M+NH_4]^+$: 352.1222; observed $[M+NH_4]^+$: 352.1238.

Compound **3.17**: 3,5-Di-*tert*-butylbenzyl bromide (0.38 g, 1.36 mmol) was used as a precursor to yield the trisulfide **3.17** as transparent viscous liquid. Reaction time: 24 h, Yield: 72% (0.22 g); R_f = 0.5 (100 % petroleum ether). ^{1}H NMR ($CDCl_3$, 600 MHz): δ (ppm): 1.32 (s, 18H), 4.06 (s, 2H), 7.15 (d, *J* = 1.7 Hz, 2H), 7.33 (t, *J* = 1.7 Hz, 1H). ^{13}C NMR ($CDCl_3$, 150 MHz): δ (ppm): 31.4, 34.8, 44.2, 121.6, 123.6, 135.4, 151.0. ESI-MS: *m/z* calcd for $C_{30}H_{50}\,N\,S_3$ $[M+NH_4]^+$: 520.3106, observed $[M+NH_4]^+$: 520.3097.

Compound **3.18**: 2,4-Dichlorobenzyl chloride (0.28 g, 1.36 mmol) was used as a precursor to yield the trisulfide **3.18** as white amorphous solid. Reaction time: 4 h, Yield: 89% (0.26 g); M.P: 84 - 86 ºC; R_f = 0.5 (100 % petroleum ether). ^{1}H NMR ($CDCl_3$, 400 MHz) δ (ppm): 4.09 (s, 2H), 7.20 – 7.25 (m, 2H), 7.40 (s, 1H). ^{13}C NMR ($CDCl_3$, 150 MHz) δ (ppm): 39.7, 127.0, 129.6, 132.3, 132.8, 134.2, 134.9.

Compound **3.19**: 2-(Chloromethyl)naphthalene (0.30 g, 1.36 mmol) was used as a precursor to yield the trisulfide **3.19** as white solid. Reaction time: 4 h, Yield: 96% (0.25 g); M.P: 118 – 121 ºC; R_f = 0.5 (100 % petroleum ether). ^{1}H NMR ($CDCl_3$, 400 MHz) δ (ppm): 4.17 (s,. 2H), 7.40 – 7.47 (m, 4H), 7.47 – 7.45 (m, 2H), 7.70 (s, 1H), 7.79 (s, 4H). ^{13}C NMR ($CDCl_3$, 100 MHz) δ (ppm): 43.5, 126.0, 126.3, 127.2, 127.7, 127.8, 128.3, 128.5, 132.7, 133.3, 133.9. ESI-MS: *m/z* calcd for $C_{22}H_{22}\,N\,S_3$ $[M+NH_4]^+$: 396.0909; observed $[M+NH_4]^+$: 396.0873.

3.5.4. **Bulk-scale synthesis of a representative trisulfide 3.4**: To validate our method for a large scale synthesis of trisulfides, a representative trisulfide **3.4** was synthesized

using the method as shown above. The Bunte salt was prepared using 4-methyl benzyl bromide (5.00 g, 27.00 mmol) and $Na_2S_2O_3.5H_2O$ (8.7 g, 35.1 mmol) in 30% ethanol-water system (50.0 mL) at room temperature for 5 h. The crude Bunte salt was reacted with $Na_2S.9H_2O$ (3.24 g, 13.5 mmol) in water (150.0 mL) at 0 °C for 5 h. After the usual work-up the crude trisulfide **3.4** was obtained (3.24 g, 82%). Purity of the crude product was analyzed by ^{1}H NMR and reverse-phase analytical HPLC method (Figure A4.91).

3.5.5. **Synthesis of unsymmetrical trisulfide 3.22**: To an aqueous solution (16.0 mL) of the column purified Bunte salts **3.20** and **3.21** (0.37 mmol) corresponding to 4-methylbenzyl bromide and 4-Isopropylbenzyl bromide, respectively was added an aqueous solution (16.0 mL) of sodium sulfide nonahydrate (0.37 mmol) in a drop-wise manner at 0 °C and the mixture was stirred for 5 h at that temperature. The progress of the reaction was monitored by TLC analysis. Upon completion, the reaction mixture was diluted with ethyl acetate and washed with brine solution. The combined organic layer was dried over anhydrous sodium sulfate and the solvent was evaporated under reduced pressure to afford the crude trisulfide mixture containing symmetrical and unsymmetrical trisulfides (**3.4**, **3.5** and **3.22**) at reasonably good yields. The crude mixture was then analyzed by a reverse-phase C-18 column in an analytical HPLC system to identify the trisulfides present in the mixture (Figure 3.5a).

3.5.6. **General synthesis of disulfides**: To a stirred ethanolic solution (3.5 mL) of Bunte salt (1.36 mmol, 1.0 equiv), was added the aqueous solution (1.5 mL) of sodium sulfide nonahydrate (0.68 mmol, 0.50 equiv) at room temperature and the mixture was heated at 50 °C and the progress of the reaction was monitored by TLC analysis. Upon the completion of reaction, the ethanol component was evaporated at reduced pressure and residual mixture was diluted with ethyl acetate and washed with brine solution. The combined organic layer was dried over anhydrous sodium sulfate and the solvent was evaporated under reduced pressure to afford the crude disulfides. For compounds DADS, **3.3a**, **3.17a** and **3.19a**, higher equivalents of sodium sulfite (5.0 equiv) was added in the reaction mixture to enhance the selectivity towards disulfide formation.

Compound DBDS: Benzyl bromide (0.23 g, 1.36 mmol) was used to as a precursor yield the disulfide DBDS as white solid product. Reaction time: 8 h, Yield: 79% (0.18 g); M.P: 69 - 71 ºC; R_f = 0.5 (100 % petroleum ether). ^{1}H NMR ($CDCl_3$, 400 MHz) δ (ppm): 3.60 (s, 2H), 7.23 – 7.34 (m, 5H). ^{13}C NMR ($CDCl_3$, 150 MHz) δ (ppm): 43.2, 127.4,

128.5, 129.4, 137.3. ESI-MS: *m/z* calcd for $C_{14}H_{15}S_2$ $[M+H]^+$: 247.0615. Observed $[M+H]^+$: 247.0617.

Compound DADS:[27] Allyl bromide (1.00 g, 8.46 mmol) was used as a precursor in the presence of Na_2SO_3 (5.33 g, 42.33 mmol) to yield the disulfide DADS as a yellow liquid. Reaction time: 8 h, Yield: 65% (0.40 g); R_f = 0.9 (100 % petroleum ether). ^{1}H NMR ($CDCl_3$, 600 MHz) δ (ppm): 3.34 (d, *J* = 7.3 Hz, 2H), 5.14 – 5.21 (m, 2H), 5.81 – 5.87 (m, 1H). ^{13}C NMR ($CDCl_3$, 150 MHz) δ (ppm): 42.3, 118.5, and 133.5.

Compound **3.1a**: 5-Bromopent-1-ene (0.50 gm, 3.35 mmol) was used as a precursor to yield the disulfide **3.1a** as a colorless liquid. Reaction time: 12 h, Yield: 26% (0.20 g); R_f = 0.7 (100 % petroleum ether). ^{1}H NMR ($CDCl_3$, 400 MHz) δ (ppm): 1.75 – 1.82 (m, 2H), 2.13 – 2.19 (m, 2H), 2.68 (t, *J* = 7.2 Hz, 2H), 4.97 - 5.06 (m, 2H), 5.73 – 5.82 (m, 1H). ^{13}C NMR ($CDCl_3$, 100 MHz) δ (ppm): 27.9, 32.4, 38.1, 115.5, and 137.5.

Compound **3.2a**[15]: *n*-Propyl bromide (0.50 g, 4.06 mmol) was used as a precursor to yield the disulfide **3.2a** as liquid product. Reaction time: 5 h, Yield: 72% (0.23 g); R_f = 0.8 (100 % petroleum ether). ^{1}H NMR ($CDCl_3$, 400 MHz) δ (ppm): 1.00 (t, *J* = 7.3 Hz, 6H), 1.67 – 1.76 (m, 2H), 2.66 (t, *J* = 7.1 Hz, 4H). ^{13}C NMR ($CDCl_3$, 100 MHz) δ (ppm): 12.1, 21.5, 40.2.

Compound **3.3a**[29]: *n*-Butyl bromide (0.50 g, 4.06 mmol) was used as a precursor to yield the disulfide **3.3a** as liquid product. Reaction time: 5 h, Yield: 50% (0.20 g); R_f = 0.7 (100 % petroleum ether). ^{1}H NMR ($CDCl_3$, 400 MHz) δ (ppm): 0.91 - 0.95 (t, *J* = 8.0 Hz, 3H), 1.40 – 1.44 (m, 2H), 1.64 – 1.73 (m, 2H), 2.68 (t, *J* = 7.4 Hz, 3H). ^{13}C NMR ($CDCl_3$, 100 MHz) δ (ppm): 12.7, 20.6, 30.3, 37.9.

Compound **3.4a**: 4-Methylbenzyl bromide (0.25 g, 1.36 mmol) was used as a precursor to yield the disulfide **3.4a** as white solid. Reaction time: 4 h, Yield: 65% (0.12 g); M.P: 46 - 48 ºC; R_f = 0.5 (100 % Petroleum ether). ^{1}H NMR ($CDCl_3$, 600 MHz) δ (ppm): 2.33 (s, 3H), 3.60 (s, 2H), 7.14 – 7.17 (m, 4H). ^{13}C NMR ($CDCl_3$, 150 MHz) δ (ppm): 21.2, 43.0, 129.2, 129.3, 134.3, 137.1. ESI-MS: *m/z* calcd for $C_{16}H_{19}S_2$ $[M+H]^+$: 275.0923, Observed $[M+H]^+$: 275.0941.

Compound **3.5a**: 4-Isopropylbenzyl bromide (0.30 g, 1.36 mmol) was used as a precursor to yield the disulfide **3.5a** as liquid product. Reaction time: 4 h, Yield: 75% (0.20 g); R_f = 0.5 (100 % petroleum ether). ^{1}H NMR ($CDCl_3$, 600 MHz) δ (ppm): 1.23

(d, *J* = 6.9 Hz, 3H), 2.86 - 2.92 (m, 1H), 3.59 (s, 2H), 7.19 – 7.14 (m, 2H). ^{13}C NMR ($CDCl_3$, 150 MHz) δ (ppm): 24.0, 33.8, 43.0, 126.5, 129.4, 134.6, 148.2. ESI-MS: *m/z* calcd for $C_{20}H_{30}NS_2$ $[M+NH_4]^+$: 348.1814, Observed $[M+NH_4]^+$: 348.1951.

Compound **3.6a**: 4-*tert*-Butylbenzyl chloride (0.25 g, 1.36 mmol) was used as a precursor to yield the disulfide **3.6a** as semi solid product. Reaction time: 16 h, Yield: 95% (0.23 g); M.P: 63 – 64 ºC; R_f = 0.5 (100 % petroleum ether). ^{1}H NMR (400 MHz, $CDCl_3$,): δ (ppm): 1.31 – 1.30 (m, 9H), 3.60 (s, 2H) 7.17 (d, *J* = 8.3 Hz, 2H), 7.34 (d, *J* = 8.3 Hz, 2H). ^{13}C NMR (150 MHz, $CDCl_3$): δ (ppm): 31.4, 43.0, 125.4, 129.1, 134.2, 150.5. ESI-MS: *m/z* calcd for $C_{22}H_{34}NS_2$ $[M+NH_4]^+$: 276.2127, Observed $[M+NH_4]^+$: 276.2156.

Compound **3.7a**: 4-Fluorobenzyl bromide (0.26 g, 1.36 mmol) was used as a precursor to yield the disulfide **3.7a** as white solid product. Reaction time: 4 h, Yield: 86% (0.13 g); M.P: 59 - 61 ºC; R_f = 0.5 (100 % petroleum ether). ^{1}H NMR ($CDCl_3$, 600 MHz) δ (ppm): 3.58 (s, 2H), 7.01 (t, *J* = 8.7 Hz, 2H), 7.24 – 7.28 (m, 2H). ^{13}C NMR ($CDCl_3$, 150 MHz) δ (ppm): 42.4, 115.3, 115.5, 130.8, 130.9, 133.1, 133.1, 161.4, 163.0. ESI-MS: *m/z* calcd for $C_{14}H_{13}F_2S_2$ $[M+H]^+$: 283.0421, Observed $[M+H]^+$: 283.1897.

Compound **3.8a**:[30] 4-Chlorobenzyl chloride (0.22 g, 1.36 mmol) was used as a precursor to yield the disulfide **3.8a** as white solid product. Reaction time: 5 h, Yield: 79% (0.20 g); M.P: 57 – 59 ºC; R_f = 0.5 (100 % petroleum ether). ^{1}H NMR ($CDCl_3$, 600 MHz) δ (ppm): 3.57 (s, 2H), 7.15 (d, *J* = 8.4 Hz, 2H), 7.30 (d, *J* = 8.4 Hz, 2H). ^{13}C NMR ($CDCl_3$, 150 MHz) δ (ppm): 42.4, 128.7, 130.6, 133.4, 135.8.

Compound **3.9a**: 4-Bromobenzyl bromide (0.34 g, 1.36 mmol) was used as a precursor to yield the disulfide **3.9a** as reddish amorphous solid. Reaction time: 20 h, Yield: 81% (0.22 g); M.P: 77 – 79 ºC; R_f = 0.5 (100 % petroleum ether). ^{1}H NMR ($CDCl_3$, 400 MHz) δ (ppm): 3.72 (s,. 2H), 7.09 (d, *J* = 8.3 Hz, 2H), 7.45 (d, *J* = 8.4 Hz, 2H). ^{13}C NMR ($CDCl_3$, 100 MHz) δ (ppm): 42.6, 121.5, 131.0, 131.7, 136.6. ESI-MS: *m/z* calcd for $C_{14}H_{16}Br_2NS_2$ $[M+NH_4]^+$: 419.9085, Observed $[M+NH_4]^+$: 419.0412.

Compound **3.10a**:[31] 4-Trifluromethylbenzyl bromide (0.26 g, 1.36 mmol) was used as a precursor to yield the disulfide **3.10a** as white amorphous solid. Reaction time: 16 h, Yield: 73% (0.20 g); M.P: 64 – 66 ºC; R_f = 0.5 (100 % petroleum ether).^{1}H NMR ($CDCl_3$, 400 MHz) δ (ppm): 3.64 (s, 2H), 7.32 (d, *J* = 8.0 Hz, 2H), 7.58 (d, *J* = 8.1 Hz,

2H). ^{13}C NMR ($CDCl_3$, 150 MHz) δ (ppm): 42.6, 123.2, 125.0, 125.4 – 125.5 (q, J_1 = 12.0 Hz, J_2 = 18.0 Hz), 129.6, 129.7, 129.4.

Compound **3.11a**: 2-Nitrobenzyl bromide (0.30 g, 1.36 mmol) was used as a precursor to yield the disulfide **3.11a** as yellow solid product. Reaction time: 2 h, Yield: 71% (0.20 g); M.P: 107 – 109 ºC; R_f = 0.5 (10 % ethyl acetate in petroleum ether). ^{1}H NMR ($CDCl_3$, 600 MHz) δ (ppm): 4.03 (s, 2H), 7.35 (d, *J* = 7.6 Hz, 1H), 7.46 (t, *J* = 8.3 Hz, 1H), 7.58 (t, *J* = 7.3 Hz, 1H), 8.05 (d, *J* = 8.2 Hz, 1H). ^{13}C NMR ($CDCl_3$, 150 MHz) δ (ppm): 41.0, 125.5, 128.7, 132.8, 133.4, 133.4, 147.9. ESI-MS: *m/z* calcd for $C_{14}H_{12}N_2O_4S_2$ Na $[M + Na]^+$: 359.0136, Observed $[M+Na]^+$: 359.0223.

Compound **3.12a**: 2-Methylbenzyl bromide (0.25 g, 1.36 mmol) was used as a precursor to yield the disulfide **3.12a** as white solid. Reaction time: 16 h, Yield: 50% (0.10 g); M.P: 77 – 78 ºC; R_f = 0.5 (in 100% Petroleum ether). ¹H NMR (400 MHz, $CDCl_3$,): δ (ppm): 2.37 (s, 3H), 3.66 (s, 2H), 7.13 – 7.19 (m, 4H). ¹³C NMR (100 MHz, $CDCl_3$): δ (ppm):19.3, 41.6, 125.9, 127.8, 130.5, 130.5, 135.1, 136.8. ESI-MS: *m/z* calcd for $C_{16}H_{19}S_2$ $[M + H]^+$ = 275.0923, Observed $[M+H]^+$: 275.0973.

Compound **3.13a**: 3-Nitrobenzyl bromide (0.23 g, 1.36 mmol) was used as a precursor to yield the disulfide **3.13a** as white amorphous solid. Reaction time: 30 h, Yield: 96% (0.22 g); M.P: 101 – 102 ºC; R_f = 0.5 (10% ethyl acetate in petroleum ether).^{1}H NMR ($CDCl_3$, 400 MHz) δ (ppm): 3.72 (s, 2H), 7.58 – 7.53 (m, 2H), 8.06 (s, 1H), 8.16 (dt, *J* = 7.8, 1.8 Hz, 2H). ^{13}C NMR ($CDCl_3$, 100 MHz) δ (ppm): 42.1, 122.7, 124.1, 129.6, 135.3, 139.3. ESI-MS: *m/z* calcd for $C_{14}H_{12}N_2O_4S_2Na$ $[M + Na]^+$: 359.0136, Observed $[M+Na]^+$: 359.0155.

Compound **3.14a**: 3- Chlorobenzyl chloride (0.22 g, 1.36 mmol) was used as a precursor to yield the disulfide **3.14a** as white amorphous solid. Reaction time: 18 h, Yield: 89% (0.10 g); M.P: 122 – 123 ºC; R_f = 0.8 (100 % petroleum ether).^{1}H NMR ($CDCl_3$, 400 MHz) δ (ppm): 3.56 (s, 2H), 7.13 – 7.10 (m, 1H), 7.23 (s, 1H), 7.23 - 7.27 (m, 2H). ^{13}C NMR ($CDCl_3$, 100 MHz) δ (ppm): 42.7, 127.5, 127.7, 129.5, 129.8, 134.3, 139.3. ESI-MS: *m/z* calcd for $C_{14}H_{16}$ N Cl_2S_2 $[M + NH_4]^+$ = 332.0096, Observed $[M+ NH_4]^+$: 332.2070.

Compound **3.15a**: 3-Bromobenzyl bromide (0.34 g, 1.36 mmol) was used as a precursor to yield the disulfide **3.15a** as reddish amorphous solid. Reaction time: 21 h, Yield: 98%

(0.27 g); M.P: 56 – 58 ºC; R_f = 0.5 (100% petroleum ether).^{1}H NMR ($CDCl_3$, 400 MHz) δ (ppm): 3.96 (s, 2H), 7.19 (dt, *J* = 14.2, 7.7 Hz, 2H), 7.42 (dt, *J* = 7.6, 1.5 Hz, 1H), 7.40 – 7.38 (m, 1H). ^{13}C NMR ($CDCl_3$, 100 MHz) δ (ppm): 42.4, 122.6, 128.1, 130.2, 130.7, 132.4, 138.8. ESI-MS: *m/z* calcd for $C_{14}H_{12}Br_2S_2K$ $[M + K]^+$ = 440.8384, Observed $[M + K]^+$ = 440.1956.

Compound **3.16a**: 3,5-Dimethylbenzyl bromide (0.27 g, 1.36 mmol) was used as a precursor to yield the disulfide **3.16a** as reddish semi solid compound. Reaction time: 21 h, Yield: 83% (0.17 g); R_f = 0.6 (100 % petroleum ether). ^{1}H NMR ($CDCl_3$, 400 MHz): δ (ppm): 2.31 (s, 6H), 3.57 (s, 2H), 6.86 (s, 1H). 6.90 (s, 2H). ^{13}C NMR ($CDCl_3$, 100 MHz): δ (ppm): 21.2, 43.4, 127.2, 129.1, 137.1, and 138.0.

Compound **3.17a**: In this reaction, the corresponding trisulfide **3.17** was obtained as the major product even in the presence of 5.0 equiv of sodium sulfite.

Compound **3.18a**:[32] 2,4- Dichlorobenzyl chloride (0.27 g, 1.36 mmol) was used as a precursor to yield the disulfide **3.18a** as white amorphous solid. Reaction time: 24 h, Yield: 92% (0.24 g); M.P: 119 – 120 ºC; R_f = 0.8 (100 % petroleum ether). ^{1}H NMR ($CDCl_3$, 400 MHz) δ (ppm): 3.76 (s, 2H), 7.20 – 7.17 (m, 2H), 7.39 (d, *J* = 1.8 Hz, 1H). ^{13}C NMR ($CDCl_3$, 150 MHz) δ (ppm): 40.4, 127.0, 129.6, 132.2, 133.5, 134.1, 134.8.

Compound **3.19a**: 2-(Chloromethyl)naphthalene (0.30 g, 1.36 mmol) was used as a precursor in the presence of Na_2SO_3 (0.34 g, 2.72 mmol) to yield the disulfide **3.19a** as white solid. Reaction time: 4 h, Yield: 96% (0.25 g); M.P: 121 – 122 ºC; R_f = 0.5 (100 % petroleum ether). ^{1}H NMR ($CDCl_3$, 400 MHz) δ (ppm): 3.72 (s, 2H), 7.32 – 7.34 (m, 1H), 7.46 – 7.51 (m, 3H), 7.75 – 7.82 (m, 3H). ^{13}C NMR ($CDCl_3$, 100 MHz) δ (ppm): 43.7, 126.0, 126.7, 127.3, 127.7, 127.8, 128.2, 128.3, 132.7, 133.3, 134.6. ESI-MS: *m/z* calcd for $C_{22}H_{19}S_2$ $[M+H]^+$: 347.0923; observed $[M+H]^+$: 347.2515.

3.5.7. **Synthesis of unsymmetrical disulfide 3.22a**: To an ethanolic solution (3.5 mL) of the column purified Bunte salts **3.20** and **3.21** (0.92 mmol) of 4-Methylbenzyl bromide and 4-Isopropylbenzyl bromide, was added an aqueous solution (1.5 mL) of sodium sulfide nonahydrate (0.92 mmol) in a drop-wise manner at 50 °C and the mixture was stirred for 3 h at that temperature. The progress of the reaction was monitored by TLC study. Upon the completion, the reaction mixture was diluted with ethyl acetate and washed with brine solution. The combined organic layer was dried over anhydrous

sodium sulfate and the solvent was evaporated under reduced pressure to afford crude disulfide mixture (**3.4a**, **3.5a** and **3.22a**) at reasonably good yields. The crude mixture was then analyzed by a reverse-phase C-18 column in an analytical HPLC system to identify the disulfides present in the mixture (Figure 3.5b).

3.5.8. Synthesis of monosulfide 3.11b

To a stirred solution of sodium sulfide nonahydrate (0.05g, 0.23 mmol) in ethanol (5.0 mL), 2-nitrobenzyl bromide (0.10 g, 0.46 mmol) was added at room temperature and the mixture was stirred at room temperature for 3 h. The progress of the reaction was monitored by TLC study. After completion of the reaction, ethanol was evaporated under reduced pressure and the reaction mixture was diluted with ethyl acetate and washed with brine solution. The combined organic layer was dried over anhydrous sodium sulfate and the solvent was evaporated under reduced pressure to afford the crude monosulfide **3.11b** as crystalline yellow solid. Yield: 58% (0.04 g); M.P: 118 – 122 ºC; R_f = 0.5 (10% ethyl acetate in petroleum ether). ^{1}H NMR ($CDCl_3$, 400 MHz) δ (ppm): 4.02 (s, 4H), 7.37 – 7.41 (m, 4H), 7.49 – 7.53 (m, 2H), 7.93 (d, *J* = 8.1 Hz, 2H). ^{13}C NMR ($CDCl_3$, 100 MHz) δ (ppm): 32.6, 124.3, 127.3, 130.8, 132.0, 132.4, 147.7. ESI-MS: *m/z* calcd for $C_{14}H_{13}N_2O_4S$ $[M+H]^+$: 305.0591, observed $[M+H]^+$: 305.0281.

3.5.9. HPLC analysis

The HPLC analysis of the test compounds was performed using HPLC grade solvents. 2-Nitro-substituted benzylic compounds **3.11**, **3.11a**, and **3.11b** were analyzed using (70 to 95%) of acetonitrile and (30 to 5%) water system for 10 min in a linear gradient mode and (95:5) ratio of acetonitrile and water system in isocratic mode for another 10 min, respectively (Figure 3.4). Compounds **3.4**, **3.5** and **3.22** were analyzed using (85 to 97%) acetonitrile and (15 to 3%) water system for 10 min in a linear gradient mode followed by (97:3) acetonitrile and water system in an isocratic mode for another 10 min (Figure 3.5a). Compounds **3.4a**, **3.5a** and **3.22a** were analyzed by using acetonitrile (92 to 98%) and water (8 to 2%) in a linear gradient mode for 10 min followed by (98:2) ratio of acetonitrile and water in an isocratic mode for another 10 min (Figure 3.5b). Final test compounds for biological study were purified by reverse-phase semi-prep column (Luna ®, polar C-18, 250×21.2 mm) on a semi-prep HPLC system (Thermo scientific Dionex, Ultimate 3000 pump with DAD).

3.5.10. DFT calculations

The geometries of the all the considered reactants, transition states (TS) and products were fully optimized at M06/6-31+G(d) level of theory using Gaussian-09 program.[33] Effect of water solvent we included in all the calculations using IEF-PCM method.[34] The optimizations were followed by frequency calculations at the same level to characterize the obtained stationary points as minima or transition state on the potential energy surface. Intrinsic reaction coordinate (IRC) calculations,[35] with mass weighted coordinates at the same level of theory, were also performed wherever necessary to validate the reaction path and to follow the reaction profile. Single point energy calculations at various levels were carried out to analyze the effect of methods and basis set on the energy profile of the reaction. Effect of zero point correction and Gibbs free energy on the profile is summarized in (Table A4.4 - A4.11).

3.5.11. X-Ray crystallography

Single crystal X-ray diffraction data was collected on a Bruker AXS SMART APEX CCD diffractometer or Super Nova, Single source at offset, Eos diffractometer. The data refinement and cell reductions were carried out by CrysAlisPro at room temperature (293 K). The X-ray generator was operated at 50 KV and 35 mA using Mo-Kα radiation (λ = 0.71073 Å). The data was collected using SMART software package. The data were reduced by SAINTPLUS, an empirical absorption correction was applied using the package SADABS and XPREP were used to determine the space group. The crystal structure was solved by direct methods using SIR92[36] and refined by full-matrix least-squares method using SHELXL-97.[37] All non-hydrogen atoms were refined anisotropically and hydrogen atoms were assigned at idealized locations. **CCDC 1905587** (compound **3.11**), **CCDC 1905588** (compound **3.11a**) and **CCDC 1905589** (compound **3.11b**) contain the supplementary crystallographic data for this paper. These data can be obtained free of charge from The Cambridge Crystallographic Data Centre *via* www.ccdc.cam.ac.uk/data_request/cif.

3.5.12. Cell culture

Human breast carcinoma cell line MCF-7 was obtained from the National Centre for Cell Science (NCCS), India. MCF-7 was cultured in DMEM medium (Gibco) supplemented with 10% (v/v) FBS (Gibco) and 1% Pen-Strep (Gibco). Cells were

cultured as a monolayer in a humidified incubator at 37 °C in the presence of 5% CO_2 level.

3.5.13. Cellular morphology and viability studies

The synthesized compounds were primarily screened in breast cancer cell line (MCF-7, passage no 41-50). Stock solution of the synthesized compounds was prepared in DMSO (HiMedia) and serially diluted in the culture media for the preparation of working solutions of different concentrations. The cells were seeded at a density of 1×10^4 cells per 100.0 µL in 96-well plates and incubated overnight. The cells were treated with test compounds (10.0 µM and 25.0 µM) and incubated for 72 h in the CO_2 incubator. Cellular morphology was carefully observed and imaged in a Bio-rad ZOE™ fluorescent cell imager before and after (24 h, 48 h and 72 h interval) the treatment of test compounds. Preliminary screening with cell viability assay was performed for the cells in the presence of test compounds after 72 h and compared with the control experiments without any test compound. Trisulfides that exhibited significant potencies in preliminary studies were selected and purified further by a reverse-phase HPLC method. The purified trisulfides were screened for their anti-proliferative activities. Stock solution of the synthesized compounds was prepared in DMSO (HiMedia) and serially diluted in the culture media for the preparation of working solutions of different concentrations. The cells (MCF-7) were plated in 96-well culture plates at a density of 1×10^4 cells/100.0 µL/well and treated with test compounds (up to 25.0 µM) for 0 h (Set 1) and 72 h (Set 2). At the end of treatment period, the cells were washed with DPBS and 100.0 µL of 0.5 mg/mL of MTT in fresh DPBS was added to each well (Set 1) and incubated for 2 h. Following the 2 h incubation, the culture media from the plate was removed and the purple formazan crystals were dissolved using 100.0 µL of DMSO (HiMedia) and the absorbance at 570 nm was measured using a microplate reader (Thermo Scientific Multiskan™ GO Microplate spectrophotometer). In Set 2, similar MTT treatment protocol was followed only after 72 h. The mean ΔOD values were calculated by the subtraction of mean OD values of 0 h plate (Set 1) from the mean OD values of identical wells at 72 h plate (Set 2) and the percentage proliferation was calculated keeping the mean ΔOD of untreated control as 100%.

3.5.14. Detection of Hydrogen sulfide (H_2S) release by MB assay

Generation of H_2S by the synthesized trisulfides and disulfides in the presence of thiols such as glutathione (GSH) was monitored using methylene blue assay in an UV-Vis spectrophotometer.[38] H_2S generation was initiated by adding trisulfide or disulfide donors (50.0 μM) into PBS buffer (pH 7.4, 50.0 mM) solution containing thiol (500.0 μM). Formation of methylene blue was monitored at 670 nm in UV-Vis spectrophotometer in different time intervals after adding 500.0 μL of the above solution to 500.0 μL of methylene blue cocktail (100.0 μL of zinc acetate (1% w/v), 200.0 μL of *N*,*N*-dimethyl-1,4-phenylenediamine sulfate (20.0 mM in 7.2 M HCl), and 200.0 μL of ferric chloride (30.0 mM in 1.2 M HCl) in a cuvette. The H_2S concentration of each sample was calculated against a calibration curve, which was obtained using known concentrations of $Na_2S.9H_2O$ solution under identical condition without any thiols.

3.5.15. H_2S release from 3.4 in cellular medium and its detection using fluorescent probe NAP-N_3

MCF-7 cells were cultured in high glucose Dulbecco's modified Eagle's medium (DMEM) supplemented with 10% fetal bovine serum (FBS) and 1% penicillin/streptomycin at 37 °C under 5% CO_2. Cells were then plated (0.7×10^4 cells/well) in poly-D-lysine coated plates (Merck) containing 2.0 mL of DMEM and incubated at 37 ºC under 5% CO_2 for 24 h. The confluent cells were washed with PBS and incubated with compound **NAP-N_3** for 10 mins. After washing with PBS, cells were fixed and imaged to check the level of endogenous H_2S in the treated MCF-7 cells. In another experiment, compound **3.4** (1.0 μM) was added to the adhered cells and kept for 10 min at 37 °C under 5% CO_2. After the incubation, cells were washed (5 times) with PBS and compound **NAP-N_3** was added. The cells were incubated for 10 mins in the incubator and washed with PBS. The cells were fixed with 4% formaldehyde and imaged under fluorescence microscope (Biorad ZOE^{TM} Fluorescent Cell Imager).

3.6. References

1. Steudel, R., *Chemical Reviews* **2002,** *102*, 3905.

2. (a) Nicolaou, K. C.; Hummel, C. W.; Nakada, M.; Shibayama, K.; Pitsinos, E. N.; Saimoto, H.; Mizuno, Y.; Baldenius, K. U.; Smith, A. L., *Journal of the American Chemical Society* **1993,** *115*, 7625; (b) Golik, J.; Dubay, G.; Groenewold, G.;

Kawaguchi, H.; Konishi, M.; Krishnan, B.; Ohkuma, H.; Saitoh, K.; Doyle, T. W., *Journal of the American Chemical Society* **1987,** *109,* 3462; (c) Pluth, M. D.; Bailey, T. S.; Hammers, M. D.; Hartle, M. D.; Henthorn, H. A.; Steiger, A. K., *Synlett* **2015,** *26,* 2633.

3. (a) Jespersen, A. M.; Christensen, T.; Klausen, N. K.; Nielsen, P. F.; SØRensen, H. H., *European Journal of Biochemistry* **1994,** *219,* 365; (b) Thakur, S. S.; Balaram, P., *Journal of the American Society for Mass Spectrometry* **2009,** *20,* 783; (c) Bernardes, G. J. L.; Marston, J. P.; Batsanov, A. S.; Howard, J. A. K.; Davis, B. G., *Chemical Communications* **2007,** 3145; (d) Yao, J. K.; Keshavan, M. S., *Antioxidants & Redox Signaling* **2010,** *15,* 2011.

4. (a) Adams, T. C.; Payette, J. N.; Cheah, J. H.; Movassaghi, M., *Organic Letters* **2015,** *17,* 4268; (b) Singh, S. V.; Powolny, A. A.; Stan, S. D.; Xiao, D.; Arlotti, J. A.; Warin, R.; Hahm, E.-R.; Marynowski, S. W.; Bommareddy, A.; Potter, D. M.; Dhir, R., *Cancer Research* **2008,** *68,* 9503.

5. Fleischauer, A. T.; Arab, L., *The Journal of Nutrition* **2001,** *131,* 1032S.

6. Song, K.; Milner, J. A., *The Journal of Nutrition* **2001,** *131,* 1054S.

7. (a) Benavides Gloria, A.; Squadrito Giuseppe, L.; Mills Robert, W.; Patel Hetal, D.; Isbell, T. S.; Patel Rakesh, P.; Darley-Usmar Victor, M.; Doeller Jeannette, E.; Kraus David, W., *Proceedings of the National Academy of Sciences* **2007,** *104,* 17977; (b) Zheng, Y.; Ji, X.; Ji, K.; Wang, B., *Acta Pharmaceutica Sinica B* **2015,** *5,* 367.

8. (a) Zysman-Colman, E.; Harpp, D. N., *The Journal of Organic Chemistry* **2003,** *68,* 2487; (b) Sato, R.; Saito, S.; Chiba, H.; Goto, T.; Saito, M., *Chemistry Letters* **1986,** *15,* 349; (c) Buckman, J. D.; Field, L., *The Journal of Organic Chemistry* **1967,** *32,* 454; (d) Hou, Y.; Abu-Yousef, I. A.; Doung, Y.; Harpp, D. N., *Tetrahedron Letters* **2001,** *42,* 8607; (e) Abe, Y.; Horii, T.; Kawamura, S.-i.; Nakabayashi, T., *Bulletin of the Chemical Society of Japan* **1979,** *52,* 3461; (f) An, H.; Zhu, J.; Wang, X.; Xu, X., *Bioorganic & Medicinal Chemistry Letters* **2006,** *16,* 4826.

9. Kiesel, V. A.; Stan, S. D., *Biochemical and Biophysical Research Communications* **2017,** *484,* 833.

10. Liu, Y.; Zhao, Y.; Wei, Z.; Tao, L.; Sheng, X.; Wang, S.; Chen, J.; Ruan, J.; Liu, Z.; Cao, Y.; Shan, Y.; Wang, A.; Chen, W.; Lu, Y., *Cellular Physiology and Biochemistry* **2018,** *50,* 1945.

11. Ali, D.; Amer, Y.; Petersen, W. F.; Kaschula, C. H.; Hunter, R., *SynOpen* **2021,** *05,* 49.

12. Harpp, D. N.; Smith, R. A., *The Journal of Organic Chemistry* **1979,** *44,* 4140.

13. Nakabayashi, T.; Tsurugi, J., *The Journal of Organic Chemistry* **1961,** *26,* 2482.

14. Bolton, S. G.; Cerda, M. M.; Gilbert, A. K.; Pluth, M. D., *Free Radical Biology and Medicine* **2019,** *131,* 393.

15. Baker, A.; Graz, M.; Saunders, R.; Evans, G. J. S.; Kaul, S.; Wirth, T., *Journal of Flow Chemistry JFC* **2013,** *3,* 118.

16. Milligan, B.; Saville, B.; Swan, J. M., *Journal of the Chemical Society (Resumed)* **1963,** 3608.

17. Sinha, P.; Kundu, A.; Roy, S.; Prabhakar, S.; Vairamani, M.; Sankar, A. R.; Kunwar, A. C., *Organometallics* **2001,** *20,* 157.

18. (a) Firouzabadi, H.; Abbassi, M.; Karimi, B., *Synthetic Communications* **1999,** *29,* 2527; (b) Witt, D., *Synthesis* **2008,** *2008,* 2491.

19. Santhosha, S. G.; Jamuna, P.; Prabhavathi, S. N., *Food Bioscience* **2013,** *3,* 59.

20. El-Bayoumy, K.; Sinha, R.; Pinto, J. T.; Rivlin, R. S., *The Journal of Nutrition* **2006,** *136,* 864S.

21. Herman-antosiewicz, A.; Powolny, A. A.; Singh, S. V., *Acta Pharmacologica Sinica* **2007,** *28,* 1355.

22. Xiao, D.; Choi, S.; Johnson, D. E.; Vogel, V. G.; Johnson, C. S.; Trump, D. L.; Lee, Y. J.; Singh, S. V., *Oncogene* **2004,** *23,* 5594.

23. (a) Hahm, E. R.; Singh, S. V., *Breast Cancer Research and Treatment* **2014,** *144,* 47; (b) Malki, A.; El-Saadani, M.; Sultan, A. S., *Cancer Biology & Therapy* **2009,** *8,* 2174; (c) Malki, A.; El-Saadani, M.; Sultan, A., *Annals of Nutrition and Metabolism* **2009,** *55,* 683.

24. Filipovic, M. R.; Zivanovic, J.; Alvarez, B.; Banerjee, R., *Chemical Reviews* **2018,** *118,* 1253.

25. Wu, Z.; Liang, D.; Tang, X., *Analytical Chemistry* **2016,** *88,* 9213.

26. Distler, H., *Angew Chem Int Ed* **1967,** *6,* 544.

27. Baker, A.; Graz, M.; Saunders, R.; Evans, G. J. S.; Kaul, S.; Wirth, T., *Journal of Flow Chemistry* **2013,** *3,* 118.

28. Ren, F. K.; He, X. Y.; Deng, L.; Li, B. H.; Shin, D. S.; Li, Z. B., *Bulletin of the Korean Chemical Society* **2009,** *30,* 687.

29. Hosono, T.; Fukao, T.; Ogihara, J.; Ito, Y.; Shiba, H.; Seki, T.; Ariga, T., *Journal of Biological Chemistry* **2005,** *280,* 41487.

30. Panduranga, V.; Prabhu, G.; Basavaprabhu; Panguluri, N. R.; Sureshbabu, V. V., *Synthesis-Stuttgart* **2016,** *48,* 1711.

31. He, W.; Ding, Y.; Tu, J. Z.; Que, C. Q.; Yang, Z. H.; Xu, J. X., *Organic & Biomolecular Chemistry* **2018,** *16,* 1659.

32. Khan, K. M.; Taha, M.; Rahim, F.; Ali, M.; Jamil, W.; Perveen, S.; Choudhary, M. I., *Letters in Organic Chemistry* **2010,** *7,* 415.

33. Frisch, M. J.; Trucks, G. W.; Schlegel, H. B.; Scuseria, G. E.; Robb, M. A.; Cheeseman, J. R.; Scalmani, G.; Barone, V.; Mennucci, B.; Petersson, G. A.; Nakatsuji, H.; Caricato, M.; Li, X.; Hratchian, H. P.; Izmaylov, A. F.; Bloino, J.; Zheng, G.; Sonnenberg, J. L.; Hada, M.; Ehara, M.; Toyota, K.; Fukuda, R.; Hasegawa, J.; Ishida, M.; Nakajima, T.; Honda, Y.; Kitao, O.; Nakai, H.; Vreven, T.; J. A. Montgomery, J.; Peralta, J. E.; Ogliaro, F.; Bearpark, M.; Heyd, J. J.; Brothers, E.; Kudin, K. N.; Staroverov, V. N.; Keith, T.; Kobayashi, R.; Normand, J.; Raghavachari, K.; Rendell, A.; Burant, J. C.; Iyengar, S. S.; Tomasi, J.; Cossi, M.; Rega, N.; Millam, J. M.; Klene, M.; Knox, J. E.; Cross, J. B.; Bakken, V.; Adamo, C.; Jaramillo, J.; Gomperts, R.; Stratmann, R. E.; Yazyev, O.; Austin, A. J.; Cammi, R.; Pomelli, C.; Ochterski, J. W.; Martin, R. L.; Morokuma, K.; Zakrzewski, V. G.; Voth, G. A.; Salvador, P.; Dannenberg, J. J.; Dapprich, S.; Daniels, A. D.; Farkas, O.; Foresman, J. B.; Ortiz, J. V.; Cioslowski, J.; Fox, D. J., *Gaussian, Inc, Wallingford CT, 2013* **2013**.

34. Miertus, S.; Scrocco, E.; Tomasi, J., *Chemical Physics* **1981,** *55,* 117.

35. Fukui, K., *Acc Chem Res* **1981,** *14,* 363.

36. (a) Altomare, A.; Giacovazzo, C.; Moliterni, A. G. G., *Acta Crystallographica Section A* **1994,** *50,* 585; (b) Altomare, A.; Cascarano, G.; Giacovazzo, G.; Guagliardi, A.; Burla, M. C.; Polidori, G.; Camalli, M., *Journal of Applied Crystallography* **1994,** *27,* 435.

37. Sheldrick, G. M., *Acta Crystallographica Section A* **2008,** *64,* 112.

38. Popowsky, J. K. F. a. M., *Analytical Chemistry* **1949,** *21,* 732.

Anti-cancer Activity of Benzylic Organotrisulfides in Triple-negative Breast Cancer: Inactivation of Wnt/β-catenin Signaling Cascade and Contribution of the Released Hydrogen Sulfide

4.1. Introduction

Hydrogen sulfide (H_2S) has recently been considered as a third member of the gasotransmitter family, along with carbon monoxide (CO) and nitric oxide (NO).[1] The endogenous production of H_2S from Cys and Hcy and its regulation is governed by a cascade of enzymes, including CSE, CBS, CAT and 3-MST.[2] Overexpression of one or more of these H_2S-synthesizing enzymes has been reported in different organ-specific cancers, indicating the cancer-promoting roles of H_2S in general.[3] While the cancer-promoting effect is reported for H_2S, which is released instantly from inorganic donors, a sustained release of H_2S from organic donors is shown to be important for the cellular homeostasis and is known to exhibit apoptotic effects in different organ-specific cancers.[4] In this direction, over the last two decades, in addition to DATS (active constituents) a number of synthetic non-fluorogenic and turn-on fluorogenic organotrisulfides/organopolysulfides have been reported as sustained donors of H_2S for their applications in disease conditions having H_2S deficiency.[5,6] Notably, among all the polysulfides, DATS is widely studied and reported to exhibit the most potent anti-cancer activity against several organ-specific cancers.[6] For example, the anti-cancer activity of DATS in different breast cancer cells was observed due to the overproduction of ROS.[7] In a recent report, Keisel and co-workers have elucidated the role of DATS against estrogen-dependent and -independent breast cancer cells by targeting alpha-secretases and notch signaling cascade.[8] In 2017, Tao and co-workers have shown the anti-cancer activity of DATS in malignant glioma cells by suppressing the Wnt/β-catenin signaling pathway.[9] In addition, this study showed that the inactivation was accompanied by the suppression of LRP6, TRIM29 and Pygo2 expression in glioma cells. In another report (2018), Han and co-workers reported the suppressing effect of DATS on colorectal cancer stem cells *via* the Wnt/β-catenin signaling pathway.[10] In the same year, Li and co-workers showed the inhibitory role of DATS in human breast cancer stem cells by suppressing the Wnt/β-catenin pathway.[11] Therefore, it is important to target an appropriate signal transduction pathway as a therapeutic strategy for the effective treatment of cancer. The aberrant Wnt/β-catenin pathway plays a crucial role in cancer stem cell self-renewal, cell survival, cell proliferation, cell migration, cell differentiation, tumor development and chemoresistance, making it a key signaling pathway in cancer.[12] Moreover, the inhibition of the Wnt/β-catenin pathway resulted in the suppression of self-renewal of breast cancer stem cells.[13] In mammals, the absence of Wnt ligands is

associated with the canonical pathway, where the concentration of cytoplasmic β-catenin is continuously monitored by the activation and stabilization of the destruction complex.[14] Under this condition, phosphorylation of β-catenin by casein kinase 1α (CK-1α) and glycogen synthase kinase-3β (GSK-3β) helps its recognition by β-TrCP and E3 ligase subunits, which promote the ubiquitination-mediated proteasomal degradation. However, the binding of Wnt ligands with the Frizzled/ LRP5/ LRP6 leads to the destabilization of the destruction complex that subsequently prevents the phosphorylation of β-catenin. The accumulated β-catenin in the cytosol eventually translocate to the nucleus and activates several downstream signals (TCF/LEF-1, BCL9 etc.) (Figure 4.1). This results in the induction of the transcriptional target genes, namely c-Myc, Cyclin D1 and other proliferation-associated genes, leading to cell proliferation.[12e, 14a] Therefore, targeting the Wnt/β-catenin signaling is considered as an innovative strategy for anti-cancer therapy. Although the mechanistic pathways for the anti-cancer activity of garlic-based trisulfide DATS highlight the suppression of the Wnt/β-catenin signaling in different Wnt-dependent cancer cells, there are few questions that need detailed investigation. First, the direct interaction of DATS and its analogues with any particular protein of the Wnt/β-catenin signaling cascade has not been elucidated to date. Second, the possible association of the H_2S released from DATS and its analogues was not considered while understanding their suppressing effects on Wnt/β-catenin signaling, although it is well-known that DATS and organotrisulfides act as sustained donors of H_2S. And lastly, why is the inhibitory potential of DATS found to be weak in most of the organ-specific cancer cells?

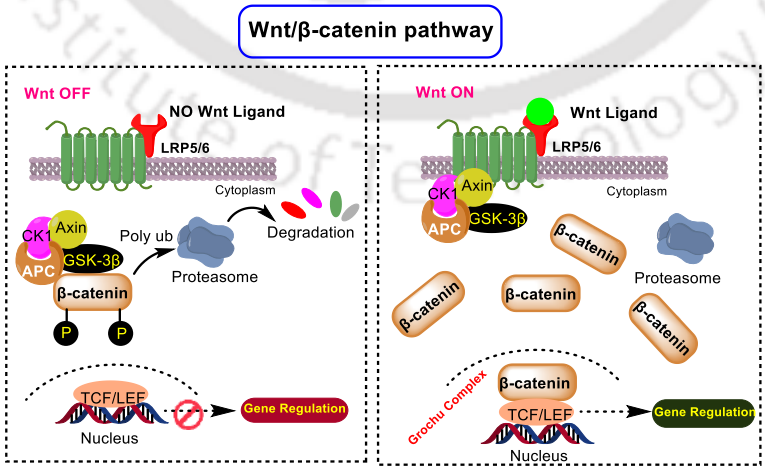

Figure 4.1. Schematic representation of canonical and non-canonical Wnt/β-catenin signaling pathway.

4.2. Outline of the chapter

In this chapter we describe, for the first time, the mechanism of action for the potent anti-cancer activity of bis(3,5-dimethoxybenzyl) trisulfide **4.1** against highly aggressive triple-negative breast cancer (MDA-MB-231) is described. Preliminary *in vitro* studies revealed potent anti-proliferative activity of the trisulfide **4.1** against TNBC with an IC_{50} value of 1.0 μM. Mechanistic studies reveal that the compound exhibited anti-cancer activity, primarily by targeting and suppressing the Wnt/β-catenin signaling pathway. The inactivation of the β-catenin level was associated with the cell cycle arrest in the G2/M phase and the significant down-regulation of downstream signaling genes such as Cyclin D1 and c-Myc expression. Several control experiments with analogous organosulfur compounds and the key enzyme inhibitors reveal that the presence of a trisulfide unit in the compound is crucial for the desired inactivation of β-catenin expression, which is promoted by GSK-3β-induced phosphorylation of β-catenin and its proteasomal degradation. Moreover, the trisulfide unit or the released H_2S induced down-regulation of the p53 expression with the possible S-sulfhydration process and led to p53-independent up-regulation of p21 expression. Therefore, the key results of this study highlighting the potency of synthetic benzylic organotrisulfide and the released H_2S towards the growth inhibition of TNBC *via* Wnt/β-catenin signaling pathway would certainly be helpful for further studies and understanding in developing small-molecule anti-cancer therapeutics in future.

4.3. Results and discussion

4.3.1. Synthesis of symmetrical benzylic organopolysulfides

In the present study, the symmetrical benzylic trisulfides, disulfides, and the corresponding monosulfides were selectively prepared using our laboratory-developed greener and catalyst/additive-free methodology, as shown in Scheme 4.1.[15] The final products could be achieved from the easily available halide precursors in 1-2 step reactions. The reaction of the halides with sodium thiosulfate in the ethanol-water system produced the corresponding Bunte salts with satisfactory yields. Subsequent reaction of the Bunte salt with sodium sulfide nonahydrate ($Na_2S.9H_20$) in 2:1 molar ratio at 0 °C temperature in water yielded the symmetrical organotrisulfides (DBTS and **4.1**) exclusively. In contrast, the corresponding symmetrical disulfides (DBDS and **4.2**) could be afforded exclusively from the reaction of Bunte salt and $Na_2S.9H_2O$ at a

slightly higher temperature (50 °C) in a water-ethanol mixture. The reaction temperature and the solvent were found to play crucial roles in accomplishing the desired selectivity of symmetrical trisulfides and disulfides from the same precursors. On the other hand, the monosulfides (DBMS and **4.3**) could be synthesized directly from the corresponding halides in the presence of $Na_2S.9H_2O$ in a methanolic solvent at room temperature (Scheme 4.1). The 3,5-dimethoxybenzyl thiol **4.5** was prepared following the literature method from 3,5-dimethoxybenzyl bromide using thiourea as the sulfur-transfer reagent.[16]

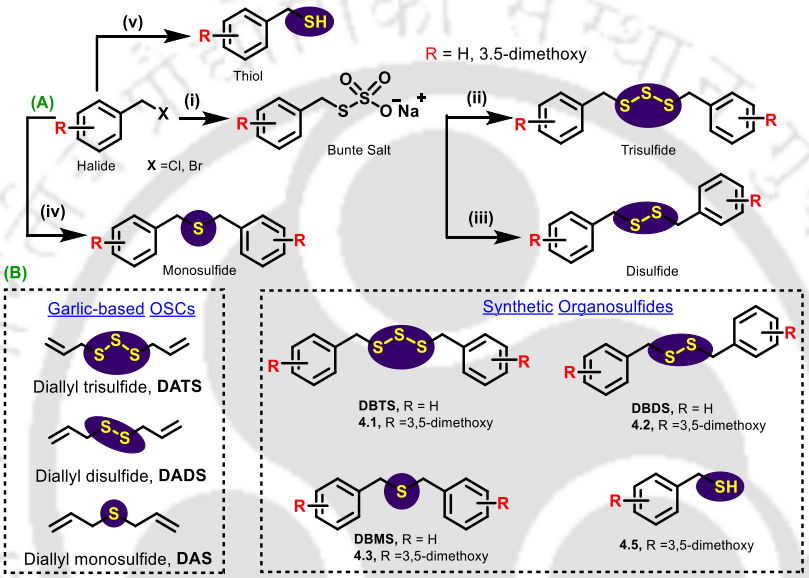

Scheme 4.1. (A) Selective synthetic schemes to symmetrical benzylic trisulfides, disulfides and monosulfides. Reagents and conditions: (i) $Na_2S_2O_3.5H_2O$, EtOH/H_2O (3:7), RT, 4 h; (ii) $Na_2S.9H_2O$, H_2O, 0 °C, 5 h; (iii) $Na_2S.9H_2O$, EtOH/H_2O (3:1), 50 °C, 5 h; (iv) $Na_2S.\ 9H_2O$, MeOH, RT, 3 h; (v) (a) Thiourea, methanol, 18 h, (b) Butylamine, 24 h (B) Chemical structures of the garlic-based organosulfides, synthetic benzylic trisulfides (DBTS, and **4.1**) and disulfides (DBDS and **4.2**) and the corresponding monosulfides (DBMS and **4.3**), and thiol (**4.5**), respectively.

4.3.2. Preliminary anti-proliferative activities

The anti-proliferative activity of garlic-based trisulfides is reported to be significantly higher than the corresponding disulfides and monosulfides in different organ-specific cancers.[7a, 15, 17] In the present study, a comparative anti-proliferative activity of the synthesized benzylic and the garlic-based allylic organosulfur compounds has been studied in a representative TNBC cell line (MDA-MB-231) at three different concentrations (5.0, 10.0 and 25.0 µM). As shown in Figures 4.2a and 4.2b, **4.1**

exhibited higher anti-proliferative activity among the compounds studied herein. Moreover, as bis(3,5-dimethoxybenzyl) trisulfide **4.1** exhibited the highest potency at all three concentrations, the dose-dependent inhibitory potential of compound **4.1** was evaluated further in breast cancer cells (MDA-MB-231 and MCF-7). It should be mentioned here that, compound **4.1** was chosen for studying its anti-cancer activity with the detailed mechanistic insights based on the initial screening of a series of analogous benzylic trisulfides (Figure 4.2). In chapter 3, we have screened several trisulfides for their anti-proliferative activities against MCF-7 cells. Interestingly, compound **3.4-3.18** were found to exhibit potent anti-proliferative activities against MCF-7 cells. Further, we have screened those compounds for their preliminary anti-proliferative activity against MDA-MB-231. A non-tumorogenic cells HEK-293 was considered for understanding the selectivity of the trisulfides towards cancer cells over the normal cells. These preliminary studies indicated compound **4.1** to be the most potent with high selectivity towards the cancer cells over the normal cells (Figure 4.2). [15]

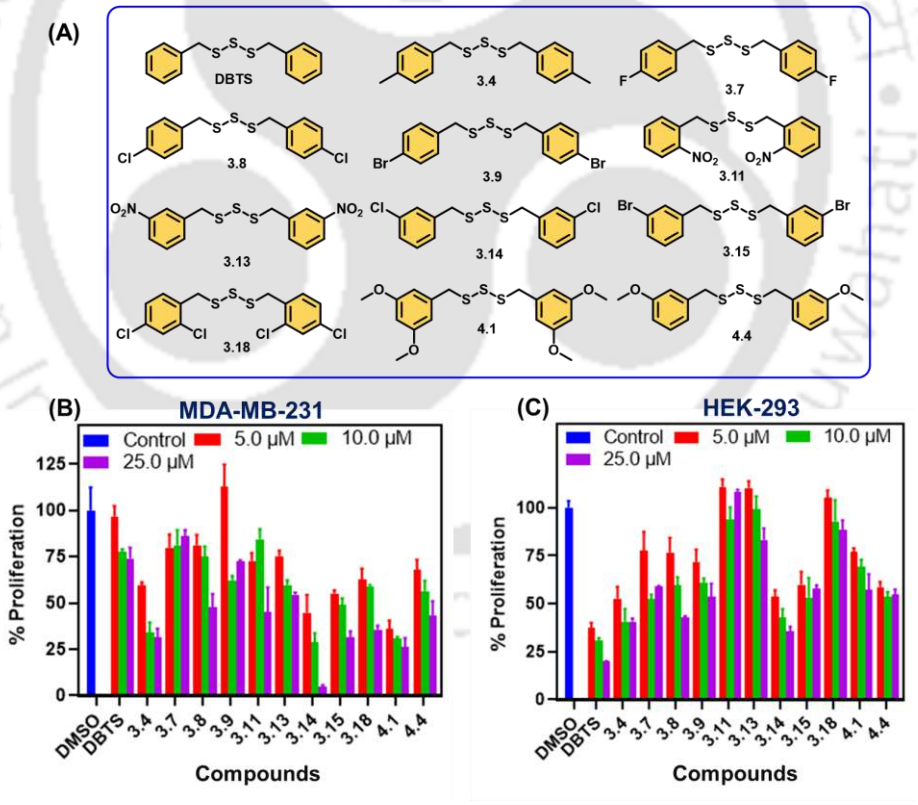

Figure 4.2. (A) Chemical structures of different benzylic trisulfides and their anti-proliferative activities in (B) MDA-MB-231 cells and (C) HEK-293 cells at 5.0, 10.0 and 25.0 μM concentrations after an incubation for 48 h.

The IC_{50} value of compound **4.1** was found to be around 1.0 µM and 2.8 µM in MDA-MB-231 and MCF-7 cells, respectively (Figures 4.3a and 4.3b). On the other hand, the corresponding disulfide **4.2** (IC_{50} > 10.0 µM) and the monosulfide **4.3** (IC_{50} > 50.0 µM) exhibited much weaker anti-proliferative activity under the identical condition (Figure 4.3a). These preliminary results indicated the importance of the number of sulfur atoms in 3,5-dimethoxybenzylic compounds **4.1**, **4.2** and **4.3**. A similar difference in preliminary anti-proliferative activity of compounds DBTS, DBDS and DBMS was reported earlier by Pluth and co-workers.[18] The lead compound **4.1** was evaluated further in several organ-specific cancer cell lines such as ER+ breast cancer cells (MCF-7), human colon carcinoma (HCT-116), human prostate adenocarcinoma (PC-3), human cervical carcinoma (HeLa) and in a representative normal human embryonic kidney cells (HEK-293). As shown in Figure 4.3c, compound **4.1** exhibited potent anti-proliferative activities in all the organ-specific cancer cells. Interestingly, a significantly lower potency in the HEK-293 cell line indicated the selectivity of compound **4.1** towards cancer cells over the normal cells. Based on these observations, bis(3,5-dimethoxybenzyl) trisulfide **4.1** was considered for studying the mechanistic insights for its potent anti-cancer activities. Next, the morphological changes of MDA-MB-231 cells by compound **4.1** (5.0 and 15.0 µM) in the presence of DAPI was studied upon incubating up to 48 h. A considerable morphological damage with the cellular killing profile was observed at both concentrations in the presence of DAPI (Figure 4.3d) with the indication of nuclear aberration and DNA damage. Similar morphological changes were also observed in the lentivirus-transduced MDA-MB-231 cells stably expressing green fluorescent protein (GFP) upon the treatment with compound **4.1** (Figure 4.3d). As shown in Figure 4.3d, upon the treatment of Lenti-GFP expressed cells with compound **4.1** (5.0 and 15.0 µM) for 48 h the cellular morphology changed abruptly with a highly reduced intensity of GFP expression. These observations indicate the apoptosis/necrosis-inducing potential of compound **4.1** in MDA-MB-231 cells. Considering the high rate of metastasis of TNBC cells, the anti-migratory activity of compound **4.1** (5.0 and 15.0 µM) was studied using a scratch assay. While the cells migrated to the scratched area and almost compensated the vacant spaces over 48 h in the absence of the compound (DMSO control), prevention of such migration was observed in the presence of compound **4.1** in a dose-dependent manner over time (Figures 4.3e and 4.3f). These results indicate the anti-migratory activity of compound **4.1** towards MDA-MB-231

cells. A similar anti-migratory activity of TNBC cells by a benzimidazole-based organoselenocyanate has been reported recently (Figures 4.3e and 4.3f).[19]

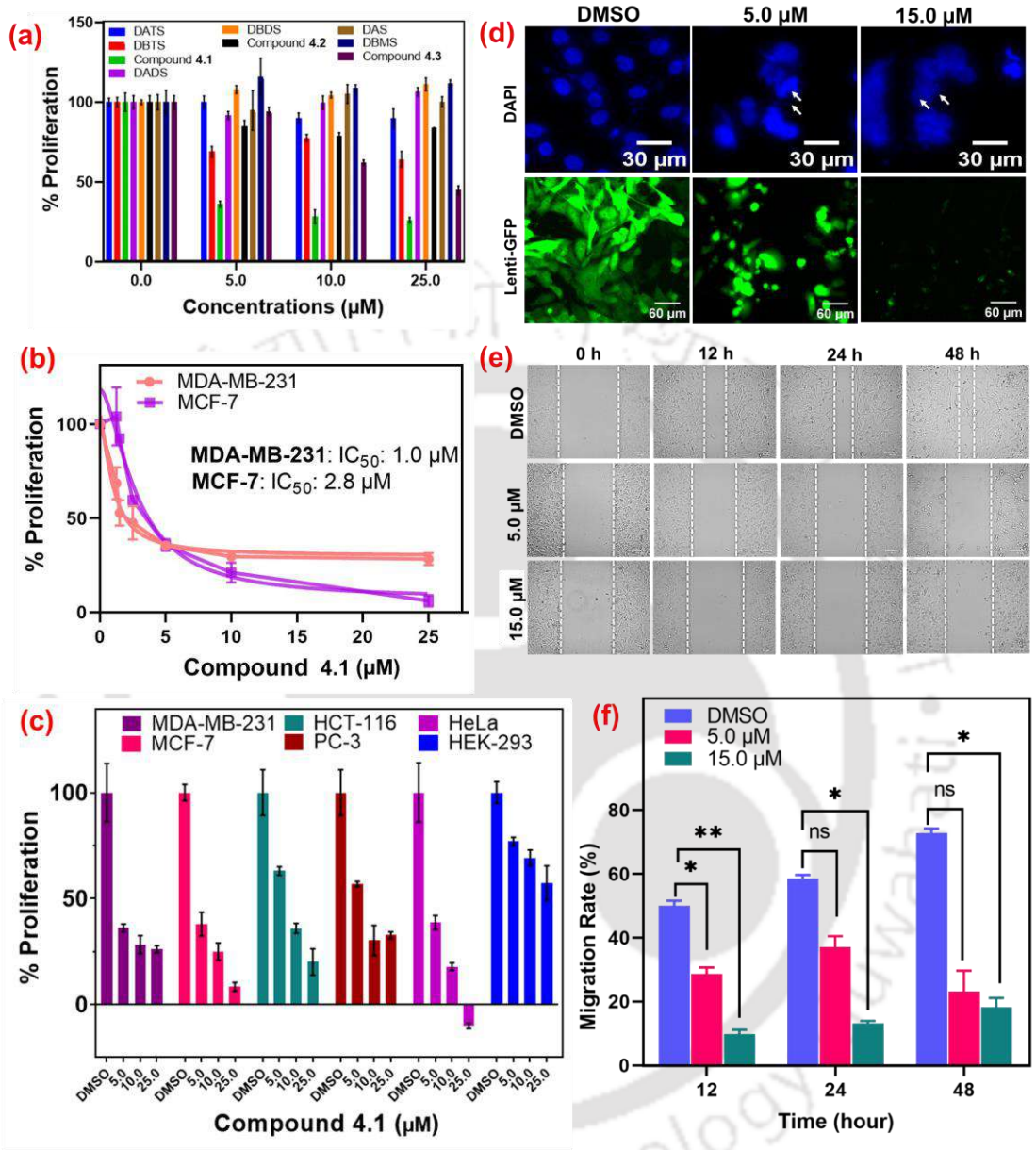

Figure 4.3. (a) Anti-proliferative activity of test compounds (5.0, 10.0 and 25.0 μM) in MDA-MB-231 cells after an incubation for 48 h. (b) Determination of IC_{50} value of compound **4.1** in MDA-MB-231 and MCF-7 cells. (c) Anti-proliferative activity of compound **4.1** in different organ-specific cell lines (MDA-MB-231, MCF-7, HCT-116, PC-3, HeLa and HEK-293) after an incubation for 48 h. (d) Visualization of nuclear morphological changes of MDA-MB-231 cells upon the treatment of compound **4.1** (5.0 and 15.0 μM) for 48 h followed by the staining with DAPI (3.0 nM). Scale bar represents 30 μm; Evaluation of cellular morphology in lentivirus-transduced MDA-MB-231 cells stably expressing GFP upon the treatment of compound **4.1** (5.0 and 15.0 μM) for 48 h.

Scale bar: 60 µm. (e) The anti-migratory activity of compound **4.1** (5.0 and 15.0 µM) in MDA-MB-231 cells at different time intervals (0, 12, 24 and 48 h). Scale bar: 100 µm. (f) Bar plot of anti-migratory effect of compound **4.1** in MDA-MB-231 cells. Experiments were performed in n = 3 replicates. The quantitative data shown are mean ± SD (n=3). **p*<0.05; ***p*<0.01. *p* values < 0.05 were considered statistically significant based on the one-way ANOVA.

4.3.3. Modulation of cell cycle of TNBC cells by compounds 4.1 and 4.2

As proper regulation of the cell cycle is crucial for the cellular homeostasis and cellular development, it is important to modulate different phases of cell cycle to control the proliferation and progression of cancer cells. To understand the impact of compound **4.1** on the cell cycle of MDA-MB-231 cells, the cellular distribution was analyzed by flow cytometry using the fluorogenic dye propidium iodide (PI). Cell cycle distribution was studied upon the incubation of cells with compound **4.1** (2.5, 5.0 and 10.0 µM) for 48 h. As shown in Figure 4.4a and Figure 4.4c, a noticeable alteration of cellular distribution was observed in the presence of compound **4.1**. Interestingly, the cellular population at G2/M phase was considerably enhanced in the presence of compound **4.1**, and the population of cells in G1 phase was decreased accordingly. For example, the cellular population in G2/M phase is increased to 34.1 ± 12.1% and 55.4 ± 11.6% from 13.1 ± 0.3% in the presence of 5.0 and 10.0 µM of compound **4.1**, respectively. Similarly, the population in G1 phase decreased to 30.1 ± 13.0% and 15 ± 8.5% from 56.4 ± 0.9% in the presence of 5.0 and 10.0 µM of compound **4.1**, respectively. These results clearly indicate the cell cycle arresting (in G2/M phase) ability of compound **4.1** (Figure 4.4a and Figure 4.4c). A similar G2/M phase arrest by DATS in C6 and U87 cells was reported by Tao and co-workers in 2017.[9] In contrast to the trisulfide **4.1** the corresponding disulfide **4.2** did not exhibit any G2/M phase arresting activity, rather it induced G1 phase arrest with a significant decrease in G2/M phase population at 10.0 µM concentration (Figures 4.4b and 4.4d). It is well established that two important checkpoint markers for G1 to S phase progression are regulated by Cyclin D, Cyclin E and their CDKs.[20] They promote the G1 to S phase transition through retinoblastoma phosphorylation and E2F-dependent gene induction. Accumulation of Cyclin D1 regulates G1 progression, which is crucial for DNA synthesis and cellular proliferation.[21] Therefore, with the information of G2/M phase arrest by compound **4.1**, the expression level of Cyclin D1 was examined using western blot analysis.

Interestingly, as shown in Figure 4.4e, a significant down-regulation of Cyclin D1 expression in MDA-MB-231 cells was observed by compound **4.1** in a dose-dependent manner. The down-regulation of Cyclin D1 is well correlated with the cell cycle distribution, in which a dose-dependent inhibition of G1 to S phase progression was markedly observed (Figures 4.4e and 4.4g). Furthermore, no significant changes in the expression level of Cyclin D1 was observed for compound **4.2** in the Western blot experiment (Figure 4.4f). These observations indicate the probable mechanistic differences in their mode of action in TNBC cells.

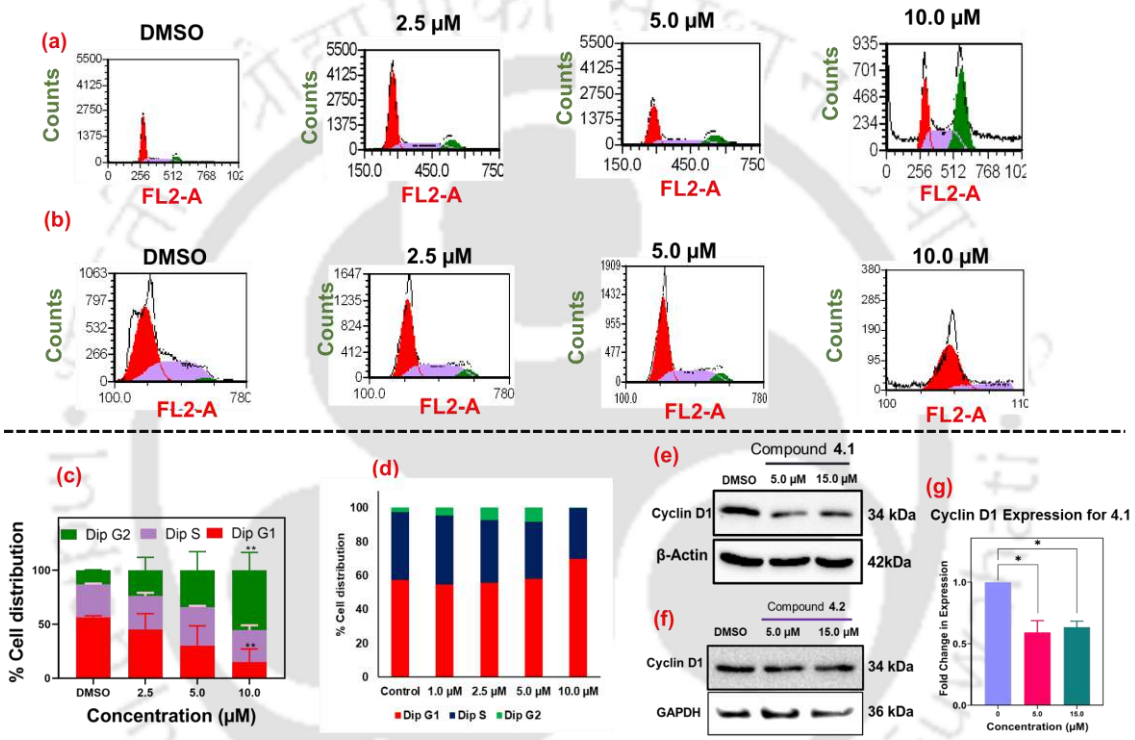

Figure 4.4. (a, b) Cell cycle analysis of MDA-MB-231 cells in the presence of compounds **4.1** and**4.2** (2.5, 5.0, 10.0 µM) upon an incubation for 48 h. (c, d) Cell cycle distribution plot for **4.1** and **4.2**, respectively. (e, f) Western blot analysis for the estimation of Cyclin D1 expression in MDA-MB-231 cells in the presence of compounds **4.1** and **4.2** (5.0 and 15.0 µM) for 48 h, respectively. (g) Bar diagram of cyclin D1 expression upon treatment of compound **4.1**. Equal protein loading was confirmed by the analysis of β-Actin expression. Experiments were performed in n = 2 replicates. The quantitative data shown are mean ± SD (n=2). **p*<0.05; ***p*<0.01. *p* values < 0.05 were considered to be statistically significant based on the one-way ANOVA.

4.3.4. Apoptosis study and the expression of key cancer marker proteins in TNBC

With the understanding of potent anti-proliferative activity of compound **4.1**, we next investigated the mode of cell death (apoptosis/necrosis) for its anti-proliferative activity in MDA-MB-231 cells. The TNBC cells were incubated with compound **4.1** (0.0, 2.5, 5.0 and 10.0 μM) for 48 h and subsequently stained with FITC-conjugated Annexin V/PI and analyzed using flow cytometry. As shown in Figure 4.5a, compound **4.1** induced late apoptosis in a dose-dependent manner. For example, while only around 6% of cells underwent late apoptosis in the absence of compound **4.1** (DMSO control), the PI population increased to 18% and 29% in the presence of 5.0 and 10.0 μM of compound **4.1**, respectively. The changes in the cellular population in the Annexin V channel were insignificant (Figure 4.5a), indicating the late apoptosis-inducing activity of compound **4.1** in MDA-MB-231 cells. Next, the changes in expression level of some key marker proteins (Bcl2, Survivin, Procaspase 3 and COX-2) associated with cancer progression and apoptosis were evaluated in the presence of compound **4.1** (5.0 and 15.0 μM) upon an incubation for 48 h. Interestingly, the level of Bcl2 and Survivin were found to be down-regulated in the presence of compound **4.1** in a dose-dependent manner (Figure 4.5c). Similarly, the expression level of Procaspase 3, a zymogen of caspase 3, responsible for apoptosis, was also down-regulated in the presence of compound **4.1**. Moreover, compound **4.1** induced the down-regulation of COX-2 expression in a dose-dependent manner. It is noteworthy that, the expression of COX-2 is regulated by the Wnt/β-catenin signaling *via* upregulating the β-catenin level.[22] Therefore, the down-regulation of COX-2 level by compound **4.1** could possibly be correlated with the β-catenin expression and regulation. Moreover, the COXIB family of drugs, which are selective inhibitors of COX-2, are reported to have a potent effect on the downstream transcription factors such as Axin and c-Myc, which are important players in the Wnt/β-catenin signaling cascade.[23] Therefore, it was important to understand the regulation of Wnt/β-catenin signaling pathway in the presence of compound **4.1**. It has also been reported that, the down-regulation of Cyclin D1 followed by the G2/M phase arrest is also mediated by the overproduction of intracellular ROS levels (Figures 4.4c and 4.5b).[24] Therefore, the ROS-inducing ability of the trisulfide **4.1** was studied using the conventional DCFDA fluorogenic assay. Herein, MDA-MB-231 cells were pre-incubated with compound **4.1** (5.0 and 15.0 μM) over 12 h, and the ROS-inducing ability was qualitatively visualized by monitoring the fluorescence emission of DCF dye

using fluorescence microscopy (Figure 4.5b). The enhanced emission intensity of the cells was observed in the presence of compound **4.1** in a dose-dependent manner, indicating the ROS-inducing capacity of **4.1**, which is well correlated with the significant down-regulation of Cyclin D1. A similar enhancement of ROS was also observed upon the treatment of cells with 1% H_2O_2. Furthermore, the enhancement of the ROS-level by **4.1** (15.0 µM) could be quenched upon the subsequent treatment of the antioxidant NAC (2.0 mM).

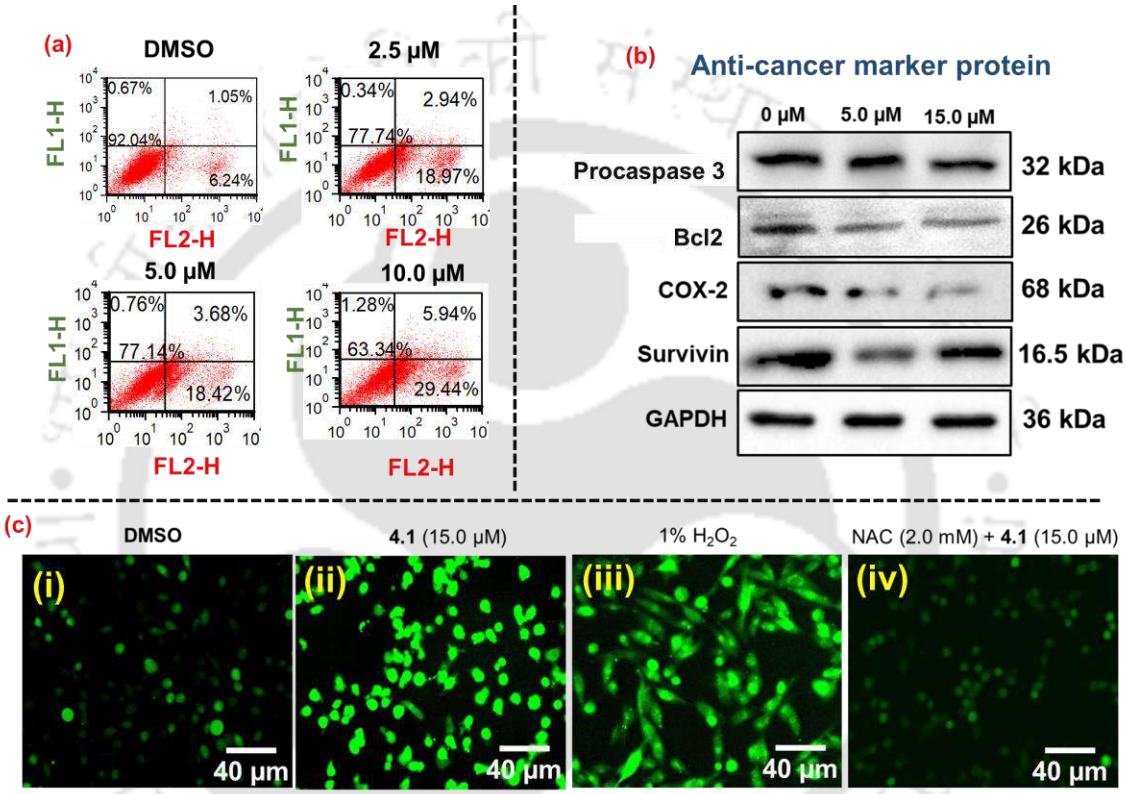

Figure 4.5. (a) Detection of apoptosis of MDA-MB-231 cells by Annexin V/PI double-stained flow cytometric assay in the presence of compound **4.1** (2.5, 5.0 and 10.0 µM) upon an incubation for 48 h. (b) Western blot for estimating the expression of key marker proteins in MDA-MB-231 cells in the presence of compound **4.1** (5.0 and 15.0 µM) for 48 h. Equal protein loading was confirmed by the analysis of GAPDH expression. (c) Visualization of the intracellular level of ROS in MDA-MB-231 cells in the presence of compounds **4.1** (15.0 µM) with an incubation of 12 h. (i) DMSO control; (ii) compound **4.1** (15.0 µM); (iii) 1% H_2O_2; (iv) compound **4.1** (15.0 µM) followed by NAC (2.0 mM). (i) DMSO control; (ii) compound **4.1** (15.0 µM); (iii) 1% H_2O_2; (iv) compound **4.1** (15.0 µM) followed by the NAC (2.0 mM). Scale bar represents 40 µm.

4.3.5. Regulation of Wnt/β-catenin signaling by compound 4.1

To understand the impact of trisulfide **4.1** on the regulation of Wnt/β-catenin signaling in MDA-MB-231 cells, the expression of β-catenin and c-Myc (Wnt/β-catenin downstream signaling pathway protein) was studied. Interestingly, the incubation of MDA-MB-231 cells with compound **4.1** (5.0 and 15.0 μM) over 48 h led to a significant down-regulation of both β-catenin and c-Myc expression in a dose-dependent manner (Figures 4.6a and 4.6b). A similar down-regulation of β-catenin and c-Myc expression by compound **4.1** was also observed in another Wnt-dependent ER+ breast cancer cell line such as MCF-7 (Figures 4.6c and 4.6d). However, no such inhibition of β-catenin expression was observed in the presence of the corresponding disulfide analogue **4.2** (Figure 4.6e). These observations indicate the possible selectivity of a trisulfide moiety towards the Wnt/β-catenin signaling pathway. As compound **4.1** mediated the down-regulation of β-catenin level, the expression of β-catenin in the sub-cellular compartments such as the cytoplasm and nucleus was investigated next using subcellular fractionation. Upon the treatment of MDA-MB-231 cells with compound **4.1**, the cytoplasmic and nuclear fractions were extracted at different time courses (12 h, 24 h and 48 h) and the level of β-catenin in both the fractions was analyzed by Western blot analysis. As shown in Figure 4.6f, the expression of total β-catenin is noticeably decreased in the presence of compound **4.1** (5.0 μM) in both cytoplasm and nucleus as compared to that of the untreated control. Moreover, analysis of β-catenin level at different time intervals provided important information about the nuclear translocation of β-catenin. For example, while the nuclear translocation was found to be partial after 12 h, the translocation was almost complete by 24 h as the level of cytoplasmic β-catenin was found to be nominal at 24 h and 48 h (Figure 4.6f). As the total β-catenin in the nucleus was relatively low in the presence of compound **4.1**, the observation is in agreement with the overall down-regulation of the downstream transcription factors (c-Myc and Cyclin D1) in the whole-cell lysate (Figures 4.4c, 4.4d, and 4.6a). A similar down-regulation of c-Myc and Cyclin D1 expression was also observed for the inhibition of breast cancer stem cells by DATS that followed Wnt/β-catenin signaling pathway.[11]

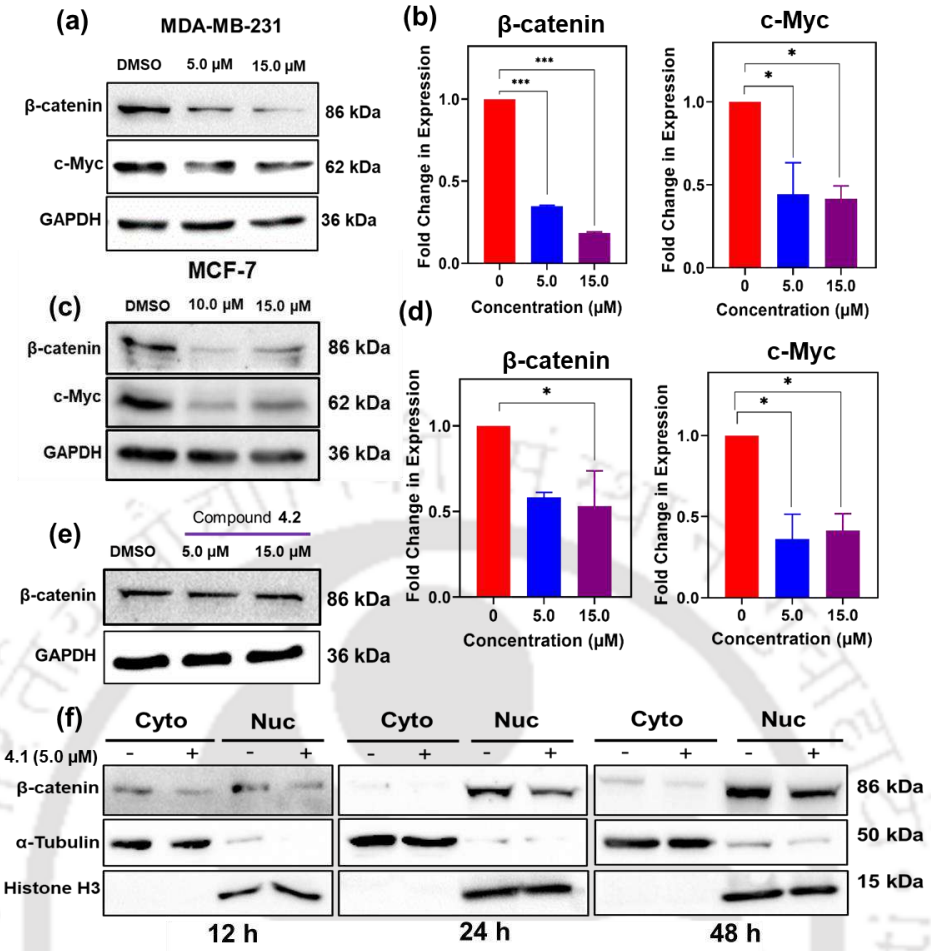

Figure 4.6. Western blot analysis for the estimation of β-catenin and c-Myc expressions in (a-b) MDA-MB-231 cells and (c-d) MCF-7 cells in the presence of compound **4.1** (5.0 and 15.0 μM) for 48 h. Experiments were performed in n = 2 replicates. The quantitative data shown are mean ± SD (n=2). **p*<0.05; ***p*<0.01, ****p*<0.001. *p* values < 0.05 were considered statistically significant based on the one-way ANOVA. GAPDH was taken as a loading control. (e) Western blot analysis for the estimation of β-catenin expression levels in MDA-MB-231 cells upon the treatment of compound **4.2**. GAPDH housekeeping was used as loading control. (f) Western blot for the estimation of β-catenin expression levels in sub-cellular fractions (cytoplasm and nucleus) of MDA-MB-231 cells in the presence of compound **4.1** (5.0 μM) at different time intervals (12 h, 24 h and 48 h). Histone-H3 and α-Tubulin were taken as loading controls for nucleus and cytoplasm, respectively.

4.3.6. Mechanistic insights for the inhibition of β-catenin by compound 4.1

To understand the underlying mechanism of the β-catenin down-regulation in the presence of compound **4.1**, we have examined the proteins involved in the Wnt/β-catenin

signaling cascade. Generally, GSK-3β negatively regulates the total β-catenin level by inducing the phosphorylation at serine/threonine residues of the N-terminal.[25] The phosphorylated β-catenin undergoes subsequent proteasomal degradation. With the initial results that compound **4.1** induced a significant down-regulation of β-catenin expression as well as its target genes such as c-Myc and Cyclin D1, the involvement of GSK-3β was investigated in the presence of a classical GSK-3β inhibitor i.e., lithium chloride (LiCl).[10] An optimal dose of LiCl activates the Wnt/β-catenin signaling by inhibiting the expression of GSK-3β through phosphorylation at Ser9 residue.[11] The treatment of MDA-MB-231 cells with LiCl (20.0 mM) led to an elevation of β-catenin level as the GSK-3β-mediated phosphorylation of β-catenin was probably hampered (Figure 4.7a). In contrast, the treatment of cells with compound **4.1** alone or in combination with LiCl led to a decrease in β-catenin level, although the expression level of total GSK-3β was almost unaltered (Figure 4.7a).[11] These results indicate that the activation of Wnt/β-catenin signaling by LiCl can be suppressed by compound **4.1**. A similar suppressing effect for LiCl-induced Wnt/β-catenin signaling was also observed for the garlic-based trisulfide DATS in breast cancer stem cells.[11] Unlike the opposing effect of LiCl and **4.1** on the level of β-catenin, down-regulation of the expression of Cyclin D1 was observed in the presence of both (Figure 4.7a). A similar down-regulation of Cyclin D1 expression in RPMI-8226 cells in the presence of LiCl (40.0 mM) was reported by Yao and co-workers.[26] As the down-regulation of Cyclin D1 expression is associated with the arrest in G2/M phase, the effect of LiCl on the distribution of cell cycle (MDA-MB-231 cells) was analyzed. Similar to compound **4.1**, LiCl (20.0 mM) alone and in combination with compound **4.1**, noticeably enhanced the population of cells in the G2/M phase (Figure 4.7b). These results indicate that, both LiCl and compound **4.1** down-regulate Cyclin D1 and arrest cells in G2/M phase. The inactivation of Wnt/β-catenin signaling and the down-regulation of β-catenin level by compound **4.1** prompted us to investigate the role of proteasomes. A down-regulation of β-catenin could be possible by promoting the phosphorylation of β-catenin followed by the possible proteasomal degradation, instead of its nuclear translocation. To test this possibility, the expression of β-catenin in MDA-MB-231 cells was studied in the presence of a known and selective proteasomal inhibitor (R)-MG132 (selective 26s proteasome inhibitor).[14c] As shown in Figure 4.7c, an up-regulation of β-catenin expression was observed in the presence of (R)-MG132 (40.0 μM) in a time-dependent

manner (2 h, 4 h and 6 h), and a significant up-regulation of β-catenin expression was observed after 4 h. To understand the effect of compound **4.1** on the proteasomal degradation, we studied the expression of β-catenin in the presence of (R)-MG132 alone and in combination with compound **4.1**. As the down-regulation and up-regulation of β-catenin was observed in the presence of compound **4.1** (5.0 µM) and (R)-MG132 (40.0 µM) alone, respectively, their combined impact on the expression of β-catenin in MDA-MB-231 cells was studied further. This was performed in three different manners with 5 h intervals such as pre-treatment (**4.1** was treated before), co-treatment (treated together) and post-treatment ((R)-MG132 was treated before) followed by an incubation for 24 h. From the Western blot analysis, it is evident that the proteasomal degradation induced by compound **4.1** was substantially suppressed by (R)-MG132 with a resultant elevation of β-catenin level (Figure 4.7d). Furthermore, the proteasomal inhibition led to an up-regulation of the downstream signaling gene such as c-Myc. These observations confirm the probable promotion of GSK-3β-mediated phosphorylation of β-catenin by compound **4.1** and subsequent proteasomal degradation as the major pathway for the inactivation of the Wnt/β-catenin signaling (Figure 4.1).

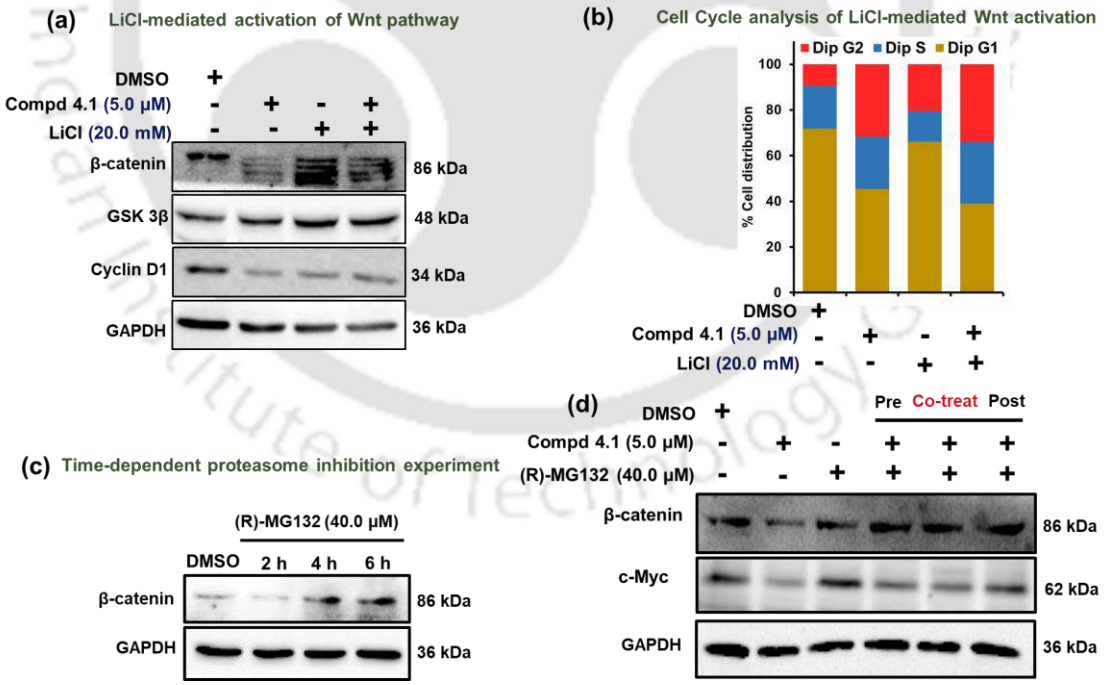

Figure 4.7. (a) LiCl-induced inhibition of GSK-3β. Western blot for the estimation of β-catenin, GSK-3β and Cyclin D1 in MDA-MB-231 cells by compound **4.1** in the presence and absence of 20.0 mM of LiCl for 12 h. (b) Cell cycle analysis of MDA-MB-231 cells in the presence and absence of compound **4.1** (5.0 µM) and LiCl (20.0 mM) after 24 h of

the incubation. (c) Expression of β-catenin in MDA-MB-231 cells at different time intervals upon the treatment of (R)-MG132 (40.0 μM). (d) Estimation of β-catenin and c-Myc in the presence of (R)-MG132 (40.0 μM) and compound **4.1** (5.0 μM) at various sequences of treatment; ***Pre***: compound **4.1** was treated before 5 h of (R)-MG132; ***Co-treat***: compound **4.1** and (R)-MG132 were treated together; ***Post***: (R)-MG132 was treated 5 h before compound **4.1**. GAPDH was taken as a loading control.

4.3.7. Feasibility of H_2S donation from compound 4.1, DBTS and DATS

With the confirmation of potent anti-proliferative activity of trisulfide **4.1** in TNBC cells *via* the inactivation of Wnt/β-catenin signaling, we next elucidated the structural aspects of compound **4.1** and their possible implications for the observed anti-proliferative activities. Considering the feasibility of H_2S release from the natural and synthetic trisulfides in the presence of biothiols, the H_2S donation from compound **4.1** (25.0 μM) was studied using methylene blue (MB) assay and was compared to that of DATS (25.0 μM) and DBTS (25.0 μM). As shown in Figure 4.8a, both DBTS and **4.1** exhibited sustained H_2S release profiles in the presence of GSH, although the release profiles were significantly lower than that of DATS. A similar difference in H_2S donation feasibility was also reported earlier for the DBTS and DATS as well as 4-methyl-substituted benzylic trisulfide and DATS in the presence of GSH.[15, 18] The GSH-responsive release of H_2S from compound **4.1** was validated further using the reported and selective turn-on fluorogenic sensor of H_2S **WSP2** (10.0 μM).[27] As shown in Figure 4.8b, a remarkable enhancement in the fluorescence emission intensity upon the reaction of released H_2S from compound **4.1** + GSH with **WSP2** was observed. The probe **WSP2**, which is known as a selective sensor of H_2S, is known to react selectively with H_2S and undergo intramolecular cyclization with the release of free fluorophore (Figure 4.8c). The feasibility of H_2S release from compound **4.1** was then investigated in MDA-MB-231 cells using **WSP2**. Treatment of cells with **WSP2** (5.0 μM) led to the turn-on fluorescence emission under the blue channel, indicating the presence of intracellular level of H_2S. Interestingly, a further enhancement of emission intensity in the presence of compound **4.1** indicated the exogenous donation of H_2S from compound **4.1** in the presence of intracellular GSH (Figures 4.8c and 4.8d). Involvement of endogenous GSH for triggering the H_2S release from compound **4.1** and also the participation of endogenous H_2S for the fluorescence turn-on was validated further with the evidence of very weak emission upon the pre-treatment of cells with *N*-ethylmaleimide (NEM,

scavenger of biothiols) and *D,L*-propargyl glycine (PAG, inhibitor of cystathionine γ-lyase). These observations reveal the H_2S donating capacity of compound **4.1** in the cellular medium (Figure 4.8d).

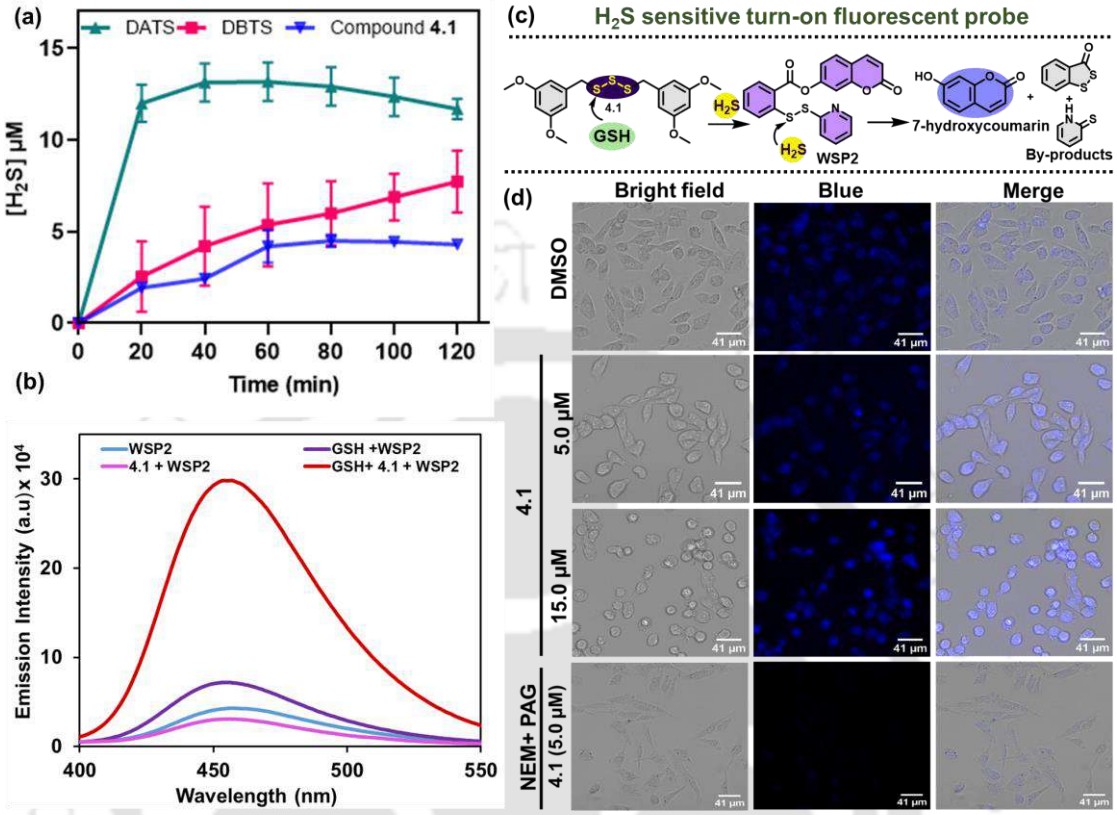

Figure 4.8. (a) Determination of H_2S release profile of DATS (25.0 µM), DBTS (25.0 µM) and **4.1** (25.0 µM) in the presence of GSH (500.0 µM) over 120 min using the MB assay. (b) Emission spectra of **WSP2** (10.0 µM) upon the reaction with the released H_2S from compound **4.1** (15.0 µM) in the presence and absence of GSH (500.0 µM) in phosphate buffered saline (20.0 mM) of pH 7.4 after an incubation of 60 min. (c) Schematic representation of H_2S release from compound **4.1** and its reaction with **WSP2** with turn-on fluorescence. (d) Fluorescence microscopic images (bright field, blue channel and merged) for the detection of released H_2S from compound **4.1** (5.0 and 15.0 µM) in MDA-MB-231 cells using the H_2S-selective probe **WSP2** (5.0 µM). In the control experiment, cells were incubated with NEM (2.0 mM) and PAG (50.0 µM) for 2 h and subsequently compound **4.1** (5.0 µM) was added. The scale bar represents 41 µm.

4.3.8. Sustained release of H_2S from organic donors and its anti-proliferative activity

It has been well-established that, in contrast to the instantaneous donors of H_2S that promote proliferation, sustained donors of H_2S rather induce anti-proliferative activity to cancerous cells without affecting the healthy normal cells.[4] For example, the potent anti-proliferative activity in several organ-specific cancer cells has been reported for the organosulfur compound GYY4137, which is known to release H_2S in a sustained manner.[28] The anti-cancer activity of garlic-based trisulfide DATS has also been studied in different organ-specific cell lines, including breast cancer.[6] To elucidate the role of released H_2S from the organotrisulfide-based compounds towards the growth profile of MDA-MB-231 cells, we have chosen two organotrisulfides such as DATS (a fast donor of H_2S) and compound **4.1** (slow and sustained donor of H_2S). The cellular viability and the expression level of few key oncogenic marker proteins were analyzed using MTT and Western blot analyses, respectively. Interestingly, while compound **4.1** exhibited potent anti-proliferative activity at 15.0 µM concentration, DATS did not show any noticeable anti-proliferative activity at that concentration, and even it was found to be almost inactive at 100.0 µM concentrations under the identical condition (Figure 4.9a). This indicates the importance of the controlled release of H_2S from the organic donors for an effective anti-proliferative activity. Moreover, the garlic-based compounds DADS and DAS, which do not release any H_2S, were also found to be almost inactive at 100.0 µM concentration. With the previous reports on the cytoprotective and chemopreventive activity of DATS in the literature,[29] we have investigated this property using the combined treatment strategy. The cellular viability of MDA-MB-231 cells was studied with compound **4.1** (15.0 µM) in combination with DATS (100.0 µM), DADS (100.0 µM) and DAS (100.0 µM). Interestingly, although DADS and DAS could not alter the cellular viability, the combination of DATS with compound **4.1** could significantly increase the cellular viability of MDA-MB-231 cells (Figure 4.9a). This observation clearly indicates the cytoprotective activity of DATS, unlike the analogous disulfide (DADS) and the monosulfides (DAS). The changes in the expression of oncogenic proteins such as Bcl2, Survivin and GSK-3β in MDA-MB-231 cells by compound **4.1** (15.0 µM) was studied alone as well as in combination with 100.0 µM of DATS, DADS and DAS using Western blot analysis. While the expression of Bcl2 was down-regulated by compound **4.1**, it was found to be compensated by the addition of DATS. However,

unlike the trisulfide (DATS), the analogous disulfide (DADS) and monosulfide (DAS) could not alter the down-regulation of Bcl2 induced by compound **4.1**. This is in agreement with the observation in the MTT assay that the combination of compound **4.1** with DATS significantly enhanced the cellular viability (Figure 4.9b). This could be associated with the impact of rapidly released H_2S from DATS, which is not feasible from DADS and DAS. The contrasting behavior was also observed on the expression level of Survivin. While both DADS and DAS did not significantly alter the expression of Survivin in MDA-MB-231 cells, its down-regulation was observed in the presence of DATS as well as compound **4.1** alone (Figures 4.9c and 4.9d). However, the level was found to be comparable to that of the control in the combined treatment of compound **4.1** and DATS (Figure 4.9b).

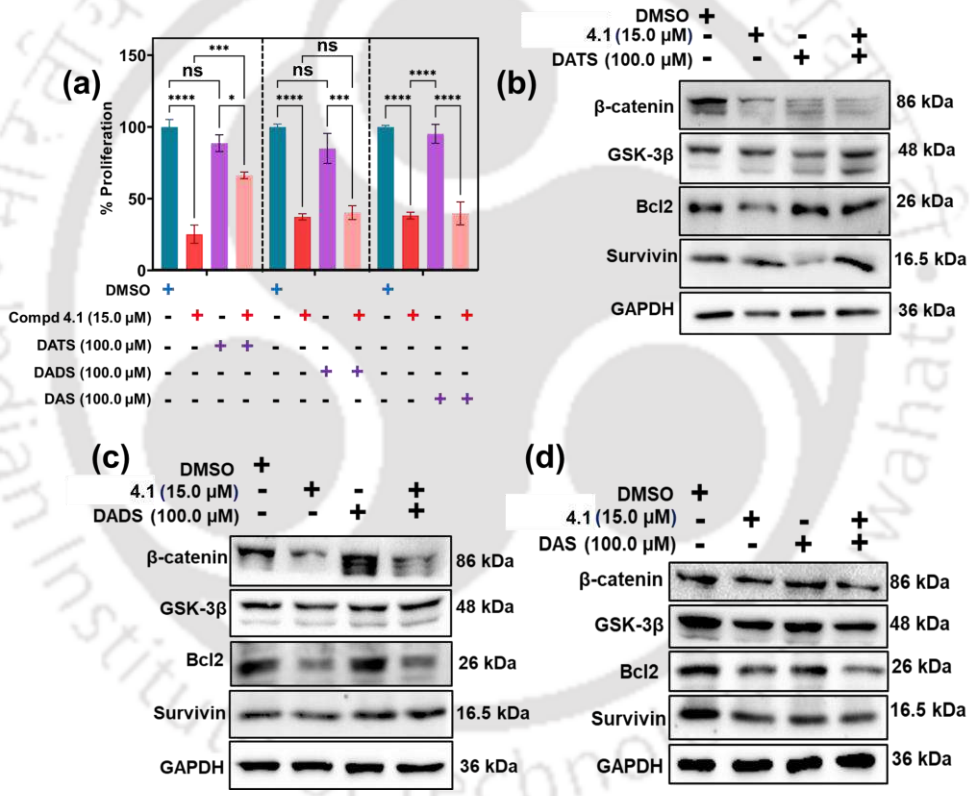

Figure 4.9. (a) Anti-proliferative activity of compounds **4.1**, DATS, DADS and DAS alone and in combination against MDA-MB-231 cells after 48 h of incubation. Experiments were performed in n = 2 replicates. The quantitative data shown are mean ± SD (n=2). **p*<0.05; ***p*<0.01, ****p*<0.001, ****p*<0.0001. *p* values < 0.05 were considered to be statistically significant based on the one-way ANOVA. (b-d) Western blot for the estimation of β-catenin, GSK-3β, Bcl2, and Survivin, upon the treatment of **4.1**, DATS, DADS and DAS alone or in combination. GAPDH was taken as a loading control.

To understand the contribution of the generated thiol intermediate **4.5** from the trisulfide **4.1** towards the observed anti-cancer activity of **4.1**, the thiol intermediate **4.5** was prepared and purified. The preliminary anti-proliferative activity of the intermediate **4.5** in MDA-MB-231 cells was evaluated using MTT assay. As shown in figure 4.10B, compound **4.5** did not exhibit any anti-proliferative activity up to 25.0 μM concentration. To further understand the possible impact of this intermediate on the expression level of key marker proteins, Western blot was carried out in the presence of compound **4.5** (5.0 and 15.0 μM) and the expression of Wnt/β-catenin signaling (β-catenin, c-Myc, and Cyclin D1) and oncogenic marker proteins (Bcl2 and Survivin) was analyzed. However, unlike trisulfide **4.1**, compound **4.5** did not alter the expression level of the targeted marker proteins (Figures 4.10A and 4.10C). These observations reveal very minimum contribution of the generated thiol intermediate **4.5** towards the overall anti-cancer activity of the trisulfide **4.1** in MDA-MB-231 cells. The control experiments further emphasize the major contributions of the generated H_2S or the corresponding perthiol (intermediate 2, Figure 4.10A) towards the overall anti-cancer activity of compound **4.1**.

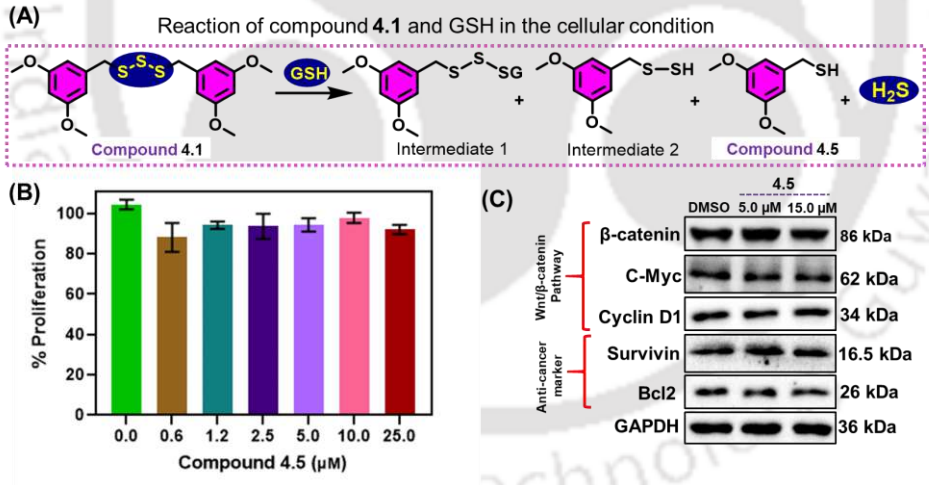

Figure 4.10. (A) Plausible reaction mechanism for the reaction of compound **4.1** with biothiol in the cellular condition. (B) Anti-proliferative activity of compound **4.5** in MDA-MB-231 cells at 5.0, 10.0 and 25.0 μM concentrations after an incubation for 48 h. Western blot analysis for the estimation of Wnt/β-catenin and anti-cancer marker protein expression levels in MDA-MB-231 cells upon treatment of compound **4.5**. GAPDH housekeeping was taken as loading control.

The role of a trisulfide linker on the down-regulation of β-catenin level was confirmed after performing several control experiments with compound **4.1**, the analogous DBTS, and the known garlic-based organosulfur compounds such as DATS, DADS and DAS. Interestingly, while, a down-regulation of β-catenin was observed in the presence of compound **4.1** and DATS and DBTS having trisulfide moieties (Figures 4.9b, 4.11a and 4.11b), the level of β-catenin was almost unaltered in the presence of disulfide **4.2** (Figure 4.6e), DADS and DAS (Figures 4.9b and 4.9c). These results clearly highlight the importance of a trisulfide moiety in compound **4.1** and analogous compounds in down-regulating the expression of β-catenin in MDA-MB-231 cells. Similarly, upon treatment with DBTS in MDA-MB-231 cells significant down-regulation of c-Myc has been observed after 48 h of treatment. With this information, we performed *in silico* docking studies to determine the binding affinity of compound **4.1** with β-catenin-TCF-4 complex (PDB: 2GL7)[30] and compared that with MSAB, which is the reported selective inhibitor of β-catenin.[14c] Interestingly, compound **4.1** exhibited good binding affinity with the β-catenin-TCF-4 complex, assisted by multiple non-bonding interactions (Figure 4.11c and 4.11d). Moreover the affinity of compound **4.1** towards β-catenin was found to be slightly higher than the DBTS, which did not have any non-bonding interaction with the proximal amino acids.

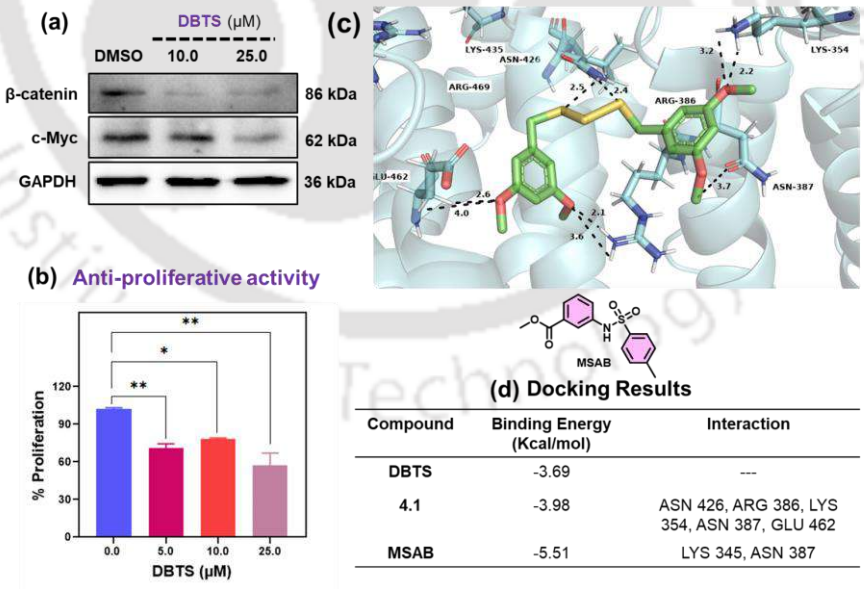

Compound	Binding Energy (Kcal/mol)	Interaction
DBTS	-3.69	---
4.1	-3.98	ASN 426, ARG 386, LYS 354, ASN 387, GLU 462
MSAB	-5.51	LYS 345, ASN 387

Figure 4.11. (a) Western blot analysis for the estimation of β-catenin and c-Myc expression levels in MDA-MB-231 cells upon treatment of DBTS for the incubation period of 48 h. GAPDH was taken as a loading control. (b) Estimation of the anti-proliferative activity of DBTS against MDA-MB-231 after 48 h of incubation.

Experiments were performed in n = 2 replicates. The quantitative data shown are mean ± SD (n=2). **p*<0.05; ***p*<0.01, *p* values < 0.05 were considered to be statistically significant based on the one-way ANOVA. (c) Molecular docking experiment of compound **4.1** and MSAB with β-catenin-TCF-4 complex (**PDB**: **2GL7**). (d) Consolidated docking result of compound DBTS, **4.1** and MSAB highlighting the non-bonded interactions with the proximal amino acids of β-catenin-TCF-4 complex.

4.3.9. Modulation of p53 and P21 expression by the released H_2S from compound 4.1

It is well documented that the sustained donation of H_2S from organic donors are associated with the anti-proliferation of cancer cells. In 2018, Jurkowska *et al*. have reported the anti-proliferative activity of 4-hydroxybenzyl isothiocyanate (HBITC), which acts as a sustained donor of H_2S.[31] The anti-proliferative activity of human neuroblastoma cells (SH-SY5Y) by HBITC was shown to be associated with the down-regulation of p53 expression and an up-regulation of p21 expression. The released H_2S from HBITC was reported to play important role in the S-sulfhydration of the sulfhydryl groups of p53 protein. Therefore, to understand the direct impact of the released H_2S from compound **4.1** and DATS on the expression level of p53 and p21 proteins, MDA-MB-231 cells were incubated with compound **4.1** (15.0 µM) and DATS (100.0 µM) alone or in combination for 48 h and the protein expression was measured. A significant down-regulation of p53 expression was observed in MDA-MB-231 cells in the presence of both compound **4.1** and DATS (Figure 4.12a). Moreover, the down-regulation of p53 was further enhanced upon their combined treatment. This could be correlated with the H_2S-induced S-sulfhydration of the sulfhydryl groups of p53 followed by its proteasomal degradation. A similar S-glutathionylation of p53 is also reported to take place under oxidative-stress conditions.[32] Therefore, the down-regulation of p53 by compound **4.1** *via* S-sulfhydration is not surprising as it releases H_2S (Figure 4.8) as well as induces ROS in MDA-MB-231 cells (Figure 4.5c). It has been reported that Glutathione-S-transferase P1 (GSTP1) is a downstream transcriptional gene, which is up-regulated by the wild-type p53 to combat xenobiotics. Moreover, the S-glutathionylation of p53 is reported to be catalyzed by the GSTP1 enzyme,[30, 33] which is up-regulated by DATS and DADS *via* ERK-AP-1 and JNK-AP-1 signaling pathways.[34] Therefore, to understand the impact of GSTP1 on the down-regulation of p53 and the possible S-glutathionylation in the presence of compound **4.1** and DATS, the expression of p53 was analyzed in the presence of a selective and potent inhibitor of GSTP1 (NBD-

HEX).[35] The cells were pre-treated with NBD-HEX (1.0 µM) for 12 h followed by the treatment with compound **4.1** (15.0 µM) and DATS (100.0 µM) for 48 h. Interestingly, it is evident from the Western blot that, NBD-HEX pre-treatment substantially increased the p53 expression level in comparison to the cells treated with compound **4.1** or DATS without any inhibitor (Figure 4.12b). This observation clearly indicates the induction of S-glutathionylation of p53 by GSTP1 expression, which is probably positively regulated by compound **4.1** or DATS. Similarly, a significant up-regulation of p21 expression was also observed upon the addition of compound **4.1** (Figure 4.12c). Importantly, a down-regulation of Cyclin D1 was also observed upon the treatment of compound **4.1** to MDA-MB-231 cells (Figure 4.12c). An up-regulation of p21 expression was also observed for DATS in PC-3 and DU145 cells. The up-regulation was well correlated with the G2/M phase arrest.[17] Therefore, the p53-independent up-regulation of p21 by compound **4.1** could possibly be one of the reasons for the G2/M phase arrest and the inhibition of cyclin D1.

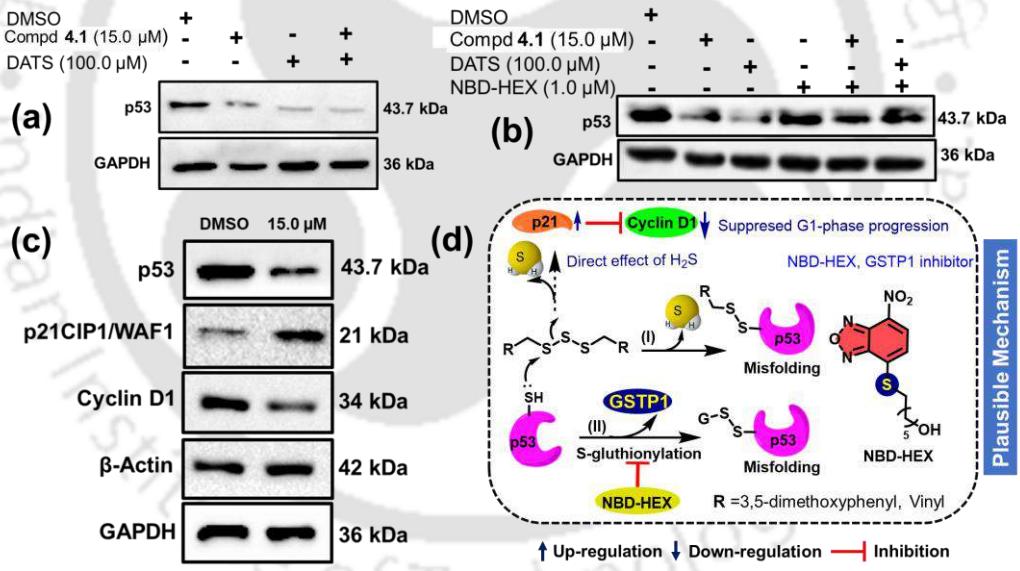

Figure 4.12. Impact of the released H_2S on the expression level of various proteins. Western blot for the estimation of (a) p53 in the presence or absence of compound **4.1** (15.0 µM) and DATS (100.0 µM) for 48 h; (b) p53 upon the pre-treatment of NBD-HEX (1.0 µM) for 12 h followed by compound **4.1** (15.0 µM) or DATS (100.0 µM) for 48 h. GAPDH and/or β-actin were taken as loading controls. (c) p53, p21CIP1/WAF1, and Cyclin D1 in the presence of compound **4.1** (15.0 µM) for 48 h; (d) Proposed schematics for the involvement of the released H_2S from compound **4.1** towards the

regulation of p53, p21CIP1/WAF1 and Cyclin D1. Proposed pathways of S-sulfhydration of p53 by compound **4.1** as well as GSTP1 is highlighted.

4.3.10. Proposed mechanistic pathway for the anti-proliferative activity of compound 4.1

The results of potent anti-proliferative activity followed by the understanding on detailed mechanistic studies with compound **4.1** and related analogues in MDA-MB-231 cells imply several key features. The results cumulatively indicate that compound **4.1** targets the canonical Wnt/β-catenin pathway *via* significant down-regulation of β-catenin expression. The down-regulation of β-catenin is mediated by GSK-3β-driven phosphorylation and the subsequent proteasomal degradation process. However, the suppression of β-catenin level could also be tuned by COX-2 expression. Moreover, the anti-proliferative activity of compound **4.1** was associated with the suppression of several oncogenic proteins such as procaspase 3, Bcl2, and Survivin. The cell cycle analysis revealed G2/M phase arrest by compound **4.1** with the down-regulation of Cyclin D1, which is one of the downstream regulators of mitosis and β-catenin. The impact of the released H_2S from compound **4.1** and DATS on several oncogenic proteins was studied by Western blot analyses and provided useful information. The induction of S-glutathionylation of p53 by GSTP1 expression, which is probably positively regulated by the released H_2S from compound **4.1** or DATS, could be suppressed using the potent inhibitor of GSTP1 (NBD-HEX). Compound **4.1** could also regulate the expression of p53 by direct S-sulfhydration process. Considering these deciphering events, a mechanistic pathway for the overall anti-cancer activity of compound **4.1** against the TNBC cells is proposed in Scheme 4.2. In addition to the generation of H_2S from the trisulfide **4.1**, formation of the corresponding persulfide could also take place. The generated persulfide can react directly with the oxidized proteins for the protein post-translational modifications or it can react with the possible biologically relevant radicals *via* H-atom transfer (HAT) reactions as reported by Pratt and co-workers.[36] However such reactions were not investigated in the present study.

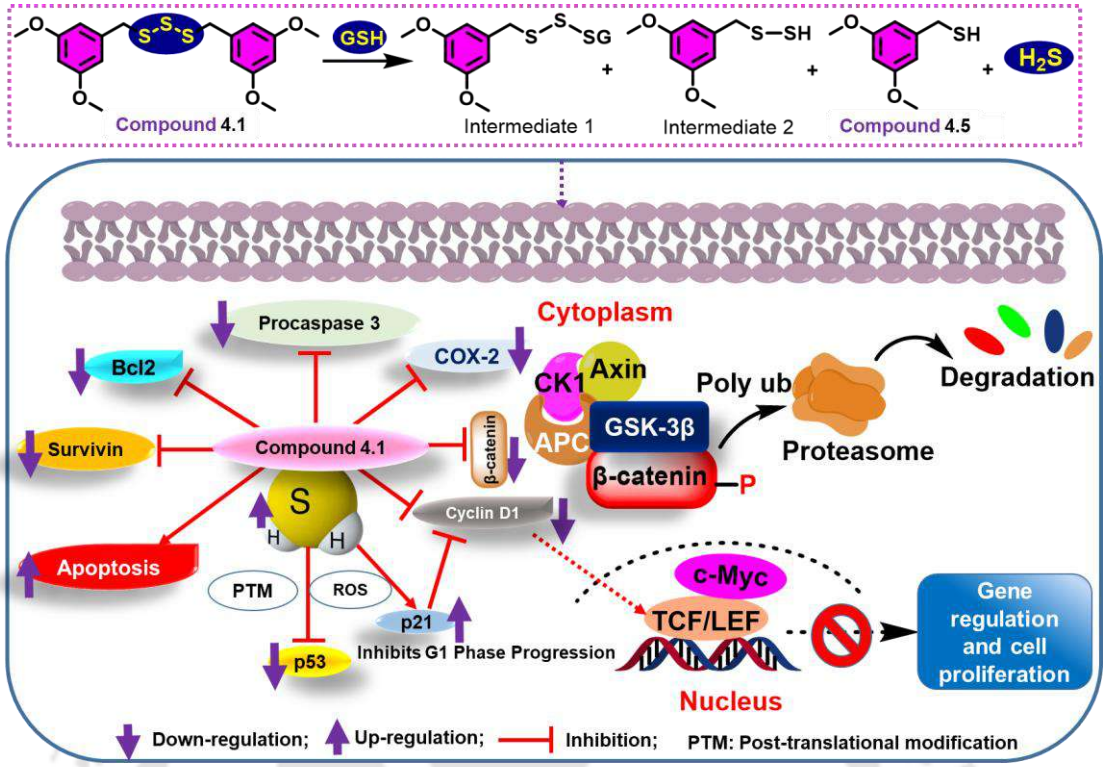

Scheme 4.2. Proposed mechanistic pathway for the anti-cancer activity of compound **4.1** against MDA-MB-231 cells.

4.4. Conclusions

In summary, the potent anti-proliferative activity of the benzylic organotrisulfide **4.1** against highly aggressive triple-negative breast cancer is described. The compound exhibits anti-cancer activity mainly by targeting and suppressing Wnt/β-catenin signaling pathway. The detailed mechanistic studies reveal that compound **4.1** facilitates the GSK-3β-induced phosphorylation of β-catenin and subsequent proteasomal degradation, which was supported by the G2/M phase arrest and with the down-regulation of downstream signaling genes such as Cyclin D1 and c-Myc. Unlike disulfide and monosulfide, the presence of a trisulfide unit capable of releasing H_2S was found to be important for the desired inactivation of β-catenin expression. The trisulfide **4.1** or the released H_2S induced down-regulation of the p53 gene, possibly through S-sulfhydration process. Taken together, this is the first report highlighting the involvement of released H_2S from the synthetic benzylic trisulfide in inhibiting the growth of triple-negative breast cancer *via* Wnt/β-catenin suppression. These novel findings could certainly help further in understanding the molecular mechanisms of small-molecule anti-cancer therapeutics for aggressive breast cancers in the future.

4.5. Experimental section

4.5.1. Materials and method

Thin layer chromatographic (TLC) analyses were carried out on pre-coated silica gel on aluminium sheets (F_{254}), purchased from Merck, and spots were visualized by UV irradiation at λ = 254 nm and/or iodine staining. All the solvents used for chromatographic separations were distilled before use. The melting point of the synthesized compounds was recorded in a Büchi B540 melting point apparatus. The NMR spectra (^{1}H, ^{13}C) were recorded with a Bruker AVANCE (400 or 500 MHz) spectrometers, respectively. Chemical shifts are cited with respect to TMS (Me_4Si) as an internal standard (^{1}H and ^{13}C nuclei). Mass spectra were obtained using an Agilent 6520 Accurate-Mass Quadrupole Time-of-Flight (Q-TOF) LC/MS spectrometer. UV-Vis spectroscopic analyses were performed on an Agilent Carey UV-Vis spectrophotometer and fluorescence emission spectra were recorded on a Fluoromax-4 spectrophotometer (FluoroMax-4 - Horiba Jobin Yvon). All the mammalian cells were purchased from NCCS Pune cell repository division. Cells were cultured under purified air class II biosafety cabinet (Thermo Scientific™). Finally, cells were incubated in CO_2 incubator (Eppendorf, Galaxy 170S). Cell viability assay was performed using Thermo Scientific Multiskan™ GO Microplate spectrophotometer. Cellular morphology was visualized and imaged under Bio-Rad ZOE™ fluorescent cell imager. Cell cycle experiment and Annexin/PI-mediated apoptosis experiment was performed using Flow Cytometer (BD Bioscience). A small molecule-based proteasome inhibitor (+R)-MG-132 was purchased from Sigma-Aldrich. The fluorescent sensor of H_2S (**WSP2**) and GSTP1 inhibitor (NBD-HEX) were synthesized following the reported methods.[27, 37]

4.5.2. Synthesis of Bunte salt

Bunte salts were prepared following the literature method with minor modifications.[38] To a stirred solution of sodium thiosulfate pentahydrate ($Na_2S_2O_3.5H_2O$) (1.77 mmol, 1.3 equiv) in 30% of ethanol-water mixture (5.0 mL), was added the corresponding halide precursor (1.36 mmol, 1.0 equiv) and stirred at room temperature for 4-5 h. Progress of the reaction was monitored by the TLC study. Upon completion of the reaction, the ethanol component was removed under reduced pressure and the residue was used for the next step in general without any further purification. The crude Bunte

salt **2** was purified using neutral alumina column chromatographic method with ethyl acetate and methanol as eluents.[15]

4.5.3. Synthesis of compound 4.1

To a stirred solution of the crude 3,5-dimethoxybenzyl Bunte salt (0.38 g, 1.36 mmol, considering 100% conversion of halides to Bunte salts) in water (20.0 mL), was added an aqueous solution (25.0 mL) of sodium sulfide nonahydrate (0.16 g, 0.68 mmol) at 0 °C in a dropwise manner and the mixture was stirred at that temperature for 5 h. A white-coloured suspension appeared upon completion of the addition of sodium sulfide. The progress of the reaction was monitored by the TLC study. Upon the completion of the reaction, the mixture was diluted with ethyl acetate and washed with brine solution. The combined organic layer was dried over anhydrous sodium sulfate and the solvent was evaporated under reduced pressure to afford crude trisulfides. 3,5-dimethoxybenzyl bromide (0.31 g, 1.36 mmol) was used to yield the trisulfide **4.1** as a white amorphous solid. The product was purified using semi-preparative HPLC method to afford the pure trisulfide. Yield: 86% (0.23 g); M.P: 100 - 102 ºC; R_f = 0.5 (100 % petroleum ether).^{1}H NMR ($CDCl_3$, 400 MHz) δ (ppm): 3.78 (s, 6H), 3.97 (s, 2H), 6.37 (*t*, 1H, *J* = 4.0 Hz), 6.47 (d, 2H, *J* = 4.0 Hz). ^{13}C NMR ($CDCl_3$, 100 MHz) δ (ppm): 43.7, 55.4, 99.8, 107.3, 138.8, 160.9. ESI-MS: *m/z* calcd. for $C_{18}H_{23}O_4S_3$ $[M+H]^+$: 399.0753; observed: 399.0746.

4.5.4. Synthesis of compound 4.2[39]

To a stirred ethanolic solution (3.5 mL) of 3,5-dimethoxybenzyl Bunte salt (0.38 g, 1.36 mmol), was added the aqueous solution (1.5 mL) of sodium sulfide nonahydrate (0.16 g, 0.68 mmol) at room temperature and the mixture was heated at 50 °C for 5 h. Progress of the reaction was monitored by TLC studies. Upon the completion of the reaction, the ethanol component was evaporated at reduced pressure and the residual mixture was diluted with ethyl acetate and washed with brine solution. The combined organic layer was dried over anhydrous sodium sulfate and the solvent was evaporated under reduced pressure to afford the crude disulfide. 3,5-dimethoxybenzyl bromide (0.31 g, 1.36 mmol) was used to yield the disulfide **4.2** as a white amorphous solid. Yield: 64% (0.25 g); M.P: 100 - 102 ºC; R_f = 0.5 (100% petroleum ether).^{1}H NMR ($CDCl_3$, 400 MHz) δ (ppm): 3.59 (s, 2H), 3.79 (s, 6H), 6.37 (t, 1H, *J* = 4.0 Hz), 6.42 (d, 2H, *J* = 4.0 Hz). ^{13}C

NMR ($CDCl_3$, 100 MHz) δ (ppm): 43.6, 55.3, 99.6, 107.3, 139.6, and 160.8. ESI-MS: *m/z* calcd. for $C_{18}H_{23}O_4S_2$ $[M+H]^+$: 367.1032; observed: 367.1029.

4.5.5. Synthesis of compound 4.3

To a stirred solution of sodium sulfide nonahydrate (0.05 g, 0.23 mmol) in ethanol (5.0 mL), 3,5-dimethoxybenzyl bromide (0.10 g, 0.46 mmol) was added at room temperature and the mixture was stirred at room temperature for 3 h. The progress of the reaction was monitored by the TLC study. After completion of the reaction, ethanol was evaporated under reduced pressure and the reaction mixture was diluted with ethyl acetate and washed with brine solution. The combined organic layer was dried over anhydrous sodium sulfate and the solvent was evaporated under reduced pressure to afford the almost pure monosulfide **4.3** as a crystalline yellow solid. Yield: 74% (0.32 g); M.P: 118 - 122 ºC; R_f = 0.5 (10% ethyl acetate in petroleum ether). ^{1}H NMR ($CDCl_3$, 500 MHz) δ (ppm): 3.78 (s, 6H), 3.56 (s, 2H), 6.35 (br s, 1H), 6.46 (br s, 2H). ^{13}C NMR ($CDCl_3$, 125 MHz) δ (ppm): 36.0, 55.3, 99.2, 107.0, 140.4, and 160.8. ESI-MS: *m/z* calcd. for $C_{18}H_{23}O_4S$ $[M+H]^+$: 335.1312; observed: 335.1347.

4.5.6. Synthesis of compound 4.5[16]

A methanolic solution (5.0 mL) of 3,5-dimethoxybenzyl bromide (0.050 g, 0.21 mmol) in a 2-neck flask under an inert condition was stirred at room temperature for 15 min. To the stirred solution, thiourea (0.024 g, 0.31 mmol) was added in one portion under N_2 atmosphere and the solution was stirred at room temperature for overnight (18 h). The progress of the reaction was monitored by TLC analysis. Next day, the reaction mixture was concentrated under vacuum and the thiouronium intermediate was subsequently suspended in de-gassed chloroform (5.0 mL). Butylamine (0.031 g, 42.0 µL, 0.42 mmol) was added dropwise to the suspension, which dissolved slowly over the period of around 24 h resulting a bright yellow colored clear solution. After the completion of reaction, the excess solvent was evaporated under reduced pressure to yield a semi-solid sticky brownish compound. The crude product was then purified by flash chromatography using silica gel (230 – 400 mesh) column to afford the pure product **4.5** as an off-white semi-solid material Yield: 50% (0.03 g). R_f = 0.5 (100% pet. ether) ^{1}H NMR ($CDCl_3$, 400 MHz) δ (ppm): 1.77 (t, 1H, *J* = 8.0 Hz), 3.67 (d, 2H, *J* = 8.0 Hz), 3.79 (s, 6H), 6.34 (t, 1H, *J* = 2.0 Hz), 6.48 (d, 1H, *J* = 2.0 Hz). ^{13}C NMR ($CDCl_3$, 100 MHz) δ (ppm): 29.2, 55.3, 99.1, 106.1, 143.4, and 161.0.

4.5.7. HPLC analysis

The purity of the synthesized compounds was analyzed by high-performance liquid chromatography (HPLC) using Agilent 1220 Infinity II LC system using reverse-phase C-18 column (Luna®, 5 µM, 100 Å, 205×4.6 mm) and HPLC grade solvents. Compounds were analyzed using (85 to 95%) of acetonitrile and (15 to 5%) water system for 10 min in a linear gradient mode and (95:5) ratio of acetonitrile and water system in the isocratic mode for another 5 min. Finally compound **4.1** was purified by semi-preparative HPLC system (Thermo Scientific^{TM} Dionex, Ultimate 3000 pump with DAD) using reverse-phase semi-preparative column (Luna ®, polar C-18, 250×21.2 mm) (Figure A5.4).

4.5.8. Detection of H_2S release by MB assay

The generated H_2S from the donors in the presence of GSH was monitored using methylene blue assay using UV-Vis spectrophotometer.[40] H_2S generation was initiated by adding trisulfide donor (25.0 µM) into PBS buffer (pH 7.4, 50.0 mM) solution containing thiol (500.0 µM). The formation of methylene blue was monitored at 670 nm in UV-Vis spectrophotometer at different time intervals after adding 500.0 µL of the above solution to 500.0 µL of methylene blue cocktail (100.0 µL of zinc acetate (1% w/v), 200.0 µL of *N*,*N*-dimethyl-1,4-phenylenediamine sulfate (20.0 mM in 7.2 M HCl), and 200.0 µL of ferric chloride (30.0 mM in 1.2 M HCl) in a cuvette. The H_2S concentration of each sample was calculated against a calibration curve, which was obtained using known concentrations of $Na_2S.9H_2O$ solution under the identical condition without any thiols.

4.5.9. Measurement of the released H_2S using the turn-on fluorogenic probe WSP2

The released H_2S from the donors in the presence of GSH (500.0 µM) was monitored using the H_2S-sensitive turn-on fluorogenic probe **WSP2** (10.0 µM) using fluorescence spectrophotometer.[27, 41] Initially, the probe **WSP2** (10.0 µM) was pre-incubated with GSH (500.0 µM) for 60 min in PBS buffer (20.0 mM, pH 7.4) and the emission spectra were measured to saturate the possible reaction of **WSP2** with thiols. Subsequently, the aliquot from the experimental solution of test compounds (15.0 µM) + GSH (500.0 µM) was added to the above mixture and measured the emission intensity after an incubation of 60 min to understand the reaction of **WSP2** with the generated H_2S from test compounds (10.0 µM) + GSH (500.0 µM).

4.5.10. Cell Culture

The triple-negative breast cancer (TNBC) cells (MDA-MB-231), Michigan Cancer Foundation-7 (MCF-7), Human Embryonic Kidney cells (HEK-293), Prostate cancer cell (PC-3), Human cervical cancer cell line (HeLa) and Human colon cancer cells (HCT-116) were obtained from National Centre for Cell Science (NCCS), Pune, India. The cells were cultured in DMEM medium (Gibco) supplemented with 10% (v/v) FBS (Gibco) and 1% Pen-Strep (Gibco). Cells were cultured as a monolayer in a humidified incubator at 37 °C in the presence of 5% CO_2 level.

4.5.11. Cell viability Assay

The synthesized compounds were screened for their anti-proliferative activities using the conventional MTT assay. Cells (MDA-MB-231) were seeded in 96-well culture plates at a density of 2×10^4 cells /100.0 µL/well and treated with the freshly prepared test compounds (DATS, DADS, DAS and compounds **4.1**-**4.5**) (0.0, 5.0, 10.0 and 25.0 µM) for 0 h (control) and 48 h (experimental), respectively. The IC_{50} of the best compound (**4.1**) was further evaluated in two different breast cancer cell types (MDA-MB-231 and MCF-7). The best active compound (**4.1**) was screened against several organ-specific cancer cells (MDA-MB-231, MCF-7, PC-3, HeLa, HCT-116) a representative non-tumorigenic cells (HEK-293). At the end of the treatment period, 10.0 µL of 5.0 mg/mL of MTT (Sigma Aldrich) was added to the plate (control) and incubated for 4 h. Following the 4 h incubation, the reagent from the plate was removed and the purple formazan crystals were dissolved using 100.0 µL of DMSO (Avra Synthesis Pvt Ltd) and the absorbance at 570 nm was measured using a microplate reader. In the experimental set, a similar MTT treatment protocol was followed only after 48 h. The mean ΔOD values were calculated by the subtraction of mean OD values of 0 h plate (control) from the mean OD values of identical wells at 48 h plate (experimental) and the percentage proliferation was calculated, keeping the mean ΔOD of untreated control as 100%.

4.5.12. Effect of compound 4.1 on cellular morphology (nuclear staining dye DAPI)

MDA-MB-231 cells (2×10^4 cells/ 2.0 mL) were plated in 35 mm dishes and maintained in a CO_2-regulated humidified (95% air/5% CO_2 atmosphere) incubator at 37 °C. The next day, cells were treated with text compounds (5.0 and 15.0 µM), and DMSO as vehicle control. The cells were imaged (Bright field) under fluorescent cell imager after

0 h, 12 h, 24 h and 48 h of time intervals, respectively. The nuclear aberration was analyzed upon staining the compound (5.0 and 15.0 µM) treated cells with DAPI (3.0 nM). After the treatment with compound **4.1** for 48 h, cells were washed with ice-cold DPBS for three times and fixed the cells with 4 % formaldehyde (Merck) and incubated for 10 min at room temperature. After the incubation, cells were washed and incubated further for 10 min with DAPI (Sigma Aldrich). Finally, cells were washed with DPBS for three times and imaged under fluorescent imager.

4.5.13. GFP-lentivirus production and evaluation of cellular morphology after treatment with 4.1

Second-generation lentiviral vectors were packaged in HEK293T cells using the calcium phosphate transfection method. Briefly, 6×10^6 HEK293T cells were seeded in a 100 mm 0.1% gelatin-coated dish and then grown to 75-80% confluency in complete growth medium. Once the culture attained the confluency, the medium was replaced with a transfection medium containing advanced DMEM (Invitrogen) supplemented with 2% FBS, 1X Penstrep, and 1X non-essential amino acids (NEAA; Invitrogen), 1-2 h prior to transfection. The calcium phosphate transfection mixture was then prepared by mixing 12 µg lentiviral backbone plasmid, 7.7 µg psPAX2 (Addgene plasmid 12260), 4.3 µg pMD2.G (Addgene plasmid 12259), tissue-culture grade water, and 125.0 mM $CaCl_2$ with 2X HBS buffer (1:1), and incubated for 15 min at room temperature. Subsequently, this mixture was added to the cells dropwise in the presence of 25.0 µM chloroquine. After 5-6 h of transfection, the medium was replaced with a virus production medium containing advanced DMEM supplemented with 5% FBS, 1X Pen-strep, and 1X NEAA. The medium was then replaced with a fresh medium after 12-16 h post-transfection. Subsequently, the GFP-lentiviral supernatant was then harvested at 24, 36, and 48 h of incubation, pooled, concentrated (centrifugation at 14000 rpm for 2 h), aliquoted for storage at -80 °C. Finally, the viral supernatant (200.0 µL) was added to the MDA MB-231 cells and incubated for 24 h (2% FBS in DMEM). Next day, cells were washed with DPBS and complete DMEM (10% FBS, 1% PS) was added and incubated for another three days for complete expression of GFP. Finally, cells were treated with compound **4.1** (5.0 and 15.0 µM) and incubated for 48 h at cell culture conditions. Post-incubation, cells were washed with ice-cold PBS and imaged under fluorescent imager.

4.5.14. Wound healing (Scratch) assay

MDA-MB-231 cells were seeded in a 24-well plate at a concentration of 6×10^5 cells per 0.5 mL per well and incubated in a CO_2 incubator at 37 °C to form a monolayer of cells. After the monolayer formation, the cells were pre-incubated in serum-free medium (DMEM without FBS) for 6 h. Using a 10.0 µL tip, a scratch was made on the monolayer and the debris was removed by washing with DPBS (1X). Cells were treated with the test compound (5.0 and 15.0 µM) and the scratch was observed under fluorescent imager at regular intervals (0, 12, 24 and 48 h). The same experiment was repeated three times under identical conditions. The extension of wounds depicts the anti-migratory property of the test compound.

4.5.15. Cell cycle analysis

MDA-MB-231 cells (6×10^5 cells per 5.0 mL) were seeded in 60 mm dish and treated with 0.0, 1.0, 2.5, 5.0 and 10.0 µM of text compound (**4.1**, **4.2**) and incubated for 48 h in a CO_2 incubator at 37 °C. After completion of the treatment, cells were harvested and washed with DPBS (1X) for the successful removal of media components. Finally, the cells were fixed with 70% ethanol (gentle vortexing while dropwise addition) and kept at -20 °C overnight. Next day, cells were centrifuged (8000 rpm for 8 min) at 4°C and the supernatant was discarded. Cells were washed with cold PBS (1X) and centrifuged down to remove the excess amount of ethanol from the tube. To eliminate the RNA content from the cells, RNAaseA (type I-AS from bovine pancreas, Sigma-Aldrich) was added (100.0 µg/mL) and incubated in a 37 °C water bath for 30 min. Finally, cells were washed with cold PBS (1X) and PI was added (50.0 µg/ml) and kept at 4 °C for 30 min and analyzed using Flow cytometry.

4.5.16. FITC-Annexin V/ PI dead cell apoptosis assay

MDA-MB-231 cells (6×10^5 cells per 5.0 mL) were seeded in 60 mm dish and treated with 0, 2.5, 5.0 and 10.0 µM of compound **4.1** and incubated for 48 h in a CO_2 incubator at 37 °C. After completion of the treatment, cells were harvested and washed with ice-cold DPBS (1X) for the successful removal of media components. Cells were resuspended in 0.5 mL cold 1X binding buffer. Finally, Annexin V-FITC (1.25 µL) (Invitrogen) was added according to the manufacturer's protocol. Then cells were incubated at room temperature for 15 min in a dark place. After incubation, cells were centrifuged (800 rpm for 8 min) at 4°C and the supernatant was carefully discarded. The

cells were again washed with 0.5 mL cold 1X binding buffer. Finally, Propidium iodide (PI, 0.6 µg/mL) was added and the samples were placed on ice in a dark chamber to protect from the light exposure. Finally, cells were analyzed by Flow cytometry using corresponding fluorescence channels as per the prescribed manufacturer protocol.

4.5.17. Estimation of ROS profile after treatment with 4.1 using DCFDA fluorescence microscopy-based assay

To estimate the intracellular ROS production, MDA MB-231 cells were in high glucose Dulbecco's modified Eagle's medium (DMEM) supplemented with 10% fetal bovine serum (FBS) and 1% penicillin/streptomycin at 37 °C under 5% CO_2 atmosphere. Cells were then plated (3.0×10^5 cells/2.0 mL) in 35 mm cell culture petridishes containing 2.0 mL of DMEM and incubated at 37 °C under 5% CO_2 for 24 h. The confluent cells were washed with DPBS and finally incubated with the test compound (5.0 and 15.0 µM) at 37 °C under 5% CO_2 for 12 h. Additionally, for the control experiment, *N*-acetyl cysteine (NAC, a well-known ROS scavenger) (2.0 mM) and compound **4.1** (2.5 µM) were incubated for 1 h at 37 °C to affirm the quenching of the endogenous ROS level. Finally, after sequential washing with DPBS (2 times), a freshly prepared H_2DCFDA (5.0 µM) was added in DMEM and incubated at dark condition for 30 min. Cells were finally washed with ice-cold DPBS (2 times) and imaged under fluorescent imager.

4.5.18. Intracellular H_2S detection

MDA MB-231 cells (2×10^5 cells per 2.0 mL) were plated and incubated 37 °C under 5% CO_2 for 24 h. The confluent cells were then washed with DPBS (2 times) and treated with compound **4.1** (0, 5.0 and 15.0 µM) or DATS (100.0 µM) and incubated for 2 h under 5% CO_2 condition. After the completion of treatment, cells were washed with DPBS (2 times) and treated with **WSP2** (5.0 µM) and incubated under 5% CO_2 condition for 2 h. For the negative control experiment, cells were pre-treated with *N*-ethylmalemide (NEM, a well-known thiol quencher) (2.0 mM) and *D*,*L*-propargyl glycine (PAG) (25.0 µM) for 1 h to ensure the complete quenching of intracellular thiols and H_2S respectively. After this treatment, cells were washed with DPBS (2 times) and incubated with compound **4.1** (5.0 and 15.0 µM) and incubated for another 2 h under % CO_2 condition. Finally, cells were washed with DPBS (2 times) and incubated with the probe (**WSP2**, 5.0 µM) for another 2 h under 5% CO_2 condition. Cells were finally washed with DPBS (2 times) and imaged under fluorescent cell imager.

4.5.19. Western blot analysis

MDA MB-231 cells (5 × 10^5 cells per 5.0 mL) were treated with test compounds and incubated for respected time points. After treatment, cells were washed with cold DPBS for three times. Finally, the whole-cell protein was extracted using RIPA cell lysis buffer (150.0 mM of NaCl, 1% (v/v) NP-40 (Himedia), 0.5% Sodium deoxycholate (Himedia), 0.1% SDS, 25.0 mM of Tris, 10 mg/ml PMSF (Sigma Aldrich). Equal volumes of protein was loaded and separated on 2% sodium dodecyl sulfate (SDS)-polyacrylamide gel by electrophoresis and transferred to a nitrocellulose membrane (Bio-Rad). Protein transfer was confirmed by Ponceau-S (HiMedia) staining. The blots were blocked with 5% (w/v) non-fat dry milk in 1X TBST buffer for 1 h at room temperature. Finally, the blots were incubated with the primary antibodies specific for Survivin, Procaspase 3, Bcl2, p53, β-catenin, c-Myc, GSK-3β, α-Tubulin, Histone-3, Cyclin D1, p21cip1/WAF1, β-Actin or GAPDH (Cell Signaling, Abcam, Invitrogen) overnight at 4 °C. Following the primary antibody incubation (1:5000), the blots were washed with TBST (1X) buffer and incubated with IgG-HRP-conjugated secondary antibodies (anti-rabbit, anti-mouse) (1:10000, 1:5000) (Abcam/Invitrogen) for 1 h and developed using Clarity™ Western ECL Substrate (Bio-Rad) and imaged using ChemiDoc XRS+ System equipped with Image Lab software (Bio-Rad, California, USA). The housekeeping genes such as GAPDH and β-Actin were used as a loading control.

4.5.20. Subcellular fractionation

MDA-MB-231 cells (5 × 10^5 cells) were treated with compound **4.1** (5.0 µM) and incubated for different time points (12 h, 24 h and 48 h). After the incubation period was over, cells were washed with ice cold PBS and 200.0 µL of SF (Cytosolic fraction) buffer (250.0 mM Sucrose, 20.0 mM HEPES (pH 7.4), 10.0 mM KCl, 1.5 mM EDTA, 1.0 mM EGTA, fresh 1.0 mM DTT and 1X protease cocktail inhibitor (Sigma Aldrich)) was added in plate on ice. The cell lysate was collected in an Eppendorf tube and agitated at 4 °C for 30 min at around 30-50 rpm on the tube roller. Then, cell lysate was centrifuged at 720 × g at 4 °C for 7 min. Finally, the supernatant was transferred to a new tube and further centrifuged at 10,000 × g at 4 °C for 10 min. The cytosolic and membrane supernatant was collected for the immunoblot experiments. The pellet collected at the first step was further washed with SF buffer and centrifuged at 20 × g at 4 °C for 10 min. After removal of the supernatant, the pellet was resuspended in NL

(Nuclear fraction) buffer (50.0 mM Tris HCl (pH 8.0), 150.0 mM NaCl, 1% NP-40 (HiMedia), 0.5% sodium deoxycholate (HiMedia), 0.1% SDS and fresh Protease cocktail 1X, and 10% glycerol). The pellet was further sonicated on ice (2×3 sec, separated by 3 s resting under 30% amplitude power). The nuclear fraction was subjected for an immunoblot experiment. To evaluate the lysate purity and internal loading control, α-Tubulin and Histone-H3 were used.[42]

4.5.21. Molecular docking studies

4.5.21.1. Protein preparation

For docking studies, the recently published crystal structures of the β-catenin-TCF-4 complex (PDB: 2GL7) were extracted from the RCSB (Protein Data Bank) (https://www.rcsb.org/).[43] Before beginning our docking experiment, the protein structures were subjected to preparation using AutoDock 4.2 Tools (MGLTools 1.5.6) and the PyMol (Schrödinger LLC) software package.[44] Initially, the protein structure was assembled into the original form having all the important subunits depicted by the crystallographic study. During the protein preparation, missing hydrogens were added and Gasteiger charges were applied.

4.5.21.2. Ligand preparation

The 2D chemical structures of compound **4.1** and MSAB were drawn and converted to 3D structures using ChemDraw 3D Version 20.0.0.41.[14c] All the 3D structures were subjected to MM2 energy minimization calculation and assigned all the bond orders. Finally, for docking studies, an extended PDB format, termed PDBQT, was used for coordinate files, which included atomic partial charges and atom types. Torsion angles were calculated to assign the fixable and non-bonded rotation of molecules (Compound **4.1** and MSAB exhibits 10 and 5 rotatable bonds, respectively).

4.5.21.3. Receptor grid generation and docking method

In the present study, we used the crystal structure of the β-catenin-TCF-4 complex (PDB: 2GL7). The grid was generated around the cysteine-rich site (N426, K435, R469, H470, and K508) to understand the interaction with ligand binding sites. Finally, minimized protein structure was subjected to perform AutoGrid to build a grid box. The grid size was set to 42 × 40 × 46 points with a grid spacing of 0.497 Å. The other points were center x = 12.126, center y = 15.236, and center z = 56.861. Docking simulation

was performed in the AutoDock 4.2 program. Ten search attempts (i.e., ga_run parameter) were performed for each ligand. The maximum number of energy evaluations before the termination of the LGA run was 250 000 and the maximum number of generations of LGA run before termination was 27 000. Other docking parameters were set to the default values of the AutoDock 4.2 program.

4.5.22. Statistical analysis

A statistical test (One-way Anova analysis followed by Dunnett's multiple comparison test) was performed to analyze the results obtained from MTT, migration assay and Western Blotting using Graphpad Prism 9 software. p values ≤ 0.05 were considered to be statistically significant.

4.6. References

1. (a) Vandiver, M. S.; Snyder, S. H., *Journal of Molecular Medicine-Jmm* **2012,** *90,* 255; (b) Fukuto, J. M.; Carrington, S. J.; Tantillo, D. J.; Harrison, J. G.; Ignarro, L. J.; Freeman, B. A.; Chen, A.; Wink, D. A., *Chemical Research in Toxicology* **2012,** *25,* 769.
2. (a) Wu, D.; Si, W.; Wang, M.; Lv, S.; Ji, A.; Li, Y., *Nitric oxide* **2015,** *50,* 38; (b) Predmore, B. L.; Lefer, D. J.; Gojon, G., *Antioxidants & Redox Signaling* **2012,** *17,* 119; (c) Stipanuk, M. H.; Ueki, I., *Journal of Inherited Metabolic Disease* **2011,** *34,* 17.
3. (a) Bhattacharyya, S.; Saha, S.; Giri, K.; Lanza, I. R.; Nair, K. S.; Jennings, N. B.; Rodriguez-Aguayo, C.; Lopez-Berestein, G.; Basal, E.; Weaver, A. L.; Visscher, D. W.; Cliby, W.; Sood, A. K.; Bhattacharya, R.; Mukherjee, P., *Plos One* **2013,** *8,* e79167; (b) Szabo, C.; Coletta, C.; Chao, C.; Módis, K.; Szczesny, B.; Papapetropoulos, A.; Hellmich, M. R., *Proceedings of the National Academy of Sciences* **2013,** *110,* 12474.
4. Wu, D.; Li, M.; Tian, W.; Wang, S.; Cui, L.; Li, H.; Wang, H.; Ji, A.; Li, Y., *Scientific Reports* **2017,** *7,* 5134.
5. (a) Szabo, C.; Papapetropoulos, A., *Pharmacological Reviews* **2017,** *69,* 497; (b) Hartle, M. D.; Pluth, M. D., *Chemical Society Reviews* **2016,** *45,* 6108; (c) Zhao, Y.; Biggs, T. D.; Xian, M., *Chemical Communications* **2014,** *50,* 11788; (d)

Powell, C. R.; Dillon, K. M.; Matson, J. B., *Biochemical Pharmacology* **2018,** *149,* 110; (e) Powell, C. R.; Kaur, K.; Dillon, K. M.; Zhou, M.; Alaboalirat, M.; Matson, J. B., *Acs Chemical Biology* **2019,** *14,* 1129; (f) Zhou, M.; Qian, Y.; Zhu, Y.; Matson, J., *Chemical Communications* **2020,** *56,* 1085; (g) Zheng, Y.; Yu, B.; Ji, K.; Pan, Z.; Chittavong, V.; Wang, B., *Angewandte Chemie* **2016,** *55,* 4514.

6. Asemani, Y.; Zamani, N.; Bayat, M.; Amirghofran, Z., *Phytotherapy Research* **2019,** *33,* 3019.
7. (a) Na, H. K.; Kim, E. H.; Choi, M. A.; Park, J. M.; Kim, D. H.; Surh, Y. J., *Biochemical Pharmacology* **2012,** *84,* 1241; (b) Hahm, E. R.; Singh, S. V., *Breast Cancer Res Treat* **2014,** *144,* 47; (c) Chandra-Kuntal, K.; Lee, J.; Singh, S. V., *Breast Cancer Research and Treatment* **2013,** *138,* 69.
8. Kiesel, V. A.; Stan, S. D., *Biochemical and Biophysical Research Communications* **2017,** *484,* 833.
9. Tao, Q.; Wu, C.; Xu, R.; Niu, L.; Qin, J.; Liu, N.; Zhang, P.; Wang, C., *Cell and Tissue Research* **2017,** *370,* 379.
10. Zhang, Q.; Li, X.-T.; Chen, Y.; Chen, J.-Q.; Zhu, J.-Y.; Meng, Y.; Wang, X.-Q.; Li, Y.; Geng, S.-S.; Xie, C.-F.; Wu, J.-S.; Zhong, C.-Y.; Han, H.-Y., *Cancer Chemotherapy and Pharmacology* **2018,** *81,* 969.
11. Li, X.; Meng, Y.; Xie, C.; Zhu, J.; Wang, X.; Li, Y.; Geng, S.; Wu, J.; Zhong, C.; Li, M., *Journal of Cellular Biochemistry* **2018,** *119,* 4134.
12. (a) Klaus, A.; Birchmeier, W., *Nat Rev Cancer* **2008,** *8,* 387; (b) Yu, Q. C.; Verheyen, E. M.; Zeng, Y. A., *Cancers* **2016,** *8*; (c) Yu, S.; Wang, Z.; Su, Z.; Song, J.; Zhou, L.; Sun, Q.; Liu, S.; Li, S.; Li, Y.; Wang, M.; Zhang, G.-Q.; Zhang, X.; Liu, Z.-J.; Lu, D., *BMC Complementary Medicine and Therapies* **2018,** *18,* 59; (d) King, T. D.; Suto, M. J.; Li, Y., *Journal of Cellular Biochemistry* **2012,** *113,* 13; (e) Zhan, T.; Rindtorff, N.; Boutros, M., *Oncogene* **2017,** *36,* 1461.
13. Xu, L.; Zhang, L.; Hu, C.; Liang, S.; Fei, X.; Yan, N.; Zhang, Y.; Zhang, F., *International Journal of Oncology* **2016,** *48,* 1175.
14. (a) MacDonald, B. T.; Tamai, K.; He, X., *Developmental Cell* **2009,** *17,* 9; (b) Behrens, J.; Jerchow, B.-A.; Würtele, M.; Grimm, J.; Asbrand, C.; Wirtz, R.; Kühl, M.; Wedlich, D.; Birchmeier, W., *Science* **1998,** *280,* 596; (c) Hwang, S.-

Y.; Deng, X.; Byun, S.; Lee, C.; Lee, S.-J.; Suh, H.; Zhang, J.; Kang, Q.; Zhang, T.; Westover, K. D.; Mandinova, A.; Lee, S. W., *Cell Reports* **2016,** *16,* 28.

15. Bhattacherjee, D.; Sufian, A.; Mahato, S. K.; Begum, S.; Banerjee, K.; De, S.; Srivastava, H. K.; Bhabak, K. P., *Chemical Communications* **2019,** *55,* 13534.
16. Dillon, K. M.; Carrazzone, R. J.; Wang, Y.; Powell, C. R.; Matson, J. B., *ACS Macro Letters* **2020,** *9,* 606.
17. Xiao, D.; Herman-Antosiewicz, A.; Antosiewicz, J.; Xiao, H.; Brisson, M.; Lazo, J. S.; Singh, S. V., *Oncogene* **2005,** *24,* 6256.
18. Bolton, S. G.; Cerda, M. M.; Gilbert, A. K.; Pluth, M. D., *Free Radical Biology and Medicine* **2019,** *131*, 393.
19. Banerjee, K.; Bhattacherjee, D.; Raina, K.; Thummer, R. P.; Bhabak, K. P., *New Journal of Chemistry* **2022**.
20. (a) Bertoli, C.; Skotheim, J. M.; de Bruin, R. A. M., *Nature Reviews Molecular Cell Biology* **2013,** *14,* 518; (b) Resnitzky, D.; Reed, S. I., *Molecular and Cellular Biology* **1995,** *15,* 3463.
21. Dowdy, S. F.; Hinds, P. W.; Louie, K.; Reed, S. I.; Arnold, A.; Weinberg, R. A., *Cell* **1993,** *73,* 499.
22. Nuñez, F.; Bravo, S.; Cruzat, F.; Montecino, M.; De Ferrari, G. V., *PLOS ONE* **2011,** *6,* e18562.
23. Majchrzak-Celińska, A.; Misiorek, J. O.; Kruhlenia, N.; Przybyl, L.; Kleszcz, R.; Rolle, K.; Krajka-Kuźniak, V., *BMC Cancer* **2021,** *21*, 493.
24. Pyo, C.-W.; Choi, J. H.; Oh, S.-M.; Choi, S.-Y., *Biochimica Et Biophysica Acta* **2013,** *1830*, 5316.
25. Liu, C.; Li, Y.; Semenov, M.; Han, C.; Baeg, G.-H.; Tan, Y.; Zhang, Z.; Lin, X.; He, X., *Cell* **2002,** *108*, 837.
26. Yao, R.; Sun, X.; Xie, Y.; Liu, L.; Han, D.; Yao, Y.; Li, H.; Li, Z.; Xu, K., *American Journal of Translational Research* **2018,** *10,* 2610.
27. Peng, B.; Chen, W.; Liu, C.; Rosser, E. W.; Pacheco, A.; Zhao, Y.; Aguilar, H. C.; Xian, M., *Chemistry—A European Journal* **2014,** *20,* 1010.
28. Lee, Z. W.; Zhou, J.; Chen, C.-S.; Zhao, Y.; Tan, C.-H.; Li, L.; Moore, P. K.; Deng, L.-W., *PLOS ONE* **2011,** *6,* e21077.
29. Antony, M. L.; Singh, S. V., *Indian Journal of Experimental Biology* **2011,** *49,* 805.

30. Low, J.-L.; Du, W.; Gocha, T.; Oguz, G.; Zhang, X.; Chen, M. W.; Masirevic, S.; Yim, D. G. R.; Tan, I. B. H.; Ramasamy, A.; Fan, H.; DasGupta, R., *iScience* **2021,** *24*, 102544.
31. Jurkowska, H.; Wróbel, M.; Szlęzak, D.; Jasek-Gajda, E., *Amino Acids* **2018,** *50*, 699.
32. Kim, D.-H.; Kundu, J. K.; Surh, Y.-J., *Molecular Carcinogenesis* **2011,** *50*, 222.
33. (a) Velu, C. S.; Niture, S. K.; Doneanu, C. E.; Pattabiraman, N.; Srivenugopal, K. S., *Biochemistry* **2007,** *46*, 7765; (b) Lo, H.-W.; Stephenson, L.; Cao, X.; Milas, M.; Pollock, R.; Ali-Osman, F., *Molecular Cancer Research* **2008,** *6*, 843.
34. Tsai, C. W.; Chen, H. W.; Yang, J. J.; Sheen, L. Y.; Lii, C. K., *Journal of Agricultural and Food Chemistry* **2007,** *55*, 1019.
35. Turella, P.; Filomeni, G.; Dupuis, M. L.; Ciriolo, M. R.; Molinari, A.; De Maria, F.; Tombesi, M.; Cianfriglia, M.; Federici, G.; Ricci, G.; Caccuri, A. M., *Journal of Biological Chemistry* **2006,** *281*, 23725.
36. Chauvin, J.-P. R.; Griesser, M.; Pratt, D. A., *Journal of the American Chemical Society* **2017,** *139*, 6484.
37. Fulci, C.; Rotili, D.; De Luca, A.; Stella, L.; Morozzo della Rocca, B.; Forgione, M.; Di Paolo, V.; Mai, A.; Falconi, M.; Quintieri, L.; Caccuri, A. M., *Journal of Enzyme Inhibition and Medicinal Chemistry* **2017,** *32*, 240.
38. Milligan, B.; Swan, J. M., *Journal of the Chemical Society* **1962,** 2172.
39. Takaguchi, Y.; Suzuki, S.; Ohta, K.; Motoyoshiya, J.; Aoyama, H., *Phosphorus Sulfur Silicon Related Elements* **2001,** *176*, 61.
40. Popowsky, J. K. F. a. M., *Analytical Chemistry* **1949,** *21*, 732.
41. Mahato, S. K.; Bhattacherjee, D.; Barman, P.; Bhabak, K. P., *Journal of Materials Chemistry B* **2022,** *10*, 2183.
42. Yu, Z.; Huang, Z.; Lung, M. L., *Bio-protocol* **2013,** *3*, e754.
43. Sampietro, J.; Dahlberg, C. L.; Cho, Uhn S.; Hinds, T. R.; Kimelman, D.; Xu, W., *Molecular Cell* **2006,** *24*, 293.
44. Morris, G. M.; Huey, R.; Lindstrom, W.; Sanner, M. F.; Belew, R. K.; Goodsell, D. S.; Olson, A. J., *Journal of Computational Chemistry* **2009,** *30*, 2785.

Thesis Summary and Future Perspectives

The present thesis entitled "***Benzylic Organosulfides and Analogues: Greener Synthesis, Anti-cancer Activities and the Feasibilities of H_2S Donation***" brings forward the design and synthesis of benzylic Organosulfides and some related diselenides. Particular emphasis was towards the synthesis of organotrisulfides and their hydrogen sulfide (H_2S) donation feasibilities and its impact for the possible treatment strategy of the most aggressive triple-negative breast cancer.

The dual characteristics of the H_2S towards cancer progression and metastasis have been documented in many reports. The signaling property of H_2S toward cancer has been studied through several control experiments using instantaneous donors of H_2S-like inorganic salts (NaHS and Na_2S). Over the last two decades, inorganic salts-mediated H_2S donation (Na_2S and NaHS) and their detailed biological studies have been covered throughout the literature. It is noteworthy that, inorganic salts are considered as instantaneous donors of H_2S, therefore, the concentration of H_2S cannot be maintained throughout the study due to its volatile nature. To counter that problem higher dose of salts (upto milimolar concentration) have been used to maintain the level of H_2S in the study, which is therapeutically not justified. Therefore, various organosulfur compounds were identified in some selective dietary vegetables (allium and cruciferous) and in some plants (shrubs) for the donation of H_2S as well as for their medicinal properties. The medicinal properties (particularly for cancer) of garlic in general and some of the key organosulfur compounds (DAS, DADS and DATS) in garlic were evaluated extensively over last few decades to understand their anti-cancer activities. However, it is not clear whether the anti-cancer activity of the organosulfur compounds in garlic could be enhanced further with some synthetic analogues or not. Previous reports on organopolysulfide-mediated H_2S donation for cancer treatment sparked our interest in designing a selective synthetic strategy for synthesizing garlic-inspired organopolysulfides. In addition, the mechanisms of their anti-cancer activity and their H_2S donation capacity were studied in cellular medium.

In search of developing newer derivatives of DADS with potential anti-cancer activities, a series of benzylic disulfides and diselenides have been synthesized and purified and evaluated for their anti-cancer activities. According to the preliminary anti-proliferative activity, diselenides were found to be significantly more potent than the

corresponding disulfide analogues. Our study further revealed that the activity of benzylic disulfides/diselenides could be increased several fold upon the introduction of a cyano group at the *para*-position of the benzene ring (Chapter 2, compounds **2.3** and **2.8**).

In the chapter 3, we describe a very simple and convenient method for the selective synthesis of allyl sulfides and related derivatives utilizing alkyl, alkenyl and benzylic halides as precursors under a greener and catalyst-free condition. We show herein for the first time that a selectivity among symmetrical trisulfides, disulfides and monosulfides could be achieved using Na_2S as a sulfur-transfer agent by the variation of reaction conditions and parameters. Interestingly, compound **3.4** was found to donate H_2S in a sustained manner in the aqueous as well as cellular medium in the presence of biothiols.

Finally, in chapter 4, for the first time, the mechanism of action for the potent anti-cancer activity of the trisulfide **4.1** against the highly aggressive triple-negative breast cancer cells (MDA-MB-231) was studied. Mechanistic studies reveal that the compound exhibited anti-cancer activity primarily by targeting and suppressing the Wnt/β-catenin signaling pathway. Moreover, cell cycle arrest in the G2/M phase was associated with the inactivation of β-catenin and significant downregulation of downstream signaling genes such as Cyclin D1 and c-Myc. Several control experiments with the analogous organosulfur compounds and the key enzyme inhibitors reveal that the presence of a trisulfide unit in the compound is crucial for the desired inactivation of β-catenin expression, which is promoted by GSK-3β-induced phosphorylation of β-catenin and its proteasomal degradation. Moreover, the trisulfide unit or the released H_2S reduced the expression of p53 through the S-sulfhydration process and increased the expression of p21 independent of p53.

In summary, with the synthesis of diverse series of organosulfides followed by the evaluation of their anti-cancer activities, we could identify several key compounds having potent pharmacological implications. With the available resources and facilities, we have undertaken preliminary mechanistic studies with the synthesized organosulfides towards their *in vitro* anti-proliferative activities to identify the potent compounds as described in this thesis. Further investigations suggested that compound **4.1** exhibit selectivity towards Wnt/β-catenin signaling pathway. In addition, some more mechanistic aspects may be considered as important future perspectives of the present thesis to take the potent compounds forward up to their applications.

1. A preliminary anti-proliferative study of compound **2.8** showed potent anti-cancer activities. Further detailed mechanistic exploration might aid in designing more

potent and less toxic diselenides. Apart from its anti-cancer activities, diselenide compound can be explored against anti-leishmanial, anti-viral activities.

2. In chapter 3, we reported a new synthetic methodology for the selective synthesis of symmetrical trisulfides. Preliminary studies revealed the potent anti-cancer activities and H_2S donation capacities of compound **3.4** in a cellular medium. However, the synthesis of selective tetrasulfides can be further explored and new series of H_2S donors can be screened in a cellular medium.
3. In chapter 4, we reported for the first time, organotrisulfide-mediated inhibition of the Wnt/β-catenin signaling pathway in TNBC cells. Additionally, mechanistic studies depicted the H_2S-mediated protein degradation (p53) by compound **4.1**. This warrants further investigations on the design of organopolysulfides for the persulfidation-driven protein modification and degradation.

List of publications and conferences

Thesis Publications

1. **Bhattacherjee, D**.; Raina, K.; Mandal, T. K.; Thummer, R. P.*; Bhabak, K. P.* Targeting Wnt/ β-catenin signaling pathway in triple-negative breast cancer by benzylic organotrisulfides: contribution of the released hydrogen sulfide towards potent anti-cancer activity. *Free Radical Biology and Medicine* **2022**, *191*, 82-96.

2. **Bhattacherjee, D**.; Sufian, A.; Mahato, S. K.; Begum, S.; Banerjee, K.; De, S.; Srivastava, H. K.* Bhabak, K. P.* Trisulfides over disulfides: highly selective synthetic strategies, anti-proliferative activities and sustained H_2S release profiles. *Chemical Communication* **2019**, *55*, 13534-13537.

3. **Bhattacherjee, D**.; Basu, C.; Bhardwaj, Q.; Mal, S.; Sahu, S.; Sur, R.; Bhabak, K. P.* Design, synthesis and anti-cancer activities of benzyl analogues of garlic-derived diallyl disulfide (DADS) and the corresponding diselenides. *ChemistrySelect* **2017**, *2*, 7399-7406.

Other Publications

1. Sufian, A.; **Bhattacherjee, D**.; Barman, P.; Srivastava, A.; Thummer, R. P.; Bhabak, K. P.* Stimuli-responsive prodrug of non-steroidal anti-inflammatory drug diclofenac: self-immolative drug release with turn-on near-infrared fluorescence. *Chemical Communication* **2022**, *58*, 7833-7836.

2. Banerjee, K.; **Bhattacherjee, D**.; Raina, K.; Thummer, R. P.*; Bhabak, K. P.* Benzimidazole-based Ionic and Non-ionic Organoselenium Compounds: Innovative Synthetic Strategies, Structural Characterizations and Preliminary Anti-Proliferative Activities. *New Journal of Chemistry* **2022**, *46*, 11910-11926.

3. Mahato,S. K.; **Bhattacherjee, D**.; Barmana, P.; Bhabak K. P.*; Thioredoxin reductase-triggered fluorogenic donor of hydrogen sulfide: a model study with a symmetrical organopolysulfide probe with turn-on near-infrared fluorescent emission. *Journal of Materials Chemistry B* **2022**, *10*, 2183-2193.

4. Banerjee, K.; **Bhattacherjee, D**.; Mahato, S. K.; Sufian, A., Bhabak, K. P.* Benzimidazole-and imidazole-Fused selenazolium and selenazinium selenocyanates: ionic organoselenium compounds with efficient peroxide scavenging activities. *Inorganic Chemistry* **2021**, 60, *17*, 12984–12999.

5. Ghosh, S.; **Bhattacherjee, D**.; Satpati, P*.; Bhabak K. P.* Venetoclax: A promising repurposed drug against SARS-CoV-2 main protease. *Journal of Biomolecular Structure and Dynamics* **2021**, 1-12.

6. Sufian, A.; **Bhattacherjee, D**.; Mishra, T.; Bhabak, K. P.* Peroxide-responsive boronate ester-coupled turn-on fluorogenic probes: Direct linkers supersede selfimmolative linkers for sensing peroxides. *Dyes and Pigments* **2021**, *191*, 109363.

7. Mahato, S. K.; **Bhattacherjee, D**.; Bhabak, K. P.* Biothiol-triggered organotrisulfidebased self-immolative fluorogenic donors of hydrogen sulfide enabling lysosomal trafficking. *Chemical Communication* **2020**, *56*, 7769-7772.
8. Malviya, N.; Sonkar, C.; Ganguly, R.; **Bhattacherjee, D**.; Bhabak, K. P.; Mukhopadhyay, S.* Novel approach to generate self-deliverable anticancer Ru(II) agent in the self-reacting confined gel space. *ACS Applied Materials & Interfaces* **2019**, *11*, 47606-47618.
9. Banerjee, K.; Padmavathi, G.; **Bhattacherjee, D**.; Saha, S.; Kunnumakkara, A. B.; Bhabak, K. P.* potent anti-proliferative activities of organochalcogenocyanates towards breast cancer. *Organic and Biomolecular Chemistry* **2018**, *16*, 8769-8782.
10. Mandal, P.; Kundu, B. K.; Vyas, K.; Sabu, V.; Helen, A.; Dhankhar, S. S.; Nagaraja, C. M.; **Bhattacherjee, D.**; Bhabak, K. P.; Mukhopadhyay, S.* Ruthenium(II) arene NSAID complexes: inhibition of cyclooxygenase and antiproliferative activity against cancer cell lines. *Dalton Transaction* **2018**, *47*, 517-527.
11. Saha, M.; Vyas, K. M.; Martins, L. M.; Martins, N. M. R.; Pombeiro, A. J. L.; Mobin, S. M.; **Bhattacherjee, D**.; Bhabak, K. P.; Mukhopadhyay, S. Copper (II) tetrazolato complexes: Role in oxidation catalysis and protein binding. *Polyhedron* **2017**, *132*, 53-63.
12. **Bhattacherjee, D**.; Bhabak, K. P.* Atom based 3D-QSAR studies on 2,4-dioxopyrimidine-1-carboxamide analogs: Validation of experimental inhibitory potencies towards acid ceramidase. *European Journal of Pharmaceutical Sciences* **2016**, *83*, 8-18.

Conferences

1. **Bhattacherjee, D**., Bhabak, K.P. A Highly Selective Synthetic Strategies to Symmetrical Diorganotrisulfides with Hydrogen Sulfide Donation Capacities. Participated as oral presenter at JNOST-2020, IISc Bangalore.
2. **Bhattacherjee, D**., Mahato, S.K., Bhabak, K.P. Organotrisulfide-based Donors of Hydrogen Sulfide: Synthetic Strategies and Biothiol-triggered H_2S Donation Efficacies. Participated as oral presenter at GASO2020 (American Gasotransmitter Symposium 2020 twitter poster event).
3. **Bhattacherjee, D**., Bhabak, K.P. Garlic-derived Organosulfur Compounds and Analogues: Synthesis and Anti-cancer Activities. Participated as oral presenter and received '**Best Oral Presentation Award**' at Research Conclave-2019, IIT Guwahati, India.
4. **Bhattacherjee, D**., Bhabak, K.P. Garlic-derived Organosulfur Compounds and Analogues: An Efficient Synthetic Methodology and Antiproliferative Activities, Participated as oral presenter at "Frontiers in Chemical Sciences, 2018", IIT Guwahati, India.
5. **Bhattacherjee, D**., Bhabak, K.P. Garlic-derived Organosulfur Compounds and Analogues: An Efficient Synthetic Methodology and Anti-proliferative Activities.

Participated as poster presenter at International Conference on Chemistry for Human Development (ICCHD-2018), India.

6. **Bhattacherjee, D**., Bhabak, K.P. Atom-based 3D-QSAR studies on 2,4-dioxopyrimidine-1-carboxamide analogs: Validation of experimental inhibitory potencies towards acid ceramidase. Participated as oral presenter and received '**Best Oral Presentation Award**' at "Frontiers in Chemical Sciences, 2016", IIT Guwahati, India.

Supplementary data of Chapter 2

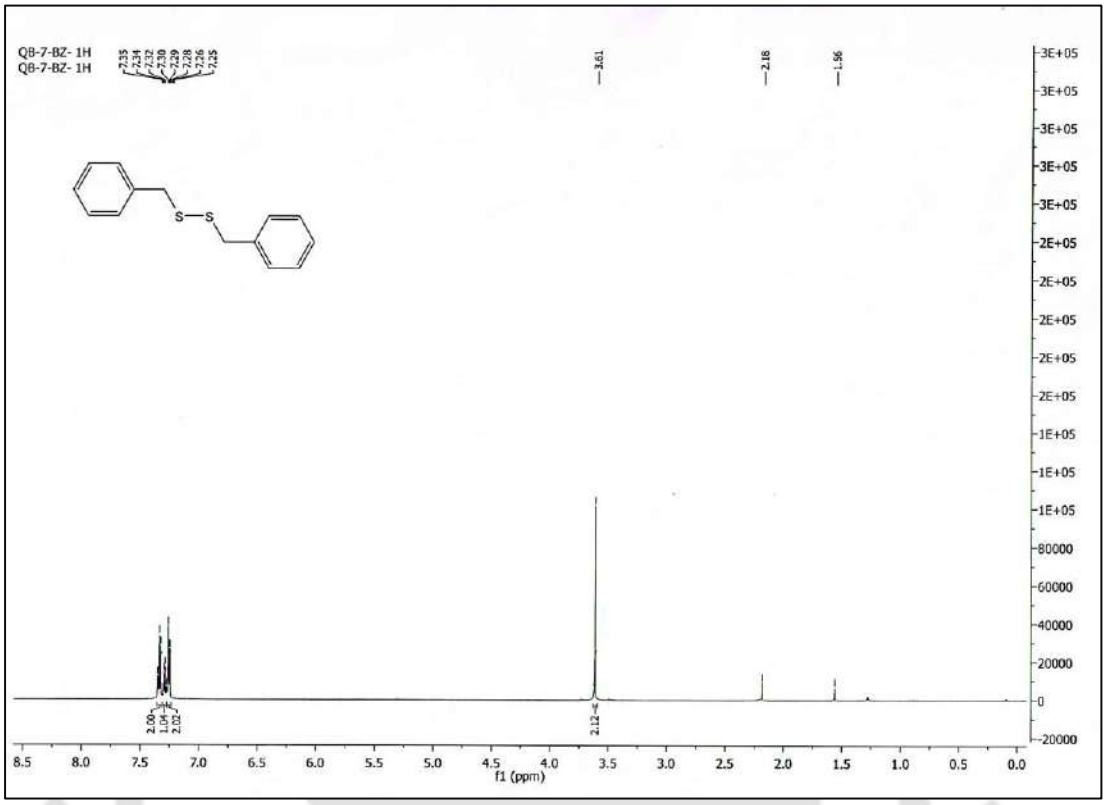

Figure A3.1. ^{1}H NMR ($CDCl_3$, 600 MHz, ppm) spectrum of compound DBDS.

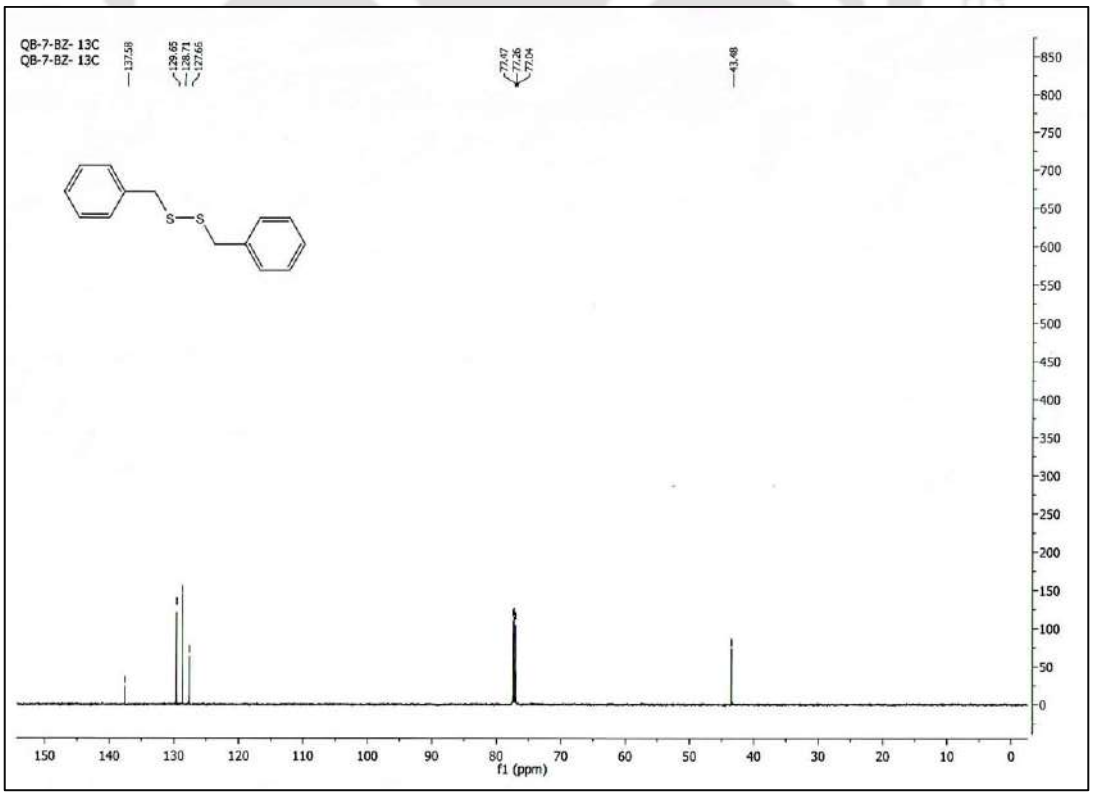

Figure A3.2. ^{13}C NMR ($CDCl_3$, 150 MHz, ppm) spectrum of compound DBDS.

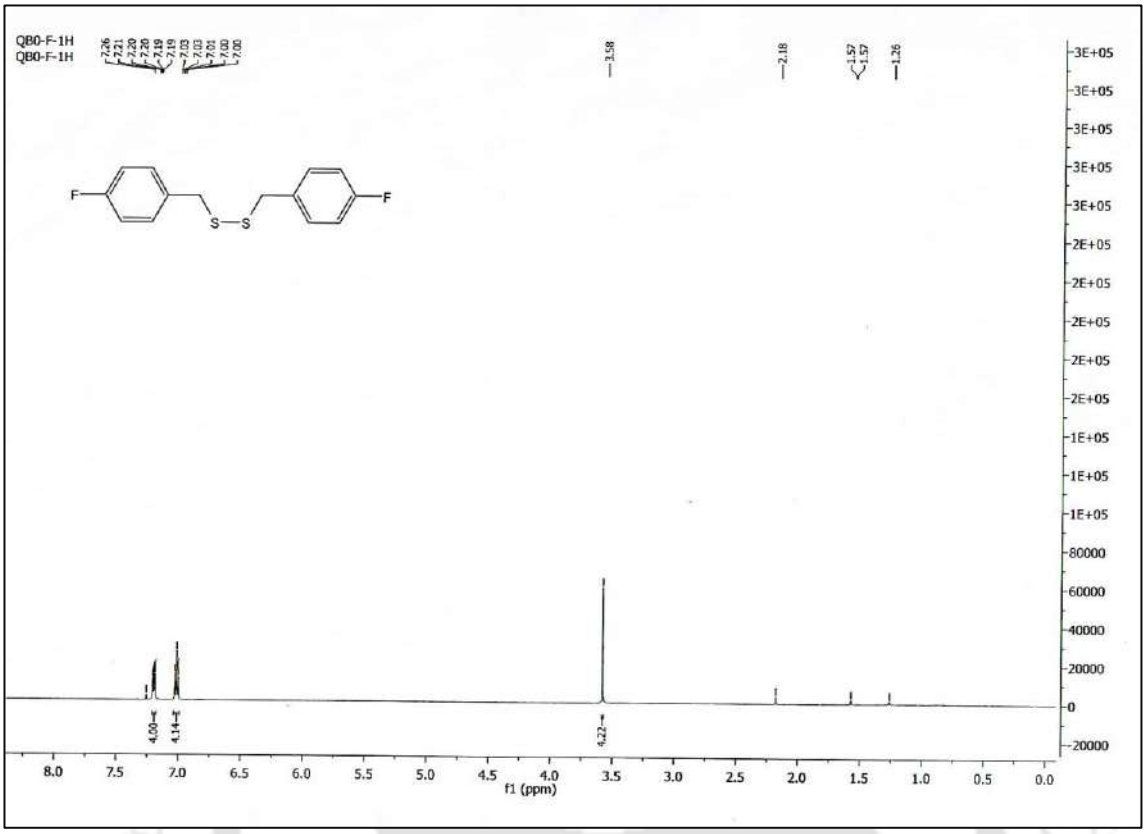

Figure A3.3. ^{1}H NMR ($CDCl_3$, 600 MHz, ppm) spectrum of compound **2.2**.

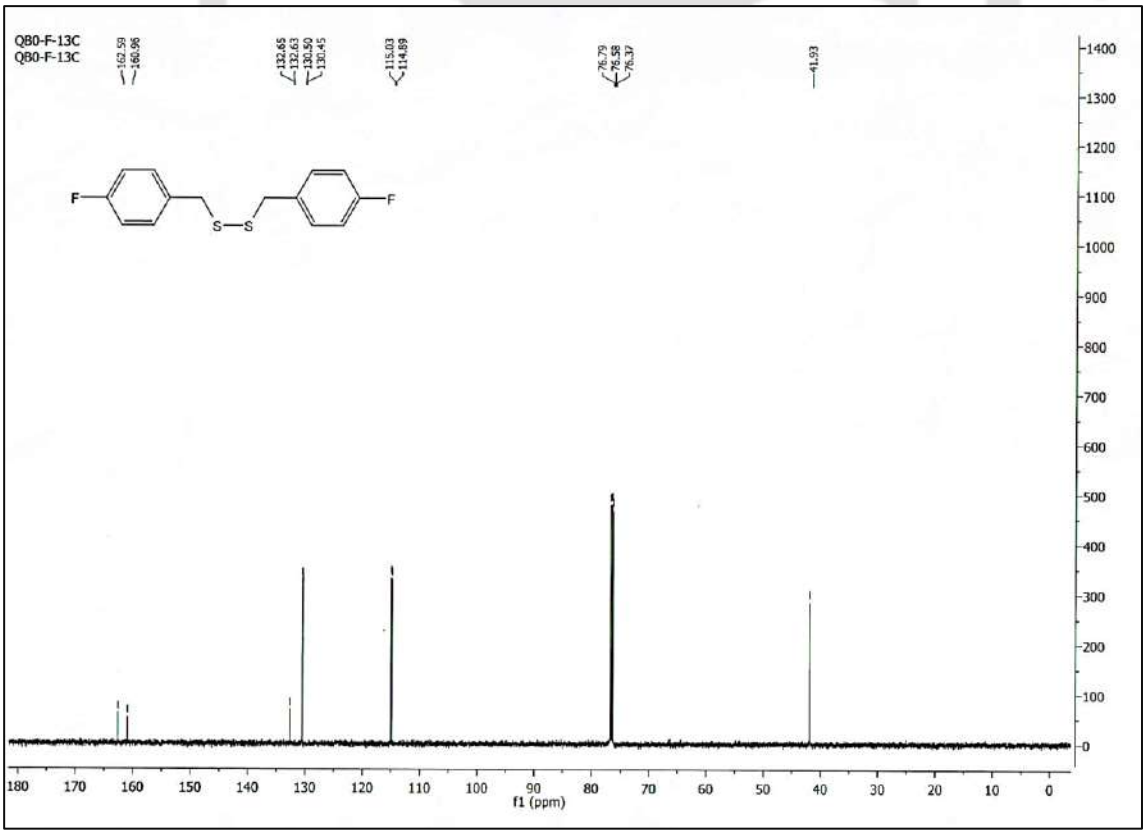

Figure A3.4. ^{13}C NMR ($CDCl_3$, 150 MHz, ppm) spectrum of compound **2.2**.

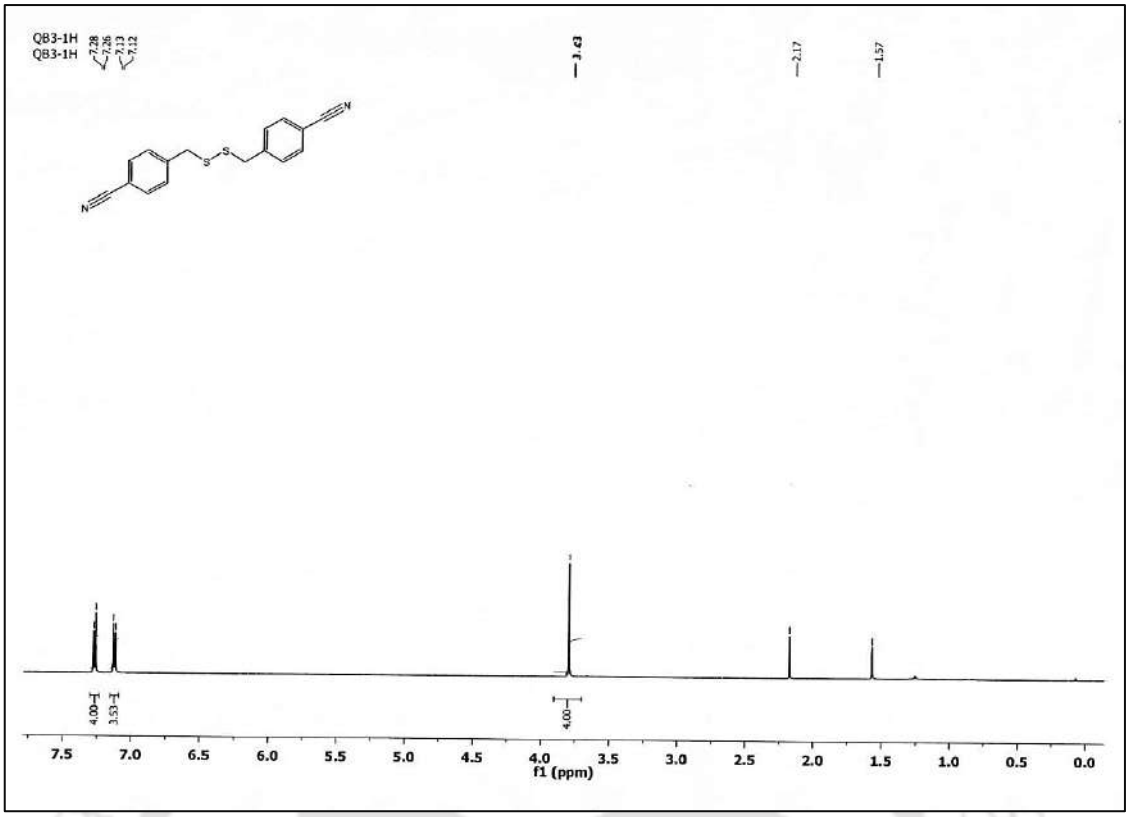

Figure A3.5. ^{1}H NMR ($CDCl_3$, 600 MHz, ppm) spectrum of compound **2.3**.

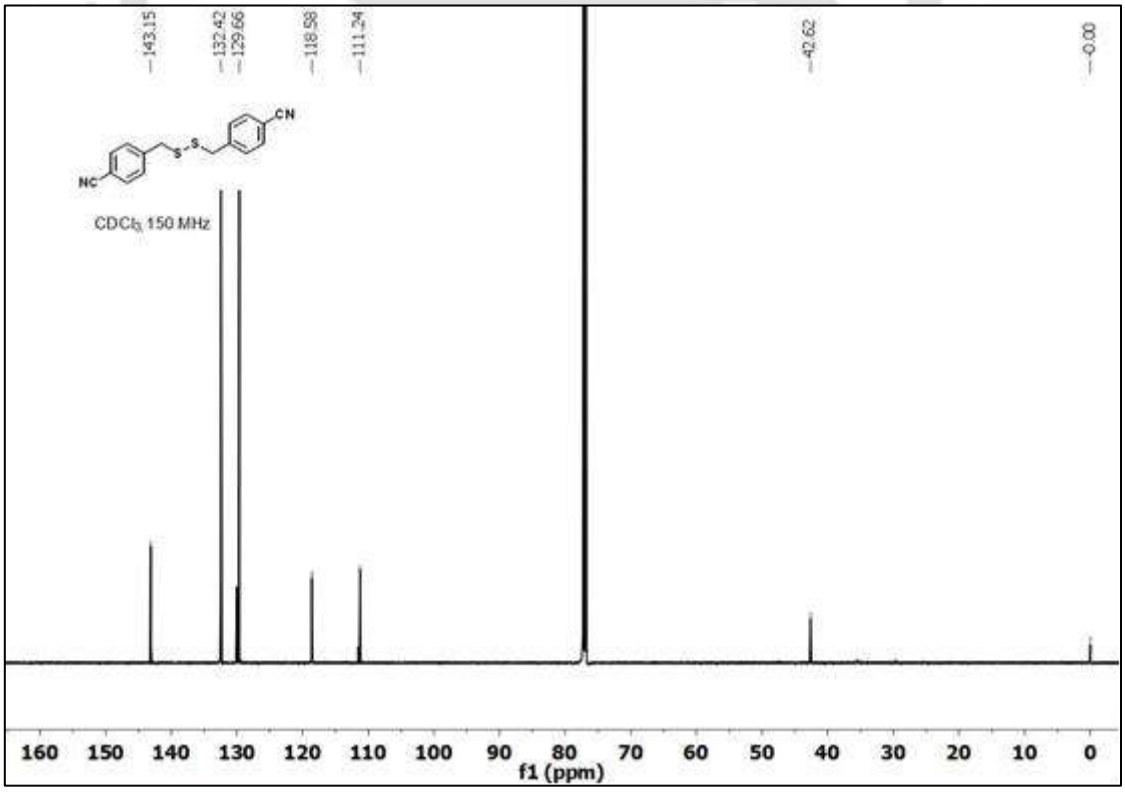

Figure A3.6. ^{13}C NMR ($CDCl_3$, 150 MHz, ppm) spectrum of compound **2.3**.

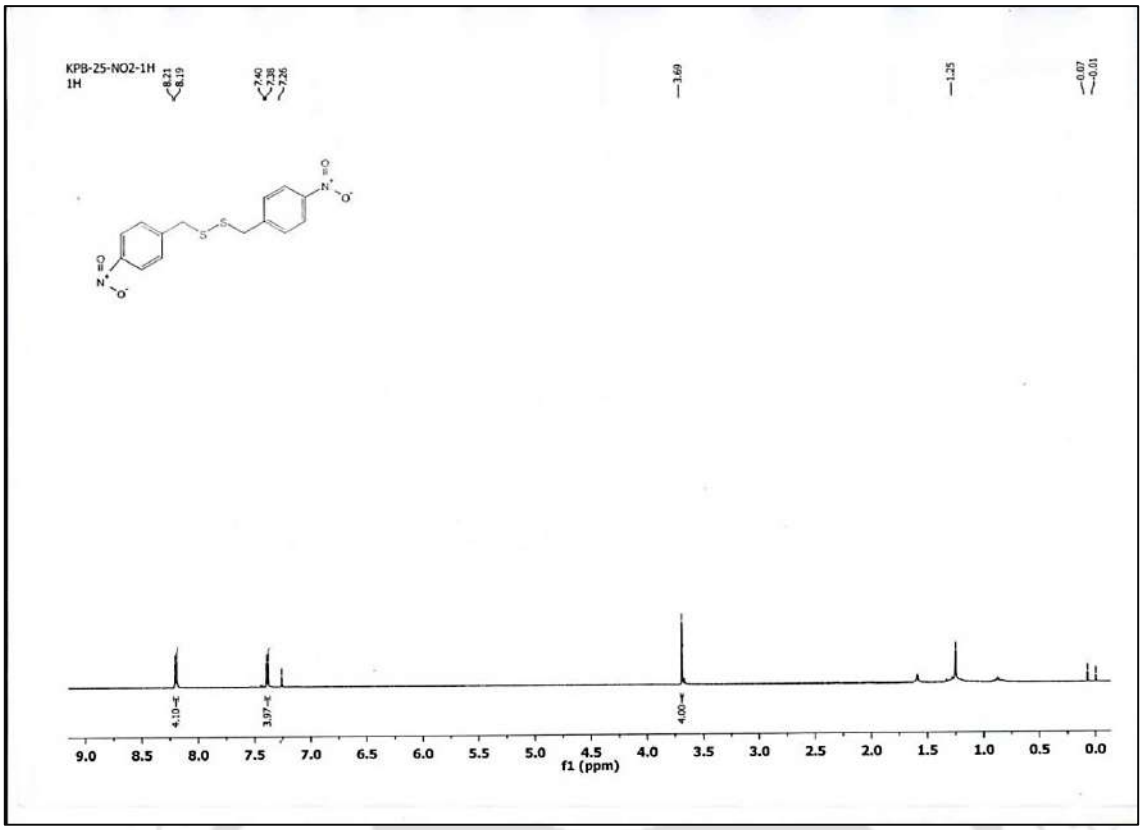

Figure A3.7. ^{1}H NMR ($CDCl_3$, 600 MHz, ppm) spectrum of compound **2.4**.

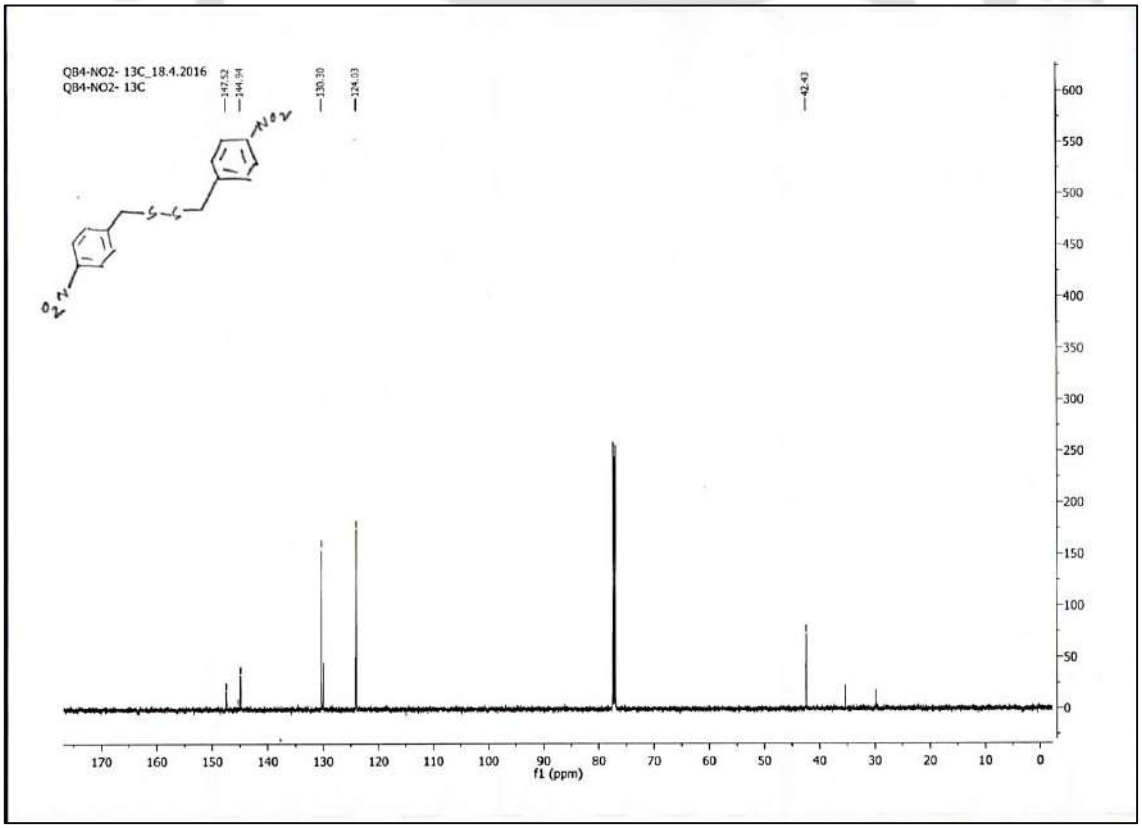

Figure A3.8. ^{13}C NMR ($CDCl_3$, 150 MHz, ppm) spectrum of compound **2.4**.

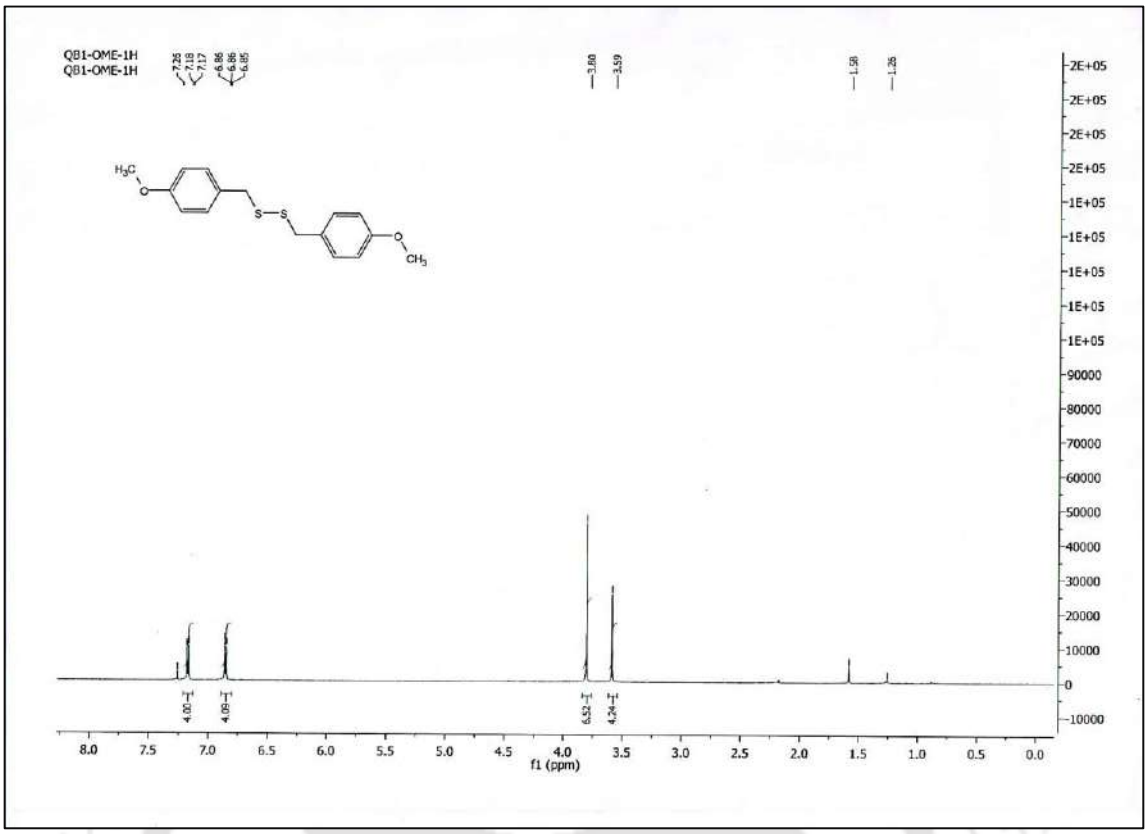

Figure A3.9. ^{1}H NMR ($CDCl_3$, 600 MHz, ppm) spectrum of compound **2.5**.

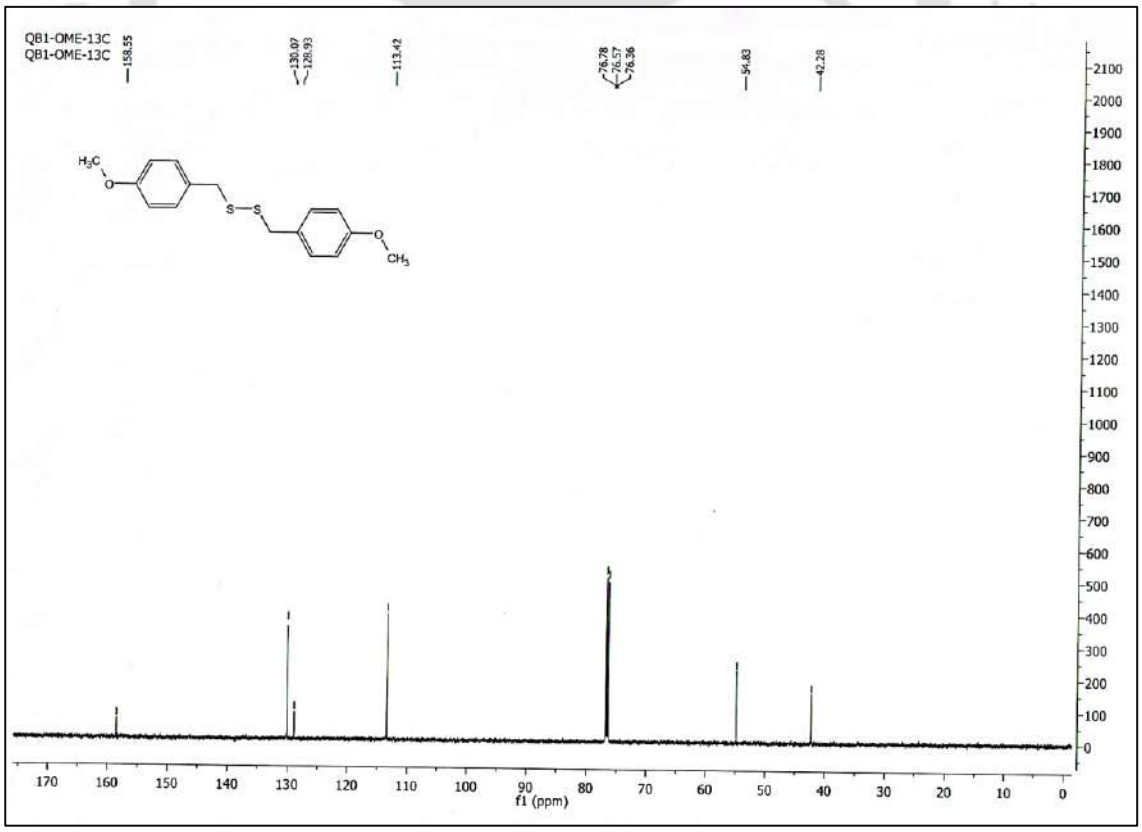

Figure A3.10. ^{13}C NMR ($CDCl_3$, 150 MHz, ppm) spectrum of compound **2.5**.

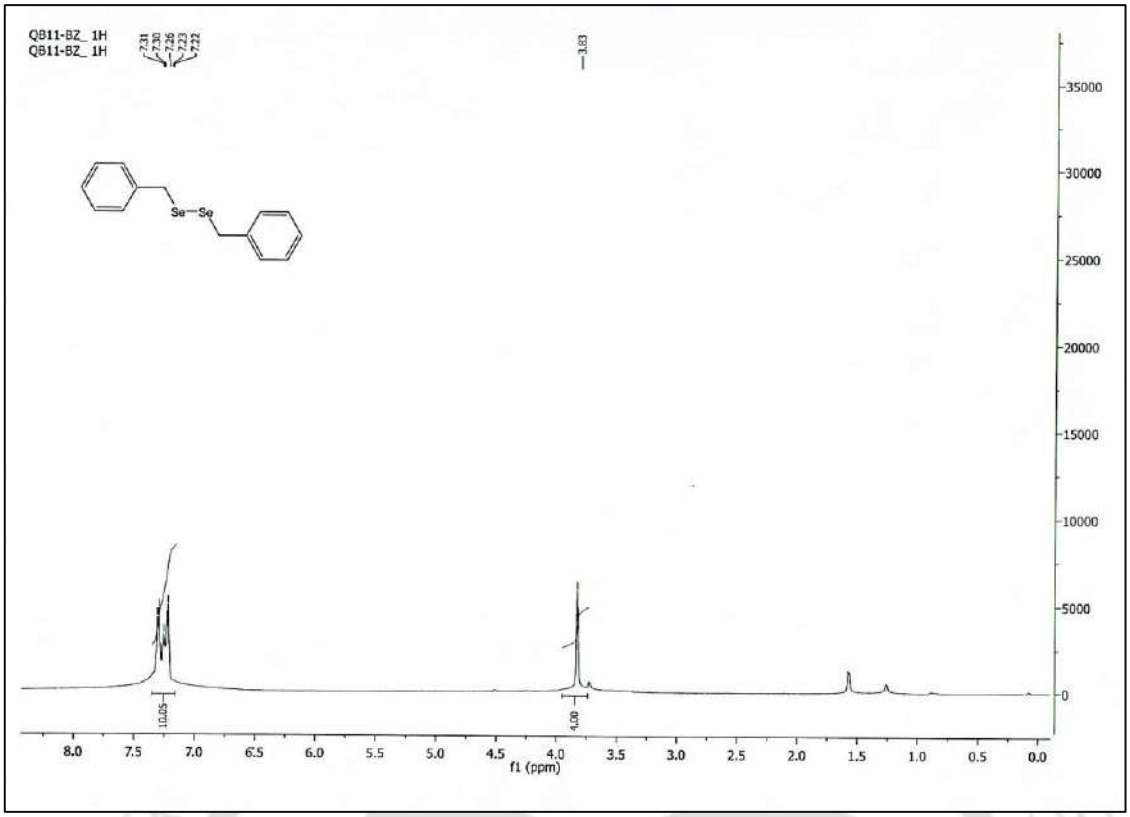

Figure A3.11. ^{1}H NMR ($CDCl_3$, 600 MHz, ppm) spectrum of compound **2.6**.

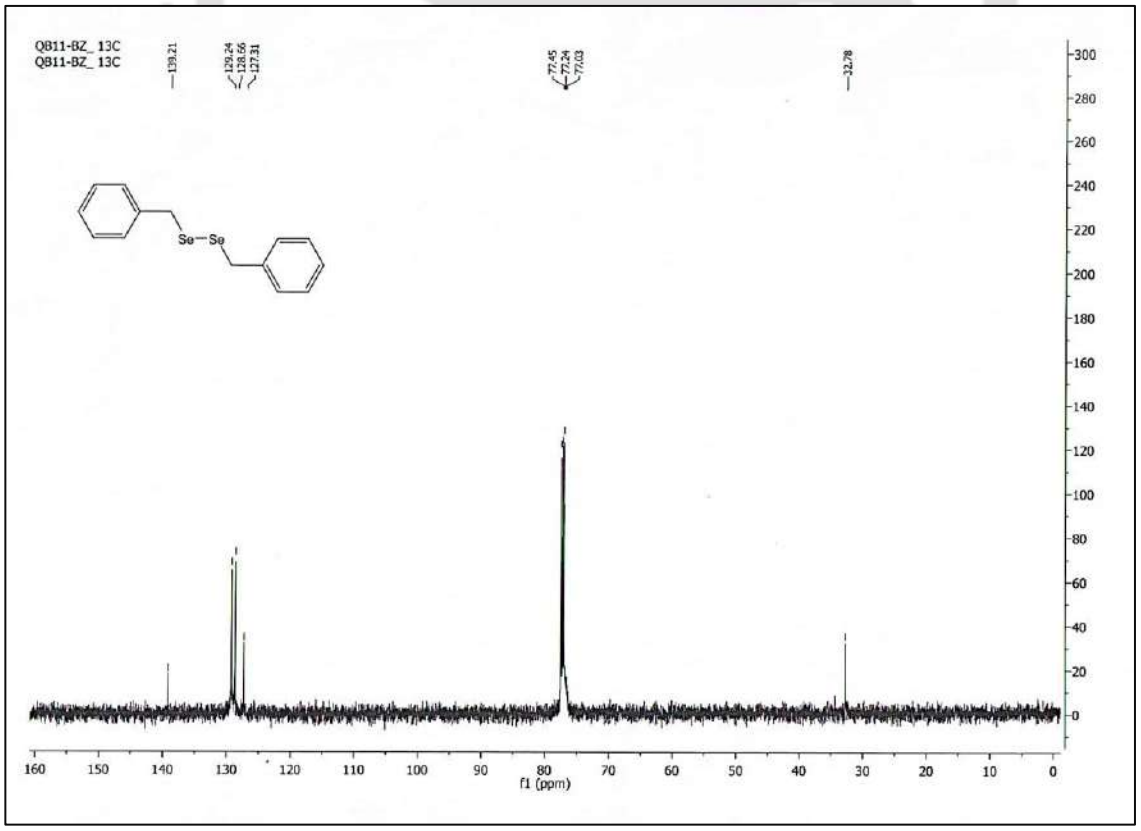

Figure A3.12. ^{13}C NMR ($CDCl_3$, 150 MHz, ppm) spectrum of compound **2.6**.

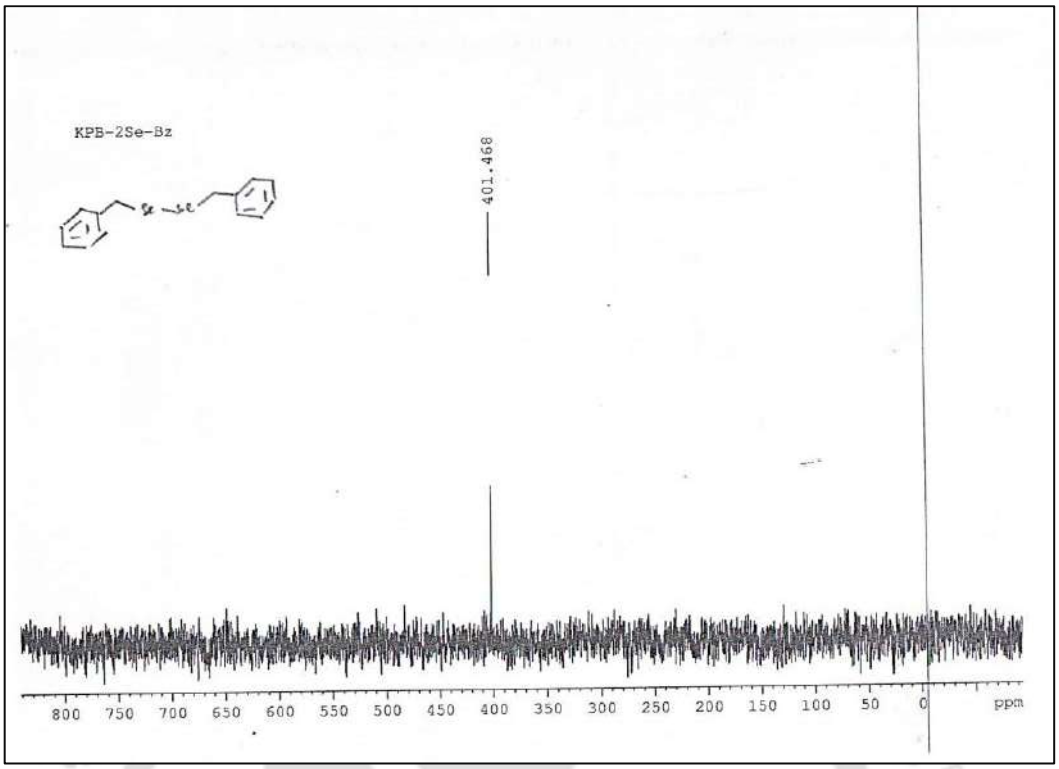

Figure A3.13. ^{77}Se NMR ($CDCl_3$, 114 MHz, ppm) spectrum of compound **2.6**.

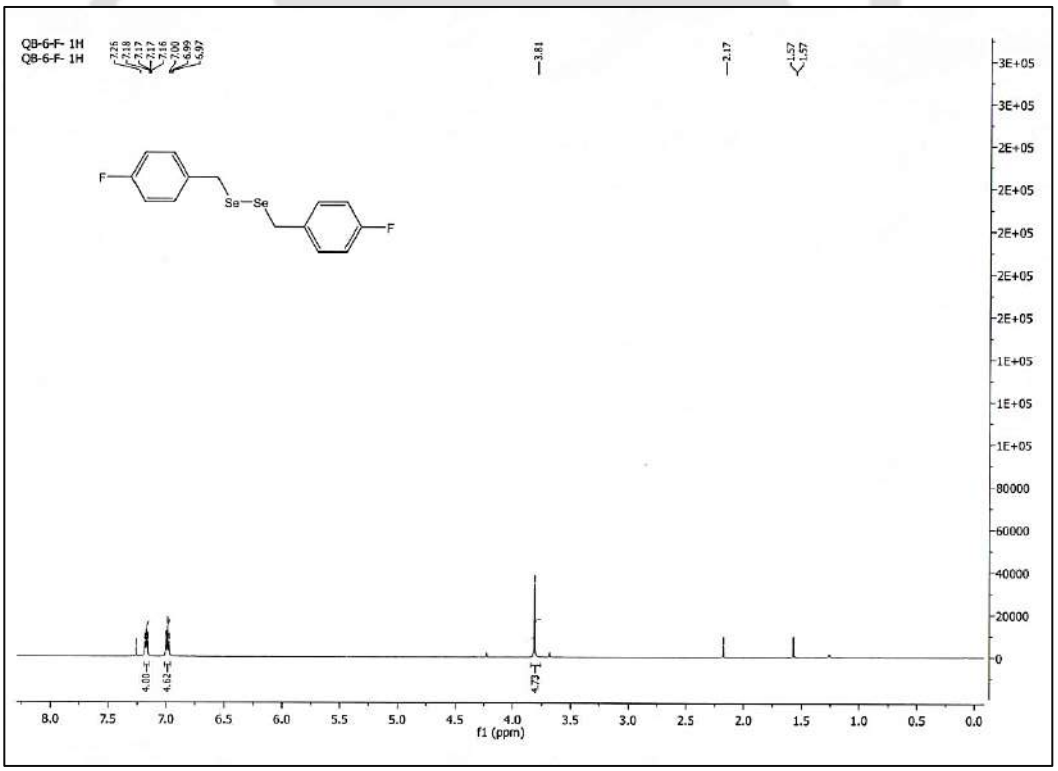

Figure A3.14. ^{1}H NMR ($CDCl_3$, 600 MHz, ppm) spectrum of compound **2.7**.

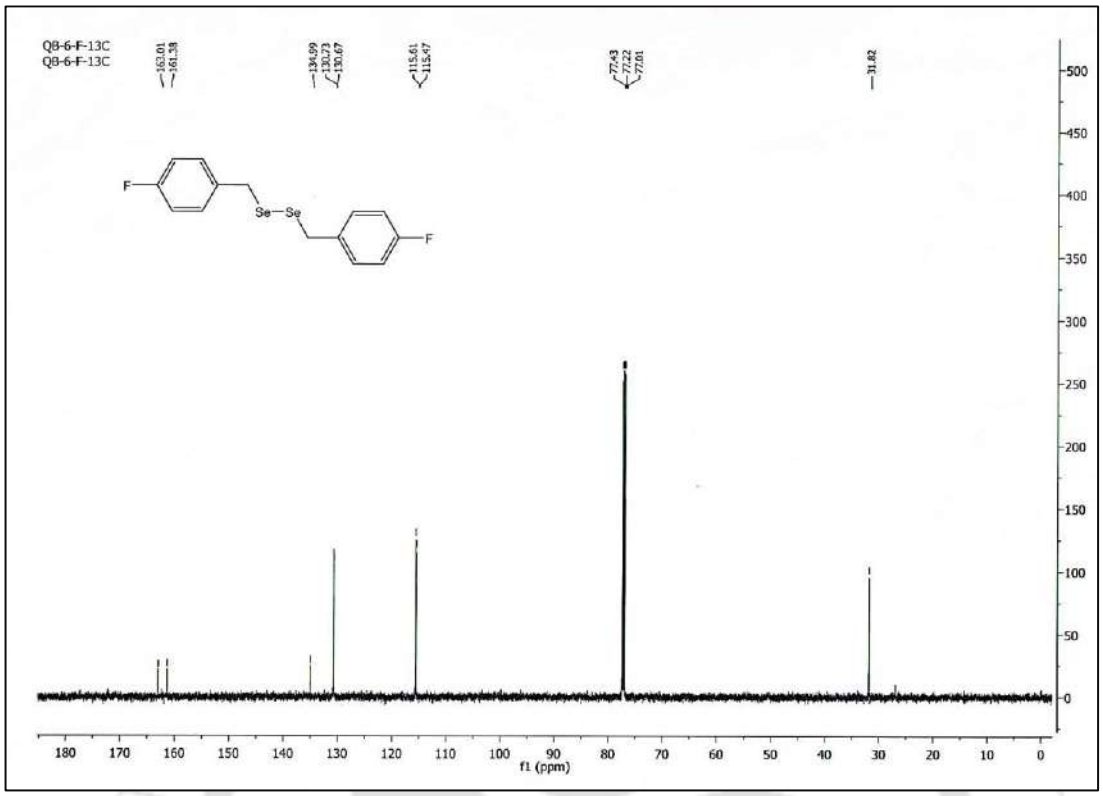

Figure A3.15. ^{13}C NMR ($CDCl_3$, 150 MHz, ppm) spectrum of compound **2.7**.

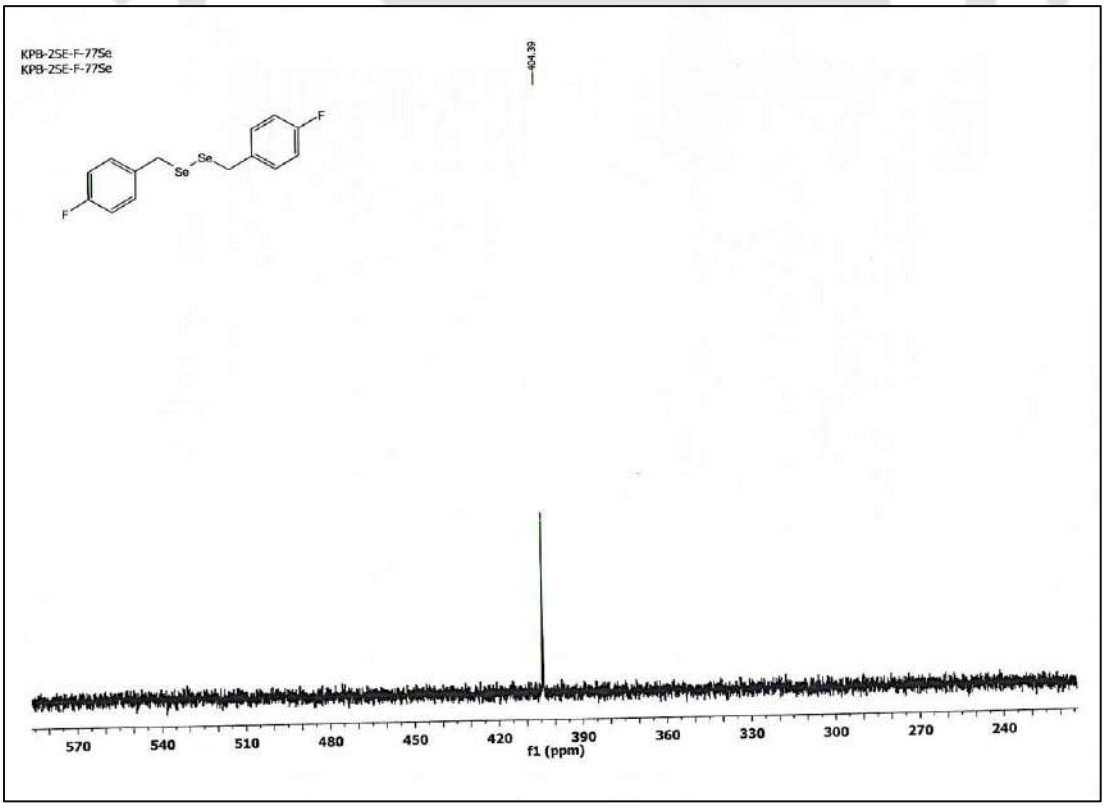

Figure A3.16. ^{77}Se NMR ($CDCl_3$, 114 MHz, ppm) spectrum of compound **2.7**.

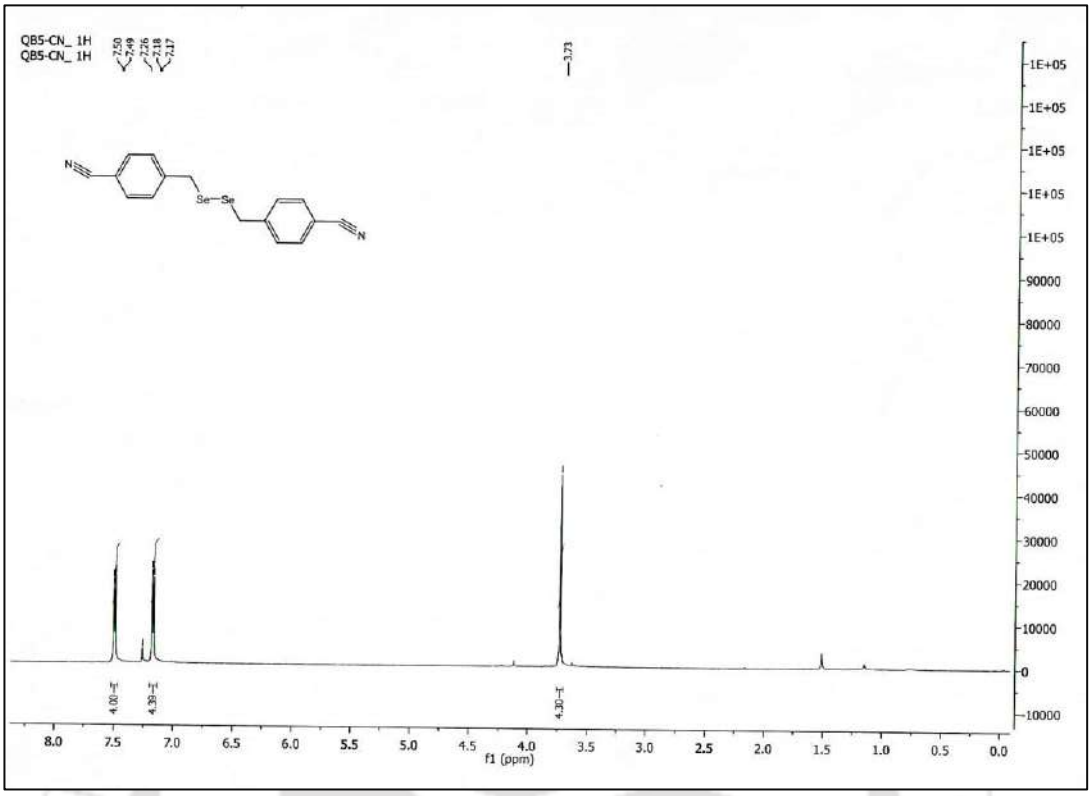

Figure A3.17. ^{1}H NMR ($CDCl_3$, 600 MHz, ppm) spectrum of compound **2.8**.

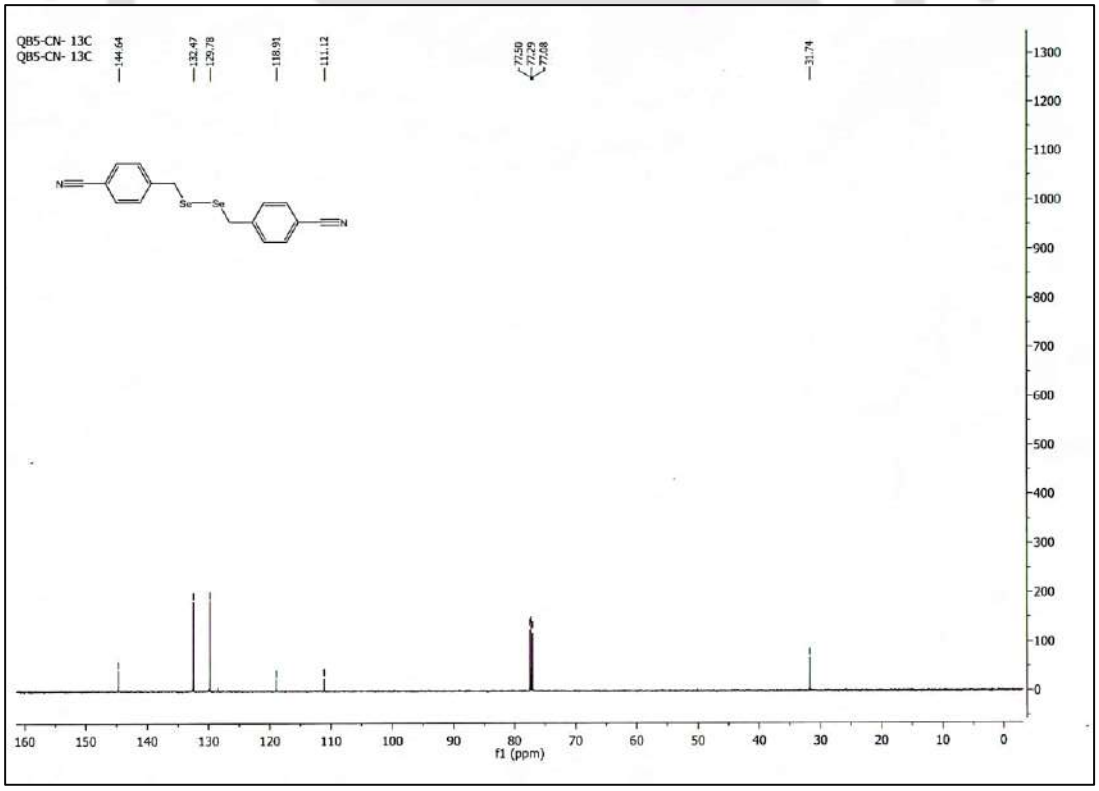

Figure A3.18. ^{13}C NMR ($CDCl_3$, 150 MHz, ppm) spectrum of compound **2.8**.

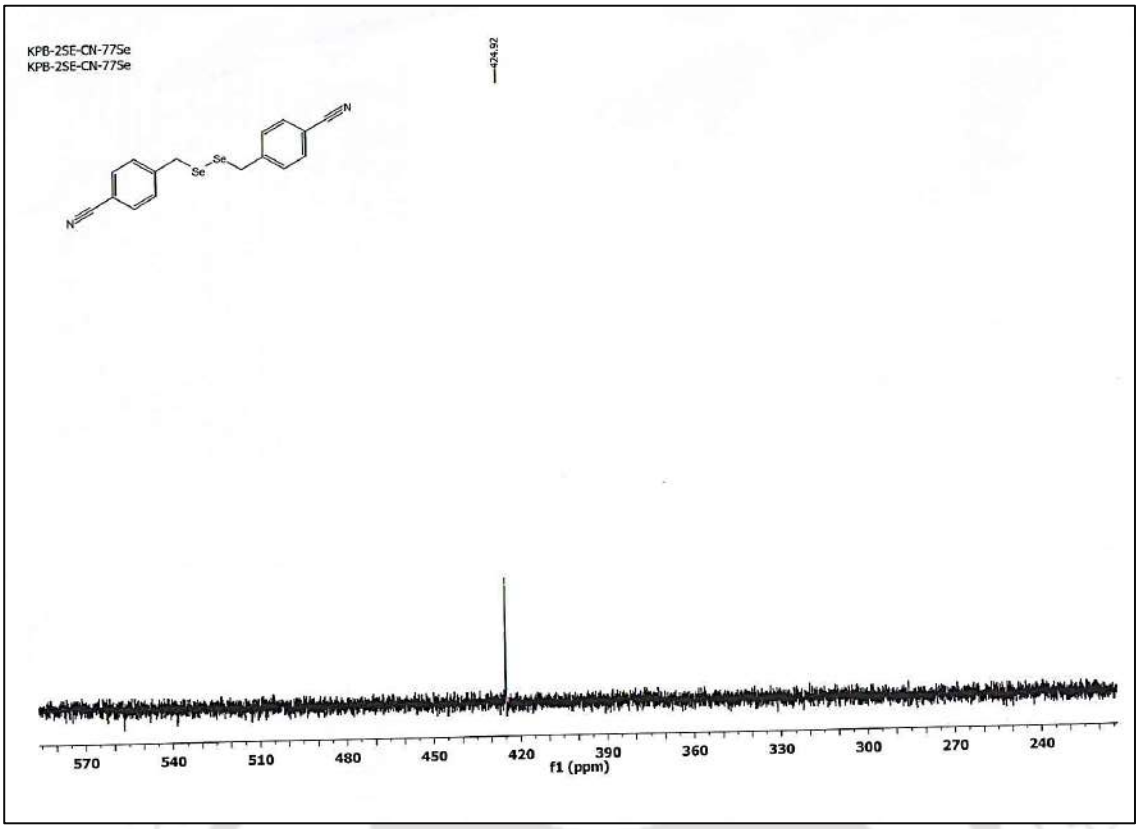

Figure A3.19. ^{77}Se NMR ($CDCl_3$, 114 MHz, ppm) spectrum of compound **2.8**.

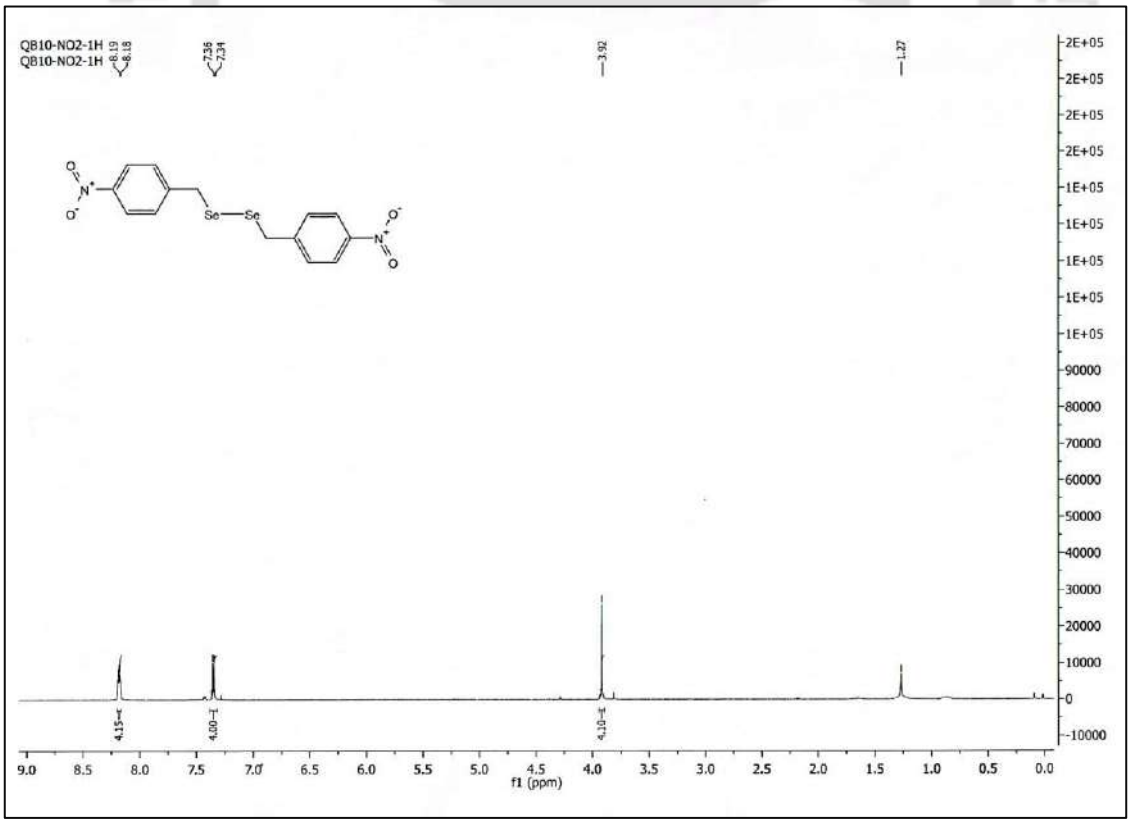

Figure A3.20. ^{1}H NMR ($CDCl_3$, 600 MHz, ppm) spectrum of compound **2.9**.

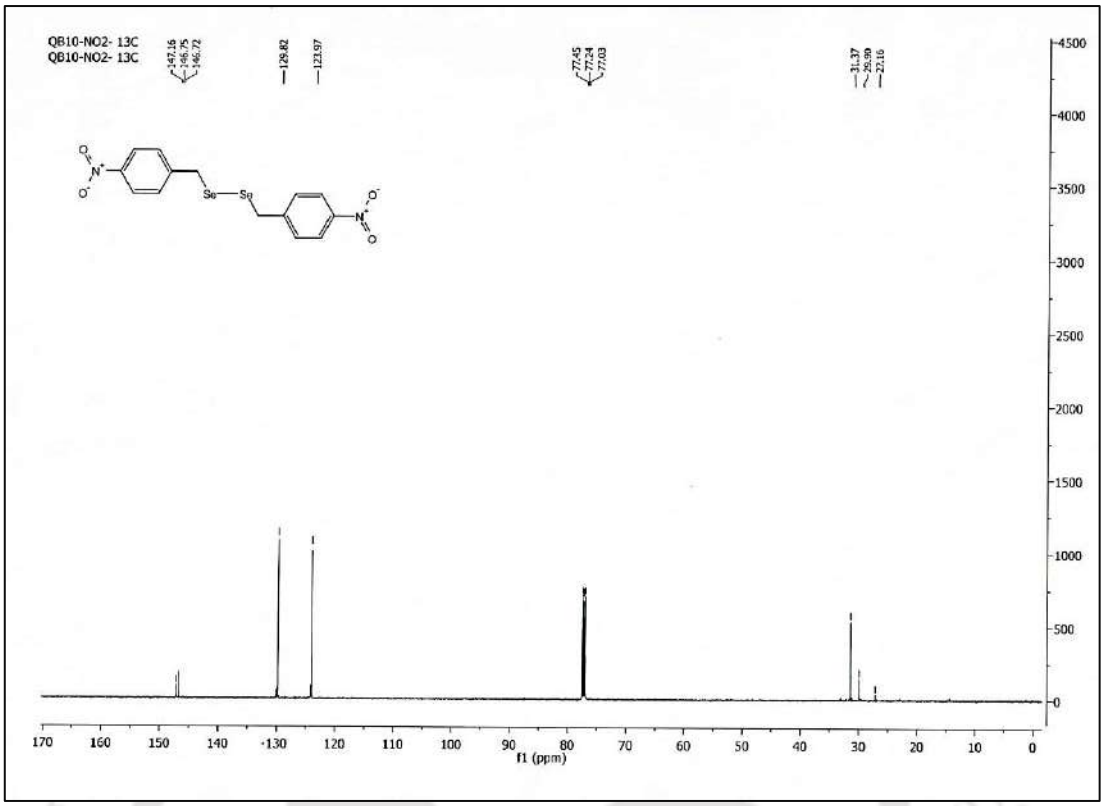

Figure A3.21. ^{13}C NMR ($CDCl_3$, 150 MHz, ppm) spectrum of compound **2.9**.

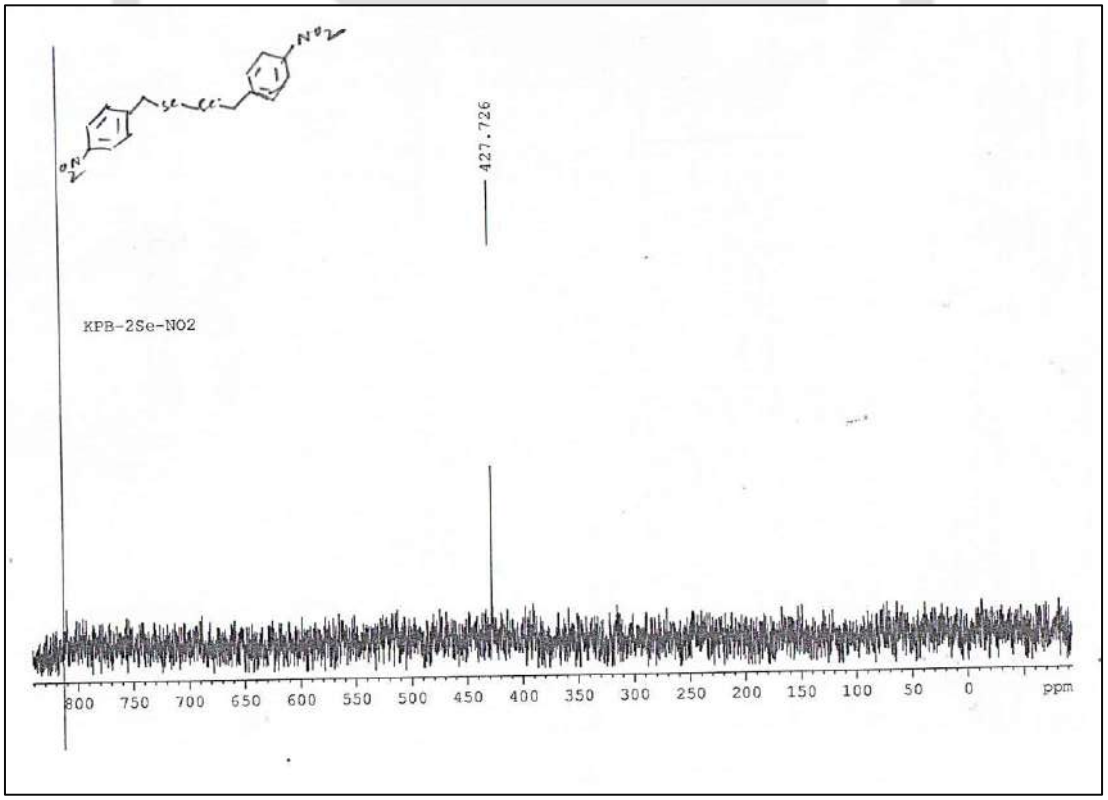

Figure A3.22. ^{77}Se NMR ($CDCl_3$, 114 MHz, ppm) spectrum of compound **2.9**.

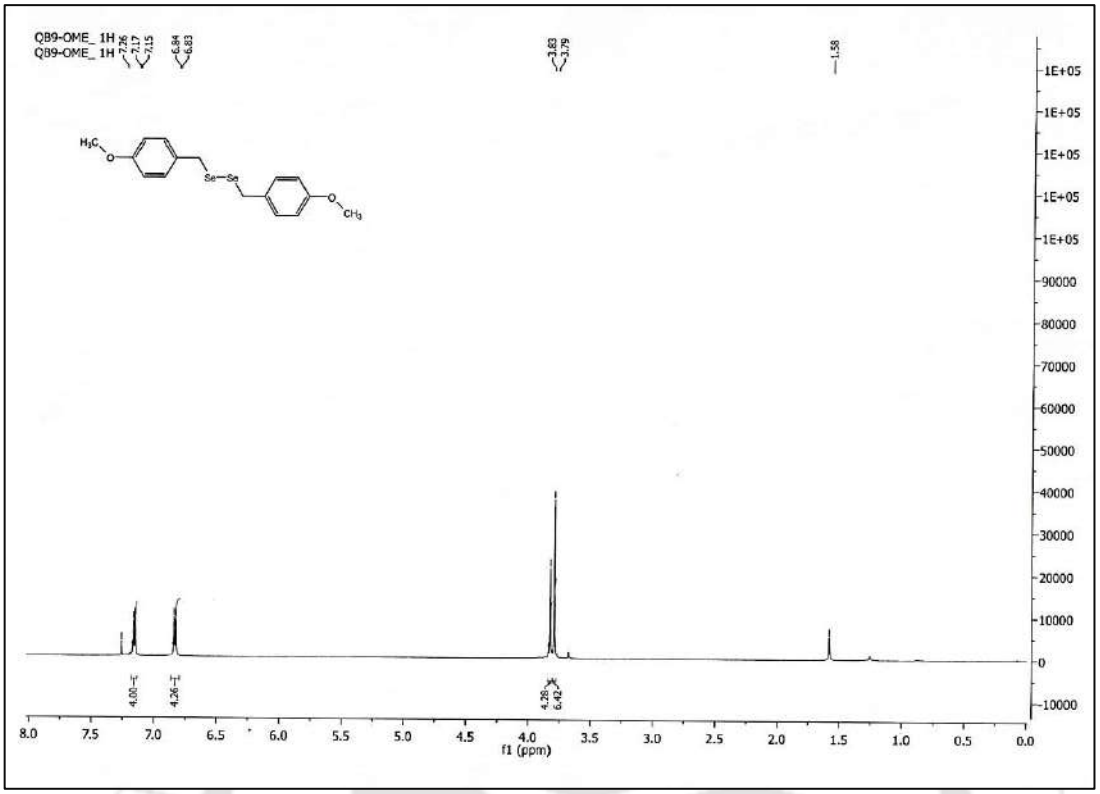

Figure A3.23. ^{1}H NMR ($CDCl_3$, 600 MHz, ppm) spectrum of compound **2.10**.

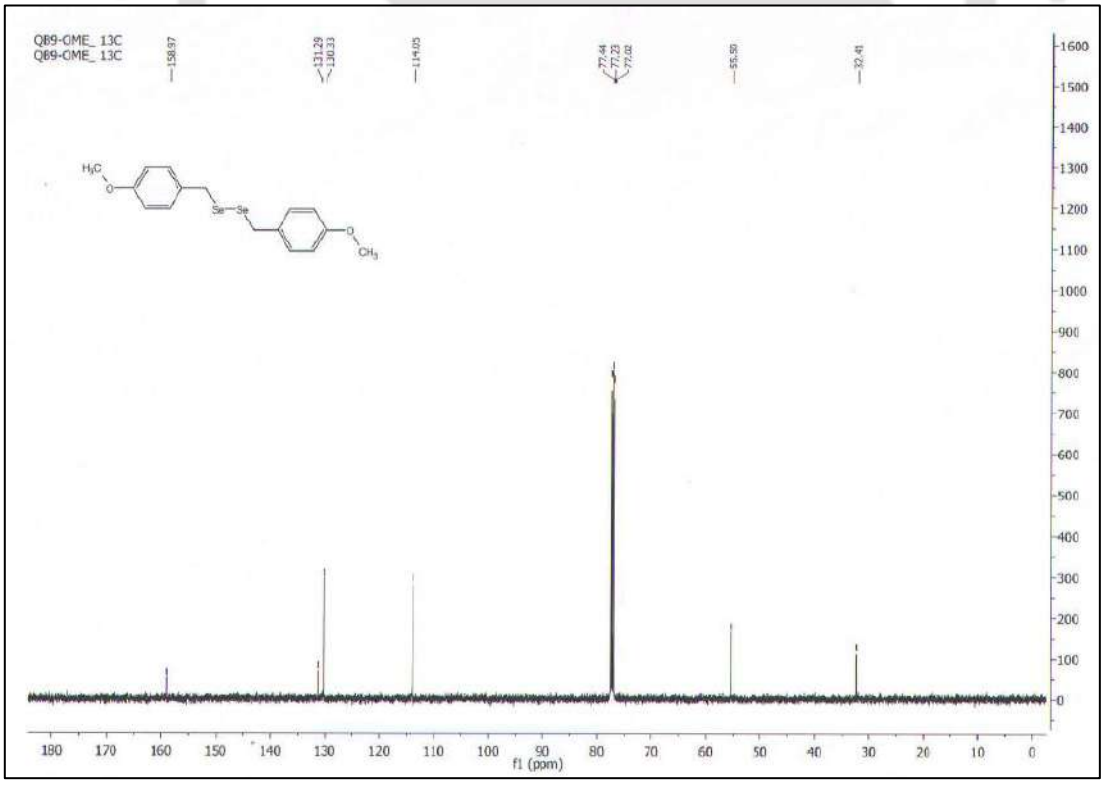

Figure A3.24. ^{13}C NMR ($CDCl_3$, 150 MHz, ppm) spectrum of compound **2.10**.

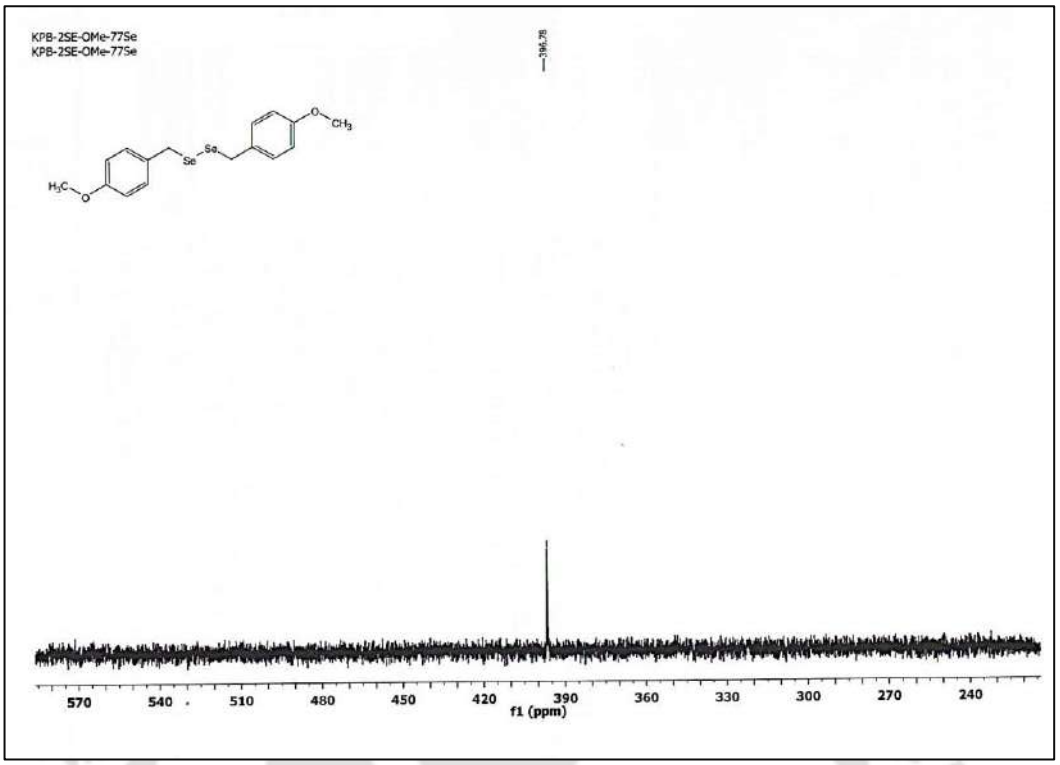

Figure A3.25. ^{77}Se NMR ($CDCl_3$, 114 MHz, ppm) spectrum of compound **2.10**.

Table A3.1. Crystal data and structure refinement for compound **2.3**

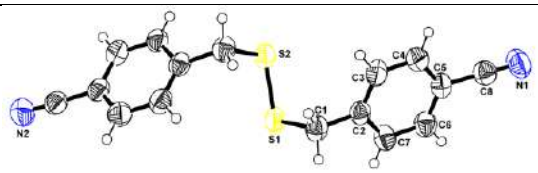	
2.3 (CCDC No: 1535430)	
Empirical formula	$C_{16}H_{12}N_2S_2$
Formula Weight	296.4
Crystal habit, color	Needle, colorless
Crystal size (mm)	0.18 × 0.1 × 0.05
Temperature, *T* (K)	293(2)
Wavelength, λ (Å)	0.71073
Crystal System	monoclinic
Space Group	P 21/n
Unit cell dimension	a = 8.4139(13) Å; b = 8.5686(13) Å; c = 20.958(5) Å; α = 90.00°, β = 98.194(18)° , γ =90.00°
Volume, V(Å^3)	1495.6(5)
Cell Formula units, Z	4
Calculated density, g/cm^3	1.316
Absorption Coefficient, μ (mm^{-1})	0.346
F(000)	616
θ range for data collection	3.1° to 28.1°
Limiting Indices	$-10 \leq h \leq 11$, $-11 \leq k \leq 10$, $-27 \leq l \leq 28$
Reflection Collected / unique	7325 / 3428
Refinement method	SHELXL-2016/4 (Sheldrick, 2016)
Data / Restraints / Parameters	3428 / 0 / 181
Goodness-of-fit on F^2	1.004
Final R indices [I>2sigma(I)]	R1 = 0.0632, wR2 = 0.1406
R indices (all data)	R1 = 0.1328, wR2 = 0.1876
Largest diff. peak and hole	0.250 and -0.632

Table A3.2. Crystal data and structure refinement for compound **2.8**

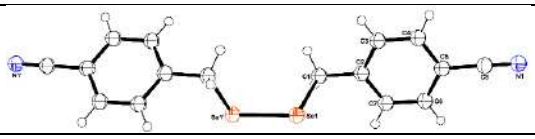	
2.8 (CCDC No: 1535431)	
Empirical formula	$C_{16}H_{12}N_2Se_2$
Formula Weight	390.2
Crystal habit, color	Needle, colorless
Crystal size (mm)	0.16 × 0.09 × 0.07
Temperature, *T* (K)	297(2)
Wavelength, λ (Å)	0.71073
Crystal System	monoclinic
Space Group	C 2/c
Unit cell dimension	a = 18.4748(9) Å; b = 5.7827(3) Å; c = 14.2201(7) Å; α = 90.00°, β = 91.609(3)° , γ =90.00°
Volume, V(Å^3)	1518.59(13)
Cell Formula units, Z	4
Calculated density, g/cm^3	1.707
Absorption Coefficient, μ (mm^{-1})	4.86
F(000)	760
θ range for data collection	2.86° to 28.29°
Limiting Indices	$-24 \leq h \leq 24$, $-7 \leq k \leq 7$, $-18 \leq l \leq 18$
Reflection Collected / unique	9655 / 1857
Refinement method	SHELXL-2016/4 (Sheldrick, 2016)
Data / Restraints / Parameters	1857 / 0 / 92
Goodness-of-fit on F2	1.072
Final R indices [I>2sigma(I)]	R1 = 0.0545, wR2 = 0.1136
R indices (all data)	R1 = 0.0775, wR2 = 0.124
Largest diff. peak and hole	1.322 and -0.700

Supplementary data of Chapter 3

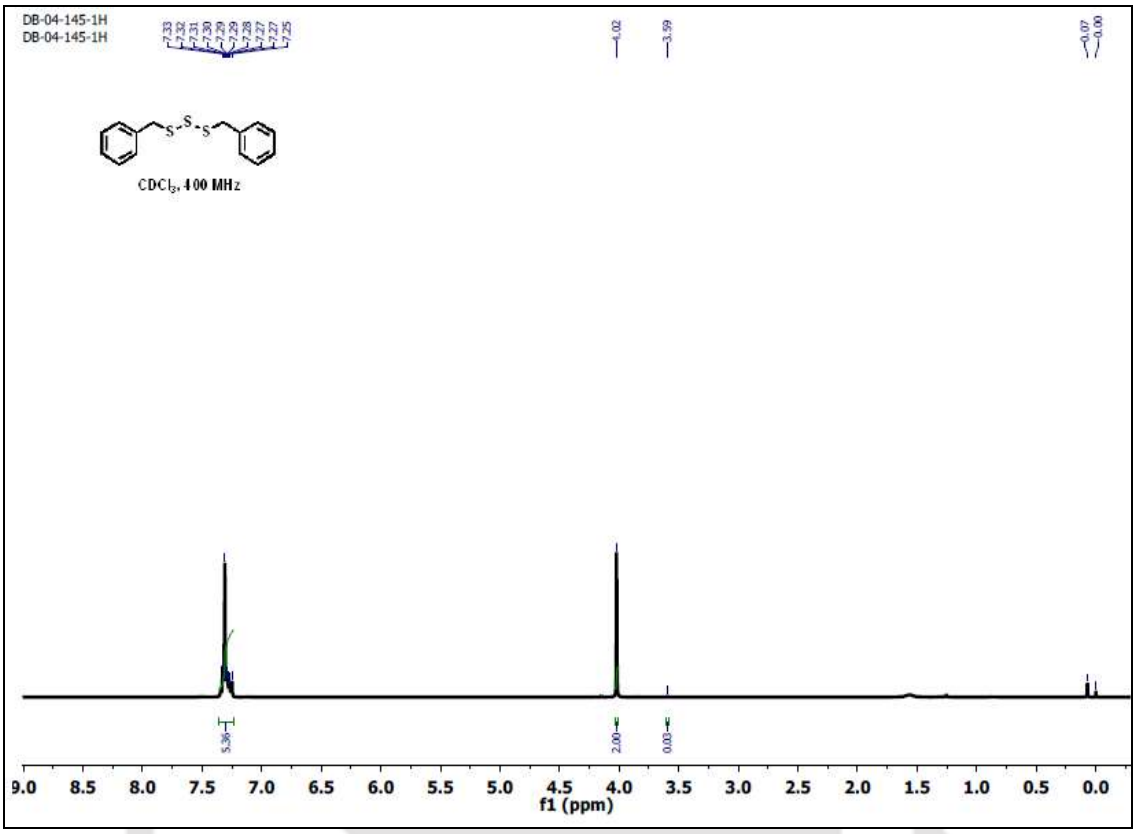

Figure A4.1. ^{1}H NMR ($CDCl_3$, 400 MHz, ppm) spectrum of compound DBTS.

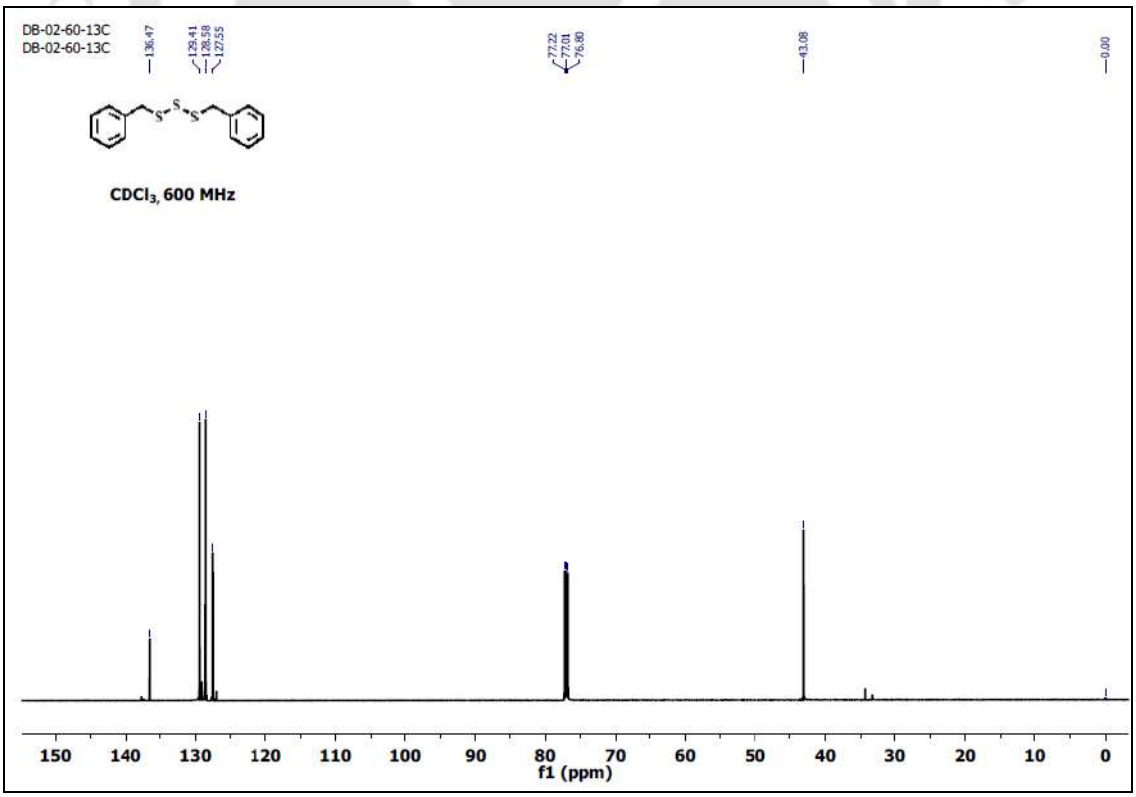

Figure A4.2. ^{13}C NMR ($CDCl_3$, 150 MHz, ppm) spectrum of compound DBTS.

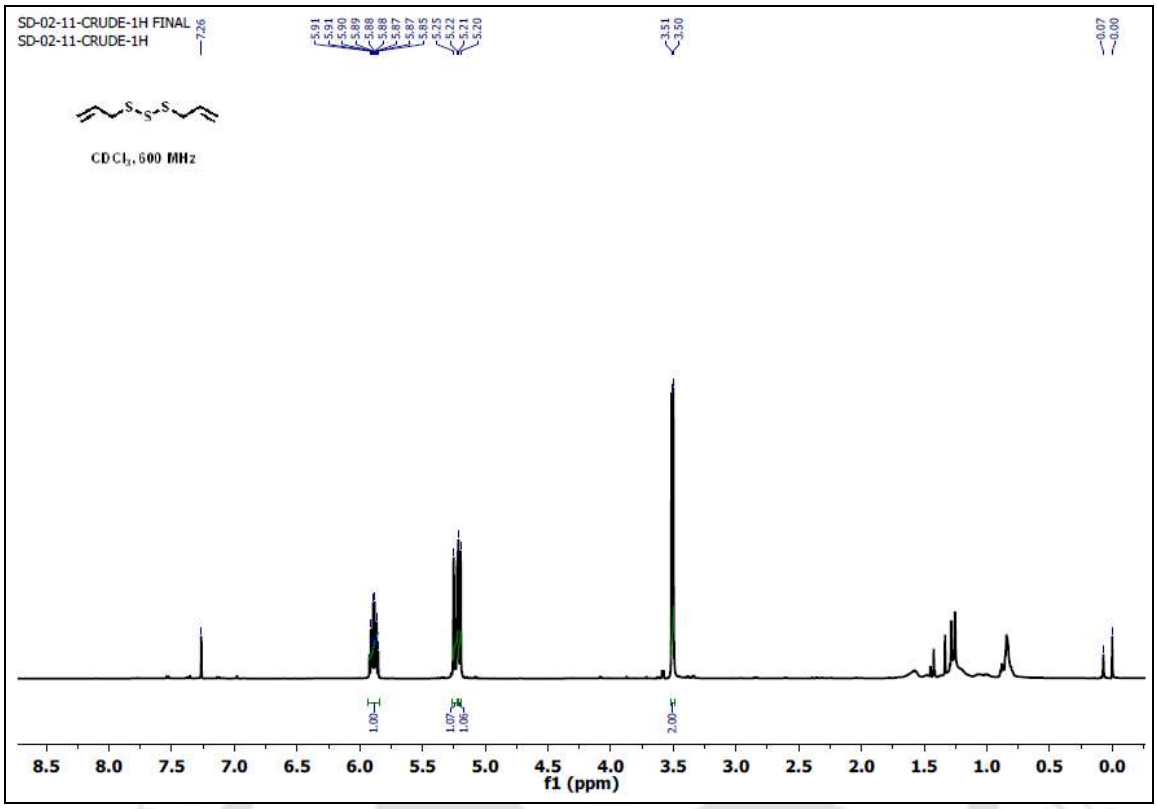

Figure A4.3. ^{1}H NMR ($CDCl_3$, 600 MHz, ppm) spectrum of compound DATS.

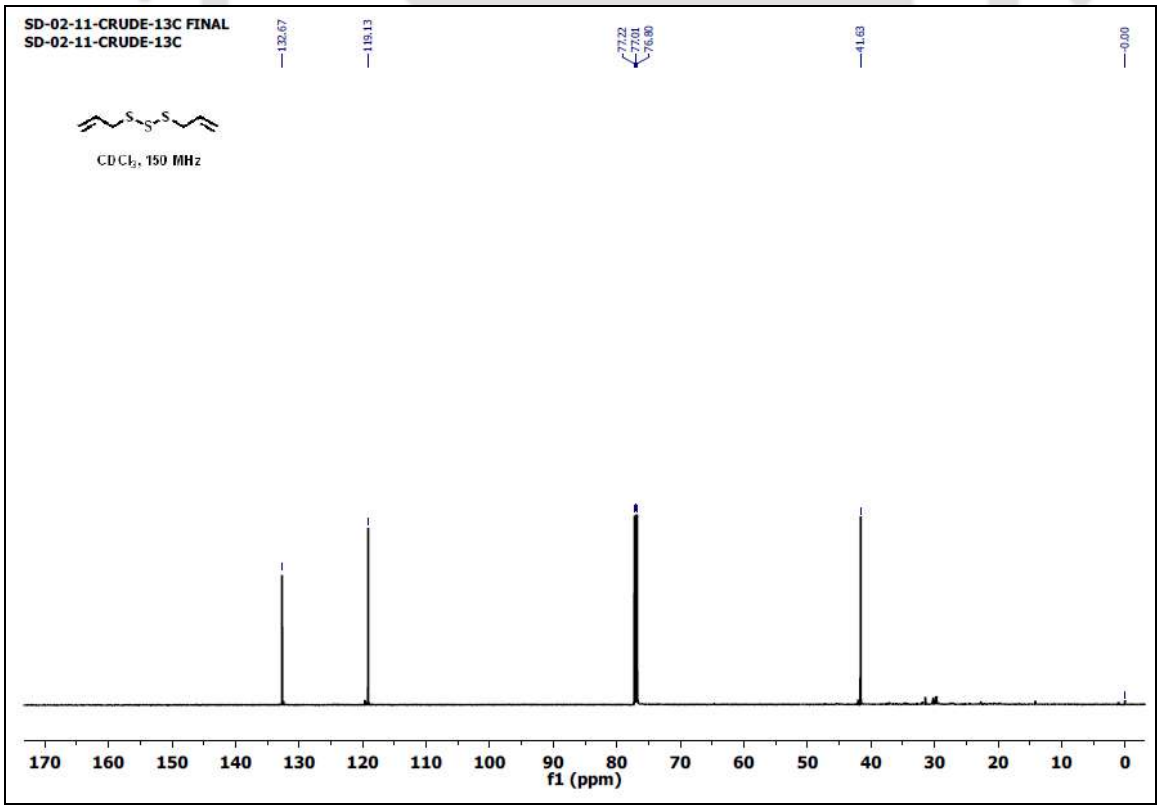

Figure A4.4. ^{13}C NMR ($CDCl_3$, 150 MHz, ppm) spectrum of compound DATS.

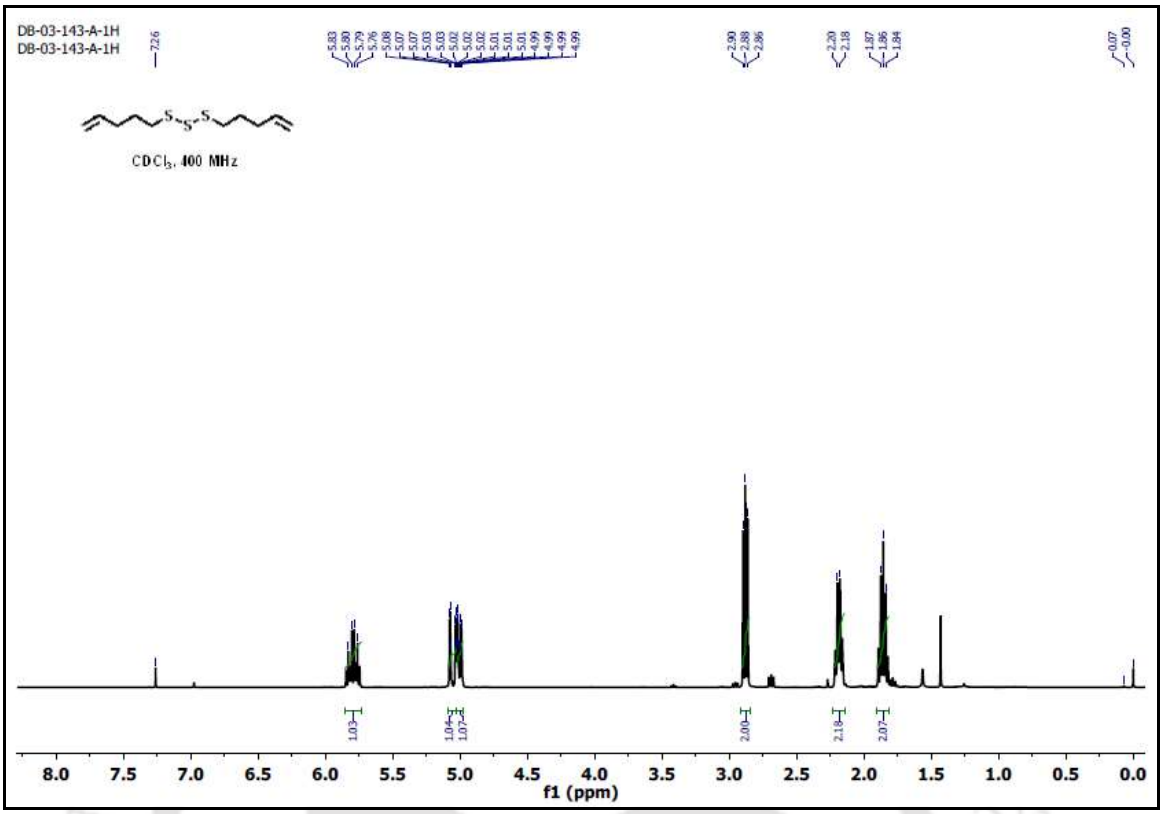

Figure A4.5. ^{1}H NMR ($CDCl_3$, 400 MHz, ppm) spectrum of compound **3.1**.

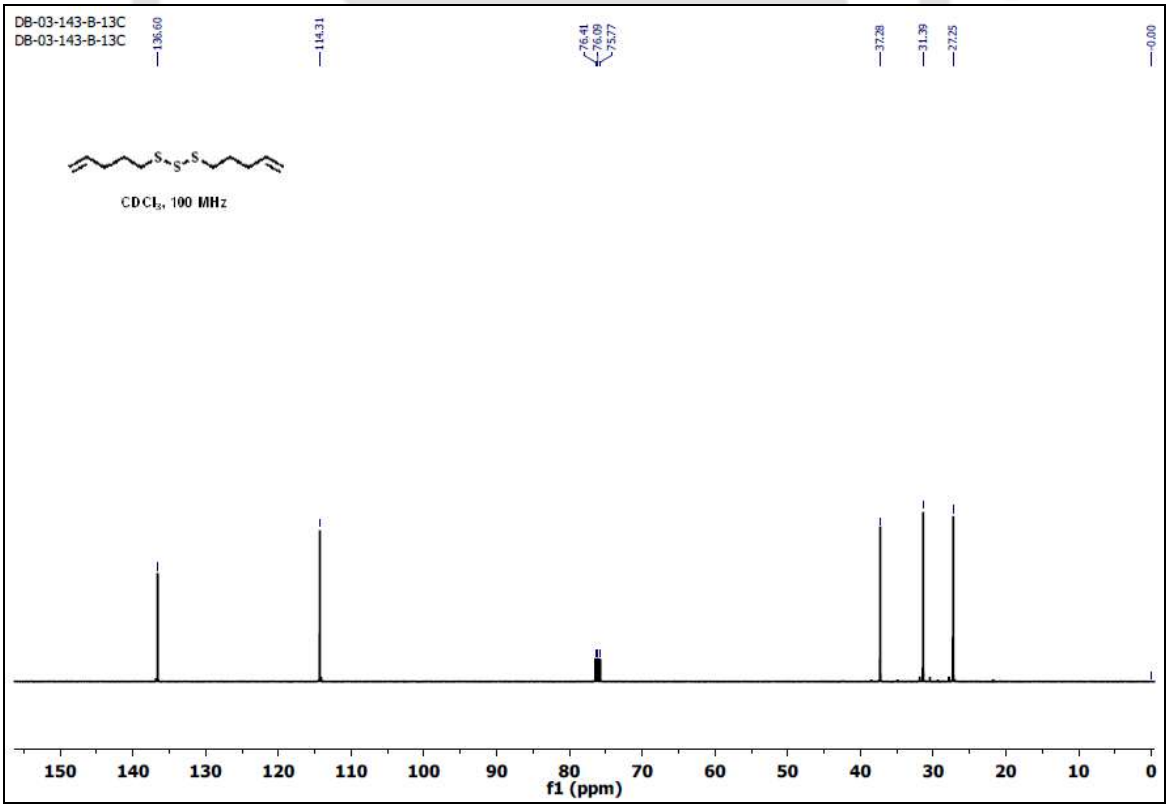

Figure A4.6. ^{13}C NMR ($CDCl_3$, 100 MHz, ppm) spectrum of compound **3.1**.

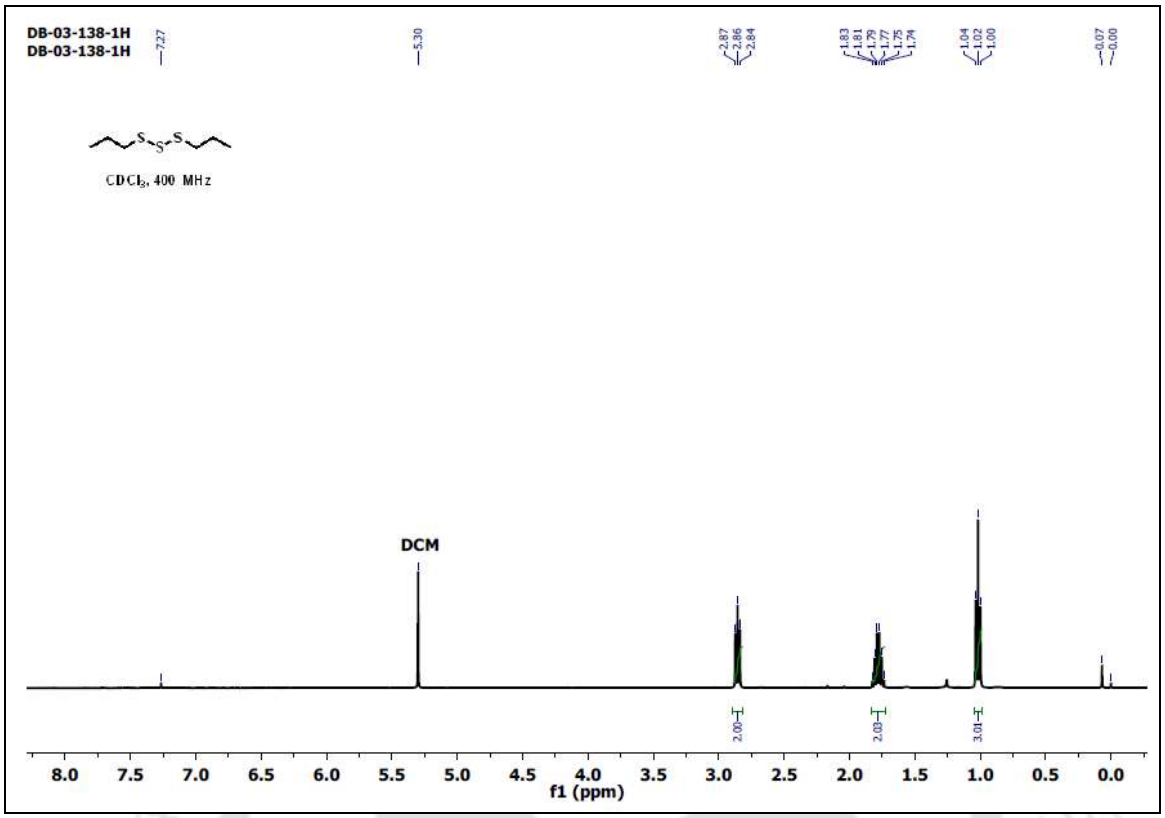

Figure A4.7. ^{1}H NMR ($CDCl_3$, 400 MHz, ppm) spectrum of compound **3.2**.

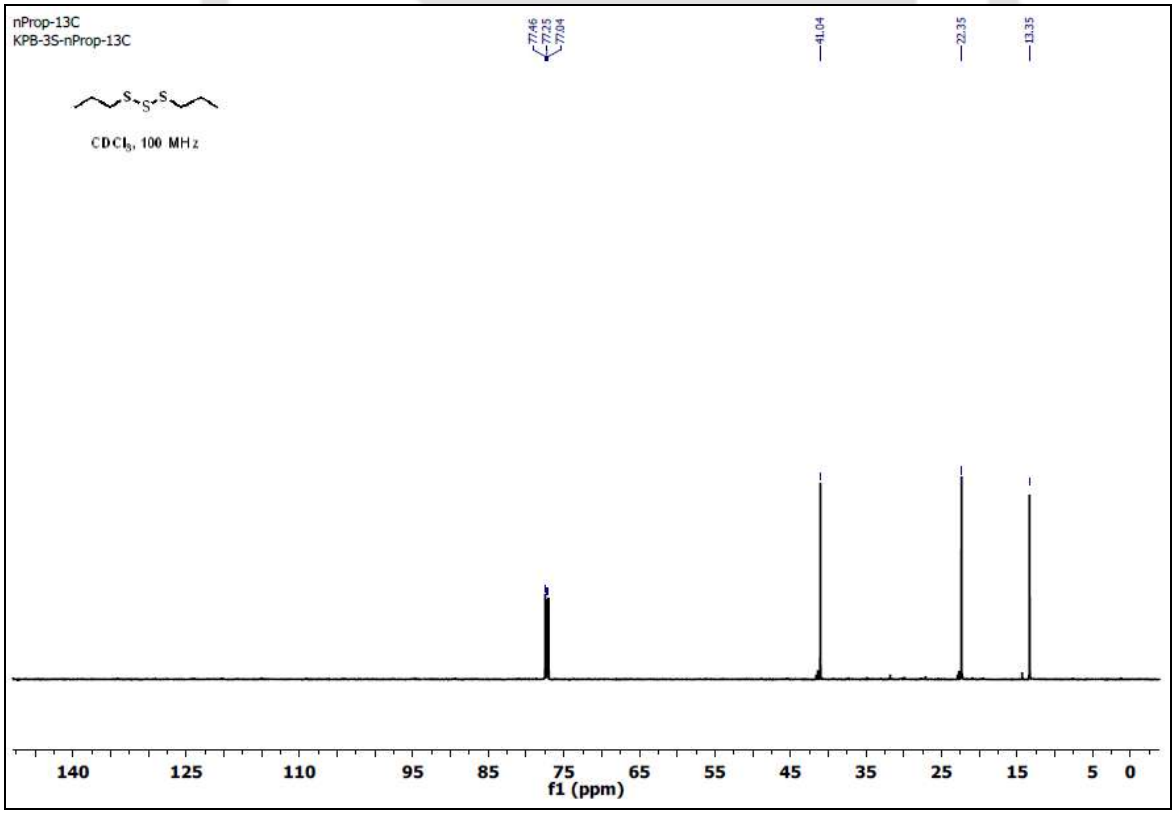

Figure A4.8. ^{13}C NMR ($CDCl_3$, 100 MHz, ppm) spectrum of compound **3.2**.

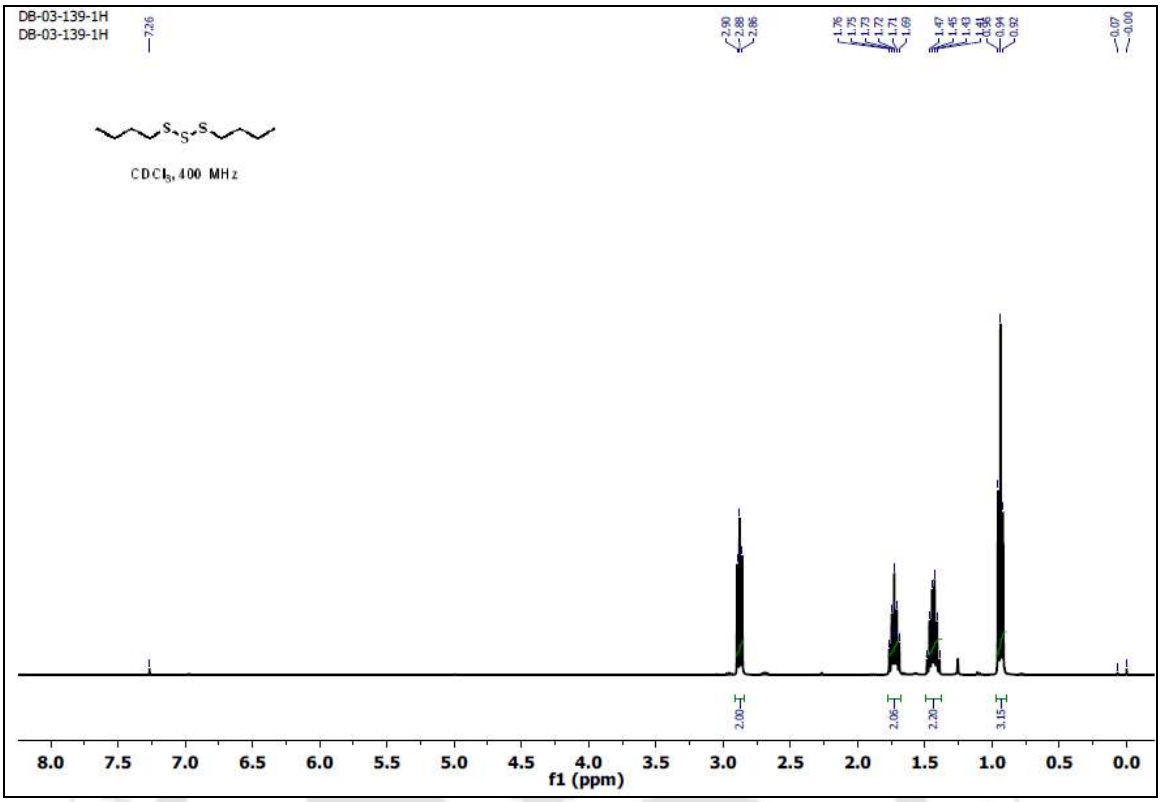

Figure A4.9. ^{1}H NMR ($CDCl_3$, 400 MHz, ppm) spectrum of compound **3.3**.

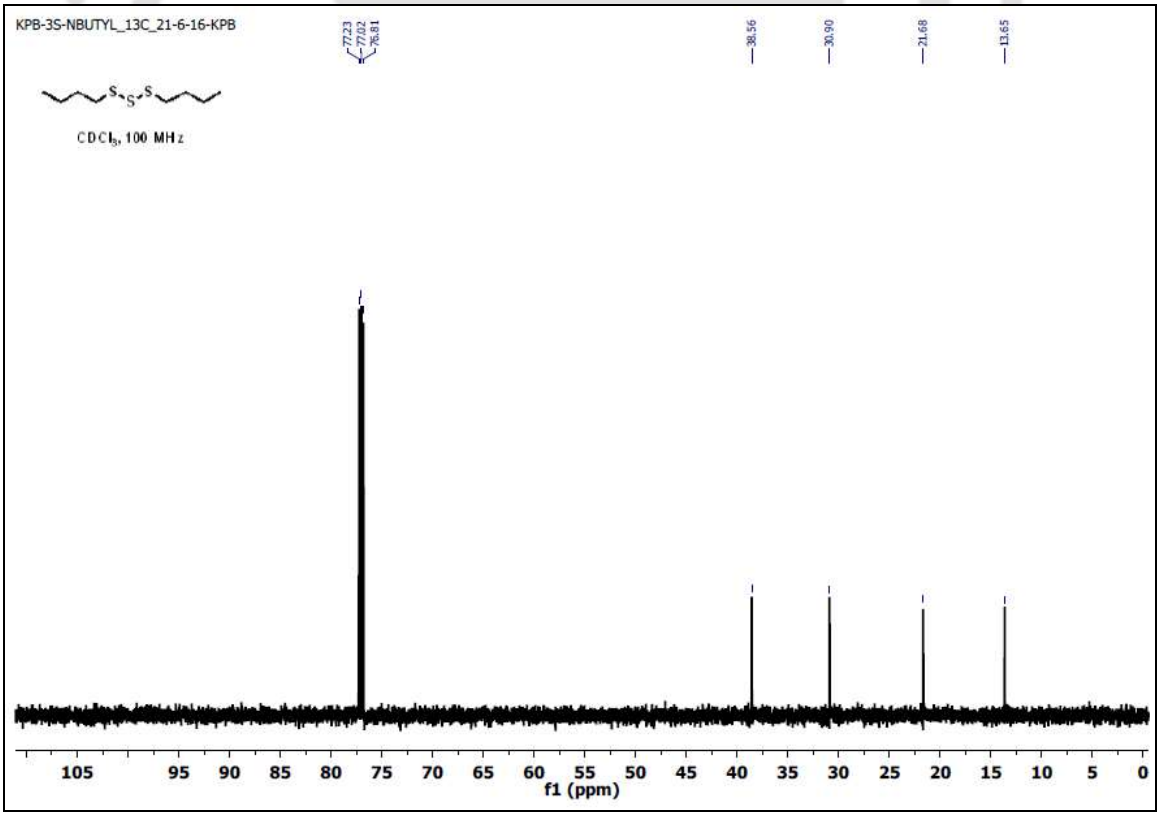

Figure A4.10. ^{13}C NMR ($CDCl_3$, 100 MHz, ppm) spectrum of compound **3.3**.

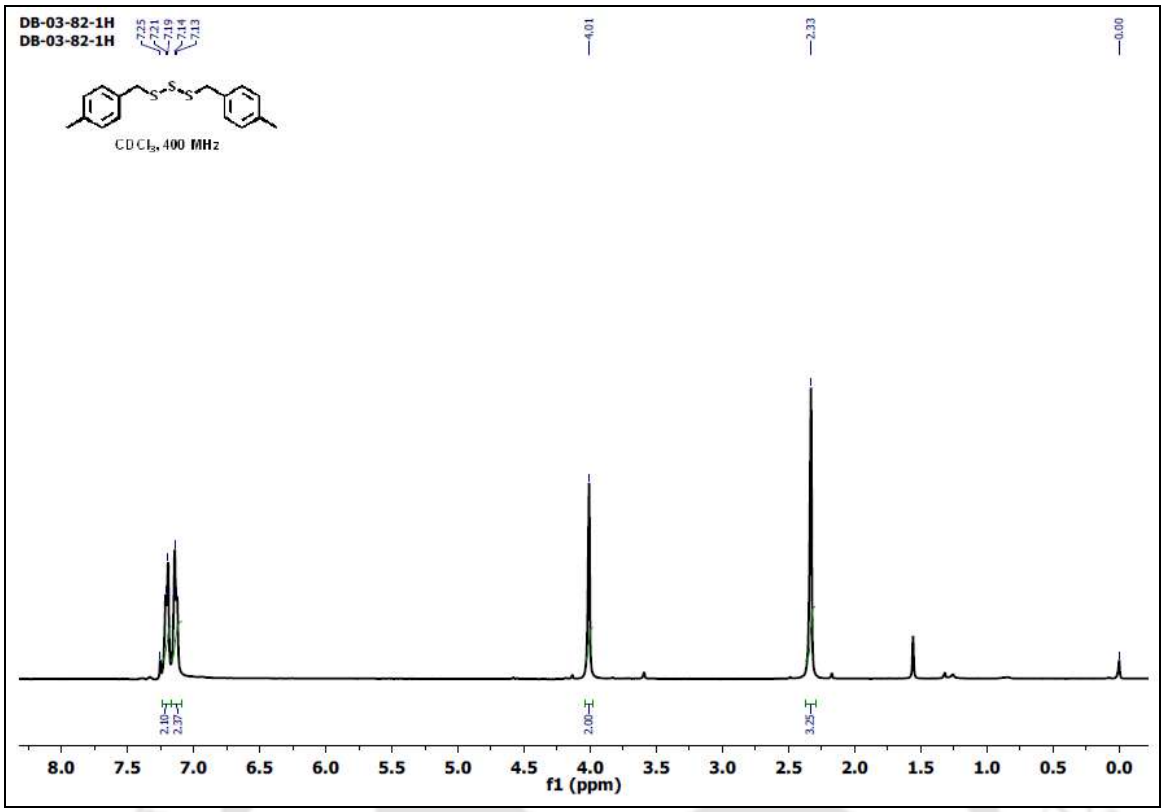

Figure A4.11. ^{1}H NMR ($CDCl_3$, 400 MHz, ppm) spectrum of compound **3.4**.

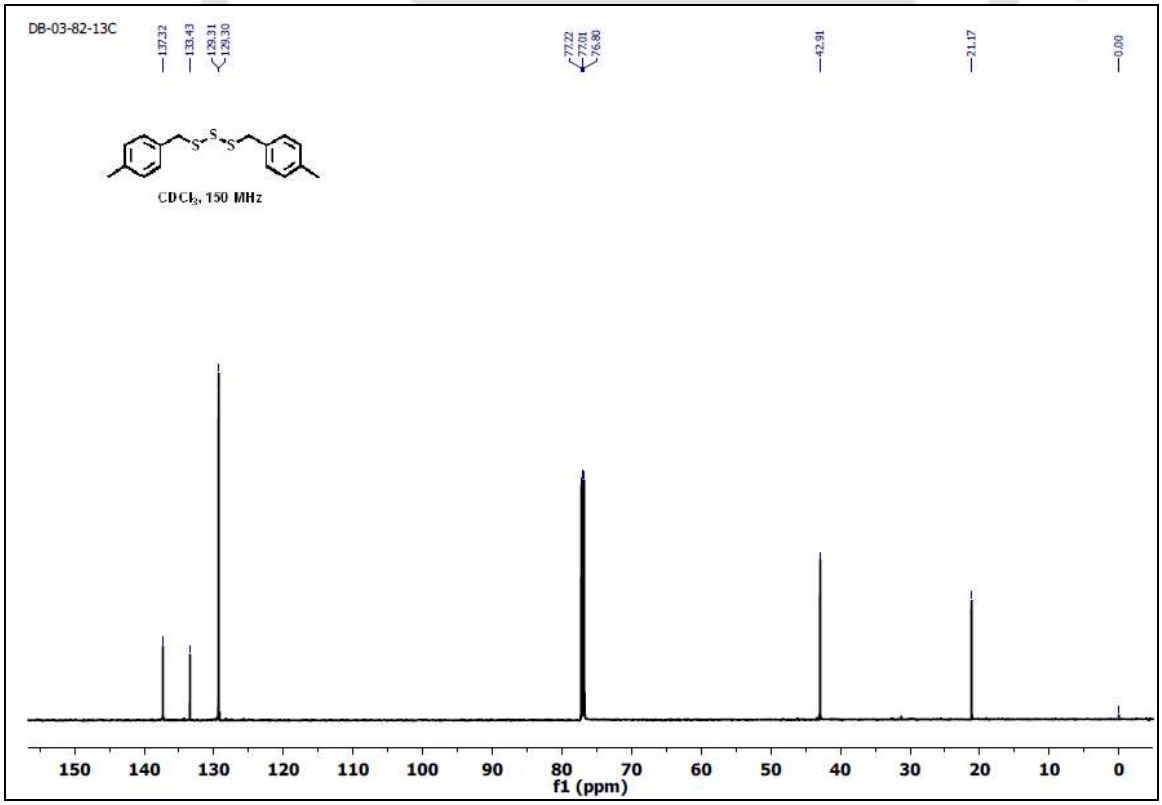

Figure A4.12. ^{13}C NMR ($CDCl_3$, 150 MHz, ppm) spectrum of compound **3.4**.

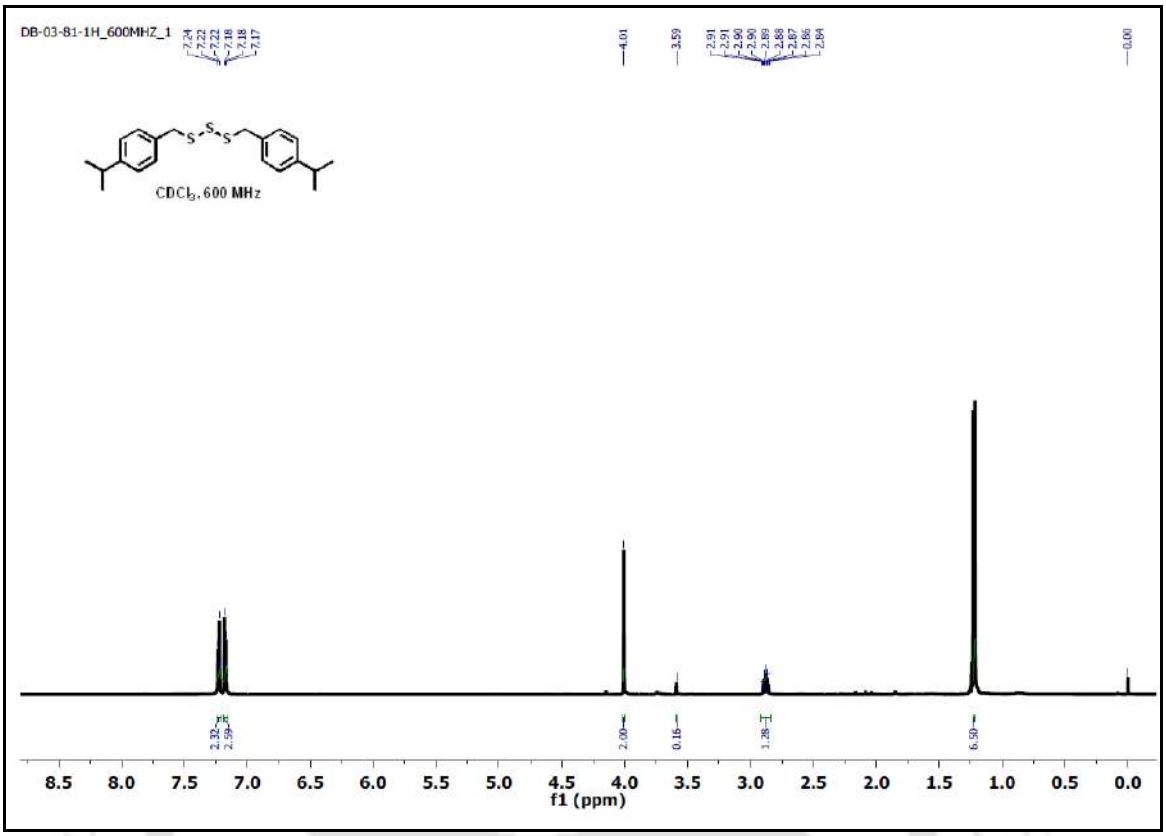

Figure A4.13. ^{1}H NMR ($CDCl_3$, 600 MHz, ppm) spectrum of compound **3.5**.

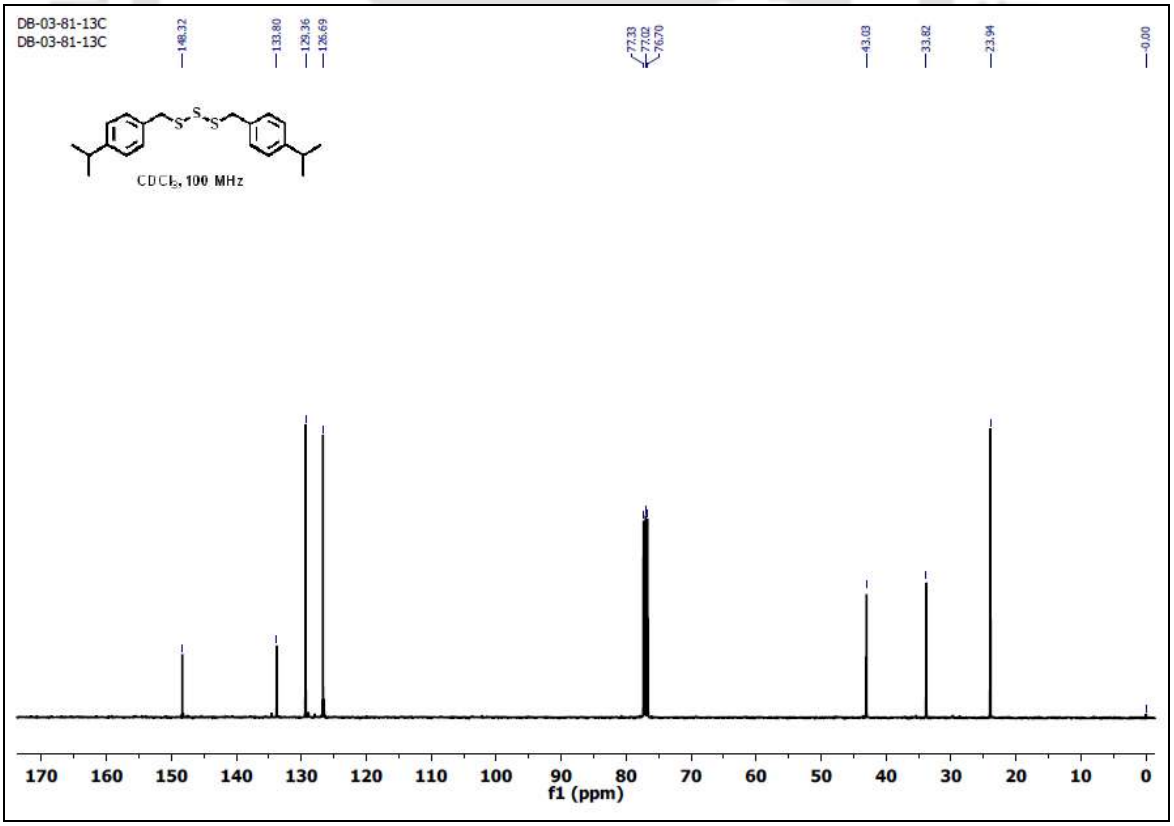

Figure A4.14. ^{13}C NMR ($CDCl_3$, 100 MHz, ppm) spectrum of compound **3.5**.

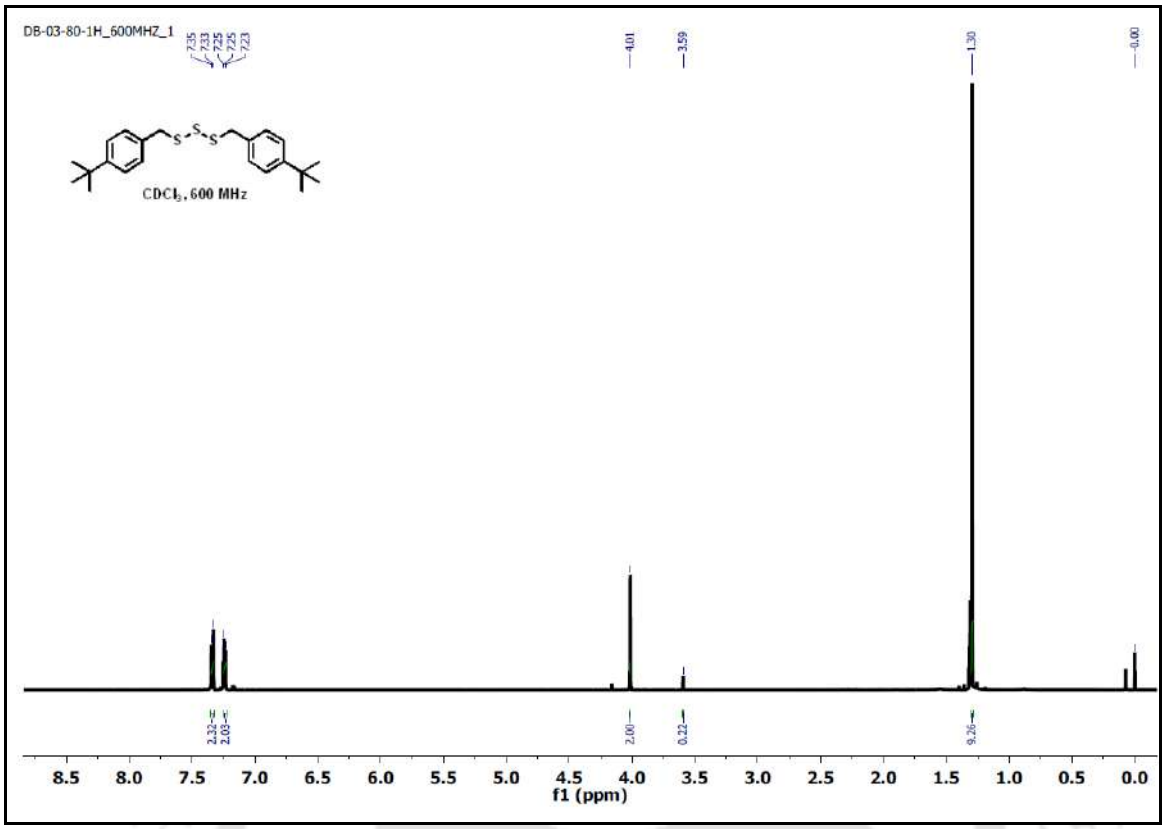

Figure A4.15. ^{1}H NMR ($CDCl_3$, 600 MHz, ppm) spectrum of compound **3.6**.

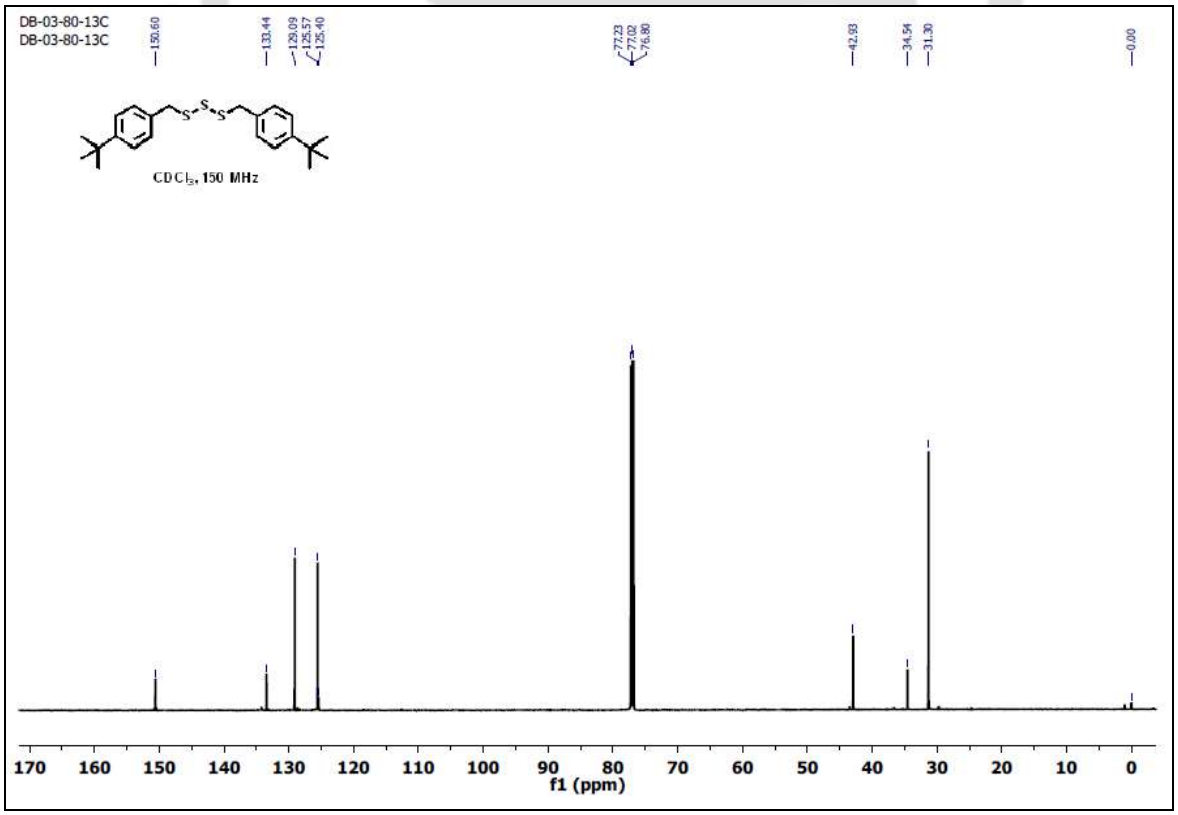

Figure A4.16. ^{13}C NMR ($CDCl_3$, 150 MHz, ppm) spectrum of compound **3.6**.

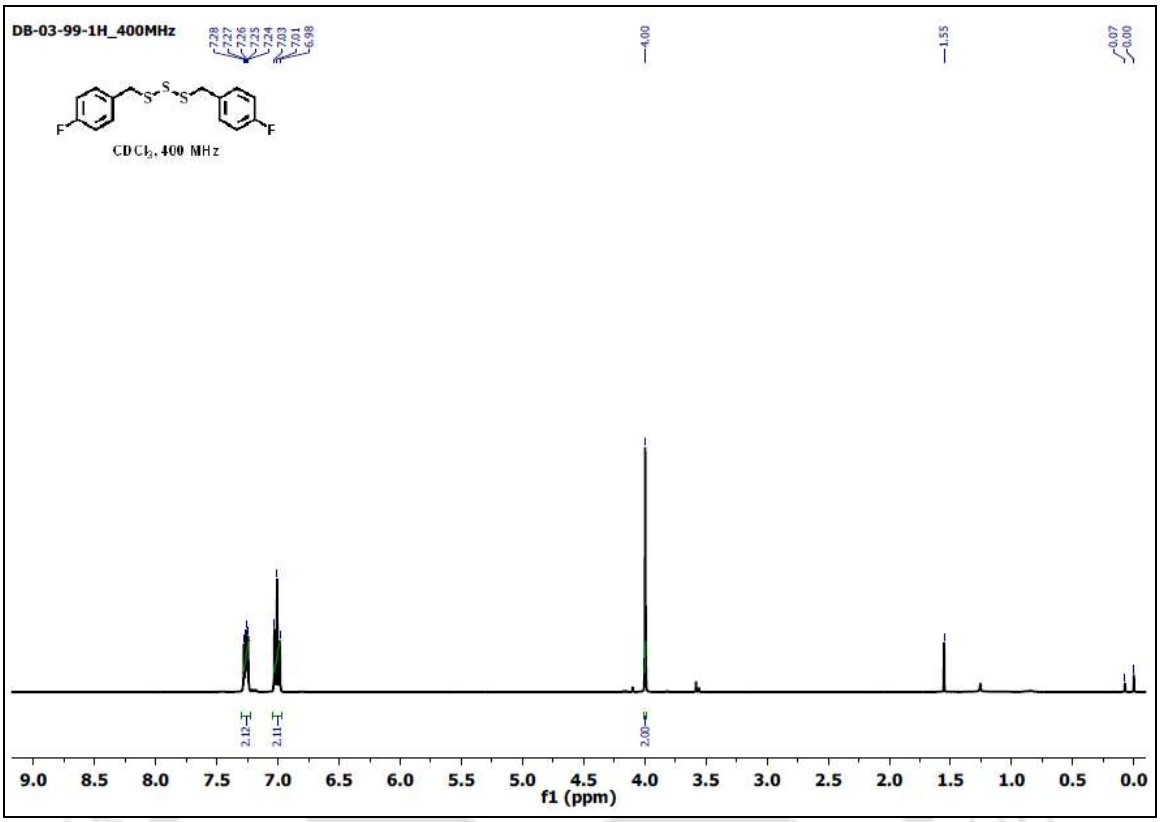

Figure A4.17. ^{1}H NMR ($CDCl_3$, 400 MHz, ppm) spectrum of compound **3.7**.

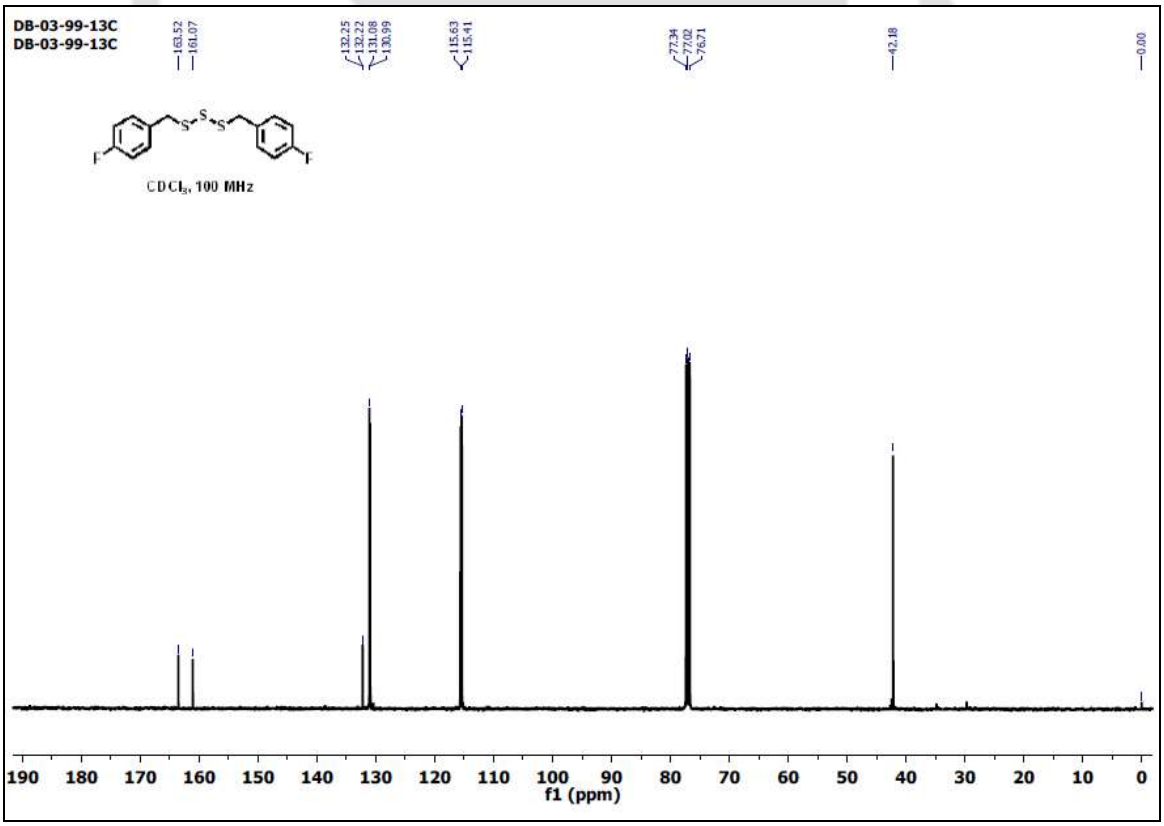

Figure A4.18. ^{13}C NMR ($CDCl_3$, 100 MHz, ppm) spectrum of compound **3.7**.

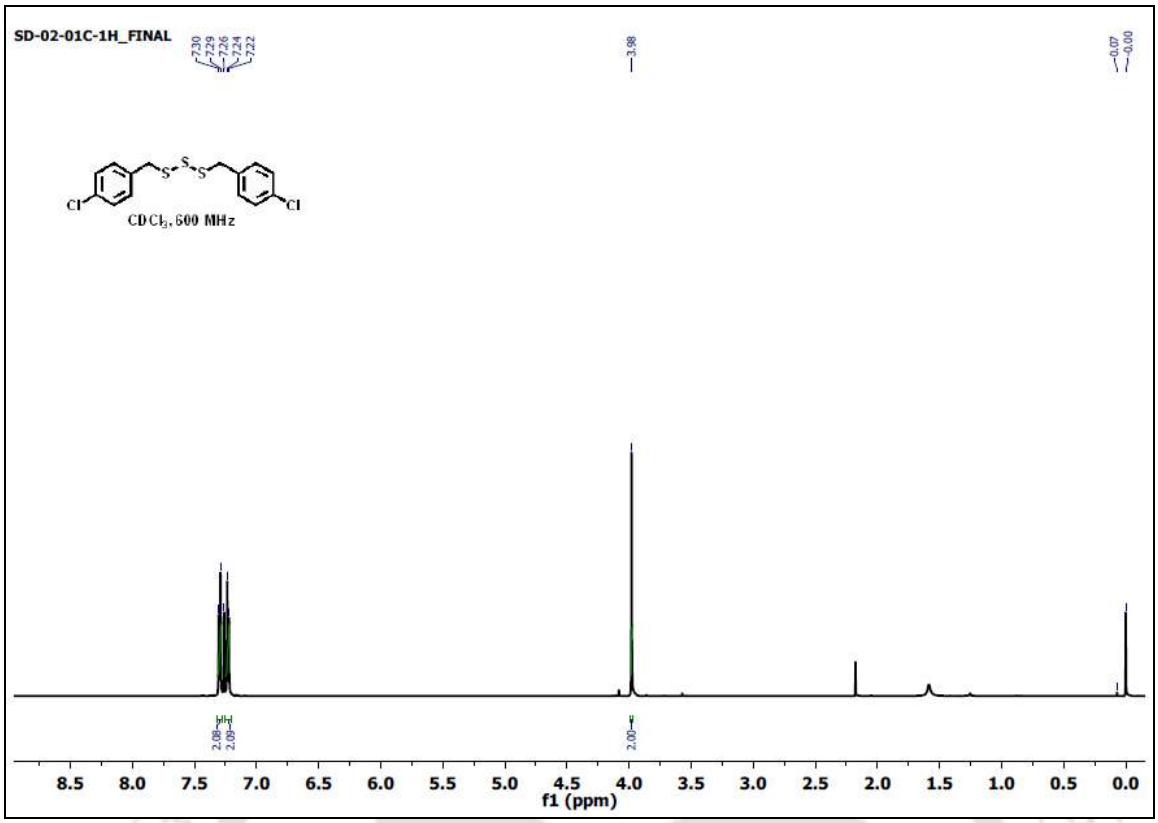

Figure A4.19. ^{1}H NMR ($CDCl_3$, 600 MHz, ppm) spectrum of compound **3.8**.

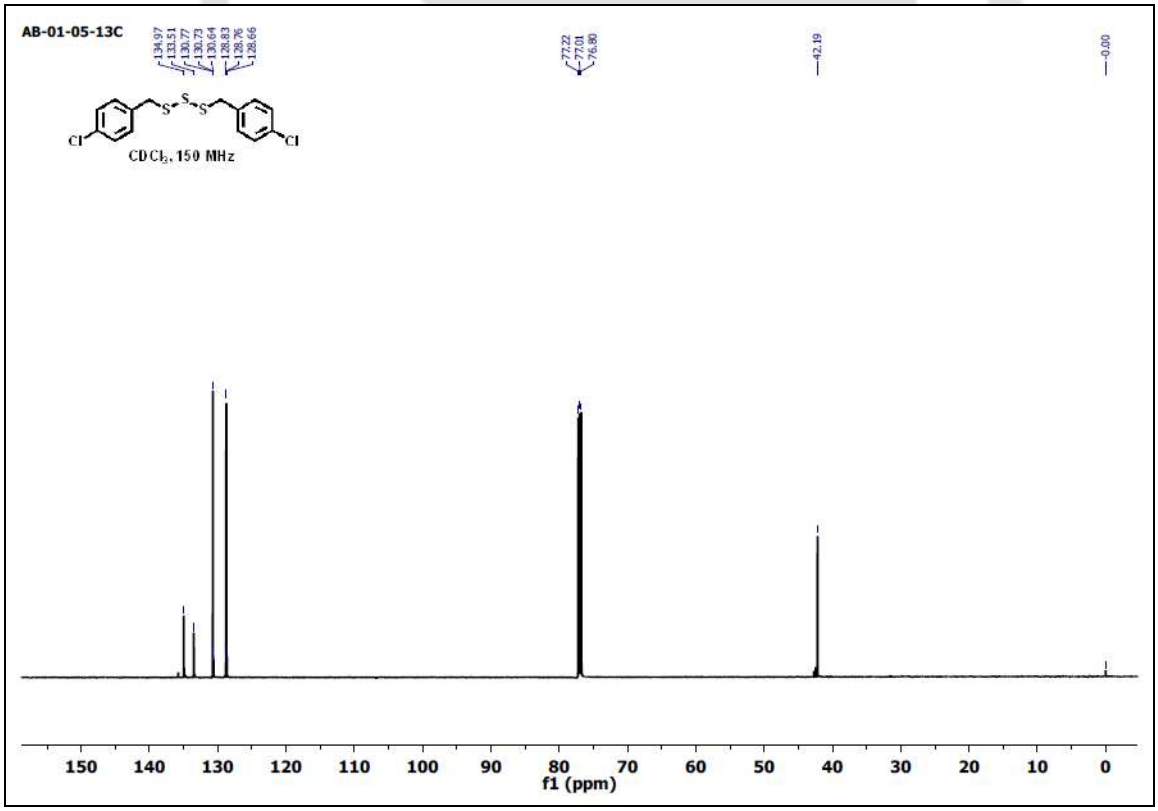

Figure A4.20. ^{13}C NMR ($CDCl_3$, 150 MHz, ppm) spectrum of compound **3.8**.

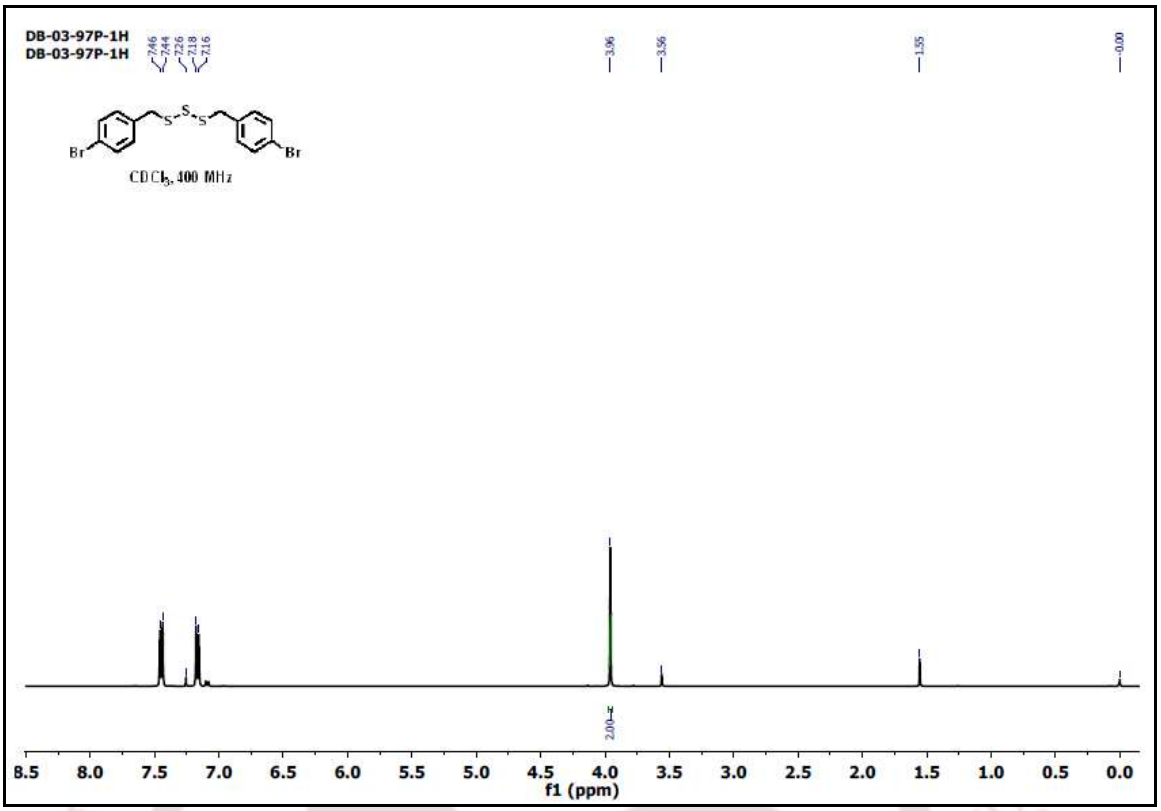

Figure A4.21. ^{1}H NMR ($CDCl_3$, 400 MHz, ppm) spectrum of compound **3.9**.

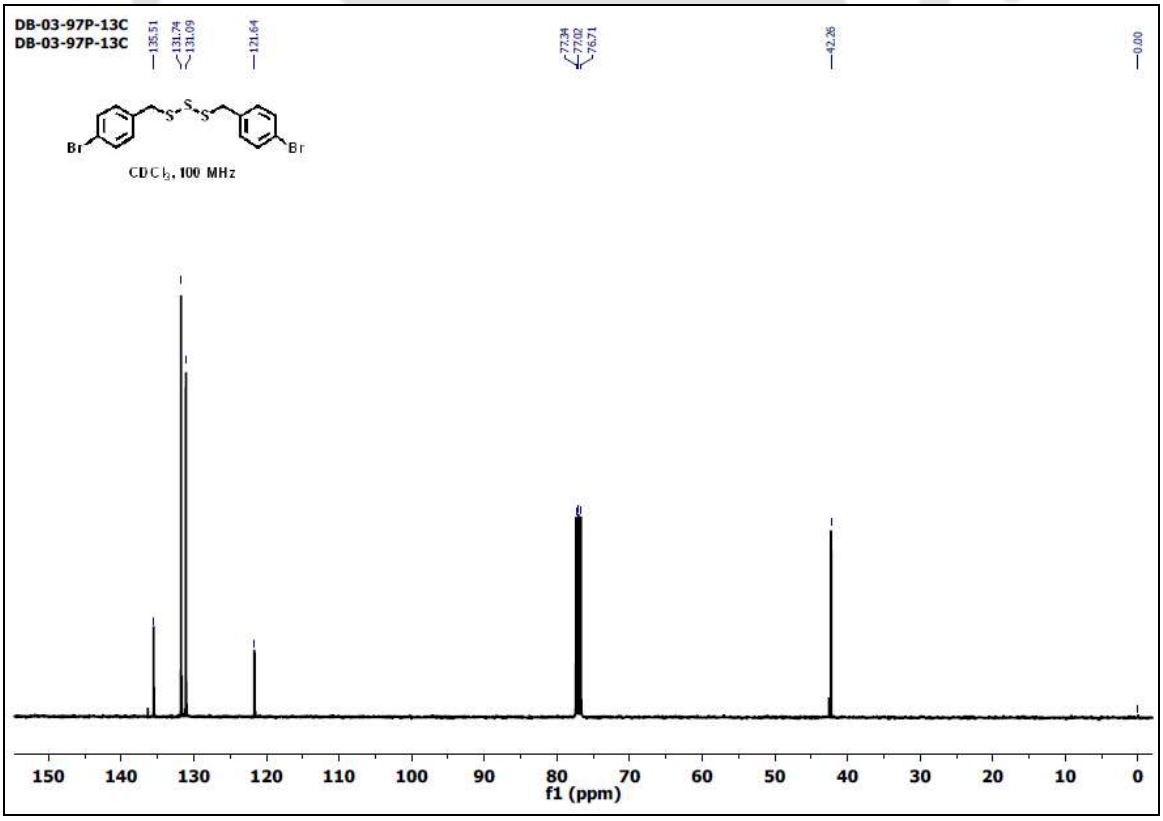

Figure A4.22. ^{13}C NMR ($CDCl_3$, 100 MHz, ppm) spectrum of compound **3.9**.

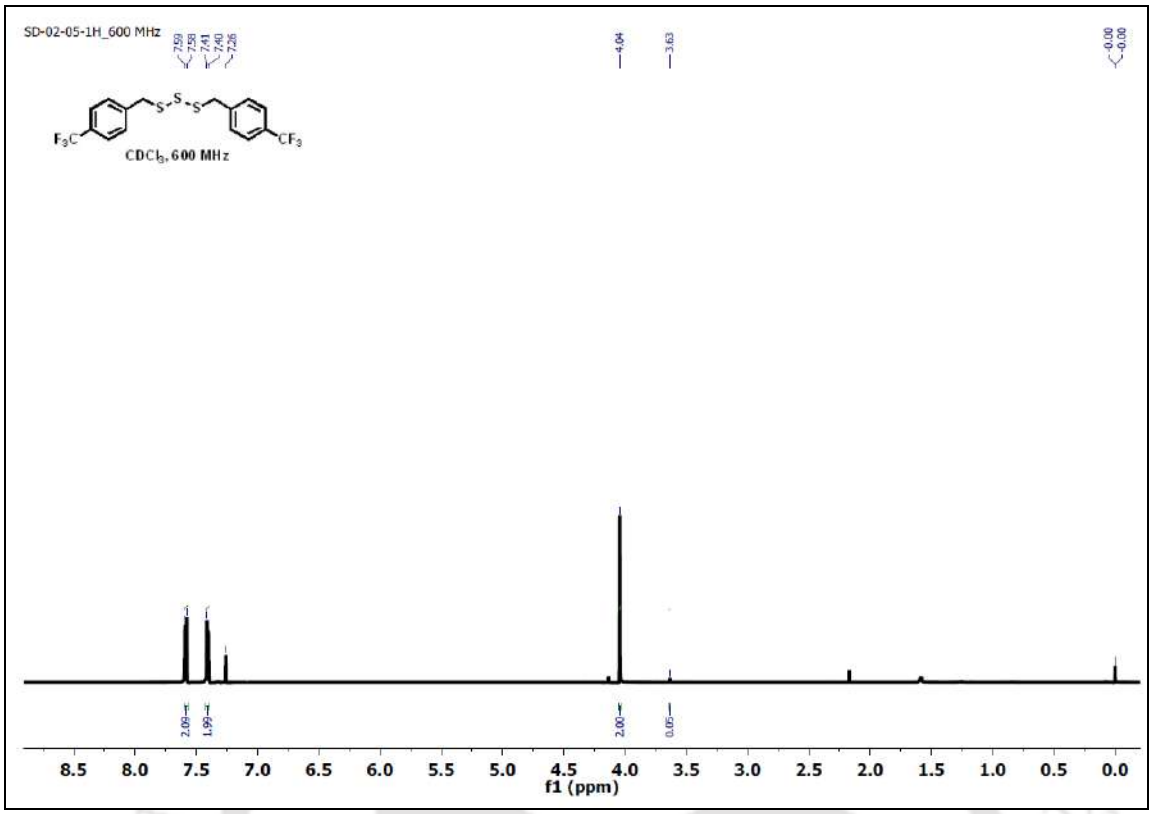

Figure A4.23. ^{1}H NMR ($CDCl_3$, 600 MHz, ppm) spectrum of compound **3.10**.

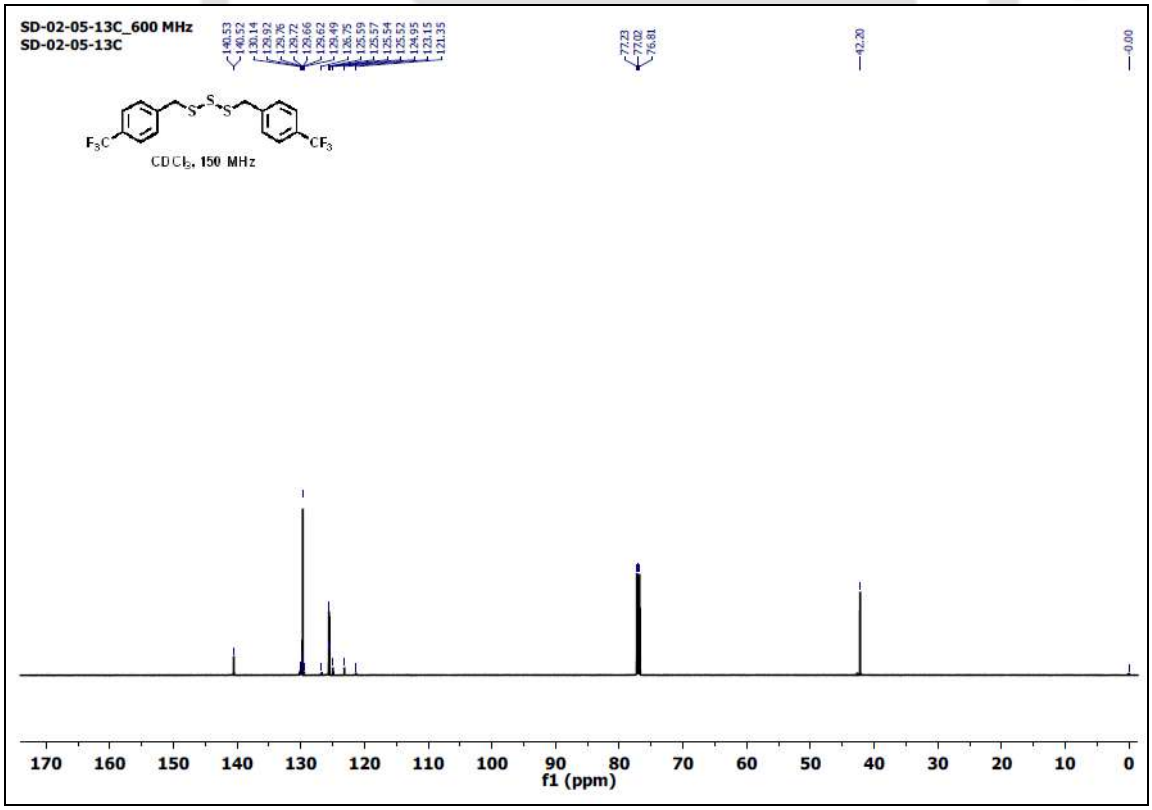

Figure A4.24. ^{13}C NMR ($CDCl_3$, 150 MHz, ppm) spectrum of compound **3.10**.

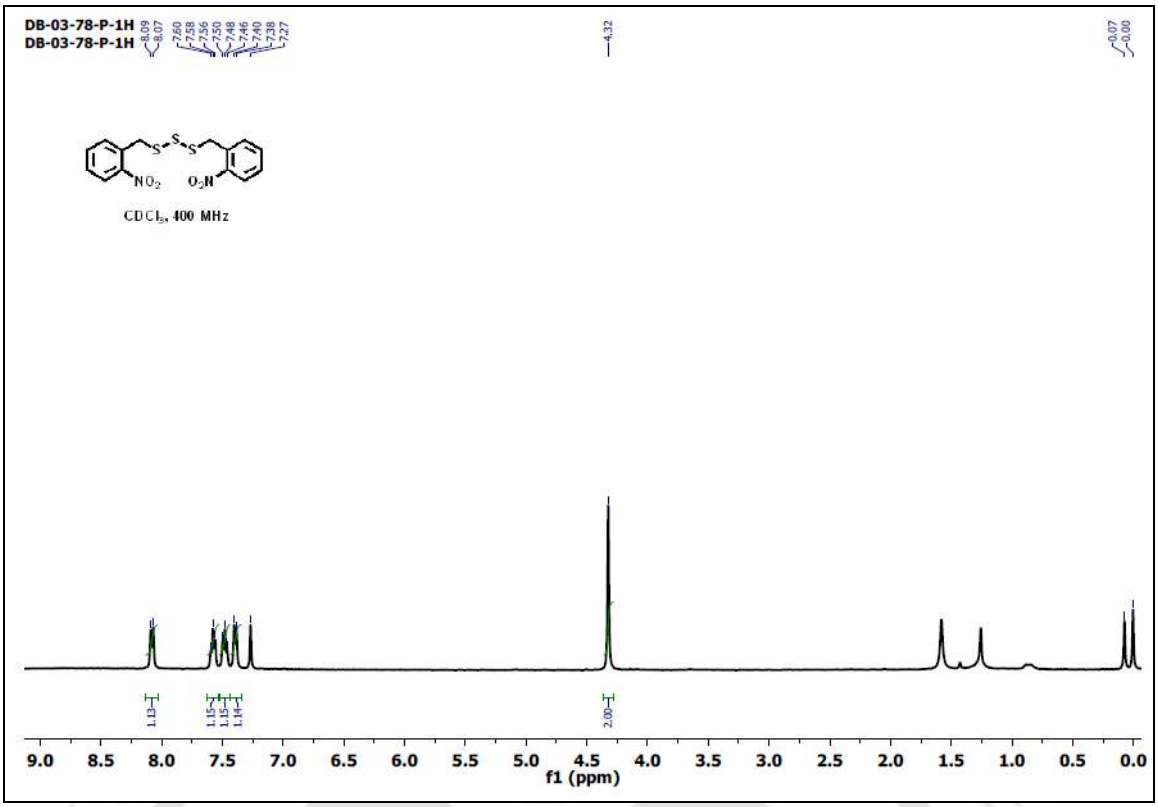

Figure A4.25. ^{1}H NMR ($CDCl_3$, 400 MHz, ppm) spectrum of compound **3.11**.

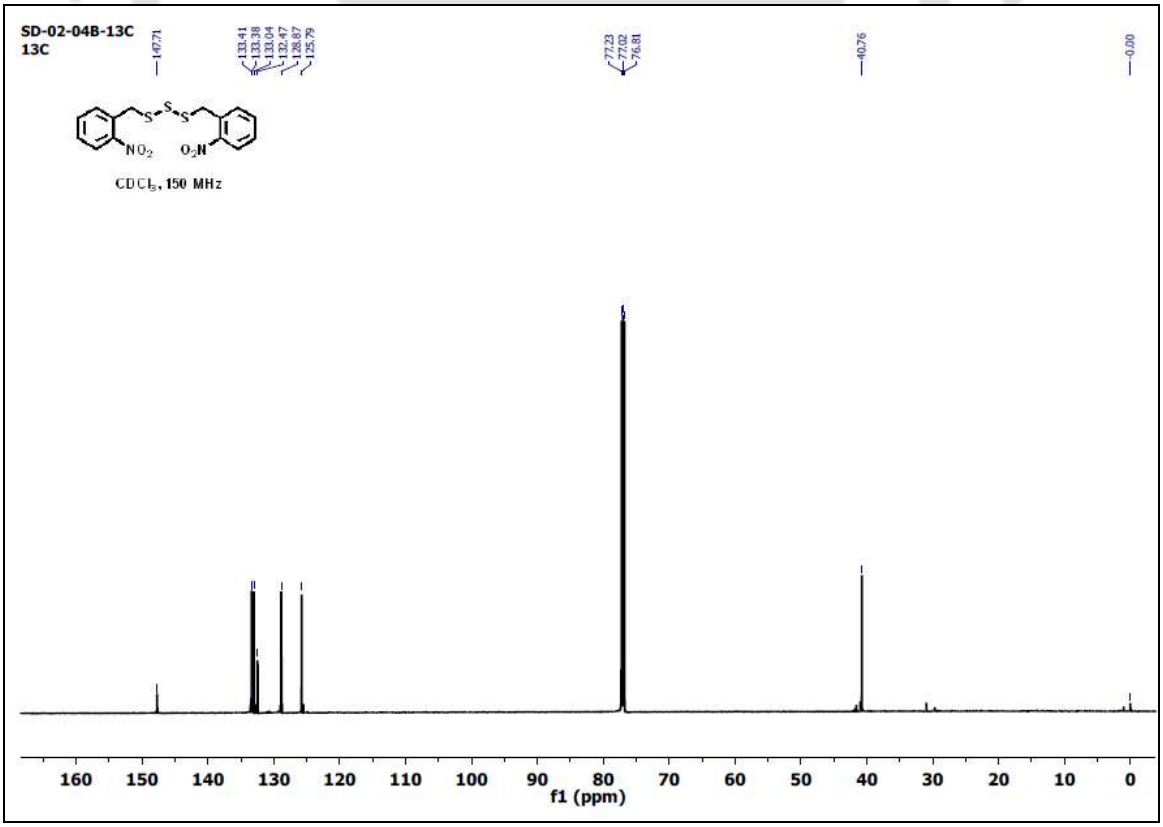

Figure A4.26. ^{13}C NMR ($CDCl_3$, 150 MHz, ppm) spectrum of compound **3.11**.

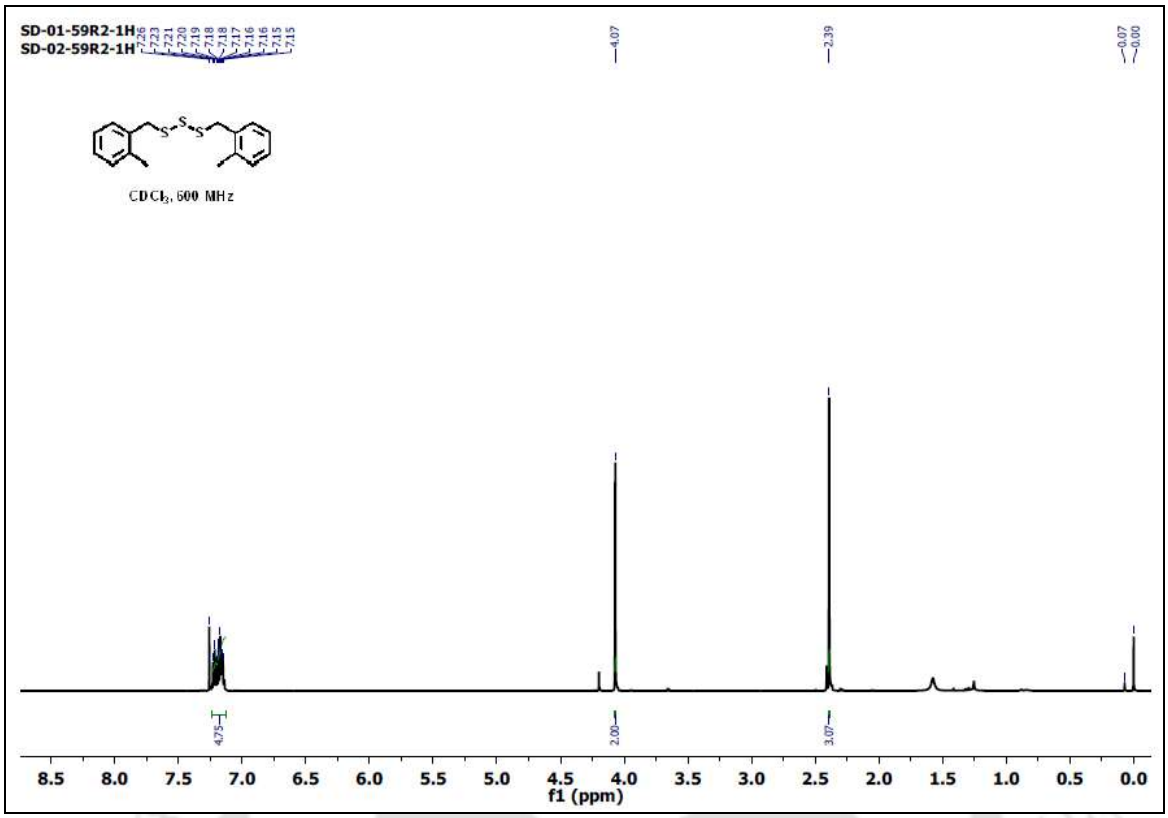

Figure A4.27. ^{1}H NMR ($CDCl_3$, 600 MHz, ppm) spectrum of compound **3.12**.

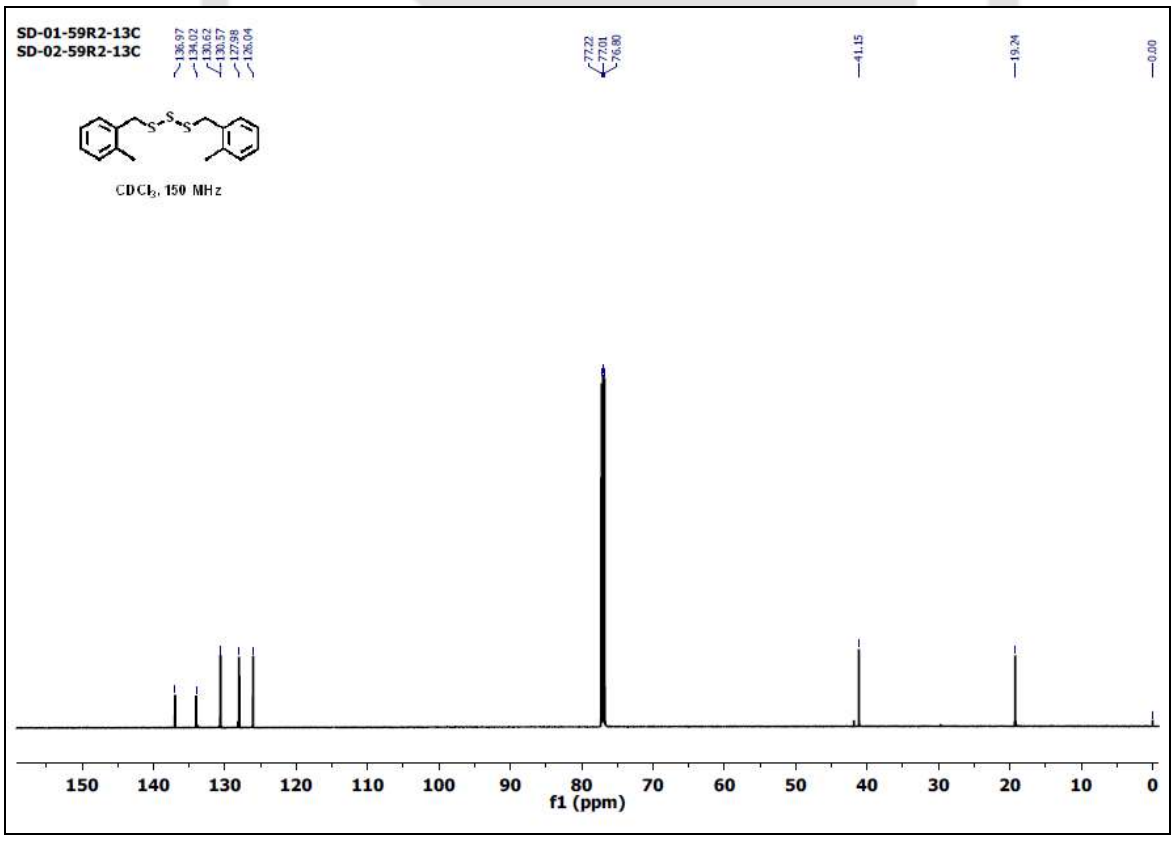

Figure A4.28. ^{13}C NMR ($CDCl_3$, 150 MHz, ppm) spectrum of compound **3.12**.

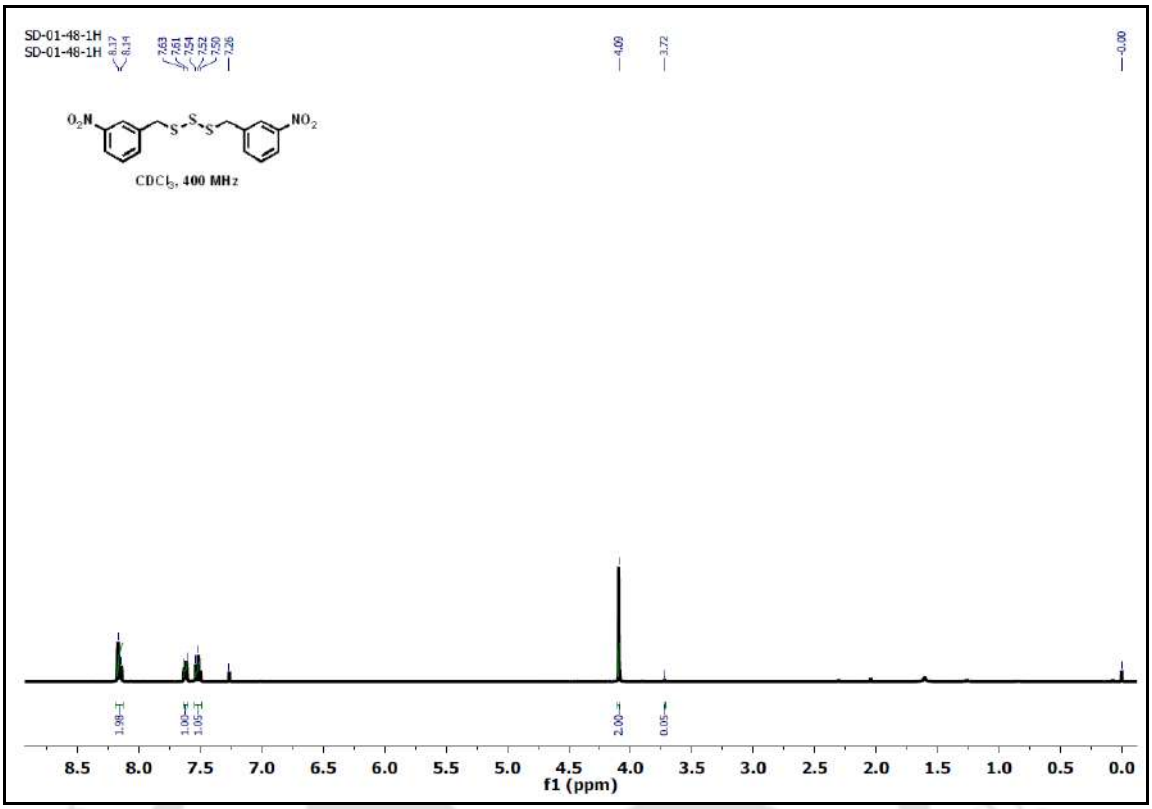

Figure A4.29. ^{1}H NMR ($CDCl_3$, 400 MHz, ppm) spectrum of compound **3.13**.

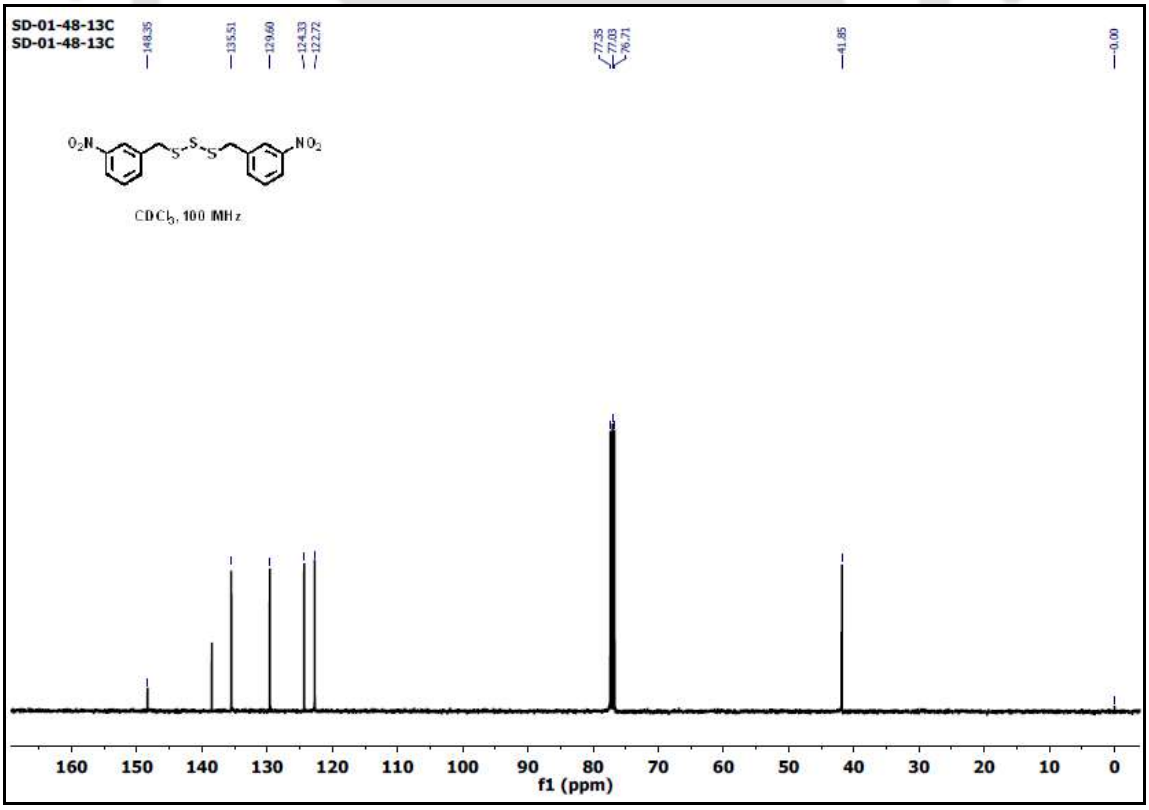

Figure A4.30. ^{13}C NMR ($CDCl_3$, 100 MHz, ppm) spectrum of compound **3.13**.

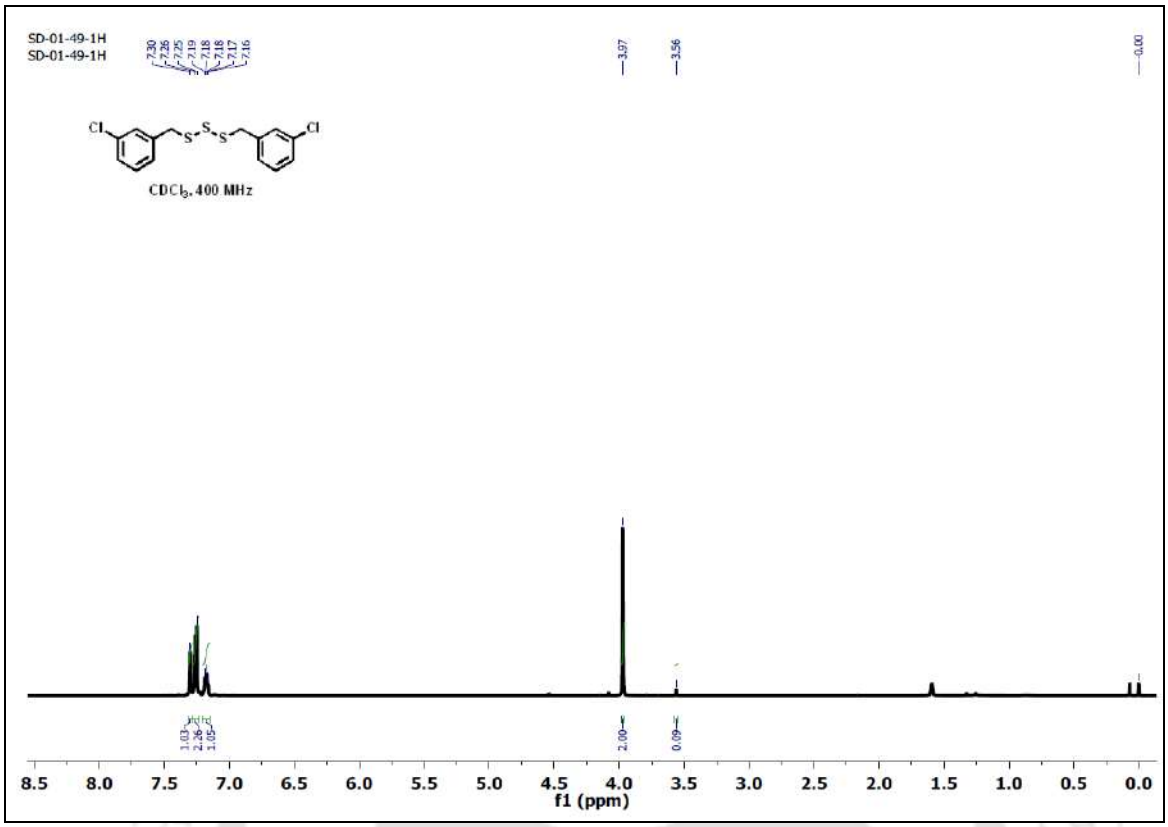

Figure A4.31. ^{1}H NMR ($CDCl_3$, 400 MHz, ppm) spectrum of compound **3.14**.

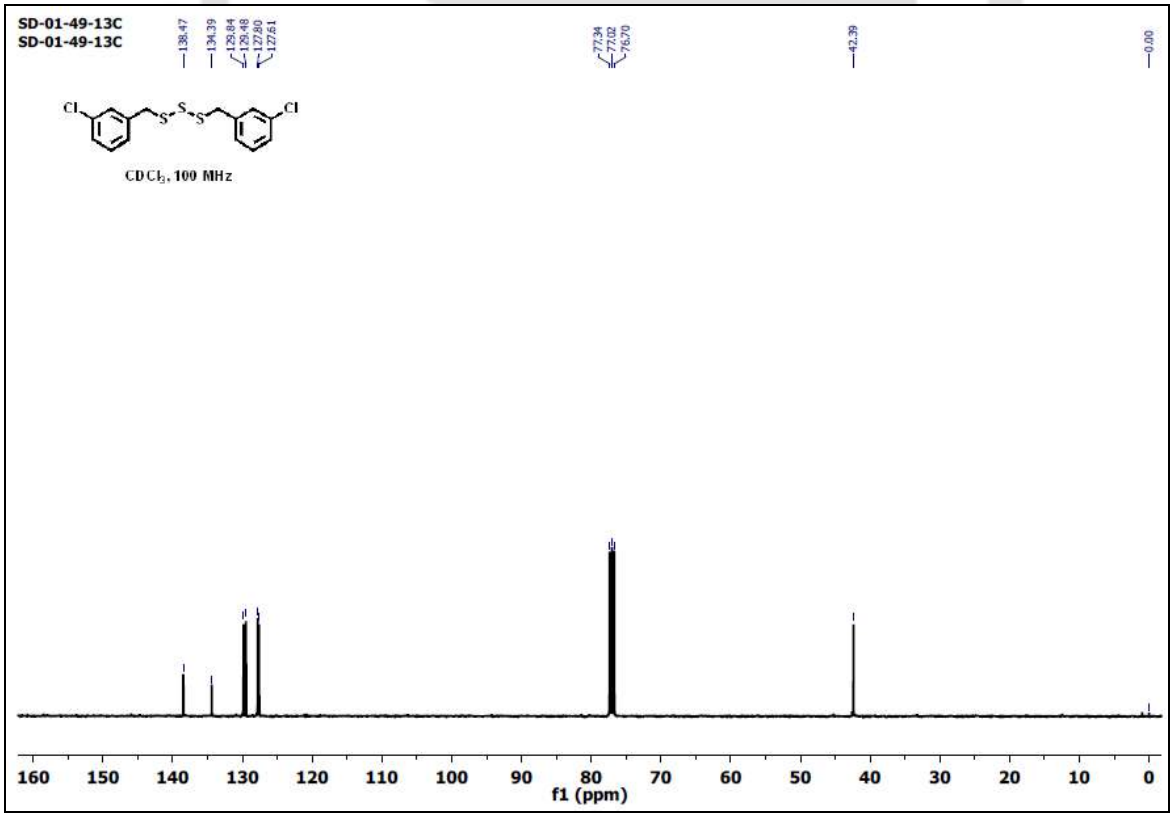

Figure A4.32. ^{13}C NMR ($CDCl_3$, 100 MHz, ppm) spectrum of compound **3.14**.

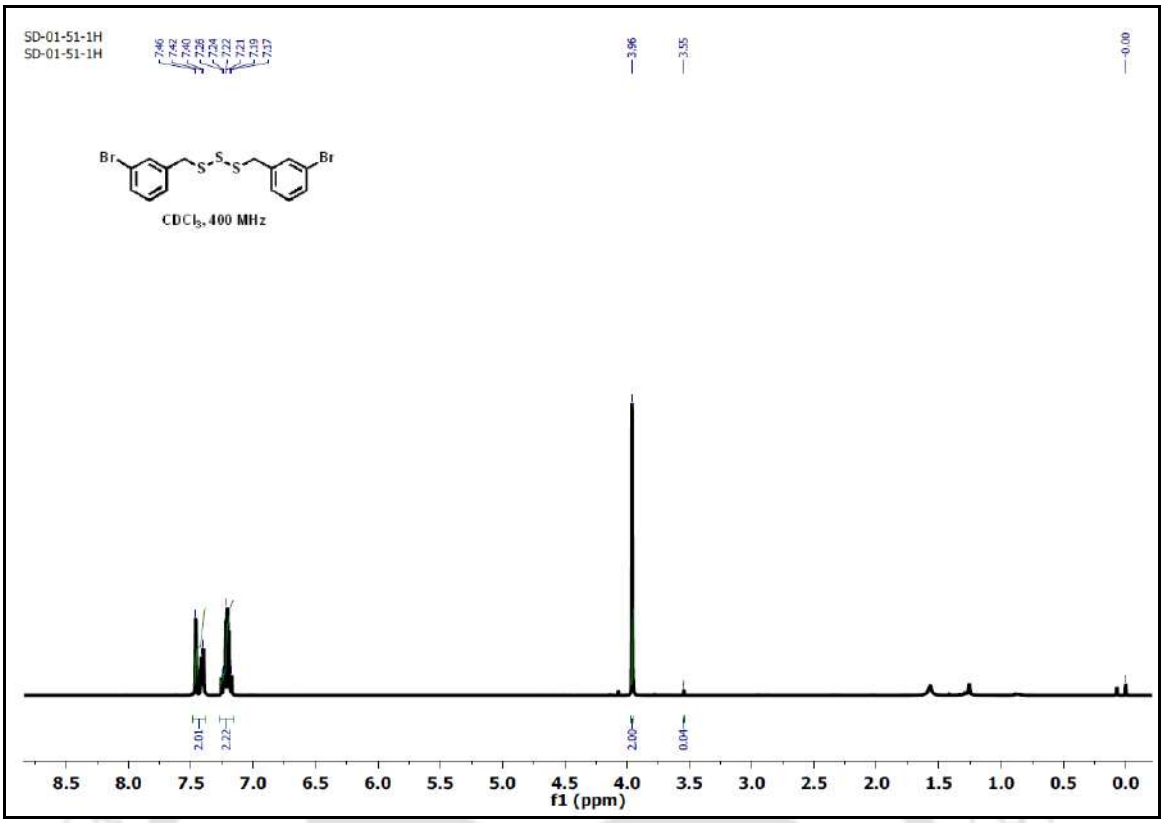

Figure A4.33. ^{1}H NMR ($CDCl_3$, 400 MHz, ppm) spectrum of compound **3.15**.

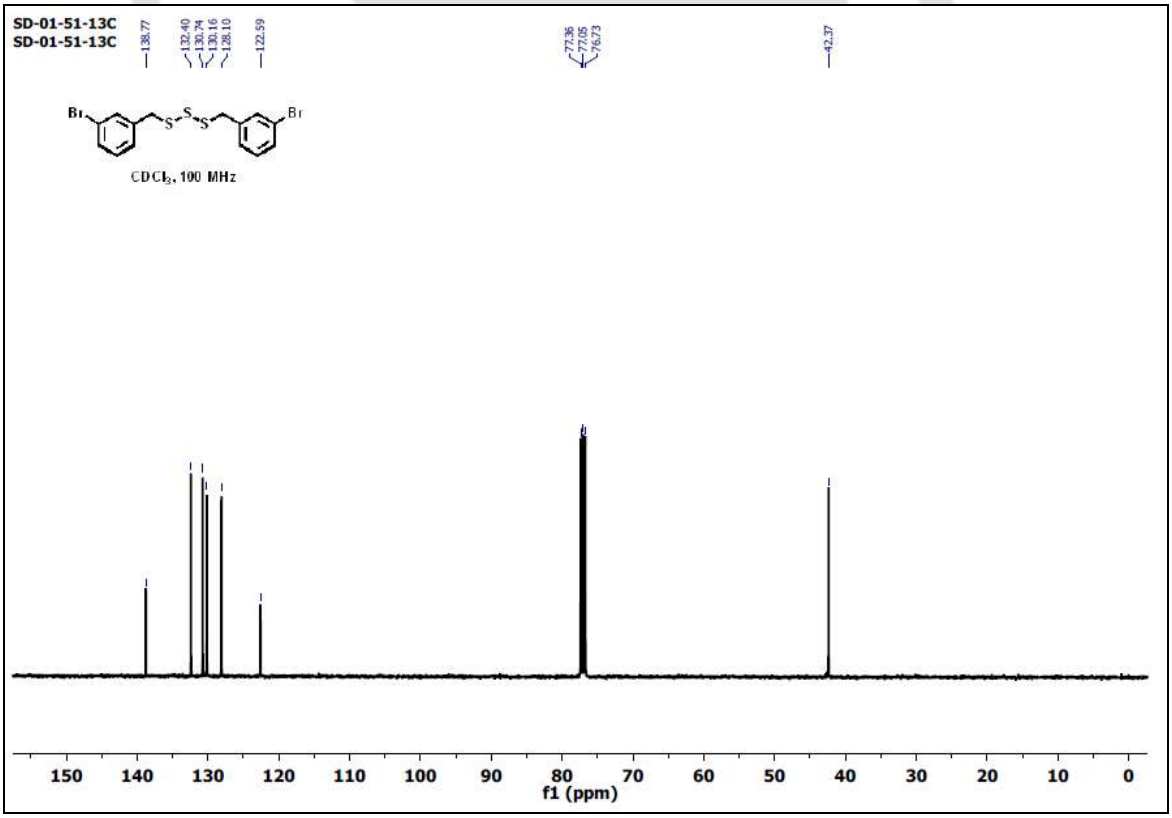

Figure A4.34. ^{13}C NMR ($CDCl_3$, 100 MHz, ppm) spectrum of compound **3.15**.

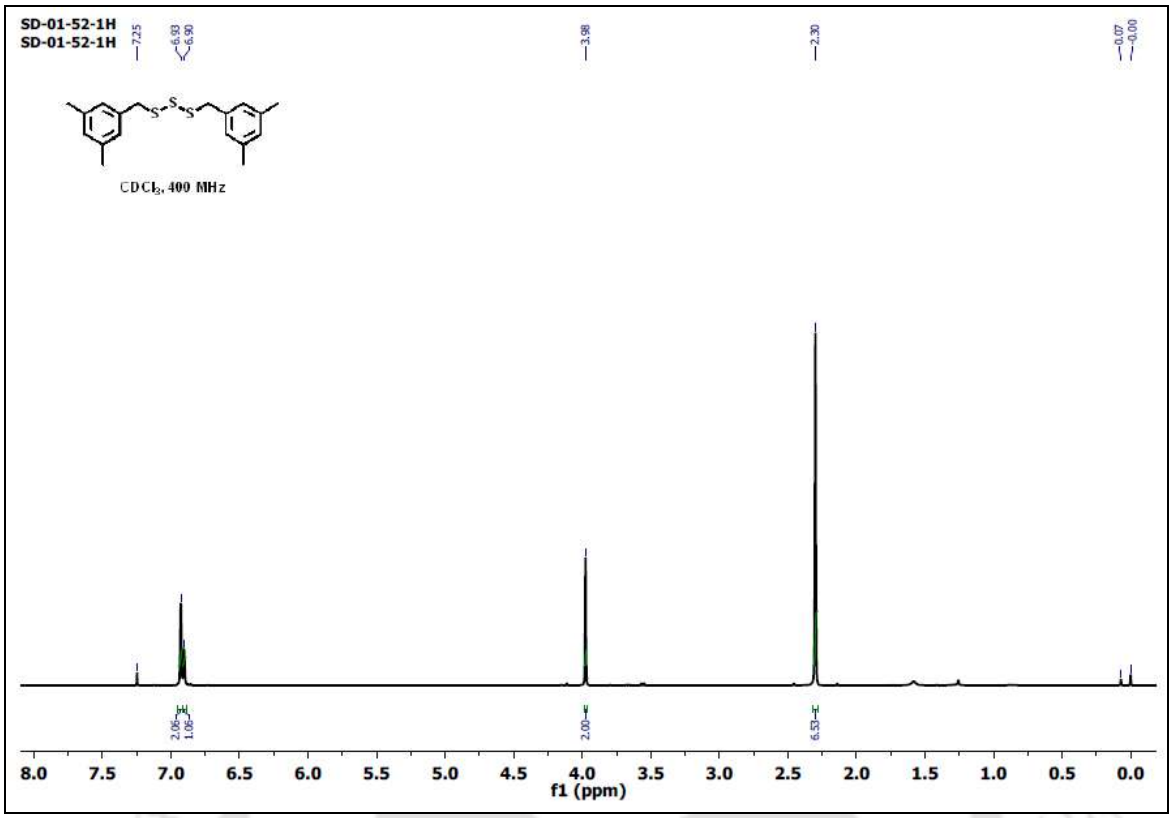

Figure A4.35. ^{1}H NMR ($CDCl_3$, 400 MHz, ppm) spectrum of compound **3.16**.

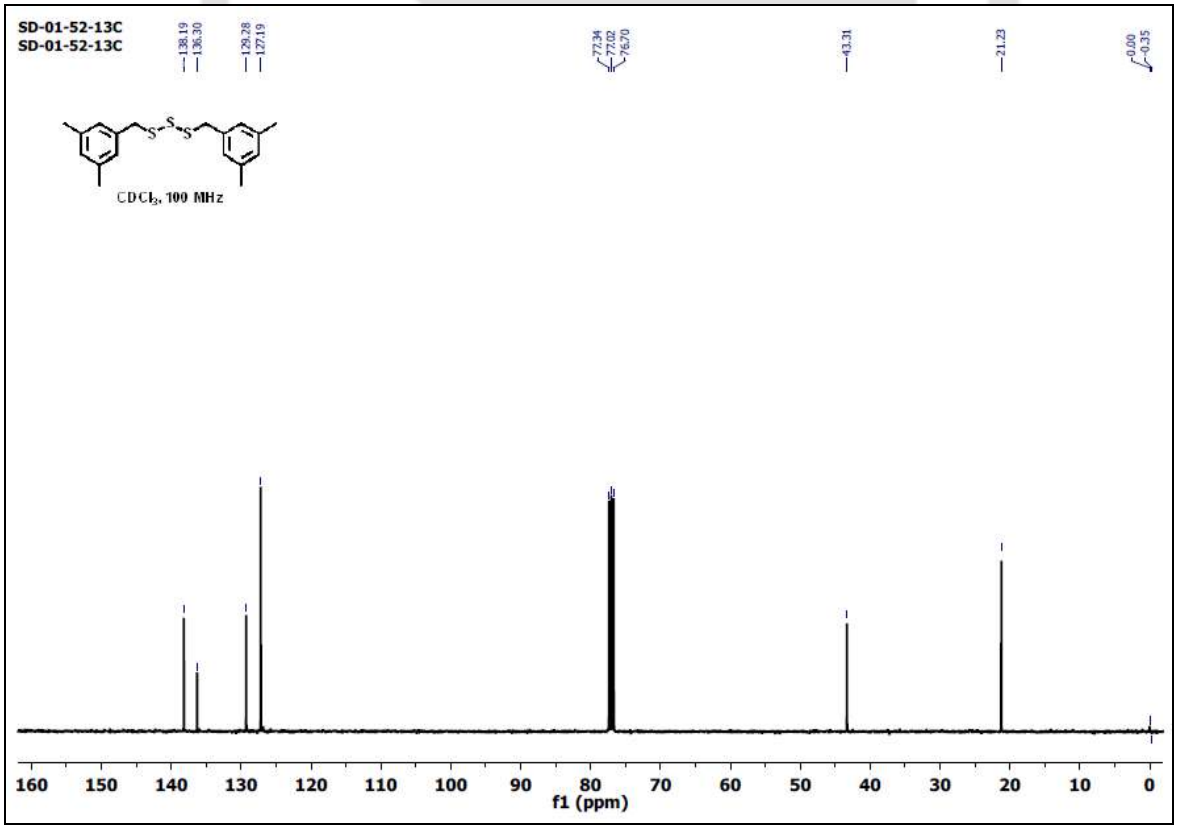

Figure A4.36. ^{13}C NMR ($CDCl_3$, 100 MHz, ppm) spectrum of compound **3.16**.

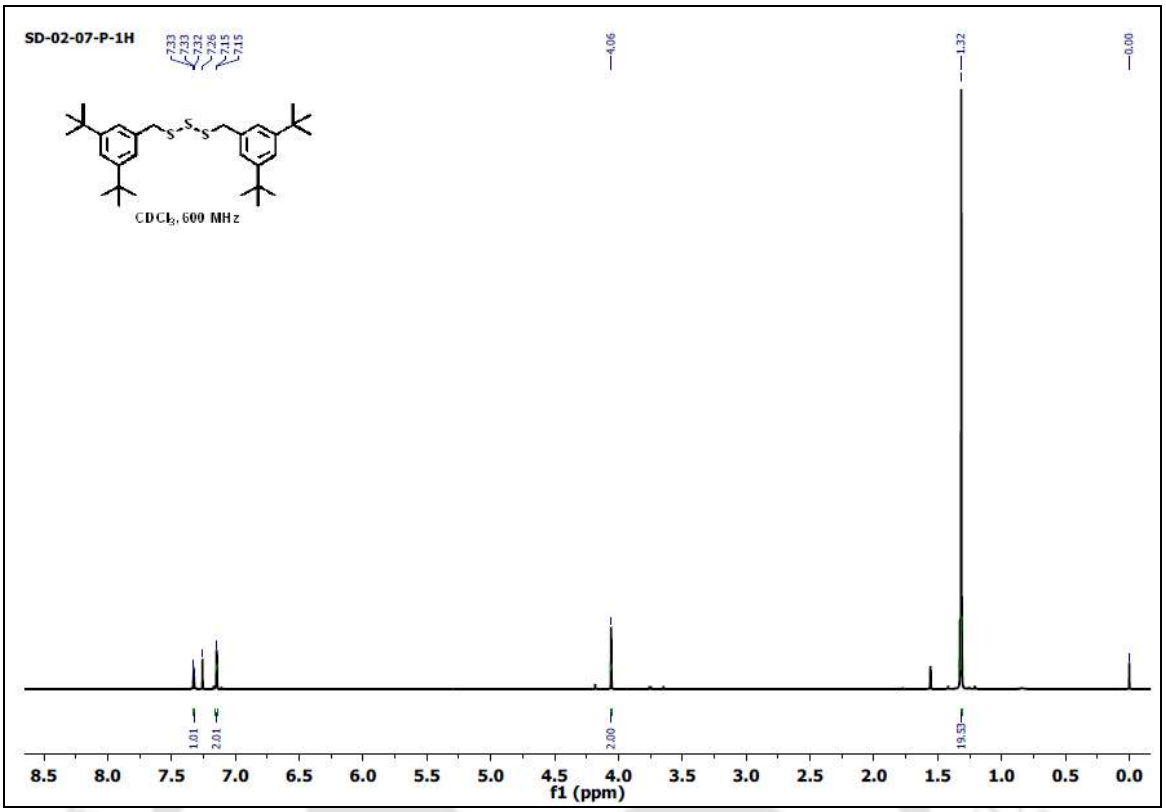

Figure A4.37. ^{1}H NMR ($CDCl_3$, 600 MHz, ppm) spectrum of compound **3.17**.

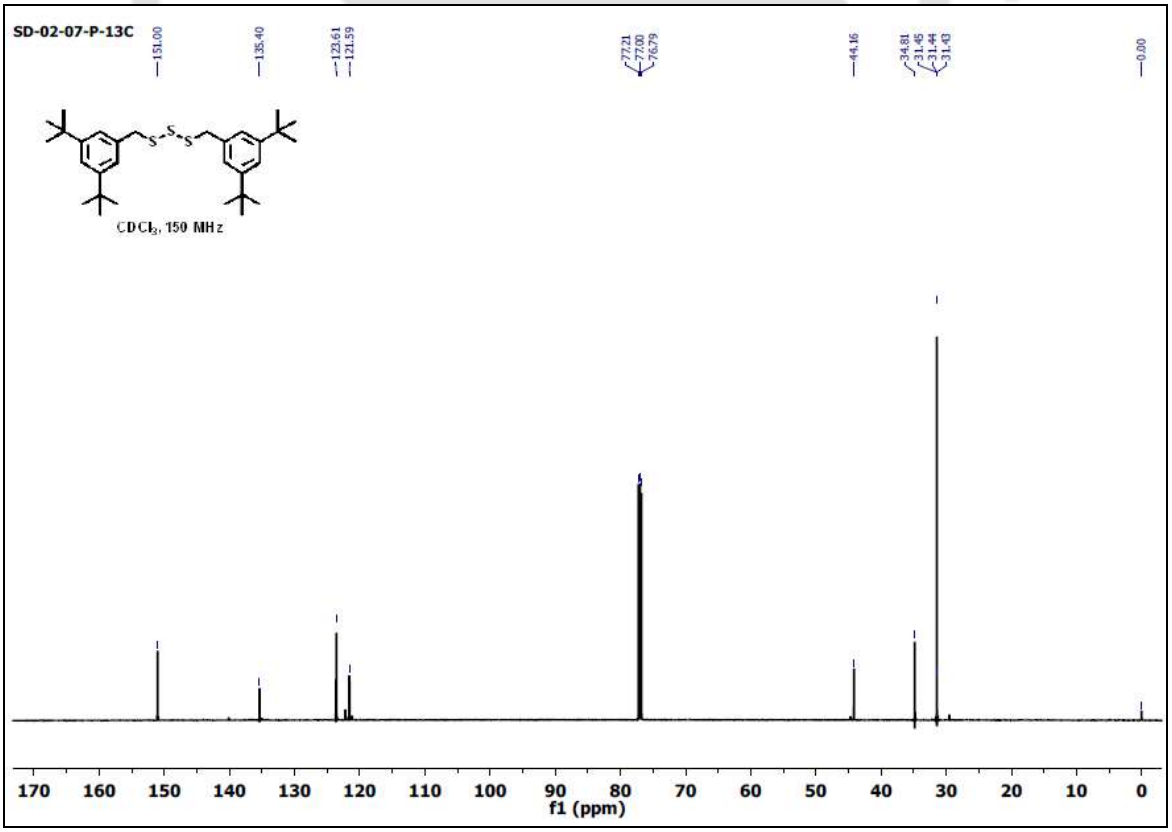

Figure A4.38. ^{13}C NMR ($CDCl_3$, 150 MHz, ppm) spectrum of compound **3.17**.

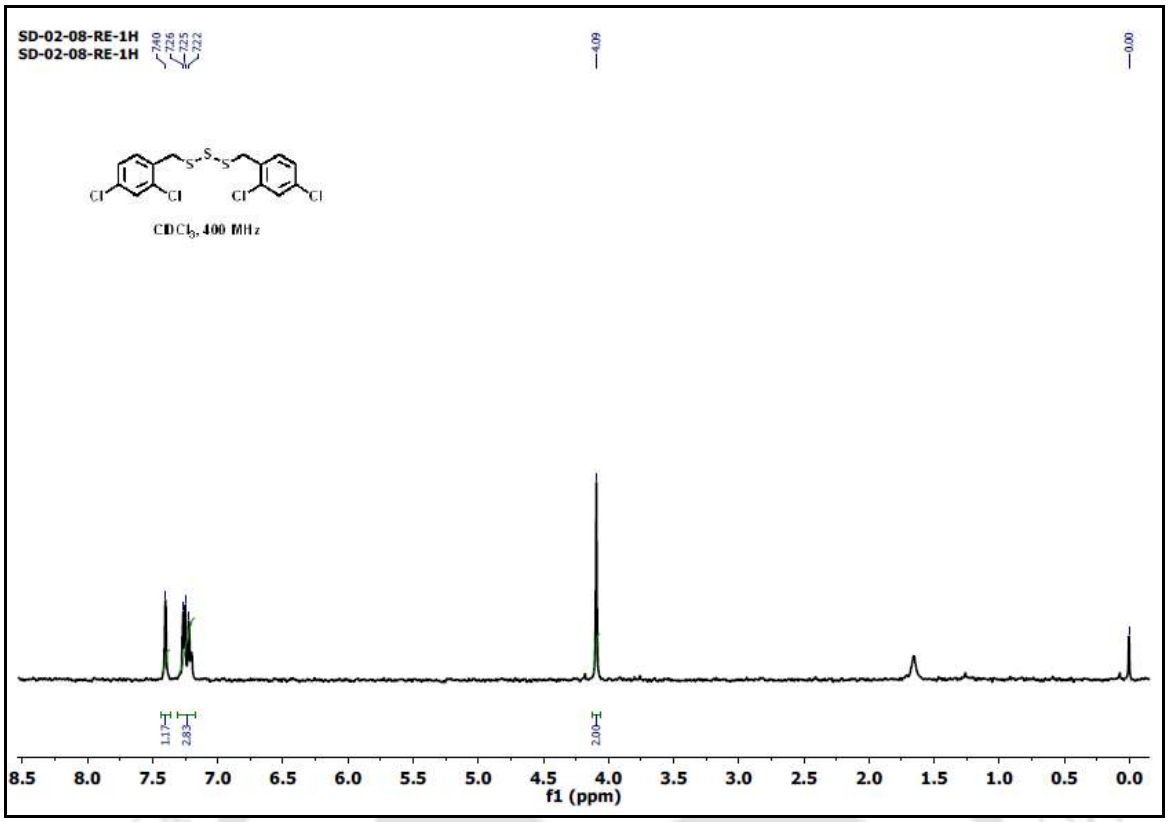

Figure A4.39. ^{1}H NMR ($CDCl_3$, 400 MHz, ppm) spectrum of compound **3.18**.

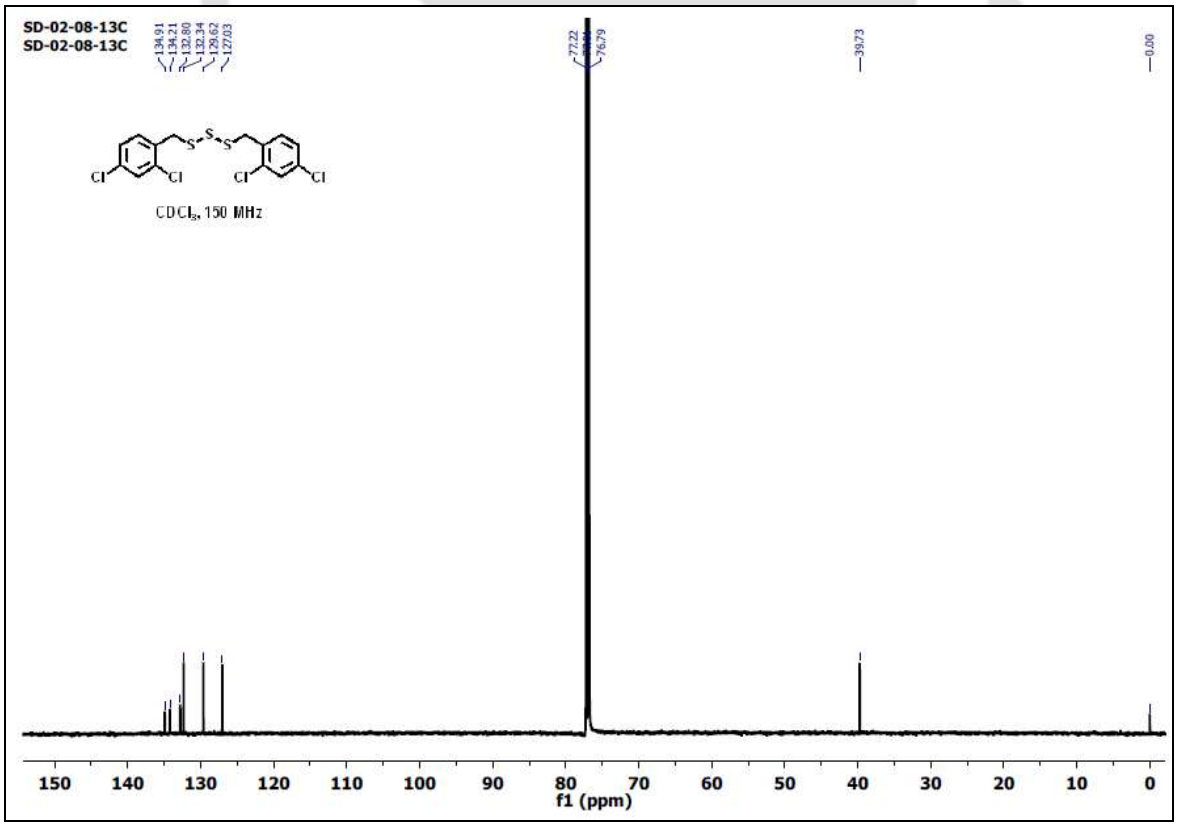

Figure A4.40. ^{13}C NMR ($CDCl_3$, 150 MHz, ppm) spectrum of compound **3.18**.

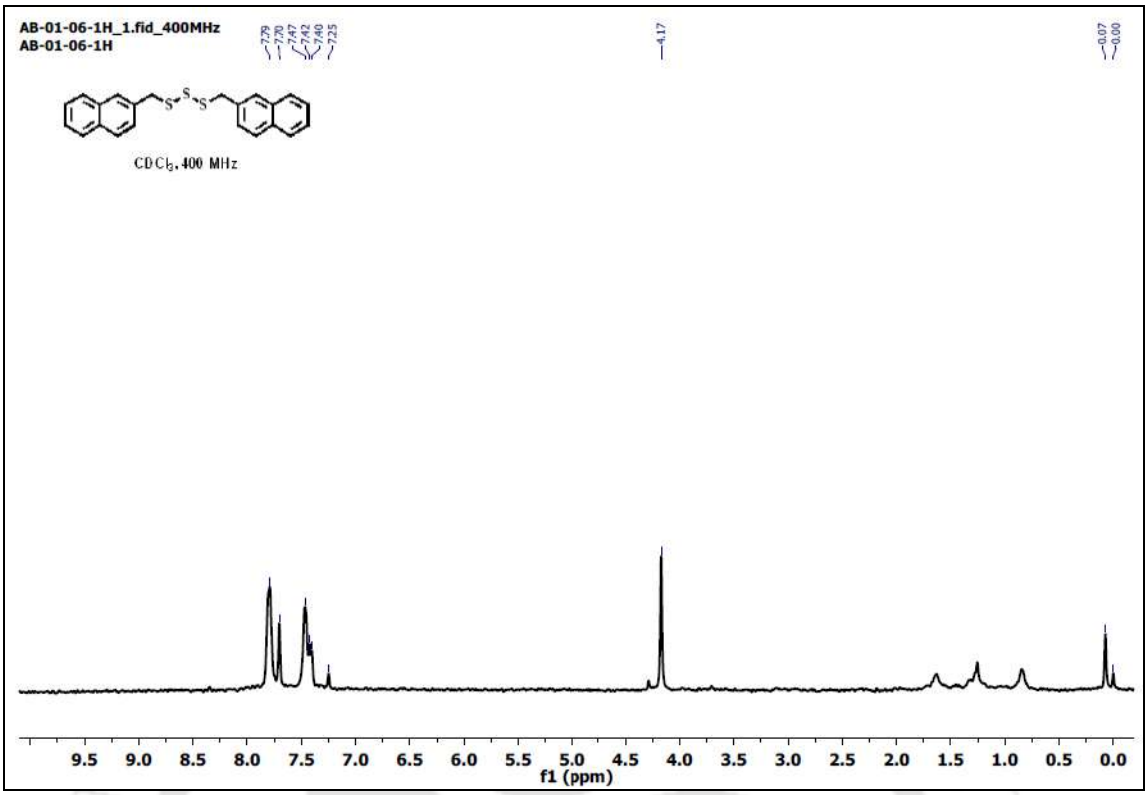

Figure A4.41. ^{1}H NMR ($CDCl_3$, 400 MHz, ppm) spectrum of compound **3.19**.

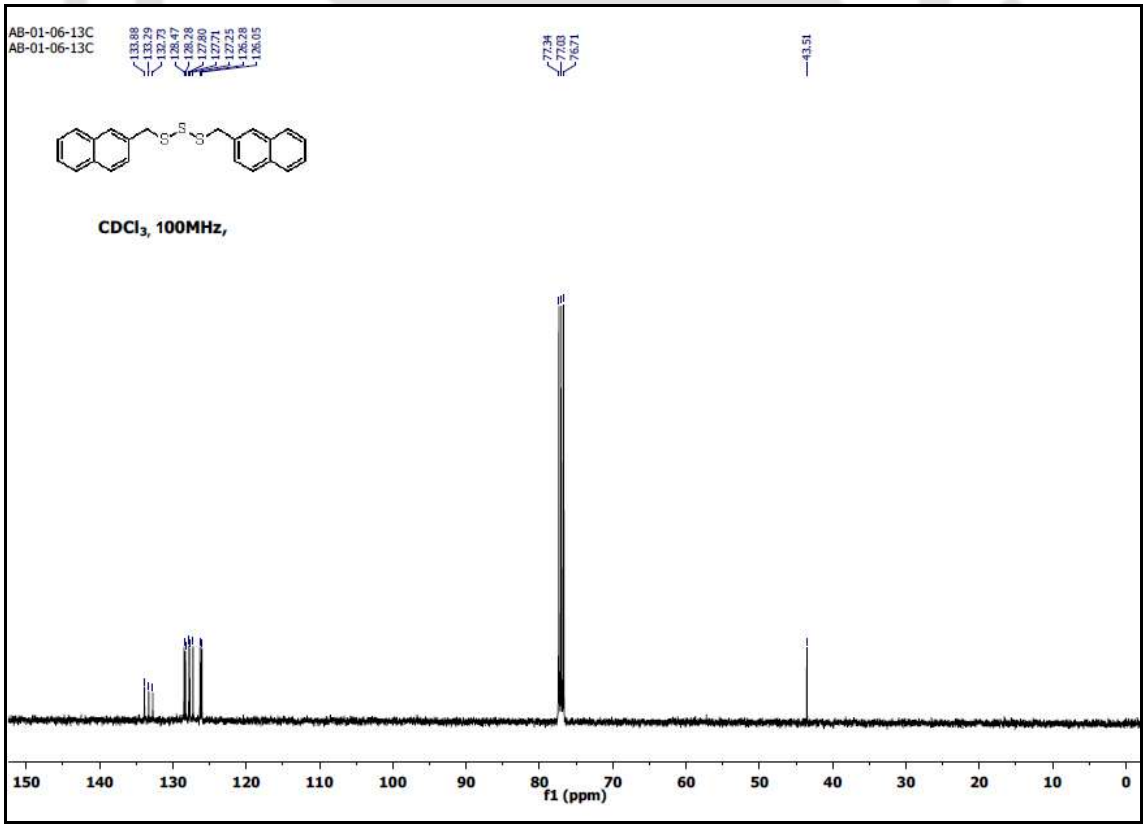

Figure A4.42. ^{13}C NMR ($CDCl_3$, 100 MHz, ppm) spectrum of compound **3.19**.

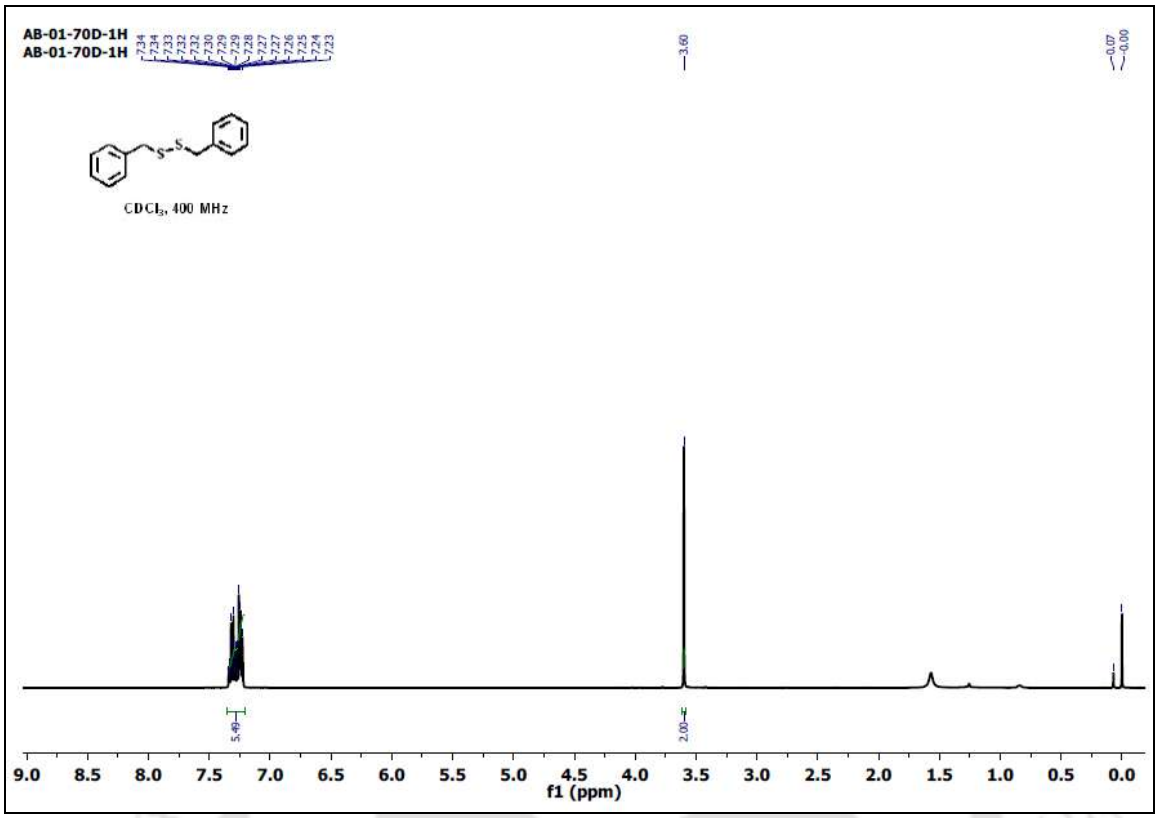

Figure A4.43. ^{1}H NMR ($CDCl_3$, 400 MHz, ppm) spectrum of DBDS.

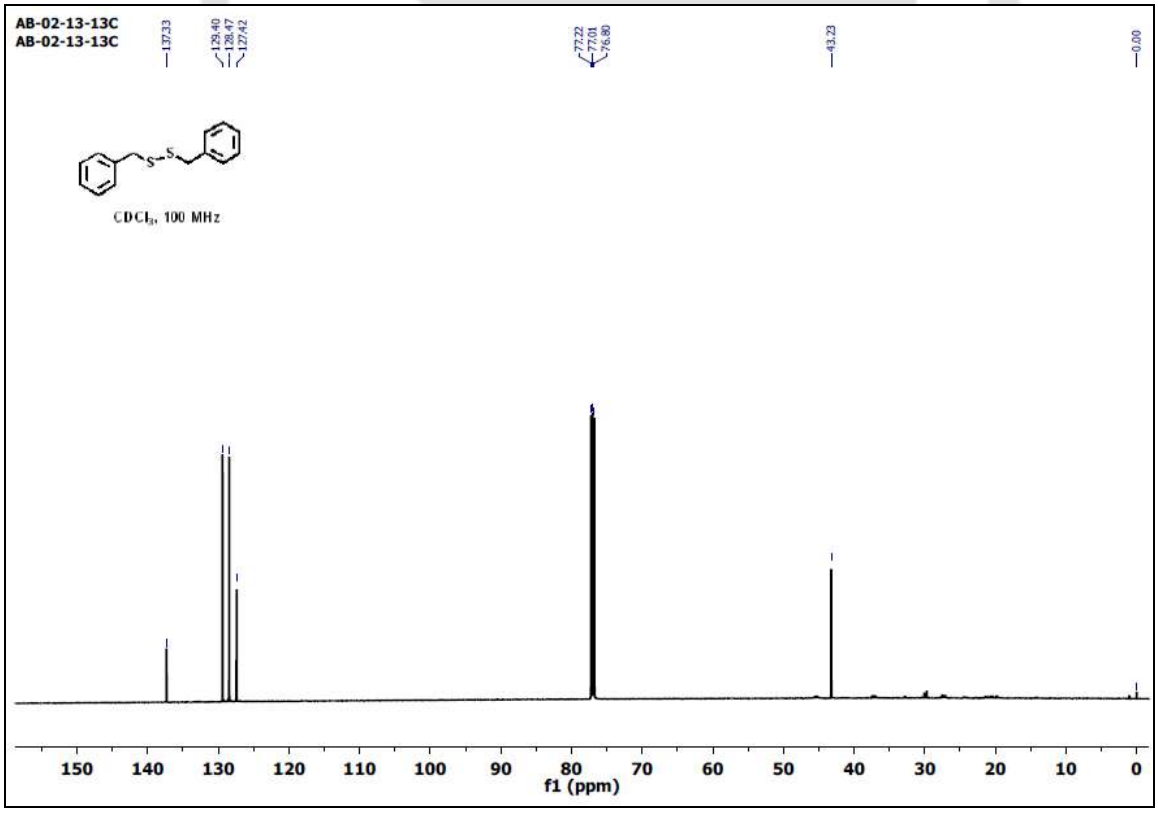

Figure A4.44. ^{13}C NMR ($CDCl_3$, 100 MHz, ppm) spectrum of DBDS.

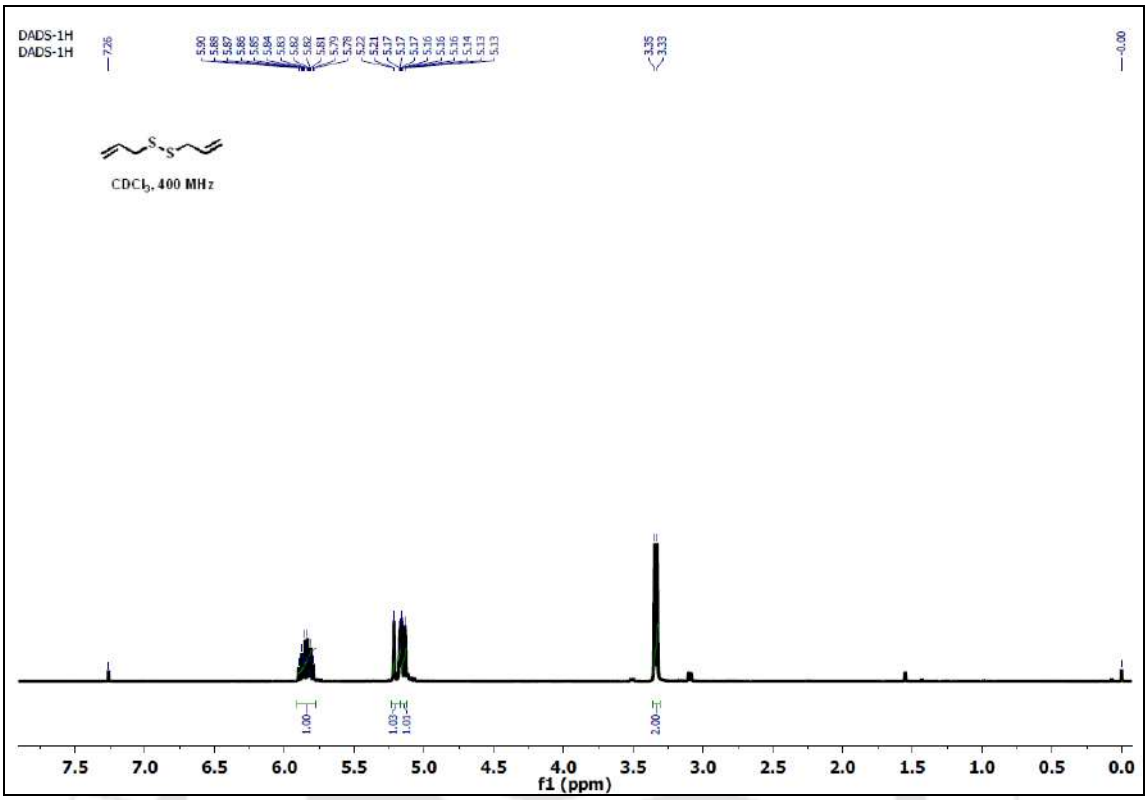

Figure A4.45. ^{1}H NMR ($CDCl_3$, 400 MHz, ppm) spectrum of compound DADS upon the addition of 5.0 equiv of Na_2SO_3 into the reaction.

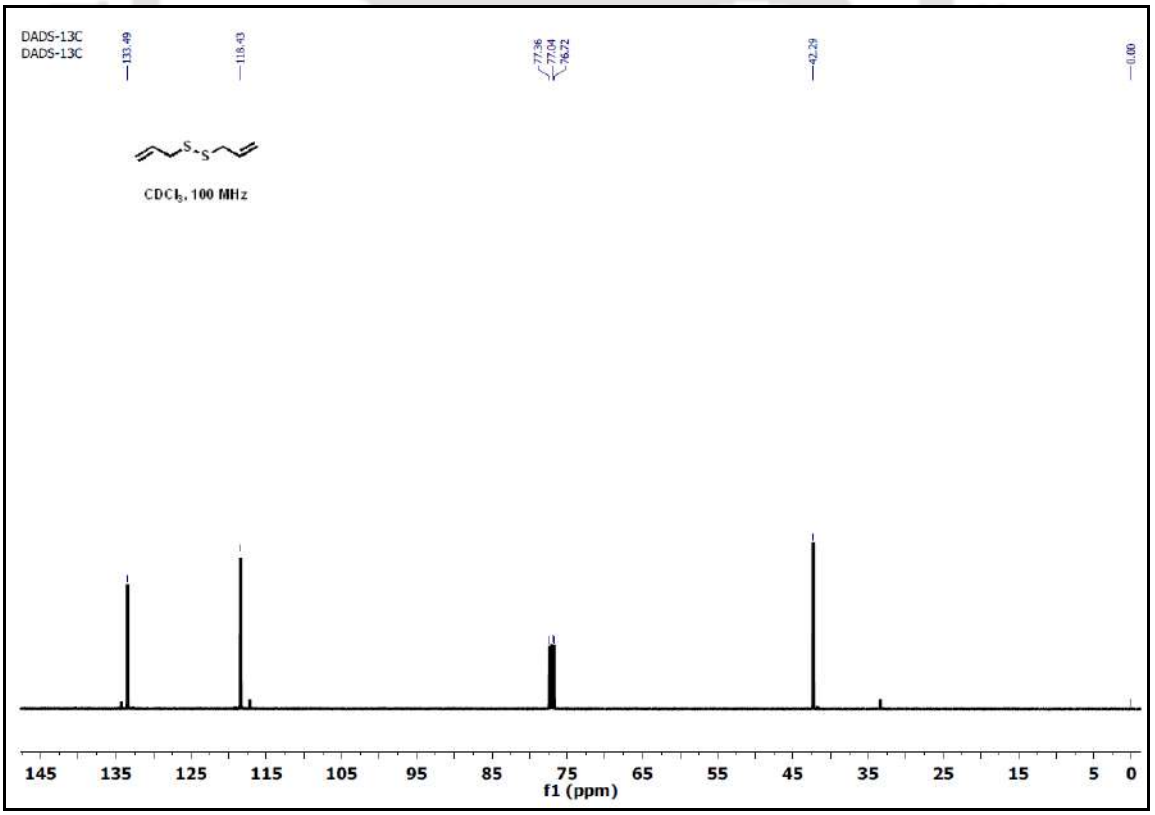

Figure A4.46. ^{13}C NMR ($CDCl_3$, 100 MHz, ppm) spectrum of compound DADS upon the addition of 5.0 equiv of Na_2SO_3 into the reaction.

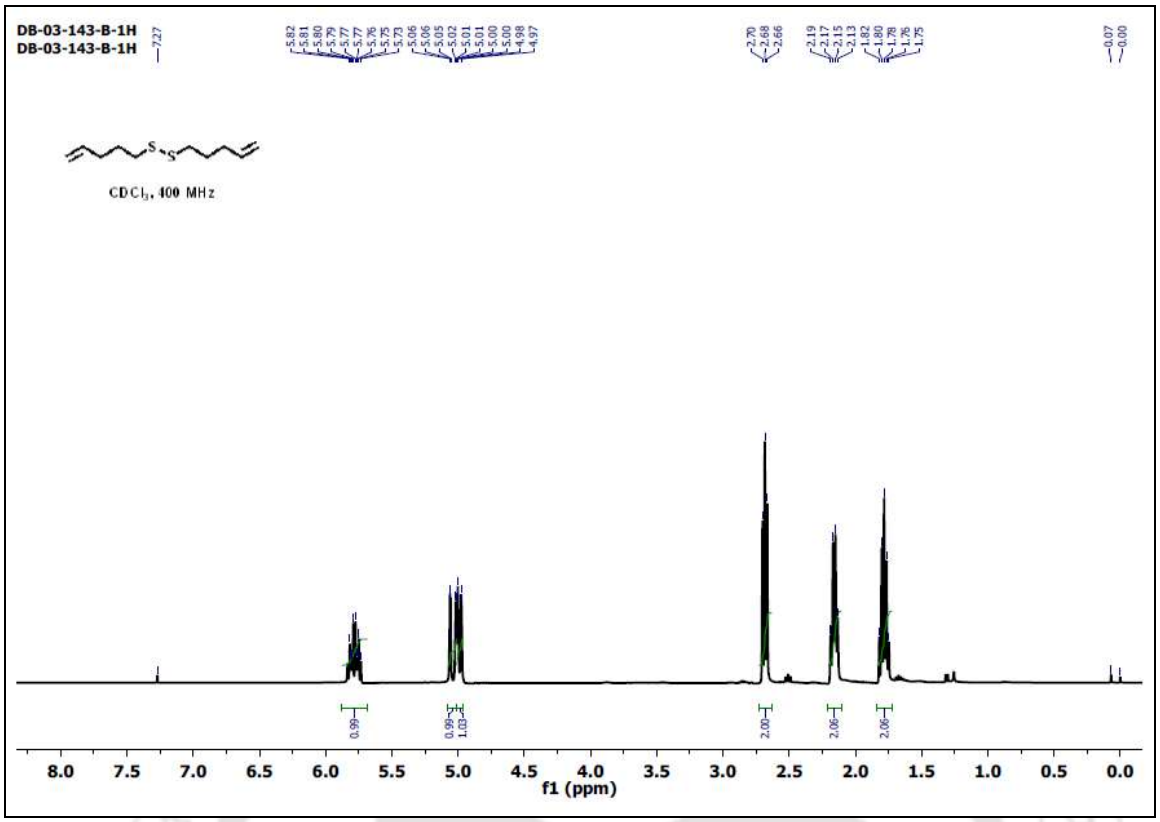

Figure A4.47. ^{1}H NMR ($CDCl_3$, 400 MHz, ppm) spectrum of compound **3.1a**.

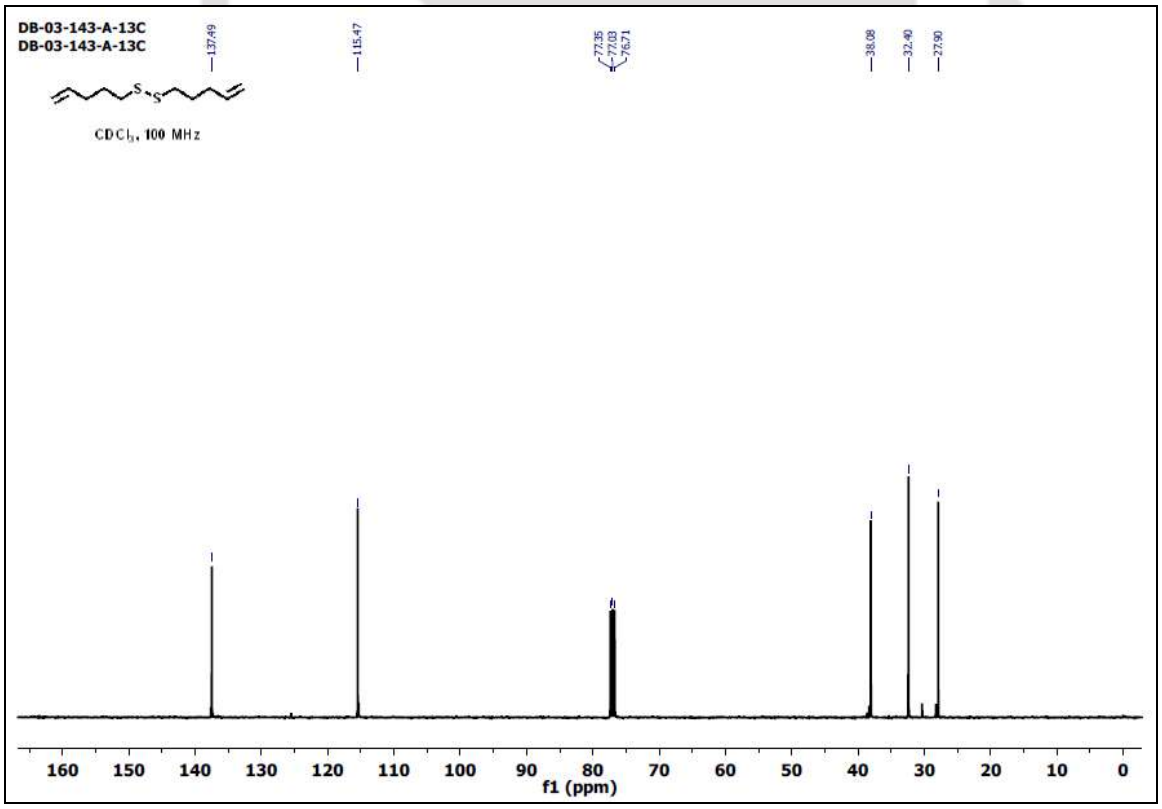

Figure A4.48. ^{13}C NMR ($CDCl_3$, 100 MHz, ppm) spectrum of compound **3.1a**.

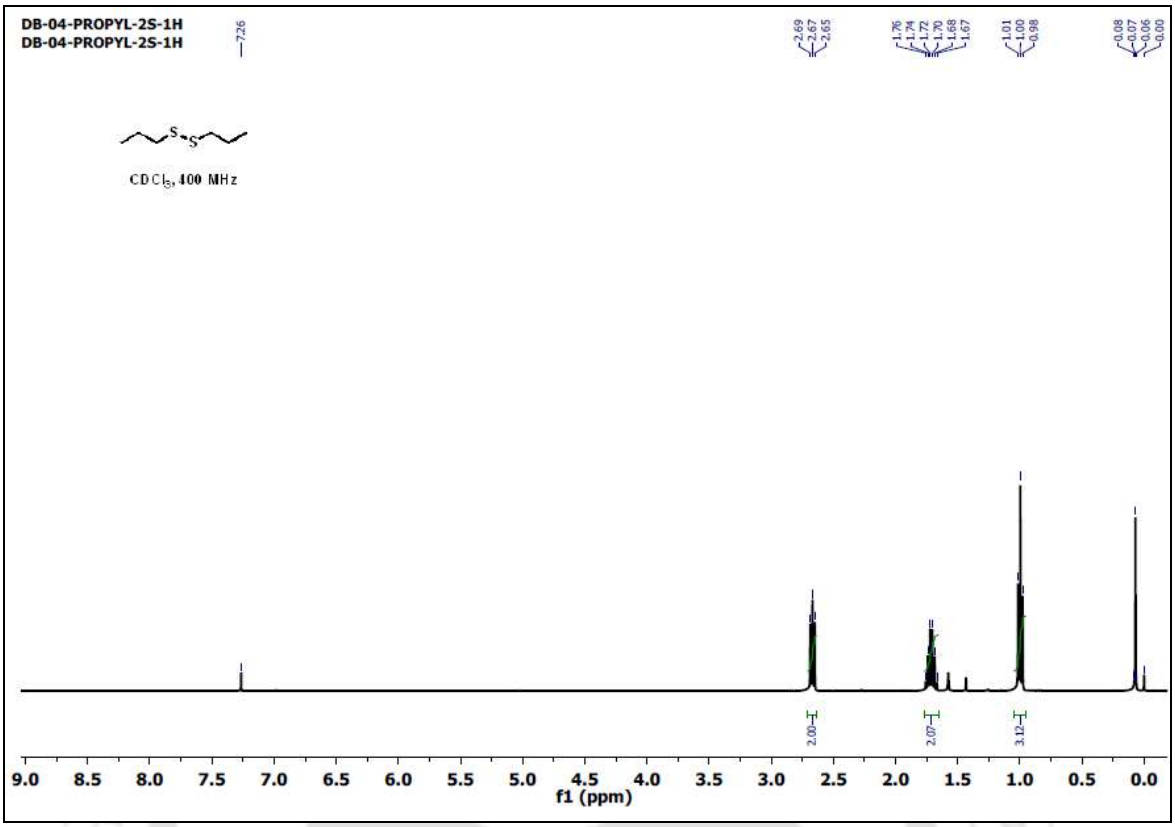

Figure A4.49. ^{1}H NMR ($CDCl_3$, 400 MHz, ppm) spectrum of compound **3.2a**.

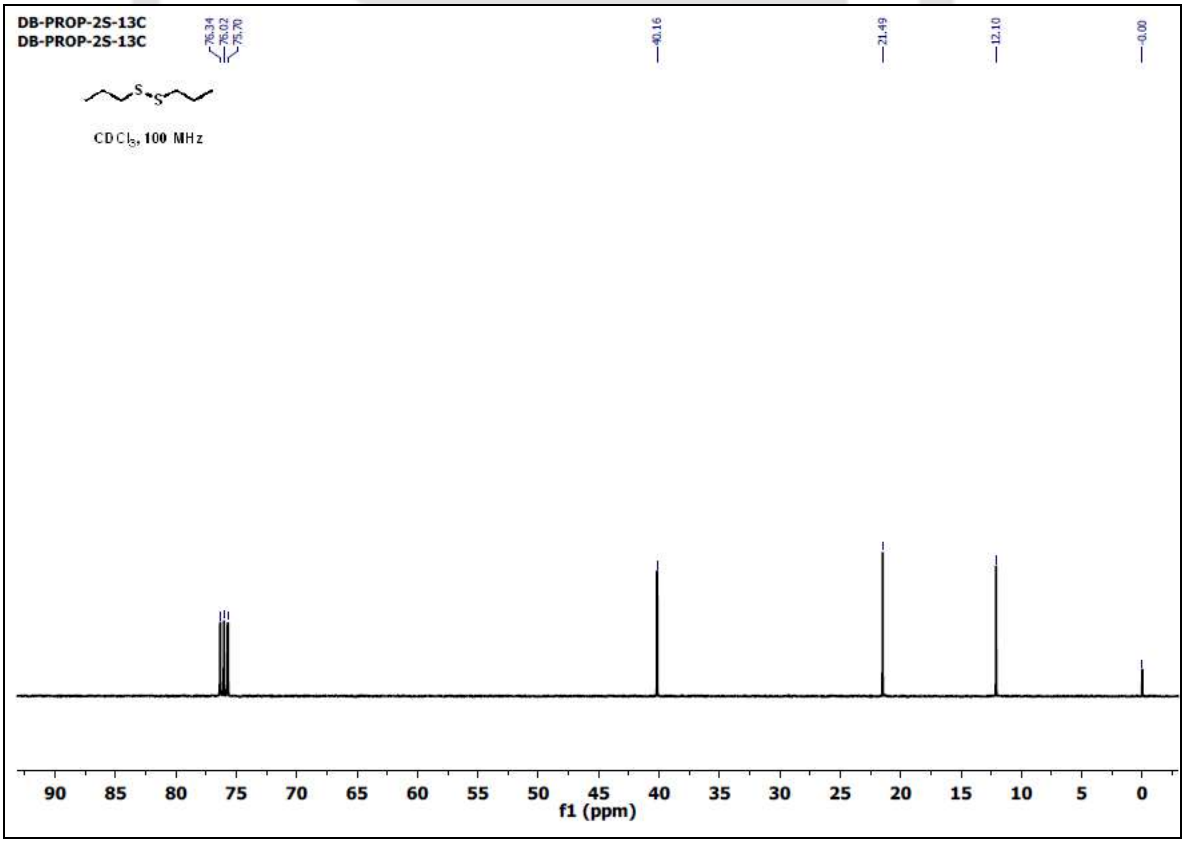

Figure A4.50. ^{13}C NMR ($CDCl_3$, 100 MHz, ppm) spectrum of compound **3.2a**.

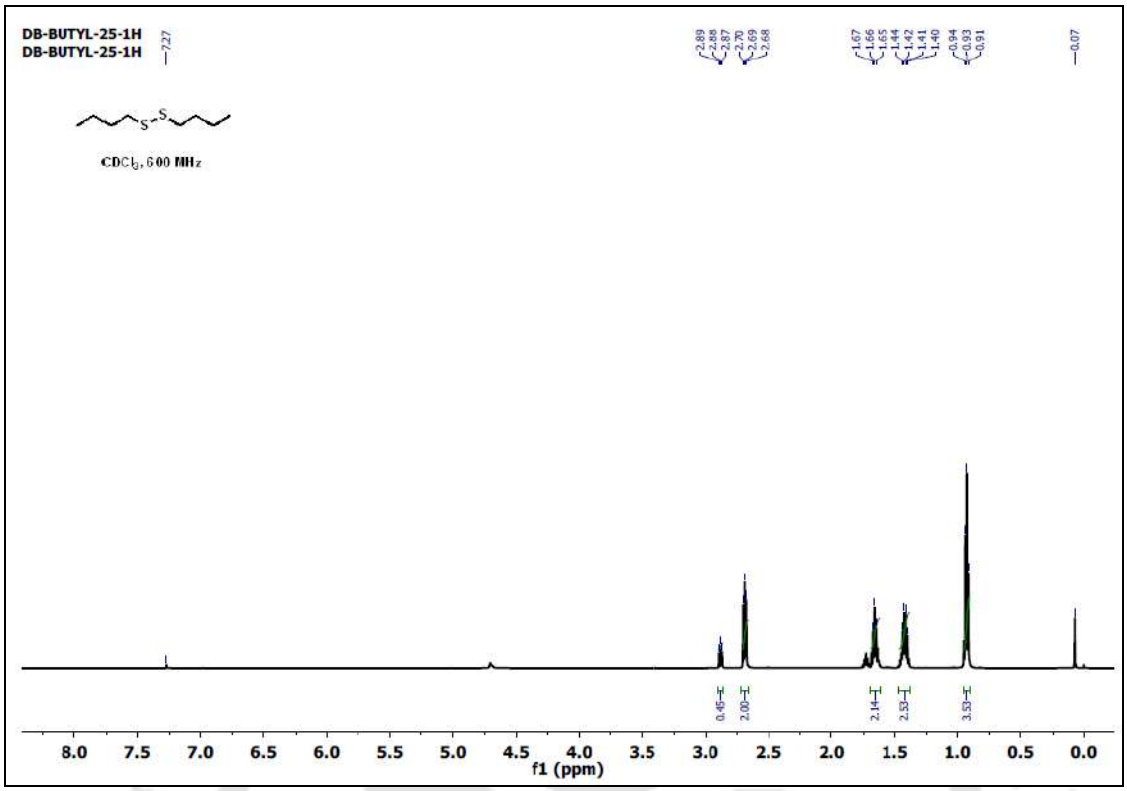

Figure A4.51. ^{1}H NMR ($CDCl_3$, 600 MHz, ppm) spectrum of compound **3.3a** upon the addition of 5.0 equiv of Na_2SO_3 into the reaction.

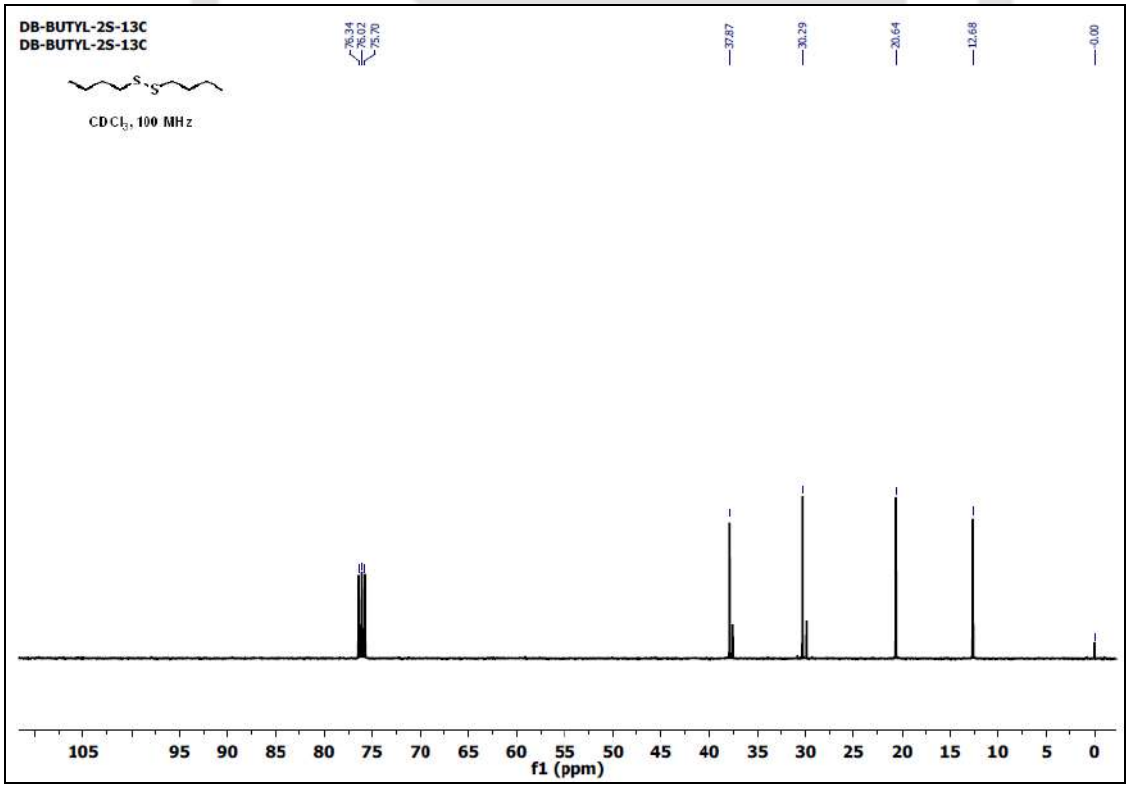

Figure A4.52. ^{13}C NMR ($CDCl_3$, 100 MHz, ppm) spectrum of compound **3.3a** upon the addition of 5.0 equiv of Na_2SO_3 into the reaction.

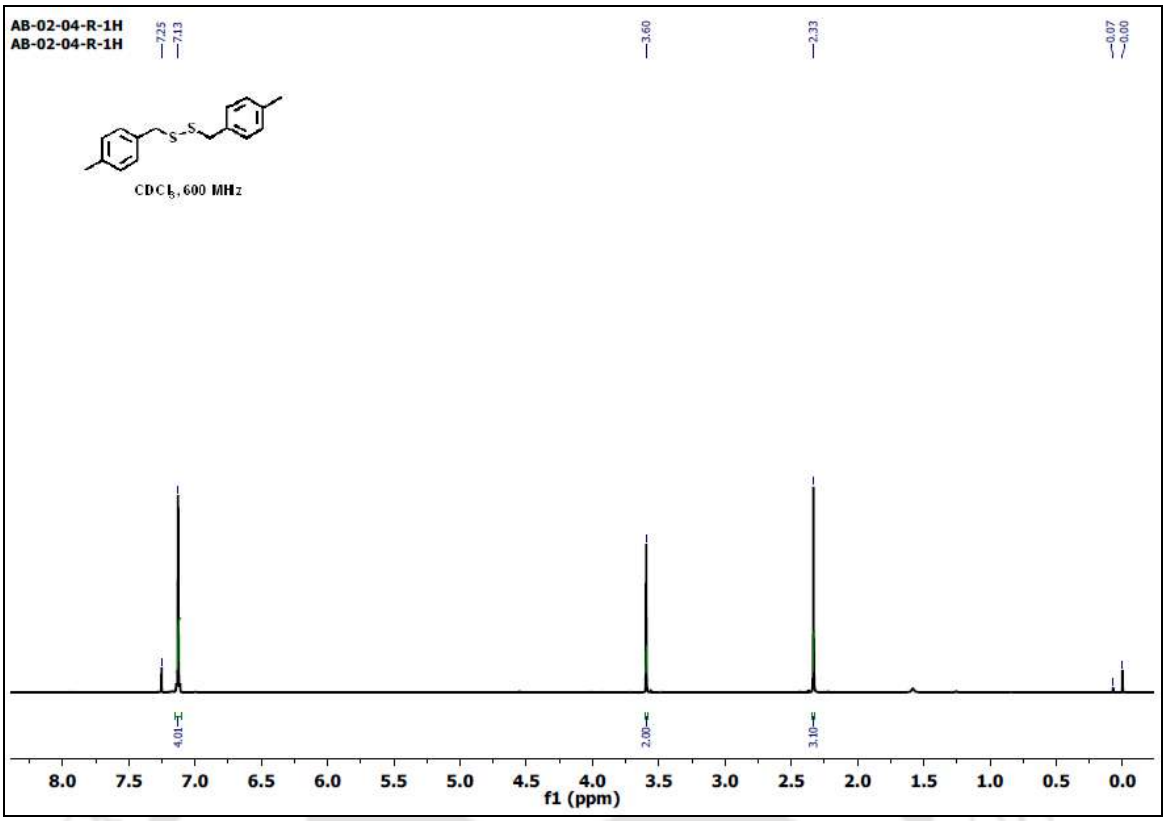

Figure A4.53. ^{1}H NMR ($CDCl_3$, 600 MHz, ppm) spectrum of compound **3.4a**.

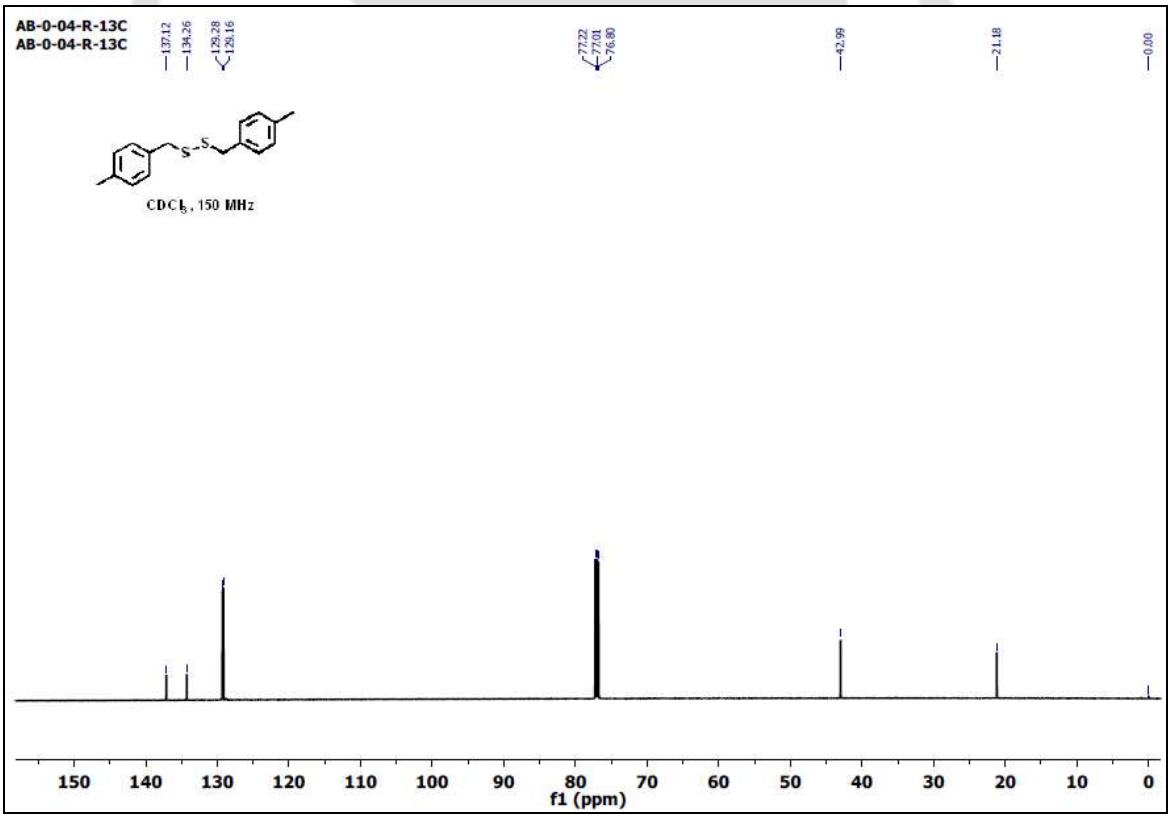

Figure A4.54. ^{13}C NMR ($CDCl_3$, 150 MHz, ppm) spectrum of compound **3.4a**.

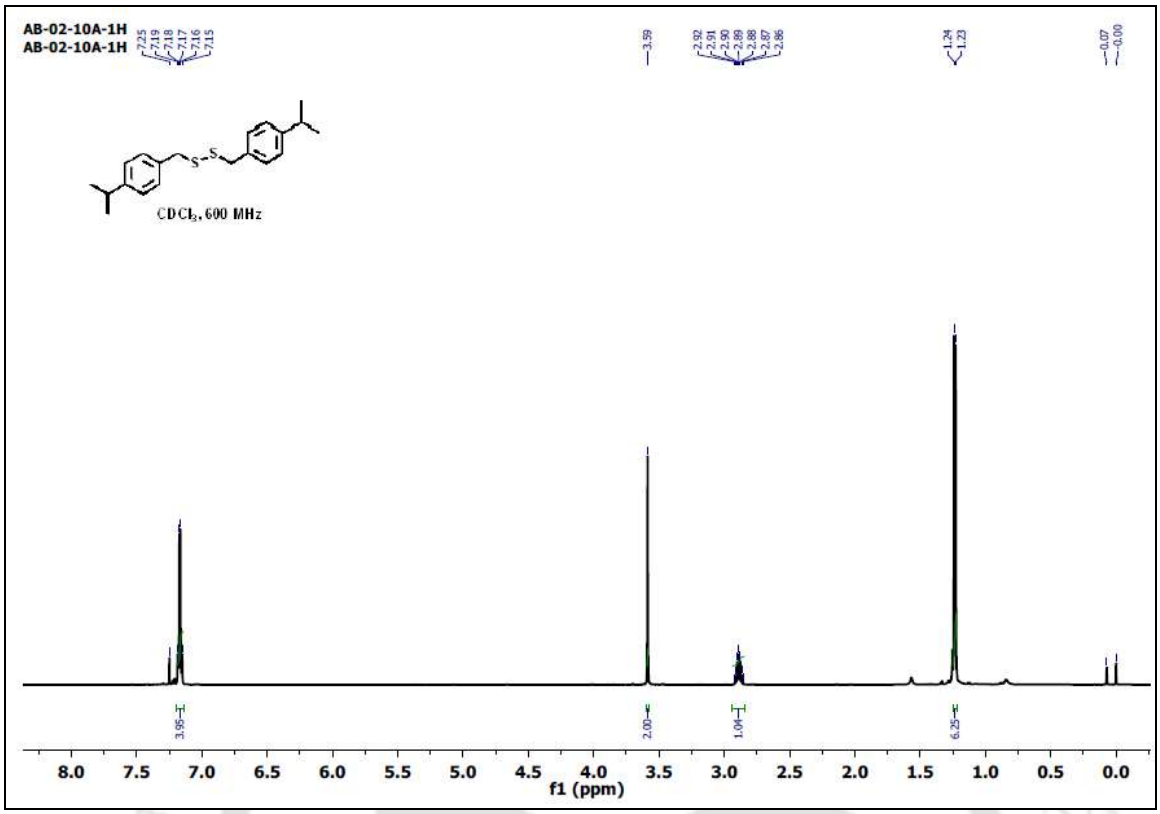

Figure A4.55. ^{1}H NMR ($CDCl_3$, 600 MHz, ppm) spectrum of compound **3.5a**.

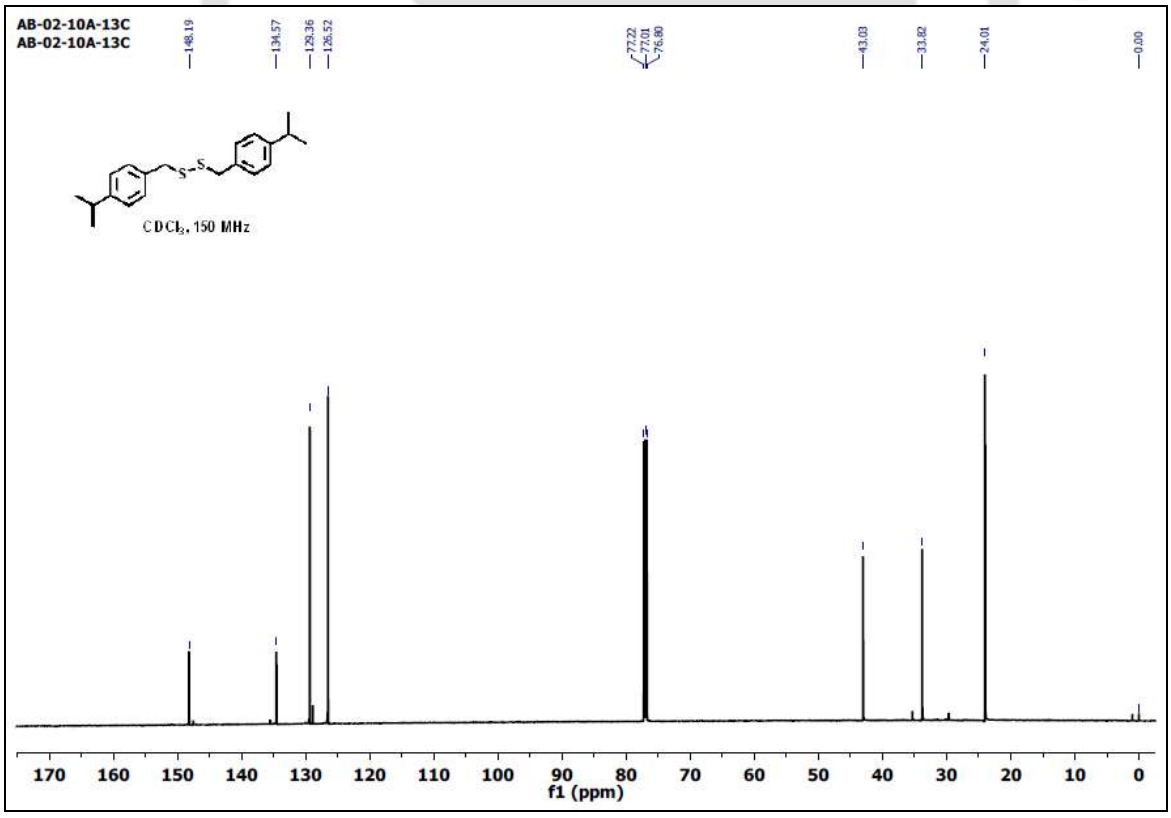

Figure A4.56. ^{13}C NMR ($CDCl_3$, 150 MHz, ppm) spectrum of compound **3.5a**.

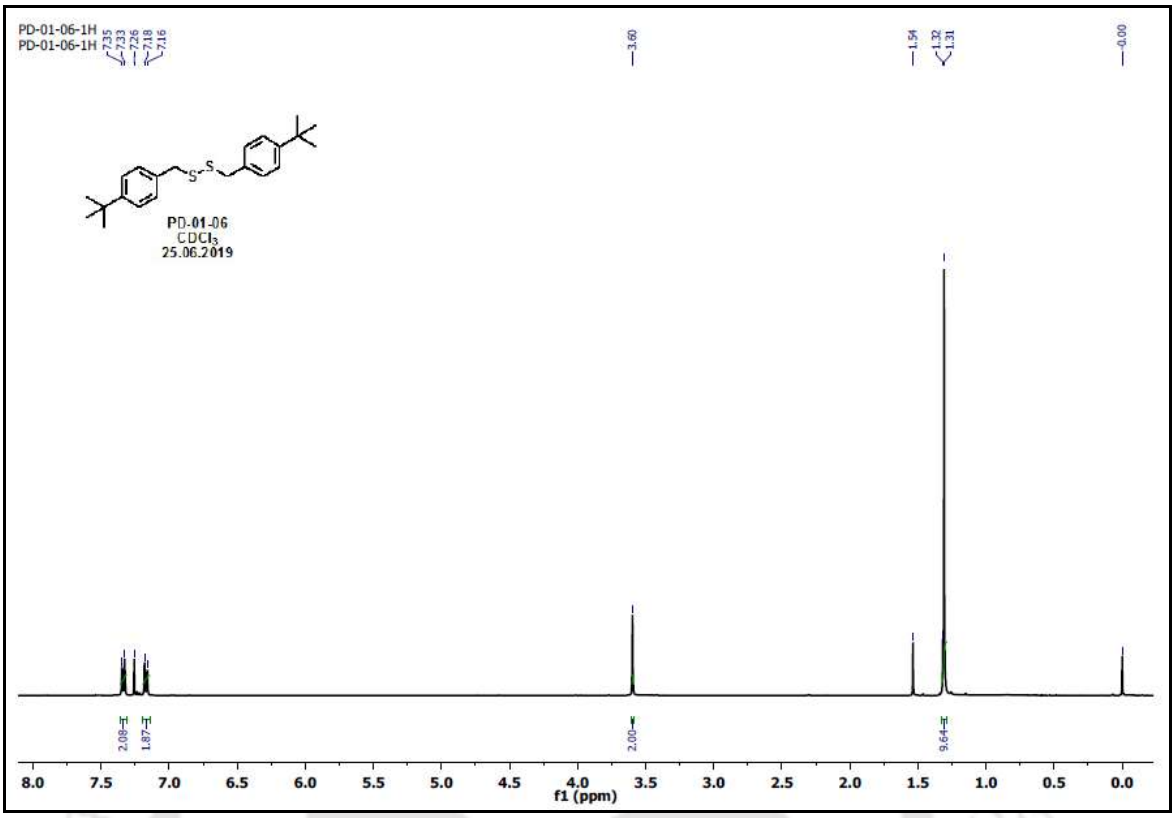

Figure A4.57. ^{1}H NMR ($CDCl_3$, 400 MHz, ppm) spectrum of compound **3.6a**.

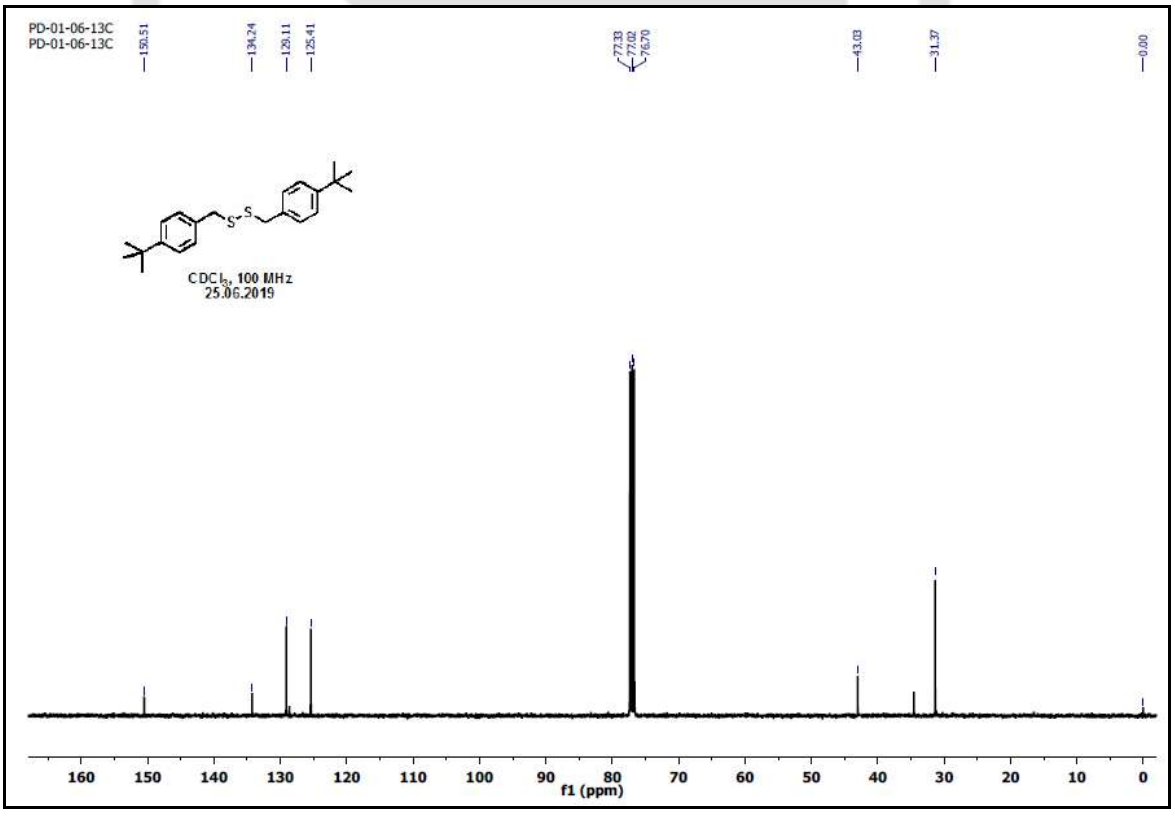

Figure A4.58. ^{13}C NMR ($CDCl_3$, 100 MHz, ppm) spectrum of compound **3.6a**.

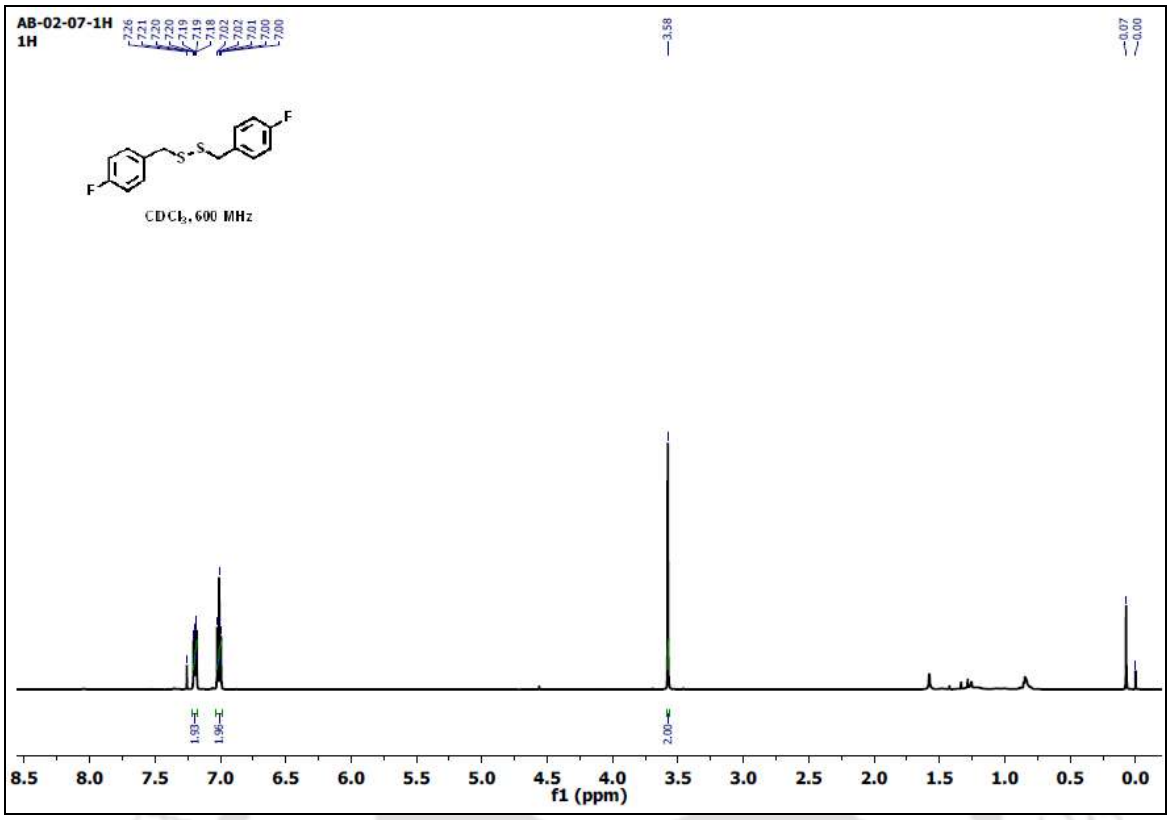

Figure A4.59. ^{1}H NMR ($CDCl_3$, 600 MHz, ppm) spectrum of compound **3.7a**.

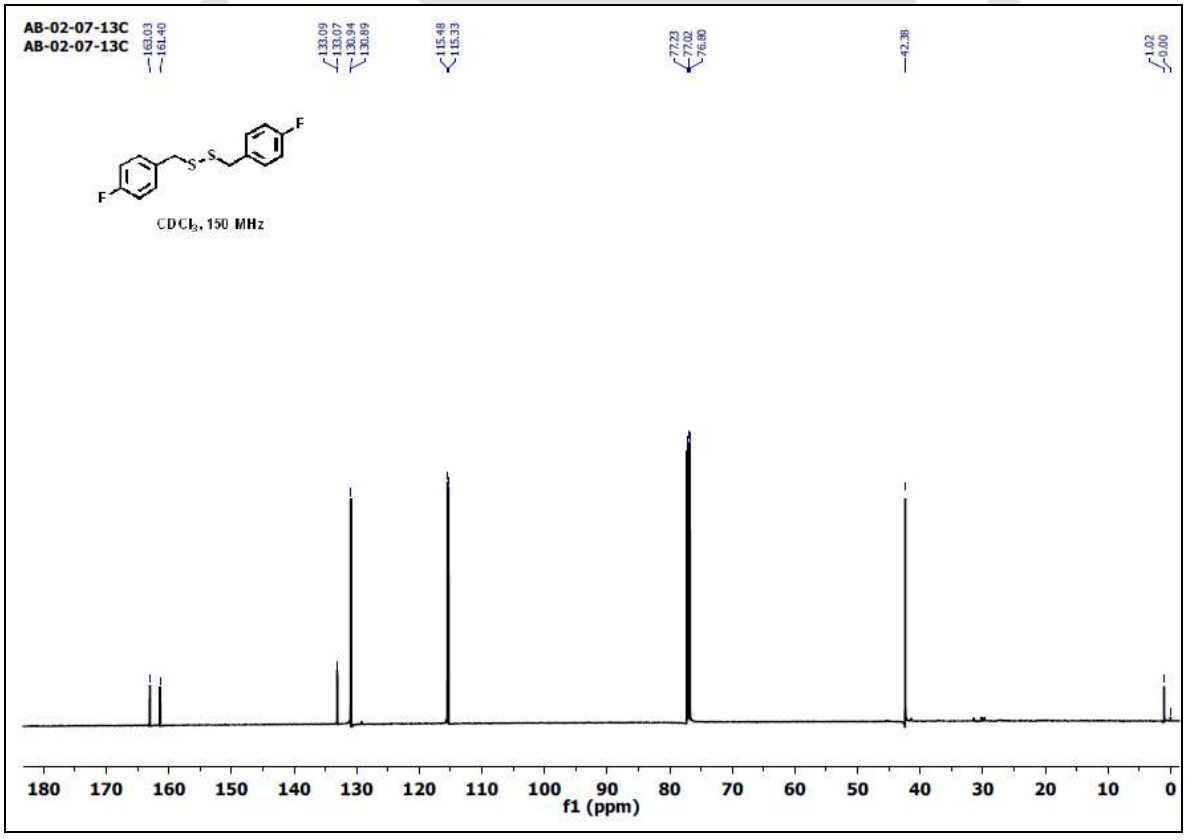

Figure A4.60. ^{13}C NMR ($CDCl_3$, 150 MHz, ppm) spectrum of compound **3.7a**.

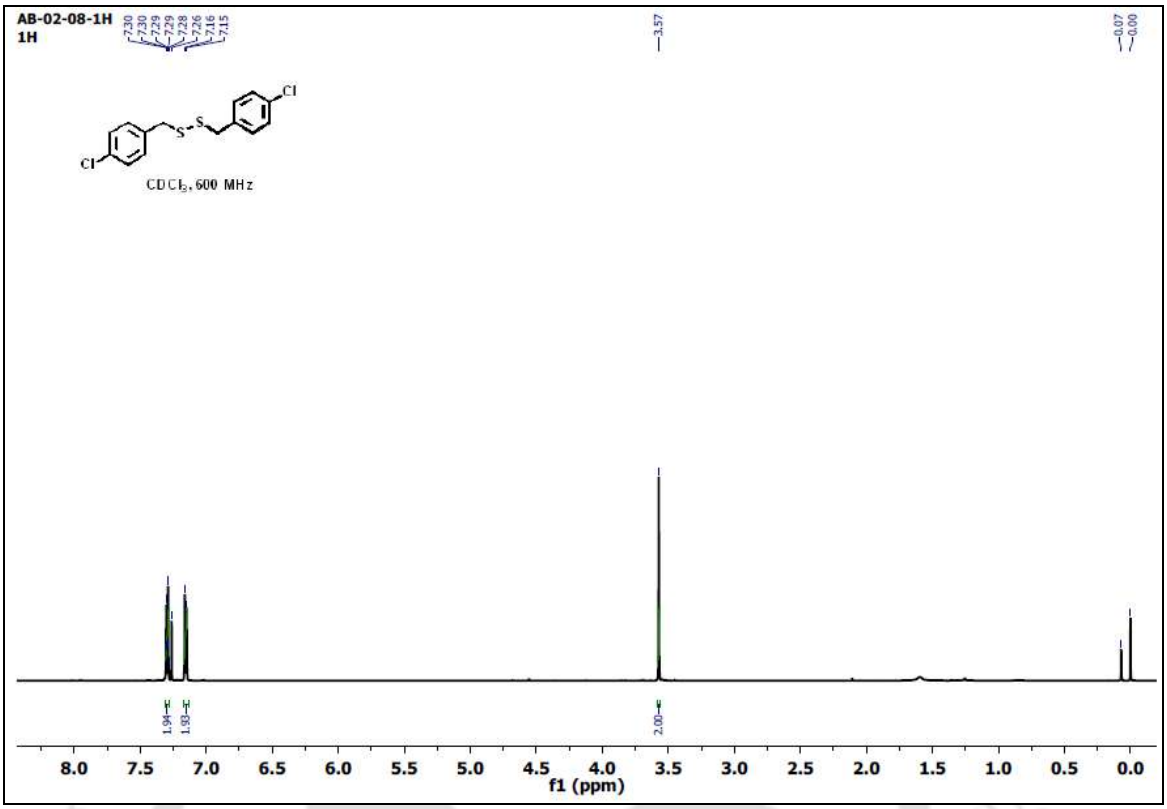

Figure A4.61. ^{1}H NMR ($CDCl_3$, 600 MHz, ppm) spectrum of compound **3.8a**.

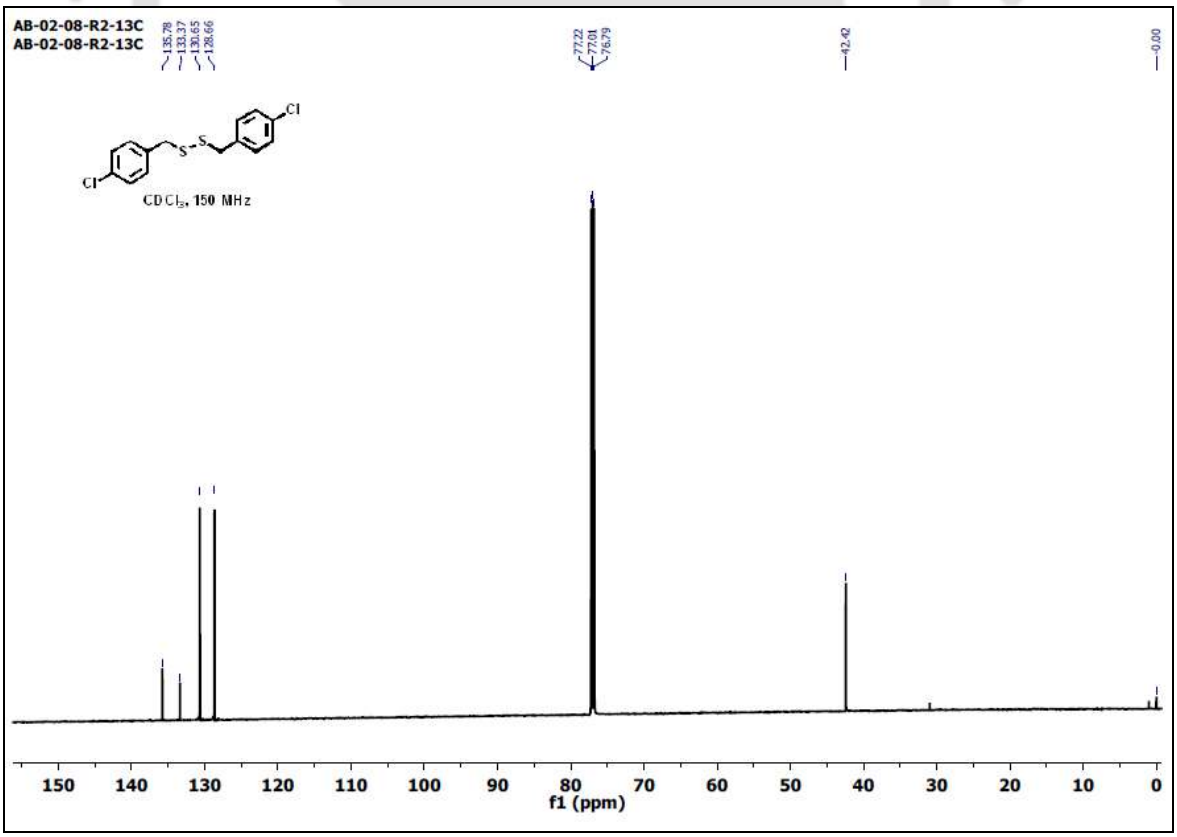

Figure A4.62. ^{13}C NMR ($CDCl_3$, 150 MHz, ppm) spectrum of compound **3.8a**.

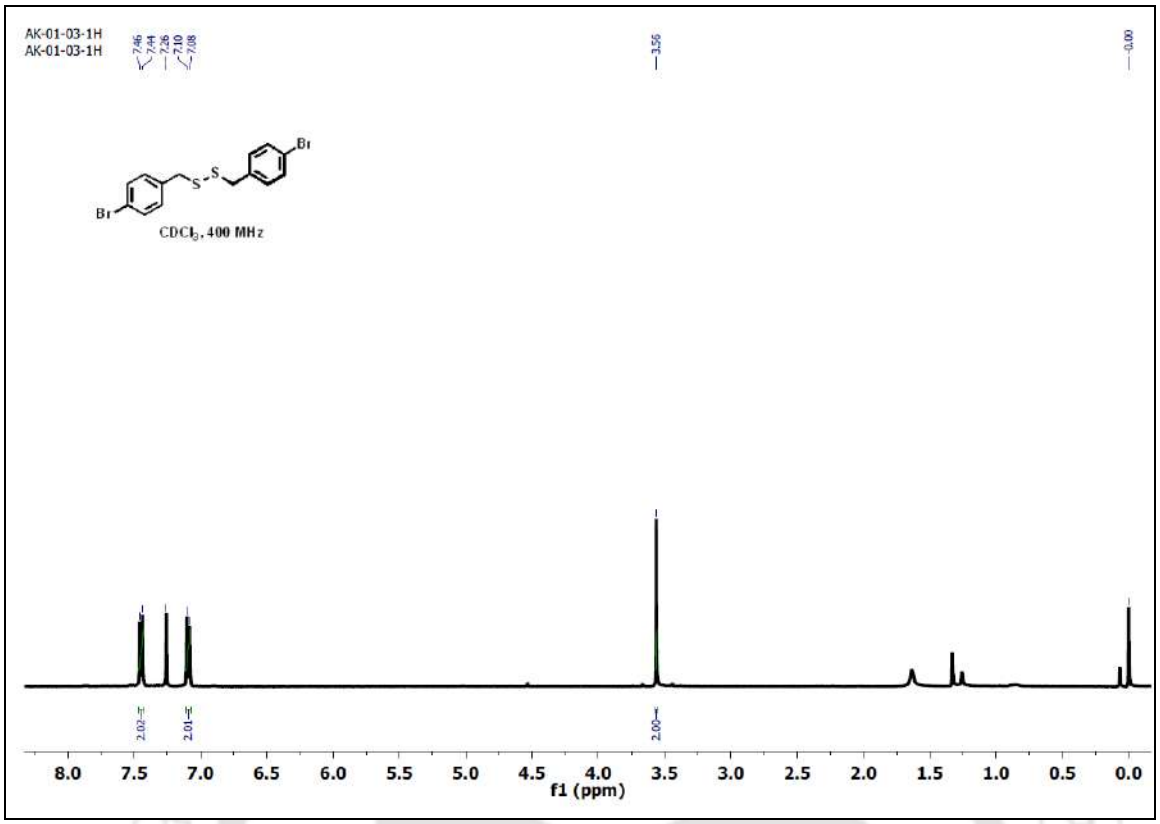

Figure A4.63. ^{1}H NMR ($CDCl_3$, 400 MHz, ppm) spectrum of compound **3.9a**.

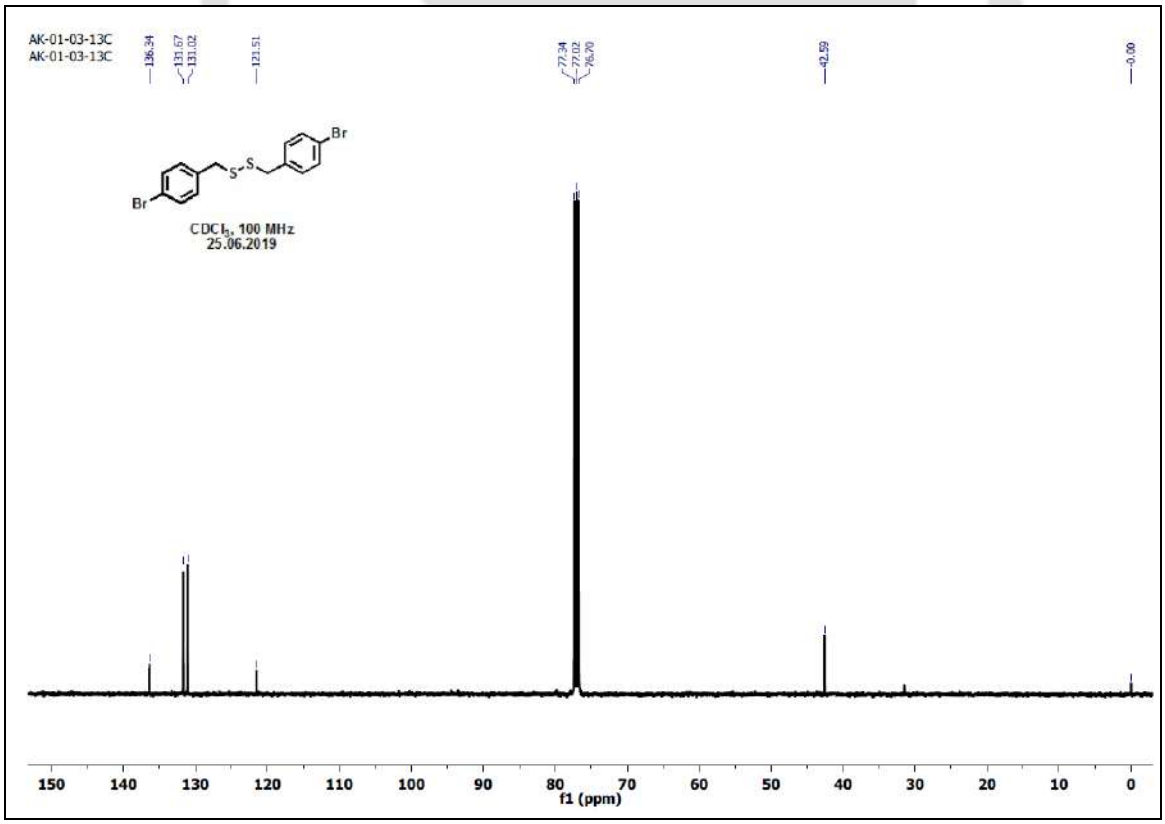

Figure A4.64. ^{13}C NMR ($CDCl_3$, 100 MHz, ppm) spectrum of compound **3.9a**.

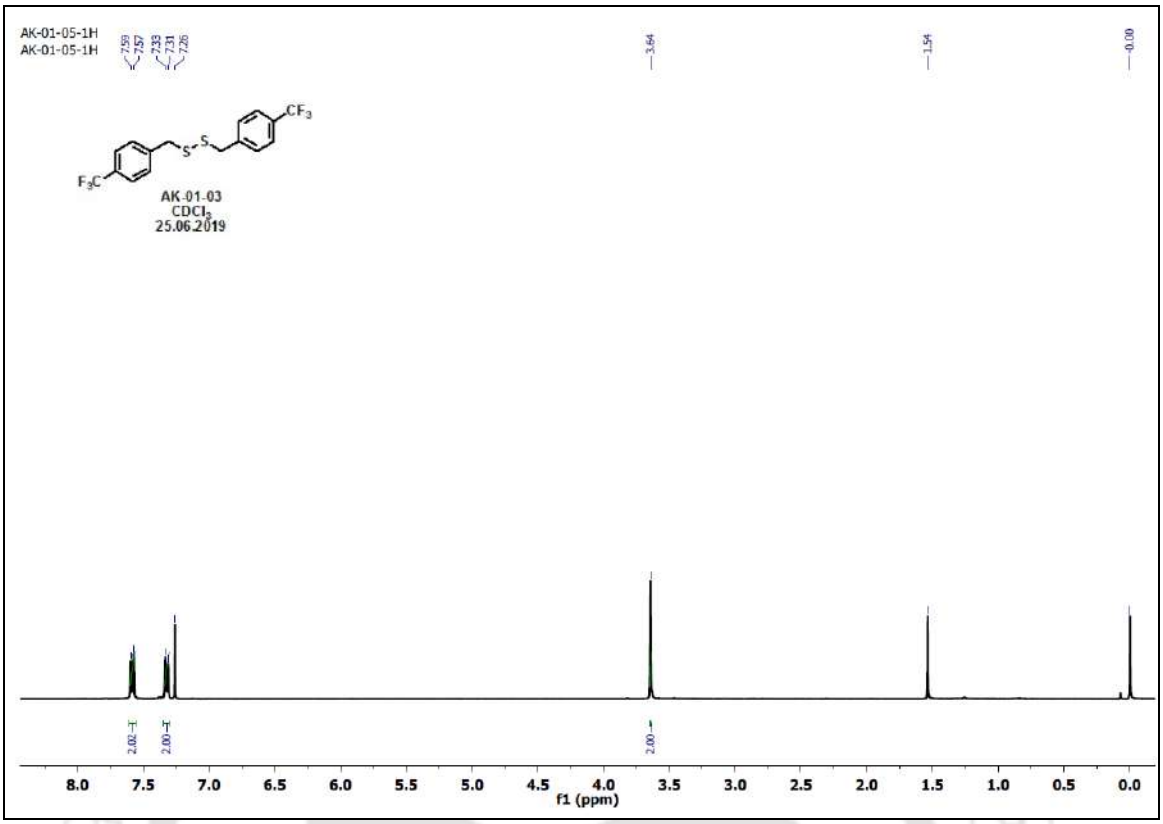

Figure A4.65. ^{1}H NMR ($CDCl_3$, 400 MHz, ppm) spectrum of compound **3.10a**.

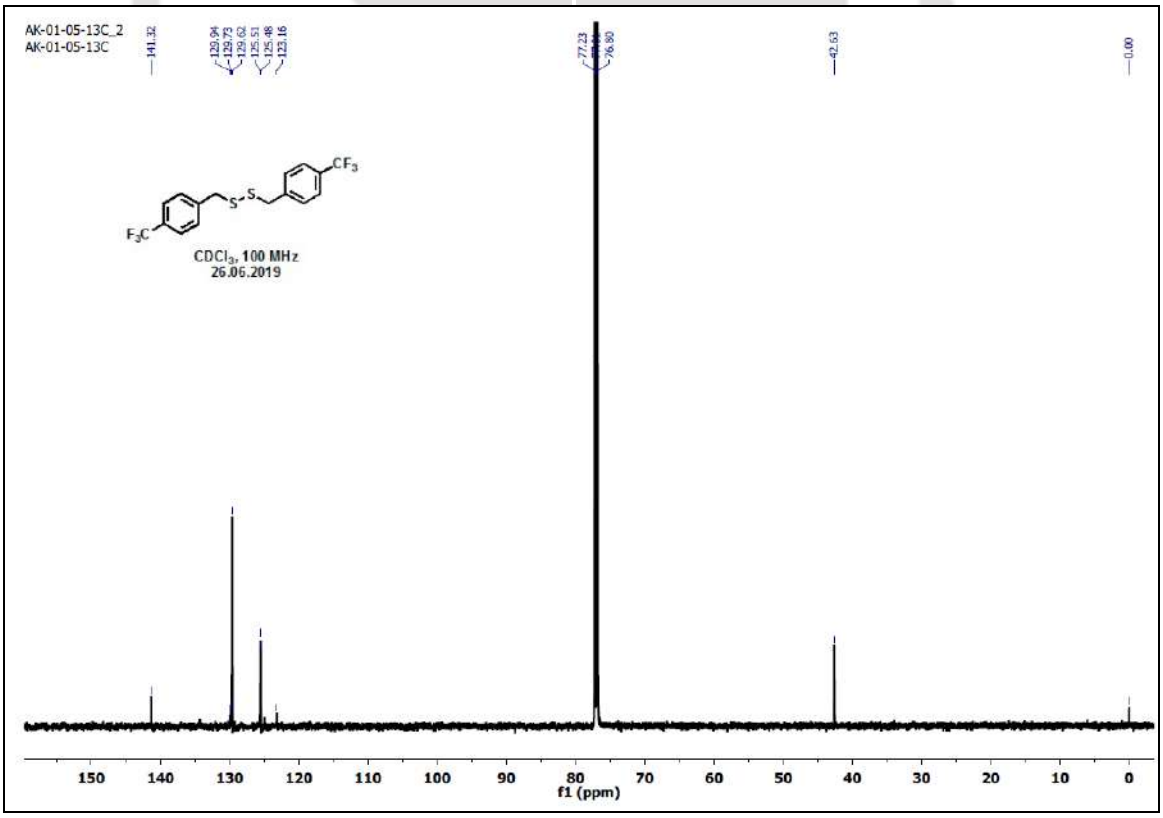

Figure A4.66. ^{13}C NMR ($CDCl_3$, 100 MHz, ppm) spectrum of compound **3.10a**.

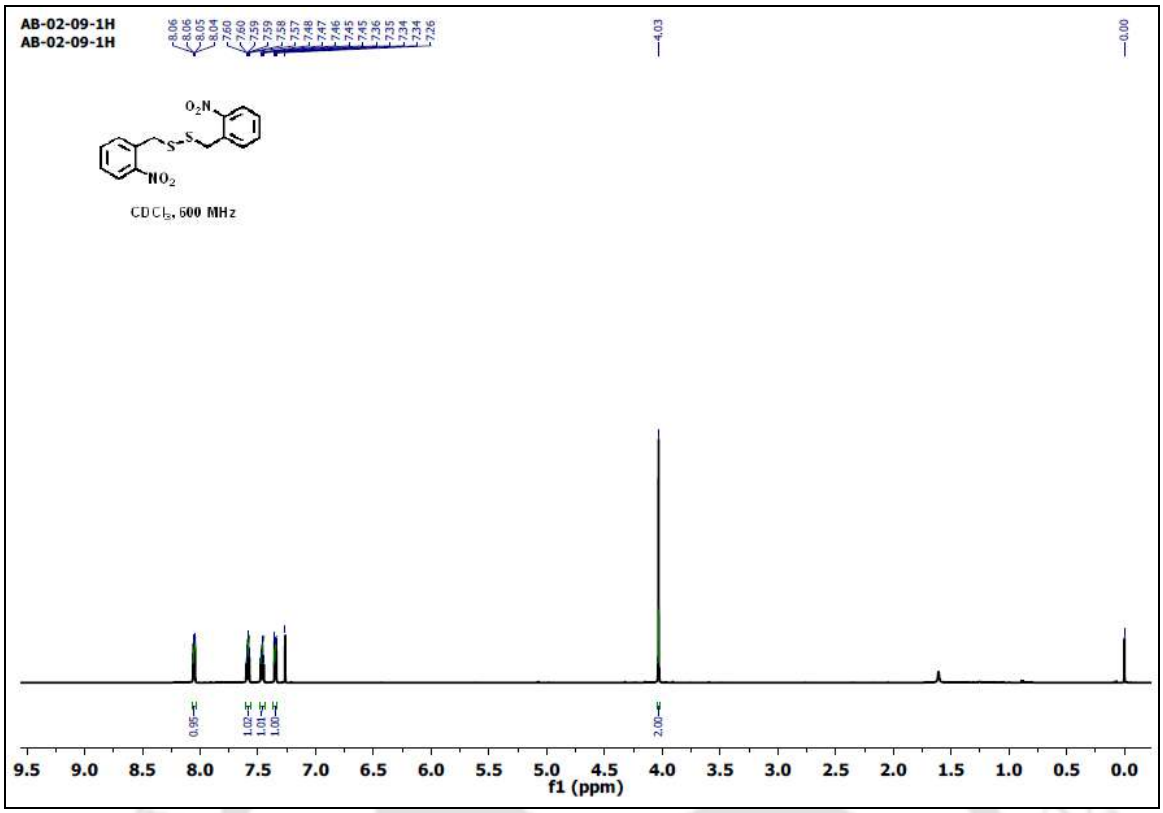

Figure A4.67. ^{1}H NMR ($CDCl_3$, 600 MHz, ppm) spectrum of compound **3.11a**.

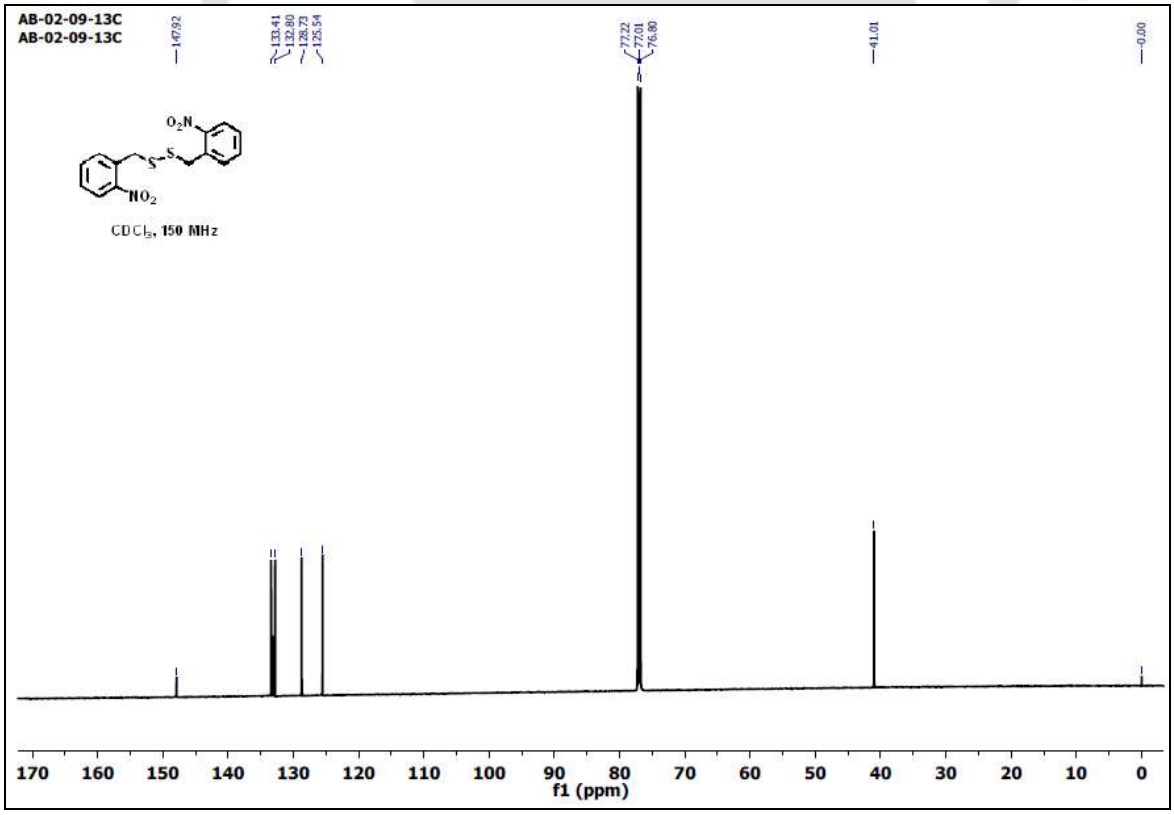

Figure A4.68. ^{13}C NMR ($CDCl_3$, 150 MHz, ppm) spectrum of compound **3.11a**.

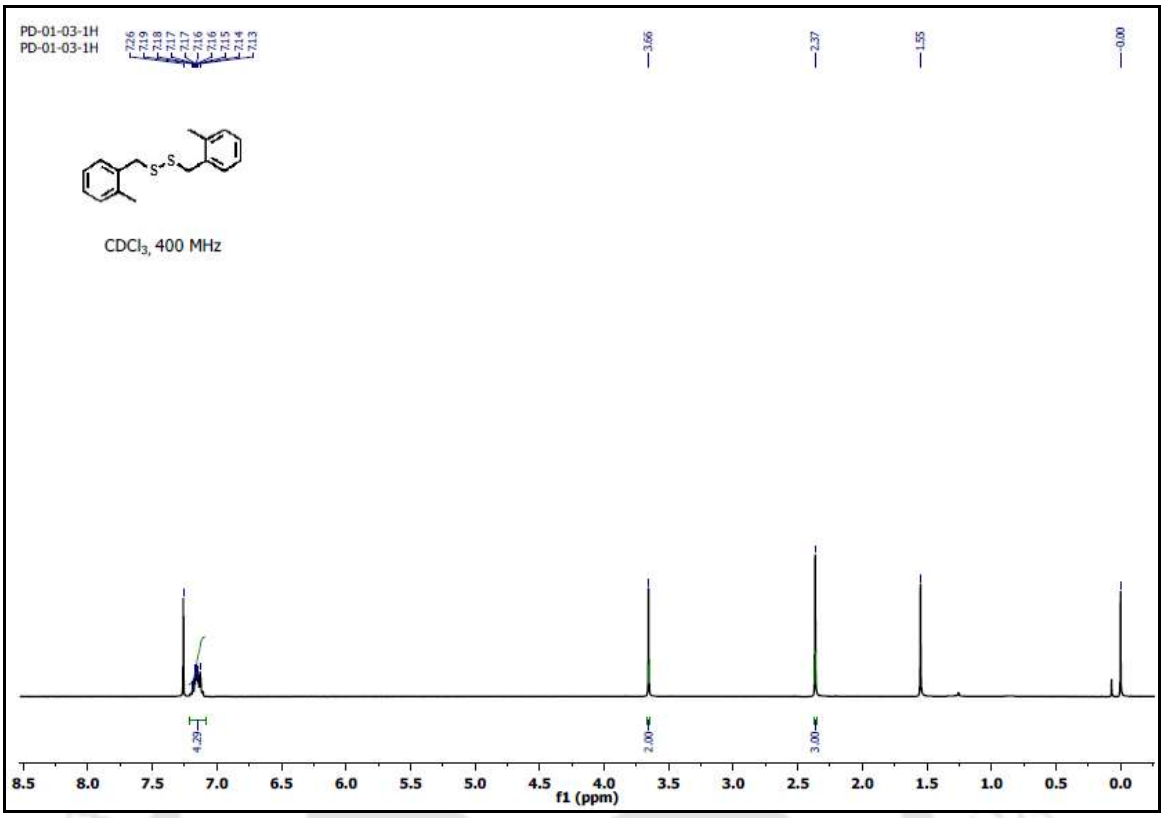

Figure A4.69. ^{1}H NMR ($CDCl_3$, 600 MHz, ppm) spectrum of compound **3.12a**.

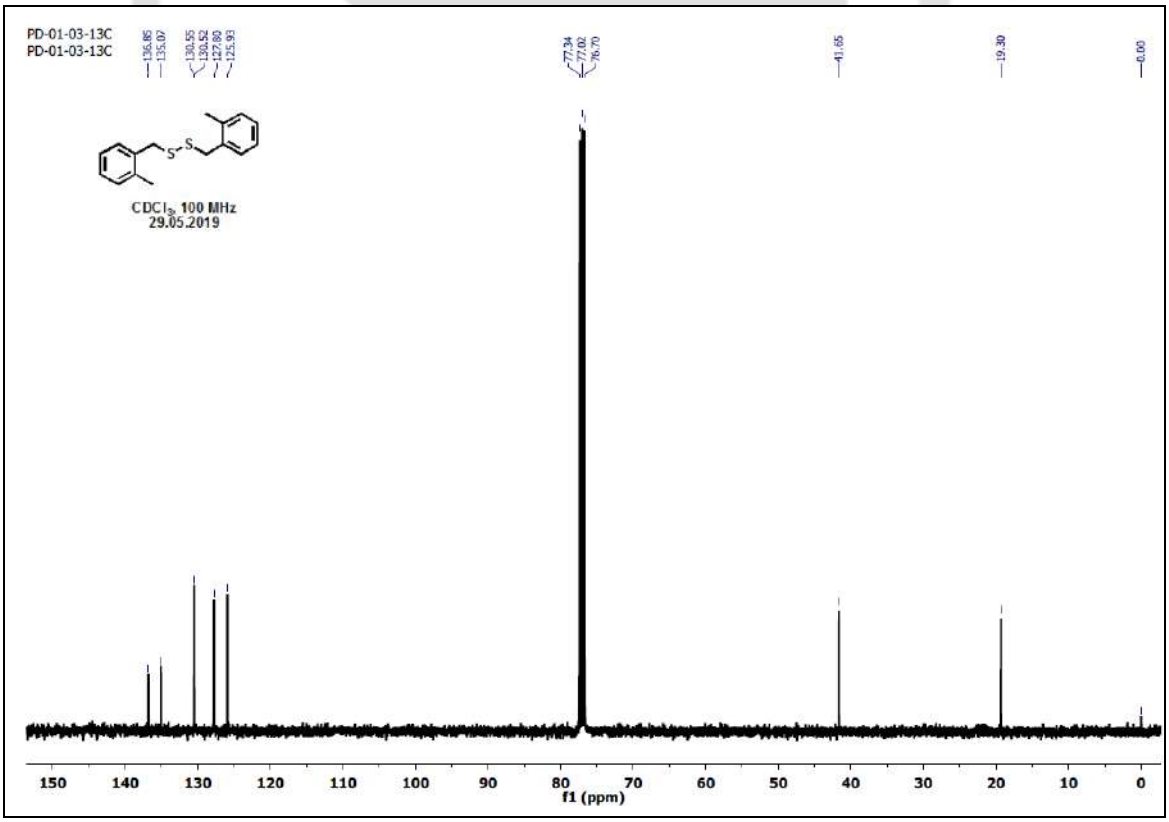

Figure A4.70. ^{13}C NMR ($CDCl_3$, 100 MHz, ppm) spectrum of compound **3.12a**.

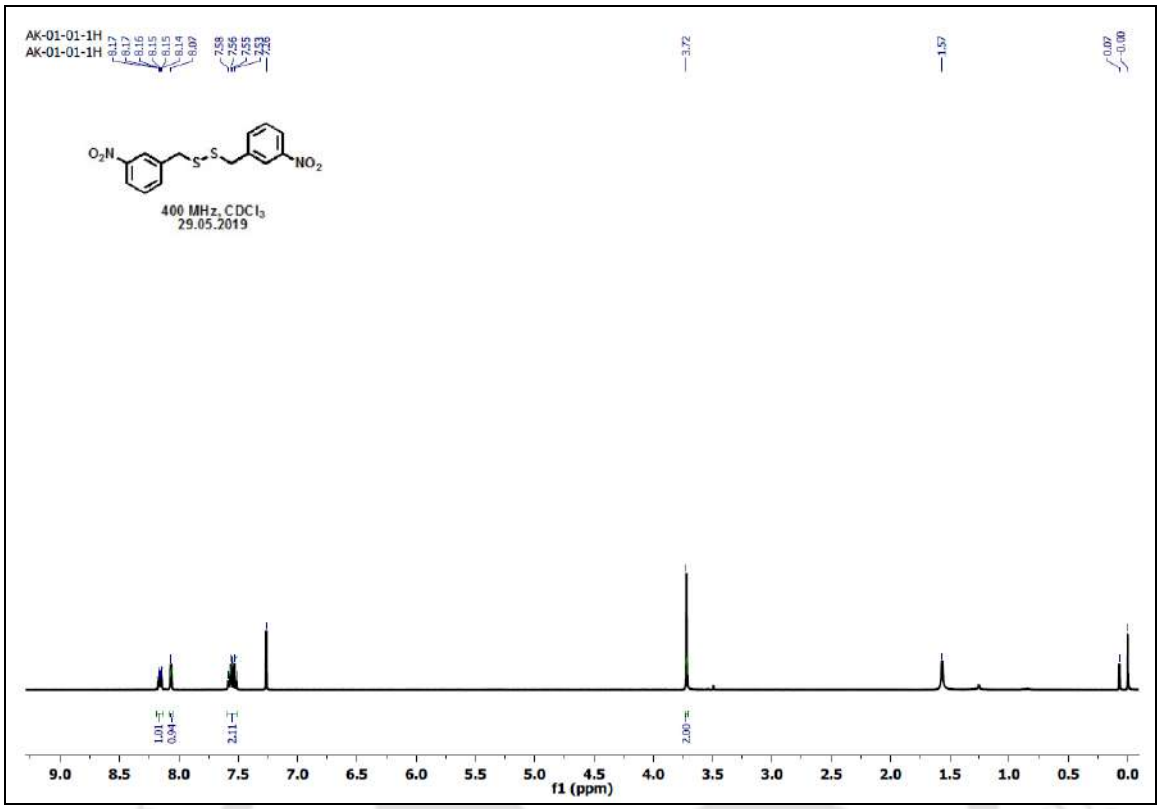

Figure A4.71. ^{1}H NMR ($CDCl_3$, 400 MHz, ppm) spectrum of compound **3.13a**.

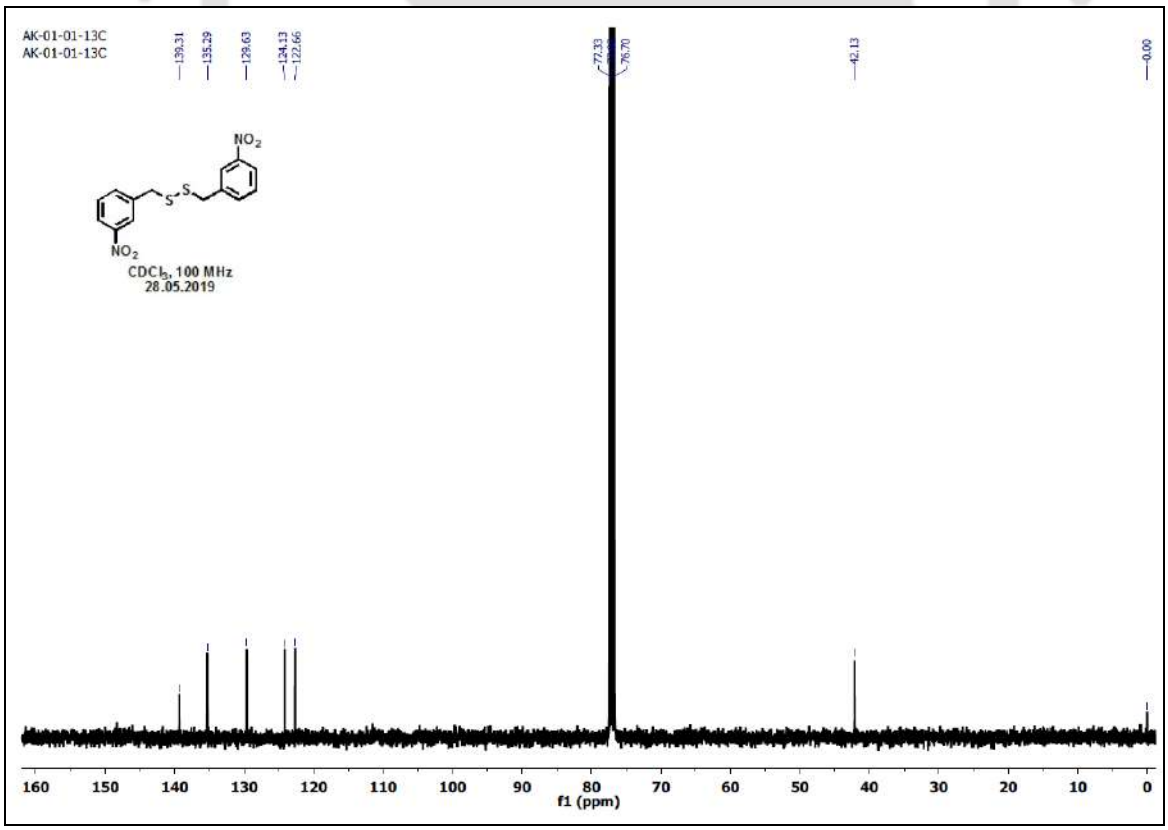

Figure A4.72. ^{13}C NMR ($CDCl_3$, 100 MHz, ppm) spectrum of compound **3.13a**.

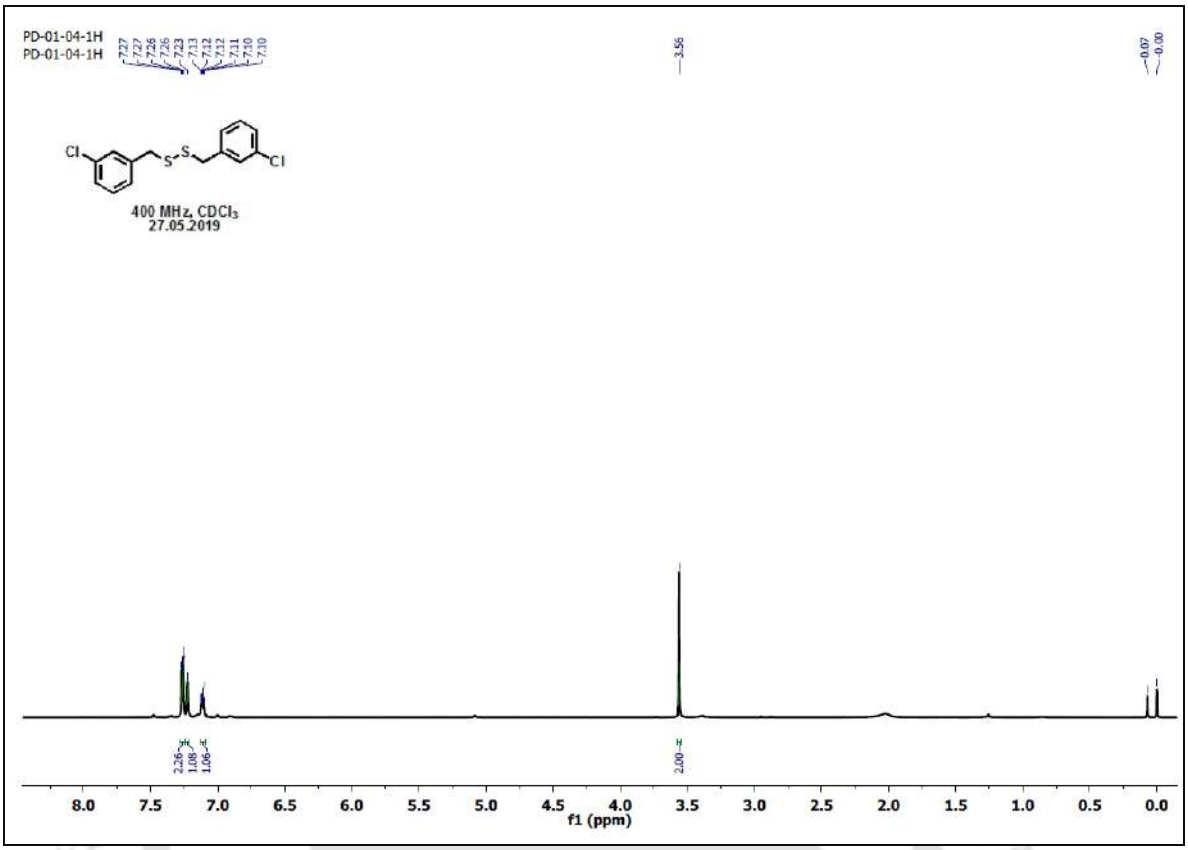

Figure A4.73. ^{1}H NMR ($CDCl_3$, 400 MHz, ppm) spectrum of compound **3.14a**.

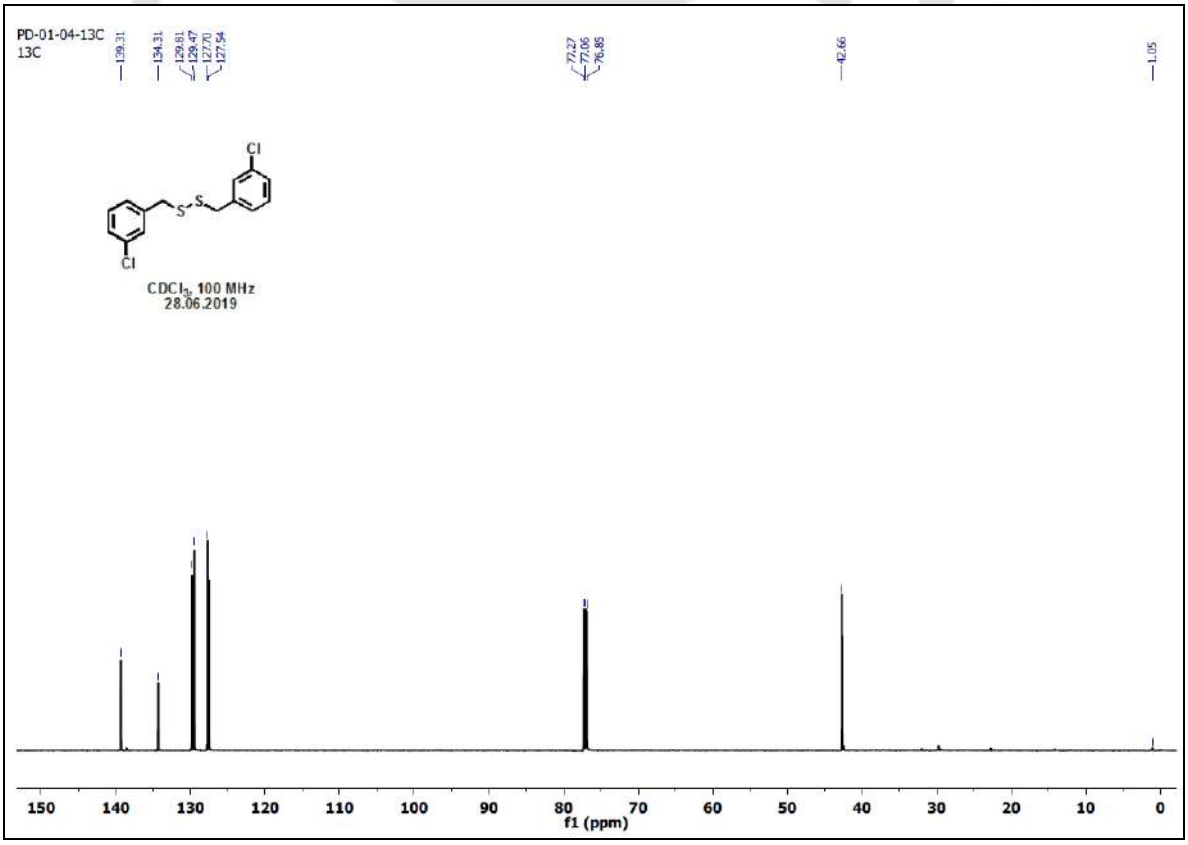

Figure A4.74. ^{13}C NMR ($CDCl_3$, 100 MHz, ppm) spectrum of compound **3.14a**.

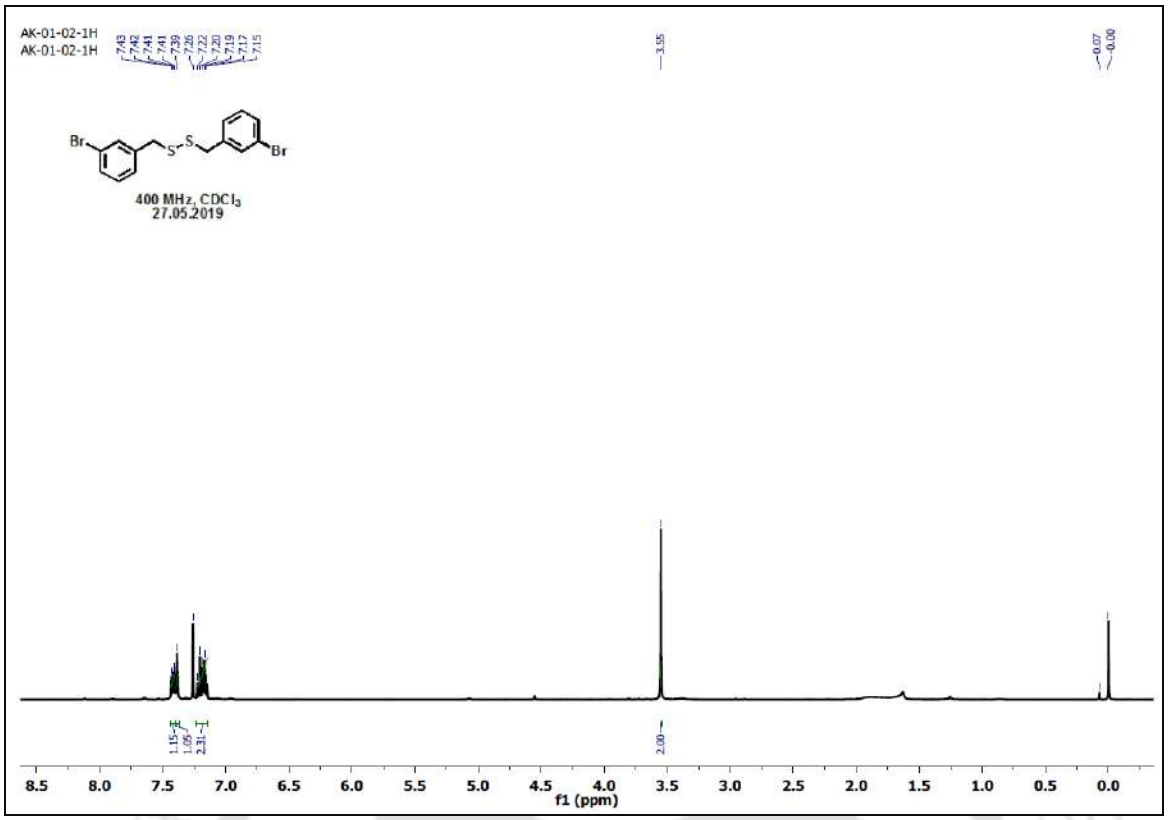

Figure A4.75. ^{1}H NMR ($CDCl_3$, 400 MHz, ppm) spectrum of compound **3.15a**.

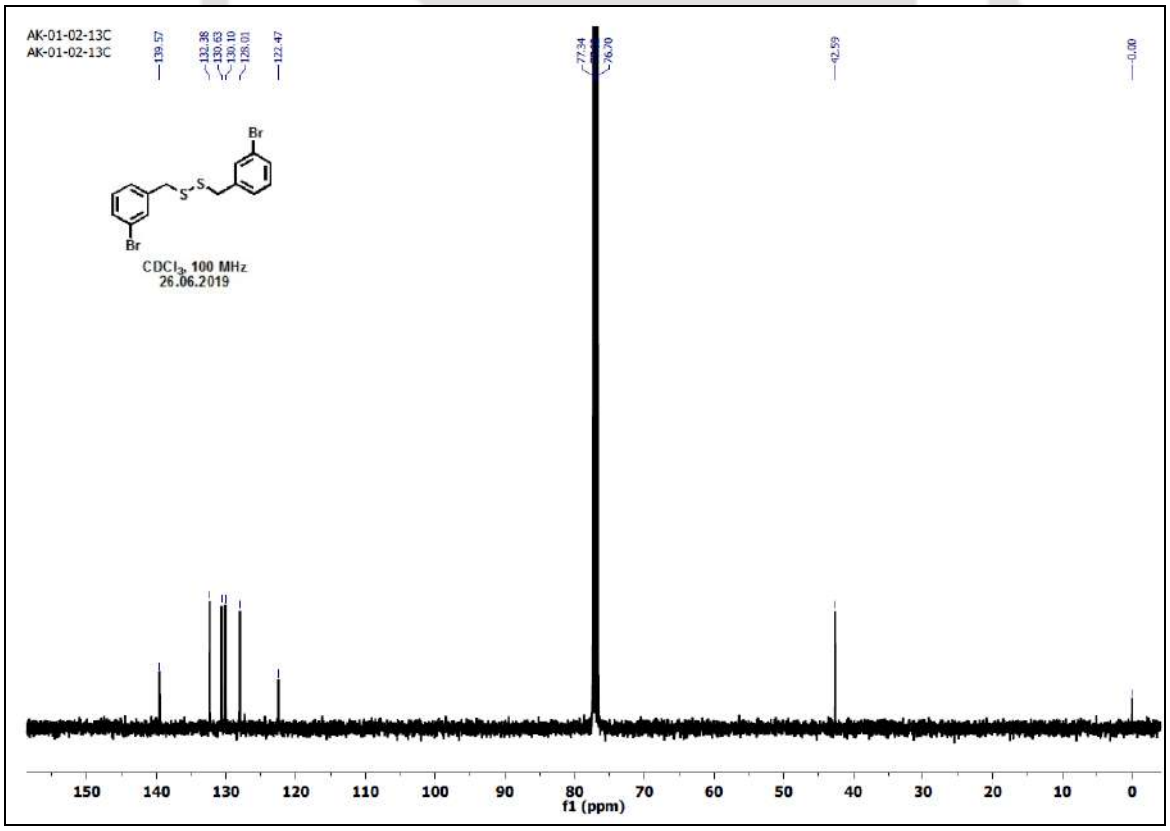

Figure A4.76. ^{13}C NMR ($CDCl_3$, 100 MHz, ppm) spectrum of compound **3.15a**.

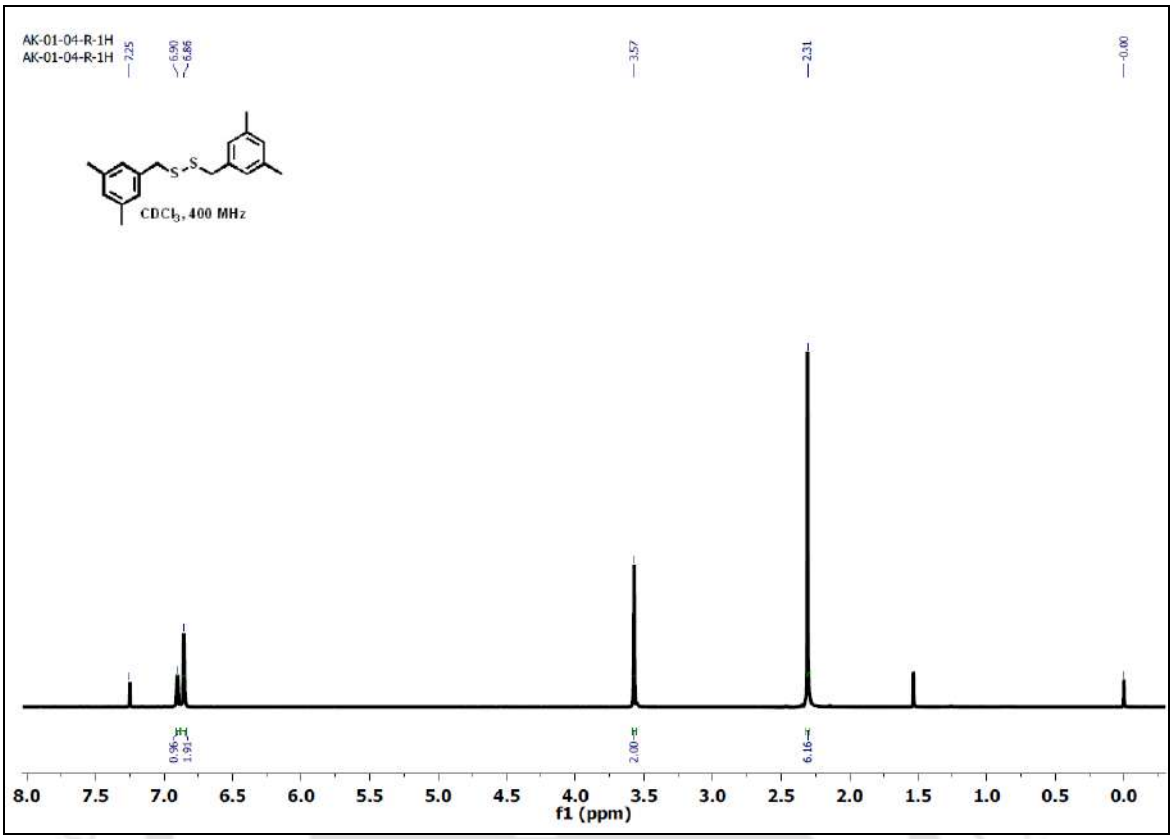

Figure A4.77. ^{1}H NMR ($CDCl_3$, 400 MHz, ppm) spectrum of compound **3.16a**.

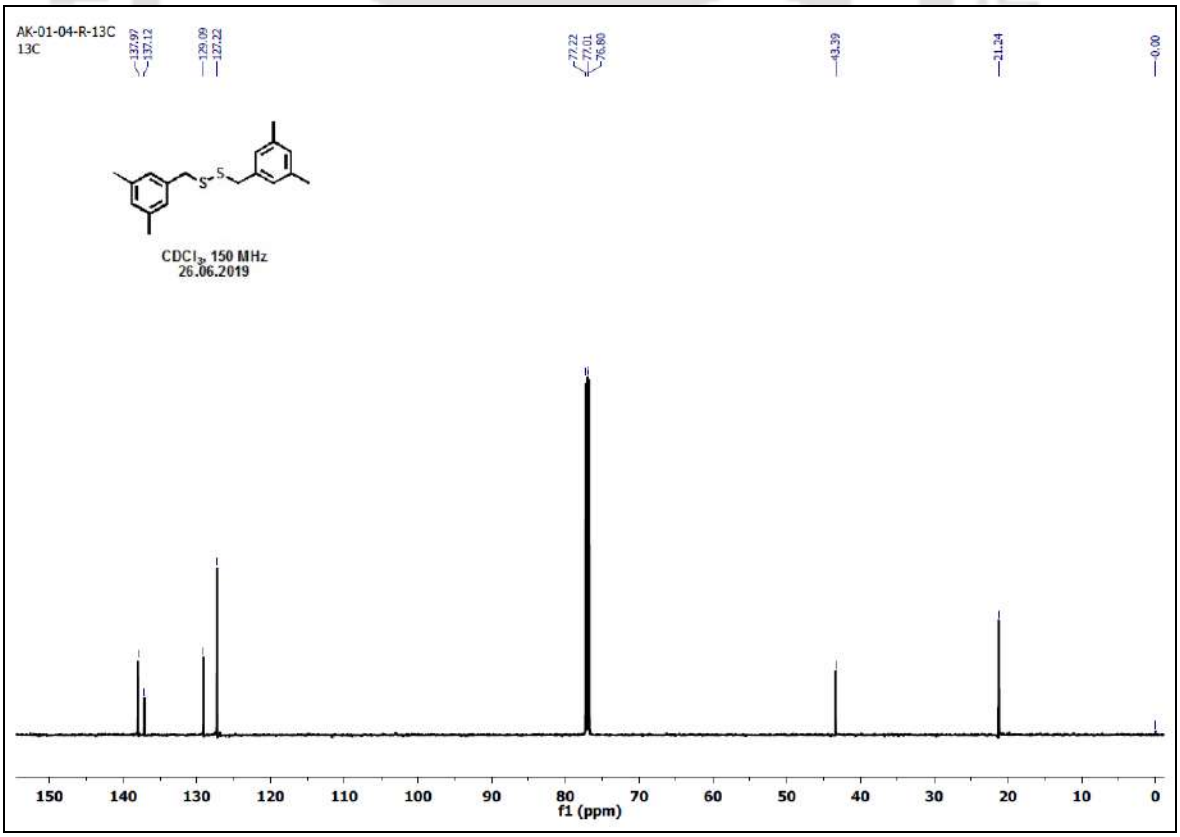

Figure A4.78. ^{13}C NMR ($CDCl_3$, 150 MHz, ppm) spectrum of compound **3.16a**.

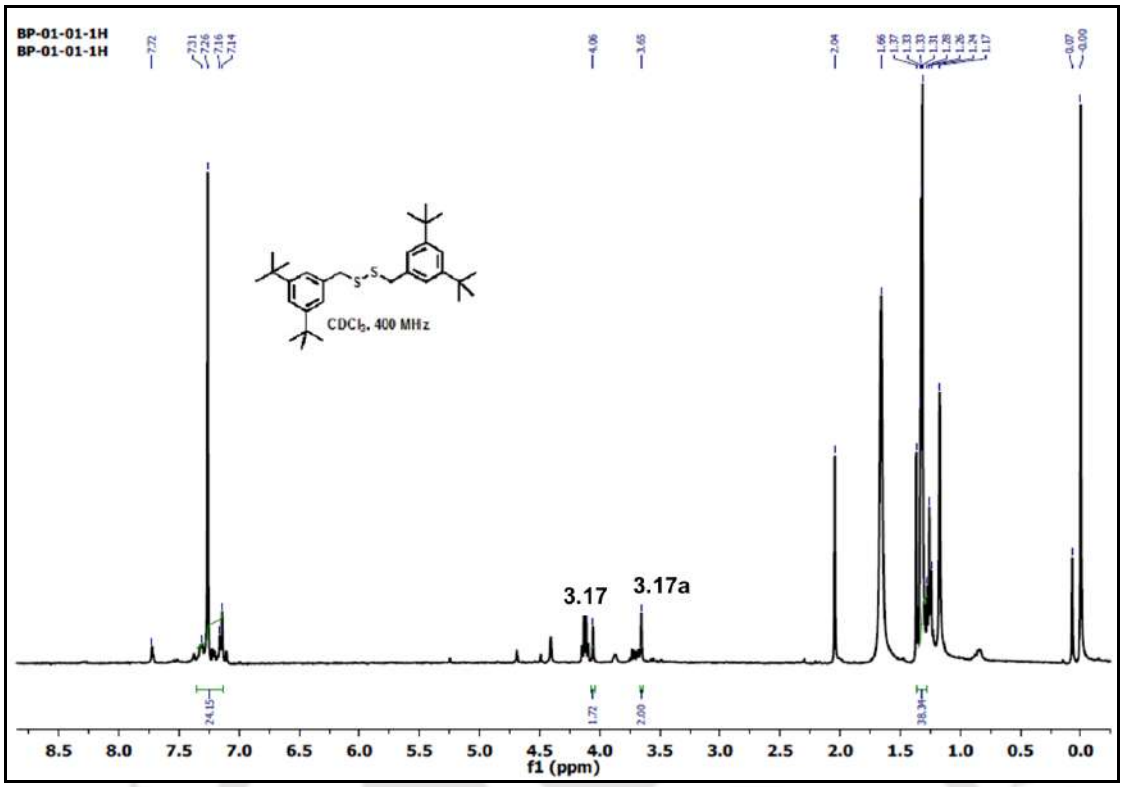

Figure A4.79. ^{1}H NMR ($CDCl_3$, 400 MHz, ppm) spectrum of compound **3.17a**. Here trisulfide **3.17** and the desired disulfide **3.17a** were present along with some higher polysulfides.

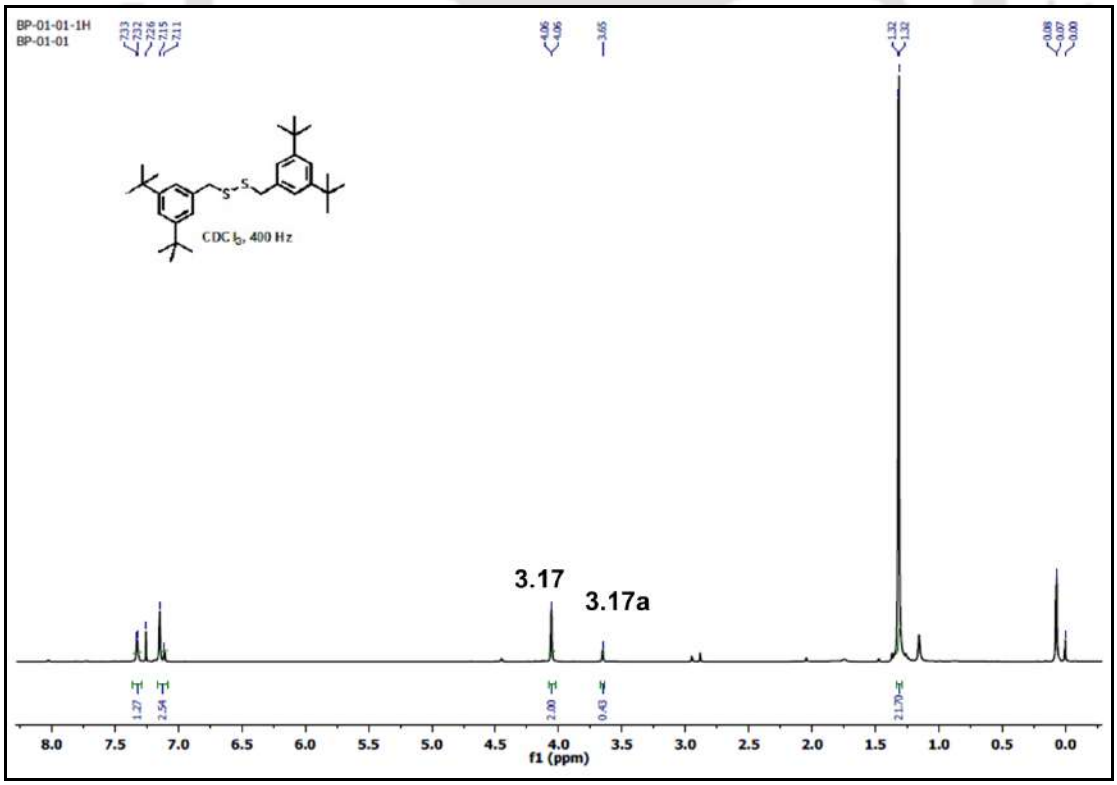

Figure A4.80. ^{1}H NMR ($CDCl_3$, 400 MHz, ppm) spectrum of compound **3.17a** upon the addition of 5.0 equiv of Na_2SO_3 into the reaction. Here the corresponding trisulfide **3.17** became the predominant product after addition of Na_2SO_3.

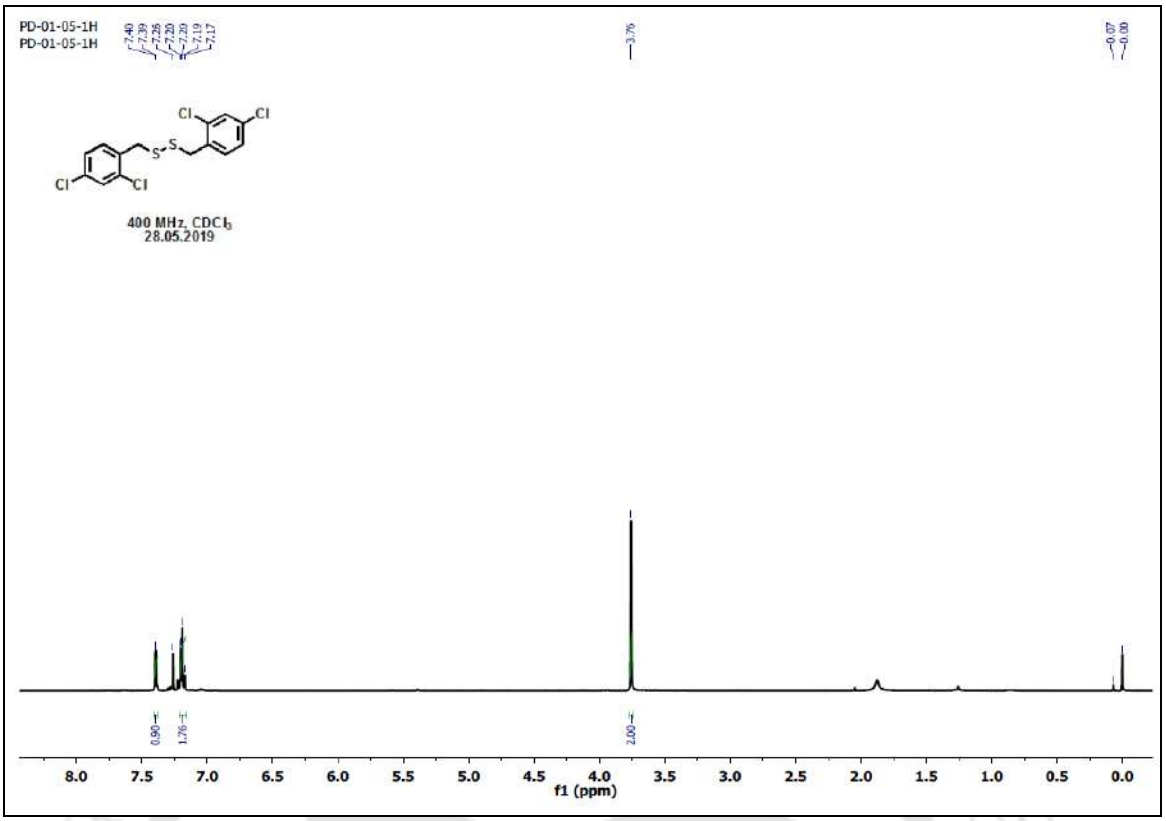

Figure A4.81. ^{1}H NMR ($CDCl_3$, 400 MHz, ppm) spectrum of compound **3.18a**.

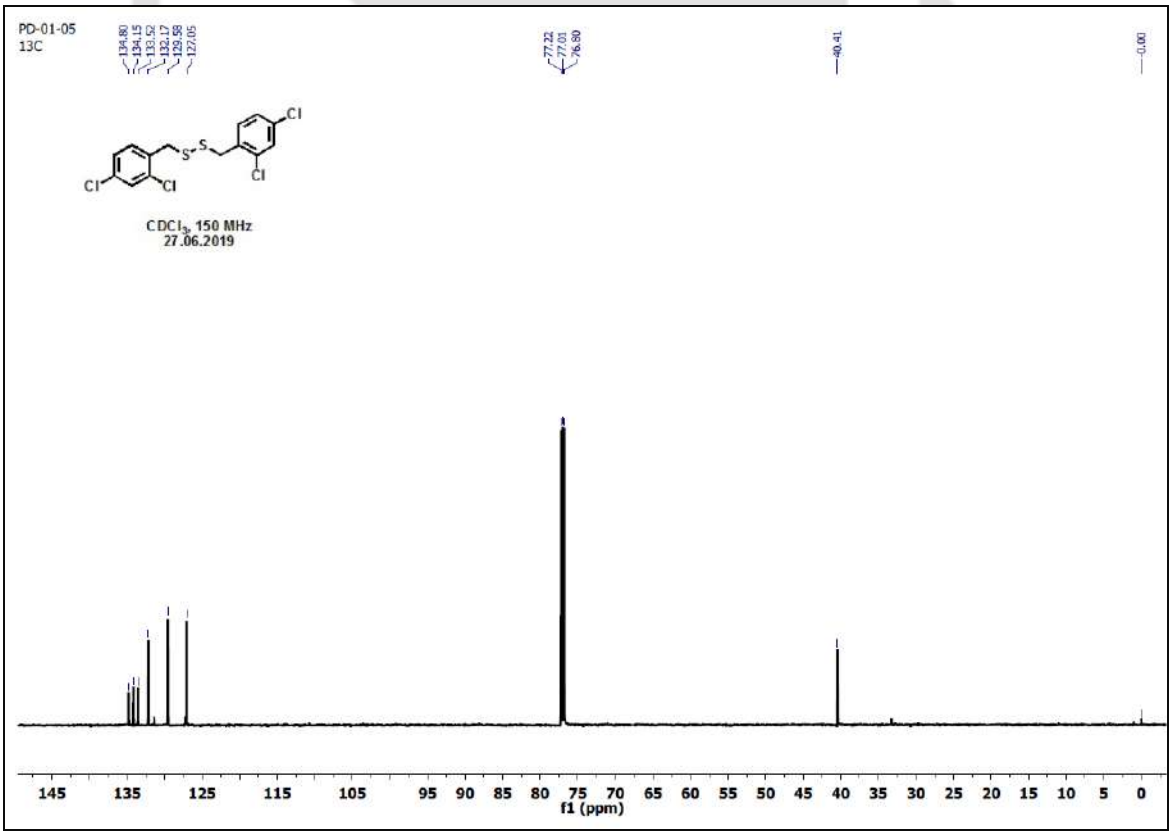

Figure A4.82. ^{13}C NMR ($CDCl_3$, 150 MHz, ppm) spectrum of compound **3.18a**.

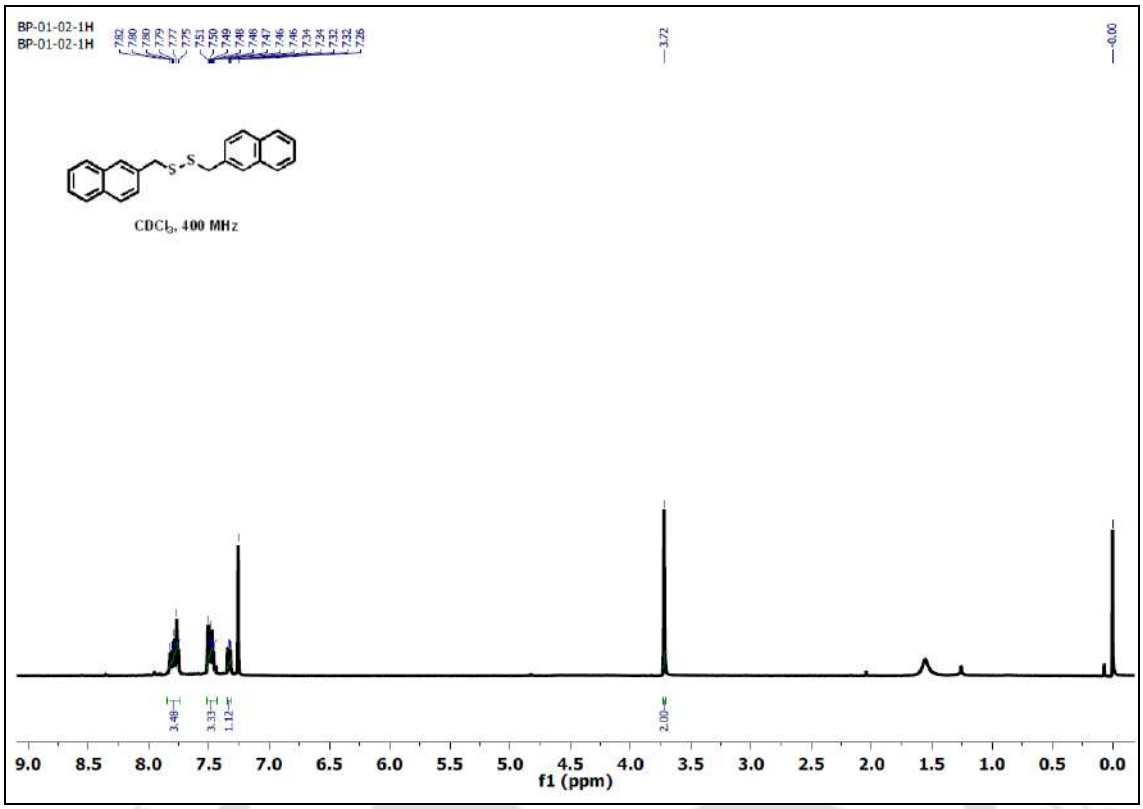

Figure A4.83. ^{1}H NMR ($CDCl_3$, 400 MHz, ppm) spectrum of compound **3.19a** upon the addition of 5.0 equiv of Na_2SO_3 into the reaction.

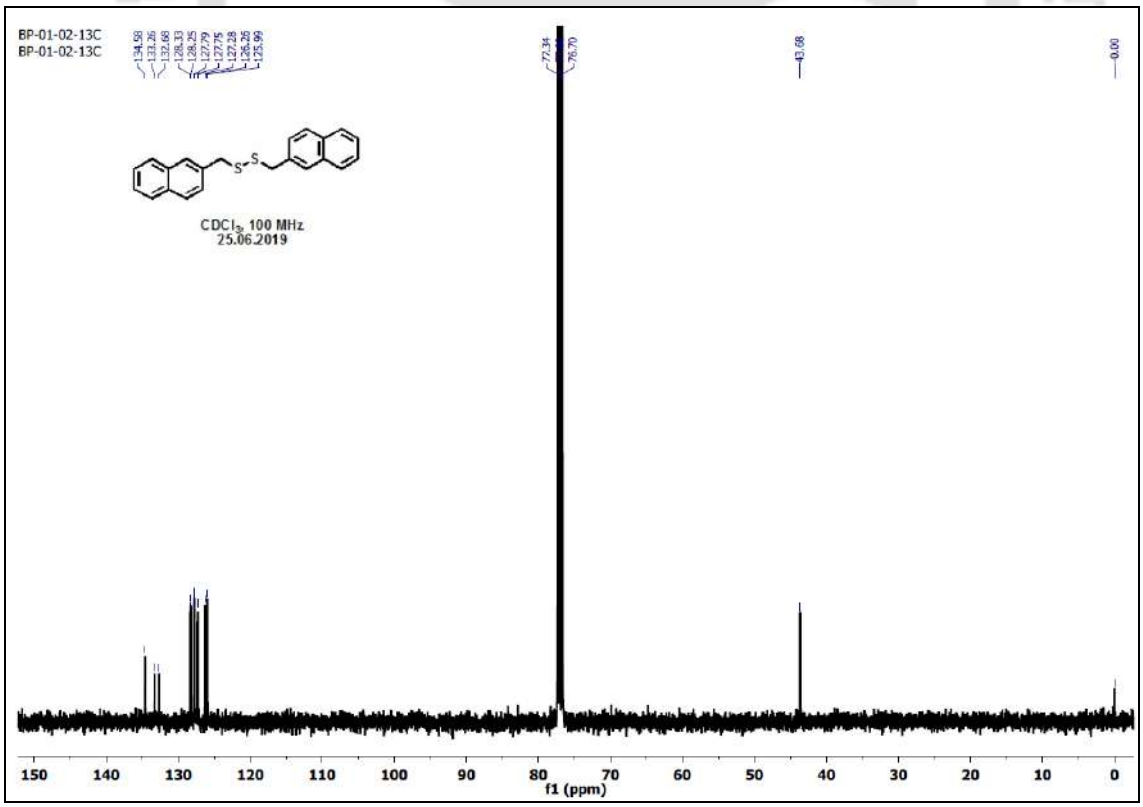

Figure A4.84. ^{13}C NMR ($CDCl_3$, 100 MHz, ppm) spectrum of compound **3.19a** upon the addition of 5.0 equiv of Na_2SO_3 into the reaction.

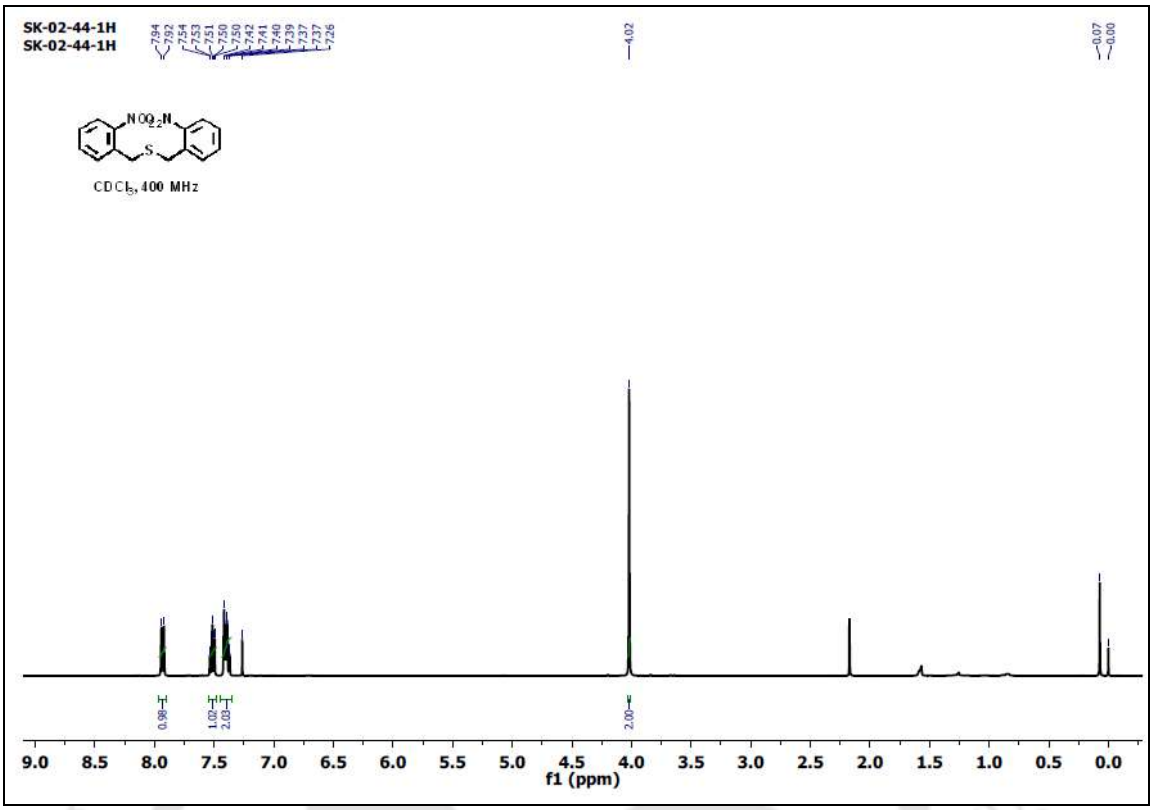

Figure A4.85. ^{1}H NMR ($CDCl_3$, 400 MHz, ppm) spectrum of compound **3.11b**.

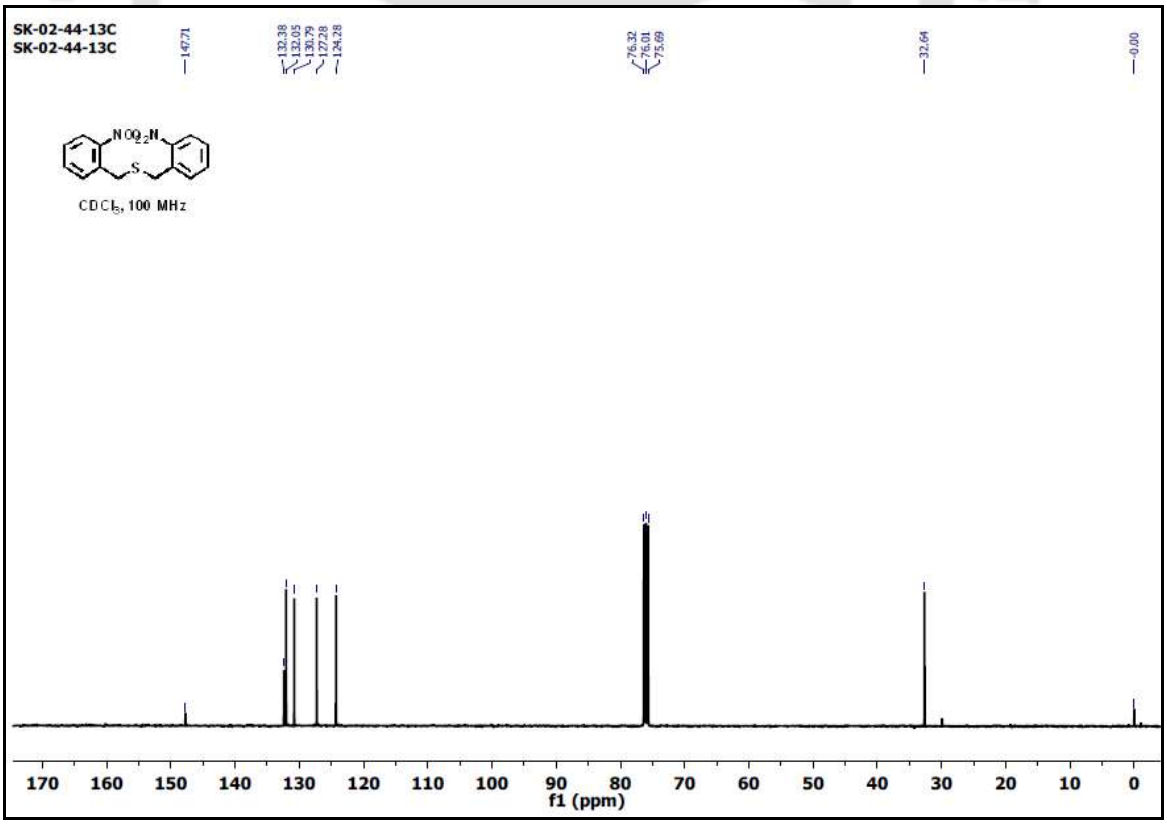

Figure A4.86. ^{13}C NMR ($CDCl_3$, 100 MHz, ppm) spectrum of compound **3.11b**.

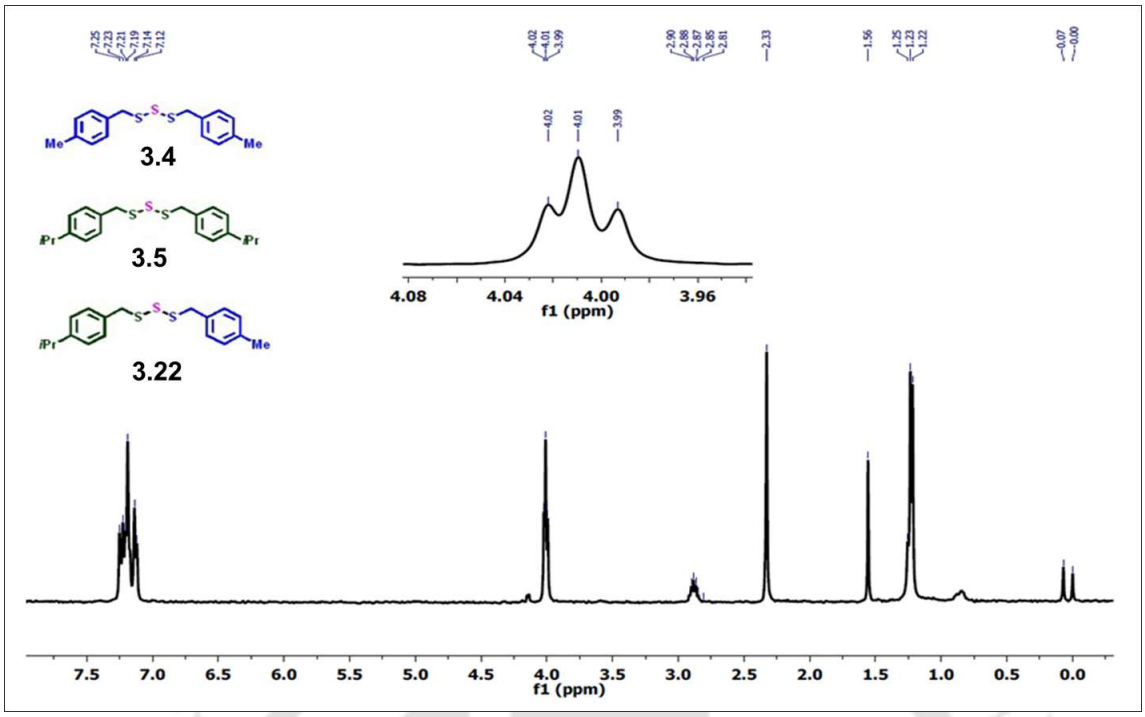

Figure A4.87. ^{1}H NMR ($CDCl_3$, 400 MHz, ppm) spectrum of the crude trisulfide mixture containing the symmetrical trisulfides **3.4** and **3.5** and the unsymmetrical trisulfide **3.22**.

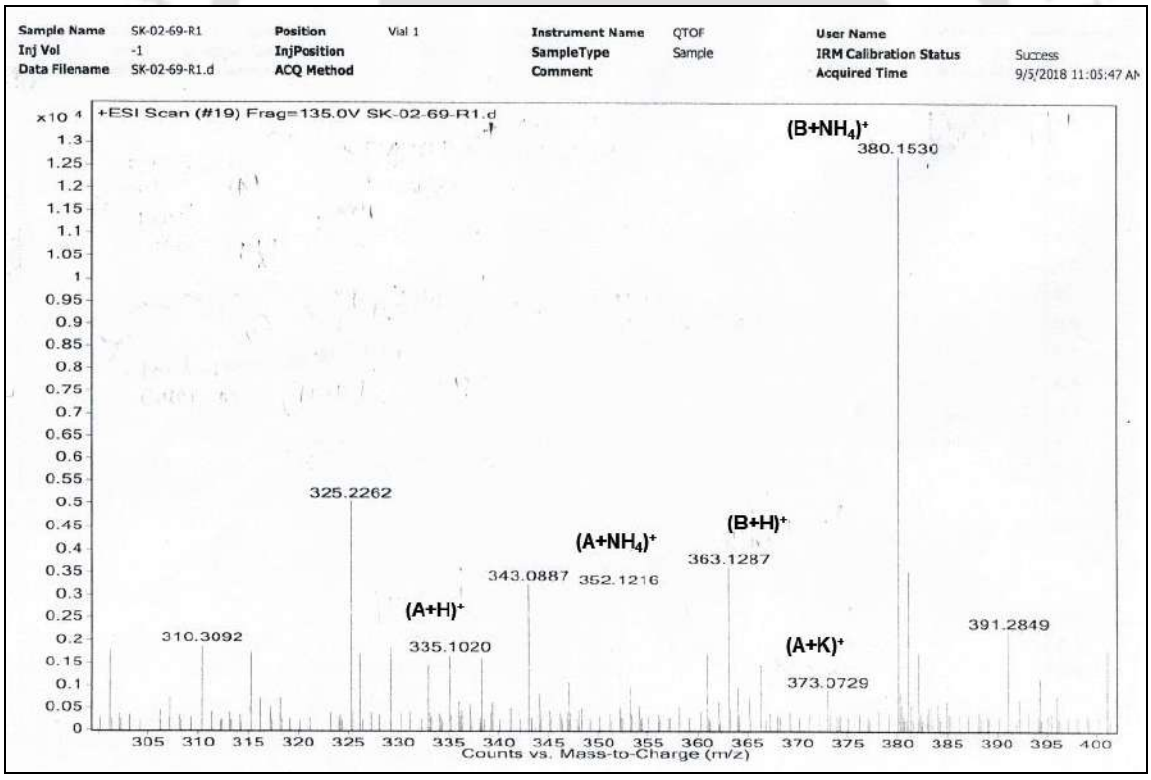

Figure A4.88. ESI-MS (+Ve) spectrum of crude trisulfide mixture with compounds **3.4**, **3.5** (B) and **3.22** (A). The molecular ion peak for **3.4** was not observed during this analysis.

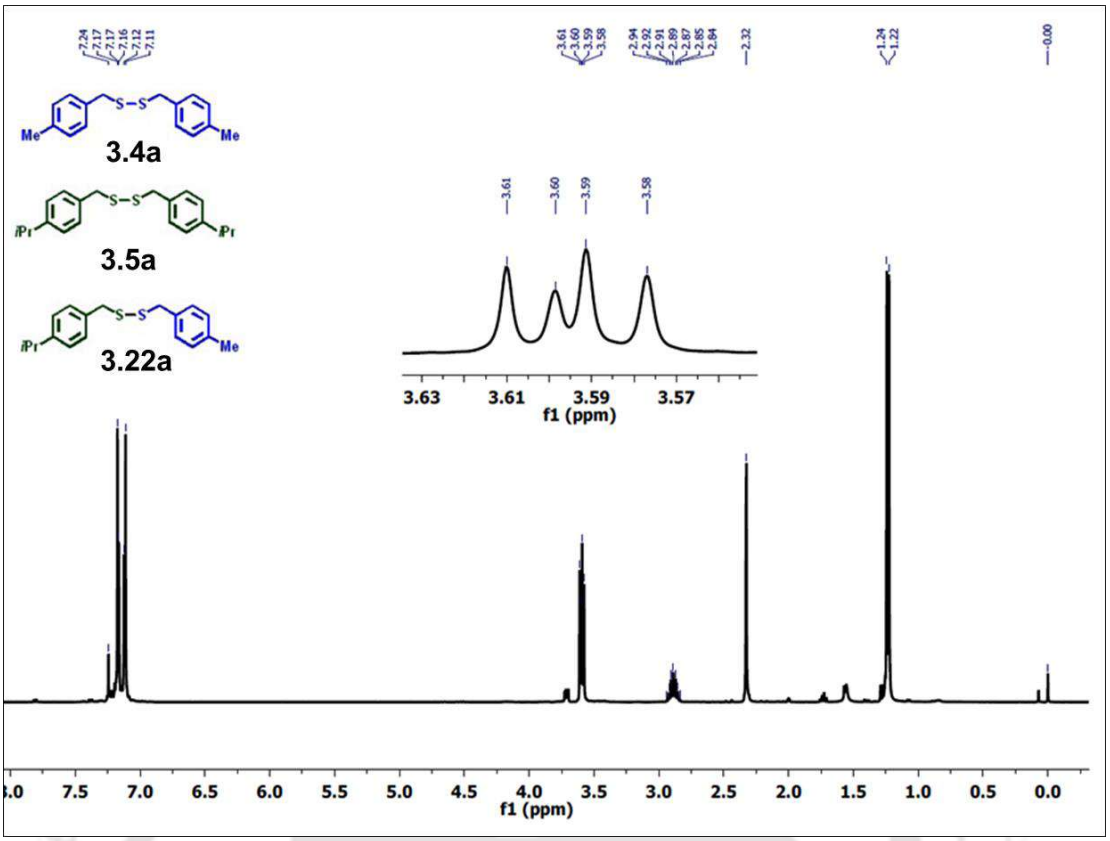

Figure A4.89. ^{1}H NMR ($CDCl_3$, 400 MHz, ppm) spectrum of the crude disulfide mixture containing the symmetrical disulfide **3.4a** and **3.5a** and the unsymmetrical disulfide **3.22a**.

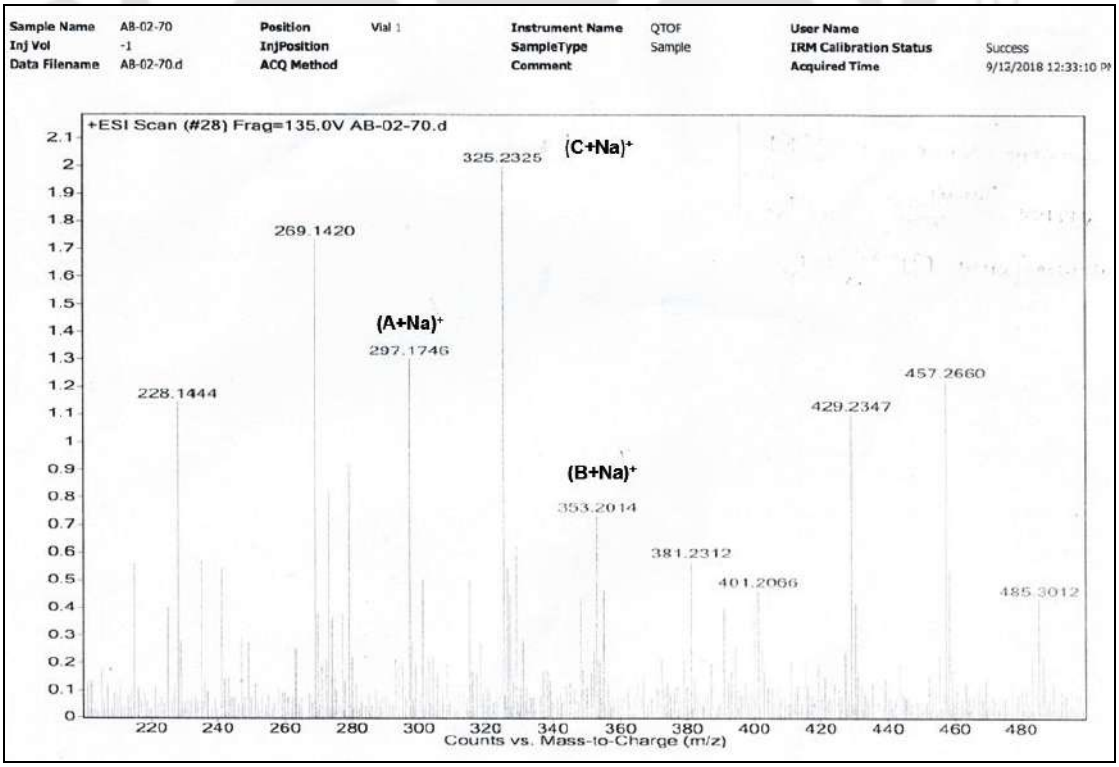

Figure A4.90. ESI-MS (+Ve) spectrum of the crude disulfide mixture [**3.4a** (A), **3.5a** (B) and **3.22a** (C)].

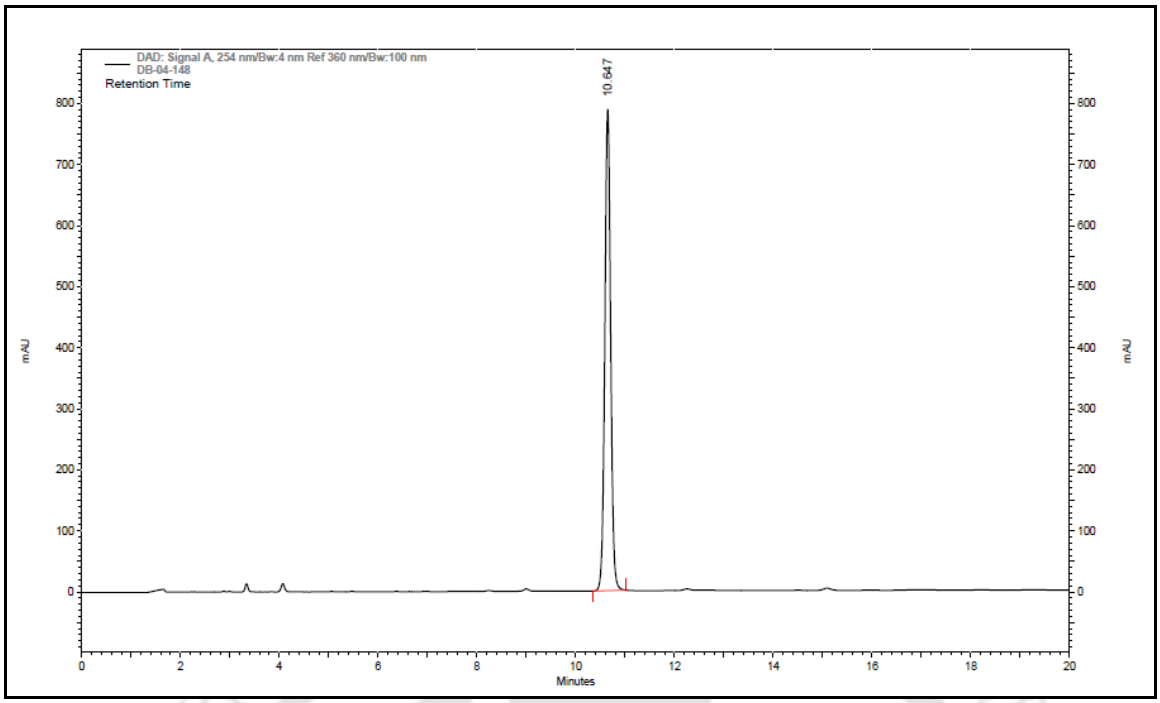

Figure A4.91. HPLC chromatogram of compound **3.4** yielded from bulk-scale reaction.

Effect of Na_2SO_3 towards the formation of disulfides

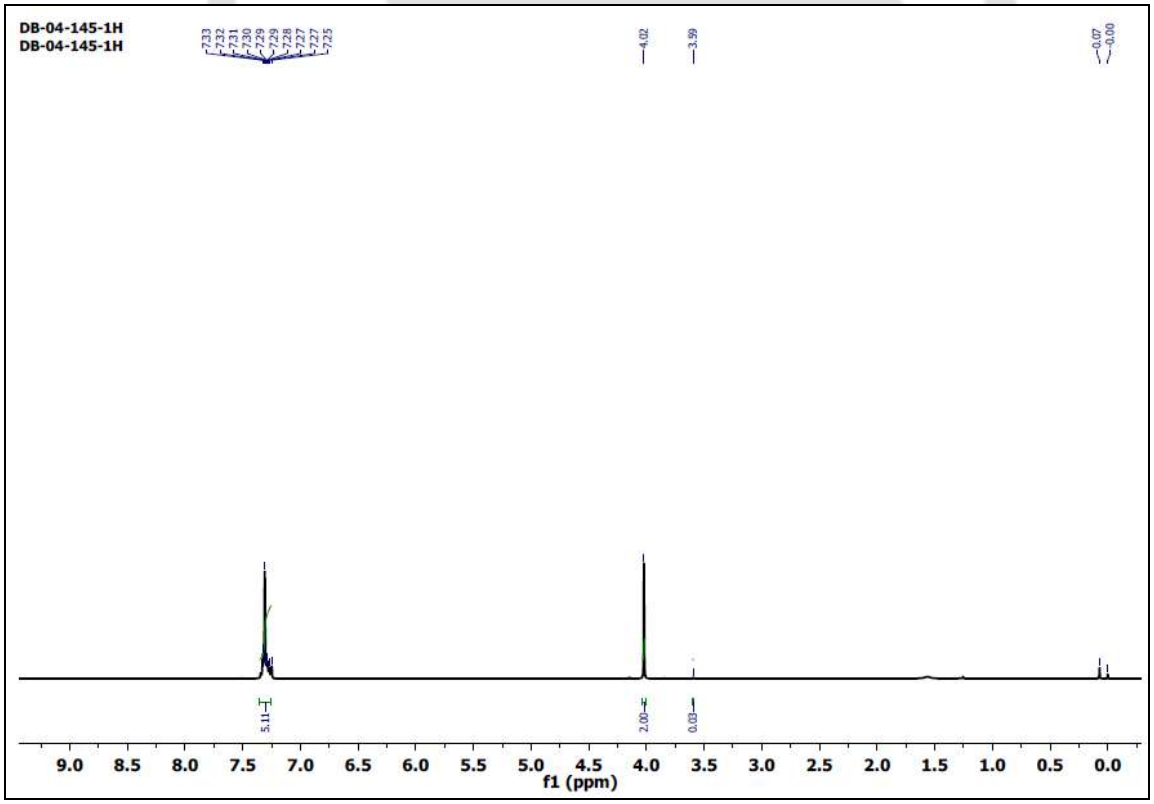

Figure A4.92. ^1H NMR ($CDCl_3$, 400 MHz, ppm) spectrum of crude product mixture from the reaction of column purified Bunte salt (1.0 equiv) of benzyl bromide with Na_2S (0.5 equiv) **without Na_2SO_3** in water at 0 ºC for 8 h. The mixture contained trisulfide DBTS with a very trace amount of disulfide DBDS (99:1).

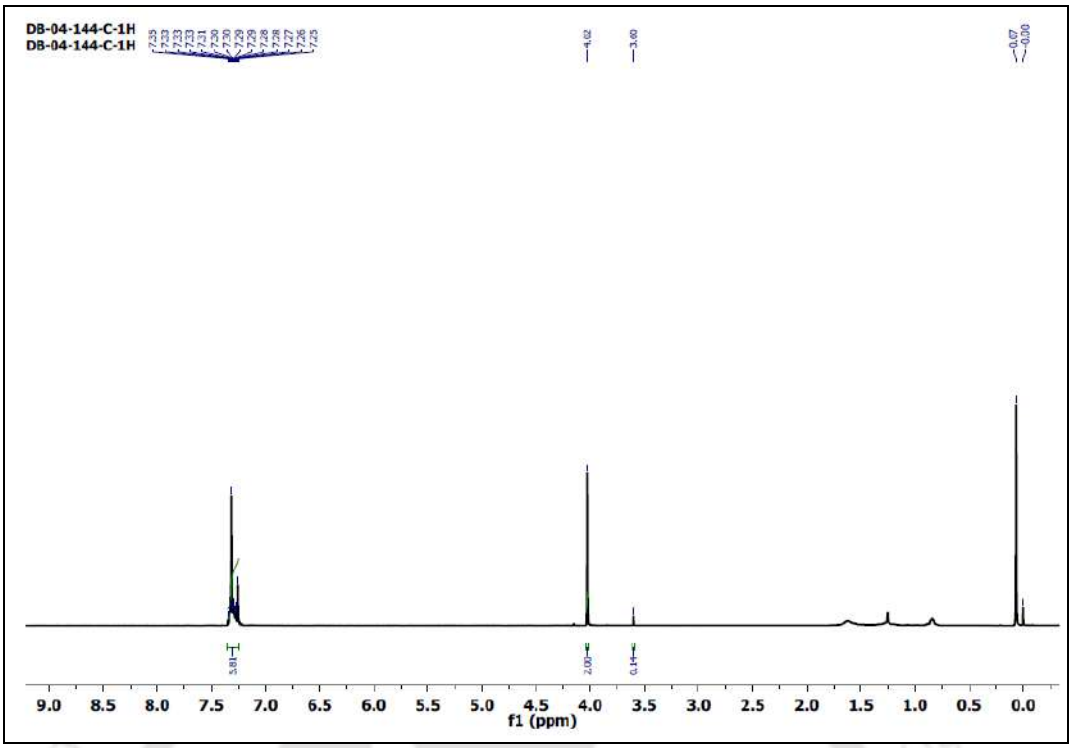

Figure A4.93. ^{1}H NMR ($CDCl_3$, 400 MHz, ppm) spectrum of crude product mixture from the reaction of column purified Bunte salt (1.0 equiv) of benzyl bromide with Na_2S (0.5 equiv) and **Na_2SO_3** (5.0 equiv) in water at 0 ºC for 8 h. The mixture contained trisulfide DBTS with a slightly increased amount of disulfide DBDS (94:6).

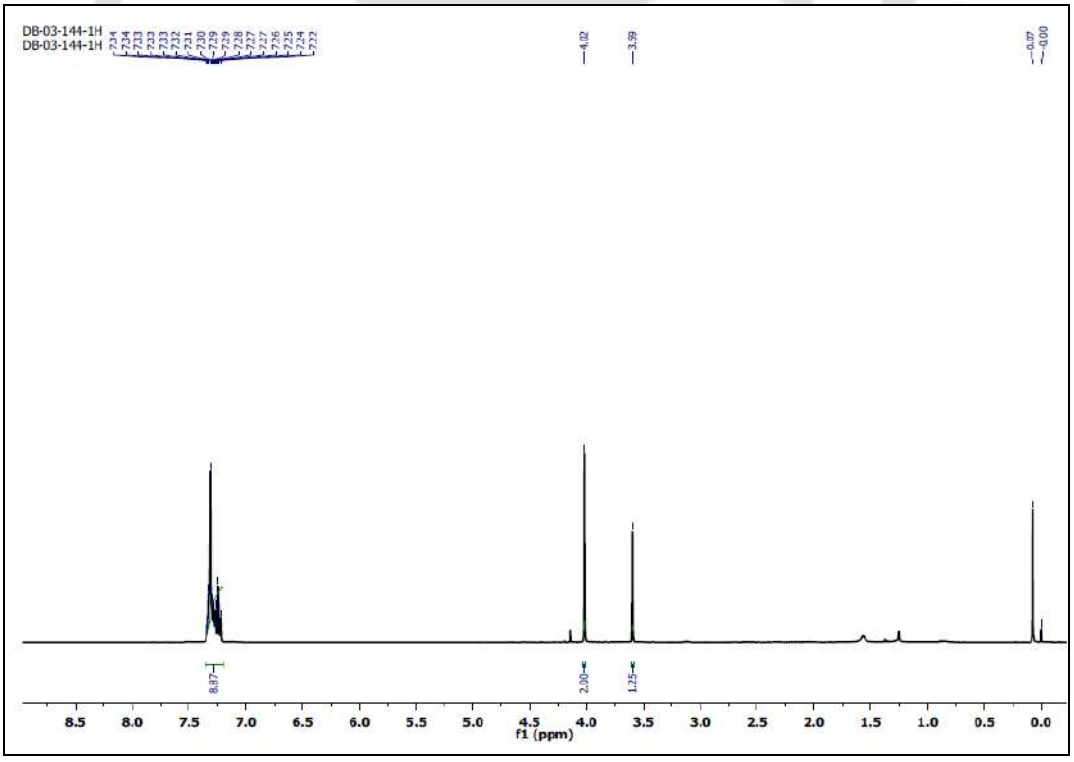

Figure A4.94. ^{1}H NMR ($CDCl_3$, 400 MHz, ppm) spectrum of crude product mixture from the reaction of column purified Bunte salt (1.0 equiv) of benzyl bromide with Na_2S (0.5 equiv) **without Na_2SO_3** in water at 50 ºC for 8 h. The mixture contained trisulfide DBTS with a significant amount of disulfide DBDS (62:38).

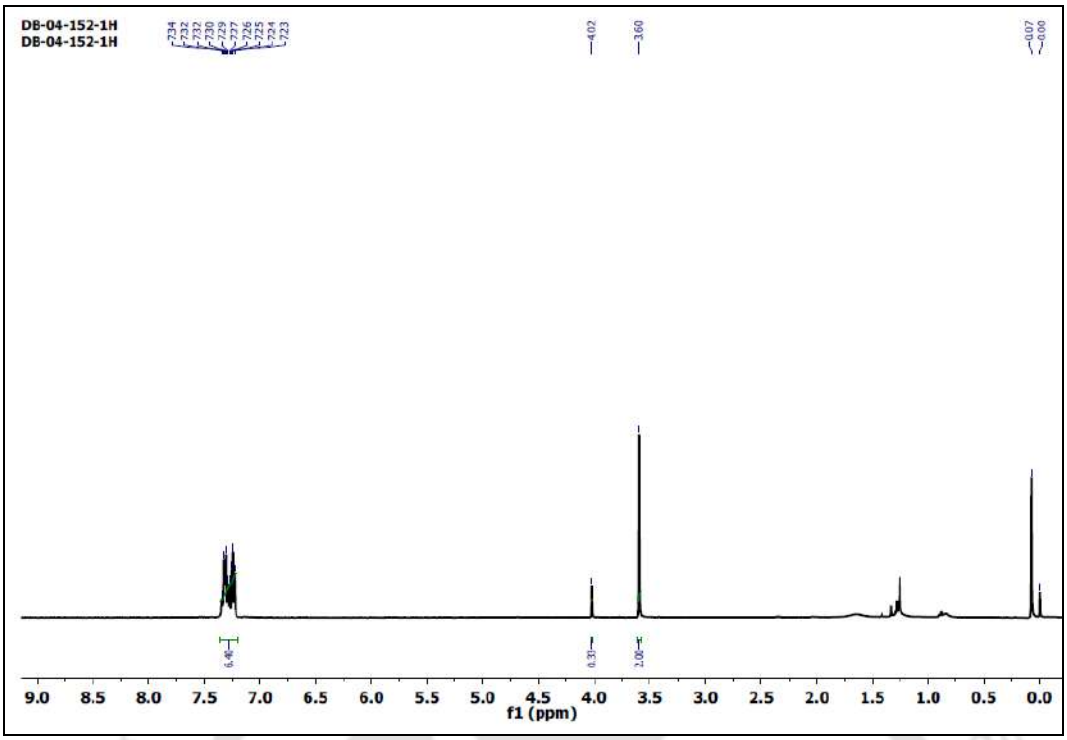

Figure A4.95. ^{1}H NMR ($CDCl_3$, 400 MHz, ppm) spectrum of crude product mixture from the reaction of column purified Bunte salt (1.0 equiv) of benzyl bromide with Na_2S (0.5 equiv) and **Na_2SO_3** (5.0 equiv) in water at 50 ºC for 8 h. The mixture contained minor amount of trisulfide DBTS and major amount of disulfide DBDS (14:86).

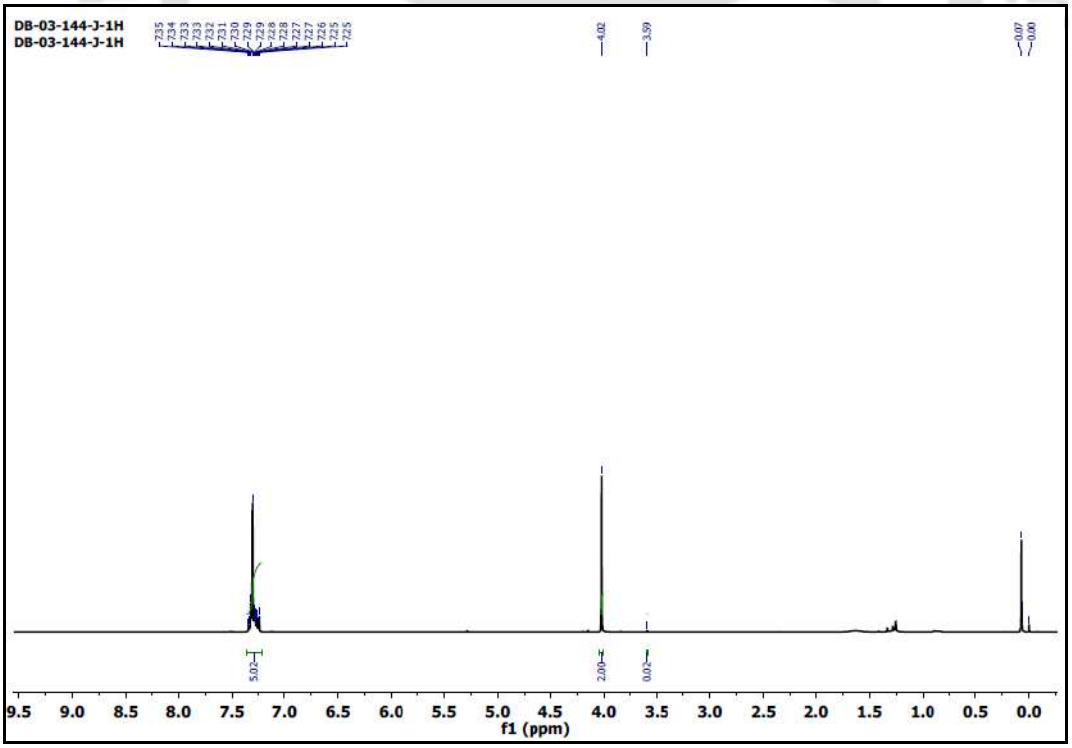

Figure A4.96. ^{1}H NMR ($CDCl_3$, 400 MHz, ppm) spectrum of crude product mixture from the reaction of previously synthesized trisulfide DBTS with **Na_2SO_3** (5.0 equiv) in water at 0 ºC for 8 h. The disulfide (DBDS) content in the crude product mixture was almost unaltered (99:1).

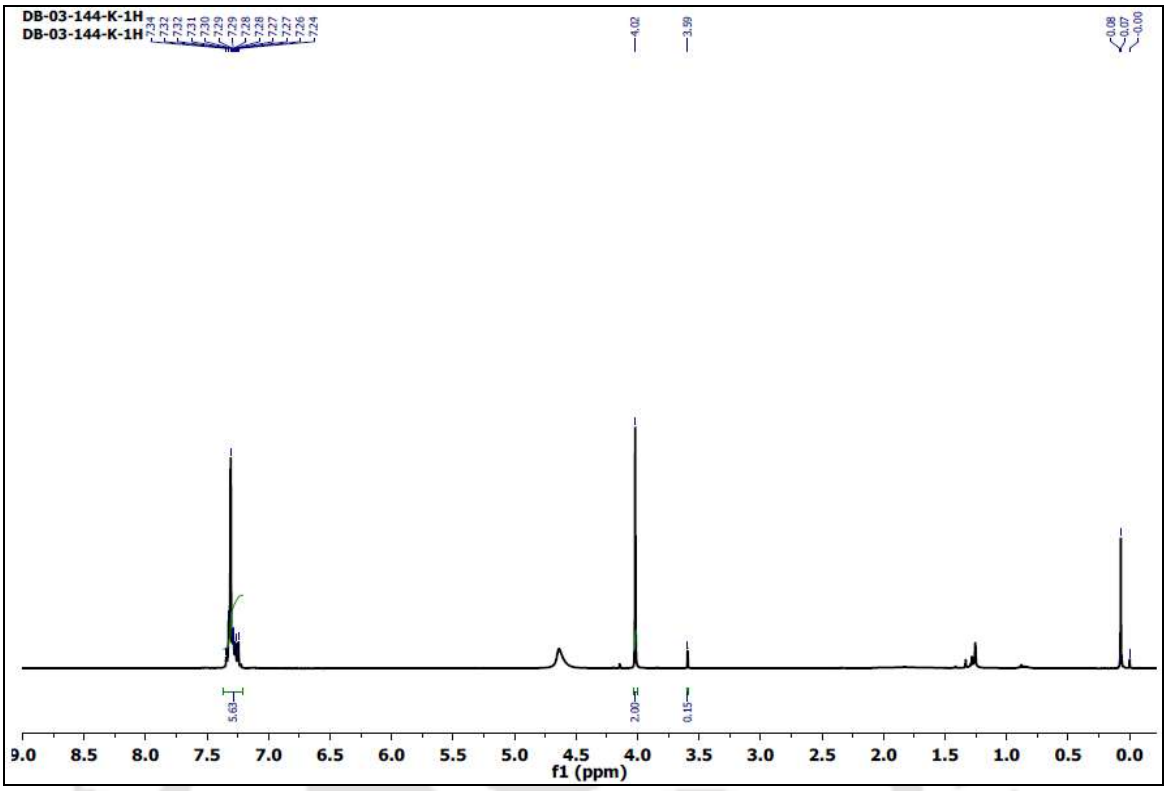

Figure A4.97. ^{1}H NMR ($CDCl_3$, 400 MHz, ppm) spectrum of crude product mixture from the reaction of previously synthesized trisulfide DBTS with **Na_2SO_3** (5.0 equiv) in water at 50 ºC for 8 h. The disulfide content in the crude product mixture was slightly enhanced (93:7).

Table A4.1. Crystal data and structure refinement for **3.11**.

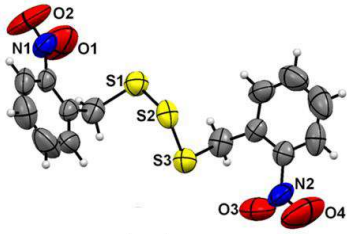	
3.11 (CCDC: 1905588)	
Empirical formula	$C_{14}H_{12}N_2O_4S_3$
Formula Weight	368.5
Crystal habit, color	Rectangular, Colorless
Crystal size	0.170 × 0.110 × 0.070
Temperature, *T* (K)	293(2)
Wavelength, λ (Å)	0.71073
Crystal System	Monoclinic
Space Group	P*21*
Unit cell dimension	a = 4.6759 (12), b = 14.3551 (42), c = 12.2530(35); α =90, β = 90.125(20), γ = 90
Volume, *V*(Å^3)	822.46(2)
Cell Formula units, Z	2
Calculated density, g/cm^3	1.49
Absorption Coefficient, μ (mm^{-1})	0.470
F(000)	380
θ range for data collection	1.662 ° - 26.372 °
Limiting Indices	-5 ≤ h ≤ 5, -17 ≤ k ≤ 15, -15 ≤ l ≤ 14
Reflection Collected / unique	5998/ 2856
Refinement method	SHELXL-2016/4
Data / Restraints / Parameters	2856/1/208
Goodness-of-fit on F^2	0.904
Final R indices [*I*>2sigma(*I*)]	R_1 = 0.047, wR_2 = 0.108
R indices (all data)	R_1= 0.100, wR_2=0.127
Largest diff. peak and hole	0.173 and -0.229

Table A4.2. Crystal data and structure refinement for **3.11a**.

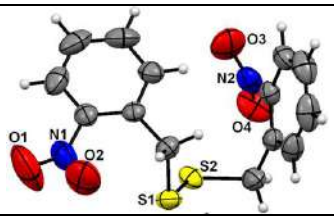	
3.11a (CCDC: 1905589)	
Empirical formula	$C_{14}H_{12}N_2O_4S_2$
Formula Weight	336.4
Crystal habit, color	Rectangular, Colorless
Crystal size	0.140 × 0.100 × 0.080
Temperature, *T* (K)	293(2)
Wavelength, λ (Å)	0.71073
Crystal System	Monoclinic
Space Group	P*21/n*
Unit cell dimension	a = 13.6592 (5), b = 7.8745 (3), c = 14.1331(5); α =90, β = 99.026(2), γ = 90
Volume, *V*(Å^3)	1501.32(5)
Cell Formula units, Z	4
Calculated density, g/cm^3	1.49
Absorption Coefficient, μ (mm^{-1})	0.373
F(000)	696
θ range for data collection	1.9 ° - 28.4 °
Limiting Indices	-17 ≤ h ≤ 18, -10 ≤ k ≤ 10, -18 ≤ l ≤ 18
Reflection Collected / unique	18795/3722
Refinement method	SHELXL-2016/4
Data / Restraints / Parameters	3722/0/199
Goodness-of-fit on F^2	1.089
Final R indices [*I*>2sigma(*I*)]	R_1 = 0.042, wR_2 = 0.109
R indices (all data)	R_1= 0.058, wR_2=0.117
Largest diff. peak and hole	0.426 and -0.328

Table A4.3. Crystal data and structure refinement for **3.11b**.

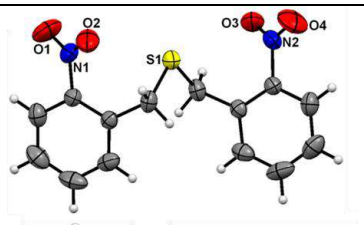	
3.11b (CCDC: 1905587)	
Empirical formula	$C_{14}H_{12}N_2O_4S$
Formula Weight	304.3
Crystal habit, color	Rectangular, Colorless
Crystal size	0.110 × 0.090 × 0.060
Temperature, *T* (K)	293(2)
Wavelength, λ (Å)	0.71073
Crystal System	Monoclinic
Space Group	C*2/c*
Unit cell dimension	a = 7.5711 (4), b = 14.0965 (8), c = 13.1401(7); α =90, β = 90.629(5); γ = 90
Volume, *V*(Å^3)	1402.31(2)
Cell Formula units, Z	4
Calculated density, g/cm^3	1.44
Absorption Coefficient, μ (mm^{-1})	0.248
F(000)	632
θ range for data collection	2.9 ° - 28.8 °
Limiting Indices	$-7 \leq h \leq 10$, $-18 \leq k \leq 8$, $-16 \leq l \leq 17$
Reflection Collected / unique	2814/1577
Refinement method	SHELXL-2016/4
Data / Restraints / Parameters	1577/0/96
Goodness-of-fit on F^2	1.072
Final R indices [*I*>2sigma(*I*)]	R_1 = 0.041, wR_2 = 0.102
R indices (all data)	R_1= 0.051, wR_2=0.109
Largest diff. peak and hole	0.279 and -0.203

Table A4.4. Energy values at various level of DFT and effect of zero point and free energy correction on the energy profiles of reactions

Structure	ΔE(1)	ΔZ	ΔG	ΔE(2)	ΔE(3)	ΔE(4)
Bn-R1	0	0	0	0	0	0
Bn-TS1	14.01	13.66	15.09	14.92	13.13	12.30
Int-1	-17.85	-17.10	-14.09	-16.65	-17.46	-22.81
Bn-TS2	-8.96	-9.13	-5.31	-7.74	-6.27	-16.08
Int-2	-37.97	-38.93	-15.37	-36.83	-34.77	-48.74
Bn-TS3	-32.51	-33.53	-7.49	-31.36	-30.78	-44.88
Int-3	-43.43	-44.61	-19.38	-42.25	-44.54	-57.12
Bn-TS4	-26.95	-28.82	-3.39	-25.58	-26.16	-38.69
Int-4	-33.91	-34.61	-10.59	-32.83	-30.94	-44.50
Bn-TS5	-33.17	-34.47	-10.19	-32.02	-30.36	-43.19
Bn-P5	-48.05	-48.06	-22.10	-46.86	-44.86	-58.38
Int-2a	-31.58	-32.79	-30.94	-30.10	-36.28	-41.39
Bn-TS6	-23.66	-24.35	-20.98	-22.28	-24.80	-31.89
Int-6	-40.73	-40.59	-38.12	-39.43	-36.94	-47.62
Bn-TS7	-31.80	-32.48	-28.63	-30.71	-28.13	-41.45
Bn-P7	-50.89	-50.99	-47.06	-49.80	-48.15	-60.75

ΔE(1):Total Energy at M06/6-31+G(d) level of DFT, **ΔZ**: Sum of electronic and zero-point Energies at M06/6-31+G(d) level of DFT, **ΔG**: Sum of electronic and Free Energies at M06/6-31+G(d) level of DFT, **ΔE(2)**: Total Energy at M06/6-31++G(d,p)//M06/6-31+G(d) level of DFT, **ΔE(3)**: Total Energy at B3LYP/6-31++G(d,p)//M06/6-31+G(d) level of DFT, **ΔE(4)**: Total Energy at M06/AUG-cc-pVDZ//M06/6-31+G(d) level of DFT, Effect of water solvent was included in all calculations. See computational methodology for details. **ΔE(1):** values were used for making energy profile diagrams.

Table A4.5. Optimized XYX coordinates of Bn-R1 and Bn-TS

Bn-R1				Bn-TS1			
C	-0.72469	2.926357	-0.76419	C	-3.52462	1.965627	-0.46424
C	-0.42354	1.58803	-0.5246	C	-2.41815	1.162645	-0.71057
C	-1.27668	0.805354	0.259012	C	-1.84269	0.417073	0.325697
C	-2.44473	1.371226	0.777821	C	-2.39276	0.485199	1.611443
C	-2.74229	2.71048	0.544633	C	-3.49395	1.29497	1.859251
C	-1.88188	3.490312	-0.22831	C	-4.06223	2.036583	0.822091
H	-0.04993	3.534261	-1.36544	H	-3.96986	2.541387	-1.27373
H	0.482197	1.131536	-0.92821	H	-1.99362	1.101767	-1.7139
H	-3.11366	0.757531	1.383369	H	-1.93811	-0.09224	2.417404
H	-3.64676	3.147483	0.965113	H	-3.9133	1.350634	2.86228
H	-2.11194	4.539307	-0.40936	H	-4.92626	2.669523	1.017048
O	3.523608	1.050084	-0.8603	O	2.54223	0.585074	-1.60052
S	3.119586	-0.30526	-0.36333	S	2.641162	0.363697	-0.12584
S	2.814429	-0.24426	1.646444	S	1.055061	1.383067	0.732163
O	4.235953	-1.27944	-0.67872	O	3.910553	0.907205	0.440036

O	1.87506	-0.78828	-1.04904	O	2.51219	-1.08552	0.217719
C	-0.92985	-0.60674	0.558139	C	-0.66589	-0.39571	0.077973
H	0.14151	-0.81238	0.479082	H	-0.19977	-0.41247	-0.89933
H	-1.32192	-0.94416	1.521072	H	-0.18974	-0.95154	0.872975
Br	-1.77263	-1.82338	-0.76239	Br	-1.81051	-2.54076	-0.5346
Na	5.780568	0.385449	-1.48753	Na	4.5002	-1.33449	1.523615
Na	2.766418	-2.85119	-1.83162	Na	0.958073	2.218033	-2.23823

Table A4.6. Optimized XYX coordinates of Int-1 and Bn-TS2

Int-1				**Bn-TS2**			
C	-4.42229	0.950849	-0.56632	C	2.465671	-3.17381	-0.25613
C	-3.13286	0.731238	-1.04915	C	1.404179	-2.4497	-0.79882
C	-2.05233	0.630664	-0.16973	C	1.324317	-1.06357	-0.6354
C	-2.28291	0.763526	1.204461	C	2.343938	-0.40987	0.069295
C	-3.5687	0.980508	1.689289	C	3.402785	-1.13177	0.61449
C	-4.64271	1.074788	0.803276	C	3.466433	-2.51701	0.45592
H	-5.25558	1.023817	-1.26359	H	2.509032	-4.25379	-0.39063
H	-2.95992	0.631832	-2.12152	H	0.62092	-2.96758	-1.35289
H	-1.44123	0.693612	1.896456	H	2.292698	0.674147	0.189203
H	-3.73558	1.074955	2.76125	H	4.186397	-0.6091	1.161914
H	-5.64949	1.243245	1.182193	H	4.295672	-3.07947	0.882605
C	-0.66665	0.394102	-0.68405	C	0.190755	-0.29455	-1.24569
H	-0.12228	-0.31208	-0.03303	H	0.564188	0.467656	-1.94401
H	-0.6786	-0.0076	-1.70406	H	-0.47476	-0.96462	-1.80027
O	2.483635	0.653094	0.640555	O	1.410549	2.776389	-0.24795
S	2.240789	1.2374	-0.70429	S	-0.04492	2.64588	-0.56623
O	3.045199	2.436423	-0.98793	O	-0.89417	3.553432	0.286874
S	0.247731	1.996389	-0.70394	S	-0.87984	0.598525	-0.02868
O	2.290679	0.185769	-1.74938	O	-0.32234	2.948085	-2.02029
S	0.621304	-2.69097	1.31377	S	-2.16377	-1.73454	0.647412
Na	-2.07755	-2.89804	0.914975	Na	-3.63294	-0.15832	-1.06471
Na	2.528649	-1.89827	-0.51499	Na	0.065242	-1.61722	2.21963
Na	1.479695	-0.38454	2.521584	Na	-1.962	4.679813	-1.57243

Table A4.7. Optimized XYX coordinates of Int-2 and Bn-TS3

Int-2				**Bn-TS3**			
C	0.822982	2.569235	-1.6643	C	0.293585	2.685883	1.358449
C	0.736703	1.809885	-0.50089	C	0.390963	2.113632	0.093816
C	1.463184	2.165153	0.64045	C	-0.75261	1.902075	-0.68447
C	2.293188	3.288729	0.5886	C	-1.99595	2.276524	-0.16487
C	2.38353	4.050558	-0.57548	C	-2.09737	2.84779	1.102083
C	1.647803	3.69384	-1.7049	C	-0.9515	3.055332	1.867943
H	0.244735	2.277202	-2.54169	H	1.19264	2.839636	1.955223
H	0.097674	0.924674	-0.47228	H	1.363652	1.802901	-0.29354

H	2.86816	3.56931	1.472806	H	-2.89425	2.119115	-0.76468
H	3.029214	4.927432	-0.59942	H	-3.07348	3.134838	1.490871
H	1.718964	4.289698	-2.6137	H	-1.02731	3.503018	2.857783
C	1.388163	1.310252	1.863067	C	-0.66193	1.248991	-2.02652
H	1.604846	1.876483	2.778895	H	-1.42532	1.639292	-2.71175
H	0.402389	0.833946	1.962449	H	0.323997	1.38742	-2.48525
S	2.632349	-0.0447	1.697707	S	-0.91734	-0.59315	-1.89165
S	2.246248	-1.25883	3.376518	S	0.807414	-1.42744	-2.70796
C	2.833305	-3.08553	-1.36901	C	-1.08158	-3.17258	1.312712
C	1.580145	-3.26656	-0.78578	C	0.089857	-3.20382	0.556863
C	0.490771	-2.48669	-1.18107	C	1.09384	-2.2541	0.754335
C	0.674417	-1.51984	-2.17572	C	0.910347	-1.27265	1.735196
C	1.925025	-1.336	-2.75699	C	-0.25891	-1.23668	2.488979
C	3.008464	-2.11959	-2.35728	C	-1.2616	-2.18514	2.278455
H	3.67276	-3.70133	-1.04936	H	-1.8563	-3.91925	1.142513
H	1.443926	-4.02081	-0.00922	H	0.223872	-3.97232	-0.20593
H	-0.17109	-0.89892	-2.47664	H	1.6943	-0.52902	1.893469
H	2.056995	-0.57861	-3.52894	H	-0.38989	-0.46326	3.246094
H	3.985963	-1.97655	-2.81526	H	-2.17685	-2.15464	2.86828
C	-0.84891	-2.68863	-0.54493	C	2.345611	-2.29966	-0.06853
H	-1.66274	-2.69067	-1.28125	H	3.238048	-2.38382	0.566952
H	-0.8922	-3.64379	-0.00867	H	2.339345	-3.16712	-0.73763
O	-2.19236	0.268879	-1.56408	O	3.898707	0.374291	1.639832
S	-2.79444	-0.33499	-0.34876	S	4.368378	-0.02732	0.258441
O	-3.16153	0.705613	0.646318	O	4.818414	1.236975	-0.46912
S	-1.26407	-1.38873	0.702113	S	2.623904	-0.80781	-1.13306
O	-3.8569	-1.31176	-0.64531	O	5.55109	-0.96787	0.341964
Na	-2.78003	2.662612	-0.76163	Na	4.378321	2.740174	1.34013
Na	4.537804	0.175603	4.289813	Na	7.099004	0.523591	-0.77349

Table A4.8.Optimized XYX coordinates of Int-3 and Bn-TS4

Int-3				**Bn-TS4**			
C	0.34121	3.10667	1.904426	C	-1.93371	-4.11536	-0.47815
C	1.312199	2.249576	2.421831	C	-1.0141	-3.36032	0.249689
C	2.373677	1.81423	1.626101	C	-1.44926	-2.38338	1.148375
C	2.446993	2.250138	0.297954	C	-2.82449	-2.17996	1.310738
C	1.479491	3.102279	-0.22196	C	-3.74421	-2.92952	0.586226
C	0.422772	3.534653	0.582049	C	-3.29977	-3.90058	-0.31346
H	-0.47927	3.440593	2.537954	H	-1.57953	-4.87366	-1.17517
H	1.246954	1.914355	3.457904	H	0.056254	-3.52966	0.12183
H	3.268219	1.90527	-0.33321	H	-3.17288	-1.41698	2.009659
H	1.547899	3.432047	-1.25806	H	-4.81128	-2.76056	0.724268
H	-0.32945	4.211368	0.179072	H	-4.01857	-4.48997	-0.88075
C	3.393076	0.870116	2.176922	C	-0.46632	-1.55304	1.90454

H	4.413775	1.153089	1.883738	H	-0.79797	-1.37295	2.937066
H	3.353853	0.822442	3.271677	H	0.524985	-2.022	1.944658
S	3.235091	-0.84891	1.515353	S	-0.26365	0.158179	1.237501
S	1.408817	-1.46344	2.307833	S	0.612213	-0.17052	-0.6071
C	3.081673	-3.46394	-1.55528	C	-1.2852	3.98072	0.792092
C	1.919749	-3.37626	-0.78862	C	-0.93997	3.302099	-0.37729
C	0.989322	-2.36166	-1.0228	C	-1.88745	2.554483	-1.08087
C	1.23247	-1.43425	-2.04339	C	-3.20005	2.517491	-0.59413
C	2.38904	-1.5248	-2.8108	C	-3.55108	3.193936	0.569308
C	3.320479	-2.53626	-2.56574	C	-2.59062	3.924737	1.2729
H	3.799762	-4.25963	-1.36118	H	-0.52864	4.552828	1.328385
H	1.73362	-4.10161	0.005028	H	0.084954	3.348843	-0.74942
H	0.500891	-0.64249	-2.23248	H	-3.94943	1.937854	-1.13634
H	2.568116	-0.80238	-3.60664	H	-4.57815	3.154551	0.930928
H	4.226437	-2.60306	-3.16666	H	-2.86334	4.453577	2.185213
C	-0.22635	-2.23226	-0.16487	C	-1.50916	1.79436	-2.31553
H	-1.12197	-1.97734	-0.7507	H	-2.21758	2.007867	-3.12862
H	-0.43152	-3.14765	0.402925	H	-0.51347	2.109114	-2.65941
O	-1.32	0.80685	-2.63723	O	3.022134	-0.34138	1.686844
S	-2.22941	0.558665	-1.40852	S	2.800453	-0.38684	0.198226
O	-2.85093	1.966959	-1.10796	O	3.598746	0.743594	-0.44284
S	-0.1142	-0.82221	1.029582	S	-1.5079	-0.03563	-2.07523
O	-3.42873	-0.28629	-1.90173	O	3.276467	-1.68723	-0.40185
Na	-1.55932	3.13911	-2.67136	Na	4.472042	1.669906	1.583563
Na	-5.05625	1.37998	-1.6094	Na	4.718888	-0.66407	-2.06452

Table A4.9.Optimized XYX coordinates of Int-4, Bn-TS4 and Bn-P5

Int-4				**Bn-TS5**				**Bn-P5**			
C	-0.35006	4.32103	-0.71828	C	-1.09548	4.32426	-0.22595	C	-1.43942	3.03886	0.64621
C	0.224522	3.10212	-1.07743	C	-0.31851	3.28164	-0.73084	C	-0.60455	1.96750	0.34808
C	-0.51592	1.91847	-1.01694	C	-0.83422	1.98715	-0.8289	C	-0.86839	1.14572	-0.75482
C	-1.84692	1.97636	-0.58564	C	-2.14555	1.74989	-0.39794	C	-1.98071	1.42145	-1.5529
C	-2.42182	3.19088	-0.22623	C	-2.92216	2.78768	0.10723	C	-2.81857	2.49535	-1.25502
C	-1.67479	4.36817	-0.29201	C	-2.40099	4.08015	0.19217	C	-2.54961	3.30680	-0.15638
H	0.240916	5.23436	-0.77107	H	-0.67676	5.32744	-0.15714	H	-1.22092	3.67353	1.50447
H	1.261715	3.06525	-1.41354	H	0.70626	3.47117	-1.05511	H	0.27218	1.75339	0.96497
H	-2.43421	1.05690	-0.52217	H	-2.5521	0.73673	-0.44858	H	-2.19405	0.78444	-2.41359
H	-3.45963	3.22124	0.104123	H	-3.94229	2.58923	0.43515	H	-3.68584	2.69644	-1.88311
H	-2.12653	5.31862	-0.01174	H	-3.01123	4.89193	0.58551	H	-3.20391	4.14579	0.07775
C	0.10308	0.61885	-1.4095	C	-0.00427	0.89050	-1.41834	C	0.05157	0.01785	-1.0831
H	-0.58058	-0.00232	-2.00447	H	-0.51105	0.429881	-2.27382	H	-0.11224	-0.36396	-2.09806
H	1.040095	0.757724	-1.96141	H	0.97113	1.261676	-1.75342	H	1.100667	0.33781	-1.00194
S	0.467604	-0.5108	0.013922	S	0.315438	-0.52501	-0.26484	S	-0.01334	-1.43752	0.059512
S	1.896101	0.577674	1.064194	S	1.764406	0.65348	1.055882	S	2.729342	0.262013	1.678188

C	-5.51017	-0.47004	0.449108	C	-5.37356	-1.20921	0.286114	C	-5.58926	-0.17917	-0.5413
C	-4.68921	-1.53063	0.077241	C	-4.34131	-1.99009	-0.2241	C	-4.73504	-1.27637	-0.51755
C	-3.41882	-1.69465	0.644342	C	-3.09768	-2.05008	0.417072	C	-3.76754	-1.40606	0.485167
C	-3.00192	-0.77082	1.607456	C	-2.92026	-1.31336	1.591162	C	-3.6752	-0.41552	1.465758
C	-3.82052	0.293117	1.985916	C	-3.95182	-0.52967	2.108354	C	-4.52646	0.687835	1.441097
C	-5.07672	0.450574	1.405498	C	-5.18119	-0.47218	1.456427	C	-5.48588	0.807421	0.439842
H	-6.49497	-0.36099	-0.00467	H	-6.33394	-1.17677	-0.2275	H	-6.34127	-0.09293	-1.3246
H	-5.03029	-2.24635	-0.67349	H	-4.49087	-2.56191	-1.14184	H	-4.817	-2.04893	-1.28458
H	-2.01342	-0.88335	2.056055	H	-1.95682	-1.35131	2.101603	H	-2.92777	-0.51244	2.254931
H	-3.46943	1.006749	2.731403	H	-3.79142	0.041218	3.022561	H	-4.43507	1.457772	2.206417
H	-5.71591	1.28384	1.695235	H	-5.98759	0.141163	1.856496	H	-6.15073	1.67004	0.420344
C	-2.52958	-2.82132	0.214815	C	-1.98614	-2.87452	-0.15618	C	-2.8685	-2.59704	0.517063
H	-1.72534	-2.95386	0.953117	H	-1.19553	-3.01852	0.594927	H	-2.39853	-2.72827	1.499257
H	-3.10531	-3.75788	0.190714	H	-2.35456	-3.87138	-0.4353	H	-3.423	-3.51866	0.29038
O	3.520757	0.598682	-1.38858	O	3.413644	0.977751	-1.33962	O	3.04605	1.685506	-0.83949
S	3.713678	0.117052	-0.01	S	3.536172	0.293751	-0.03554	S	3.813387	0.731845	0.005252
O	3.929933	-1.34845	0.086937	O	3.674524	-1.19173	-0.19208	O	4.069005	-0.56192	-0.74469
S	-1.78329	-2.54762	-1.46115	S	-1.23602	-2.12377	-1.66471	S	-1.52028	-2.63977	-0.75061
O	4.717573	0.870981	0.784141	O	4.625667	0.817833	0.830339	O	5.14518	1.296717	0.406629
Na	0.870723	-3.5214	-1.27922	Na	2.197534	-2.36146	-1.66551	Na	3.202675	-2.42927	0.381876
Na	5.923314	-1.16982	1.61652	Na	5.67187	-1.43984	1.25247	Na	6.475063	-0.4225	-0.61484

Table A4.10.Optimized XYX coordinates of Int-2a and Bn-TS6

Int-2a				**Bn-TS6**			
C	-0.48748	-0.05043	-0.05675	C	1.101423	1.105082	-0.6571
C	0.690913	-0.47933	0.549224	C	1.269375	-0.27566	-0.62384
C	1.819765	0.345296	0.578358	C	1.82678	-0.90787	0.495898
C	1.748451	1.606566	-0.02263	C	2.19404	-0.11802	1.590395
C	0.572393	2.038606	-0.63058	C	2.031091	1.267408	1.56004
C	-0.54953	1.210695	-0.64797	C	1.487198	1.884132	0.435708
H	-1.36059	-0.70143	-0.06556	H	0.664527	1.577767	-1.53604
H	0.74106	-1.4667	1.010935	H	0.974384	-0.88266	-1.48199
H	2.626957	2.254027	-0.00759	H	2.612871	-0.59898	2.475107
H	0.530241	3.025503	-1.08925	H	2.326086	1.8653	2.421712
H	-1.4705	1.548494	-1.12057	H	1.357453	2.965142	0.411041
C	3.094305	-0.13419	1.193793	C	2.043448	-2.38837	0.50024
H	3.676278	0.690684	1.627667	H	2.186308	-2.75314	1.526843
H	2.911936	-0.88205	1.976964	H	1.17017	-2.90461	0.077689
O	10.27353	-3.36442	2.158401	O	7.772956	-2.86025	3.210539
S	9.160346	-2.7038	3.00871	S	7.114656	-1.64189	2.56067
O	8.221531	-3.84096	3.482399	O	6.602971	-0.70993	3.661436
S	4.123909	-0.92874	-0.11843	S	3.507311	-2.90785	-0.50103
O	9.903256	-2.26006	4.318485	O	8.264189	-0.87047	1.862212
S	5.83961	-1.5337	0.946654	S	5.32956	-2.28821	1.015738
Na	6.653886	1.088675	0.232277	Na	4.753237	-0.16635	-0.78924

Na	8.761056	-3.7114	5.75887	Na	8.097469	1.059563	3.204266
Na	12.05204	-2.9208	3.623937	Na	9.934008	-2.48064	2.314903

Table A4.11. Optimized XYX coordinates of Int-6, Bn-TS7 and Bn-P7

Int-6				**Bn-TS7**				**Bn-P7**			
C	13.80873	-3.0361	1.541253	C	-0.87667	2.873728	-1.82362	C	-3.63899	2.300091	-0.27277
C	13.32932	-1.84169	1.007496	C	-1.17952	1.915338	-0.86117	C	-2.55239	2.255951	0.599725
C	14.08148	-1.13325	0.067344	C	-0.95716	2.175578	0.496877	C	-1.25782	2.055018	0.113708
C	15.32286	-1.63717	-0.33193	C	-0.44587	3.421934	0.86498	C	-1.06054	1.917575	-1.26633
C	15.80265	-2.83101	0.198513	C	-0.14071	4.384196	-0.09747	C	-2.14412	1.971286	-2.13772
C	15.04592	-3.53361	1.136778	C	-0.34917	4.110248	-1.44672	C	-3.43696	2.157537	-1.64425
H	13.21239	-3.58037	2.271927	H	-1.05022	2.654943	-2.87689	H	-4.6439	2.452252	0.119117
H	12.36111	-1.45025	1.32579	H	-1.57828	0.941629	-1.15879	H	-2.70905	2.37324	1.673538
H	15.91376	-1.0767	-1.05803	H	-0.27787	3.640504	1.920351	H	-0.04372	1.752906	-1.63605
H	16.76858	-3.21795	-0.12283	H	0.264081	5.347969	0.209033	H	-1.98229	1.866229	-3.21022
H	15.42034	-4.46846	1.55083	H	-0.10606	4.856346	-2.20188	H	-4.28387	2.196663	-2.32791
C	13.57827	0.162134	-0.48316	C	-1.26535	1.143689	1.539133	C	-0.09621	1.970421	1.046812
H	13.92976	0.329674	-1.50845	H	-1.04705	1.526119	2.543097	H	0.819581	2.4063	0.620793
H	12.48249	0.202362	-0.49705	H	-2.32559	0.856485	1.518344	H	-0.30669	2.441112	2.015008
O	16.36734	1.693711	-1.37867	O	-2.50717	-1.2425	-1.04463	O	3.095343	2.226685	0.284863
S	15.29661	2.618244	-0.94338	S	-2.34313	-1.53961	0.44596	S	3.463408	1.380219	-0.96061
O	15.82606	3.773008	-0.18064	O	-3.64243	-1.09705	1.121228	O	3.823615	-0.02578	-0.36122
S	14.14352	1.60241	0.534238	S	-0.33192	-0.4448	1.352692	S	0.479008	0.247798	1.379935
O	14.36748	2.981141	-2.03547	O	-2.1099	-3.01401	0.65864	O	2.147526	1.127942	-1.73772
S	11.46952	5.030288	-0.08946	S	1.728332	0.490823	2.166614	S	-0.96759	-0.56339	2.623136
C	10.29517	4.0439	0.95611	C	2.460788	1.158783	0.605299	C	-2.25421	-1.2794	1.492182
C	9.710063	2.879048	0.220199	C	2.850859	0.100996	-0.38028	C	-1.71789	-2.10203	0.367634
C	8.690489	3.071464	-0.72187	C	3.985945	-0.68926	-0.16425	C	-1.0708	-3.3196	0.604138
C	10.17043	1.57571	0.437494	C	2.095837	-0.11693	-1.53622	C	-1.86079	-1.65866	-0.94896
C	8.159457	2.001373	-1.4351	C	4.356318	-1.67283	-1.07588	C	-0.58111	-4.07851	-0.45408
H	8.316875	4.082251	-0.89601	H	4.58123	-0.52688	0.736268	H	-0.95056	-3.67105	1.630185
C	9.641494	0.498677	-0.27575	C	2.462108	-1.10307	-2.45202	C	-1.37595	-2.41882	-2.01292
H	10.95368	1.406894	1.180883	H	1.212534	0.497302	-1.72084	H	-2.35907	-0.70659	-1.14201
C	8.636749	0.707439	-1.21748	C	3.592477	-1.88476	-2.22475	C	-0.73456	-3.63107	-1.76793
H	7.366233	2.174057	-2.16172	H	5.245253	-2.27517	-0.89203	H	-0.08432	-5.0272	-0.25579
H	10.00857	-0.51071	-0.08729	H	1.862767	-1.25846	-3.34841	H	-1.50015	-2.06004	-3.03402
H	8.221789	-0.13238	-1.77276	H	3.880615	-2.65399	-2.93985	H	-0.35541	-4.22771	-2.59618
H	10.82327	3.685434	1.851038	H	1.745477	1.861702	0.158079	H	-2.85343	-1.88226	2.189491
H	9.488972	4.708809	1.297535	H	3.3426	1.734936	0.918208	H	-2.88423	-0.46424	1.118308
Na	12.00567	3.171574	-2.16294	Na	1.576878	2.594807	4.221995	Na	3.66283	0.609338	1.894392
Na	18.17706	3.120271	-0.04792	Na	-4.55288	-0.04811	-0.80547	Na	1.943363	-1.14967	-1.22795

Supplementary data of Chapter 4

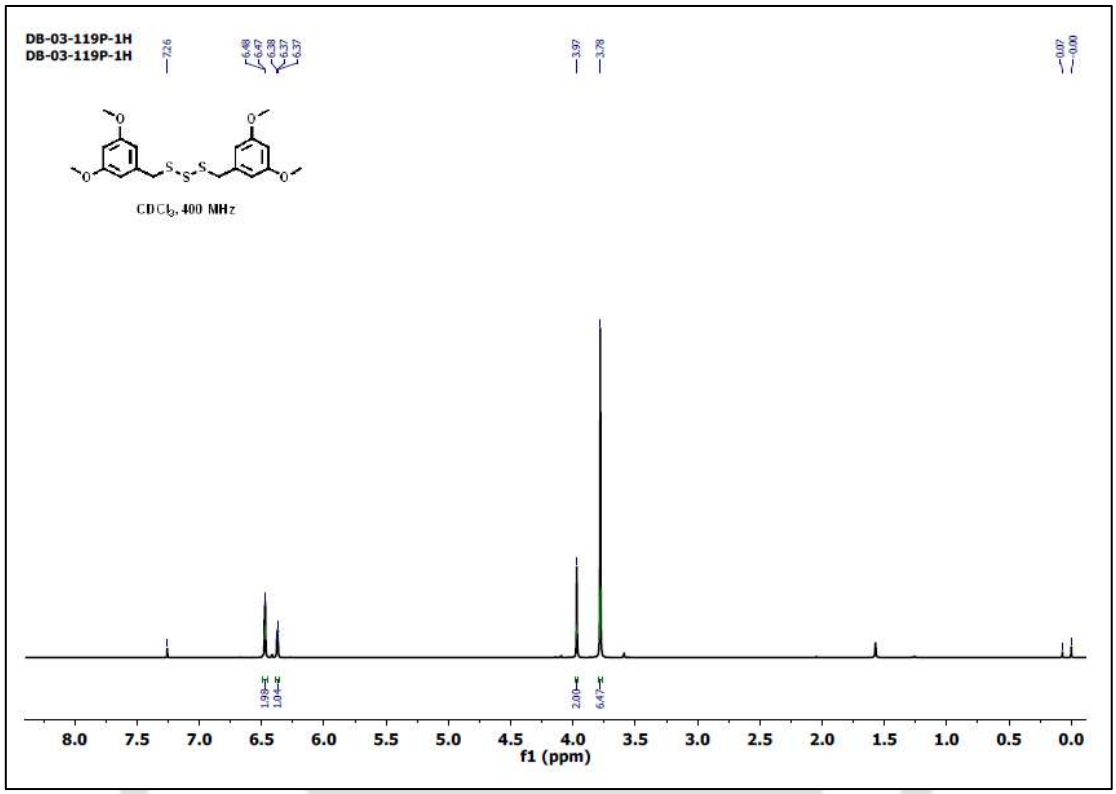

Figure A5.1. ^{1}H NMR ($CDCl_3$, 400 MHz, ppm) spectrum of compound **4.1**.

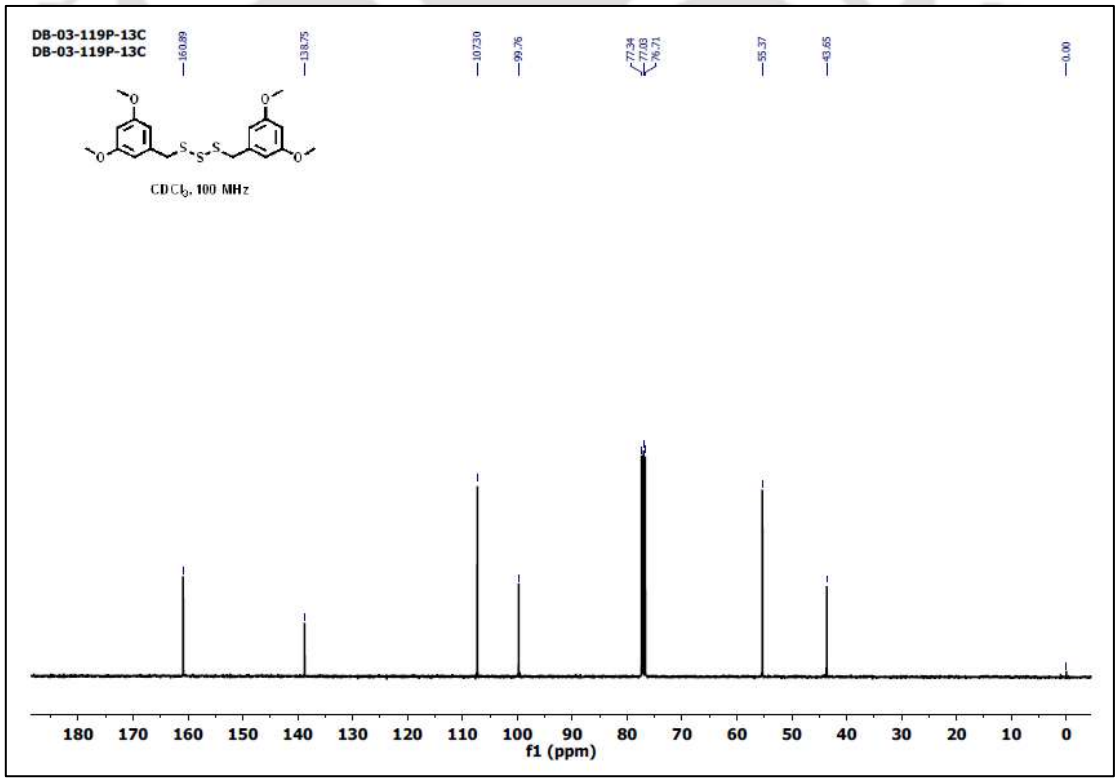

Figure A5.2. ^{13}C NMR ($CDCl_3$, 100 MHz, ppm) spectrum of compound **4.1**.

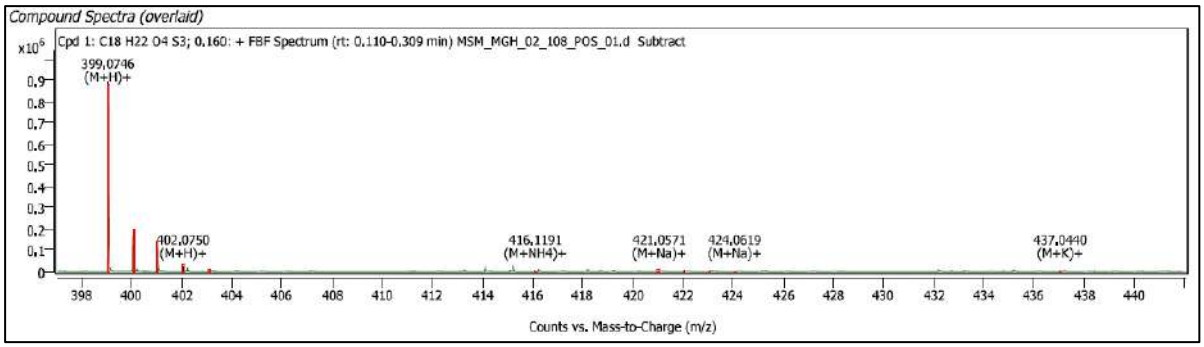

Figure A5.3. ESI-MS (+ve) spectrum of compound **4.1**. ESI-MS: *m*/*z* calcd. for $C_{18}H_{22}O_4S_3$ $[M+H]^+$: 399.0753; observed: 399.0746.

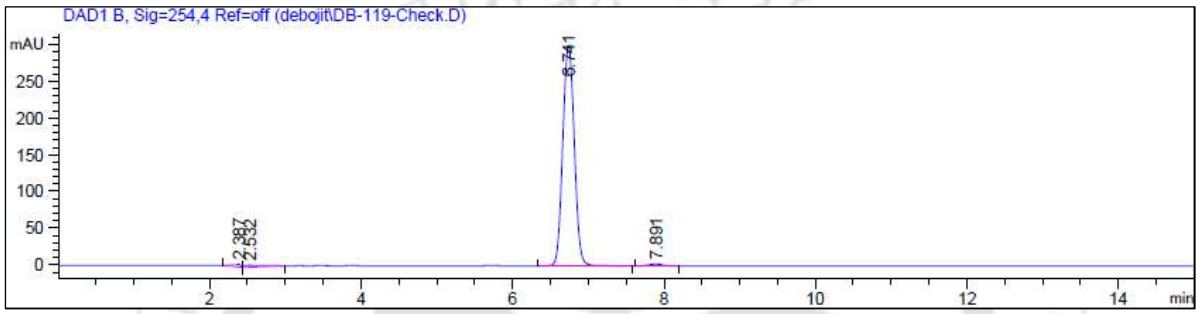

Figure A5.4. HPLC chromatogram of pure symmetrical trisulfide **4.1**.

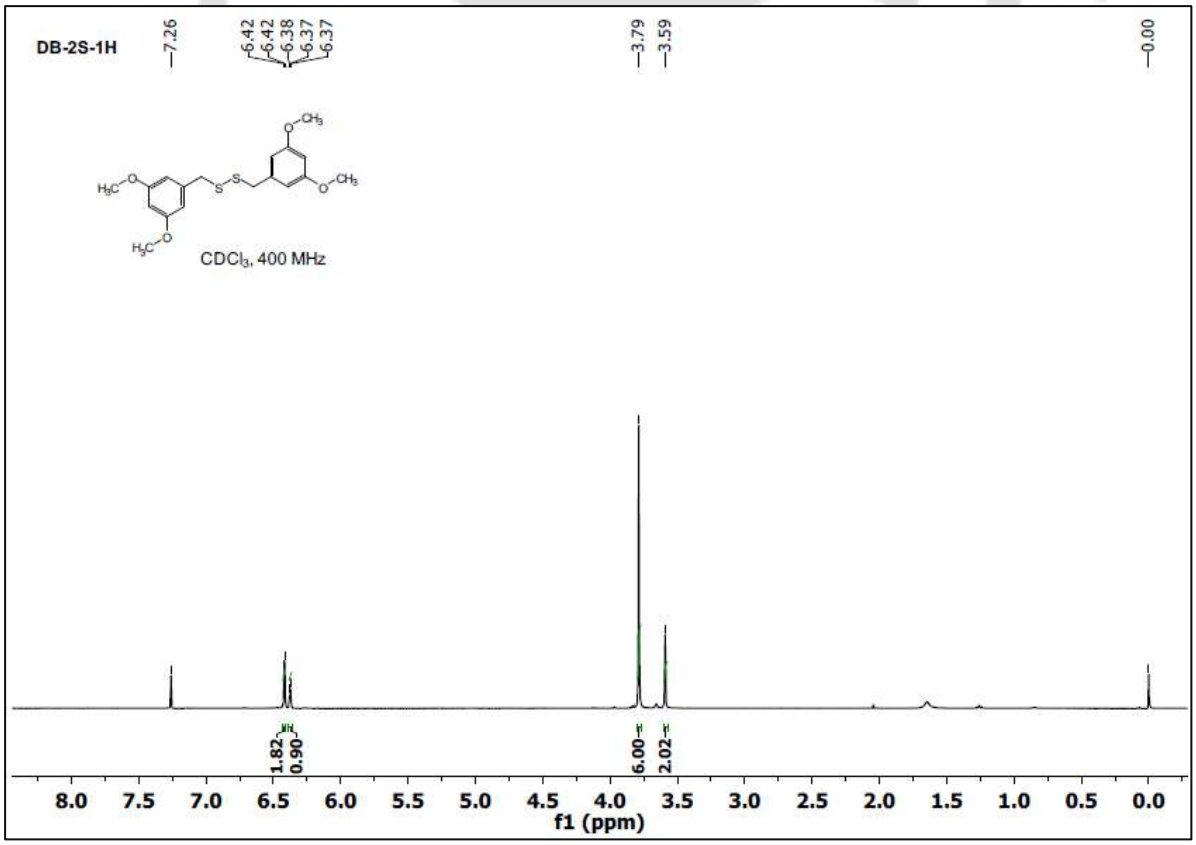

Figure A5.5. ^{1}H NMR ($CDCl_3$, 400 MHz, ppm) spectrum of compound **4.2**.

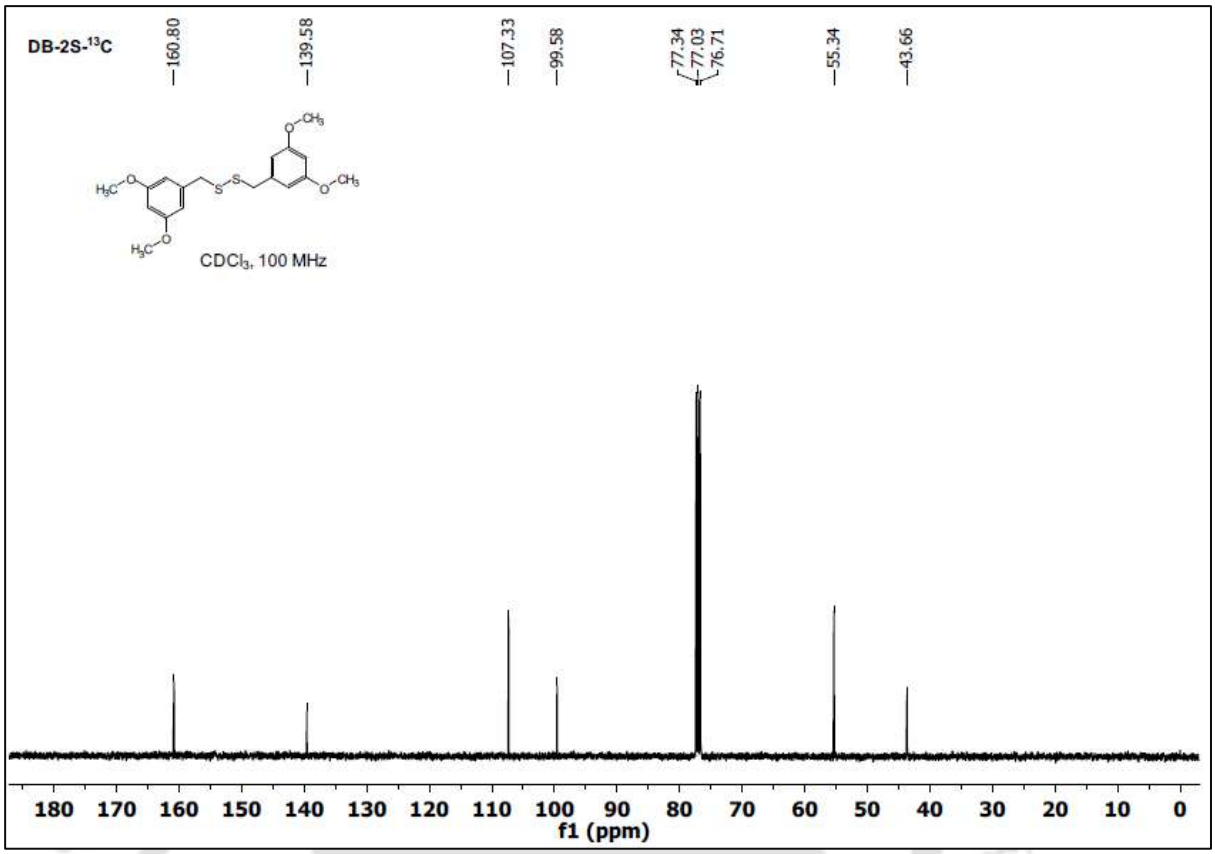

Figure A5.6. ^{13}C NMR ($CDCl_3$, 100 MHz, ppm) spectrum of compound **4.2**.

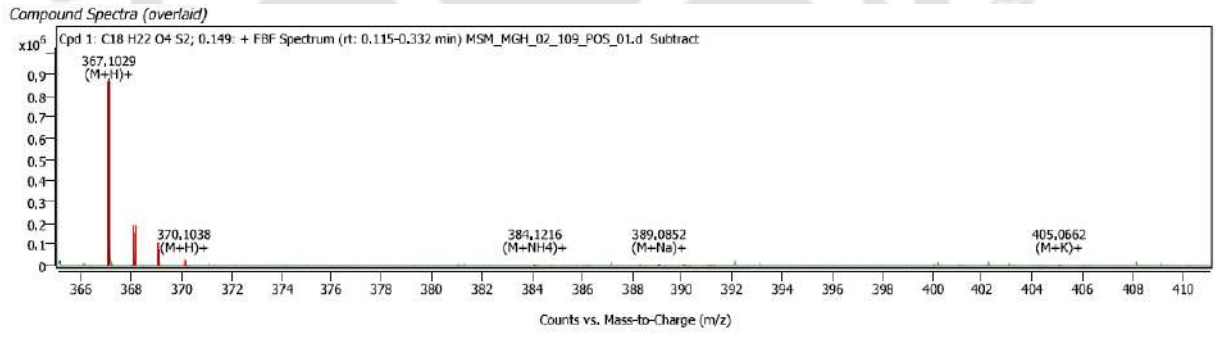

Figure A5.7. ESI-MS spectrum of compound **4.2**. ESI-MS (+ve): *m*/*z* calcd. For $C_{18}H_{22}O_4S_2$ $[M+H]^+$: 367.1032; observed: 367.1029.

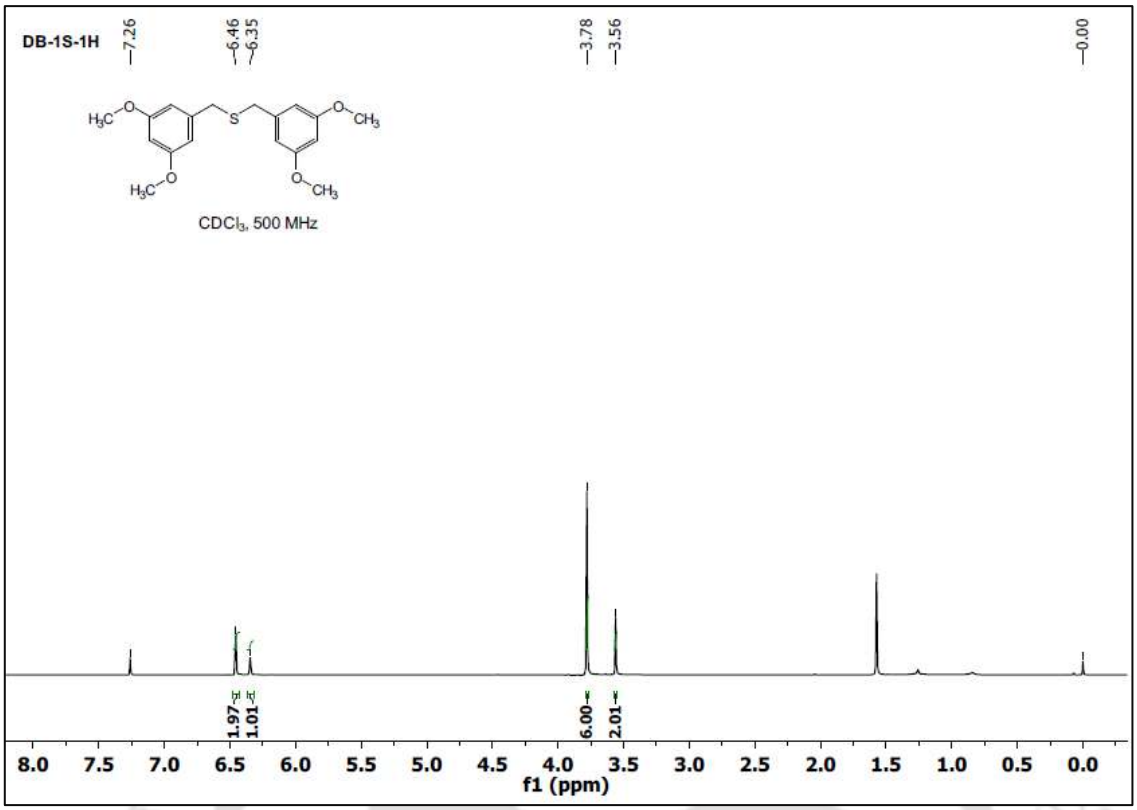

Figure A5.8. ^{1}H NMR ($CDCl_3$, 500 MHz, ppm) spectrum of compound **4.3**.

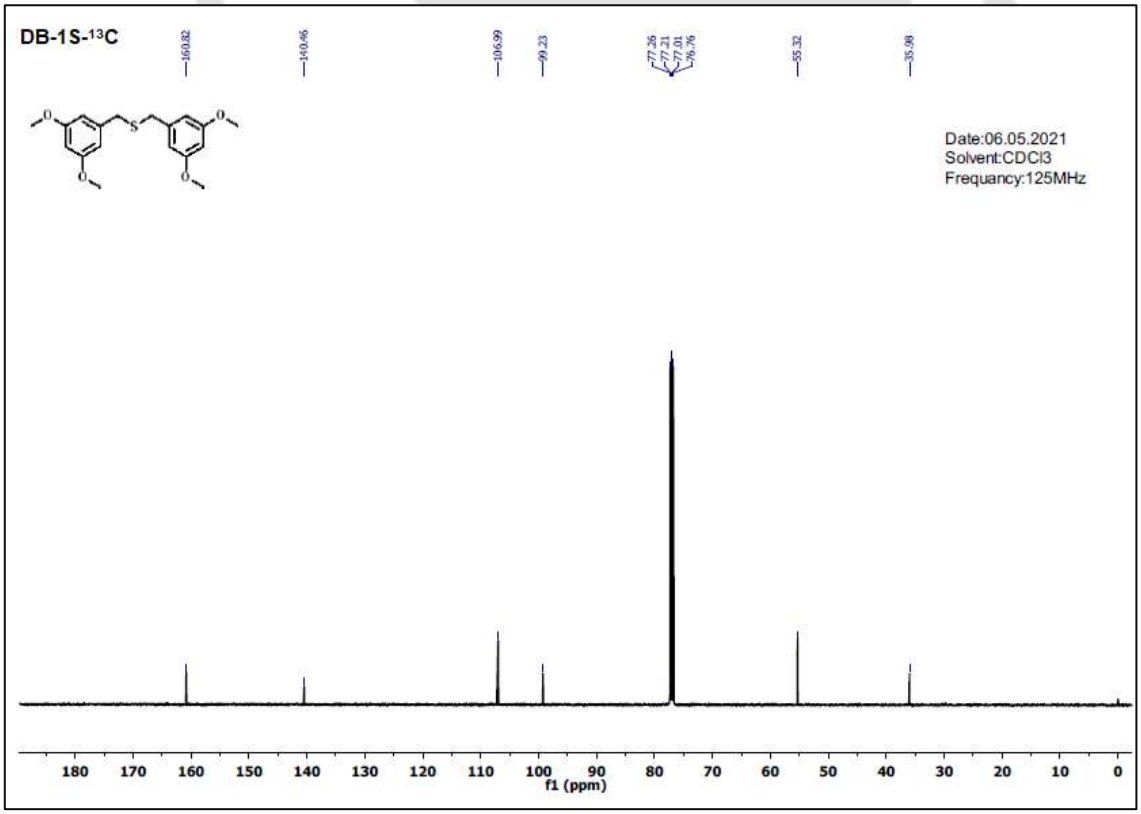

Figure A5.9. ^{13}C NMR ($CDCl_3$, 125 MHz, ppm) spectrum of compound **4.3**.

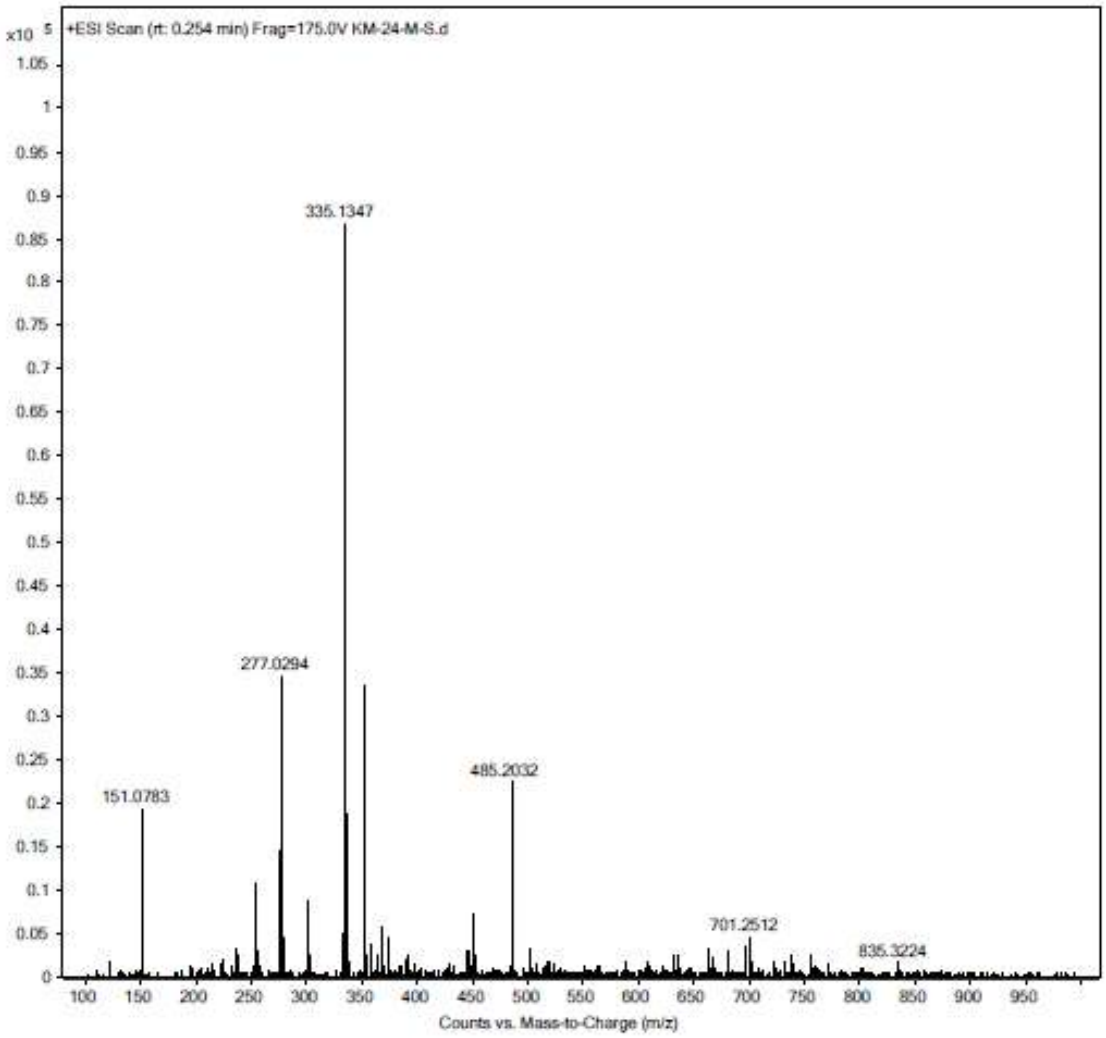

Figure A5.10. ESI-MS spectrum of compound **4.3**. ESI-MS (+ve): *m*/*z* calcd. for $C_{18}H_{22}O_4S$ $[M+H]^+$: 335.1312; observed: 335.1347.

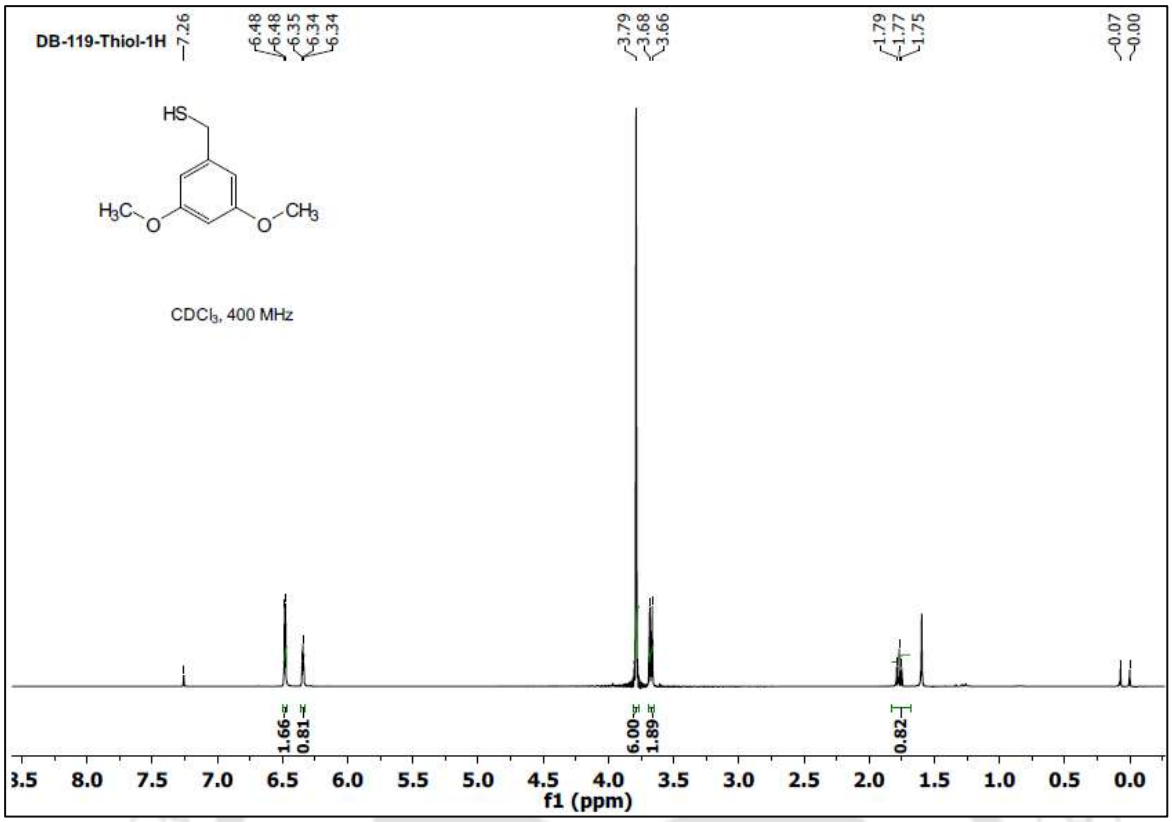

Figure A5.11. ^{1}H NMR ($CDCl_3$, 400 MHz, ppm) spectrum of compound **4.5**.

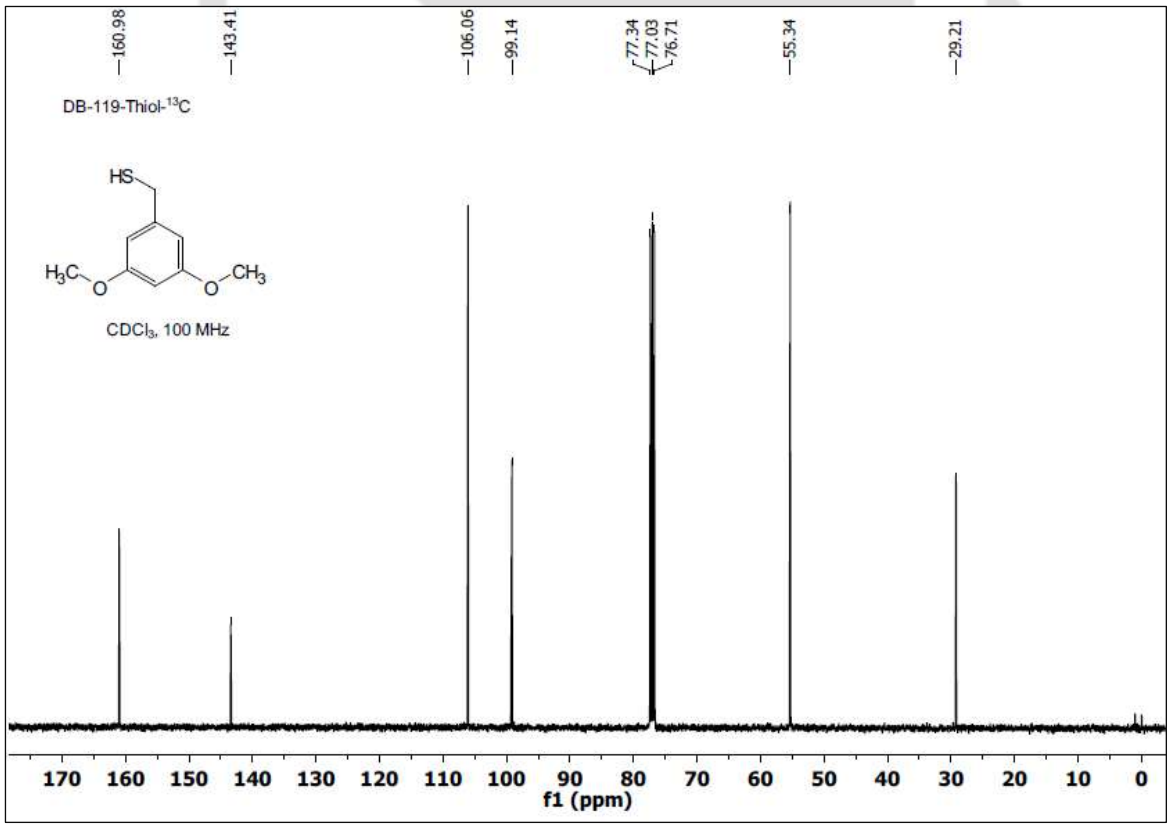

Figure A5.12. ^{13}C NMR ($CDCl_3$, 100 MHz, ppm) spectrum of compound **4.5**.
